Flight Dynamics Principles

M. V. Cook

BSc, MSc, CEng, FRAeS, CMath, FIMA
Senior Lecturer in the College of Aeronautics
Cranfield University

BUTTERWORTH HEINEMANN

OXFORD • AUCKLAND • BOSTON • JOHNANNESBURG • MELBOURNE • NEW DELHI

Butterworth-Heinemann
Linacre House, Jordan Hill, Oxford OX2 8DP
225 Wildwood Avenue, Woburn, MA 01801-2041
A division of Reed Educational and Professional Publishing Ltd

A member of the Reed Elsevier plc group

First published 1997
Reprinted by Reed Educational & Professional Publishing Ltd.
Transferred to Digital Printing 2004

British Library Cataloguing in Publication Data
A catalogue record for this book is available from the British Library

Library of Congress Cataloguing in Publication Data
A catalogue record for this book is available from the Library of Congress

ISBN 0 340 63200 3

For more information on all Butterworth-Heinemann publications please visit our web site www.bh.com

Typeset in 10/12 Times by AFS Image Setters Ltd, Glasgow

Preface

When I joined the staff of the College of Aeronautics some years ago I was presented with a well-worn collection of lecture notes and invited to teach *Aircraft Stability and Control* to postgraduate students. Inspection of the notes revealed the unmistakable signs that their roots reached back to the work of W. J. Duncan, which is perhaps not surprising since Duncan was the first Professor of Aerodynamics at Cranfield some 50 years ago. It is undoubtedly a privilege and, at first, was very daunting to be given the opportunity to follow in the footsteps of such a distinguished academic. From that humble beginning my interpretation of the subject has continuously evolved to its present form, which provided the basis for this book.

The classical linearized theory of the stability and control of aircraft is timeless, it is brilliant in its relative simplicity and it is very securely anchored in the domain of the aerodynamicist. So what is new? The short answer is: not a great deal. However, today the material is used and applied in ways that have changed considerably, due largely to the advent of the digital computer. The computer is used as the principal tool for analysis and design, and it is also the essential component of the modern flight control system on which all advanced-technology aeroplanes depend. It is the latter development in particular which has had, and continues to have, a major influence on the way in which the material of the subject is now used. It is no longer possible to guarantee good flying and handling qualities simply by tailoring the stability and control characteristics of an advanced-technology aeroplane by aerodynamic design alone. Flight control systems now play an equally important part in determining the flying and handling qualities of an aeroplane by augmenting the stability and control characteristics of the airframe in a beneficial way. Therefore, the subject has had to evolve in order to facilitate integration with flight control and, today, the integrated subject is much broader in scope and is more frequently referred to as *Flight Dynamics*.

The treatment of the material in this book reflects my personal experience of using, applying and teaching it over a period of many years. My formative experience was gained as a Systems Engineer in the avionics industry where the emphasis was on the design of flight control systems. In more recent years, in addition to teaching a formal course in the subject, I have been privileged to have spent very many hours teaching the classical material in the College of Aeronautics' airborne laboratory aircraft. This experience has enabled me to develop the material from the classical treatment introduced by Duncan in the earliest days of the College of Aeronautics to the present

treatment, which is biased towards modern systems applications. However, the vitally important aerodynamic origins of the material remain clear and for this I can take no credit.

Modern flight dynamics tends to be concerned with the wider issues of flying and handling qualities rather than with the traditional, and more limited, issues of stability and control. The former is, of course, largely shaped by the latter and for this reason the emphasis is on dynamics and its importance to flying and handling qualities.

The material is developed using dimensional or normalized dimensional forms of the aircraft equations of motion only. These formulations are in common use, with minor differences, on both sides of the North Atlantic. The understanding of the dimensionless equations of motion has too often been a major stumbling block for many students and, in my experience, I have never found it necessary, or even preferable, to work with the classical dimensionless equations of motion. The dimensionless equations of motion are a creation of the aerodynamicist and are referred to only in so far as is necessary to explain the origins and interpretation of the dimensionless aerodynamic stability and control derivatives. However, it remains most appropriate to use dimensionless derivatives to describe the aerodynamic properties of an airframe.

It is essential that the modern flight dynamicist has not only a thorough understanding of the classical theory of the stability and control of aircraft, but also some knowledge of the role and structure of flight control systems. Consequently, a basic understanding of the theory of control systems is necessary and then it becomes obvious that the aircraft may be treated as a *system* that may be manipulated and analysed using the tools of the control engineer. As a result, it is common to find control engineers looking to modern aircraft as an interesting challenge for the application of their skills. Unfortunately, it is also too common to find control engineers who have little or no understanding of the dynamics of their *plant* which, in my opinion, is unacceptable. It has been my intention to address this problem by developing the classical theory of the stability and control of aircraft in a systems context in order that it should become equally accessible to both the aeronautical engineer and to the control engineer. This book, then, is an aeronautical text which borrows from the control engineer rather than a control text which borrows from the aeronautical engineer.

This book is primarily intended for undergraduate and postgraduate students studying aeronautical subjects and those students studying avionics, systems engineering, control engineering, mathematics, etc, who wish to include some flight dynamics in their studies. Of necessity, the scope of the book is limited to linearized small perturbation aircraft models since the material is intended for those coming to the subject for the first time. However, a good understanding of the material should give the reader the basic skills and confidence to analyse and evaluate aircraft flying qualities and to initiate preliminary augmentation system design. It should also provide a secure foundation from which to move on into non-linear flight dynamics, simulation and advanced flight control.

M. V. Cook
College of Aeronautics
Cranfield University

Acknowledgements

Over the years I have been fortunate to have worked with a number of very able people from whom I have learned a great deal. My own understanding and interpretation of the subject has benefited enormously from that contact and it is appropriate to acknowledge the contributions of those individuals.

My own formal education was founded on the text by W. J. Duncan and, later, on the first text by A. W. Babister, and as a result the structure of the present book has many similarities to those earlier texts. This, I think, is inevitable since the treatment and presentation of the subject has not really been bettered in the intervening years.

During my years at what is now GEC-Marconi Avionics Ltd I worked with David Sweeting, John Corney and Richard Smith on various flight control system design projects. This activity also brought me into contact with Brian Gee, John Gibson and Arthur Barnes at British Aerospace (Military Aircraft Division) all three of whom are now retired. Of the many people with whom I worked these individuals in particular were, in some way, instrumental in helping me to develop a greater understanding of the subject in its widest modern context.

During my early days at Cranfield my colleagues Angus Boyd, Harry Ratcliffe, Dr Peter Christopher and Dr Martin Eshelby were especially helpful with advice and guidance at a time when I was establishing my teaching activities. I also consider myself extremely fortunate to have spent hundreds of hours flying with a small but distinguished group of test pilots, Angus McVitie, Ron Wingrove and Roger Bailey as we endeavoured to teach and demonstrate the rudiments of flight mechanics to generations of students. My contribution to the experimental flying programme was an invaluable experience, which has enhanced my understanding of the subtleties of aircraft behaviour considerably. In more recent years, the development of the postgraduate course in Flight Dynamics brought me into contact with my present colleagues, Peter Thomasson, John Lewis and Dr Sandra Fairs, with all of whom it is a delight to work. Their cooperative interest and enthusiasm, and indeed their forbearance during the long preparation of this book, has been, and continues to be, most encouraging. I must also acknowledge my former colleague Jim Lipscombe, now retired, whose knowledgeable advice and guidance has been directly instrumental in determining the way in which my material has developed more recently. On a practical note, I am indebted to Chris Daggett who obtained some of the experimental flight data for me which has been used to illustrate the examples based on the College of Aeronautics' Jetstream aircraft.

The numerous bright young people who have been my students have unwittingly contributed to this material by providing the all important 'customer feedback'. Since this is the audience to which the work is directed it is fitting that what has probably been the most important contribution to its development is gratefully acknowledged.

Finally, I am indebted to David Ross of Arnold who has had the unenviable task of transforming my original material into the volume you now have before you.

To the above mentioned I am extremely grateful and to all of them I extend my most sincere thanks.

M. V. Cook

Cover pictures

Front cover

The front cover photograph shows the College of Aeronautics Handley Page Jetstream laboratory aircraft which is used for teaching and research in Experimental Flight Mechanics.

Back cover

The back cover photograph shows the Cranfield A1 aircraft. This fully aerobatic aeroplane was designed and built by the College of Aeronautics to a specification by the late Neil Williams, sometime European aerobatic champion.

All photography by the Photographic Unit of Cranfield University Press and reproduced with the kind permission of Cranfield University.

Nomenclature

Of the very large number of symbols required by the subject, many have more than one meaning. Usually the meaning is clear from the context in which the symbol is used.

a	Wing or wing–body lift curve slope. Acceleration. Local speed of sound
a'	Inertial or absolute acceleration
a_0	Speed of sound at sea level. Tailplane zero incidence lift coefficient
a_1	Tailplane lift curve slope
a_{1_F}	Fin lift curve slope
a_2	Elevator lift curve slope
a_3	Elevator tab lift curve slope
a_∞	Lift curve slope of an infinite span wing
a_h	Local lift curve slope at coordinate h
a_y	Local lift curve slope at spanwise coordinate y
ac	Aerodynamic centre
A	Aspect ratio
$\mathbf{A}$	State matrix
b	Wing-span
b_1	Elevator hinge moment derivative with respect to α_T
b_2	Elevator hinge moment derivative with respect to η
b_3	Elevator hinge moment derivative with respect to β_η
$\mathbf{B}$	Input matrix
c	Chord. Viscous damping coefficient. Command input
$\bar{c}$	Standard mean chord (*smc*)
$\bar{\bar{c}}$	Mean aerodynamic chord (*mac*)
$\bar{\bar{c}}_\eta$	Mean elevator chord aft of hinge line
c_h	Local chord at coordinate h
c_y	Local chord at spanwise coordinate y
cg	Centre of gravity
cp	Centre of pressure
C	Command path transfer function
$\mathbf{C}$	Output matrix
C_D	Drag coefficient

C_{D_0} Zero lift drag coefficient
C_l Rolling moment coefficient
C_L Lift coefficient
C_{L_w} Wing or wing–body lift coefficient
C_{L_T} Tailplane lift coefficient
C_H Elevator hinge moment coefficient
C_m Pitching moment coefficient
C_{m_0} Pitching moment coefficient about aerodynamic centre of wing
C_{m_α} Slope of C_m–α plot
C_n Yawing moment coefficient
D Drag
D' Drag in a lateral-directional perturbation
$\mathbf{D}$ Direction cosine matrix. Direct matrix
D_c Drag due to camber
D_α Drag due to incidence
F Aerodynamic force. Feed-forward path transfer function
F_c Aerodynamic force due to camber
F_α Aerodynamic force due to incidence
F_η Elevator control force
g Acceleration due to gravity
g_η Elevator stick to surface mechanical gearing constant
G Controlled system transfer function
h Height. Centre of gravity position on reference chord. Spanwise coordinate along wing sweep line
h_0 Aerodynamic centre position on reference chord
h_F Fin height coordinate above roll axis
h_m Controls fixed manoeuvre point position on reference chord
h'_m Controls free manoeuvre point position on reference chord
h_n Controls fixed neutral point position on reference chord
h'_n Controls free neutral point position on reference chord
H Elevator hinge moment. Feedback path transfer function
H_F Fin span measured perpendicular to the roll axis
H_m Controls fixed manoeuvre margin
H'_m Controls free manoeuvre margin
i_x Dimensionless moment of inertia in roll
i_y Dimensionless moment of inertia in pitch
i_z Dimensionless moment of inertia in yaw
i_{xz} Dimensionless product of inertia about ox and oz axes
I' Normalized inertia
I_x Moment of inertia in roll
I_y Moment of inertia in pitch
I_z Moment of inertia in yaw
$\mathbf{I}$ Identity matrix
I_{xy} Product of inertia about ox and oy axes
I_{xz} Product of inertia about ox and oz axes
I_{yz} Product of inertia about oy and oz axes
j The complex variable ($\sqrt{-1}$)
k General constant. Spring stiffness coefficient

k_q Pitch rate transfer function gain constant
k_u Axial velocity transfer function gain constant
k_w Normal velocity transfer function gain constant
k_θ Pitch attitude transfer function gain constant
k_τ Turbo-jet engine gain constant
K Feedback gain
$\mathbf{K}$ Feedback gain matrix
K_n Controls fixed static stability margin
K'_n Controls free static stability margin
l_f Fin arm measured between wing and fin quarter chord points
l_t Tail arm measured between wing and tailplane quarter chord points
l_F Fin arm measured between *cg* and fin quarter chord point
l_T Tail arm measured between *cg* and tailplane quarter chord point
L Lift. Rolling moment
L' Lift in a lateral-directional perturbation
L_c Lift due to camber
L_w Wing or wing–body lift
L_F Fin lift
L_T Tailplane lift
L_α Lift due to incidence
m Mass
m' Normalized mass
M Local Mach number
M_0 Free stream Mach number
M_{crit} Critical Mach number
M Pitching moment
$\mathbf{M}$ 'Mass' matrix
M_0 Wing–body pitching moment about wing aerodynamic centre
M_T Tailplane pitching moment about tailplane aerodynamic centre
n Total normal load factor
n_α Normal load factor per unit angle of attack
n' Inertial normal load factor
N Yawing moment
o Origin of axes
p Roll rate perturbation. Trim reference point. System pole
Q Dynamic pressure
q Pitch rate perturbation
r Yaw rate perturbation. General response variable
R Radius of turn
s Wing semi-span. Laplace operator
S Wing reference area
S_B Projected body side reference area
S_F Fin reference area
S_T Tailplane reference area
S_η Elevator area aft of hinge line
t Time. Maximum aerofoil section thickness
T Time constant
T_r Roll mode time constant

T_s Spiral mode time constant
T_u Numerator zero in axial velocity transfer function
T_w Numerator zero in normal velocity transfer function
T_θ Numerator zero in pitch rate and attitude transfer functions
T_τ Turbo-jet engine time constant
T_2 Time to double amplitude
u Axial velocity perturbation
$\mathbf{u}$ Input vector
U Total axial velocity
U_e Axial component of steady equilibrium velocity
U_E Axial velocity component referred to datum-path earth axes
v Lateral velocity perturbation
$\mathbf{v}$ Eigenvector
V Perturbed total velocity. Total lateral velocity
V_e Lateral component of steady equilibrium velocity
V_E Lateral velocity component referred to datum-path earth axes
V_0 Steady equilibrium velocity
$\bar{V}_F$ Fin volume ratio
$\bar{V}_T$ Tailplane volume ratio
$\mathbf{V}$ Eigenvector matrix
w Normal velocity perturbation
W Total normal velocity
W_e Normal component of steady equilibrium velocity
W_E Normal velocity component referred to datum-path earth axes
x Longitudinal coordinate in axis system
$\mathbf{x}$ State vector
X Axial force component
y Lateral coordinate in axis system
y_B Lateral body 'drag' coefficient
$\mathbf{y}$ Output vector
Y Lateral force component
z Normal coordinate in axis system. System zero
$\mathbf{z}$ Transformed state vector
Z Normal force component

Greek letters

α Angle of attack or incidence perturbation
α' Incidence perturbation
α_e Equilibrium incidence
α_T Local tailplane incidence
β Sideslip angle perturbation
β_e Equilibrium sideslip angle
β_η Elevator trim tab angle
γ Flight path angle perturbation. Imaginary part of a complex number
γ_e Equilibrium flight path angle
Γ Wing dihedral angle
δ Control angle. Increment. Unit impulse function

δ_ξ Roll control stick angle
δ_η Pitch control stick angle
δ_ζ Rudder pedal control angle
δm Mass increment
Δ Characteristic polynomial. Transfer function denominator
ε Throttle lever angle. Downwash angle at tailplane. Closed loop system error
ζ Rudder angle perturbation. Damping ratio
ζ_d Dutch roll damping ratio
ζ_p Phugoid damping ratio
ζ_s Short period pitching oscillation damping ratio
η Elevator angle perturbation
η_T Tailplane setting angle
θ Pitch angle perturbation. A general angle
θ_e Equilibrium pitch angle
λ Eigenvalue
Λ Wing sweep angle
$\mathbf{\Lambda}$ Eigenvalue matrix
μ_1 Longitudinal relative density factor
μ_2 Lateral relative density factor
ξ Aileron angle perturbation
ρ Air density
σ Aerodynamic time parameter. Real part of a complex number
τ Engine thrust perturbation. Time parameter
ϕ Roll angle perturbation. Phase angle. A general angle
$\mathbf{\Phi}$ State transition matrix
ψ Yaw angle perturbation
ω Undamped natural frequency
ω_b Bandwidth frequency
ω_d Dutch roll undamped natural frequency
ω_n Damped natural frequency
ω_p Phugoid undamped natural frequency
ω_s Short period pitching oscillation undamped natural frequency

Subscripts

0 Datum axes. Normal earth fixed axes. Wing or wing–body aerodynamic centre. Free stream flow conditions
1/4 Quarter chord
2 Double or twice
∞ Infinite span
a Aerodynamic
b Aeroplane body axes. Bandwidth
B Body or fuselage
c Control. Chord. Compressible flow. Camber line
d Atmospheric disturbance. Dutch roll
D Drag
e Equilibrium, steady or initial condition
E Datum-path earth axes

F Fin
g Gravitational
H Elevator hinge moment
i Incompressible flow
l Rolling moment
le Leading edge
L Lift
m Pitching moment. Manoeuvre
n Damped natural frequency
n Neutral point. Yawing moment
p Power. Phugoid
p Roll rate
q Pitch rate
r Roll mode
r Yaw rate
s Short period pitching oscillation. Spiral mode
T Tailplane
u Axial velocity
v Lateral velocity
w Aeroplane wind or stability axes. Wing or wing–body
w Normal velocity
x ox axis
y oy axis
z oz axis

α Angle of attack or incidence
ε Throttle lever
ζ Rudder
η Elevator
θ Pitch
ξ Ailerons
τ Thrust

Examples of other symbols and notation

x_u A shorthand notation to denote a concise derivative, a dimensional derivative divided by the appropriate mass or inertia parameters
X_u A shorthand notation to denote the dimensionless derivative $\frac{\partial \hat{X}}{\partial \hat{u}}$
$\mathring{X}_u$ A shorthand notation to denote the dimensional derivative $\frac{\partial X}{\partial u}$
$N_u^y(t)$ A shorthand notation to denote a transfer function numerator polynomial relating the output response y to the input u
$(^*)$ A superscript to denote a complex conjugate
$\hat{u}$ A shorthand notation to denote that the variable u is dimensionless

Please note that although the pronoun 'he' has been used throughout for clarity, it is not intended to imply that piloting and flight dynamics analysis are gender specific.

1
Introduction

1.1 Overview

This book is primarily concerned with the provision of good flying and handling qualities in the conventional aeroplane. Consequently it is also very much concerned with the stability, control and dynamic characteristics which are fundamental to the determination of those qualities. Since flying and handling qualities are of critical importance to safety and to the piloting task it is essential that their origins are properly understood. Here then, the intention is to set out the basic principles of the subject at an introductory level and to illustrate the application of those principles by means of worked examples.

Following the first flights made by the Wright brothers in December 1903, the pace of aeronautical development quickened and the progress made in the following decade or so was dramatic. However, the stability and control problems that faced the early aviators were sometimes considerable since the flying qualities of their aeroplanes were often less than satisfactory. Many investigators were studying the problems of stability and control at the time, although it is the published works of Bryan (1911) and Lanchester (1908) which are usually accredited with laying the first really secure foundations for the subject. By conducting many experiments with flying models Lanchester was able to observe and successfully describe mathematically some dynamic characteristics of aeroplanes. The beauty of Lanchester's work was its practicality and theoretical simplicity, thereby lending itself to easy application and interpretation. Bryan, on the other hand, was a mathematician who chose to apply his energies, with the assistance of a Mr Harper, to the problems of the stability and control of the aeroplane. Bryan developed the general equations of motion of a rigid body with six degrees of freedom to describe successfully the motion of the aeroplane. His treatment, with very few changes, is still in everyday use. What has changed is the way in which the material is now used, due largely to the advent of the digital computer as an analysis tool. The stability and control of aeroplanes is a subject which has its origins in aerodynamics and the classical theory of the subject is traditionally expressed in the language of the aerodynamicist. The objective of the present work is to revisit the development of the classical theory and to express it in the language of the systems engineer where it is more appropriate to do so.

Flight Dynamics is about the relatively short term motion of an aeroplane in response to a control input or to an external disturbance such as atmospheric turbulence. The

motion of interest can vary from small excursions about trim to very large amplitude manoeuvring when normal aerodynamic behaviour may well become very non-linear. Since the treatment of the subject in this book is introductory, a discussion of large amplitude dynamics is beyond the scope of the present work. The dynamic behaviour of an aeroplane is significantly shaped by its stability and control properties, which in turn have their roots in the aerodynamics of the airframe. Previously the achievement of good stability characteristics in an aeroplane usually ensured good flying qualities, all of which depended only on good aerodynamic design. Expanding flight envelopes and the increasing dependence on *automatic flight control systems* (AFCS) for stability augmentation means that good flying qualities are no longer a guaranteed product of good aerodynamic design and good stability characteristics. The reasons for this apparent inconsistency are now reasonably well understood and, put very simply, result from the addition of flight control system dynamics to those of the airframe. Flight control system dynamics are, of course, a necessary, but not always desirable, by-product of stability augmentation.

Modern flight dynamics is concerned not only with the dynamics, stability and control of the basic airframe but also with the sometimes complex interaction between aeroplane and flight control system. Since the flight control system comprises motion sensors, a control computer, control actuators and other items of control hardware, a study of the subject becomes a multi-disciplinary activity. Therefore, it is essential that the modern flight dynamicist has, not only a thorough understanding of the classical stability and control theory of aeroplanes but also a working knowledge of control theory and of the use of computers in a flight critical environment. Thus, the aeroplane together with the flight control equipment may be treated as a whole *system* using the traditional tools of the aerodynamicist together with the analytical tools of the control engineer.

Thus, in a modern approach to the analysis of stability and control it is convenient to treat the aeroplane as a system component. This leads to the derivation of mathematical models which describe the aeroplane in terms of aerodynamic transfer functions. Described in this way, the stability, control and dynamic characteristics of the aeroplane are readily interpreted with the aid of very powerful computational systems engineering tools. It follows that the mathematical model of the aeroplane is immediately compatible with, and provides the foundation for, integration with flight control system studies. This is an ideal state of affairs since, today, it is most likely that stability and control investigations are a precursor to flight control system development.

Today, the modern flight dynamicist tends to be concerned with the wider issues of flying and handling qualities rather than with the traditional, and more limited issues of stability and control. The former is, of course, largely determined by the latter. The present treatment of the material is shaped by answering the following questions which a newcomer to the subject might be tempted to ask.

(i) *How are the stability and control characteristics of an aeroplane determined and how do they influence flying qualities?*

The answer to this question involves the establishment of a suitable mathematical framework for the problem, the development of the equations of motion, the solution of the equations of motion, investigation of response to controls and the general interpretation of dynamic behaviour.

(ii) *What are acceptable flying qualities, how are the requirements defined, interpreted and applied, and how do they limit flight characteristics?*

The answer to this question involves a review of standard flying qualities requirements documents and the evaluation and interpretation of the detail requirements.

(iii) *When an aeroplane has unacceptable flying qualities how may its dynamic characteristics be augmented?*

The answer to this question involves an introduction to the rudiments of feedback control as the means for augmenting the stability of the basic airframe.

1.2 Flying and handling qualities

The flying and handling qualities of an aeroplane are those properties which describe the ease and effectiveness with which it responds to pilot commands in the execution of some flight task. In the first instance, therefore, flying and handling qualities are described qualitatively and are formulated in terms of *pilot opinion*, consequently they tend to be rather subjective. The process involved in the pilot perception of flying and handling qualities may be interpreted in the form of a signal flow diagram as shown in Fig. 1.1. The solid lines represent physical, mechanical or electrical signal flow paths, whereas the dashed lines represent sensory feedback information to the pilot. The author's interpretation distinguishes between *flying qualities* and *handling qualities* as indicated. The pilot's perception of flying qualities is considered to comprise a qualitative description of how well the aeroplane carries out the commanded task. On the other hand, the pilot's perception of handling qualities is considered a qualitative description of the adequacy of the short term dynamic response to controls in the execution of the flight task. The two *qualities* are therefore very much interdependent and, in practice, are probably inseparable. Thus, to summarize, the flying qualities may be regarded as being task related, whereas the handling qualities may be regarded as being response related. When the airframe characteristics are augmented by a flight control system, the way in which the flight control system may influence the flying and handling qualities is clearly shown in Fig. 1.1.

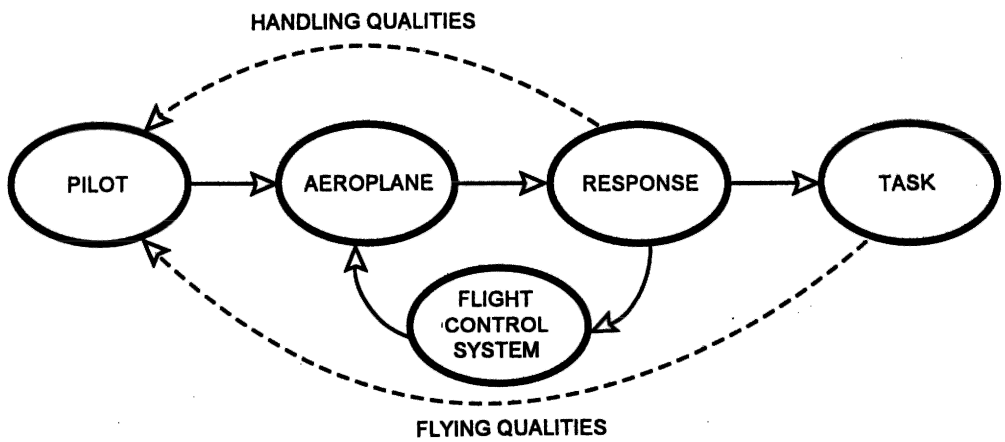

Fig. 1.1 Flying and handling qualities of the conventional aeroplane

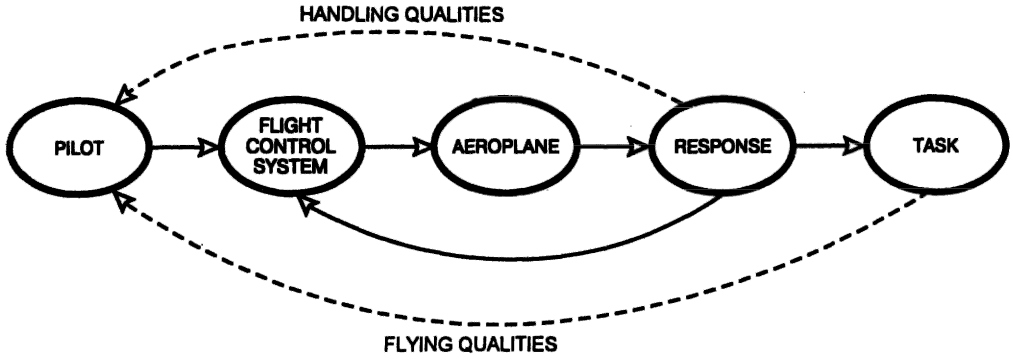

Fig. 1.2 Flying and handling qualities of the FBW aeroplane

An increasing number of advanced modern aeroplanes employ *fly-by-wire* (FBW) primary flight controls and these are usually integrated with the stability augmentation system. In this case, the interpretation of the flying and handling qualities process is modified to that shown on Fig. 1.2. Here then, the flight control system becomes an integral part of the primary signal flow path and the influence of its dynamic characteristics on flying and handling qualities is of critical importance. The need for very careful consideration of the influence of the flight control system in this context cannot be overemphasized.

Now the pilot's perception of the flying and handling qualities of an aeroplane will be influenced by many factors: for example, the stability, control and dynamic characteristics of the airframe, flight control system dynamics, response to atmospheric disturbances and the less tangible effects of cockpit design. This last factor includes considerations such as control inceptor design, instrument displays and field of view from the cockpit. Not surprisingly the quantification of flying qualities remains difficult. However, there is an overwhelming necessity for some sort of numerical description of flying and handling qualities for use in engineering design and evaluation. It is very well established that the flying and handling qualities of an aeroplane are intimately dependent on the stability and control characteristics of the airframe including the flight control system when one is installed. Since stability and control parameters are readily quantified these are usually used as indicators and measures of the likely flying qualities of the aeroplane. Therefore, the prerequisite for almost any study of flying and handling qualities is a descriptive mathematical model of the aeroplane which is capable of providing an adequate quantitative indication of its stability, control and dynamic properties.

1.3 General considerations

In a systematic study of the principles governing the flight dynamics of an aeroplane it is convenient to break the problem down into manageable descriptive elements. Thus before attempting to answer the questions posed in Section 1.1, it is useful to consider and define a suitable framework in which the essential mathematical development may take place.

1.3.1 BASIC CONTROL–RESPONSE RELATIONSHIPS

It is essential to define and establish a description of the basic input–output relationships on which the flying and handling qualities of an unaugmented aeroplane depend. These relationships are described by the aerodynamic transfer functions which provide the simplest and most fundamental description of airframe dynamics. They describe the control–response relationship as a function of flight condition and may include the influence of atmospheric disturbances when appropriate. These basic relationships are illustrated in Fig. 1.3.

Central to this framework is a mathematical model of the aeroplane which is usually referred to as *the equations of motion*. The equations of motion provide a complete description of the response to controls, subject only to modelling limitations defined at the outset, and are measured in terms of displacement, velocity and acceleration variables. The flight condition describes the conditions under which the observations are made and includes such parameters as Mach number, altitude, aeroplane geometry, mass and trim state. When the airframe is augmented with a flight control system the equations of motion are modified to model this configuration. The response transfer functions, derived from the mathematical solution of the equations of motion, are then no longer the basic aerodynamic transfer functions but are obviously the transfer functions of the augmented aeroplane.

1.3.2 MATHEMATICAL MODELS

From the foregoing it is apparent that it is necessary to derive mathematical models to describe the aeroplane, its control systems, atmospheric disturbances and so on. The success of any flight dynamics analysis hinges on the suitability of the models for the problem in hand. Often the temptation is to attempt to derive the most accurate model

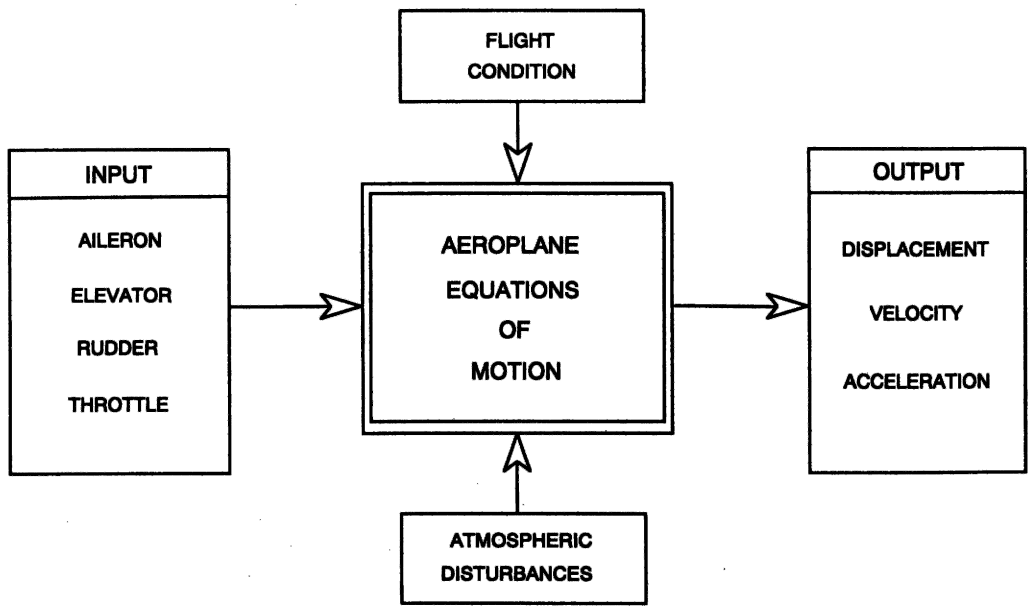

Fig. 1.3 Basic control–response relationship

possible. High fidelity models are capable of reproducing aeroplane dynamics accurately but are seldom simple. Their main drawback is the lack of functional visibility. It may be difficult, or even impossible, to relate response to the simple physical aerodynamic properties of the airframe, or to the properties of the control system components. For the purposes of the investigation of flying and handling qualities it is frequently adequate to use simple approximate models which have the advantage of maximizing functional visibility. Such models have the potential to enhance the visibility of the physical principles involved thereby facilitating the interpretation of flying and handling qualities enormously. Often, the deterioration in the fidelity of the response resulting from the use of approximate models may be relatively insignificant. For a given problem, it is necessary to develop a model which balances the desire for response fidelity against the requirement to maintain functional visibility. As is so often the case in many fields of engineering, simplicity is a most desirable virtue.

1.3.3 STABILITY AND CONTROL

Flying and handling qualities are substantially dependent on, and are usually described in terms of, the stability and control characteristics of an aeroplane. It is therefore essential to be able to describe and to quantify stability and control parameters completely. Analysis may then be performed using the stability parameters. Static stability analysis enables the *control displacement* and the *control force* characteristics to be determined for both steady and manoeuvring flight conditions. Dynamic stability analysis enables the *response to controls* and to atmospheric disturbances to be determined for various flight conditions.

1.3.4 STABILITY AND CONTROL AUGMENTATION

When an aeroplane has flying and handling qualities deficiencies it becomes necessary to correct, or augment, the aerodynamic characteristics which give rise to those deficiencies. To a limited extent, this could be achieved by modification of the aerodynamic design of the aeroplane. In this event it is absolutely essential to understand the relationship between the aerodynamics of the airframe and controls and the stability and control characteristics of that airframe. However, today, many aeroplanes are designed with their aerodynamics optimized for performance over a very large flight envelope, and a consequence of this is that their flying qualities are often deficient, the intent at the outset being to rectify those deficiencies with a stability augmentation system. Therefore, the alternative to aerodynamic design modification is the introduction of a flight control system. In this case it becomes essential to understand how feedback control techniques may be used to modify artificially the apparent aerodynamic characteristics of the airframe. So once again, but for different reasons, it is absolutely essential to understand the relationship between the aerodynamics of the airframe and its stability and control characteristics. Further, it becomes very important to appreciate the effectiveness of servo-systems for autostabilization whilst acknowledging the attendant advantages, disadvantages and limitations introduced by the system hardware. At this stage of consideration it is beginning to become obvious why flight dynamics is now a complex multi-disciplinary subject. However, since this work is introductory, the subject of stability augmentation is treated at the most elementary level only.

1.4 Aircraft equations of motion

The equations of motion of an aeroplane are the foundation on which the entire framework of flight dynamics is built and provide the essential key to a proper understanding of flying and handling qualities. At their simplest, the equations of motion can describe a small perturbation motion about trim only. At their most complex they can be completely descriptive, embodying static stability, dynamic stability, aeroelastic effects, atmospheric disturbances and control system dynamics simultaneously for a given aeroplane configuration. The equations of motion enable the rather intangible description of flying and handling qualities to be related to quantifiable stability and control parameters, which in turn may be related to identifiable aerodynamic characteristics of the airframe. For initial studies the theory of small perturbations is applied to the equations to ease their analytical solution and to enhance their functional visibility. However, for more advanced applications, which are beyond the scope of the present work, the fully descriptive non-linear form of the equations might be retained. In this case the equations are difficult to solve analytically and recourse would be made to computer simulation techniques to effect a solution.

1.5 Aerodynamics

1.5.1 SCOPE

The aerodynamics of an airframe and its controls make a fundamental contribution to the determination of the stability and control characteristics of the aeroplane. It is usual to incorporate aerodynamic descriptions in the equations of motion in the form of *aerodynamic stability and control derivatives.* Since it is necessary to constrain the motion to well-defined limits in order to obtain the derivatives so the scope of the resulting aeroplane model is similarly constrained in its application. It is, however, quite common to find aeroplane models constrained in this way being used to predict flying and handling qualities at conditions well beyond the imposed limits. This is not a recommended practice! An important aspect of flight dynamics is concerned with the proper definition of aerodynamic derivatives as functions of common aerodynamic parameters. It is also most important that the values of the derivatives are compatible with the scope of the problem to which the aeroplane model is to be applied. The processes involved in the estimation or measurement of aerodynamic derivatives provide an essential contribution to a complete understanding of aeroplane behaviour.

1.5.2 SMALL PERTURBATIONS

The aerodynamic properties of an aeroplane vary considerably over the flight envelope and mathematical descriptions of those properties are approximations at best. The limit of the approximation is determined by the ability of mathematics to describe the physical phenomena involved, or by the acceptable complexity of the description, the aim being to obtain the simplest approximation consistent with adequate physical representation. In the first instance, this aim is best met when the motion of interest is constrained to *small perturbations* about a steady flight condition, which is usually, but not necessarily, trimmed equilibrium. This means that the aerodynamic characteristics can be approximated by linearizing about the chosen flight condition. Simple approxi-

mate mathematical descriptions of aerodynamic stability and control derivatives then follow relatively easily. This is the approach pioneered by Bryan (1911) and it usually works extremely well provided the limitations of the model are recognized from the outset.

1.6 Computers

No discussion of flight dynamics would be complete without mention of the very important role played by the computer in all aspects of the subject. It is probably true to say that the development of today's very advanced aeroplanes would not have been possible without parallel developments in computer technology. In fact there is ample evidence to suggest that the demands of aeronautics have forced the pace of computer development. Computers are used for two main purposes, as a general purpose tool for design and analysis and to provide the 'intelligence' in flight control systems.

1.6.1 ANALYTICAL COMPUTERS

In the past, all electronic computation whether for analysis, simulation or airborne flight control would have been analogue. Analogue computer technology developed rapidly during and immediately after World War II and by the late 1960s had reached its highest level of development following the introduction of the electronic integrated operational amplifier. Its principal role was that of simulation and its main advantages were its ability to run in real time and its high level of functional visibility. Its main disadvantage was the fact that the electronic hardware required was directly proportional to the functional complexity of the problem to be simulated. This meant that complex aeroplane models with complex flight control systems required physically large, and very costly, electronic computer hardware. During the 1960s and 1970s electronic digital computing technology advanced very rapidly and soon displaced the analogue computer as the primary tool for design and analysis. However, it took somewhat longer before the digital computer had acquired the capacity and speed necessary to meet the demands of simulation. Today, most of the computational requirements for design, analysis and simulation can be provided by a modest Personal Computer (PC).

1.6.2 FLIGHT CONTROL COMPUTERS

In the present context flight control is taken to mean *flight critical stability augmentation*, where a computer malfunction or failure might hazard the continued safe operation of the aeroplane. In the case of an FBW computer, a total failure would mean loss of the aeroplane. Therefore, hardware integrity is a very serious issue in flight control computer design. The modern aeroplane may also have an auto-pilot computer, air data computer, navigation computer, energy management computer, weapon systems computer and more. Many of these additional computers may be capable of exercising some degree of control over the aeroplane, but none will be quite as critical as the stability augmentation computer in the event of a malfunction.

For the last 50 years or more, computers have been used in aeroplanes for flight control. For much of that time the dedicated analogue electronic computer was unchallenged because of its relative simplicity and its excellent safety record. Towards the end of the 1970s the digital computer had reached the stage of development where its

use in flight critical applications became a viable proposition. The pursuit of increasingly sophisticated performance goals led to an increase in the complexity of the aerodynamic design of aeroplanes. This, in turn, placed greater demands on the flight control system for the maintenance of good flying and handling qualities. The attraction of the digital computer for flight control is its capability for handling very complex control functions easily. The disadvantage is its lack of functional visibility and the consequent difficulty of ensuring safe trouble-free operation. However, the digital flight critical computer is here to stay and is now in use in most advanced-technology aeroplanes. Research continues to improve the hardware, software and application. Confidence in digital flight control systems is now such that applications include full FBW civil transport aeroplanes.

These functionally very complex flight control systems have given the modern aeroplane hitherto unobtainable performance benefits. But nothing is free! The consequence of using such systems is the unavoidable introduction of unwanted control system dynamics. These usually manifest themselves as control phase lag and can intrude on the piloting task in an unacceptable way, resulting in an aircraft with poor flying and handling qualities. This problem is still a subject of research and is very much beyond the scope of this book. However, the essential foundation material on which such studies are built is set out in the following chapters.

1.6.3 COMPUTER SOFTWARE TOOLS

Many computer software tools, which are suitable for flight dynamics analysis, are now available. Most packages are intended for control systems applications, are ideal for handling aeronautical system problems and may be installed on a modest Personal Computer. Software tools used regularly by the author are listed below, but it must be appreciated that the list is by no means exhaustive, nor is it implied that the programs listed are the best or necessarily the most appropriate.

CODAS-II is a low cost control system design and simulation package which is limited to classical linear and non-linear applications only. It is very easy to use and its screen graphics are good.

MATLAB or *PC MATLAB* is a very powerful control system design and analysis tool which is intended for application to systems configured in state space format. As a result all computation is handled in matrix format. Its screen graphics are good.

Program CC is also a very powerful control system design and analysis tool. It is capable of handling classical control problems in transfer function format as well as modern state space control problems in matrix format. An advantage is that it was written by flight dynamicists for flight dynamicists and as a result its use becomes intuitive once the commands have been learned. Its screen graphics are good and have some flexibility of presentation.

MATHCAD is a general purpose mathematical problem solving tool. It is not particularly easy to use for repetitive calculations but it comes into its own for solving difficult non-linear equations. It is also capable of undertaking complex algebraic computations. Its screen graphics are generally very good and are very flexible.

ACSL (axle) is a very powerful simulation language which is capable of simulating the most complex of non-linear flight dynamics problems.

Low cost student editions of *MATLAB* and *MATHCAD* are available which are sufficient for handling all of the material in this book. A text book on control by Golten

and Verwer (1991) is also available which is based on the use of *CODAS* and includes a version of the software. References for the above software tools are given below.

1.7 Summary

An attempt has been made in Chapter 1 to give a broad appreciation of what flight dynamics is all about. Clearly, to produce a comprehensive text on the subject would require many volumes, assuming that it were even possible. To reiterate, the present intention is to set out the fundamental principles of the subject only. However, where appropriate, pointers are included in the text to indicate the direction in which the material in question might be developed for more advanced studies.

References

Bryan, G. H. 1911: *Stability in Aviation*. Macmillan and Co, London.

CODAS-II. Golten and Verwer Partners, Cheadle Hulme, Cheshire.

Golten, J. and Verwer, A. 1991: *Control System Design and Simulation*. McGraw-Hill Book Company (UK) Ltd.

Lanchester, F. W. 1908: *Aerodonetics*. Constable and Co Ltd, London.

MATHCAD. MathSoft Inc, Cambridge, Massachusetts 02142.

MathSoft Inc. 1995: *MATHCAD 6.0 for Windows: Student Edition*. McGraw-Hill International (UK) Ltd.

PC MATLAB. The Math Works Inc, Natick, Massachusetts 01760.

Program CC. Peter M. Thompson, Systems Technology Inc, Hawthorne, California.

The Advanced Continuous Simulation Language (ACSL). Mitchell and Gauthier Associates, Concord, Massachusetts 01742-3096.

The Student Edition of MATLAB, version 4, 1995: Prentice-Hall Inc.

2

Systems of Axes and Notation

Before commencing the main task of developing mathematical models of the aeroplane, it is first necessary to put in place an appropriate and secure foundation on which to build the models. The foundation comprises a mathematical framework in which the equations of motion can be developed in an orderly and consistent way. Since aeroplanes have six degrees of freedom, the description of their motion can be relatively complex. Therefore, motion is usually described by a number of variables that are related to a suitably chosen system of axes. In the UK the scheme of notation and nomenclature in common use is based on that developed by Hopkin (1970) and a simplified summary may be found in the appropriate ESDU (1987) data item. As far as is reasonably possible, the notation and nomenclature used throughout this book corresponds with that of Hopkin (1970). By making the appropriate choice of axis systems, order and consistency may be introduced to the process of model building. The importance of order and consistency in the definition of the mathematical framework cannot be over-emphasized since, without either, misunderstanding and chaos will surely follow. Only the most basic commonly used axes systems appropriate to aeroplanes are discussed in the following sections. In addition to the above-named references, a more expansive treatment may be found in Etkin (1972) or in McRuer *et al.* (1973) for example.

2.1 Earth axes

Since normal atmospheric flight only is considered, it is usual to measure aeroplane motion with reference to an earth fixed framework. The accepted convention for defining earth axes determines that a reference point o_0 on the surface of the earth is the origin of a right-handed orthogonal system of axes $(o_0x_0y_0z_0)$, where o_0x_0 points to the north, o_0y_0 points to the east and o_0z_0 points vertically 'down' along the gravity vector. Conventional earth axes are illustrated on Fig. 2.1.

Clearly, the plane $(o_0x_0y_0)$ defines the local horizontal plane which is tangential to the surface of the earth. Thus, the flight path of an aeroplane flying in the atmosphere in the vicinity of the reference point o_0 may be completely described by its coordinates in the axis system. This therefore assumes a *flat earth*, where the vertical is 'tied' to the gravity vector. This model is quite adequate for localized flight although it is best suited to navigation and performance applications where flight path trajectories are of primary interest.

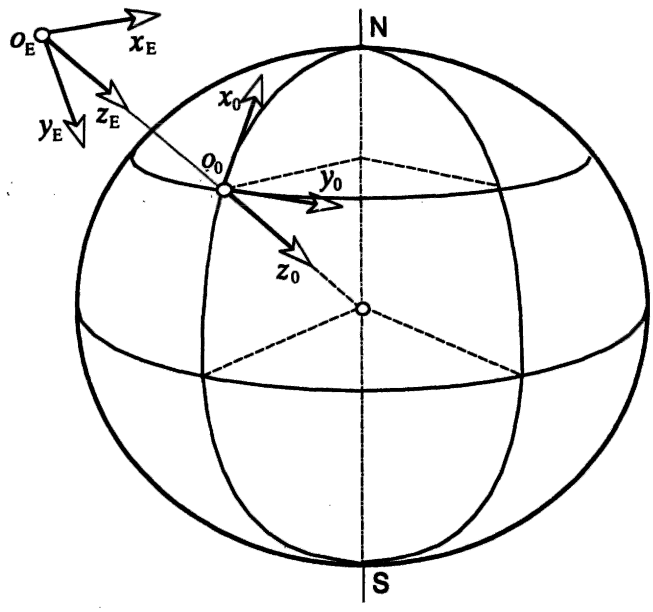

Fig. 2.1 Conventional earth axes

For investigations involving trans-global navigation, the axis system described is inappropriate, a spherical coordinate system being preferred. Similarly, for trans-atmospheric flight involving the launch and re-entry of space vehicles a spherical coordinate system would be more appropriate. However, since in such an application the angular velocity of the earth becomes important it is necessary to define a fixed spatial axis system to which the spherical earth axis system may be referenced.

For flight dynamics applications, a simpler definition of earth axes is preferred. Since short term motion only is of interest, it is perfectly adequate to assume flight above a flat earth. The most common consideration is that of motion about *straight and level* flight. Straight and level flight assumes flight in a horizontal plane at a constant altitude and, whatever the subsequent motion of the aeroplane might be, the *attitude* is determined with respect to the horizontal. Referring again to Fig. 2.1 the horizontal plane is defined by $(o_E x_E y_E)$ and is parallel to the plane $(o_0 x_0 y_0)$ at the surface of the earth. The only difference is that the $o_E x_E$ axis points in the arbitrary direction of flight of the aeroplane rather than to the north. The $o_E z_E$ axis points vertically down as before. Therefore, it is only necessary to place the origin o_E in the atmosphere at the most convenient point, which is frequently coincident with the origin of the aeroplane body fixed axes. Earth axes $(o_E x_E y_E z_E)$ defined in this way are called *datum-path earth axes*, are 'tied' to the earth by means of the gravity vector and provide the inertial reference frame for short term aeroplane motion.

2.2 Aeroplane body fixed axes

2.2.1 GENERALIZED BODY AXES

It is usual practice to define a right-handed orthogonal axis system fixed in the aeroplane and constrained to move with it. Thus, when the aeroplane is disturbed from its initial

flight condition the axes move with the airframe and the motion is quantified in terms of perturbation variables referred to the moving axes. The way in which the axes may be fixed in the airframe is arbitrary, although it is preferable to use an accepted standard orientation. The most general axis system is known as a *body axis* system ($ox_by_bz_b$) which is fixed in the aeroplane as shown in Fig. 2.2. The (ox_bz_b) plane defines the plane of symmetry of the aeroplane and it is convenient to arrange the ox_b axis such that it is parallel to the geometrical *horizontal fuselage datum*. Thus, in normal flight attitudes, the oy_b axis is directed to starboard and the oz_b axis is directed 'downwards'. The origin o of the axes is fixed at a convenient reference point in the airframe which is usually, but not necessarily, coincident with the centre of gravity (cg).

2.2.2 *AERODYNAMIC, WIND OR STABILITY AXES*

It is often convenient to define a set of aeroplane fixed axes such that the ox axis is parallel to the total velocity vector V_0 as shown on Fig. 2.2. Such axes are called *aerodynamic*, *wind* or *stability* axes. In steady symmetric flight, wind axes ($ox_wy_wz_w$) are just a particular version of body axes which are rotated about the oy_b axis through the steady body incidence angle α_e until the ox_w axis aligns with the velocity vector. Thus, the plane (ox_wz_w) remains the plane of symmetry of the aeroplane and the oy_w and the oy_b axes are coincident. Now there is a unique value of body incidence α_e for every flight condition, therefore the wind axes orientation in the airframe is different for every flight condition. However, for any given flight condition the wind axes orientation is defined and fixed in the aeroplane at the outset and is constrained to move with it in subsequent disturbed flight. Typically the body incidence might vary in the range $-10° \leqslant \alpha_e \leqslant 20°$ over a normal flight envelope.

2.2.3 *PERTURBATION VARIABLES*

The motion of the aeroplane is described in terms of force, moment, linear and angular velocities and attitude resolved into components with respect to the chosen aeroplane

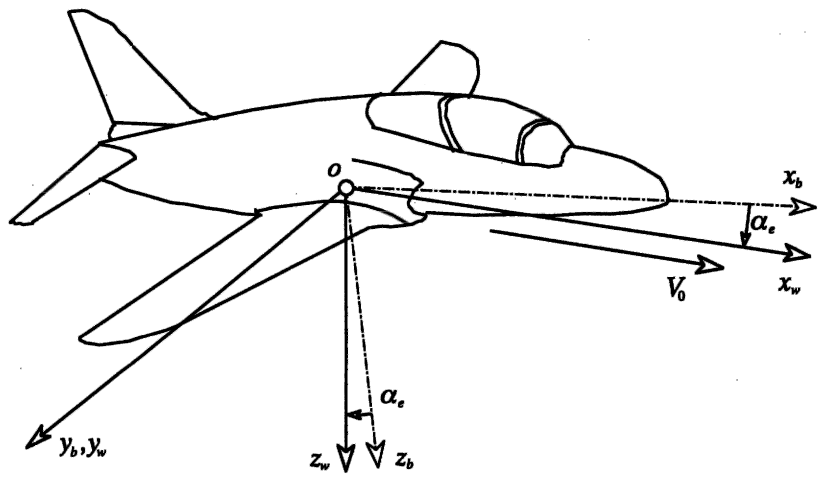

Fig. 2.2 Moving axes systems

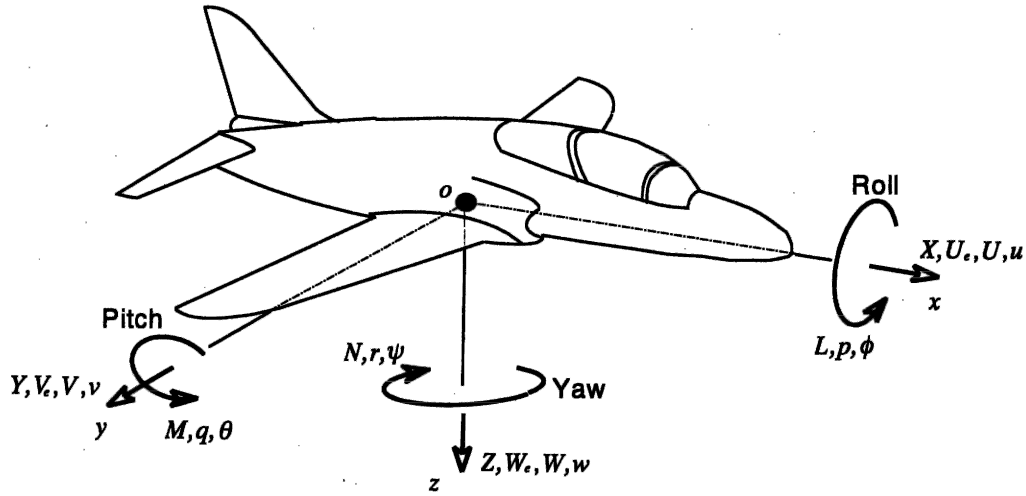

Fig. 2.3 Motion variables notation

fixed axis system. For convenience it is preferable to assume a generalized body axis system in the first instance. Thus, initially, the aeroplane is assumed to be in steady rectilinear, but not necessarily level, flight when the body incidence is α_e and the steady velocity V_0 resolves into components U_e, V_e and W_e as indicated in Fig. 2.3. In steady non-accelerating flight the aeroplane is in equilibrium and the forces and moments acting on the airframe are in balance and sum to zero. This initial condition is usually referred to as *trimmed equilibrium.*

Whenever the aeroplane is disturbed from equilibrium the force and moment balance is upset and the resulting transient motion is quantified in terms of the perturbation variables. The perturbation variables are shown in Fig. 2.3 and summarized in Table 2.1.

The positive sense of the variables is determined by the choice of a right-handed axis system. Components of linear quantities, force, velocity, etc, are positive when their direction of action is the same as the direction of the axis to which they relate. The positive sense of the components of rotary quantities, moment, velocity, attitude, etc, is a right-handed rotation and may be determined as follows. Positive *roll* about the *ox* axis is such that the *oy* axis moves toward the *oz* axis, positive *pitch* about the *oy* axis is such that the *oz* axis moves toward the *ox* axis and positive *yaw* about the *oz* axis is such that the *ox* axis moves toward the *oy* axis. Therefore, positive roll is right wing down, positive pitch is nose up and positive yaw is nose to the right as seen by the pilot.

Table 2.1 Summary of motion variables

	Trimmed equilibrium			Perturbed		
Aeroplane axis	*ox*	*oy*	*oz*	*ox*	*oy*	*oz*
Force	0	0	0	X	Y	Z
Moment	0	0	0	L	M	N
Linear velocity	U_e	V_e	W_e	U	V	W
Angular velocity	0	0	0	p	q	r
Attitude	0	θ_e	0	ϕ	θ	ψ

Table 2.2 The perturbation variables

X	Axial 'drag' force	Sum of the components of
Y	Side force	aerodynamic, thrust and
Z	Normal 'lift' force	weight forces
L	Rolling moment	Sum of the components of
M	Pitching moment	aerodynamic, thrust and
N	Yawing moment	weight moments
p	Roll rate	Components of angular
q	Pitch rate	velocity
r	Yaw rate	
U	Axial velocity	Total linear velocity
V	Lateral velocity	components of the *cg*
W	Normal velocity	

A simple description of the perturbation variables is given in Table 2.2. The intention is to provide some insight into the physical meaning of the many variables used in the model. Note that the components of the total linear velocity perturbations (U, V, W) are given by the sum of the steady equilibrium components and the transient perturbation components (u, v, w) thus,

$$\left.\begin{aligned} U &= U_e + u \\ V &= V_e + v \\ W &= W_e + w \end{aligned}\right\} \tag{2.1}$$

2.2.4 *ANGULAR RELATIONSHIPS IN SYMMETRIC FLIGHT*

Since it is assumed that the aeroplane is in steady rectilinear, but not necessarily level, flight, and that the axes fixed in the aeroplane are body axes then it is useful to relate the steady and perturbed angles as shown in Fig. 2.4.

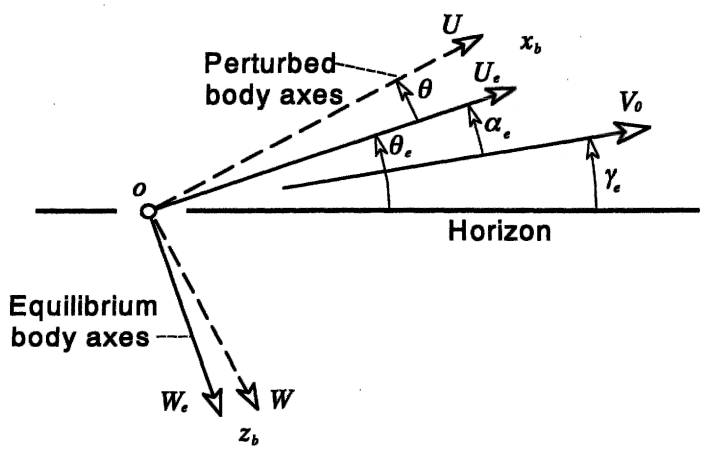

Fig. 2.4 Generalized body axes in symmetric flight

With reference to Fig. 2.4, the steady velocity vector V_0 defines the flight path and γ_e is the steady flight path angle. As before, α_e is the steady body incidence and θ_e is the steady pitch attitude of the aeroplane. The relative angular change in a perturbation is also shown in Fig. 2.4 where it is implied that the axes have moved with the airframe and the motion is viewed at some instant during the disturbance. Thus, the steady flight path angle is given by

$$\gamma_e = \theta_e - \alpha_e \tag{2.2}$$

In the case when the aeroplane fixed axes are wind axes rather than body axes then

$$\alpha_e = 0 \tag{2.3}$$

and in the special case when the axes are wind axes and when the initial condition is level flight

$$\alpha_e = \theta_e = 0 \tag{2.4}$$

It is also useful to note that the perturbation in pitch attitude θ and the perturbation in body incidence α are the same; thus, it is convenient to write

$$\tan(\alpha_e + \theta) \equiv \tan(\alpha_e + \alpha) = \frac{W}{U} \equiv \frac{W_e + w}{U_e + u} \tag{2.5}$$

2.2.5 CHOICE OF AXES

Having reviewed the definition of aeroplane fixed axis systems, the obvious question must be: *when is it appropriate to use wind axes and when is it appropriate to use body axes?* The answer to this question depends on the use to which the equations of motion are to be put. The best choice of axes simply facilitates the analysis of the equations of motion. When starting from first principles it is preferable to use generalized body axes since the resulting equations can cater for most applications. It is then reasonably straightforward to simplify the equations to a wind axis form if the application warrants it. On the other hand, to extend wind axis based equations to cater for the more general case is not as easy.

When dealing with numerical data for an existing aeroplane, it is not always obvious which axis system has been used in the derivation of the model. However, by reference to equations (2.3) or (2.4) and the quoted values of α_e and θ_e it should become obvious which axis system has been used.

When it is necessary to make experimental measurements in an actual aeroplane, or in a model, which are to be used subsequently in the equations of motion, it is preferable to use a generalized body axis system. Since the measuring equipment is installed in the aeroplane its location is precisely known in terms of body axis coordinates which, therefore, determines the best choice of axis system. In a similar way, most aerodynamic measurements and computations are referenced to the free stream velocity vector. For example, in wind tunnel work the obvious reference is the tunnel axis, which is coincident with the velocity vector. Thus, for aerodynamic investigations involving the equations of motion, a wind axis reference is to be preferred. Traditionally, all aerodynamic data for use in the equations of motion are referenced to wind axes.

Thus, to summarize, it is not particularly important which axis system is chosen provided it models the flight condition to be investigated; the end result does not depend on the choice of axis system. However, when compiling data for use in the equations of motion of an

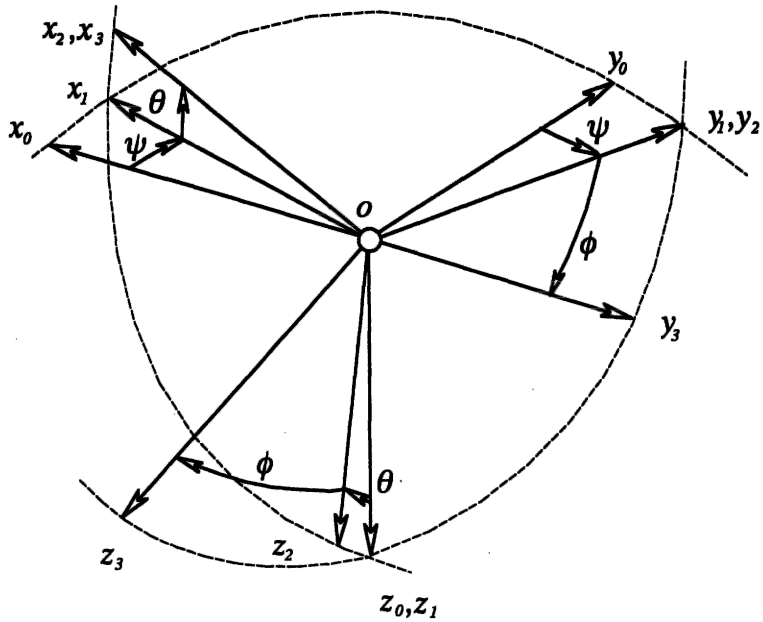

Fig. 2.5 The Euler angles

aeroplane it is quite common for some data to be referred to wind axes and for some data to be referred to body axes. It therefore becomes necessary to have available the mathematical tools for transforming data between different reference axes.

2.3 Euler angles and aeroplane attitude

The angles defined by the right-handed rotation about the three axes of a right-handed system of axes are called *Euler angles*. The sense of the rotations and the order in which the rotations are considered about the three axes in turn are very important since angles do not obey the commutative law. The attitude of an aeroplane is defined as the angular orientation of the airframe fixed axes with respect to earth axes. Attitude angles, therefore, are a particular application of Euler angles. With reference to Fig. 2.5 $(ox_0y_0z_0)$ are datum or reference axes and $(ox_3y_3z_3)$ are aeroplane fixed axes, either generalized body axes or wind axes. The attitude of the aeroplane, with respect to the datum axes, may be established by considering the rotation about each axis in turn required to bring $(ox_3y_3z_3)$ into coincidence with $(ox_0y_0z_0)$. Thus, first rotate about ox_3 through the *roll* angle ϕ to $(ox_2y_2z_2)$. Second, rotate about oy_2 through the *pitch* angle θ to $(ox_1y_1z_1)$ and third, rotate about oz_1 through the *yaw* angle ψ to $(ox_0y_0z_0)$. Clearly, when the attitude of the aeroplane is considered with respect to earth axes then $(ox_0y_0z_0)$ and $(o_Ex_Ey_Ez_E)$ are coincident.

2.4 Axes transformations

It is frequently necessary to transform motion variables and other parameters from one system of axes to another. Clearly, the angular relationships used to describe

attitude may be generalized to describe the angular orientation of one set of axes with respect to another. A typical example might be to transform components of linear velocity from aeroplane wind axes to body axes. Thus, with reference to Fig. 2.5, $(ox_0y_0z_0)$ may be used to describe the velocity components in wind axes, $(ox_3y_3z_3)$ may be used to describe the components of velocity in body axes and the angles (ϕ, θ, ψ) then describe the generalized angular orientation of one set of axes with respect to the other. It is usual to retain the angular description of *roll*, *pitch* and *yaw* although the angles do not necessarily describe attitude strictly in accordance with the definition given in Section 2.3.

2.4.1 LINEAR QUANTITIES TRANSFORMATION

Let, for example, (ox_3, oy_3, oz_3) represent components of a linear quantity in the axis system $(ox_3y_3z_3)$ and let (ox_0, oy_0, oz_0) represent components of the same linear quantity transformed into the axis system $(ox_0y_0z_0)$. The linear quantities of interest would be, for example, acceleration, velocity, displacement, etc. Resolving through each rotation in turn and in the correct order then, with reference to Fig. 2.5, it may be shown that:

(i) after *rolling* about ox_3 through the angle ϕ

$$\left.\begin{aligned} ox_3 &= ox_2 \\ oy_3 &= oy_2 \cos\phi + oz_2 \sin\phi \\ oz_3 &= -oy_2 \sin\phi + oz_2 \cos\phi \end{aligned}\right\} \tag{2.6}$$

Alternatively, writing equations (2.6) in the more convenient matrix form

$$\begin{bmatrix} ox_3 \\ oy_3 \\ oz_3 \end{bmatrix} = \begin{bmatrix} 1 & 0 & 0 \\ 0 & \cos\phi & \sin\phi \\ 0 & -\sin\phi & \cos\phi \end{bmatrix} \begin{bmatrix} ox_2 \\ oy_2 \\ oz_2 \end{bmatrix} \tag{2.7}$$

(ii) similarly, after *pitching* about oy_2 through the angle θ

$$\begin{bmatrix} ox_2 \\ oy_2 \\ oz_2 \end{bmatrix} = \begin{bmatrix} \cos\theta & 0 & -\sin\theta \\ 0 & 1 & 0 \\ \sin\theta & 0 & \cos\theta \end{bmatrix} \begin{bmatrix} ox_1 \\ oy_1 \\ oz_1 \end{bmatrix} \tag{2.8}$$

(iii) and after *yawing* about oz_1 through the angle ψ

$$\begin{bmatrix} ox_1 \\ oy_1 \\ oz_1 \end{bmatrix} = \begin{bmatrix} \cos\psi & \sin\psi & 0 \\ -\sin\psi & \cos\psi & 0 \\ 0 & 0 & 1 \end{bmatrix} \begin{bmatrix} ox_0 \\ oy_0 \\ oz_0 \end{bmatrix} \tag{2.9}$$

By repeated substitution equations (2.7), (2.8) and (2.9) may be combined to give the required transformation relationship

$$\begin{bmatrix} ox_3 \\ oy_3 \\ oz_3 \end{bmatrix} = \begin{bmatrix} 1 & 0 & 0 \\ 0 & \cos\phi & \sin\phi \\ 0 & -\sin\phi & \cos\phi \end{bmatrix} \begin{bmatrix} \cos\theta & 0 & -\sin\theta \\ 0 & 1 & 0 \\ \sin\theta & 0 & \cos\theta \end{bmatrix} \begin{bmatrix} \cos\psi & \sin\psi & 0 \\ -\sin\psi & \cos\psi & 0 \\ 0 & 0 & 1 \end{bmatrix} \begin{bmatrix} ox_0 \\ oy_0 \\ oz_0 \end{bmatrix} \tag{2.10}$$

or

$$\begin{bmatrix} ox_3 \\ oy_3 \\ oz_3 \end{bmatrix} = \mathbf{D} \begin{bmatrix} ox_0 \\ oy_0 \\ oz_0 \end{bmatrix} \tag{2.11}$$

where the *direction cosine matrix* **D** is given by

$$\mathbf{D} = \begin{bmatrix} \cos\theta\cos\psi & \cos\theta\sin\psi & -\sin\theta \\ \sin\phi\sin\theta\cos\psi - \cos\phi\sin\psi & \sin\phi\sin\theta\sin\psi + \cos\phi\cos\psi & \sin\phi\cos\theta \\ \cos\phi\sin\theta\cos\psi + \sin\phi\sin\psi & \cos\phi\sin\theta\sin\psi - \sin\phi\cos\psi & \cos\phi\cos\theta \end{bmatrix} \tag{2.12}$$

As shown, equation (2.11) transforms linear quantities from $(ox_0y_0z_0)$ to $(ox_3y_3z_3)$. By inverting the direction cosine matrix **D** the transformation from $(ox_3y_3z_3)$ to $(ox_0y_0z_0)$ is obtained as given by equation (2.13).

$$\begin{bmatrix} ox_0 \\ oy_0 \\ oz_0 \end{bmatrix} = \mathbf{D}^{-1} \begin{bmatrix} ox_3 \\ oy_3 \\ oz_3 \end{bmatrix} \tag{2.13}$$

EXAMPLE 2.1

To illustrate the use of equation (2.11) consider the very simple example in which it is required to resolve the velocity of the aeroplane through both the incidence angle and the sideslip angle into aeroplane axes. The situation prevailing is assumed to be steady and is shown in Fig. 2.6.

The axes $(oxyz)$ are generalized aeroplane body axes with velocity components U_e, V_e and W_e respectively. The free stream velocity vector is V_0 and the angles of incidence and sideslip are α_e and β_e respectively. With reference to equation (2.11), axes $(oxyz)$ correspond to axes $(ox_3y_3z_3)$ and V_0 corresponds to ox_0 of axes $(ox_0y_0z_0)$, therefore the following vector substitutions may be made

$$(ox_0, oy_0, oz_0) = (V_0, 0, 0) \quad \text{and} \quad (ox_3, oy_3, oz_3) = (U_e, V_e, W_e)$$

and the angular correspondence means that the following substitution may be made

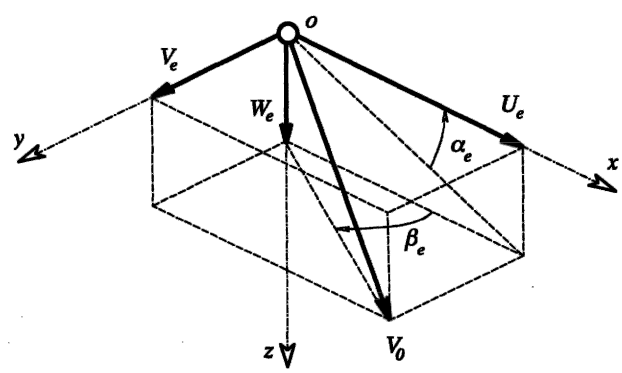

Fig. 2.6 Resolution of velocity through incidence and sideslip angles

$$(\phi, \theta, \psi) = (0, \alpha_e, -\beta_e)$$

Note that a positive sideslip angle is equivalent to a negative yaw angle. Thus, making the substitutions in equation (2.9)

$$\begin{bmatrix} U_e \\ V_e \\ W_e \end{bmatrix} = \begin{bmatrix} \cos\alpha_e \cos\beta_e & -\cos\alpha_e \sin\beta_e & -\sin\alpha_e \\ \sin\beta_e & \cos\beta_e & 0 \\ \sin\alpha_e \cos\beta_e & -\sin\alpha_e \sin\beta_e & \cos\alpha_e \end{bmatrix} \begin{bmatrix} V_0 \\ 0 \\ 0 \end{bmatrix} \tag{2.14}$$

Or, equivalently,

$$\left.\begin{aligned} U_e &= V_0 \cos\alpha_e \cos\beta_e \\ V_e &= V_0 \sin\beta_e \\ W_e &= V_0 \sin\alpha_e \cos\beta_e \end{aligned}\right\} \tag{2.15}$$

EXAMPLE 2.2

Another very useful application of the direction cosine matrix is to calculate height perturbations in terms of aircraft motion. Equation (2.13) may be used to relate the velocity components in aircraft axes to the corresponding components in earth axes as follows

$$\begin{bmatrix} U_E \\ V_E \\ W_E \end{bmatrix} = \mathbf{D}^{-1} \begin{bmatrix} U \\ V \\ W \end{bmatrix} = \begin{bmatrix} \cos\psi \cos\theta & \cos\psi \sin\theta \sin\phi & \cos\psi \sin\theta \cos\phi \\ & -\sin\psi \cos\phi & +\sin\psi \sin\phi \\ \sin\psi \cos\theta & \sin\psi \sin\theta \sin\phi & \sin\psi \sin\theta \cos\phi \\ & +\cos\psi \cos\phi & -\cos\psi \sin\phi \\ -\sin\theta & \cos\theta \sin\phi & \cos\theta \cos\phi \end{bmatrix} \begin{bmatrix} U \\ V \\ W \end{bmatrix} \tag{2.16}$$

where U_E, V_E and W_E are the perturbed total velocity components referred to earth axes. Now, since height is measured positive in the 'upwards' direction, the rate of change of height due to the perturbation in aircraft motion is given by

$$\dot{h} = -W_E$$

whence, from equation (2.16),

$$\dot{h} = U \sin\theta - V \cos\theta \sin\phi - W \cos\theta \cos\phi \tag{2.17}$$

2.4.2 *ANGULAR VELOCITIES TRANSFORMATION*

Probably the most useful angular quantities transformation relates the angular velocities p, q, r of the aeroplane fixed axes to the resolved components of angular velocity, the attitude rates $\dot{\phi}, \dot{\theta}, \dot{\psi}$ with respect to datum axes. The easiest way to deal with the algebra of this transformation whilst retaining a good grasp of the physical implications is to

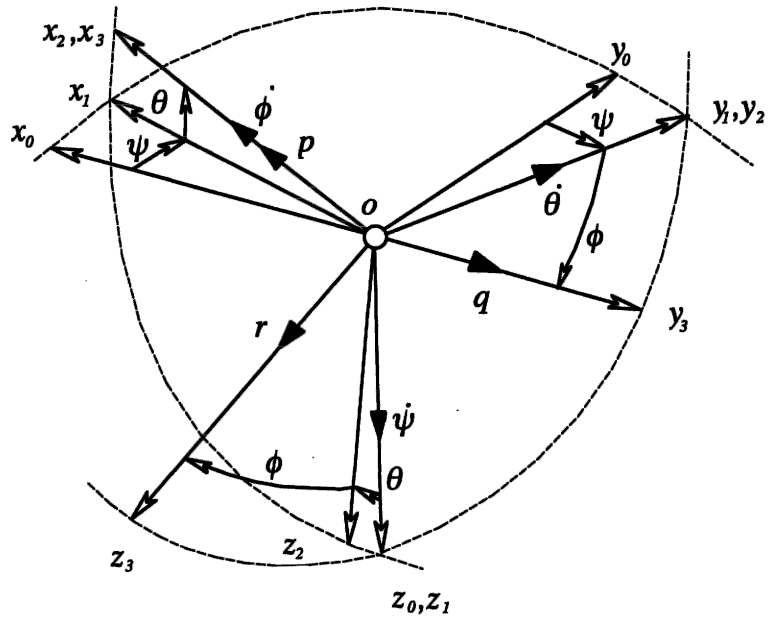

Fig. 2.7 Angular rates transformation

superimpose the angular rate vectors on to the axes shown in Fig. 2.5, and the result of this is shown in Fig. 2.7.

The angular *body rates* p, q, r are shown in the aeroplane axes $(ox_3y_3z_3)$; then consider each rotation in turn necessary to bring the aeroplane axes into coincidence with the datum axes $(ox_0y_0z_0)$. First, *roll* about ox_3 through the angle ϕ with angular velocity $\dot{\phi}$. Second, *pitch* about oy_2 through the angle θ with angular velocity $\dot{\theta}$. And third, *yaw* about oz_1 through the angle ψ with angular velocity $\dot{\psi}$. Again, it is most useful to refer the attitude rates to earth axes, in which case the datum axes $(ox_0y_0z_0)$ are coincident with earth axes $(o_Ex_Ey_Ez_E)$. The *attitude rate* vectors are clearly shown in Fig. 2.7. The relationship between the aeroplane body rates and the attitude rates, referred to datum axes, is readily established as follows.

(i) *Roll rate* p is equal to the sum of the components of $\dot{\phi}, \dot{\theta}, \dot{\psi}$ resolved along ox_3

$$p = \dot{\phi} - \dot{\psi}\sin\theta \tag{2.18}$$

(ii) *Pitch rate* q is equal to the sum of the components of $\dot{\phi}, \dot{\theta}, \dot{\psi}$ resolved along oy_3

$$q = \dot{\theta}\cos\phi + \dot{\psi}\sin\phi\cos\theta \tag{2.19}$$

(iii) *Yaw rate* r is equal to the sum of the components of $\dot{\phi}, \dot{\theta}, \dot{\psi}$ resolved along oz_3

$$r = \dot{\psi}\cos\phi\cos\theta - \dot{\theta}\sin\phi \tag{2.20}$$

Equations (2.18), (2.19) and (2.20) may be combined into the convenient matrix notation

$$\begin{bmatrix} p \\ q \\ r \end{bmatrix} = \begin{bmatrix} 1 & 0 & -\sin\theta \\ 0 & \cos\phi & \sin\phi\cos\theta \\ 0 & -\sin\phi & \cos\phi\cos\theta \end{bmatrix} \begin{bmatrix} \dot{\phi} \\ \dot{\theta} \\ \dot{\psi} \end{bmatrix} \tag{2.21}$$

and the inverse of equation (2.21) is

$$\begin{bmatrix} \dot{\phi} \\ \dot{\theta} \\ \dot{\psi} \end{bmatrix} = \begin{bmatrix} 1 & \sin\phi\tan\theta & \cos\phi\tan\theta \\ 0 & \cos\phi & -\sin\phi \\ 0 & \sin\phi\sec\theta & \cos\phi\sec\theta \end{bmatrix} \begin{bmatrix} p \\ q \\ r \end{bmatrix} \tag{2.22}$$

When the aeroplane perturbations are small, such that (ϕ, θ, ψ) may be treated as small angles, equations (2.21) and (2.22) may be approximated by

$$\left.\begin{aligned} p &= \dot{\phi} \\ q &= \dot{\theta} \\ r &= \dot{\psi} \end{aligned}\right\} \tag{2.23}$$

EXAMPLE 2.3

To illustrate the use of the angular velocities transformation, consider the situation when an aeroplane is flying in a steady level coordinated turn at a speed of 250 m/s at a bank angle of 60°. It is required to calculate the turn rate $\dot{\psi}$, the yaw rate r and the pitch rate q. The forces acting on the aeroplane are shown in Fig. 2.8.

By resolving the forces acting on the aeroplane vertically and horizontally and eliminating the lift L between the two resulting equations it is easily shown that the radius of turn is given by

$$R = \frac{V_0^2}{g\tan\phi} \tag{2.24}$$

The time to complete one turn is given by

$$t = \frac{2\pi R}{V_0} = \frac{2\pi V_0}{g\tan\phi} \tag{2.25}$$

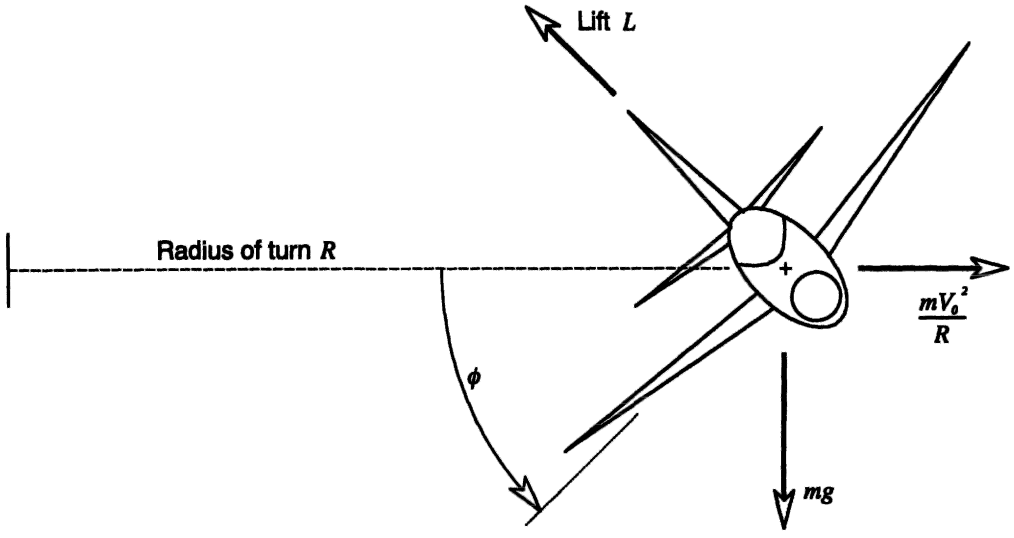

Fig. 2.8 Aeroplane in a steady banked turn

therefore the rate of turn is given by

$$\dot{\psi} = \frac{2\pi}{t} = \frac{g \tan \phi}{V_0} \tag{2.26}$$

Thus, $\dot{\psi} = 0.068$ rad/s. For the conditions applying to the turn, $\dot{\phi} = \dot{\theta} = \theta = 0$ and thus equation (2.21) may now be used to find the values of r and q

$$\begin{bmatrix} p \\ q \\ r \end{bmatrix} = \begin{bmatrix} 1 & 0 & 0 \\ 0 & \cos 60° & \sin 60° \\ 0 & -\sin 60° & \cos 60° \end{bmatrix} \begin{bmatrix} 0 \\ 0 \\ \dot{\psi} \end{bmatrix}$$

Therefore, $p = 0$, $q = 0.059$ rad/s and $r = 0.034$ rad/s. Note that p, q and r are the angular velocities that would be measured by rate gyros fixed in the aeroplane with their sensitive axes aligned with the *ox*, *oy* and *oz* aeroplane axes respectively.

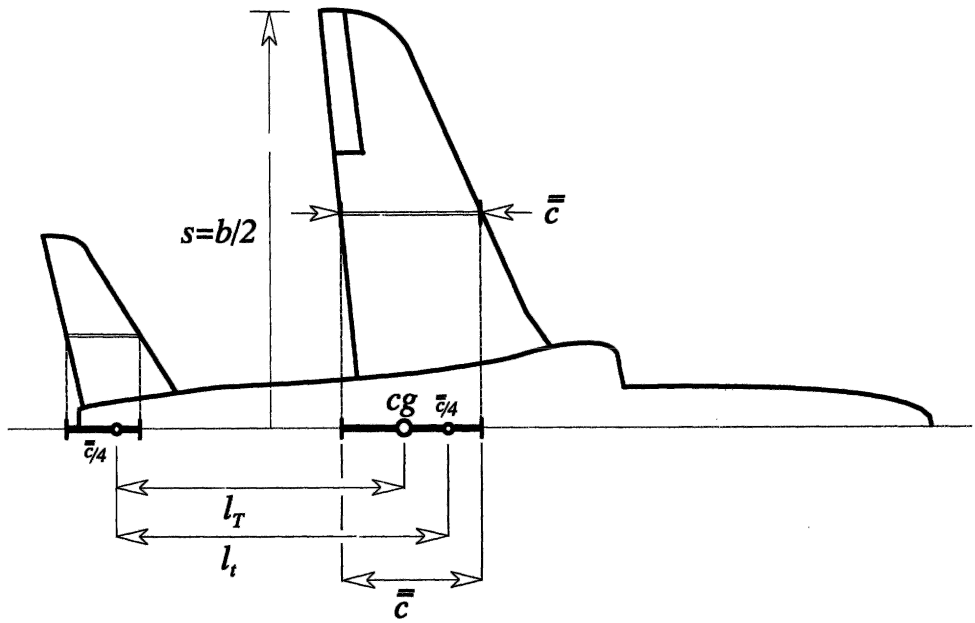

Fig. 2.9 Longitudinal reference geometry

2.5 Aeroplane reference geometry

The description of the geometric layout of an aeroplane is an essential part of the mathematical modelling process. For the purposes of flight dynamics analysis it is convenient that the geometry of the aeroplane can be adequately described by a small number of dimensional reference parameters which are defined below and illustrated in Fig. 2.9

2.5.1 WING AREA

The reference area is usually the gross plan area of the wing, including that part within the fuselage, and is denoted S where

$$S = b\bar{c} \tag{2.27}$$

where b is the wing span and $\bar{c}$ is the standard mean chord of the wing.

2.5.2 *MEAN AERODYNAMIC CHORD*

The *mean aerodynamic chord* of the wing (*mac*) is denoted $\bar{\bar{c}}$ and is defined

$$\bar{\bar{c}} = \frac{\int_{-s}^{s} c_y^2 \, dy}{\int_{-s}^{s} c_y \, dy} \tag{2.28}$$

The reference *mac* is located on the centre line of the aircraft by projecting $\bar{\bar{c}}$ from its spanwise location as shown in Fig. 2.9. Thus, for a swept wing the leading edge of the *mac* lies aft of the leading edge of the root chord of the wing. The *mac* represents the location of the root chord of a rectangular wing which has the same aerodynamic influence on the aeroplane as the actual wing. Traditionally, *mac* is used in stability and control studies since a number of important aerodynamic reference centres are located on it.

2.5.3 *STANDARD MEAN CHORD*

The *standard mean chord* of the wing (*smc*) is effectively the same as the geometric mean chord and is denoted $\bar{c}$. For a wing of symmetric planform it is defined

$$\bar{c} = \frac{\int_{-s}^{s} c_y \, dy}{\int_{-s}^{s} dy} \tag{2.29}$$

where $s = b/2$ is the semi-span and c_y is the local chord at spanwise coordinate y. For a straight tapered wing, equation (2.29) simplifies to

$$\bar{c} = \frac{S}{b} \tag{2.30}$$

The reference *smc* is located on the centre line of the aircraft by projecting $\bar{c}$ from its spanwise location in the same way that the *mac* is located. Thus, for a swept wing the leading edge of the *smc* also lies aft of the leading edge of the root chord of the wing. The *smc* is the mean chord preferred by aircraft designers since it relates very simply to the geometry of the aeroplane. For most aeroplanes the *smc* and *mac* are sufficiently similar in length and location that they are practically interchangeable. It is quite common to find references that quote a mean chord without specifying which. This is not good practice, although the error incurred by assuming the wrong chord is rarely serious. However, the reference chord used in any application should be clearly defined at the outset.

2.5.4 *ASPECT RATIO*

The aspect ratio of the aeroplane wing is a measure of its spanwise slenderness, is denoted A and is defined as follows

$$A = \frac{b^2}{S} = \frac{b}{\bar{\bar{c}}} \tag{2.31}$$

2.5.5 CENTRE OF GRAVITY LOCATION

The centre of gravity, *cg*, of an aeroplane is usually located on the reference chord as indicated in Fig. 2.9. Its position is quoted as a fraction of $\bar{\bar{c}}$ (or $\bar{c}$), denoted h, and is measured from the leading edge of the reference chord as shown. The *cg* position varies as a function of aeroplane loading, the typical variation being in the range 10% to 40% of $\bar{\bar{c}}$. Or, equivalently, $0.1 \leqslant h \leqslant 0.4$.

2.5.6 TAIL MOMENT ARM AND TAIL VOLUME RATIO

The *mac* of the horizontal tailplane, or foreplane, is defined and located in the airframe in the same way as the *mac* of the wing as indicated in Fig. 2.9. The wing and tailplane aerodynamic forces and moments are assumed to act at their respective aerodynamic centres which, to a good approximation, lie at the quarter chord points of the *mac* of the wing and tailplane respectively. The tail moment arm l_T is defined as the longitudinal distance between the centre of gravity and the aerodynamic centre of the tailplane as shown in Fig. 2.9. The *tail volume ratio* $\bar{V}_T$ is an important geometric parameter and is defined

$$\bar{V}_T = \frac{S_T l_T}{S\bar{\bar{c}}} \tag{2.32}$$

where S_T is the gross area of the tailplane. Typically, the tail volume ratio has a value in the range $0.5 \leqslant \bar{V}_T \leqslant 1.3$ and is a measure of the aerodynamic effectiveness of the tailplane as a stabilizing device.

Sometimes, especially in stability and control studies, it is convenient to measure the longitudinal tail moment about the aerodynamic centre of the *mac* of the wing. In this case the tail moment arm is denoted l_t, as shown in Fig. 2.9, and a slightly modified tail volume ratio is defined.

2.5.7 FIN MOMENT ARM AND FIN VOLUME RATIO

The *mac* of the fin is defined and located in the airframe in the same way as the *mac* of the wing as indicated in Fig. 2.10. As for the tailplane, the fin moment arm l_F is defined

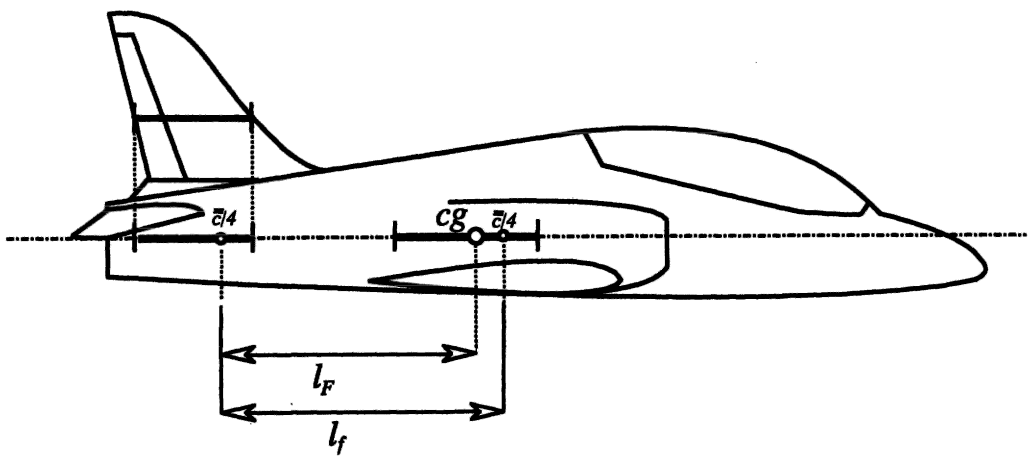

Fig. 2.10 Fin moment arm

as the longitudinal distance between the centre of gravity and the aerodynamic centre of the fin as shown in Fig. 2.10. The *fin volume ratio* $\bar{V}_F$ is also an important geometric parameter and is defined

$$\bar{V}_F = \frac{S_F l_F}{S\bar{\bar{c}}} \tag{2.33}$$

where S_F is the gross area of the fin. Again, the fin volume ratio is a measure of the aerodynamic effectiveness of the fin as a directional stabilizing device.

As stated above it is sometimes convenient to measure the longitudinal moment of the aerodynamic forces acting at the fin about the aerodynamic centre of the *mac* of the wing. In this case the fin moment arm is denoted l_f as shown in Fig. 2.10.

2.6 Controls notation

2.6.1 AERODYNAMIC CONTROLS

Sometimes it appears that some confusion exists with respect to the correct notation applying to aerodynamic controls, especially when unconventional control surfaces are used. Hopkin (1970) defines a notation which is intended to be generally applicable but, since a very large number of combinations of control motivators is possible, the notation relating to control inceptors may become ill-defined and hence application dependent. However, for the conventional aeroplane there is a universally accepted notation, which accords with Hopkin (1970), and it is simple to apply. Generally, a positive *control action* by the pilot gives rise to a positive aeroplane response, whereas a positive *control surface displacement* gives rise to a negative aeroplane response. Thus:

(i) **in roll:** positive right push force on the stick ⇒ positive stick displacement ⇒ right aileron up and left aileron down (negative mean) ⇒ right wing down roll response (positive).

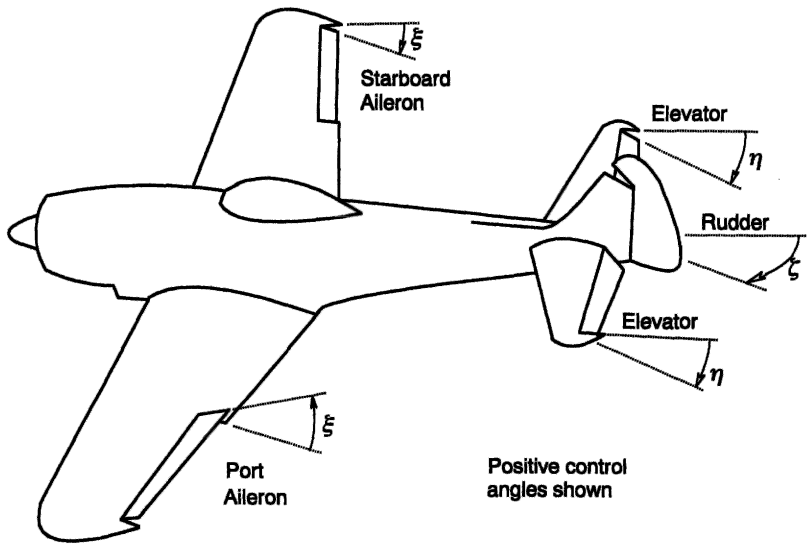

Fig. 2.11 Aerodynamic controls notation

(ii) **in pitch:** positive pull force on the stick ⇒ positive aft stick displacement ⇒ elevator trailing edge up (negative) ⇒ nose up pitch response (positive).

(iii) **in yaw:** positive push force on the right rudder pedal ⇒ positive rudder bar displacement ⇒ rudder trailing edge displaced to the right (negative) ⇒ nose to the right yaw response (positive).

Roll and pitch control stick displacements are denoted δ_ξ and δ_η respectively and rudder pedal displacement is denoted δ_ζ. Aileron, elevator and rudder surface displacements are denoted ξ, η and ζ respectively as indicated on Fig. 2.11. It should be noted that, since ailerons act differentially, the displacement ξ is usually taken as the mean value of the separate displacements of each aileron.

2.6.2 ENGINE CONTROL

Engine thrust τ is controlled by throttle lever displacement ε. Positive throttle lever displacement is usually in the forward push sense and results in a positive increase in thrust. For a turbo-jet engine the relationship between thrust and throttle lever angle is approximated by a simple first order lag transfer function

$$\frac{\tau(s)}{\varepsilon(s)} = \frac{k_\tau}{(1 + sT_\tau)} \tag{2.34}$$

where k_τ is a suitable gain constant and T_τ is the lag time constant, which is typically of the order of two to three seconds.

2.7 Aerodynamic reference centres

With reference to Fig. 2.12, the *centre of pressure*, *cp*, of an aerofoil, wing or complete aeroplane is the point at which the resultant aerodynamic force F acts. It is usual to resolve the force into the *lift* component perpendicular to the velocity vector and the *drag* component parallel to the velocity vector, denoted L and D respectively in the usual way. The *cp* is located on the *mac* and thereby determines an important aerodynamic reference centre.

Now simple theory establishes that the resultant aerodynamic force F generated by an aerofoil comprises two components, that due to camber F_c and that due to angle of attack F_α, both of which resolve into lift and drag forces as indicated. The aerodynamic force due to camber is constant and acts at the mid point of the aerofoil chord and for a symmetric aerofoil section this force is zero. The aerodynamic force due to angle of attack acts at the quarter chord point and varies directly with angle of attack at angles below the stall. This also explains why the zero lift angle of attack of a cambered aerofoil is usually a small negative value since, at this condition, the lift due to camber is equal and opposite to the lift due to angle of attack. Thus, at low speeds, when the angle of attack is generally large, most of the aerodynamic force is due to the angle of attack dependent contribution and the *cp* is nearer to the quarter chord point. On the other hand, at high speeds, when the angle of attack is generally small, a larger contribution to the aerodynamic force is due to the camber dependent component and the *cp* is nearer to the mid point of the chord. Thus, in the limit, the *cp* of an aerofoil generally lies between the quarter chord and mid chord points. More generally, the interpretation for an aeroplane recognizes that the *cp* moves as a function of angle of attack, Mach

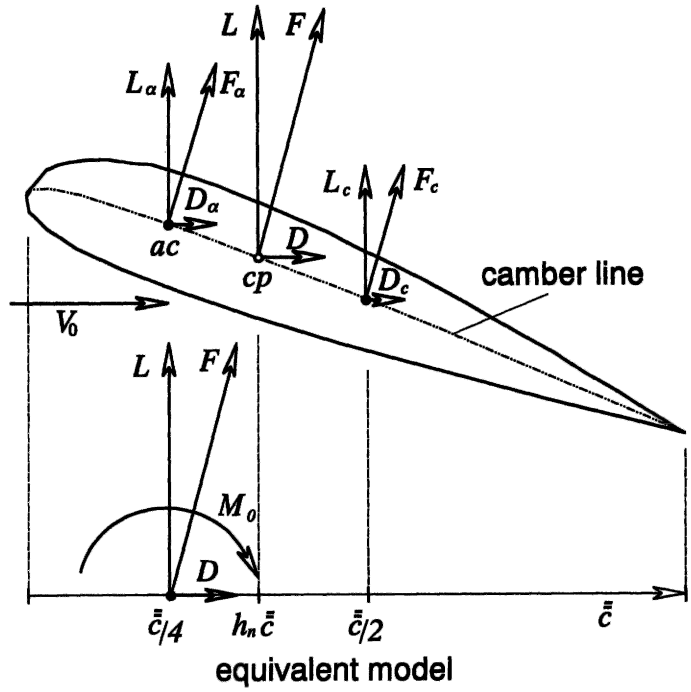

Fig. 2.12 Aerodynamic reference centre

number and configuration. For example, at low angles of attack and high Mach numbers the *cp* tends to move aft and vice versa. Consequently, the *cp* is of limited use as an aerodynamic reference point in stability and control studies. It should be noted that the *cp* of the complete aeroplane in trimmed equilibrium flight corresponds to the *controls fixed neutral point* $h_n\bar{\bar{c}}$ which is discussed in Chapter 3.

If, instead of the *cp*, another *fixed* point on the *mac* is chosen as an aerodynamic reference point then, at this point, the total aerodynamic force remains the same but is accompanied by a pitching moment about the point. Clearly, the most convenient reference point on the *mac* is the quarter chord point since the pitching moment is the moment of the aerodynamic force due to camber and remains constant with variation in angle of attack. This point is called the *aerodynamic centre*, denoted *ac*, and at low Mach numbers lies at, or very close to, the quarter chord point, $\bar{\bar{c}}/4$. It is for this reason that the *ac*, or equivalently, the quarter chord point of the reference chord, is preferred as a reference point. The corresponding equivalent aerofoil model is shown in Fig. 2.12. Since the *ac* remains essentially fixed in position during small perturbations about a given flight condition, and since the pitching moment is nominally constant about the *ac*, it is used as a reference point in stability and control studies. It is important to appreciate that as the flight condition Mach number is increased so the *ac* moves aft and, in supersonic flow conditions, it is located at, or very near to, $\bar{\bar{c}}/2$.

The definition of aerodynamic centre given above applies most strictly to the location of the *ac* on the chord of an aerofoil. However, it also applies reasonably well to its location on the *mac* of a wing and is also used extensively for locating the *ac* on the *mac* of a wing–body combination without too much loss of validity. It should be appreciated that the complex aerodynamics of a wing and body combination might result in an *ac*

location which is not at the quarter chord point although, typically, it would not be too far removed from that point.

References

ESDU 1987: *Introduction to Aerodynamic Derivatives, Equations of Motion and Stability.* Engineering Sciences Data Unit, Data Item No. 86021. Aerodynamics Series, Vol. 9a, Stability of Aircraft. Engineering Sciences Data, ESDU International Ltd.

Etkin, B. 1972: *Dynamics of Atmospheric Flight.* John Wiley and Sons, Inc, New York.

Hopkin, H. R. 1970: *A Scheme of Notation and Nomenclature for Aircraft Dynamics and Associated Aerodynamics.* Aeronautical Research Council, Reports and Memoranda No. 3562.

McRuer, D., Ashkenas, I. and Graham, D. 1973: *Aircraft Dynamics and Automatic Control.* Princeton University Press, Princeton, New Jersey.

3

Static Equilibrium and Trim

3.1 Trim equilibrium

3.1.1 PRELIMINARY CONSIDERATIONS

In normal flight it is usual for the pilot to adjust the controls of an aeroplane such that on releasing the controls it continues to fly at the chosen flight condition. By this means the pilot is relieved of the tedium of constantly maintaining control inputs, and the associated control forces, which may be tiring. The aeroplane is then said to be trimmed, and the trim state defines the initial condition about which the dynamics of interest may be studied. Thus, all aeroplanes are equipped with a means for pre-setting, or adjusting, the *datum* or *trim* setting of the primary control surfaces.

The ailerons, elevator and rudder are all fitted with *trim tabs* which, in all except the smallest aeroplanes, may be adjusted from the cockpit in flight. However, all aeroplanes are fitted with a continuously adjustable elevator trim tab. It is an essential requirement that an aeroplane must be stable if it is to remain in equilibrium following trimming. In particular, the static stability characteristics about all three axes largely determine the *trimmability* of an aeroplane. Thus, static stability is concerned with the control actions required to establish equilibrium and with the characteristics required to ensure that the aeroplane remains in equilibrium. Dynamic stability is also important of course, and largely determines the characteristics of the transient motion, following a disturbance, about a trimmed flight condition.

The object of trimming is to bring the forces and moments acting on the aeroplane into a state of equilibrium. That is, the condition when the axial, normal and side forces and the roll, pitch and yaw moments are all zero. The force balance is often expressed approximately as the requirement for the lift to equal the weight and the thrust to equal the drag. Provided that the aeroplane is stable it will then stay in equilibrium until it is disturbed by pilot control inputs or by external influences such as turbulence. The transient motion following such a disturbance is characterized by the dynamic stability characteristics and the stable aeroplane will eventually settle to its equilibrium state once more.

The maintenance of trimmed equilibrium requires the correct simultaneous adjustment of the main flight variables in all six degrees of freedom and is dependent on airspeed, or Mach number, flight path angle, airframe configuration, weight and *cg* position. As these parameters change during the course of a typical flight so trim

adjustments are made as necessary. Fortunately, the task of trimming an aeroplane is not as challenging as it might at first seem. The symmetry of a typical airframe confers symmetric aerodynamic properties on the airframe, which usually reduces the task to that of longitudinal trim only. Lateral-directional trim adjustments are only likely to be required when the aerodynamic symmetry is lost, due to loss of an engine in a multi-engined aeroplane, for example.

Lateral-directional stability is designed-in to most aeroplanes and ensures that in roll the aeroplane remains *wings level* and that in yaw it tends to *weathercock* into wind when the ailerons and rudder are at their zero or datum positions. Thus, under normal circumstances the aeroplane will naturally seek lateral-directional equilibrium without interference by the pilot. This applies even when significant changes are made to airspeed, configuration, weight and *cg* position, for example, since the symmetry of the airframe is retained throughout. However, such variations in flight condition can lead to dramatic changes in longitudinal trim.

Longitudinal trim involves the simultaneous adjustment of elevator angle and thrust to give the required airspeed and flight path angle for a given airframe configuration. Equilibrium is only achievable if the aeroplane is longitudinally stable and the control actions to trim depend on the *degree* of longitudinal static stability. Since the longitudinal flight condition is continuously variable it is very important that trimmed equilibrium is possible at all conditions. For this reason considerable emphasis is given to the problems of ensuring adequate longitudinal static stability and adequate longitudinal trim control. Because of its importance *static stability and trim* is often interpreted to mean *longitudinal static stability and trim.*

The commonly used theory of longitudinal static stability was developed by Gates and Lyon (1944), and derives from a full, static and dynamic, stability analysis of the equations of motion of an aeroplane. An excellent and accessible summary of the findings of Gates and Lyon is given in Duncan (1959) and also in Babister (1961). In the interests of understanding and physical interpretation the theory is often reduced to a linearized form retaining only the principal aerodynamic and configuration parameters. It is in this simplest form that the theory is reviewed here since it is only required as the basis on which to build the small perturbation dynamics model. It is important to appreciate that although the longitudinal static stability model is described only in terms of the aerodynamic properties of the airframe, the control and trim properties as seen by the pilot must conform to the same physical interpretation even when they are augmented by a flight control system. It is also important to note that static and dynamic stability are, in reality, inseparable. However, the separate treatment of static stability is a useful means for introducing the concept of stability insofar as it determines the control and trim characteristics of the aeroplane.

3.1.2 CONDITIONS FOR STABILITY

The static stability of an aeroplane is commonly interpreted to describe its tendency to converge on the initial equilibrium condition following a small disturbance from trim. Dynamic stability, on the other hand, describes the transient motion involved in the process of recovering equilibrium following the disturbance. Figure 3.1 includes two illustrations showing the effects of static stability and static instability in an otherwise dynamically stable aeroplane. Following an initial disturbance displacement, for example in pitch, at time $t = 0$ the subsequent response time history is shown and is

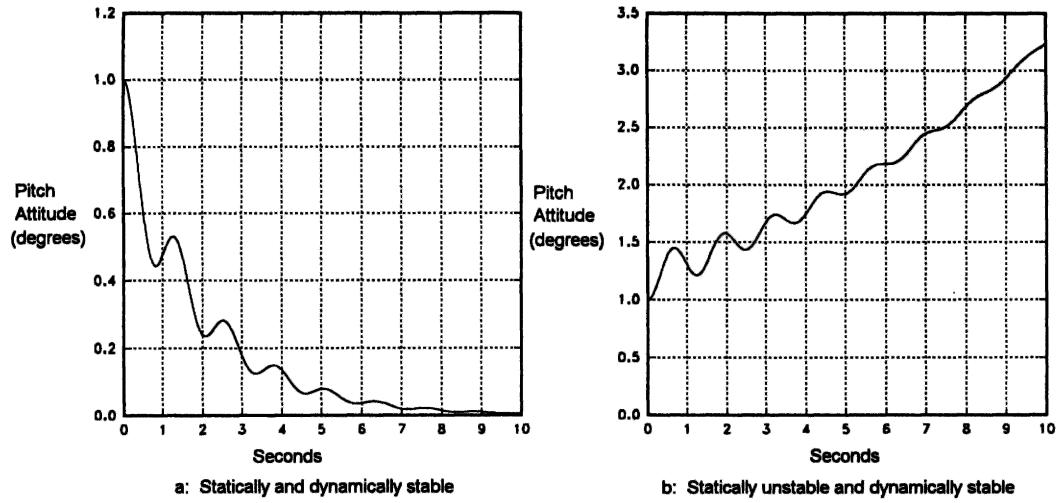

Fig. 3.1 Stability

clearly dependent on the stability of the aeroplane. It should be noted that the damping of the dynamic oscillatory component of the responses shown was deliberately chosen to be low in order to illustrate best the static and dynamic stability characteristics.

In establishing trim equilibrium the pilot adjusts the elevator angle and thrust to obtain a lift force sufficient to support the weight and thrust sufficient to balance the drag at the desired speed and flight path angle. Since the airframe is symmetric the equilibrium side force is of course zero. Provided that the speed is above the minimum drag speed then the force balance will remain stable with speed. Therefore, the static stability of the aeroplane reduces to a consideration of the effects of angular disturbances about the three axes. Following such a disturbance the aerodynamic forces and moments will no longer be in equilibrium and in a statically stable aeroplane the resultant moments will cause the aeroplane to converge on its initial condition. The condition for an aeroplane to be statically stable is therefore easily deduced.

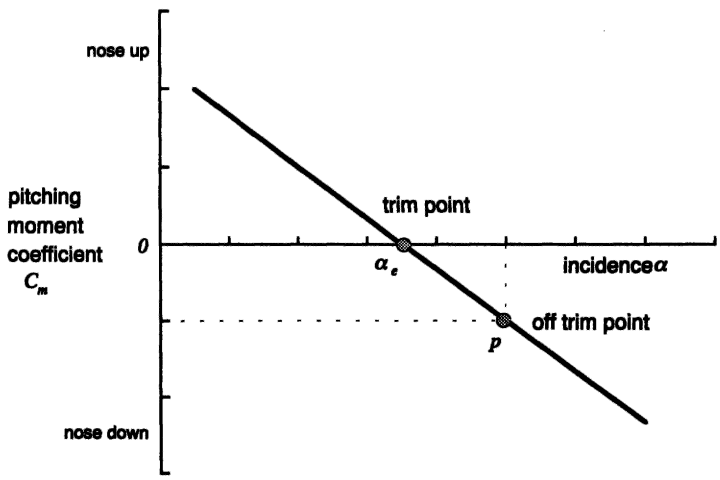

Fig. 3.2 Pitching moment variation with incidence for a stable aeroplane

Consider a positive pitch, or incidence, disturbance from equilibrium. This is in the nose up sense and results in an increase in incidence α and hence in lift coefficient C_L. In a stable aeroplane the resulting pitching moment must be restoring, that is in the negative or nose down sense. And of course the converse must be true following a nose down disturbance. Thus, the condition for longitudinal static stability may be determined by plotting pitching moment M, or pitching moment coefficient C_m, for variation in incidence α about the trim value α_e as shown in Fig. 3.2. The nose up disturbance increases α and takes the aeroplane to the out-of-trim point p where the pitching moment coefficient becomes negative and is therefore restoring. Clearly, a nose down disturbance leads to the same conclusion. As indicated, the aeroplane is stable when the slope of this plot is negative. Thus, the condition for stable trim at incidence α_e may be expressed

$$C_m = 0 \tag{3.1}$$

and

$$\frac{dC_m}{d\alpha} < 0 \tag{3.2}$$

The above observation is only strictly valid when it is assumed that the aerodynamic force and moment coefficients are functions of incidence only. This is usually an acceptable approximation for subsonic aeroplanes and, indeed, the plot of pitching moment coefficient against incidence may well be very nearly linear as shown in Fig. 3.2. However, this argument becomes increasingly inappropriate with increasing Mach number. As compressibility effects become significant so the aerodynamic force and moment coefficients become functions of both incidence and Mach number. When this occurs, equation (3.2) may not always guarantee that stable trim can be obtained. The rather more complex analysis by Gates and Lyon (1944) takes speed effects into account and defines a general requirement for longitudinal static stability as

$$\frac{dC_m}{dC_L} < 0 \tag{3.3}$$

For subsonic aeroplanes, equations (3.2) and (3.3) are completely interchangeable since α and C_L are linearly, or very nearly linearly, related by the lift curve slope a.

In a similar way the conditions for lateral-directional static stability may be deduced as

$$\frac{dC_l}{d\phi} < 0 \tag{3.4}$$

and

$$\frac{dC_n}{d\beta} < 0 \tag{3.5}$$

where C_l and C_n are rolling moment and yawing moment coefficients respectively and ϕ and β are roll angle and sideslip angle respectively.

3.1.3 DEGREE OF STABILITY

It was shown above that the condition for an aeroplane to possess static stability about all three axes at a given trim condition is that the slopes of the C_m–α, C_l–ϕ and C_n–β

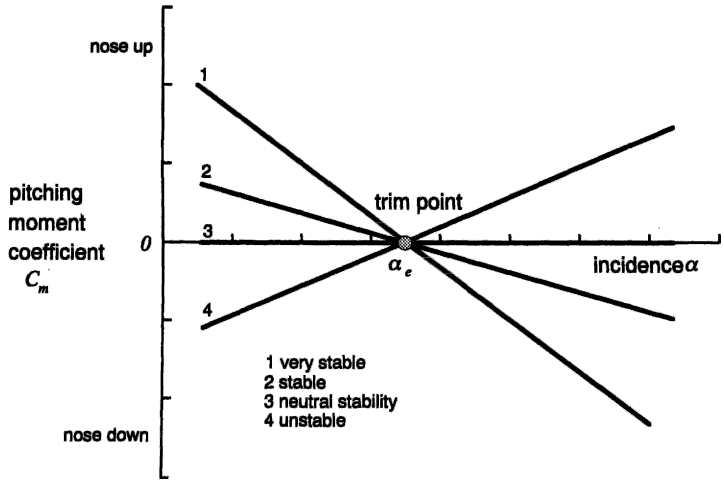

Fig. 3.3 The degree of longitudinal static stability

plots must be negative. Now, obviously, a very large range of negative slopes is possible and the magnitude of the slope determines the *degree of stability* possessed by the aeroplane. Variation in the degree of longitudinal static stability is illustrated in Fig. 3.3. The degree of stability is described in terms of *stability* margin which quantifies how much stability the aeroplane has over and above zero or neutral stability. Thus, for example, the longitudinal static stability margin is directly related to the slope of the C_m–α plot.

With reference to Fig. 3.3 and for a given disturbance in α it is clear that the corresponding restoring pitching moment C_m is greatest for a very stable aeroplane. The magnitude of the restoring moment decreases as the degree of stability, or stability margin, is reduced and becomes zero at neutral stability. Clearly, when the aeroplane is unstable the moment is of the opposite sign and is therefore divergent. Thus, the higher the degree of stability the greater is the restoring moment following a disturbance. This means that a very stable aeroplane will be very resistant to upset. This in turn means that greater control actions will be needed to encourage the aeroplane to change its trim state or to manoeuvre. It follows then that the stability margins determine the magnitude of the control actions required to trim the aeroplane. It is easy to appreciate that a consequence of this is that too much stability can be as hazardous as too little stability since the available control power is limited.

As mentioned before, the lateral-directional static stability of the aeroplane is usually fixed by design and usually remains more-or-less constant throughout the flight envelope. The lateral-directional stability margins therefore remain substantially constant for all flight conditions. This situation may well break down when large amplitude manoeuvring is considered. Under such circumstances, normally linear aerodynamic behaviour may well become very non-linear and cause dramatic changes to observed lateral-directional stability and control characteristics. Although of considerable interest to the flight dynamicist, non-linear behaviour is beyond the scope of this book and constant lateral-directional static stability is assumed throughout.

3.1.4 VARIATION IN STABILITY

Changes in the aerodynamic operating conditions of an aeroplane, which result in pitching moment changes, inevitably lead to variation in longitudinal static stability. Such variation in stability is normally manifest as a non-linear version of the C_m–C_L characteristic shown in Fig. 3.2. For the subsonic classical aeroplane, such changes are usually small and may result in some non-linearity of the pitching moment characteristic with change in trim. In general, the variation in the degree of stability is acceptably small.

For the modern supersonic high performance aeroplane, the situation is not so well defined. Large flight envelopes and significant variation in flight condition can lead to dramatic changes in static stability. For example, it is possible for such an aeroplane to be stable at some conditions and unstable at others. It easy to see how such variations might arise in a physical sense but it is much more difficult to describe the variations in mathematical terms. A brief review of some of the more obvious sources of variation in stability follows.

3.1.4.1 Power effects

Probably the most significant variation in longitudinal static stability arises from the effects of power. Direct effects result from the point of application and line of action of the thrust forces with respect to the *cg*. Clearly, as illustrated in Fig. 3.4, a high thrust line results in a nose down pitching moment and vice versa. In normal trimmed flight the thrust moment is additive to the aerodynamic moment and the total pitching moment would be trimmed to zero by adjustment of the elevator. However, any aerodynamic perturbation about trim that results in a thrust perturbation is potentially capable of giving rise to a non-linear stability characteristic. The precise nature of the variation in stability is dependent on the operating characteristics of the installed power unit, which may not be easy to identify.

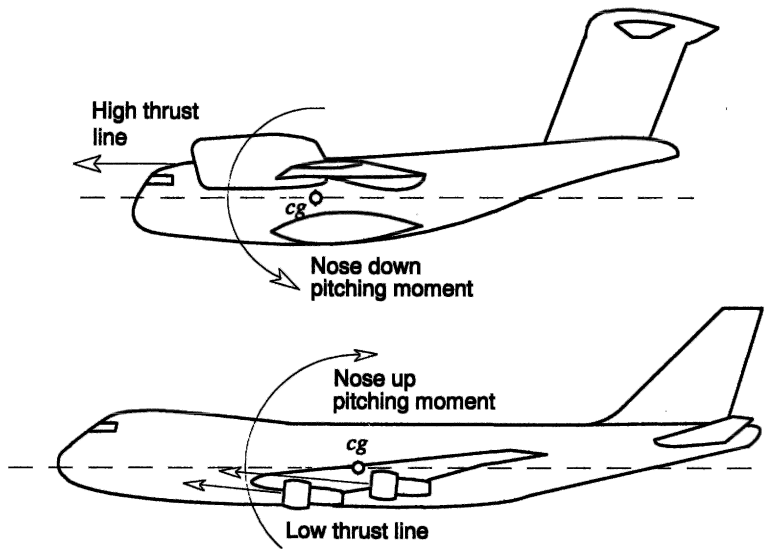

Fig. 3.4 Typical thrust line effects on pitching moment

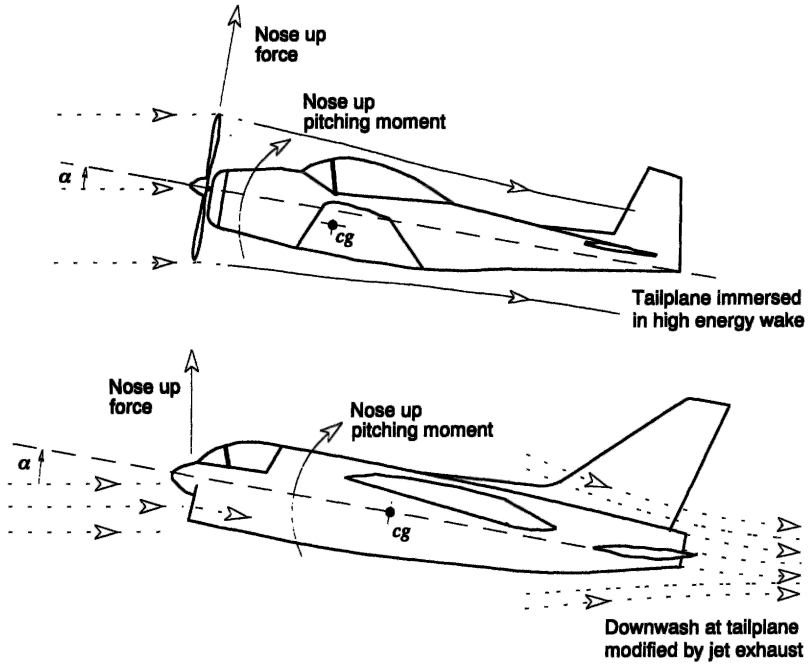

Fig. 3.5 Typical induced flow effects on pitching moment

Indirect power effects are caused by the induced flow associated with a propeller and its wake or the intake and exhaust of a gas turbine engine. Some of the more obvious induced flow effects are illustrated in Fig. 3.5. The process of turning the incident flow through the body incidence angle into the propeller disc or into the engine intake creates a normal force at the propeller or engine intake as shown. In general, this effect gives rise to a nose up pitching moment. The magnitude of the normal force is dependent on the body incidence angle and on the increase in flow energy at the propeller disc or engine intake. The force will therefore vary considerably with trim condition. The force is also sensitive to aerodynamic perturbations about trim, it is therefore easy to appreciate its contribution to pitching moment non-linearity.

The wake behind a propeller is a region of high energy flow which modifies the aerodynamic operating conditions over parts of the wing and tailplane. The greatest effect on pitching moment arises from the tailplane. The effectiveness of the tailplane is enhanced simply because of the increased flow velocity and the reduction in downwash angle. These two effects together increase the nose down pitching moment available and hence increase the degree of stability of the aeroplane.

The induced flow effects associated with the propeller driven aeroplane can have a significant influence on its longitudinal static stability. These effects also change with aerodynamic conditions especially at high angles of attack. It is therefore quite common to see some non-linearity in the pitching moment trim plot for such an aeroplane at high values of lift coefficient. It should also be noted that the propeller wake rotates about the longitudinal axis. Although less significant, the rotating flow has some influence on the lateral-directional static stability of the aeroplane.

The exhaust from a jet engine, being a region of very high velocity and reduced pressure, creates an inflow field as indicated in Fig. 3.5. Clearly the influence on

pitching moment will depend on the relative location of the aerodynamic surfaces of the aeroplane and the engine exhausts. When the tailplane is immersed in this induced flow field then there is a change in the downwash angle. Thus, the effect is to increase the static stability when the downwash angle is reduced and vice versa. In general this effect is not very significant, except perhaps for the aeroplane with engines mounted in pods on the rear fuselage and in which the tailplane is very close to the exhaust wake.

3.1.4.2 Other effects

Although power effects generally make the most significant contribution to variation in longitudinal static stability, other potentially important contributory sources also exist. For example, wing sweep back and aeroplane geometry, which result in significant variation in downwash at the tailplane, generally tend to reduce the available stability, an effect which is clearly dependent on the aerodynamic trim condition. The fuselage alone is usually unstable and the condition worsens with increasing Mach number. On the other hand, at high subsonic and supersonic Mach numbers the aerodynamic centres of the wing and tailplane move aft. This has the effect of increasing the available nose down pitching moment which is a stabilizing characteristic. Finally, since all airframes have some degree of flexibility, the structure distorts under the influence of aerodynamic loads. Today aeroelastic distortion of the structure is carefully controlled by design and is not usually significant in influencing static stability. However, in very large civil transport aeroplanes, the relative geometric disposition of the wing and tailplane changes with loading conditions. Some contribution to the variation in pitching moment is therefore inevitable but its contribution to variation in stability is usually small.

Taking all of these effects together, the prospect of ever being able quantitatively to define the longitudinal static stability of an aeroplane may seem daunting. Fortunately, these effects are well understood and can be minimized by design. The result for most aeroplanes is a pitching moment trim characteristic with some non-linear tendency at higher values of trim lift coefficient. In extreme cases the stability of the aeroplane can actually reverse at high values of lift coefficient, which results in an unstable pitch up characteristic. A typical pitching moment trim plot for an aeroplane with a pitch up characteristic is shown in Fig. 3.6.

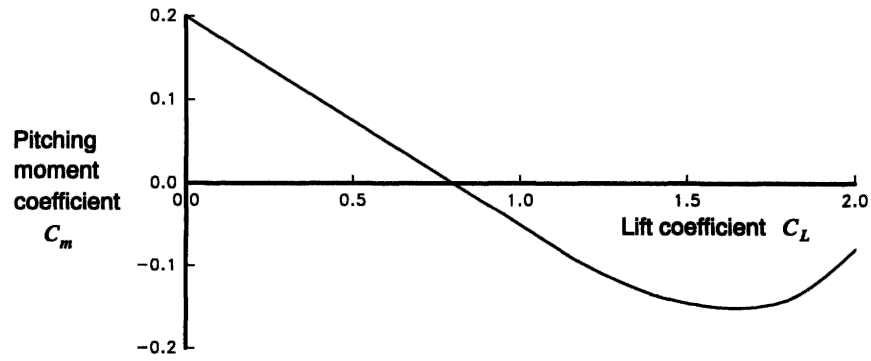

Fig. 3.6 Stability reversal at high lift coefficient

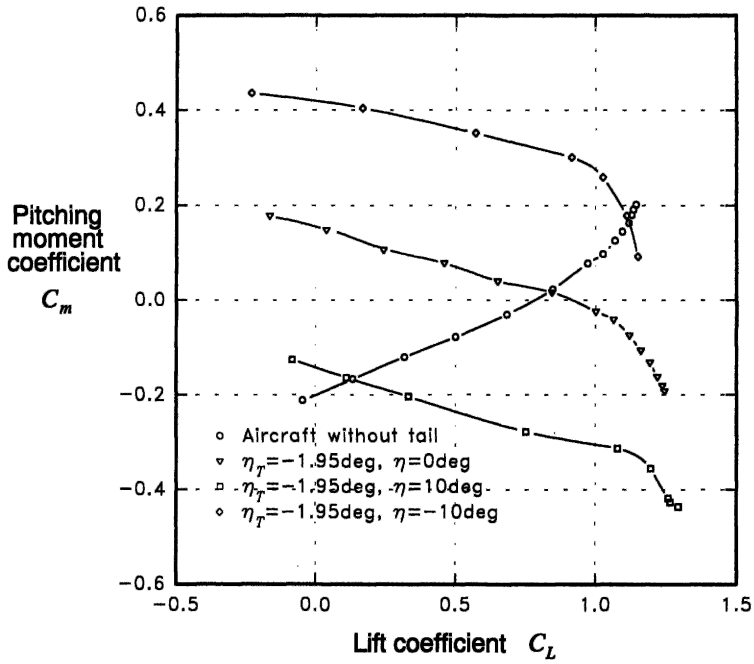

Fig. 3.7 C_m–C_L plots for a 1/6th scale model of the Handley Page Jetstream

EXAMPLE 3.1

To illustrate the variation in the pitching moment characteristic for a typical subsonic aeroplane, the relevant data obtained from wind tunnel experiments on a 1/6th scale model of the Handley Page HP-137 are shown plotted in Fig. 3.7. The data were extracted from the report by Storey (1966), were obtained at a tunnel speed of 200 ft/s and the Reynolds number was $Re = 1.2 \times 10^6$, based on mean aerodynamic chord $\bar{\bar{c}}$. The HP-137 is, in fact, the well-known Jetstream; however, it is not known if the data shown are representative of the actual aeroplane flying today.

The plots show the characteristics for the aeroplane without tail and for the aeroplane with tail at various combinations of setting angle η_T and elevator angle η. Clearly, all of the plots are reasonably linear at all values of lift coefficient up to the stall. Without a tailplane the aeroplane is unstable since the slope of the plot is positive. With a tailplane the slope, and hence the degree of stability, is more or less constant. Assuming that the trim ($C_m = 0$) range of lift coefficient is approximately $-0.2 \leqslant C_L \leqslant 1.0$ then, by interpolation, it can be seen that this can be obtained with an elevator angle range of approximately $-6° \leqslant \eta \leqslant 0°$. Clearly this is well within the control capability of the tailplane and elevator configuration shown in this example.

This kind of experimental analysis would be used to confirm the geometric design of the tailplane and elevator. In particular, it is essential to establish that the aeroplane has an adequate stability margin across the trim envelope, that the elevator angle required to trim the aeroplane is within its aerodynamic capability and that a sufficient margin of elevator control range remains for manoeuvring.

3.2 The pitching moment equation

Having established the importance of the pitching moment in the determination of longitudinal static stability, further analysis of stability requires the development of the pitching moment equation. A fully representative general pitching moment equation is difficult to develop since it is very dependent on the geometry of the aeroplane. However, it is possible to develop a simple approximation to the pitching moment equation, which is sufficiently representative for most preliminary studies and which provides considerable insight into the basic requirements for static stability and trim.

3.2.1 SIMPLE DEVELOPMENT OF THE PITCHING MOMENT EQUATION

For the development of the simplest possible pitching moment equation it is usual to define a model showing only the normal forces and pitching moments acting on the aeroplane. It is assumed that, in steady level flight, the thrust and drag are in equilibrium and act at the *cg* and, further, for small disturbances in incidence, changes in this equilibrium are insignificant. This assumption therefore implies that small disturbances in incidence cause significant changes in lift forces and pitching moments only. The model defined in these terms is shown in Fig. 3.8.

For the purposes of modelling pitching behaviour the model comprises two parts, the wing and fuselage combination and the tailplane. It is then assumed that the wing and fuselage behave aerodynamically like a wing alone. Clearly, this is not true since the fuselage may make significant aerodynamic contributions and, in any event, its presence will interfere with the aerodynamic properties of the wing to a greater or lesser extent. However, for conventional subsonic aeroplanes with a reasonably high aspect ratio wing this is a very satisfactory approximation. The tailplane is treated as a separate component since it provides the principal aerodynamic mechanism for controlling longitudinal static stability and trim. The following analysis establishes the fundamental importance of the tailplane parameters in the provision of longitudinal static stability.

Referring to Fig. 3.8, it is seen that the wing–fuselage lift L_w and residual pitching moment M_0 act at the aerodynamic centre *ac* of the combination, which is assumed to be coincident with the aerodynamic centre of the wing alone. In a similar way the lift L_T

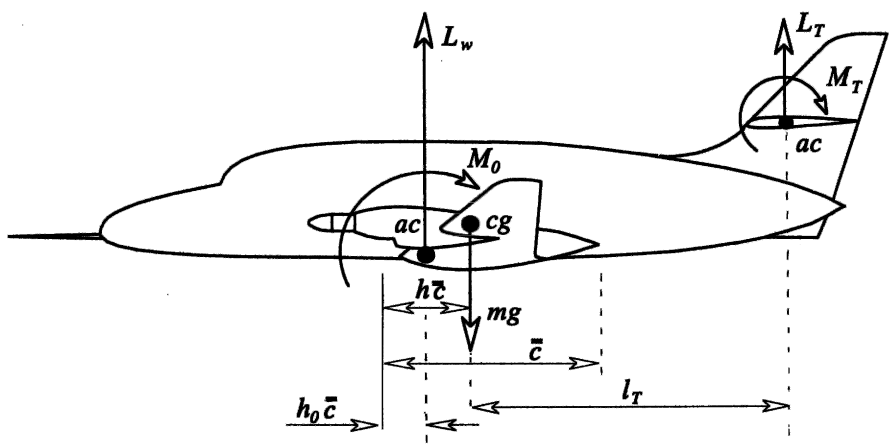

Fig. 3.8 Simple pitching moment model

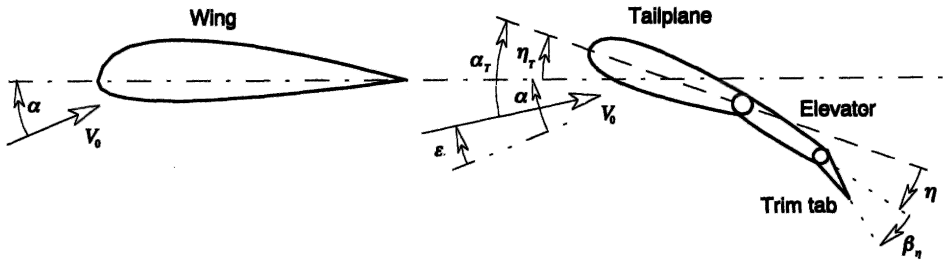

Fig. 3.9 Wing–tailplane flow geometry

and pitching moment M_T of the tailplane are assumed to act at its aerodynamic centre. The longitudinal geometry of the model is entirely related to the mean aerodynamic chord *mac* as shown in Fig. 3.8. An expression for the total pitching moment M about the *cg* may therefore be written

$$M = M_0 + L_w(h - h_0)\bar{c} - L_T l_T + M_T \tag{3.6}$$

If, as is usual, it is assumed that the tailplane aerofoil section is symmetric then M_T becomes zero. Thus, in the more convenient coefficient form, equation (3.6) may be written

$$C_m = C_{m_0} + C_{L_w}(h - h_0) - C_{L_T}\bar{V}_T \tag{3.7}$$

To facilitate further analysis of pitching moment it is necessary to express the tailplane lift coefficient C_{L_T} in terms of more accessible tailplane parameters. Tailplane lift coefficient may be expressed

$$C_{L_T} = a_0 + a_1\alpha_T + a_2\eta + a_3\beta_\eta \tag{3.8}$$

where a_0, a_1, a_2 and a_3 are constant aerodynamic coefficients, α_T is the local incidence, η is the elevator angle and β_η is the elevator trim tab angle. Note that since a symmetric tailplane aerofoil section is assumed, a_0 is also zero. The local tailplane incidence is influenced by the *tailplane setting angle* η_T and the local flow distortion due to the effect of the downwash field behind the wing. The flow geometry is shown in Fig. 3.9.

Clearly the angle of attack of the tailplane is given by

$$\alpha_T = \alpha - \varepsilon + \eta_T \tag{3.9}$$

where ε is the downwash angle at the tailplane. Since, to a good approximation, for small disturbances the downwash angle is a function of wing–body incidence α only

$$\alpha - \varepsilon = \alpha\left(1 - \frac{d\varepsilon}{d\alpha}\right) = \frac{C_{L_w}}{a}\left(\frac{d\varepsilon}{d\alpha}\right) \tag{3.10}$$

whence

$$\alpha_T = \frac{C_{L_w}}{a}\left(1 - \frac{d\varepsilon}{d\alpha}\right) + \eta_T \tag{3.11}$$

Now substituting the expression for α_T given by equation (3.11) into equation (3.8), substituting the resulting expression for C_{L_T} into equation (3.7) and noting that a_0 is zero, then the pitching moment equation in its simplest and most general form is obtained

$$C_m = C_{m_0} + C_{L_w}(h - h_0) - \bar{V}_T\left(C_{L_w}\frac{a_1}{a}\left(1 - \frac{d\varepsilon}{d\alpha}\right) + a_2\eta + a_3\beta_\eta + a_1\eta_T\right) \tag{3.12}$$

3.2.2 ELEVATOR ANGLE TO TRIM

It has already been shown, in equation (3.1), that the condition for trim is that the total pitching moment can be adjusted to zero, i.e. $C_m = 0$. Applying this condition to equation (3.12) the elevator angle required to trim the aeroplane is given by

$$\eta = \frac{1}{\bar{V}_T a_2}(C_{m_0} + C_{L_w}(h - h_0)) - \frac{C_{L_w}}{a}\left(\frac{a_1}{a_2}\right)\left(1 - \frac{d\varepsilon}{d\alpha}\right) - \frac{a_3}{a_2}\beta_\eta - \frac{a_1}{a_2}\eta_T \tag{3.13}$$

When the elevator tab is set at its neutral position, $\beta_\eta = 0$ and for a given *cg* position h the elevator angle to trim varies only with lift coefficient. For any other tab setting a different elevator angle is required to trim. Therefore, to an extent, elevator and elevator tab provide interchangeable means for achieving longitudinal trim.

3.2.3 TEST FOR LONGITUDINAL STATIC STABILITY

The basic requirement for an aeroplane to be statically stable at a given trim condition is stated in equation (3.2). By differentiating equation (3.12) with respect to C_L, or equivalently C_{L_w}, and noting that η_T and, by definition, C_{m_0} are constants then the condition for the aeroplane to be stable is given by

$$\frac{dC_m}{dC_{L_w}} < 0$$

where

$$\frac{dC_m}{dC_{L_w}} = (h - h_0) - \bar{V}_T\left(\frac{a_1}{a}\left(1 - \frac{d\varepsilon}{d\alpha}\right) + a_2\frac{d\eta}{dC_{L_w}} + a_3\frac{d\beta_\eta}{dC_{L_w}}\right) \tag{3.14}$$

Thus, at a given *cg* position h, the longitudinal static stability of the aeroplane and the aerodynamic control characteristics, that is *elevator angle to trim*, $d\eta/dC_{L_w}$, and *elevator tab angle to trim*, $d\beta_\eta/dC_{L_w}$, are interdependent. Further analysis is usually carried out by separating the effects of elevator angle and tab angle in equation (3.14). *Controls fixed stability* is concerned with the interdependence of elevator angle to trim and stability, whereas *controls free stability* is concerned with the interdependence of elevator tab angle to trim and stability.

3.3 Longitudinal static stability

3.3.1 CONTROLS FIXED STABILITY

The condition described as *controls fixed* is taken to mean the condition when the elevator and elevator tab are held at constant settings corresponding to the prevailing trim condition. In practice, this means that the pilot is flying the aeroplane with his hands on the controls and is holding the controls at the *fixed* setting required to trim. This, of course, assumes that the aeroplane is stable and remains in trim.

Since the controls are fixed

$$\frac{d\eta}{dC_{L_w}} = \frac{d\beta_\eta}{dC_{L_w}} = 0 \tag{3.15}$$

and equation (3.14) may be written

$$\frac{dC_m}{dC_{L_w}} = (h - h_0) - \bar{V}_T \frac{a_1}{a}\left(1 - \frac{d\varepsilon}{d\alpha}\right) \tag{3.16}$$

Or, writing

$$K_n = -\frac{dC_m}{dC_{L_w}} = h_n - h \tag{3.17}$$

where K_n is the *controls fixed stability margin*, the slope of the C_m–C_L plot. The location of the *controls fixed neutral point* h_n on the mean aerodynamic chord $\bar{c}$ is therefore given by

$$h_n = h_0 + \bar{V}_T \frac{a_1}{a}\left(1 - \frac{d\varepsilon}{d\alpha}\right) \tag{3.18}$$

For a statically stable aeroplane the stability margin K_n is positive, and the greater its value the greater the degree of stability possessed by the aeroplane. With reference to equation (3.17) it is clear that the aeroplane will be stable when the *cg* position h is ahead of the controls fixed neutral point h_n. The acceptable margins of stability therefore determine the permitted range of *cg* position in a given aeroplane. The aft limit often corresponds to the controls fixed neutral point, whereas the forward limit is determined by the maximum permissible stability margin. Remember, Section 3.1.3, that too much stability can be as hazardous as too little stability.

The meaning of controls fixed stability is easily interpreted by considering the pilot actions required to trim an aeroplane in a controls fixed sense. It is assumed at the outset that the aeroplane is, in fact, stable and hence can be trimmed to an equilibrium flight condition. When the aeroplane is in a trimmed initial equilibrium state the pitching moment is zero and equation (3.12) may be written

$$0 = C_{m_0} + C_{L_w}(h - h_0) - \bar{V}_T\left(C_{L_w}\frac{a_1}{a}\left(1 - \frac{d\varepsilon}{d\alpha}\right) + a_2\eta + a_3\beta_\eta + a_1\eta_T\right) \tag{3.19}$$

It is assumed that the pilot is holding the controls at the required elevator angle, the power is set to give steady level flight and the elevator tab is set at its datum, $\beta_\eta = 0$. Now, to retrim the aeroplane at a new flight condition in a controls fixed sense it is necessary for the pilot to move the controls to the new elevator setting and then to hold the controls at that setting. For example, to retrim at a higher speed in a more nose down attitude, the pilot would move the control column forward until his new condition was established and would then simply hold the column at that position. This would, of course, leave the aeroplane in a descending condition unless the power were increased sufficient to maintain level flight at the higher speed. However, power variations are not allowed for in the simple model reviewed here.

Thus, to trim a stable aeroplane at any condition in its speed envelope simply requires the selection of the correct elevator angle, all other parameters remaining constant. Therefore, the variable in controls fixed stability analysis is elevator angle to trim. Differentiating equation (3.19) with respect to C_{L_w} and making the same assumptions as before but allowing elevator angle η to vary with trim, then after some rearrangement it may be shown that

$$\frac{d\eta}{dC_{L_w}} = \frac{-1}{\bar{V}_T a_2}(h_n - h) = \frac{-1}{\bar{V}_T a_2} K_n \tag{3.20}$$

Thus, since $\bar{V}_T$ and a_2 are constants, the *elevator angle to trim* characteristic $d\eta/dC_{L_w}$ is proportional to the controls fixed stability margin K_n. Measurements of elevator angle to trim for a range of flight conditions, subject to the assumptions described, provide a practical means for determining controls fixed stability characteristics from flight experiments. However, in such experiments it is not generally possible to eliminate completely the effects of power on the results.

EXAMPLE 3.2

The practical evaluation of controls fixed static stability centres on the application of equations (3.13), (3.19) and (3.20) to a stable aeroplane. It is relatively straightforward to obtain measurements of the elevator angle η required to trim an aeroplane at a chosen value of lift coefficient C_L. Provided that the power and elevator trim tab angle β_η are maintained at constant settings throughout the measurement process then the above-mentioned equations apply directly. A flight test exercise conducted in a Handley Page Jetstream by the author under these conditions provided the trim data plotted in Fig. 3.10 for three different *cg* positions. At any given value of lift coefficient C_L the corresponding value of elevator angle to trim η is given by the solution of equation (3.13), or alternatively equation (3.19). The plots are clearly non-linear and the non-linearity in this aeroplane is almost entirely due to the effects of power.

Since the slopes of the plots shown in Fig. 3.10 are all negative the aeroplane is statically stable in accordance with equation (3.20). However, for any given *cg* position the slope varies with lift coefficient, indicating a small variation in stability margin. In a detailed analysis the stability margin would be evaluated at each value of trimmed lift coefficient in order to quantify the variation in stability. In the present example the

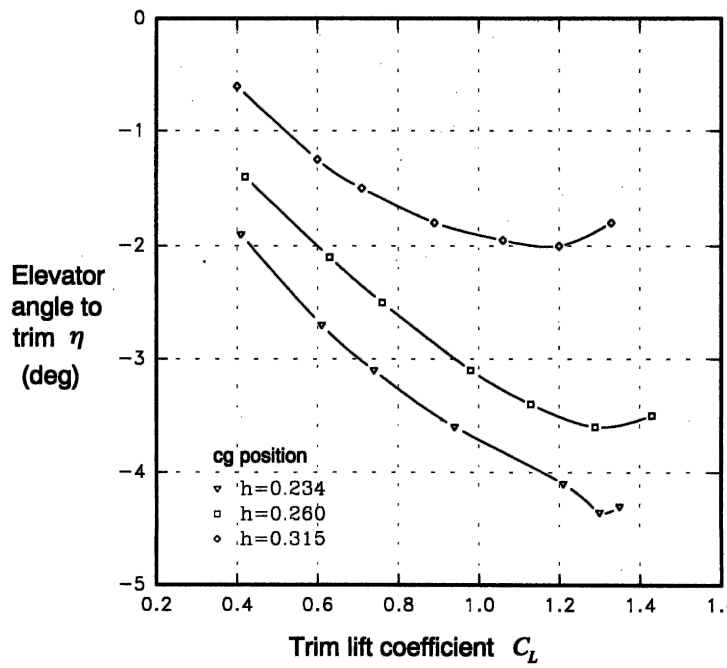

Fig. 3.10 Plot of elevator angle to trim

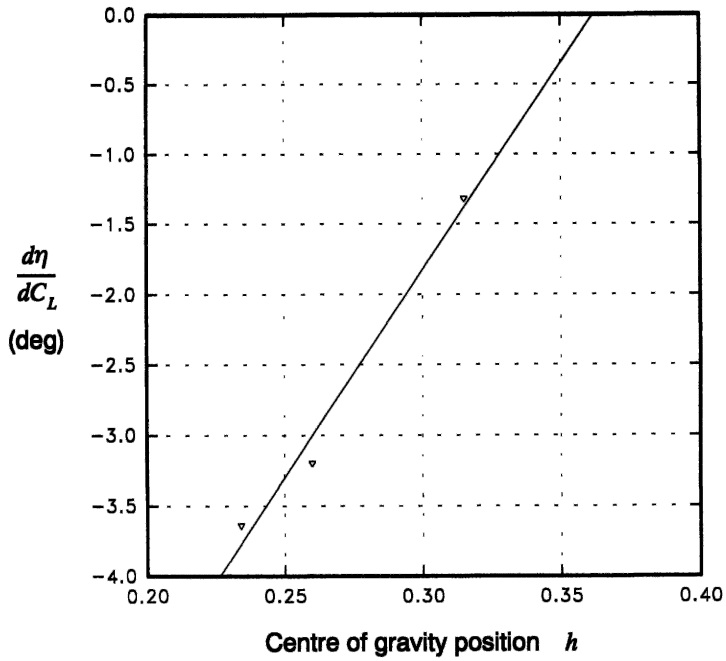

Fig. 3.11 Determination of controls fixed neutral point

quality of the data was not good enough to allow such a complete analysis. To establish the location of the controls fixed neutral point h_n, equation (3.20) must be solved at each value of trim lift coefficient. This is most easily done graphically as shown in Fig. 3.11.

Equation (3.20) is solved by plotting $d\eta/dC_L$ against *cg* position h as shown. In this example the mean slope for each *cg* position is plotted rather than the value at each trim point. Since equation (3.20) represents a linear plot a straight line may be fitted to the three data points as shown. Extrapolation to the neutral stability point at which $d\eta/dC_L = 0$ corresponds to a *cg* position of approximately $h = 0.37$. Clearly, three data points through which to draw a line are barely adequate for this kind of evaluation. A controls fixed neutral point h_n at 37% of *mac* correlates well with the known properties of the aeroplane. The most aft *cg* position permitted is in fact at 37% of *mac*. Having established the location of the controls fixed neutral point the controls fixed stability margin K_n for each *cg* position follows from the application of equation (3.20).

In a more searching stability evaluation rather more data points would be required and data of much better quality would be essential. Although limited, the present example does illustrate the typical controls fixed longitudinal static stability characteristics of a well-behaved classical aeroplane.

3.3.2 CONTROLS FREE STABILITY

The condition described as *controls free* is taken to mean the condition when the elevator is free to float at an angle corresponding to the prevailing trim condition. In practice, this means that the pilot can fly the aeroplane with his hands off the controls whilst the

aeroplane remains in its trimmed flight condition. Again, it is assumed that the aeroplane is stable, otherwise it will diverge when the controls are released. Now this situation can only be obtained if the controls can be adjusted such that the elevator will float at the correct angle for the desired *hands-off* trim condition. This is arranged by adjusting the elevator trim tab until the required trim is obtained. Thus, controls free stability is concerned with the trim tab and its control characteristics.

When the controls are free, the elevator hinge moment H is zero and the elevator floats at an indeterminate angle η. It is therefore necessary to eliminate elevator angle from the pitching moment equation (3.12) in order to facilitate the analysis of controls free stability. The elevator hinge moment coefficient is given by the expression

$$C_H = b_1\alpha_T + b_2\eta + b_3\beta_\eta \tag{3.21}$$

where b_1, b_2 and b_3 are constants determined by the design of the elevator and trim tab control circuitry. Substituting for local tailplane incidence α_T as given by equation (3.11), equation (3.21) may then be rearranged to determine the angle at which the elevator floats. Thus

$$\eta = \frac{1}{b_2}C_H - \frac{C_{L_w}}{a}\frac{b_1}{b_2}\left(1 - \frac{d\varepsilon}{d\alpha}\right) - \frac{b_3}{b_2}\beta_\eta - \frac{b_1}{b_2}\eta_T \tag{3.22}$$

To eliminate elevator angle from the pitching moment equation, substitute equation (3.22) into equation (3.12) to obtain

$$C_m = C_{m_0} + C_{L_w}(h - h_0) - \bar{V}_T\left(\begin{array}{l} C_{L_w}\dfrac{a_1}{a}\left(1 - \dfrac{d\varepsilon}{d\alpha}\right)\left(1 - \dfrac{a_2b_1}{a_1b_2}\right) + a_3\beta_\eta\left(1 - \dfrac{a_2b_3}{a_3b_2}\right) \\ + a_1\eta_T\left(1 - \dfrac{a_2b_1}{a_1b_2}\right) + \dfrac{a_2}{b_2}C_H \end{array}\right) \tag{3.23}$$

Now in the controls free condition $C_H = 0$ and noting that η_T, C_{m_0} and, since the tab is set at the trim value, β_η are constants, then differentiating equation (3.23) with respect to C_{L_w}

$$\frac{dC_m}{dC_{L_w}} = (h - h_0) - \bar{V}_T\frac{a_1}{a}\left(1 - \frac{d\varepsilon}{d\alpha}\right)\left(1 - \frac{a_2b_1}{a_1b_2}\right) \tag{3.24}$$

Or, writing

$$K_n' = -\frac{dC_m}{dC_{L_w}} = h_n' - h \tag{3.25}$$

where K_n' is the *controls free stability margin*, the slope of the C_m–C_L plot with the controls free. The location of the *controls free neutral point* h_n' on the mean aerodynamic chord $\bar{c}$ is given by

$$\begin{aligned} h_n' &= h_0 + \bar{V}_T\frac{a_1}{a}\left(1 - \frac{d\varepsilon}{d\alpha}\right)\left(1 - \frac{a_2b_1}{a_1b_2}\right) \\ &= h_n - \bar{V}_T\frac{a_2b_1}{ab_2}\left(1 - \frac{d\varepsilon}{d\alpha}\right) \end{aligned} \tag{3.26}$$

Thus, as before, for a statically stable aeroplane the controls free stability margin K_n' is positive and the greater its value the greater the degree of stability possessed by the aeroplane. With reference to equation (3.25) it is clear that for controls free stability the

cg position h must be ahead of the controls free neutral point h'_n. Equation (3.26) shows the relationship between the controls fixed and the controls free neutral points. The numerical values of the elevator and tab constants are such that usually $h'_n > h_n$, which means that it is common for the controls free neutral point to lie aft of the controls fixed neutral point. Thus, an aeroplane that is stable controls fixed will also usually be stable controls free and it follows that the controls free stability margin K'_n will be greater than the controls fixed stability margin K_n.

The meaning of controls free stability is readily interpreted by considering the pilot actions required to trim the aeroplane in a controls free sense. It is assumed that the aeroplane is stable and is initially in a hands-off trim condition. In this condition the pitching moment is zero and hence equation (3.23) may be written

$$0 = C_{m_0} + C_{L_w}(h - h_0) - \bar{V}_T \left(\begin{array}{l} C_{L_w} \dfrac{a_1}{a} \left(1 - \dfrac{d\varepsilon}{d\alpha}\right)\left(1 - \dfrac{a_2 b_1}{a_1 b_2}\right) \\ + a_3 \beta_\eta \left(1 - \dfrac{a_2 b_3}{a_3 b_2}\right) + a_1 \eta_T \left(1 - \dfrac{a_2 b_1}{a_1 b_2}\right) \end{array} \right) \tag{3.27}$$

Now to retrim the aeroplane it is necessary for the pilot to grasp the control column and move it to the position corresponding to the elevator angle required for the new trim condition. However, if he now releases the control it will simply move back to its original trim position since an out-of-trim elevator hinge moment, and hence stick force, will exist at the new position. To rectify the problem he must use the trim tab. Having moved the control to the position corresponding to the new trim condition he will be holding a force on the control. By adjusting the trim tab he can null the force and following which, he can release the control and it will stay in the new hands-off position as required. Thus, trim tab adjustment is equivalent to control force adjustment, which in turn is directly related to elevator hinge moment adjustment in a mechanical flying control system. To reiterate the previous illustration, consider the situation when the pilot wishes to retrim the aeroplane at a higher speed in a more nose down attitude. As before, he will *push* the control column forward until he obtains the desired condition which leaves him holding an out-of-trim force and descending. Elevator tab adjustment will enable him to reduce the control force to zero whereupon he can release the control to enjoy his new hands-off trim condition. Since he will be descending it would normally be necessary to increase power in order to regain level flight. However, as already stated, thrust variations are not allowed for in this model; if they were the analysis would be considerably more complex.

Thus, to trim a stable aeroplane at any hands-off flight condition in its speed envelope simply requires the correct selection of elevator tab angle. The variable in controls free stability analysis is therefore elevator tab angle to trim. Differentiating equation (3.27) with respect to C_{L_w} and making the same assumptions as previously but allowing elevator tab angle β_η to vary with trim, then after some rearrangement it may be shown that

$$\frac{d\beta_\eta}{dC_{L_w}} = \frac{-1}{a_3 \bar{V}_T \left(1 - \dfrac{a_2 b_3}{a_3 b_2}\right)} (h'_n - h) = \frac{-1}{a_3 \bar{V}_T \left(1 - \dfrac{a_2 b_3}{a_3 b_2}\right)} K'_n \tag{3.28}$$

Since it is usual for

$$-a_3 \bar{V}_T \left(1 - \frac{a_2 b_3}{a_3 b_2}\right) > 0 \tag{3.29}$$

then the *elevator tab angle to trim* characteristic $d\beta_\eta/dC_{L_w}$ is positive and is proportional to the controls free stability margin K'_n. Measurement of the tab angle to trim a range of flight conditions, subject to the assumptions described, provides a practical means for determining controls free stability characteristics from flight experiments. However, since tab angle, elevator hinge moment and control force are all equivalent it is often more meaningful to investigate control force to trim directly since this is the parameter of direct concern to the pilot.

To determine the equivalence between elevator tab angle to trim and control force to trim, consider the aeroplane in a stable hands-off trim state with the tab set at its correct trim value. If the pilot moves the controls in this condition the elevator hinge moment, and hence control force, will vary. Equation (3.23) is applicable and may be written

$$0 = C_{m_0} + C_{L_w}(h - h_0) - \bar{V}_T \left(\begin{array}{l} C_{L_w} \dfrac{a_1}{a} \left(1 - \dfrac{d\varepsilon}{d\alpha}\right)\left(1 - \dfrac{a_2 b_1}{a_1 b_2}\right) + a_3 \beta_\eta \left(1 - \dfrac{a_2 b_3}{a_3 b_2}\right) \\ + a_1 \eta_T \left(1 - \dfrac{a_2 b_1}{a_1 b_2}\right) + \dfrac{a_2}{b_2} C_H \end{array} \right) \tag{3.30}$$

where β_η is set at its datum trim position and is assumed constant and the hinge moment coefficient C_H is allowed to vary with trim condition. Differentiate equation (3.30) with respect to C_{L_w} subject to these constraints and rearrange to obtain

$$\frac{dC_H}{dC_{L_w}} = \frac{-1}{\bar{V}_T \dfrac{a_2}{b_2}}(h'_n - h) = \frac{-1}{\bar{V}_T \dfrac{a_2}{b_2}} K'_n \tag{3.31}$$

Comparison of equation (3.31) with equation (3.28) demonstrates the equivalence of tab angle to trim and hinge moment to trim. Further, if the elevator control force is denoted F_η and g_η denotes the mechanical gearing between the control column and elevator then

$$F_\eta = g_\eta H = \frac{1}{2} \rho V^2 S_\eta \bar{\bar{c}}_\eta g_\eta C_H \tag{3.32}$$

where S_η is the elevator area aft of the hinge line and $\bar{\bar{c}}_\eta$ is the mean aerodynamic chord of the elevator aft of the hinge line. This therefore demonstrates the relationship between control force and hinge moment although equation (3.32) shows the relationship depends on the square of the speed.

EXAMPLE 3.3

The practical evaluation of controls free static stability is undertaken in much the same way as the evaluation of controls fixed stability discussed in Example 3.2. In this case the evaluation of controls free static stability centres on the application of equations (3.30), (3.31) and (3.32) to a stable aeroplane. It is relatively straightforward to obtain measurements of the elevator stick force F_η, and hence hinge moment coefficient C_H, required to trim an aeroplane at a chosen value of lift coefficient C_L. Provided that the power and elevator trim tab angle β_η are maintained at constant settings throughout the measurement process the above-mentioned equations apply directly.

As before, a flight test exercise conducted in a Handley Page Jetstream under these

conditions provided the trim data plotted in Fig. 3.12 for three different *cg* positions. At any given value of lift coefficient C_L the corresponding value of elevator hinge moment to trim C_H is given by the solution of equation (3.30). Again, the plots are non-linear due primarily to the effects of power. However, since force measurements are involved, the influence of friction in the mechanical control runs is significant and inconsistent. The result of this is data with rather too many spurious points. In order to provide a meaningful example the obviously spurious data points have been 'adjusted' to correlate with the known characteristics of the aeroplane.

Since the slopes of the plots shown in Fig. 3.12 are all positive, the aeroplane is statically stable in accordance with equation (3.31). However, for any given *cg* position the slope varies with lift coefficient indicating rather inconsistent variations in stability margin. However, in this case, the variations are more likely to be the result of poor quality data rather than orderly changes in the aerodynamic properties of the aeroplane. Again, in a detailed analysis the stability margin would be evaluated at each value of trimmed lift coefficient in order to quantify the variation in stability. In the present example the quality of the data was clearly not good enough to allow such a complete analysis. To establish the location of the controls free neutral point h_n' equation (3.31) must be solved at each value of trim lift coefficient. This is most easily done graphically as shown in Fig. 3.13.

Equation (3.31) is solved by plotting $\mathrm{d}C_H/\mathrm{d}C_L$ against *cg* position h as shown. In this example the mean slope for each *cg* position is plotted rather than the value at each trim point. Since equation (3.31) represents a linear plot a straight line may be fitted to the three data points as shown. Extrapolation to the neutral stability point at which $\mathrm{d}C_H/\mathrm{d}C_L = 0$ corresponds to a *cg* position of approximately $h = 0.44$. A controls free neutral point h_n' at 44% of *mac* correlates reasonably well to the known

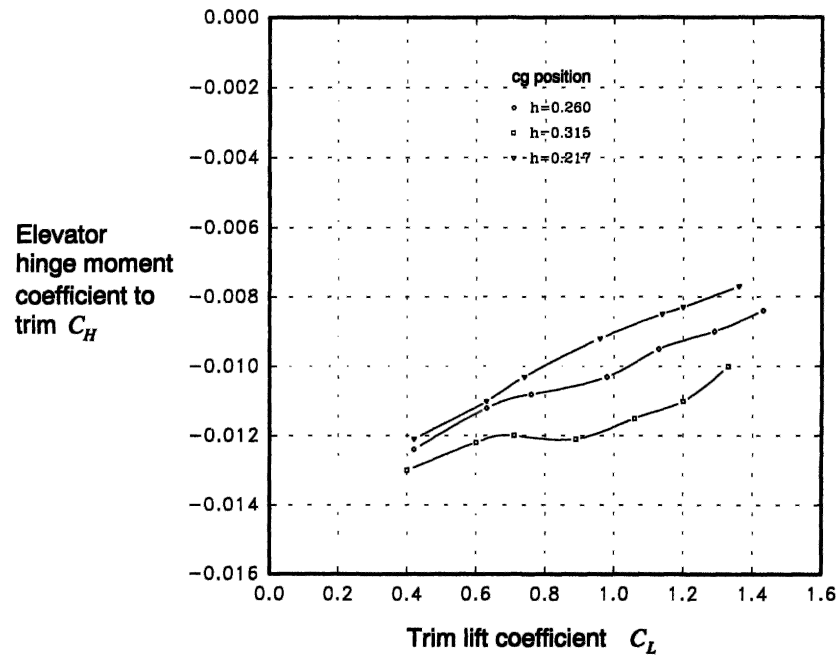

Fig. 3.12 Plot of hinge moment coefficient to trim

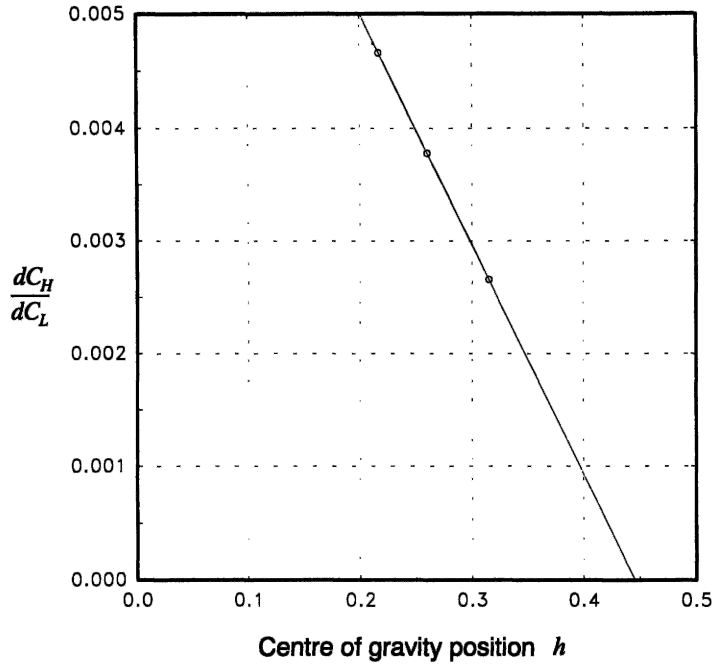

Fig. 3.13 Determination of controls free neutral point

properties of the aeroplane. Having established the location of the controls free neutral point the controls free stability margin K'_n for each *cg* position follows from the application of equation (3.25).

3.3.3 SUMMARY OF LONGITUDINAL STATIC STABILITY

A physical interpretation of the meaning of longitudinal static stability may be brought together in the summary shown in Fig. 3.14.

The important parameters are neutral point positions and their relationship to the *cg* position which, in turn, determines the stability margins of the aeroplane. The stability margins determine literally how much stability the aeroplane has in hand, in the controls fixed and free senses, over and above neutral stability. The margins therefore indicate how safe the aeroplane is. However, equally importantly, the stability margins provide a measure of the control actions required to trim the aeroplane. In particular, the controls fixed stability margin is a measure of the control displacement required to trim and the controls free stability margin is a measure of the control force required to trim. From a flying and handling qualities point of view it is the interpretation of stability in terms of control characteristics which is by far the most important consideration. In practice, the assessment of longitudinal static stability is frequently concerned only with the measurement of control characteristics, as illustrated by Examples 3.2 and 3.3.

3.4 Lateral static stability

Lateral static stability is concerned with the ability of the aeroplane to maintain wings level equilibrium in the roll sense. Wing dihedral is the most visible parameter which

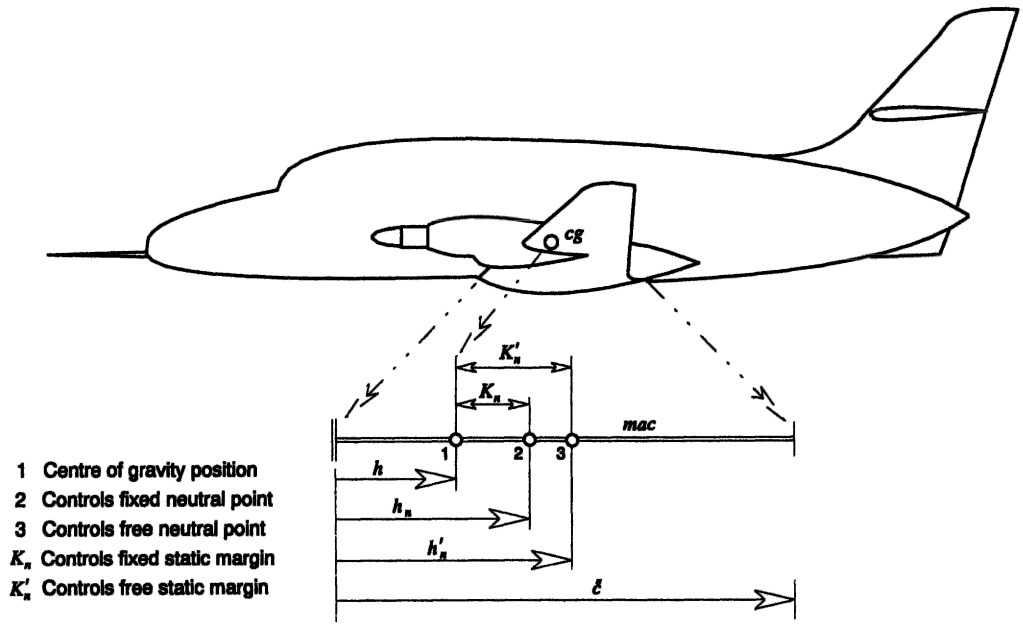

Fig. 3.14 Longitudinal stability margins

confers lateral static stability on an aeroplane although there are many other contributions, some of which are destabilizing. Since all aeroplanes are required to fly with their wings level in the steady trim state lateral static stability is designed-in from the outset. Dihedral is the easiest parameter to adjust in the design process in order to 'tune' the degree of stability to an acceptable level. Remember that too much lateral static stability will result in an aeroplane that is reluctant to manoeuvre laterally, so it is important to obtain the correct degree of stability.

The effect of dihedral as a means for providing lateral static stability is easily appreciated by considering the situation depicted in Fig. 3.15. Following a small lateral disturbance in roll, ϕ, the aeroplane will commence to slide 'downhill' sideways with a sideslip velocity v. Consider the resulting change in the aerodynamic conditions on the leading wing which has dihedral angle Γ. Since the wing has dihedral the sideslip velocity has a small component v' resolved perpendicular to the plane of the wing panel where

$$v' = v \sin \Gamma \tag{3.33}$$

The velocity component v' combines with the axial velocity component U_e to increase the angle of attack of the leading wing by α'. Since $v' \ll U_e$ the change in angle of attack α is small and the total disturbed axial velocity component $U \cong U_e$. The increase in angle of attack on the leading wing gives rise to an increase in lift which in turn gives rise to a restoring rolling moment $-L$. The corresponding aerodynamic change on the wing trailing into the sideslip results in a small decrease in lift which also produces a restoring rolling moment. The net effect therefore is to create a negative rolling moment which causes the aeroplane to recover its zero sideslip wings level equilibrium. Thus, the condition for an aeroplane to be laterally stable is that the rolling moment resulting from a positive disturbance in roll attitude must be negative, or in mathematical terms

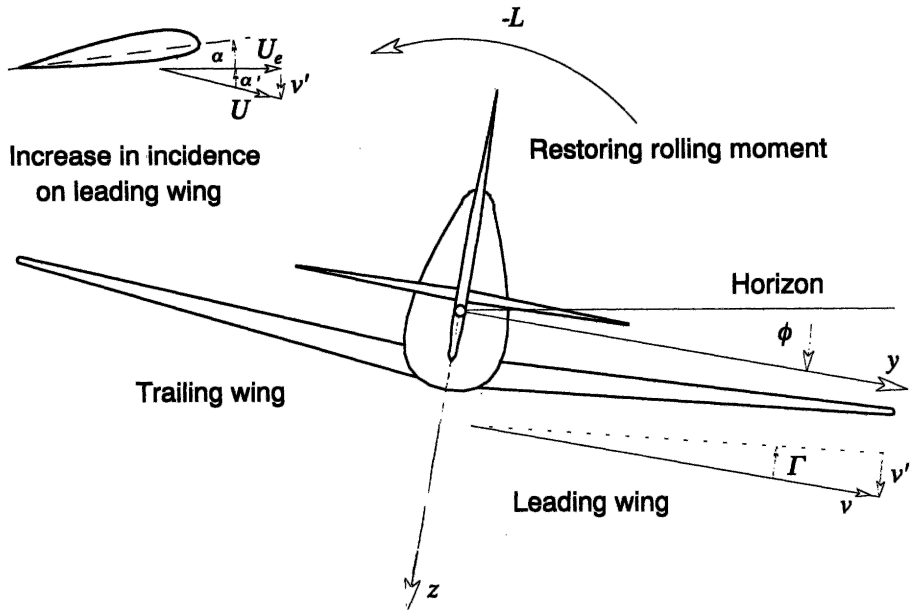

Fig. 3.15 Dihedral effect

$$\frac{dC_l}{d\phi} < 0 \tag{3.34}$$

where C_l is the rolling moment coefficient. This is shown graphically in Fig. 3.16 and may be interpreted in a similar way to the pitching moment plot shown in Fig. 3.2.

The sequence of events following a sideslip disturbance are shown for a laterally stable, neutrally stable and unstable aeroplane on Fig. 3.17. However, it must be remembered that once disturbed the resulting motion will be determined by the lateral dynamic stability characteristics as well.

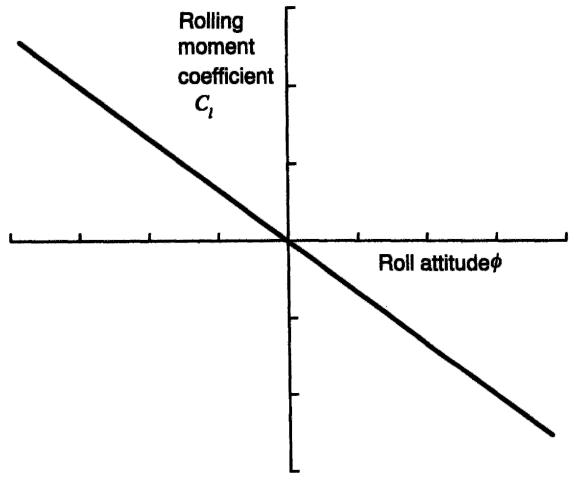

Fig. 3.16 C_l–ϕ plot for a stable aeroplane

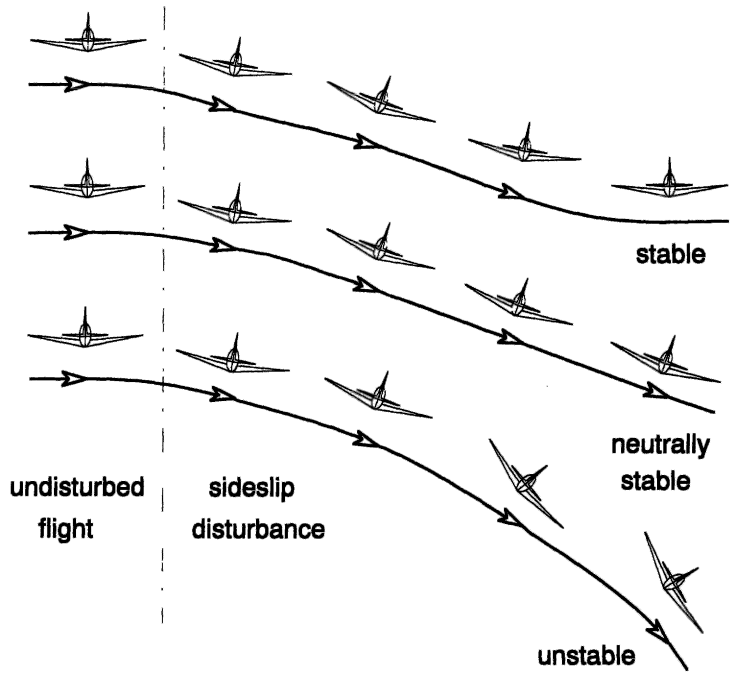

Fig. 3.17 The effect of dihedral on lateral stability

3.5 Directional static stability

Directional static stability is concerned with the ability of the aeroplane to yaw or *weathercock* into wind in order to maintain directional equilibrium. Since all aeroplanes are required to fly with zero sideslip in the yaw sense, positive directional stability is designed-in from the outset. The fin is the most visible contributor to directional static stability although, as in the case of lateral stability, there are many other contributions, some of which are destabilizing. Again, it is useful to remember that too much directional static stability will result in an aeroplane that is reluctant to manoeuvre directionally, so it is important to obtain the correct degree of stability.

Consider an aeroplane that is subject to a positive sideslip disturbance as shown in Fig. 3.18. The combination of sideslip velocity v and axial velocity component U results in a positive sideslip angle β. Note that a positive sideslip angle equates to a negative yaw angle since the nose of the aeroplane has swung to the left of the resultant total velocity vector V. Now, as shown in Fig. 3.18, in the disturbance the fin is at a non-zero angle of attack equivalent to the sideslip angle β. The fin therefore generates lift L_F which acts in the sense shown thereby creating a positive yawing moment N. The yawing moment is stabilizing since it causes the aeroplane to yaw to the right until the sideslip angle is reduced to zero. Thus, the condition for an aeroplane to be directionally stable is readily established and is

$$\frac{dC_n}{d\psi} > 0 \quad \text{or, equivalently,} \quad \frac{dC_n}{d\beta} < 0 \tag{3.35}$$

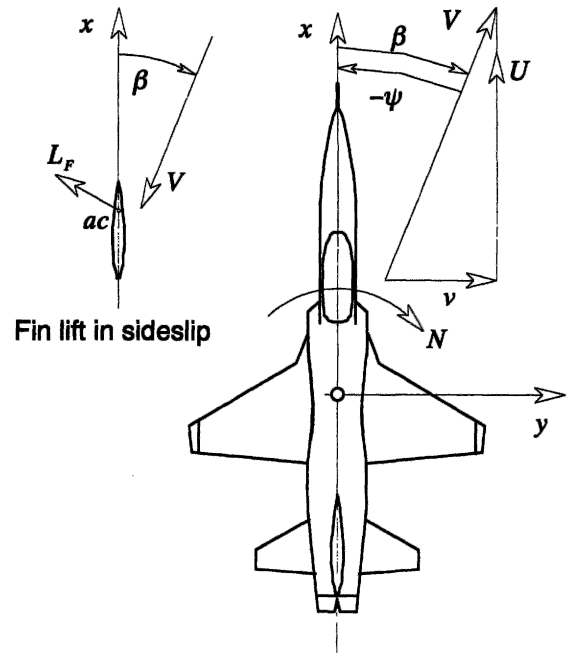

Fig. 3.18 Directional weathercock effect

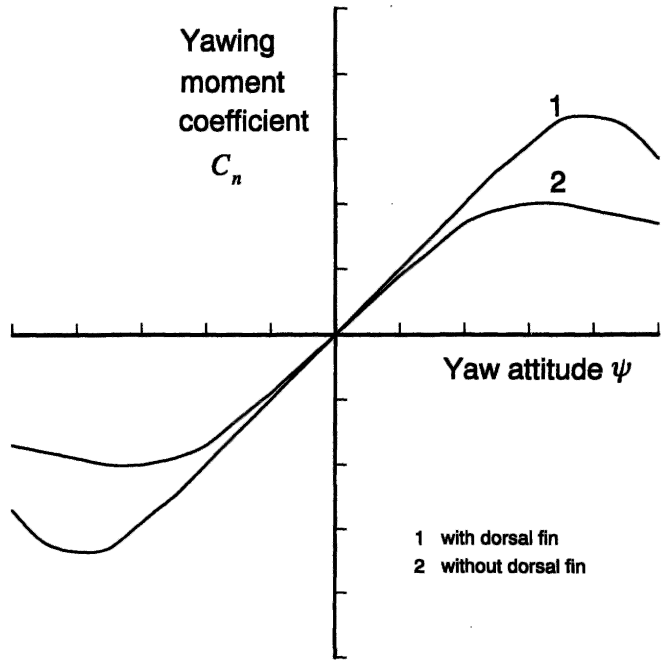

Fig. 3.19 Plot of C_n–ψ for a stable aeroplane

A typical plot of yawing moment coefficient against yaw attitude for a directionally stable aeroplane is shown in Fig. 3.19. For small disturbances in yaw the plot is reasonably linear since it is dominated by the lifting properties of the fin. However, as the fin approaches the stall its lifting properties deteriorate and other influences begin to dominate, resulting ultimately in directional instability. The main destabilizing contribution comes from the fuselage which at small yaw angles is masked by the powerful fin effect. The addition of a dorsal fin significantly delays the onset of fin stall thereby enabling directional static stability to be maintained to higher yaw disturbance angles as indicated in Fig. 3.19.

Fin effectiveness also deteriorates with increasing body incidence angle since the base of the fin becomes increasingly immersed in the forebody wake thereby reducing the effective working area of the fin. This problem has become particularly evident in a number of modern combat aeroplanes. Typically, such aeroplanes have two engines mounted side by side in the rear fuselage. This results in a broad flat fuselage ahead of the fin which creates a substantial wake to reduce fin effectiveness dramatically at moderate to high angles of incidence. For this reason many aeroplanes of this type have noticeably large fins and in some cases the aeroplanes have two fins attached to the outer edges of the upper fuselage.

References

Babister, A. W. 1961: *Aircraft Stability and Control.* Pergamon Press, London.

Duncan, W. J. 1959: *The Principles of the Control and Stability of Aircraft.* Cambridge University Press, Cambridge.

Gates, S. B. and Lyon, H. M. 1944: *A Continuation of Longitudinal Stability and Control Analysis; Part 1, General Theory.* Aeronautical Research Council, Reports and Memoranda No: 2027.

Storey, R. F. R. 1966: *H.P.137. Longitudinal and Lateral Stability Measurements on a 1/6th Scale Model.* W.T. Report No: 3021, BAC (Operating) Ltd, Weybridge, Surrey.

4

The Equations of Motion

4.1 The equations of motion of a rigid symmetric aeroplane

As stated in Chapter 1, the first formal derivation of the equations of motion for a rigid symmetric aeroplane is usually attributed to Bryan (1911). His treatment, with very few changes, remains in use today and provides the basis for the following development. The object is to realize Newton's second law of motion for each of the six degrees of freedom which simply states that

$$\text{mass} \times \text{acceleration} = \text{disturbing force} \tag{4.1}$$

For the rotary degrees of freedom the mass and acceleration become moment of inertia and angular acceleration respectively, whilst the disturbing force becomes the disturbing moment, or torque. Thus, the derivation of the equations of motion requires that equation (4.1) be expressed in terms of the motion variables defined in Chapter 2. The derivation is *classical* in the sense that the equations of motion are differential equations which are derived from first principles. However, a number of equally valid alternative means for deriving the equations of motion are frequently used, for example vector methods. The classical approach is retained here since, in the author's opinion, maximum physical visibility is maintained throughout.

4.1.1 THE COMPONENTS OF INERTIAL ACCELERATION

The first task in realizing equation (4.1) is to define the inertial acceleration components resulting from the application of disturbing force components to the aeroplane. Consider the motion referred to an orthogonal axis set ($oxyz$) with the origin o coincident with the cg of the arbitrary and, in the first instance, not necessarily rigid body shown in Fig. 4.1. The body, and hence the axes, are assumed to be in motion with respect to an external reference frame such as earth (or *inertial*) axes. The components of velocity and force along the axes ox, oy and oz are denoted (U, V, W) and (X, Y, Z) respectively. The components of angular velocity and moment about the same axes are denoted (p, q, r) and (L, M, N) respectively. The point p is an arbitrarily chosen point within the body with coordinates (x, y, z). The local components of velocity and acceleration at p relative to the body axes are denoted (u, v, w) and (a_x, a_y, a_z) respectively.

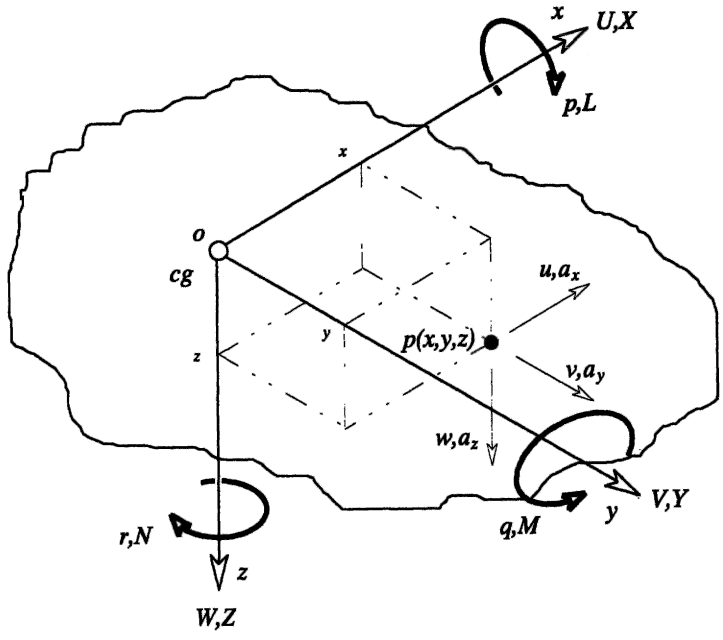

Fig. 4.1 Motion referred to generalized body axes

The velocity components at $p(x, y, z)$ relative to o are given by

$$\left.\begin{aligned} u &= \dot{x} - ry + qz \\ v &= \dot{y} - pz + rx \\ w &= \dot{z} - qx + py \end{aligned}\right\} \tag{4.2}$$

It will be seen that the velocity components each comprise a linear term and two additional terms due to rotary motion. The origin of the terms due to rotary motion in the component u, for example, is illustrated in Fig. 4.2. Both $-ry$ and qz represent *tangential velocity* components acting along a line through $p(x, y, z)$ parallel to the ox axis. The rotary terms in the remaining two components of velocity are determined in a similar way. Now, since the generalized body shown in Fig. 4.1 represents the aeroplane which is assumed to be rigid then

$$\dot{x} = \dot{y} = \dot{z} = 0 \tag{4.3}$$

and equations (4.2) reduce to

$$\left.\begin{aligned} u &= qz - ry \\ v &= rx - pz \\ w &= py - qx \end{aligned}\right\} \tag{4.4}$$

The corresponding components of acceleration at $p(x, y, z)$ relative to o are given by

$$\left.\begin{aligned} a_x &= \dot{u} - rv + qw \\ a_y &= \dot{v} - pw + ru \\ a_z &= \dot{w} - qu + pv \end{aligned}\right\} \tag{4.5}$$

Again, it will be seen that the acceleration components each comprise a linear term

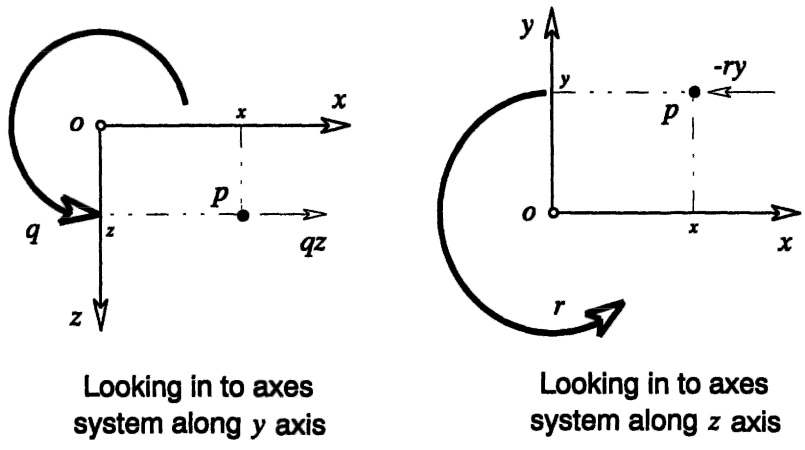

Fig. 4.2 Velocity terms due to rotary motion

and two additional terms due to rotary motion. The origin of the terms due to rotary motion in the component a_x, for example, is illustrated in Fig. 4.3. Both $-rv$ and qw represent *tangential acceleration* components acting along a line through $p(x, y, z)$ parallel to the ox axis. The accelerations arise from the mutual interaction of the linear components of velocity with the components of angular velocity. The acceleration terms due to rotary motion in the remaining two components of acceleration are determined in a similar way.

By superimposing the velocity components of the cg (U, V, W) on to the local velocity components (u, v, w) the absolute, or inertial, velocity components (u', v', w') of the point $p(x, y, z)$ are obtained. Thus

$$\left.\begin{aligned} u' &= U + u = U - ry + qz \\ v' &= V + v = V - pz + rx \\ w' &= W + w = W - qx + py \end{aligned}\right\} \tag{4.6}$$

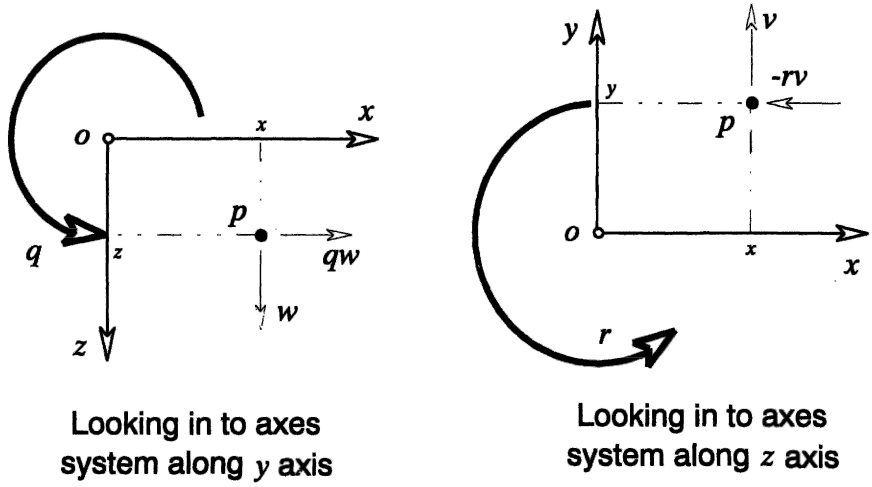

Fig. 4.3 Acceleration terms due to rotary motion

where the expressions for (u, v, w) are substituted from equations (4.4). Similarly, the components of inertial acceleration (a'_x, a'_y, a'_z) at the point $p(x, y, z)$ are obtained simply by substituting the expressions for (u', v', w'), equations (4.6), in place of (u, v, w) in equations (4.5). Whence

$$\left.\begin{aligned} a'_x &= \dot{u}' - rv' + qw' \\ a'_y &= \dot{v}' - pw' + ru' \\ a'_z &= \dot{w}' - qu' + pv' \end{aligned}\right\} \tag{4.7}$$

Differentiate equations (4.6) with respect to time and note that since a rigid body is assumed equation (4.3) applies, then

$$\left.\begin{aligned} \dot{u}' &= \dot{U} - \dot{r}y + \dot{q}z \\ \dot{v}' &= \dot{V} - \dot{p}z + \dot{r}x \\ \dot{w}' &= \dot{W} - \dot{q}x + \dot{p}y \end{aligned}\right\} \tag{4.8}$$

Thus, by substituting from equations (4.6) and (4.8) into equations (4.7) the inertial acceleration components of the point $p(x, y, z)$ in the rigid body are obtained which, after some rearrangement, may be written

$$\left.\begin{aligned} a'_x &= \dot{U} - rV + qW - x(q^2 + r^2) + y(pq - \dot{r}) + z(pr + \dot{q}) \\ a'_y &= \dot{V} - pW + rU + x(pq + \dot{r}) - y(p^2 + r^2) + z(qr - \dot{p}) \\ a'_z &= \dot{W} - qU + pV + x(pr - \dot{q}) + y(qr + \dot{p}) - z(p^2 + q^2) \end{aligned}\right\} \tag{4.9}$$

EXAMPLE 4.1

To illustrate the usefulness of equations (4.9) consider the following simple example.

A pilot in an aerobatic aeroplane performs a loop in 20 s at a steady velocity of 100 m/s. His seat is located 5 m ahead of, and 1 m above, the *cg*. What total normal load factor does he experience at the top and at the bottom of the loop?

Assuming the motion is in the plane of symmetry only, then $V = \dot{p} = p = r = 0$ and since the pilot's seat is also in the plane of symmetry $y = 0$, and the expression for normal acceleration is, from equations (4.9),

$$a'_z = \dot{W} - qU + x\dot{q} - zq^2$$

Since the manoeuvre is steady, the further simplification $\dot{W} = \dot{q} = 0$ can be made and the expression for the normal acceleration at the pilot's seat reduces to

$$a'_z = -qU - zq^2$$

Now

$$q = \frac{2\pi}{20} = 0.314 \text{ rad/s}$$

$$U = 100 \text{ m/s}$$

$$x = 5 \text{ m}$$

$$z = -1 \text{ m (above } cg \text{ hence negative)}$$

whence, $a'_z = -31.30 \text{ m/s}^2$. Now, by definition, the corresponding normal load factor

due to the manoeuvre is given by

$$n' = \frac{-a'_z}{g} = \frac{31.30}{9.81} = 3.19$$

The total normal load factor n comprises that factor due to the manoeuvre n' plus that due to gravity n_g. At the top of the loop $n_g = -1$, thus the total normal load factor is given by

$$n = n' + n_g = 3.19 - 1 = 2.19$$

and at the bottom of the loop $n_g = 1$ and in this case the total normal load factor is given by

$$n = n' + n_g = 3.19 + 1 = 4.19$$

It is interesting to note that the normal acceleration measured by an accelerometer mounted at the pilot's seat corresponds with the total normal load factor. The accelerometer would therefore give the following readings:

at the top of the loop $a_z = ng = 2.19 \times 9.81 = 21.48\,\text{m/s}^2$
at the bottom of the loop $a_z = ng = 4.19 \times 9.81 = 41.10\,\text{m/s}^2$

Equations (4.9) can therefore be used to determine the accelerations that would be measured by suitably aligned accelerometers located at any point in the airframe and defined by the coordinates (x, y, z).

4.1.2 *THE GENERALIZED FORCE EQUATIONS*

Consider now an incremental mass δm at point $p(x, y, z)$ in the rigid body. Applying Newton's second law, equation (4.1), to the incremental mass, the incremental components of force acting on the mass are given by $(\delta m a'_x, \delta m a'_y, \delta m a'_z)$. Thus the total force components (X, Y, Z) acting on the body are given by summing the force increments over the whole body, whence

$$\left.\begin{aligned} \Sigma \delta m a'_x &= X \\ \Sigma \delta m a'_y &= Y \\ \Sigma \delta m a'_z &= Z \end{aligned}\right\} \tag{4.10}$$

Substitute the expressions for the components of inertial acceleration (a'_x, a'_y, a'_z) from equations (4.9) into equations (4.10) and note that since the origin of axes coincides with the *cg*

$$\Sigma \delta m x = \Sigma \delta m y = \Sigma \delta m z = 0 \tag{4.11}$$

Therefore, the resultant components of total force acting on the rigid body are given by

$$\left.\begin{aligned} m(\dot{U} - rV + qW) &= X \\ m(\dot{V} - pW + rU) &= Y \\ m(\dot{W} - qU + pV) &= Z \end{aligned}\right\} \tag{4.12}$$

where m is the total mass of the body.

Equations (4.12) represent the force equations of a generalized rigid body and describe the motion of its *cg* since the origin of the axis system is co-located with the *cg* in the body. In some applications, for example the airship, it is often convenient to locate the origin of the axis system at some point other than the *cg*. In such cases the condition described by equation (4.11) does not apply and equations (4.12) would include rather more terms.

4.1.3 THE GENERALIZED MOMENT EQUATIONS

Consider now the moments produced by the forces acting on the incremental mass δm at point $p(x, y, z)$ in the rigid body. The incremental force components create an incremental moment component about each of the three body axes and by summing these over the whole body the moment equations are obtained. The moment equations are, of course, the realization of the rotational form of Newton's second law of motion.

For example, the total moment L about the ox axis is given by summing the incremental moments over the whole body

$$\Sigma\delta m(ya'_z - za'_y) = L \tag{4.13}$$

Substituting in equation (4.13) for a'_y and for a'_z obtained from equations (4.9) and noting that equation (4.11) applies then, after some rearrangement, equation (4.13) may be written

$$\left.\begin{aligned} &\dot{p}\Sigma\delta m(y^2 + z^2) + qr\Sigma\delta m(y^2 - z^2) \\ &+ (r^2 - q^2)\Sigma\delta myz - (pq + \dot{r})\Sigma\delta mxz + (pr - \dot{q})\Sigma\delta mxy \end{aligned}\right) = L \tag{4.14}$$

Terms under the summation sign Σ in equation (4.14) have the units of moment of inertia; thus, it is convenient to define the moments and products of inertia as set out in Table 4.1.

Equation (4.14) may therefore be rewritten

$$I_x\dot{p} - (I_y - I_z)qr + I_{xy}(pr - \dot{q}) - I_{xz}(pq + \dot{r}) + I_{yz}(r^2 - q^2) = L \tag{4.15}$$

In a similar way the total moments M and N about the oy and oz axes respectively are given by summing the incremental moment components over the whole body

$$\left.\begin{aligned} \Sigma\delta m(za'_x - xa'_z) &= M \\ \Sigma\delta m(xa'_y - ya'_x) &= N \end{aligned}\right\} \tag{4.16}$$

Substituting a'_x, a'_y and a'_z, obtained from equations (4.9), in equations (4.16), noting

Table 4.1 Moments and products of inertia

$I_x = \Sigma\delta m(y^2 + z^2)$	Moment of inertia about ox axis
$I_y = \Sigma\delta m(x^2 + z^2)$	Moment of inertia about oy axis
$I_z = \Sigma\delta m(x^2 + y^2)$	Moment of inertia about oz axis
$I_{xy} = \Sigma\delta mxy$	Product of inertia about ox and oy axes
$I_{xz} = \Sigma\delta mxz$	Product of inertia about ox and oz axes
$I_{yz} = \Sigma\delta myz$	Product of inertia about oy and oz axes

again that equation (4.11) applies and making use of the inertia definitions given in Table 4.1, then the moment M about the oy axis is given by

$$I_y\dot{q} + (I_x - I_z)pr + I_{yz}(pq - \dot{r}) + I_{xz}(p^2 - r^2) - I_{xy}(qr + \dot{p}) = M \tag{4.17}$$

and the moment N about the oz axis is given by

$$I_z\dot{r} - (I_x - I_y)pq - I_{yz}(pr + \dot{q}) + I_{xz}(qr - \dot{p}) + I_{xy}(q^2 + p^2) = N \tag{4.18}$$

Equations (4.15), (4.17) and (4.18) represent the moment equations of a generalized rigid body and describe the rotational motion about the orthogonal axes through its *cg* since the origin of the axis system is co-located with the *cg* in the body.

When the generalized body represents an aeroplane the moment equations may be simplified since it is assumed that the aeroplane is symmetric about the oxz plane and that the mass is uniformly distributed. As a result the products of inertia $I_{xy} = I_{yz} = 0$. Thus, the moment equations simplify to the following

$$\left.\begin{aligned} I_x\dot{p} - (I_y - I_z)qr - I_{xz}(pq + \dot{r}) &= L \\ I_y\dot{q} + (I_x - I_z)pr + I_{xz}(p^2 - r^2) &= M \\ I_z\dot{r} - (I_x - I_y)pq + I_{xz}(qr - \dot{p}) &= N \end{aligned}\right\} \tag{4.19}$$

The equations (4.19) describe rolling motion, pitching motion and yawing motion respectively. A further simplification can be made if it is assumed that the aeroplane body axes are aligned to be *principal inertia axes*. In this special case the remaining product of inertia I_{xz} is also zero. This simplification is not often used owing to the difficulty of precisely determining the principal inertia axes. However, the symmetry of the aeroplane determines that I_{xz} is generally very much smaller than I_x, I_y and I_z and can often be neglected.

4.1.4 DISTURBANCE FORCES AND MOMENTS

Together, equations (4.12) and (4.19) comprise the generalized six degrees of freedom equations of motion of a rigid symmetric airframe having a uniform mass distribution. Further development of the equations of motion requires that the terms on the right-hand side of the equations adequately describe the disturbing forces and moments. The traditional approach, after Bryan (1911), is to assume that the disturbing forces and moments are due to aerodynamic effects, gravitational effects, movement of aerodynamic controls, power effects and the effects of atmospheric disturbances. Thus, bringing together equations (4.12) and (4.19) they may be written to include these contributions as follows

$$\left.\begin{aligned} m(\dot{U} - rV + qW) &= X_a + X_g + X_c + X_p + X_d \\ m(\dot{V} - pW + rU) &= Y_a + Y_g + Y_c + Y_p + Y_d \\ m(\dot{W} - qU + pV) &= Z_a + Z_g + Z_c + Z_p + Z_d \\ I_x\dot{p} - (I_y - I_x)qr - I_{xz}(pq + \dot{r}) &= L_a + L_g + L_c + L_p + L_d \\ I_y\dot{q} + (I_x - I_z)pr + I_{xz}(p^2 - r^2) &= M_a + M_g + M_c + M_p + M_d \\ I_z\dot{r} - (I_x - I_y)pq + I_{xz}(qr - \dot{p}) &= N_a + N_g + N_c + N_p + N_d \end{aligned}\right\} \tag{4.20}$$

Now equations (4.20) describe the generalized motion of the aeroplane without regard for the magnitude of the motion and subject to the assumptions applying. The equations

are *non-linear* and their solution by analytical means is not generally practicable. Further, the terms on the right-hand side of the equations must be replaced with suitable expressions, which are particularly difficult to determine for the most general motion. Typically, the continued development of the non-linear equations of motion and their solution is most easily accomplished using computer modelling or simulation techniques, which are beyond the scope of this book.

In order to proceed with the development of the equations of motion for analytical purposes, they must be linearized. Linearization is very simply accomplished by constraining the motion of the aeroplane to small perturbations about the trim condition.

4.2 The linearized equations of motion

Initially, the aeroplane is assumed to be flying in steady trimmed rectilinear flight with zero roll, sideslip and yaw angles. Thus, the plane of symmetry of the aeroplane *oxz* is *vertical* with respect to the earth reference frame. At this flight condition the velocity of the aeroplane is V_0, the components of linear velocity are (U_e, V_e, W_e) and the angular velocity components are all zero. Since there is no sideslip $V_e = 0$. A stable undisturbed atmosphere is also assumed such that

$$X_d = Y_d = Z_d = L_d = M_d = N_d = 0 \tag{4.21}$$

If now the aeroplane experiences a small perturbation about trim, the components of the linear disturbance velocities are (u, v, w) and the components of the angular disturbance velocities are (p, q, r) with respect to the undisturbed aeroplane axes $(oxyz)$. Thus, the total velocity components of the *cg* in the disturbed motion are given by

$$\left.\begin{aligned} U &= U_e + u \\ V &= V_e + v = v \\ W &= W_e + w \end{aligned}\right\} \tag{4.22}$$

Now, by definition (u, v, w) and (p, q, r) are small quantities such that terms involving products and squares of these terms are insignificantly small and may be ignored. Thus, substituting equations (4.21) and (4.22) into equations (4.20), note that (U_e, V_e, W_e) are steady and hence constant, and eliminating the insignificantly small terms, the linearized equations of motion are obtained

$$\left.\begin{aligned} m(\dot{u} + qW_e) &= X_a + X_g + X_c + X_p \\ m(\dot{v} - pW_e + rU_e) &= Y_a + Y_g + Y_c + Y_p \\ m(\dot{w} - qU_e) &= Z_a + Z_g + Z_c + Z_p \\ I_x\dot{p} - I_{xz}\dot{r} &= L_a + L_g + L_c + L_p \\ I_y\dot{q} &= M_a + M_g + M_c + M_p \\ I_z\dot{r} - I_{xz}\dot{p} &= N_a + N_g + N_c + N_p \end{aligned}\right\} \tag{4.23}$$

The development of expressions to replace the terms on the right-hand side of equations (4.23) is now much simpler since it is only necessary to consider small disturbances about trim.

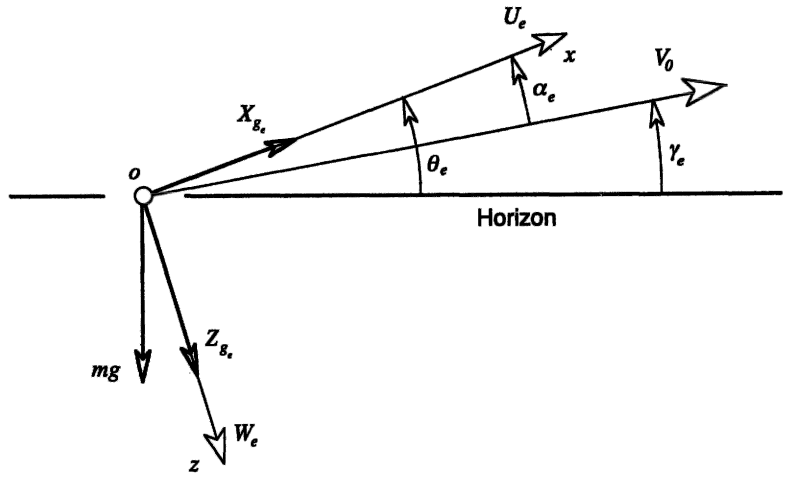

Fig. 4.4 Steady state weight components in the plane of symmetry

4.2.1 GRAVITATIONAL TERMS

The weight force mg acting on the aeroplane may be resolved into components acting in each of the three aeroplane axes. When the aeroplane is disturbed these components will vary according to the perturbations in attitude, thereby making a contribution to the disturbed motion. Thus, the gravitational contribution to equations (4.23) is obtained by resolving the aeroplane weight into the disturbed body axes. Since the origin of the aeroplane body axes is coincident with the *cg* there is no weight moment about any of the axes, therefore

$$L_g = M_g = N_g = 0 \tag{4.24}$$

Since the aeroplane is flying wings level in the initial symmetric flight condition, the components of weight only appear in the plane of symmetry as shown in Fig. 4.4. Thus, in the steady state the components of weight resolved into aeroplane axes are

$$\begin{bmatrix} X_{g_e} \\ Y_{g_e} \\ Z_{g_e} \end{bmatrix} = \begin{bmatrix} -mg\sin\theta_e \\ 0 \\ mg\cos\theta_e \end{bmatrix} \tag{4.25}$$

During the disturbance the aeroplane attitude perturbation is (ϕ, θ, ψ) and the components of weight in the disturbed aeroplane axes may be derived with the aid of the transformation equation (2.11). As, by definition, the angular perturbations are small, small angle approximations may be used in the direction cosine matrix to give the following relationship

$$\begin{bmatrix} X_g \\ Y_g \\ Z_g \end{bmatrix} = \begin{bmatrix} 1 & \psi & -\theta \\ -\psi & 1 & \phi \\ \theta & -\phi & 1 \end{bmatrix} \begin{bmatrix} X_{g_e} \\ Y_{g_e} \\ Z_{g_e} \end{bmatrix} = \begin{bmatrix} 1 & \psi & -\theta \\ -\psi & 1 & \phi \\ \theta & -\phi & 1 \end{bmatrix} \begin{bmatrix} -mg\sin\theta_e \\ 0 \\ mg\cos\theta_e \end{bmatrix} \tag{4.26}$$

Again, the products of small quantities have been neglected on the grounds that they are insignificantly small. Thus, the gravitational force components in the small perturbation equations of motion are given by

$$\left.\begin{aligned} X_g &= -mg\sin\theta_e - mg\theta\cos\theta_e \\ Y_g &= mg\psi\sin\theta_e + mg\phi\cos\theta_e \\ Z_g &= mg\cos\theta_e - mg\theta\sin\theta_e \end{aligned}\right\} \tag{4.27}$$

4.2.2 AERODYNAMIC TERMS

Whenever the aeroplane is disturbed from its equilibrium the aerodynamic balance is obviously upset. To describe explicitly the aerodynamic changes occurring during a disturbance provides a considerable challenge in view of the subtle interactions present in the motion. However, although limited in scope, the method first described by Bryan (1911) works extremely well for classical aeroplanes when the motion of interest is limited to (relatively) small perturbations. Although the approach is unchanged the rather more modern notation of Hopkin (1970) is adopted.

The usual procedure is to assume that the aerodynamic force and moment terms in equations (4.20) are dependent on the disturbed motion variables and their derivatives only. Mathematically this is conveniently expressed as a function comprising the sum of a number of Taylor series, each series involving one motion variable or derivative of a motion variable. Since the motion variables are (u, v, w) and (p, q, r), the aerodynamic term X_a in the axial force equation, for example, may be expressed

$$\begin{aligned} X_a = X_{a_e} &+ \left(\frac{\partial X}{\partial u}u + \frac{\partial^2 X}{\partial u^2}\frac{u^2}{2!} + \frac{\partial^3 X}{\partial u^3}\frac{u^3}{3!} + \frac{\partial^4 X}{\partial u^4}\frac{u^4}{4!} + \dots\right) \\ &+ \left(\frac{\partial X}{\partial v}v + \frac{\partial^2 X}{\partial v^2}\frac{v^2}{2!} + \frac{\partial^3 X}{\partial v^3}\frac{v^3}{3!} + \frac{\partial^4 X}{\partial v^4}\frac{v^4}{4!} + \dots\right) \\ &+ \left(\frac{\partial X}{\partial w}w + \frac{\partial^2 X}{\partial w^2}\frac{w^2}{2!} + \frac{\partial^3 X}{\partial w^3}\frac{w^3}{3!} + \frac{\partial^4 X}{\partial w^4}\frac{w^4}{4!} + \dots\right) \\ &+ \left(\frac{\partial X}{\partial p}p + \frac{\partial^2 X}{\partial p^2}\frac{p^2}{2!} + \frac{\partial^3 X}{\partial p^3}\frac{p^3}{3!} + \frac{\partial^4 X}{\partial p^4}\frac{p^4}{4!} + \dots\right) \\ &+ \left(\frac{\partial X}{\partial q}q + \frac{\partial^2 X}{\partial q^2}\frac{q^2}{2!} + \frac{\partial^3 X}{\partial q^3}\frac{q^3}{3!} + \frac{\partial^4 X}{\partial q^4}\frac{q^4}{4!} + \dots\right) \\ &+ \left(\frac{\partial X}{\partial r}r + \frac{\partial^2 X}{\partial r^2}\frac{r^2}{2!} + \frac{\partial^3 X}{\partial r^3}\frac{r^3}{3!} + \frac{\partial^4 X}{\partial r^4}\frac{r^4}{4!} + \dots\right) \\ &+ \left(\frac{\partial X}{\partial \dot{u}}\dot{u} + \frac{\partial^2 X}{\partial \dot{u}^2}\frac{\dot{u}^2}{2!} + \frac{\partial^3 X}{\partial \dot{u}^3}\frac{\dot{u}^3}{3!} + \dots\right) \\ &+ \left(\frac{\partial X}{\partial \dot{v}}\dot{v} + \frac{\partial^2 X}{\partial \dot{v}^2}\frac{\dot{v}^2}{2!} + \frac{\partial^3 X}{\partial \dot{v}^3}\frac{\dot{v}^3}{3!} + \dots\right) \\ &+ \text{series terms in } \dot{w}, \dot{p}, \dot{q} \text{ and } \dot{r} \\ &+ \text{series terms in higher order derivatives} \end{aligned} \tag{4.28}$$

where X_{a_e} is a constant term. Since the motion variables are small, for all practical aeroplanes only the first term in each of the series functions is significant. Further, the only significant higher order derivative terms commonly encountered are those involving $\dot{w}$. Thus, equation (4.28) is dramatically simplified to

$$X_a = X_{a_e} + \frac{\partial X}{\partial u}u + \frac{\partial X}{\partial v}v + \frac{\partial X}{\partial w}w + \frac{\partial X}{\partial p}p + \frac{\partial X}{\partial q}q + \frac{\partial X}{\partial r}r + \frac{\partial X}{\partial \dot{w}}\dot{w} \tag{4.29}$$

Using an alternative shorthand notation for the derivatives, equation (4.29) may be written

$$X_a = X_{a_e} + \mathring{X}_u u + \mathring{X}_v v + \mathring{X}_w w + \mathring{X}_p p + \mathring{X}_q q + \mathring{X}_r r + \mathring{X}_{\dot{w}}\dot{w} \tag{4.30}$$

The coefficients $\mathring{X}_u$, $\mathring{X}_v$, $\mathring{X}_w$, etc, are called *aerodynamic stability derivatives* and the symbol (°) denotes the derivatives to be *dimensional.* Since equation (4.30) has the units of force, the units of each of the aerodynamic stability derivatives are self-evident. In a similar way, the force and moment terms in the remaining equations (4.20) are determined. For example, the aerodynamic term in the rolling moment equation is given by

$$L_a = L_{a_e} + \mathring{L}_u u + \mathring{L}_v v + \mathring{L}_w w + \mathring{L}_p p + \mathring{L}_q q + \mathring{L}_r r + \mathring{L}_{\dot{w}}\dot{w} \tag{4.31}$$

4.2.3 AERODYNAMIC CONTROL TERMS

The primary aerodynamic controls are the elevator, ailerons and rudder. Since the forces and moments created by control deflections arise from the changes in aerodynamic conditions, it is usual to quantify their effect in terms of *aerodynamic control derivatives.* The assumptions applied to the aerodynamic terms are also applied to the control terms, thus, for example, the pitching moment due to aerodynamic controls may be expressed

$$M_c = \frac{\partial M}{\partial \xi}\xi + \frac{\partial M}{\partial \eta}\eta + \frac{\partial M}{\partial \zeta}\zeta \tag{4.32}$$

where aileron angle, elevator angle and rudder angle are denoted ξ, η and ζ respectively. Since equation (4.32) describes the effect of the aerodynamic controls with respect to the prevailing trim condition it is important to realize that the control angles, ξ, η and ζ are measured relative to the trim settings ξ_e, η_e and ζ_e respectively. Again, the shorthand notation may be used and equation (4.32) may be written

$$M_c = \mathring{M}_\xi \xi + \mathring{M}_\eta \eta + \mathring{M}_\zeta \zeta \tag{4.33}$$

The aerodynamic control terms in the remaining equations of motion are assembled in a similar way. If it is required to study the response of an aeroplane to other aerodynamic controls, for example flaps, spoilers, leading edge devices, etc, then additional terms may be appended to equation (4.33) and the remaining equations of motion as required.

4.2.4 POWER TERMS

Power, and hence thrust τ, is usually controlled by throttle lever angle ε and the relationship between the two variables is given, for a simple turbo-jet, by equation (2.34) in Chapter 2. Movement of the throttle lever causes a thrust change which in turn gives rise to a change in the components of force and moment acting on the aeroplane. It is mathematically convenient to describe these effects in terms of engine thrust derivatives. For example, normal force due to thrust may be expressed in the usual shorthand notation

$$Z_p = \mathring{Z}_\tau \tau \tag{4.34}$$

The contributions to the remaining equations of motion are expressed in a similar way. As for the aerodynamic controls, power changes are measured with respect to the prevailing trim setting. Therefore, τ quantifies the thrust perturbation relative to the trim setting τ_e.

4.2.5 THE EQUATIONS OF MOTION FOR SMALL PERTURBATIONS

To complete the development of the linearized equations of motion it only remains to substitute the appropriate expressions for the aerodynamic, gravitational, aerodynamic control and thrust terms into equations (4.23). The aerodynamic terms are exemplified by expressions like equations (4.30) and (4.31), expressions for the gravitational terms are given in equations (4.27), the aerodynamic control terms are exemplified by expressions like equation (4.33) and the thrust terms are exemplified by expressions like equation (4.34). Bringing all of these together the following equations are obtained

$$\begin{aligned}
m(\dot{u}+qW_e) &= X_{a_e} + \mathring{X}_u u + \mathring{X}_v v + \mathring{X}_w w + \mathring{X}_p p + \mathring{X}_q q + \mathring{X}_r r + \mathring{X}_{\dot{w}}\dot{w} \\
&\quad - mg\sin\theta_e - mg\theta\cos\theta_e + \mathring{X}_\xi \xi + \mathring{X}_\eta \eta + \mathring{X}_\zeta \zeta + \mathring{X}_\tau \tau \\
m(\dot{v}-pW_e+rU_e) &= Y_{a_e} + \mathring{Y}_u u + \mathring{Y}_v v + \mathring{Y}_w w + \mathring{Y}_p p + \mathring{Y}_q q + \mathring{Y}_r r + \mathring{Y}_{\dot{w}}\dot{w} \\
&\quad + mg\psi\sin\theta_e + mg\phi\cos\theta_e + \mathring{Y}_\xi \xi + \mathring{Y}_\eta \eta + \mathring{Y}_\zeta \zeta + \mathring{Y}_\tau \tau \\
m(\dot{w}-qU_e) &= Z_{a_e} + \mathring{Z}_u u + \mathring{Z}_v v + \mathring{Z}_w w + \mathring{Z}_p p + \mathring{Z}_q q + \mathring{Z}_r r + \mathring{Z}_{\dot{w}}\dot{w} \\
&\quad + mg\cos\theta_e - mg\theta\sin\theta_e + \mathring{Z}_\xi \xi + \mathring{Z}_\eta \eta + \mathring{Z}_\zeta \zeta + \mathring{Z}_\tau \tau \\
I_x\dot{p} - I_{xz}\dot{r} &= L_{a_e} + \mathring{L}_u u + \mathring{L}_v v + \mathring{L}_w w + \mathring{L}_p p + \mathring{L}_q q + \mathring{L}_r r \\
&\quad + \mathring{L}_{\dot{w}}\dot{w} + \mathring{L}_\xi \xi + \mathring{L}_\eta \eta + \mathring{L}_\zeta \zeta + \mathring{L}_\tau \tau \\
I_y\dot{q} &= M_{a_e} + \mathring{M}_u u + \mathring{M}_v v + \mathring{M}_w w + \mathring{M}_p p + \mathring{M}_q q + \mathring{M}_r r \\
&\quad + \mathring{M}_{\dot{w}}\dot{w} + \mathring{M}_\xi \xi + \mathring{M}_\eta \eta + \mathring{M}_\zeta \zeta + \mathring{M}_\tau \tau \\
I_z\dot{r} - I_{xz}\dot{p} &= N_{a_e} + \mathring{N}_u u + \mathring{N}_v v + \mathring{N}_w w + \mathring{N}_p p + \mathring{N}_q q + \mathring{N}_r r \\
&\quad + \mathring{N}_{\dot{w}}\dot{w} + \mathring{N}_\xi \xi + \mathring{N}_\eta \eta + \mathring{N}_\zeta \zeta + \mathring{N}_\tau \tau
\end{aligned} \tag{4.35}$$

Now in the steady trimmed flight condition all of the perturbation variables and their derivatives are, by definition, zero. Thus in the steady state equations (4.35) reduce to

$$\left.\begin{aligned}
X_{a_e} &= mg\sin\theta_e \\
Y_{a_e} &= 0 \\
Z_{a_e} &= -mg\cos\theta_e \\
L_{a_e} &= 0 \\
M_{a_e} &= 0 \\
N_{a_e} &= 0
\end{aligned}\right\} \tag{4.36}$$

Equations (4.36) therefore identify the constant trim terms which may be substituted into equations (4.35) and, following rearrangement, they may be written

$$
\begin{aligned}
&m\dot{u} - \mathring{X}_u u - \mathring{X}_v v - \mathring{X}_{\dot{w}}\dot{w} - \mathring{X}_w w \\
&\quad - \mathring{X}_p p - (\mathring{X}_q - mW_e)q - \mathring{X}_r r + mg\theta\cos\theta_e = \mathring{X}_\xi \xi + \mathring{X}_\eta \eta + \mathring{X}_\zeta \zeta + \mathring{X}_\tau \tau \\
&- \mathring{Y}_u u + m\dot{v} - \mathring{Y}_v v - \mathring{Y}_{\dot{w}}\dot{w} - \mathring{Y}_w w - (\mathring{Y}_p + mW_e)p \\
&\quad - \mathring{Y}_q q - (\mathring{Y}_r - mU_e)r - mg\phi\cos\theta_e - mg\psi\sin\theta_e = \mathring{Y}_\xi \xi + \mathring{Y}_\eta \eta + \mathring{Y}_\zeta \zeta + \mathring{Y}_\tau \tau \\
&- \mathring{Z}_u u - \mathring{Z}_v v + (m - \mathring{Z}_{\dot{w}})\dot{w} - \mathring{Z}_w w \\
&\quad - \mathring{Z}_p p - (\mathring{Z}_q + mU_e)q - \mathring{Z}_r r + mg\theta\sin\theta_e = \mathring{Z}_\xi \xi + \mathring{Z}_\eta \eta + \mathring{Z}_\zeta \zeta + \mathring{Z}_\tau \tau \\
&- \mathring{L}_u u - \mathring{L}_v v - \mathring{L}_{\dot{w}}\dot{w} - \mathring{L}_w w \\
&\quad + I_x\dot{p} - \mathring{L}_p p - \mathring{L}_q q - I_{xz}\dot{r} - \mathring{L}_r r = \mathring{L}_\xi \xi + \mathring{L}_\eta \eta + \mathring{L}_\zeta \zeta + \mathring{L}_\tau \tau \\
&- \mathring{M}_u u - \mathring{M}_v v - \mathring{M}_{\dot{w}}\dot{w} \\
&\quad - \mathring{M}_w w - \mathring{M}_p p + I_y\dot{q} - \mathring{M}_q q - \mathring{M}_r r = \mathring{M}_\xi \xi + \mathring{M}_\eta \eta + \mathring{M}_\zeta \zeta + \mathring{M}_\tau \tau \\
&- \mathring{N}_u u - \mathring{N}_v v - \mathring{N}_{\dot{w}}\dot{w} - \mathring{N}_w w \\
&\quad - I_{xz}\dot{p} - \mathring{N}_p p - \mathring{N}_q q + I_z\dot{r} - \mathring{N}_r r = \mathring{N}_\xi \xi + \mathring{N}_\eta \eta + \mathring{N}_\zeta \zeta + \mathring{N}_\tau \tau
\end{aligned}
\tag{4.37}
$$

Equations (4.37) are the small perturbation equations of motion, referred to body axes, which describe the transient response of an aeroplane about the trimmed flight condition following a small input disturbance. The equations comprise a set of six simultaneous linear differential equations written in the traditional manner with the forcing, or input, terms on the right-hand side. As written, and subject to the assumptions made in their derivation, the equations of motion are perfectly general and describe motion in which longitudinal and lateral dynamics may be fully coupled. However, for the vast majority of aeroplanes when small perturbation transient motion only is considered, as is the case here, longitudinal–lateral coupling is usually negligible. Consequently, it is convenient to simplify the equations by assuming that longitudinal and lateral motion is, in fact, fully decoupled.

4.3 The decoupled equations of motion

4.3.1 THE LONGITUDINAL EQUATIONS OF MOTION

Decoupled longitudinal motion is motion in response to a disturbance that is constrained to the longitudinal plane of symmetry, the *oxz* plane, only. The motion is therefore described by the axial force X, the normal force Z and the pitching moment M equations only. Since no lateral motion is involved the lateral motion variables v, p and r and their derivatives are all zero. Also, decoupled longitudinal–lateral motion means that the aerodynamic coupling derivatives are negligibly small and may be taken as zero, whence

$$\mathring{X}_v = \mathring{X}_p = \mathring{X}_r = \mathring{Z}_v = \mathring{Z}_p = \mathring{Z}_r = \mathring{M}_v = \mathring{M}_p = \mathring{M}_r = 0 \tag{4.38}$$

Similarly, since aileron or rudder deflections do not usually cause motion in the longitudinal plane of symmetry the coupling aerodynamic control derivatives may also be taken as zero, thus

$$\mathring{X}_\xi = \mathring{X}_\zeta = \mathring{Z}_\xi = \mathring{Z}_\zeta = \mathring{M}_\xi = \mathring{M}_\zeta = 0 \tag{4.39}$$

The equations of longitudinal symmetric motion are therefore obtained by extracting the axial force, normal force and pitching moment equations from equations (4.37) and substituting equations (4.38) and (4.39) as appropriate. Whence

$$\left.\begin{aligned} m\dot{u} - \mathring{X}_u u - \mathring{X}_{\dot{w}}\dot{w} - \mathring{X}_w w - (\mathring{X}_q - mW_e)q + mg\theta\cos\theta_e &= \mathring{X}_\eta\eta + \mathring{X}_\tau\tau \\ -\mathring{Z}_u u + (m - \mathring{Z}_{\dot{w}})\dot{w} - \mathring{Z}_w w - (\mathring{Z}_q + mU_e)q + mg\theta\sin\theta_e &= \mathring{Z}_\eta\eta + \mathring{Z}_\tau\tau \\ -\mathring{M}_u u - \mathring{M}_{\dot{w}}\dot{w} - \mathring{M}_w w + I_y\dot{q} - \mathring{M}_q q &= \mathring{M}_\eta\eta + \mathring{M}_\tau\tau \end{aligned}\right\} \quad (4.40)$$

Equations (4.40) are the most general form of the dimensional decoupled equations of longitudinal symmetric motion referred to aeroplane body axes. If it is assumed that the aeroplane is in level flight and the reference axes are wind or stability axes then

$$\theta_e = W_e = 0 \quad (4.41)$$

and the equations simplify further to

$$\left.\begin{aligned} m\dot{u} - \mathring{X}_u u - \mathring{X}_{\dot{w}}\dot{w} - \mathring{X}_w w - \mathring{X}_q q + mg\theta &= \mathring{X}_\eta\eta + \mathring{X}_\tau\tau \\ -\mathring{Z}_u u + (m - \mathring{Z}_{\dot{w}})\dot{w} - \mathring{Z}_w w - (\mathring{Z}_q + mU_e)q &= \mathring{Z}_\eta\eta + \mathring{Z}_\tau\tau \\ -\mathring{M}_u u - \mathring{M}_{\dot{w}}\dot{w} - \mathring{M}_w w + I_y\dot{q} - \mathring{M}_q q &= \mathring{M}_\eta\eta + \mathring{M}_\tau\tau \end{aligned}\right\} \quad (4.42)$$

Equations (4.42) represent the simplest possible form of the decoupled longitudinal equations of motion. Further simplification is only generally possible when the numerical values of the coefficients in the equations are known since some coefficients are often negligibly small.

EXAMPLE 4.2

Longitudinal derivative and other data for the McDonnell F-4C Phantom aeroplane were obtained from Heffley and Jewell (1972) for a flight condition of Mach 0.6 at an altitude of 35 000 ft. The original data are presented in Imperial units and in a format preferred in the USA. Normally, it is advisable to work with the equations of motion and the data in the format and units given; otherwise, conversion to another format can be tedious in the extreme and is easily subject to error. However, for the purposes of illustration, the derivative data have been converted to a form compatible with the equations developed above and the units have been changed to those of the more familiar SI system. The data are quite typical, they would normally be supplied in this, or similar, form by aerodynamicists and as such they represent the starting point in any flight dynamics analysis.

Flight path angle $\gamma_e = 0°$ — Air density $\rho = 0.3809\,\text{kg/m}^3$

Body incidence $\alpha_e = 9.4°$ — Wing area $S = 49.239\,\text{m}^2$

Velocity $V_0 = 178\,\text{m/s}$ — Mean aerodynamic chord $\bar{\bar{c}} = 4.889\,\text{m}$

Mass $m = 17\,642\,\text{kg}$ — Acceleration due to gravity $g = 9.8\,\text{m/s}^2$

Pitch moment of inertia $I_y = 165\,669\,\text{kg m}^2$

Since the flight path angle $\gamma_e = 0$ and the body incidence α_e is non-zero it may be deduced that the following derivatives are referred to a body axes system and that

$\theta_e \equiv \alpha_e$. The dimensionless longitudinal derivatives are given and any missing aerodynamic derivatives must be assumed insignificant, and hence zero. On the other hand, missing control derivatives may not be assumed insignificant although their absence will prohibit analysis of response to those controls.

$$\begin{aligned} X_u &= 0.0076 & Z_u &= -0.7273 & M_u &= 0.0340 \\ X_w &= 0.0483 & Z_w &= -3.1245 & M_w &= -0.2169 \\ X_{\dot{w}} &= 0 & Z_{\dot{w}} &= -0.3997 & M_{\dot{w}} &= -0.5910 \\ X_q &= 0 & Z_q &= -1.2109 & M_q &= -1.2732 \\ X_\eta &= 0.0618 & Z_\eta &= -0.3741 & M_\eta &= -0.5581 \end{aligned}$$

Equations (4.40) are compatible with the data although the dimensional derivatives must first be calculated according to the definitions given in Appendix 1, Tables A1.1 and A1.2. Thus, the dimensional longitudinal equations of motion, referred to body axes, are obtained by substituting the appropriate values into equations (4.40) to give

$$\begin{aligned} 17\,642\dot{u} - 12.67u - 80.62w + 512\,852.94q + 170\,744.06\theta &= 3755.77\eta \\ 1214.01u + 17\,660.33\dot{w} + 5215.44w - 3\,088\,229.7q + 28\,266.507\theta &= -22\,735.15\eta \\ -277.47u + 132.47\dot{w} + 1770.07w + 165\,669\dot{q} + 50\,798.03q &= -165\,822.03\eta \end{aligned}$$

where $W_e = V_0 \sin\theta_e = 29.07$ m/s and $U_e = V_0 \cos\theta_e = 175.61$ m/s. Note that angular variables in the equations of motion have radian units. Clearly, when written like this, the equations of motion are unwieldy. The equations can be simplified a little by dividing through by the mass or inertia as appropriate. Thus, the first equation is divided by 17642, the second equation by 17660.33 and the third equation by 165669. After some rearrangement the following rather more convenient version is obtained

$$\begin{aligned} \dot{u} &= 0.0007u + 0.0046w - 29.0700q - 9.6783\theta + 0.2129\eta \\ \dot{w} &= -0.0687u - 0.2953w + 174.8680q - 1.6000\theta - 1.2874\eta \\ \dot{q} + 0.0008\dot{w} &= 0.0017u - 0.0107w - 0.3066q - 1.0010\eta \end{aligned}$$

It must be remembered that, when written in this latter form, the equations of motion have the units of acceleration. The most striking feature of these equations, however written, is the large variation in the values of the coefficients. Terms which may, at first sight, appear insignificant are frequently important in the solution of the equations. It is therefore prudent to maintain sensible levels of accuracy when manipulating the equations by hand. Fortunately, this is an activity which is not often required.

4.3.2 THE LATERAL-DIRECTIONAL EQUATIONS OF MOTION

Decoupled lateral-directional motion involves roll, yaw and sideslip only. The motion is therefore described by the side force Y, the rolling moment L and the yawing moment N equations only. Since no longitudinal motion is involved the longitudinal motion variables u, w and q and their derivatives are all zero. Also, decoupled longitudinal–lateral motion means that the aerodynamic coupling derivatives are negligibly small and may be taken as zero, whence

$$\mathring{Y}_u = \mathring{Y}_{\dot{w}} = \mathring{Y}_w = \mathring{Y}_q = \mathring{L}_u = \mathring{L}_{\dot{w}} = \mathring{L}_w = \mathring{L}_q = \mathring{N}_u = \mathring{N}_{\dot{w}} = \mathring{N}_w = \mathring{N}_q = 0 \qquad (4.43)$$

Similarly, since the airframe is symmetric, elevator deflection and thrust variation do not usually cause lateral-directional motion and the coupling aerodynamic control derivatives may also be taken as zero, thus

$$\mathring{Y}_\eta = \mathring{Y}_\tau = \mathring{L}_\eta = \mathring{L}_\tau = \mathring{N}_\eta = \mathring{N}_\tau = 0 \tag{4.44}$$

The equations of lateral asymmetric motion are therefore obtained by extracting the side force, rolling moment and yawing moment equations from equations (4.37) and substituting equations (4.43) and (4.44) as appropriate. Whence

$$\left.\begin{aligned} \left(m\dot{v} - \mathring{Y}_v v - (\mathring{Y}_p + mW_e)p - (\mathring{Y}_r - mU_e)r \right. \\ \left. - mg\phi\cos\theta_e - mg\psi\sin\theta_e \right) &= \mathring{Y}_\xi \xi + \mathring{Y}_\zeta \zeta \\ -\mathring{L}_v v + I_x\dot{p} - \mathring{L}_p p - I_{xz}\dot{r} - \mathring{L}_r r &= \mathring{L}_\xi \xi + \mathring{L}_\zeta \zeta \\ -\mathring{N}_v v - I_{xz}\dot{p} - \mathring{N}_p p + I_z\dot{r} - \mathring{N}_r r &= \mathring{N}_\xi \xi + \mathring{N}_\zeta \zeta \end{aligned}\right\} \tag{4.45}$$

Equations (4.45) are the most general form of the dimensional decoupled equations of lateral-directional asymmetric motion referred to aeroplane body axes. If it is assumed that the aeroplane is in level flight and the reference axes are wind or stability axes then, as before,

$$\theta_e = W_e = 0 \tag{4.46}$$

and the equations simplify further to

$$\left.\begin{aligned} m\dot{v} - \mathring{Y}_v v - p\mathring{Y}_p - (\mathring{Y}_r - mU_e)r - mg\phi &= \mathring{Y}_\xi \xi + \mathring{Y}_\zeta \zeta \\ -\mathring{L}_v v + I_x\dot{p} - \mathring{L}_p p - I_{xz}\dot{r} - \mathring{L}_r r &= \mathring{L}_\xi \xi + \mathring{L}_\zeta \zeta \\ -\mathring{N}_v v - I_{xz}\dot{p} - \mathring{N}_p p + I_z\dot{r} - \mathring{N}_r r &= \mathring{N}_\xi \xi + \mathring{N}_\zeta \zeta \end{aligned}\right\} \tag{4.47}$$

Equations (4.47) represent the simplest possible form of the decoupled lateral-directional equations of motion. As for the longitudinal equations of motion, further simplification is only generally possible when the numerical values of the coefficients in the equations are known since some coefficients are often negligibly small.

4.4 Alternative forms of the equations of motion

4.4.1 THE DIMENSIONLESS EQUATIONS OF MOTION

Traditionally, the development of the equations of motion and investigations of stability and control involving their use have been securely resident in the domain of the aerodynamicist. Many aerodynamic phenomena are most conveniently explained in terms of *dimensionless aerodynamic coefficients*, for example lift coefficient, Mach number, Reynolds number, etc, and often this mechanism provides the only practical means for making progress. The advantage of this approach is that the aerodynamic properties of an aeroplane can be completely described in terms of dimensionless parameters that are independent of airframe geometry and of flight condition. A lift coefficient of 0.5, for example, has precisely the same meaning whether it applies to a Boeing 747 or to a Cessna 150. It is not surprising therefore to discover that, historically, the small perturbation equations of motion of an aeroplane were treated in the same way. This in turn leads to the concept of the *dimensionless derivative* which is just

another aerodynamic coefficient and may be interpreted in much the same way. However, the dimensionless equations of motion are of little use to the modern flight dynamicist other than as a means for explaining the origin of the dimensionless derivatives. Thus, the development of the dimensionless decoupled small perturbation equations of motion is outlined below solely for this purpose.

As formally described by Hopkin (1970) the equations of motion are rendered dimensionless by dividing each equation by a generalized force or moment parameter as appropriate. Sometimes the dimensionless equations of motion are referred to as the *aero-normalized* equations and the corresponding derivative coefficients are also referred to as *aero-normalized derivatives.* To illustrate the procedure consider the axial force equation taken from the decoupled longitudinal equations of motion (equation 4.42).

$$m\dot{u} - \mathring{X}_u u - \mathring{X}_{\dot{w}}\dot{w} - \mathring{X}_w w - q\mathring{X}_q + mg\theta = \mathring{X}_\eta \eta + \mathring{X}_\tau \tau \tag{4.48}$$

Since equation (4.48) has the units of force it may be rendered dimensionless by dividing, or normalizing, each term by the aerodynamic force parameter $\frac{1}{2}\rho V_0^2 S$, where S is the reference wing area. Defining the following parameters:

(i) dimensionless time

$$\hat{t} = \frac{t}{\sigma} \quad \text{where} \quad \sigma = \frac{m}{\frac{1}{2}\rho V_0 S} \tag{4.49}$$

(ii) the longitudinal relative density factor

$$\mu_1 = \frac{m}{\frac{1}{2}\rho S\bar{\bar{c}}} \tag{4.50}$$

where the longitudinal reference length is $\bar{\bar{c}}$, the mean aerodynamic chord

(iii) dimensionless velocities

$$\begin{aligned} \hat{u} &= \frac{u}{V_0} \\ \hat{w} &= \frac{w}{V_0} \\ \hat{q} &= q\sigma = \frac{qm}{\frac{1}{2}\rho V_0 S} \end{aligned} \tag{4.51}$$

(iv) since level flight is assumed the lift and weight are equal, thus

$$mg = \tfrac{1}{2}\rho V_0^2 S C_L \tag{4.52}$$

Thus, dividing equation (4.48) through by the aerodynamic force parameter and making use of the parameters defined in equations (4.49) to (4.52) above, the following is obtained

$$\begin{pmatrix} \dfrac{\dot{u}}{V_0}\sigma - \left(\dfrac{\mathring{X}_u}{\frac{1}{2}\rho V_0 S}\right)\dfrac{u}{V_0} - \left(\dfrac{\mathring{X}_{\dot{w}}}{\frac{1}{2}\rho S\bar{\bar{c}}}\right)\dfrac{\dot{w}\sigma}{V_0\mu_1} \\ -\left(\dfrac{\mathring{X}_w}{\frac{1}{2}\rho V_0 S}\right)\dfrac{w}{V_0} - \left(\dfrac{\mathring{X}_q}{\frac{1}{2}\rho V_0 S\bar{\bar{c}}}\right)\dfrac{q\sigma}{\mu_1} + \dfrac{mg}{\frac{1}{2}\rho V_0^2 S}\theta \end{pmatrix} = \left(\frac{\mathring{X}_\eta}{\frac{1}{2}\rho V_0^2 S}\right)\eta + \mathring{X}_\tau\left(\frac{\tau}{\frac{1}{2}\rho V_0^2 S}\right) \tag{4.53}$$

which is more conveniently written

$$\hat{\dot{u}} - X_u\hat{u} - X_{\dot{w}}\frac{\hat{\dot{w}}}{\mu_1} - X_w\hat{w} - X_q\frac{\hat{q}}{\mu_1} + C_L\theta = X_\eta\eta + X_\tau\tau \tag{4.54}$$

The derivatives denoted $X_u, X_{\dot{w}}, X_w, X_q, X_\eta$ and X_τ are the *dimensionless or aero-normalized derivatives* and their definitions follow from equation (4.53). It is in this form that the aerodynamic stability and control derivatives would usually be provided for an aeroplane by the aerodynamicists.

In a similar way the remaining longitudinal equations of motion may be rendered dimensionless. Note that the aerodynamic moment parameter used to divide the pitching moment equation is $\frac{1}{2}\rho V_0^2 S\bar{c}$. Whence

$$\left.\begin{aligned} -Z_u\hat{u} + \hat{w} - Z_{\dot{w}}\frac{\hat{\dot{w}}}{\mu_1} - Z_w\hat{w} - Z_q\frac{\hat{q}}{\mu_1} - \hat{q} &= Z_\eta\eta + Z_\tau\tau \\ -M_u\hat{u} - M_{\dot{w}}\frac{\hat{\dot{w}}}{\mu_1} - M_w\hat{w} + i_y\frac{\hat{\dot{q}}}{\mu_1} - M_q\hat{q} &= M_\eta\eta + M_\tau\tau \end{aligned}\right\} \tag{4.55}$$

where i_y is the dimensionless pitch inertia and is given by

$$i_y = \frac{I_y}{m\bar{c}^2} \tag{4.56}$$

Similarly, the lateral equations of motion (equation 4.47) may be rendered dimensionless by dividing the side force equation by the aerodynamic force parameter $\frac{1}{2}\rho V_0^2 S$ and the rolling and yawing moment equations by the aerodynamic moment parameter $\frac{1}{2}\rho V_0^2 Sb$ where, for lateral motion, the reference length is the wing-span b. Additional parameter definitions required to deal with the lateral equations are:

(v) the lateral relative density factor

$$\mu_2 = \frac{m}{\frac{1}{2}\rho Sb} \tag{4.57}$$

(vi) the dimensionless inertias

$$i_x = \frac{I_x}{mb^2}, \quad i_z = \frac{I_z}{mb^2} \quad \text{and} \quad i_{xz} = \frac{I_{xz}}{mb^2} \tag{4.58}$$

Since the equations of motion are referred to wind axes and since level flight is assumed, then equations (4.47) may be written in dimensionless form as follows

$$\left.\begin{aligned} \hat{\dot{v}} - Y_v\hat{v} - Y_p\frac{\hat{p}}{\mu_2} - Y_r\frac{\hat{r}}{\mu_2} - \hat{r} - C_L\phi &= Y_\xi\xi + Y_\zeta\zeta \\ -L_v\hat{v} + i_x\frac{\hat{\dot{p}}}{\mu_2} - L_p\frac{\hat{p}}{\mu_2} - i_{xz}\frac{\hat{\dot{r}}}{\mu_2} - L_r\frac{\hat{r}}{\mu_2} &= L_\xi\xi + L_\zeta\zeta \\ -N_v\hat{v} - i_{xz}\frac{\hat{\dot{p}}}{\mu_2} - N_p\frac{\hat{p}}{\mu_2} + i_z\frac{\hat{\dot{r}}}{\mu_2} - N_r\frac{\hat{r}}{\mu_2} &= N_\xi\xi + N_\zeta\zeta \end{aligned}\right\} \tag{4.59}$$

For convenience, the definitions of all the dimensionless aerodynamic stability and control derivatives are given in Appendix 1.

4.4.2 THE EQUATIONS OF MOTION IN STATE SPACE FORM

Today the solution of the equations of motion poses few problems since very powerful computational tools are readily available. Since computers are very good at handling numerical matrix calculations, the use of matrix methods for solving linear dynamic system problems has become an important topic in modern applied mathematics. In particular, matrix methods together with the digital computer have led to the development of the relatively new field of modern control system theory. For small perturbations, the aeroplane is a classical example of a linear dynamic system and, frequently, the solution of its equations of motion is a prelude to flight control system design and analysis. It is therefore convenient and straightforward to utilize multi-variable system theory tools in the solution of the equations of motion. However, it is first necessary to arrange the equations of motion in a suitable format.

The motion, or *state*, of any linear dynamic system may be described by a minimum set of variables called the *state variables*. The number of state variables required to describe the motion of the system completely is dependent on the number of degrees of freedom the system has. Thus, the motion of the system is described in a multi-dimensional vector space called the *state space*, the number of state variables being equal to the number of dimensions. The equation of motion, or *state equation*, of the *linear time invariant* (LTI) multi-variable system is written

$$\dot{\mathbf{x}}(t) = \mathbf{A}\mathbf{x}(t) + \mathbf{B}\mathbf{u}(t) \tag{4.60}$$

where

- $\mathbf{x}(t)$ is the column vector of n state variables, called the *state vector*;
- $\mathbf{u}(t)$ is the column vector of m input variables, called the *input vector*;
- $\mathbf{A}$ is the $(n \times n)$ *state matrix*;
- $\mathbf{B}$ is the $(n \times m)$ *input matrix*.

Since the system is LTI the matrices **A** and **B** have constant elements. Equation (4.60) is the matrix equivalent of a set of n simultaneous linear differential equations and it is a straightforward matter to configure the small perturbation equations of motion for an aeroplane in this format.

Now, for many systems some of the state variables may be inaccessible or their values may not be determined directly. Thus, a second equation is required to determine the system output variables. The output equation is written in the general form

$$\mathbf{y}(t) = \mathbf{C}\mathbf{x}(t) + \mathbf{D}\mathbf{u}(t) \tag{4.61}$$

where

- $\mathbf{y}(t)$ is the column vector of r output variables, called the *output vector*;
- $\mathbf{C}$ is the $(r \times n)$ *output matrix*;
- $\mathbf{D}$ is the $(r \times m)$ *direct matrix*;

and, typically, $r \leqslant n$. Again, for an LTI system the matrices **C** and **D** have constant elements. Together, equations (4.60) and (4.61) provide a complete description of the system. A complete description of the formulation of the general state model and the mathematics required in its analysis may be found in Barnett (1975).

For most aeroplane problems it is convenient to choose the output variables to be the state variables. Thus

$$\mathbf{y}(t) = \mathbf{x}(t) \quad \text{and} \quad r = n$$

and consequently

$\mathbf{C} = \mathbf{I}$ the $(n \times n)$ *identity* matrix;

$\mathbf{D} = \mathbf{0}$ the $(n \times m)$ *zero* matrix.

As a result, the output equation simplifies to

$$\mathbf{y}(t) = \mathbf{I}\mathbf{x}(t) \equiv \mathbf{x}(t) \tag{4.62}$$

and it is only necessary to derive the state equation from the aeroplane equations of motion.

Consider, for example, the longitudinal equations of motion (equation 4.40) referred to aeroplane body axes. These may be rewritten with the acceleration terms on the left-hand side as follows

$$\left.\begin{aligned} m\dot{u} - \mathring{X}_{\dot{w}}\dot{w} &= \mathring{X}_u u + \mathring{X}_w w + (\mathring{X}_q - mW_e)q - mg\theta\cos\theta_e + \mathring{X}_\eta\eta + \mathring{X}_\tau\tau \\ m\dot{w} - \mathring{Z}_{\dot{w}}\dot{w} &= \mathring{Z}_u u + \mathring{Z}_w w + (\mathring{Z}_q + mU_e)q - mg\theta\sin\theta_e + \mathring{Z}_\eta\eta + \mathring{Z}_\tau\tau \\ I_y\dot{q} - \mathring{M}_{\dot{w}}\dot{w} &= \mathring{M}_u u + \mathring{M}_w w + \mathring{M}_q q + \mathring{M}_\eta\eta + \mathring{M}_\tau\tau \end{aligned}\right\} \tag{4.63}$$

Since the longitudinal motion of the aeroplane is described by four state variables u, w, q and θ four differential equations are required. Thus, the additional equation is the auxiliary equation relating pitch rate to attitude rate, which for small perturbations is

$$\dot{\theta} = q \tag{4.64}$$

Equations (4.63) and (4.64) may be combined and written in matrix form

$$\mathbf{M}\dot{\mathbf{x}}(t) = \mathbf{A}'\mathbf{x}(t) + \mathbf{B}'\mathbf{u}(t) \tag{4.65}$$

where

$$\mathbf{x}^{\mathrm{T}}(t) = [u \quad w \quad q \quad \theta] \qquad \mathbf{u}^{\mathrm{T}}(t) = [\eta \quad \tau]$$

$$\mathbf{M} = \begin{bmatrix} m & -\mathring{X}_{\dot{w}} & 0 & 0 \\ 0 & (m - \mathring{Z}_{\dot{w}}) & 0 & 0 \\ 0 & -\mathring{M}_{\dot{w}} & I_y & 0 \\ 0 & 0 & 0 & 1 \end{bmatrix}$$

$$\mathbf{A}' = \begin{bmatrix} \mathring{X}_u & \mathring{X}_w & (\mathring{X}_q - mW_e) & -mg\cos\theta_e \\ \mathring{Z}_u & \mathring{Z}_w & (\mathring{Z}_q + mU_e) & -mg\sin\theta_e \\ \mathring{M}_u & \mathring{M}_w & \mathring{M}_q & 0 \\ 0 & 0 & 1 & 0 \end{bmatrix} \qquad \mathbf{B}' = \begin{bmatrix} \mathring{X}_\eta & \mathring{X}_\tau \\ \mathring{Z}_\eta & \mathring{Z}_\tau \\ \mathring{M}_\eta & \mathring{M}_\tau \\ 0 & 0 \end{bmatrix}$$

The longitudinal state equation is derived by premultiplying equation (4.65) by the inverse of the *mass matrix* $\mathbf{M}$ whence

$$\dot{\mathbf{x}}(t) = \mathbf{A}\mathbf{x}(t) + \mathbf{B}\mathbf{u}(t) \tag{4.66}$$

where

$$\mathbf{A} = \mathbf{M}^{-1}\mathbf{A}' = \begin{bmatrix} x_u & x_w & x_q & x_\theta \\ z_u & z_w & z_q & z_\theta \\ m_u & m_w & m_q & m_\theta \\ 0 & 0 & 1 & 0 \end{bmatrix} \qquad \mathbf{B} = \mathbf{M}^{-1}\mathbf{B}' = \begin{bmatrix} x_\eta & x_\tau \\ z_\eta & z_\tau \\ m_\eta & m_\tau \\ 0 & 0 \end{bmatrix}$$

The coefficients of the state matrix **A** are the aerodynamic stability derivatives, referred to aeroplane body axes, in *concise form* and the coefficients of the input matrix **B** are the control derivatives also in concise form. The definitions of the concise derivatives follow directly from the above relationships and are given in full in Appendix 1. Thus, the longitudinal state equation may be written out in full

$$\begin{bmatrix} \dot{u} \\ \dot{w} \\ \dot{q} \\ \dot{\theta} \end{bmatrix} = \begin{bmatrix} x_u & x_w & x_q & x_\theta \\ z_u & z_w & z_q & z_\theta \\ m_u & m_w & m_q & m_\theta \\ 0 & 0 & 1 & 0 \end{bmatrix} \begin{bmatrix} u \\ w \\ q \\ \theta \end{bmatrix} + \begin{bmatrix} x_\eta & x_\tau \\ z_\eta & z_\tau \\ m_\eta & m_\tau \\ 0 & 0 \end{bmatrix} \begin{bmatrix} \eta \\ \tau \end{bmatrix} \tag{4.67}$$

and the output equation is, very simply,

$$\mathbf{y}(t) = \mathbf{I}\mathbf{x}(t) = \begin{bmatrix} 1 & 0 & 0 & 0 \\ 0 & 1 & 0 & 0 \\ 0 & 0 & 1 & 0 \\ 0 & 0 & 0 & 1 \end{bmatrix} \begin{bmatrix} u \\ w \\ q \\ \theta \end{bmatrix} \tag{4.68}$$

Clearly, the longitudinal small perturbation motion of the aeroplane is completely described by the four state variables u, w, q and θ. Equation (4.68) determines that, in this instance, the output variables are chosen to be the same as the four state variables.

EXAMPLE 4.3

Consider the requirement to write the longitudinal equations of motion for the McDonnell F-4C Phantom of Example 4.2 in state space form. As the derivatives are given in dimensionless form it is convenient to express the matrices **M**, **A**′ and **B**′ in terms of the dimensionless derivatives. Substituting appropriately for the dimensional derivatives and after some rearrangement the matrices may be written

$$\mathbf{M} = \begin{bmatrix} m' & -\dfrac{X_{\dot{w}}\bar{\bar{c}}}{V_0} & 0 & 0 \\ 0 & \left(m' - \dfrac{Z_{\dot{w}}\bar{\bar{c}}}{V_0}\right) & 0 & 0 \\ 0 & -\dfrac{M_{\dot{w}}\bar{\bar{c}}}{V_0} & I'_y & 0 \\ 0 & 0 & 0 & 1 \end{bmatrix}$$

$$\mathbf{A}' = \begin{bmatrix} X_u & X_w & (X_q\bar{\bar{c}} - m'W_e) & -m'g\cos\theta_e \\ Z_u & Z_w & (Z_q\bar{\bar{c}} + m'U_e) & -m'g\sin\theta_e \\ M_u & M_w & M_q\bar{\bar{c}} & 0 \\ 0 & 0 & 1 & 0 \end{bmatrix} \qquad \mathbf{B}' = \begin{bmatrix} V_0X_\eta & V_0X_\tau \\ V_0Z_\eta & V_0Z_\tau \\ V_0M_\eta & V_0M_\tau \\ 0 & 0 \end{bmatrix}$$

where

$$m' = \frac{m}{\frac{1}{2}\rho V_0 S} \quad \text{and} \quad I'_y = \frac{I_y}{\frac{1}{2}\rho V_0 S\bar{\bar{c}}}$$

and in steady symmetric flight, $U_e = V_0 \cos\theta_e$ and $W_e = V_0 \sin\theta_e$.

Substituting the derivative values given in Example 4.2 the longitudinal state equation (4.65) may be written

$$\begin{bmatrix} 10.569 & 0 & 0 & 0 \\ 0 & 10.580 & 0 & 0 \\ 0 & 0.0162 & 20.3 & 0 \\ 0 & 0 & 0 & 1 \end{bmatrix} \begin{bmatrix} \dot{u} \\ \dot{w} \\ \dot{q} \\ \dot{\theta} \end{bmatrix}$$

$$= \begin{bmatrix} 0.0076 & 0.0483 & -307.26 & -102.29 \\ -0.7273 & -3.1245 & 1850.10 & -16.934 \\ 0.034 & -0.2169 & -6.2247 & 0 \\ 0 & 0 & 1 & 0 \end{bmatrix} \begin{bmatrix} u \\ w \\ q \\ \theta \end{bmatrix} + \begin{bmatrix} 11.00 \\ -66.5898 \\ -99.341 \\ 0 \end{bmatrix} \eta$$

This equation may be reduced to the preferred form by premultiplying each term by the inverse of **M**, as indicated above, to obtain the longitudinal state equation, referred to body axes, in concise form

$$\begin{bmatrix} \dot{u} \\ \dot{w} \\ \dot{q} \\ \dot{\theta} \end{bmatrix} = \begin{bmatrix} 7.181 \times 10^{-4} & 4.570 \times 10^{-3} & -29.072 & -9.678 \\ -0.0687 & -0.2953 & 174.868 & -1.601 \\ 1.73 \times 10^{-3} & -0.0105 & -0.4462 & 1.277 \times 10^{-3} \\ 0 & 0 & 1 & 0 \end{bmatrix} \begin{bmatrix} u \\ w \\ q \\ \theta \end{bmatrix} + \begin{bmatrix} 1.041 \\ -6.294 \\ -4.888 \\ 0 \end{bmatrix} \eta$$

This computation was carried out with the aid of *Program CC* and it should be noted that the resulting equation compares with the final equations given in Example 4.2. The coefficients of the matrices could equally well have been calculated using the concise derivative definitions given in Appendix 1, Tables A1.5 and A1.6. For the purpose of illustration some of the coefficients in the matrices have been rounded to a more manageable number of decimal places. In general this is not good practice since the rounding errors may lead to accumulated computational errors in any subsequent computer analysis involving the use of these equations. However, once the basic matrices have been entered into a computer program at the level of accuracy given, all subsequent computations can be carried out using computer-generated data files. In this way computational errors will be minimized, although it is prudent to be aware that not all computer algorithms for handling matrices can cope with poorly conditioned matrices. Occasionally, aeroplane computer models fall into this category.

The lateral small perturbation equations (4.45), referred to body axes, may be treated in exactly the same way to obtain the lateral state equation

$$\begin{bmatrix} \dot{v} \\ \dot{p} \\ \dot{r} \\ \dot{\phi} \\ \dot{\psi} \end{bmatrix} = \begin{bmatrix} y_v & y_p & y_r & y_\phi & y_\psi \\ l_v & l_p & l_r & l_\phi & l_\psi \\ n_v & n_p & n_r & n_\phi & n_\psi \\ 0 & 1 & 0 & 0 & 0 \\ 0 & 0 & 1 & 0 & 0 \end{bmatrix} \begin{bmatrix} v \\ p \\ r \\ \phi \\ \psi \end{bmatrix} + \begin{bmatrix} y_\xi & y_\zeta \\ I_\xi & I_\zeta \\ n_\xi & n_\zeta \\ 0 & 0 \\ 0 & 0 \end{bmatrix} \begin{bmatrix} \xi \\ \zeta \end{bmatrix} \tag{4.69}$$

Note that when the lateral equations of motion are referred to wind axes, equations (4.47), the lateral state equation (4.69) is reduced from fifth order to fourth order to become

$$\begin{bmatrix} \dot{v} \\ \dot{p} \\ \dot{r} \\ \dot{\phi} \end{bmatrix} = \begin{bmatrix} y_v & y_p & y_r & y_\phi \\ l_v & l_p & l_r & l_\phi \\ n_v & n_p & n_r & n_\phi \\ 0 & 1 & 0 & 0 \end{bmatrix} \begin{bmatrix} v \\ p \\ r \\ \phi \end{bmatrix} + \begin{bmatrix} y_\xi & y_\zeta \\ I_\xi & I_\zeta \\ n_\xi & n_\zeta \\ 0 & 0 \end{bmatrix} \begin{bmatrix} \xi \\ \zeta \end{bmatrix} \tag{4.70}$$

However, in this case the derivatives are referred to aeroplane wind axes rather than to body axes and will generally have slightly different values. The definitions of the concise lateral stability and control derivatives referred to aeroplane body axes are also given in Appendix 1.

Examples of the more general procedures used to create the state descriptions of various dynamic systems may be found in many books on control systems; for example, Shinners (1980) and Friedland (1987) both contain useful aeronautical examples.

EXAMPLE 4.4

Lateral derivative data for the McDonnell F-4C Phantom, referred to body axes, were also obtained from Heffley and Jewell (1972) and are used to illustrate the formulation of the lateral state equation. The data relate to the same flight condition, namely Mach 0.6 and an altitude of 35 000 ft. As before, the leading aerodynamic variables have the following values

Flight path angle $\gamma_e = 0°$ — Inertia product $I_{xz} = 2952\,\text{kg m}^2$

Body incidence $\alpha_e = 9.4°$ — Air density $\rho = 0.3809\,\text{kg m}^3$

Velocity $V_0 = 178\,\text{m/s}$ — Wing area $S = 49.239\,\text{m}^2$

Mass $m = 17\,642\,\text{kg}$ — Wing-span $b = 11.787\,\text{m}$

Roll moment of inertia $I_x = 33\,898\,\text{kg m}^2$ — Acceleration due to gravity $g = 9.81\,\text{m/s}^2$

Yaw moment of inertia $I_z = 189\,496\,\text{kg m}^2$

The dimensionless lateral derivatives, referred to body axes, are given and, as before, any missing aerodynamic derivatives must be assumed insignificant, and hence zero.

$Y_v = -0.5974$	$L_v = -0.1048$	$N_v = 0.0987$
$Y_p = 0$	$L_p = -0.1164$	$N_p = -0.0045$
$Y_r = 0$	$L_r = 0.0455$	$N_r = -0.1132$
$Y_\xi = -0.0159$	$L_\xi = 0.0454$	$N_\xi = 0.00084$
$Y_\zeta = 0.1193$	$L_\zeta = 0.0086$	$N_\zeta = -0.0741$

As for the longitudinal equations of motion, the lateral state equation (4.65) may be written in terms of the more convenient lateral dimensionless derivatives

$$\mathbf{M}\dot{\mathbf{x}}(t) = \mathbf{A}'\mathbf{x}(t) + \mathbf{B}'\mathbf{u}(t)$$

where

$$\mathbf{x}^{\mathrm{T}}(t) = [v \quad p \quad r \quad \phi \quad \psi] \qquad \mathbf{u}^{\mathrm{T}}(t) = [\xi \quad \zeta]$$

$$\mathbf{M} = \begin{bmatrix} m' & 0 & 0 & 0 & 0 \\ 0 & I'_x & -I'_{xz} & 0 & 0 \\ 0 & -I'_{xz} & I'_z & 0 & 0 \\ 0 & 0 & 0 & 1 & 0 \\ 0 & 0 & 0 & 0 & 1 \end{bmatrix}$$

$$\mathbf{A}' = \begin{bmatrix} Y_v & (Y_p b + m' W_e) & (Y_r b - m' U_e) & m' g \cos\theta_e & m' g \sin\theta_e \\ L_v & L_p b & L_r b & 0 & 0 \\ N_v & N_p b & N_r b & 0 & 0 \\ 0 & 1 & 0 & 0 & 0 \\ 0 & 0 & 1 & 0 & 0 \end{bmatrix}$$

$$\mathbf{B}' = \begin{bmatrix} V_0 Y_\xi & V_0 Y_\zeta \\ V_0 L_\xi & V_0 L_\zeta \\ V_0 N_\xi & V_0 N_\zeta \\ 0 & 0 \\ 0 & 0 \end{bmatrix}$$

where

$$m' = \frac{m}{\frac{1}{2}\rho V_0 S}, \qquad I'_x = \frac{I_x}{\frac{1}{2}\rho V_0 S b}, \qquad I'_z = \frac{I_z}{\frac{1}{2}\rho V_0 S b} \quad \text{and} \quad I'_{xz} = \frac{I_{xz}}{\frac{1}{2}\rho V_0 S b}$$

and, as before, in steady symmetric flight, $U_e = V_0 \cos\theta_e$ and $W_e = V_0 \sin\theta_e$.

Substituting the appropriate values into the above matrices and premultiplying the matrices $\mathbf{A}'$ and $\mathbf{B}'$ by the inverse of the mass matrix $\mathbf{M}$ the concise lateral state equation (4.69), referred to body axes, is obtained

$$\begin{bmatrix} \dot{v} \\ \dot{p} \\ \dot{r} \\ \dot{\phi} \\ \dot{\psi} \end{bmatrix} = \begin{bmatrix} -0.0565 & 29.072 & -175.610 & 9.6783 & 1.6022 \\ -0.0601 & -0.7979 & -0.2996 & 0 & 0 \\ 9.218 \times 10^{-3} & -0.0179 & -0.1339 & 0 & 0 \\ 0 & 1 & 0 & 0 & 0 \\ 0 & 0 & 1 & 0 & 0 \end{bmatrix} \begin{bmatrix} v \\ p \\ r \\ \phi \\ \psi \end{bmatrix}$$

$$+ \begin{bmatrix} -0.2678 & 2.0092 \\ 4.6982 & 0.7703 \\ 0.0887 & -1.3575 \\ 0 & 0 \\ 0 & 0 \end{bmatrix} \begin{bmatrix} \xi \\ \zeta \end{bmatrix}$$

Again, the matrix computation was undertaken with the aid of *Program CC*. However, the coefficients of the matrices could equally well have been calculated using the expressions for the concise derivatives given in Appendix 1, Tables A1.7 and A1.8.

References

Barnett, S. 1975: *Introduction to Mathematical Control Theory*. Clarendon Press, Oxford.

Bryan, G. H. 1911: *Stability in Aviation*. Macmillan and Co, London.

Friedland, B. 1987: *Control System Design*. McGraw-Hill Book Company, New York.

Heffley, R. K. and Jewell, W. F. 1972: *Aircraft Handling Qualities Data*. NASA Contractor Report, NASA CR-2144.

Hopkin, H. R. 1970: *A Scheme of Notation and Nomenclature for Aircraft Dynamics and Associated Aerodynamics*. Aeronautical Research Council, Reports and Memoranda No. 3562.

Shinners, S. M. 1980: *Modern Control System Theory and Application*, 2nd edn. Addison-Wesley Publishing Co, Reading, Massachusetts.

5

The Solution of the Equations of Motion

5.1 Methods of solution

The primary reason for solving the equations of motion is to obtain a mathematical, and hence graphical, description of the time histories of all the motion variables in response to a control input, or atmospheric disturbance, and to enable an assessment of stability to be made. It is also important that the chosen method of solution provides good insight into the way in which the physical properties of the airframe influence the nature of the responses.

Since the evolution of the development of the equations of motion and their solution followed in the wake of observation of aeroplane behaviour, it was no accident that practical constraints were applied that resulted in the decoupled small perturbation equations. The longitudinal and lateral decoupled equations of motion are each represented by a set of three simultaneous linear differential equations which have traditionally been solved using classical mathematical analysis methods. Although laborious to apply, the advantage of the traditional approach is that it is capable of providing excellent insight to the nature of aircraft stability and response. However, since the traditional methods of solution invariably involve the use of the dimensionless equations of motion, considerable care in the interpretation of the numerical results is required if confusion is to be avoided. A full discussion of these methods can be found in many of the earlier books on the subject, for example in Duncan (1959).

Operational methods have also enjoyed some popularity as a means for solving the equations of motion. In particular, the Laplace transform method has been, and continues to be, used extensively. By transforming the differential equations, they become algebraic equations expressed in terms of the Laplace operator s. Their manipulation to obtain a solution then becomes a relatively straightforward exercise in algebra. Thus, the problem is transformed into one of solving a set of simultaneous linear algebraic equations, a process that is readily accomplished by computational methods. Further, the input–output response relationship or transfer characteristic is described by a simple algebraic *transfer function* in terms of the Laplace operator. The time response then follows by finding the inverse Laplace transform of the transfer function for the input of interest.

Now the transfer function as a means for describing the characteristics of a linear dynamic system is the principal tool of the control systems engineer and a vast array of mathematical tools is available for analysing transfer functions. With relative ease,

analysis of the transfer function of a system enables a complete picture of its dynamic behaviour to be drawn. In particular, stability, time response and frequency response information is readily obtained. Furthermore, obtaining the system transfer function is usually the prelude to the design of a feedback control system and an additional array of mathematical tools is also available to support this task.

Since most modern aeroplanes are dependent, to a greater or lesser extent, on feedback control for their continued proper operation, it would seem particularly advantageous to be able to describe the aeroplane in terms of transfer functions. Fortunately, this is easily accomplished. The Laplace transform of the linearized small perturbation equations of motion is readily obtained and, by the subsequent application of the appropriate mathematical tools, the *response transfer functions* may be derived. An analysis of the dynamic properties of the aeroplane may then be made using control engineering tools as an alternative to the traditional methods of the aerodynamicist. Indeed, as already described in Chapter 1, many computer software packages are available which facilitate the rapid and accurate analysis of linear dynamic systems and the design of automatic control systems. Today, access to computer software of this type is essential for the flight dynamicist.

Thus, the process of solution requires that the equations of motion are assembled in the appropriate format, numerical values for the derivatives and other parameters are substituted and then the whole model is input to a suitable computer program. The output, which is usually obtained instantaneously, is most conveniently arranged in terms of response transfer functions. Thus, the objective can usually be achieved relatively easily, with great rapidity and with good accuracy. A significant shortcoming of such computational methods is the lack of *visibility*; the functional steps in the solution process are hidden from the investigator. Consequently, considerable care, and some skill, is required to analyse the solution correctly and this can be greatly facilitated if the investigator has a good understanding of the computational solution process. Indeed, it is considered essential to have an understanding of the steps involved in the solution of the equations of motion using the operational methods common to most computer software packages.

The remainder of this chapter is therefore concerned with a discussion of the use of the Laplace transform for solving the small perturbation equations of motion to obtain the response transfer functions. This is followed by a description of the computational process involving matrix methods, which is normally undertaken with the aid of a suitable computer software package.

5.2 Cramer's rule

Cramer's rule describes a mathematical process for solving sets of simultaneous linear algebraic equations and may usefully be used to solve the equations of motion algebraically. It may be found in many degree level mathematical texts, and in books devoted to the application of computational methods to linear algebra, for example in Goult *et al.* (1974). Since Cramer's rule involves the use of matrix algebra it is easily implemented in a digital computer.

To solve the system of n simultaneous linear algebraic equations described in matrix form as

$$\mathbf{y} = \mathbf{A}\mathbf{x} \tag{5.1}$$

where **x** and **y** are column vectors and **A** is a matrix of constant coefficients, then Cramer's rule states that

$$\mathbf{x} = \mathbf{A}^{-1}\mathbf{y} \equiv \left(\frac{\text{AdjointA}}{\text{DetA}}\right)\mathbf{y} \tag{5.2}$$

where the solution for x_i, the ith row of equation (5.2), is given by

$$x_i = \frac{1}{|\mathbf{A}|}(A_{1i}y_1 + A_{2i}y_2 + A_{3i}y_3 + \ldots + A_{ni}y_n) \tag{5.3}$$

The significant observation is that the numerator of equation (5.3) is equivalent to the determinant of **A** with the ith column replaced by the vector **y**. Thus, the solution of equation (5.1) to find all of the x_i reduces to the relatively simple problem of evaluating $n+1$ determinants.

EXAMPLE 5.1

To illustrate the use of Cramer's rule consider the trivial example in which it is required to solve the simultaneous linear algebraic equations

$$\begin{aligned} y_1 &= x_1 + 2x_2 + 3x_3 \\ y_2 &= 2x_1 + 4x_2 + 5x_3 \\ y_3 &= 3x_1 + 5x_2 + 6x_3 \end{aligned}$$

or, in matrix notation,

$$\begin{bmatrix} y_1 \\ y_2 \\ y_3 \end{bmatrix} = \begin{bmatrix} 1 & 2 & 3 \\ 2 & 4 & 5 \\ 3 & 5 & 6 \end{bmatrix} \begin{bmatrix} x_1 \\ x_2 \\ x_3 \end{bmatrix}$$

Applying Cramer's rule to solve for x_i

$$x_1 = \frac{\begin{vmatrix} y_1 & 2 & 3 \\ y_2 & 4 & 5 \\ y_3 & 5 & 6 \end{vmatrix}}{\begin{vmatrix} 1 & 2 & 3 \\ 2 & 4 & 5 \\ 3 & 5 & 6 \end{vmatrix}} = \frac{y_1\begin{vmatrix} 4 & 5 \\ 5 & 6 \end{vmatrix} - y_2\begin{vmatrix} 2 & 3 \\ 5 & 6 \end{vmatrix} + y_3\begin{vmatrix} 2 & 3 \\ 4 & 5 \end{vmatrix}}{-1} = y_1 - 3y_2 + 2y_3$$

$$x_2 = \frac{\begin{vmatrix} 1 & y_1 & 3 \\ 2 & y_2 & 5 \\ 3 & y_3 & 6 \end{vmatrix}}{\begin{vmatrix} 1 & 2 & 3 \\ 2 & 4 & 5 \\ 3 & 5 & 6 \end{vmatrix}} = \frac{-y_1\begin{vmatrix} 2 & 5 \\ 3 & 6 \end{vmatrix} + y_2\begin{vmatrix} 1 & 3 \\ 3 & 6 \end{vmatrix} - y_3\begin{vmatrix} 1 & 3 \\ 2 & 5 \end{vmatrix}}{-1} = -3y_1 + 3y_2 - y_3$$

and

$$x_3 = \frac{\begin{vmatrix} 1 & 2 & y_1 \\ 2 & 4 & y_2 \\ 3 & 5 & y_3 \end{vmatrix}}{\begin{vmatrix} 1 & 2 & 3 \\ 2 & 4 & 5 \\ 3 & 5 & 6 \end{vmatrix}} = \frac{y_1\begin{vmatrix} 2 & 4 \\ 3 & 5 \end{vmatrix} - y_2\begin{vmatrix} 1 & 2 \\ 3 & 5 \end{vmatrix} + y_3\begin{vmatrix} 1 & 2 \\ 2 & 4 \end{vmatrix}}{-1} = 2y_1 - y_2$$

Clearly, in this example, the numerator determinants are found by expanding about the column containing y. The denominator determinant may be found by expanding about the first row thus

$$\begin{vmatrix} 1 & 2 & 3 \\ 2 & 4 & 5 \\ 3 & 5 & 6 \end{vmatrix} = 1\begin{vmatrix} 4 & 5 \\ 5 & 6 \end{vmatrix} - 2\begin{vmatrix} 2 & 5 \\ 3 & 6 \end{vmatrix} + 3\begin{vmatrix} 2 & 4 \\ 3 & 5 \end{vmatrix} = -1 + 6 - 6 = -1$$

5.3 Aircraft response transfer functions

Aircraft response transfer functions describe the dynamic relationships between the input variables and the output variables. The relationships are indicated diagrammatically in Fig. 5.1 and, clearly, a number of possible input–output relationships exist. When the mathematical model of the aircraft comprises the decoupled small perturbation equations of motion, transfer functions relating longitudinal input variables to lateral output variables do not exist and vice versa. This may not necessarily be the case when the aircraft is described by a fully coupled set of small perturbation equations of motion. For example, such a description is quite usual when modelling the helicopter.

All transfer functions are written as a ratio of two polynomials in the Laplace operator *s*. All *proper* transfer functions have a numerator polynomial which is at least one order less than the denominator polynomial although, occasionally, *improper* transfer functions crop up in aircraft applications. For example, the transfer function describing acceleration response to an input variable is improper; the numerator and denominator polynomials are of the same order. Care is needed when working with improper transfer functions as sometimes the computational tools are unable to deal with them correctly. Clearly, this is a situation where some understanding of the physical

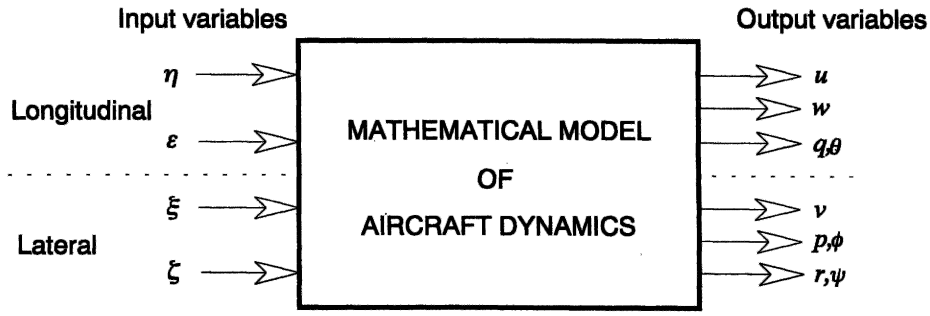

Fig. 5.1 Aircraft input–output relationships

meaning of the transfer function can be of considerable advantage. A shorthand notation is used to represent aircraft response transfer functions in this book. For example, pitch attitude $\theta(s)$ response to elevator $\eta(s)$ is denoted

$$\frac{\theta(s)}{\eta(s)} \equiv \frac{N_\eta^\theta(s)}{\Delta(s)} \tag{5.4}$$

where $N_\eta^\theta(s)$ is the unique numerator polynomial in s relating pitch attitude response to elevator input and $\Delta(s)$ is the denominator polynomial in s which is common to all longitudinal response transfer functions. Similarly, for example, roll rate response to aileron is denoted

$$\frac{p(s)}{\xi(s)} \equiv \frac{N_\xi^p(s)}{\Delta(s)} \tag{5.5}$$

where, in this instance, $\Delta(s)$ is the denominator polynomial which is common to all of the lateral response transfer functions. Since $\Delta(s)$ is context dependent its correct identification does not usually present problems.

The denominator polynomial $\Delta(s)$ is called the *characteristic polynomial* and when equated to zero defines the *characteristic equation*. Thus, $\Delta(s)$ completely describes the longitudinal or lateral stability characteristics of the aeroplane as appropriate and the roots, or *poles*, of $\Delta(s)$ describe the *stability modes* of the aeroplane. Thus, the stability characteristics of an aeroplane can be determined simply on inspection of the response transfer functions.

5.3.1 THE LONGITUDINAL RESPONSE TRANSFER FUNCTIONS

The Laplace transforms of the differential quantities $\dot{x}(t)$ and $\ddot{x}(t)$, for example, are given by

$$\left.\begin{aligned} \mathrm{L}\{\dot{x}(t)\} &= sx(s) - x(0) \\ \mathrm{L}\{\ddot{x}(t)\} &= s^2x(s) - sx(0) - \dot{x}(0) \end{aligned}\right\} \tag{5.6}$$

where $x(0)$ and $\dot{x}(0)$ are the initial values of $x(t)$ and $\dot{x}(t)$ respectively at $t = 0$. Now, taking the Laplace transform of the longitudinal equations of motion (equation 4.40), referred to body axes, assuming zero initial conditions and since small perturbation motion only is considered, write

$$\dot{\theta}(t) = q(t) \tag{5.7}$$

then

$$\left.\begin{aligned} (ms - \mathring{X}_u)u(s) - (\mathring{X}_{\dot{w}}s + \mathring{X}_w)w(s) - ((\mathring{X}_q - mW_e)s - mg\cos\theta_e)\theta(s) &= \mathring{X}_\eta\eta(s) + \mathring{X}_\tau\tau(s) \\ -\mathring{Z}_u u(s) - ((\mathring{Z}_{\dot{w}} - m)s + \mathring{Z}_w)w(s) - ((\mathring{Z}_q + mU_e)s - mg\sin\theta_e)\theta(s) &= \mathring{Z}_\eta\eta(s) + \mathring{Z}_\tau\tau(s) \\ -\mathring{M}_u u(s) - (\mathring{M}_{\dot{w}}s + \mathring{M}_w)w(s) + (I_y s^2 - \mathring{M}_q s)\theta(s) &= \mathring{M}_\eta\eta(s) + \mathring{M}_\tau\tau(s) \end{aligned}\right\} \tag{5.8}$$

Writing equations (5.8) in matrix format

$$\begin{bmatrix} (ms-\mathring{X}_u) & -(\mathring{X}_{\dot{w}}s+\mathring{X}_w) & -((\mathring{X}_q-mW_e)s-mg\cos\theta_e) \\ -\mathring{Z}_u & -((\mathring{Z}_{\dot{w}}-m)s+\mathring{Z}_w) & -((\mathring{Z}_q+mU_e)s-mg\sin\theta_e) \\ -\mathring{M}_u & -(\mathring{M}_{\dot{w}}s+\mathring{M}_w) & (I_ys^2-\mathring{M}_qs) \end{bmatrix} \begin{bmatrix} u(s) \\ w(s) \\ \theta(s) \end{bmatrix} = \begin{bmatrix} \mathring{X}_\eta & \mathring{X}_\tau \\ \mathring{Z}_\eta & \mathring{Z}_\tau \\ \mathring{M}_\eta & \mathring{M}_\tau \end{bmatrix} \begin{bmatrix} \eta(s) \\ \tau(s) \end{bmatrix} \tag{5.9}$$

Cramer's rule can now be applied to obtain the longitudinal response transfer functions: for example, to obtain the transfer functions describing response to the elevator. Assume, therefore, that the thrust remains constant, which means that the throttle is fixed at its trim setting τ_e and $\tau(s) = 0$. Therefore, after dividing through by $\eta(s)$ equation (5.9) may be simplified to

$$\begin{bmatrix} (ms-\mathring{X}_u) & -(\mathring{X}_{\dot{w}}s+\mathring{X}_w) & -((\mathring{X}_q-mW_e)s-mg\cos\theta_e) \\ -\mathring{Z}_u & -((\mathring{Z}_{\dot{w}}-m)s+\mathring{Z}_w) & -((\mathring{Z}_q+mU_e)s-mg\sin\theta_e) \\ -\mathring{M}_u & -(\mathring{M}_{\dot{w}}s+\mathring{M}_w) & (I_ys^2-\mathring{M}_qs) \end{bmatrix} \begin{bmatrix} \dfrac{u(s)}{\eta(s)} \\ \dfrac{w(s)}{\eta(s)} \\ \dfrac{\theta(s)}{\eta(s)} \end{bmatrix} = \begin{bmatrix} \mathring{X}_\eta \\ \mathring{Z}_\eta \\ \mathring{M}_\eta \end{bmatrix} \tag{5.10}$$

Equation (5.10) is of the same form as equation (5.1), Cramer's rule may be applied directly and the elevator response transfer functions are given by

$$\frac{u(s)}{\eta(s)} \equiv \frac{N_\eta^u(s)}{\Delta(s)}, \quad \frac{w(s)}{\eta(s)} \equiv \frac{N_\eta^w(s)}{\Delta(s)}, \quad \frac{\theta(s)}{\eta(s)} \equiv \frac{N_\eta^\theta(s)}{\Delta(s)} \tag{5.11}$$

Since the Laplace transform of equation (5.7) is $s\theta(s) = q(s)$ the pitch rate response transfer function follows directly

$$\frac{q(s)}{\eta(s)} \equiv \frac{N_\eta^q(s)}{\Delta(s)} = \frac{sN_\eta^\theta(s)}{\Delta(s)} \tag{5.12}$$

The numerator polynomials are given by the following determinants

$$N_\eta^u(s) = \begin{vmatrix} \mathring{X}_\eta & -(\mathring{X}_{\dot{w}}s+\mathring{X}_w) & -((\mathring{X}_q-mW_e)s-mg\cos\theta_e) \\ \mathring{Z}_\eta & -((\mathring{Z}_{\dot{w}}-m)s+\mathring{Z}_w) & -((\mathring{Z}_q+mU_e)s-mg\sin\theta_e) \\ \mathring{M}_\eta & -(\mathring{M}_{\dot{w}}s+\mathring{M}_w) & (I_ys^2-\mathring{M}_qs) \end{vmatrix} \tag{5.13}$$

$$N_\eta^w(s) = \begin{vmatrix} (ms-\mathring{X}_u) & \mathring{X}_\eta & -((\mathring{X}_q-mW_e)s-mg\cos\theta_e) \\ -\mathring{Z}_u & \mathring{Z}_\eta & -((\mathring{Z}_q+mU_e)s-mg\sin\theta_e) \\ -\mathring{M}_u & \mathring{M}_\eta & (I_ys^2-\mathring{M}_qs) \end{vmatrix} \tag{5.14}$$

$$N_\eta^\theta(s) = \begin{vmatrix} (ms-\mathring{X}_u) & -(\mathring{X}_{\dot{w}}s+\mathring{X}_w) & \mathring{X}_\eta \\ -\mathring{Z}_u & -((\mathring{Z}_{\dot{w}}-m)s+\mathring{Z}_w) & \mathring{Z}_\eta \\ -\mathring{M}_u & -(\mathring{M}_{\dot{w}}s+\mathring{M}_w) & \mathring{M}_\eta \end{vmatrix} \tag{5.15}$$

and the common denominator polynomial is given by the determinant

$$\Delta(s) = \begin{vmatrix} (ms - \mathring{X}_u) & -(\mathring{X}_{\dot{w}}s + \mathring{X}_w) & -((\mathring{X}_q - mW_e)s - mg\cos\theta_e) \\ -\mathring{Z}_u & -((\mathring{Z}_{\dot{w}} - m)s + \mathring{Z}_w) & -((\mathring{Z}_q + mU_e)s - mg\sin\theta_e) \\ -\mathring{M}_u & -(\mathring{M}_{\dot{w}}s + \mathring{M}_w) & (I_y s^2 - \mathring{M}_q s) \end{vmatrix} \tag{5.16}$$

The thrust response transfer functions may be derived by assuming the elevator to be fixed at its trim value, thus $\eta(s) = 0$, and $\tau(s)$ is written in place of $\eta(s)$. Then the derivatives $\mathring{X}_\eta$, $\mathring{Z}_\eta$ and $\mathring{M}_\eta$ in equations (5.13), (5.14) and (5.15) are replaced by $\mathring{X}_\tau$, $\mathring{Z}_\tau$ and $\mathring{M}_\tau$ respectively. Since the polynomial expressions given by the determinants are substantial they are set out in full in Appendix 2.

5.3.2 *THE LATERAL RESPONSE TRANSFER FUNCTIONS*

The lateral response transfer functions may be obtained by exactly the same means as the longitudinal transfer functions. The Laplace transform, assuming zero initial conditions, of the lateral equations of motion referred to body axes, equations (4.45), may be written in matrix form as follows

$$\begin{bmatrix} (ms - \mathring{Y}_v) & -\begin{pmatrix}(\mathring{Y}_p + mW_e)s \\ +mg\cos\theta_e\end{pmatrix} & -\begin{pmatrix}(\mathring{Y}_r - mU_e)s \\ +mg\sin\theta_e\end{pmatrix} \\ -\mathring{L}_v & (I_x s^2 - \mathring{L}_p s) & -(I_{xz}s^2 + \mathring{L}_r s) \\ -\mathring{N}_v & -(I_{xz}s^2 + \mathring{N}_p s) & (I_z s^2 - \mathring{N}_r s) \end{bmatrix} \begin{bmatrix} v(s) \\ \phi(s) \\ \psi(s) \end{bmatrix} = \begin{bmatrix} \mathring{Y}_\xi & \mathring{Y}_\zeta \\ \mathring{L}_\xi & \mathring{L}_\zeta \\ \mathring{N}_\xi & \mathring{N}_\zeta \end{bmatrix} \begin{bmatrix} \xi(s) \\ \zeta(s) \end{bmatrix} \tag{5.17}$$

where $s\phi(s) = p(s)$ and $s\psi(s) = r(s)$. By holding the rudder at its trim setting, $\zeta(s) = 0$, the aileron response transfer functions may be obtained by applying Cramer's rule to equation (5.17). Similarly, by holding the ailerons at the trim setting, $\xi(s) = 0$, the rudder response transfer functions may be obtained. For example, roll rate response to aileron is given by

$$\frac{N_\xi^p(s)}{\Delta(s)} \equiv \frac{p(s)}{\xi(s)} = \frac{s\phi(s)}{\xi(s)} \equiv \frac{sN_\xi^\phi(s)}{\Delta(s)} \tag{5.18}$$

where the numerator polynomial is given by

$$N_\xi^p(s) = s \begin{vmatrix} (ms - \mathring{Y}_v) & \mathring{Y}_\xi & -\begin{pmatrix}(\mathring{Y}_r - mU_e)s \\ +mg\sin\theta_e\end{pmatrix} \\ -\mathring{L}_v & \mathring{L}_\xi & -(I_{xz}s^2 + \mathring{L}_r s) \\ -\mathring{N}_v & \mathring{N}_\xi & (I_z s^2 - \mathring{N}_r s) \end{vmatrix} \tag{5.19}$$

and the denominator polynomial is given by

$$\Delta(s) = \begin{vmatrix} (ms - \mathring{Y}_v) & -\begin{pmatrix}(\mathring{Y}_p + mW_e)s \\ +mg\cos\theta_e\end{pmatrix} & -\begin{pmatrix}(\mathring{Y}_r - mU_e)s \\ +mg\sin\theta_e\end{pmatrix} \\ -\mathring{L}_v & (I_x s^2 - \mathring{L}_p s) & -(I_{xz}s^2 + \mathring{L}_r s) \\ -\mathring{N}_v & -(I_{xz}s^2 + \mathring{N}_p s) & (I_z s^2 - \mathring{N}_r s) \end{vmatrix} \tag{5.20}$$

Again, since the polynomial expressions given by the determinants are substantial they are also set out in full in Appendix 2.

EXAMPLE 5.2

We will obtain the transfer function describing pitch attitude response to elevator for the Lockheed F-104 Starfighter. The data were obtained from Teper (1969) and describe a sea level flight condition. Inspection of the data revealed that $\theta_e = 0$, thus it was concluded that the equations of motion to which the data relate are referred to wind axes.

$$\text{Air density } \rho = 0.00238 \text{ slug/ft}^3$$
$$\text{Axial velocity component } U_e = 305 \text{ ft/s}$$
$$\text{Aircraft mass } m = 746 \text{ slugs}$$
$$\text{Moment of inertia in pitch } I_y = 65\,000 \text{ slug ft}^2$$
$$\text{Gravitational constant } g = 32.2 \text{ ft/s}^2$$

The dimensional aerodynamic stability and control derivatives follow. Derivatives which are not quoted are assumed to be insignificant and are given a zero value, whence

$\mathring{X}_u = -26.26$ slug/s	$\mathring{Z}_u = -159.64$ slug/s	$\mathring{M}_u = 0$
$\mathring{X}_w = 79.82$ slug/s	$\mathring{Z}_w = -328.24$ slug/s	$\mathring{M}_w = -1014.0$ slug ft/s
$\mathring{X}_{\dot{w}} = 0$	$\mathring{Z}_{\dot{w}} = 0$	$\mathring{M}_{\dot{w}} = -36.4$ slug ft
$\mathring{X}_q = 0$	$\mathring{Z}_q = 0$	$\mathring{M}_q = -18\,135$ slug ft^2/s
$\mathring{X}_\eta = 0$	$\mathring{Z}_\eta = -16\,502$ slug ft/s^2/rad	$\mathring{M}_\eta = -303\,575$ slug ft/s^2/rad

The American Imperial units are retained in this example since it is preferable to work with the equations of motion and in the dimensional units appropriate to the source material. Conversion from one system of units to another often leads to confusion and error and is not therefore recommended. However, for information, factors for conversion from American Imperial units to SI units are given in Appendix 3.

These numerical values are substituted into equation (5.10) to obtain

$$\begin{bmatrix} 746s + 26.26 & -79.82 & 24\,021.2 \\ 159.64 & 746s + 328.24 & -227\,530s \\ 0 & 36.4s + 1014 & 65\,000s^2 + 18\,135s \end{bmatrix} \begin{bmatrix} u(s) \\ w(s) \\ \theta(s) \end{bmatrix} = \begin{bmatrix} 0 \\ -16\,502 \\ -303\,575 \end{bmatrix} \eta(s) \tag{5.21}$$

Cramer's rule may be applied directly to equation (5.21) to obtain the transfer function of interest

$$\frac{N_\eta^\theta(s)}{\Delta(s)} = \frac{\begin{vmatrix} 746s+26.26 & -79.82 & 0 \\ 159.64 & 746s+328.24 & -16\,502 \\ 0 & 36.4s+1014 & -303\,575 \end{vmatrix}}{\begin{vmatrix} 746s+26.26 & -79.82 & 24\,021.2 \\ 159.64 & 746s+328.24 & -227\,530s \\ 0 & 36.4s+1014 & 65\,000s^2+18\,135s \end{vmatrix}} \text{ rad/rad} \qquad (5.22)$$

whence

$$\frac{N_\eta^\theta(s)}{\Delta(s)} = \frac{-16.850\times10^{10}(s^2+0.402s+0.036)}{3.613\times10^{10}(s^4+0.925s^3+4.935s^2+0.182s+0.108)} \text{ rad/rad} \qquad (5.23)$$

Or, in the preferable factorized form,

$$\frac{N_\eta^\theta(s)}{\Delta(s)} = \frac{-4.664(s+0.135)(s+0.267)}{(s^2+0.033s+0.022)(s^2+0.893s+4.884)} \text{ rad/rad} \qquad (5.24)$$

The denominator of equation (5.24) factorizes into two pairs of complex roots (*poles*) each pair of which describes a longitudinal stability mode. The factors describing the modes may be written alternatively $(s^2+2\zeta\omega s+\omega^2)$ which is clearly the characteristic polynomial describing damped harmonic motion. The stability of each mode is determined by the damping ratio ζ and the undamped natural frequency by ω. The lower frequency mode is called the *phugoid* and the higher frequency mode is called the *short period pitching oscillation*. For the aeroplane to be completely longitudinally stable the damping ratio of both modes must be positive.

The units of the transfer function given in equation (5.24) are rad/rad, or equivalently deg/deg. Angular measure is usually, and correctly, quantified in radians and care must be applied when interpreting transfer functions since the radian is a very large angular quantity in the context of small perturbation motion of aircraft. This becomes especially important when dealing with transfer functions in which the input and output variables have different units. For example, the transfer function describing speed response to elevator for the F-104 has units ft/s/rad and one radian of elevator input is impossibly large! It is therefore very important to remember that one radian is equivalent to 57.3°. It is also important to remember that all transfer functions have units and they should always be indicated if confusion is to be avoided.

The transfer function given by equation (5.24) provides a complete description of the longitudinal stability characteristics and the dynamic pitch response to elevator of the F-104 at the flight condition in question. It is interesting to note that the transfer function has a negative sign. This means that a positive elevator deflection results in a negative pitch response which is completely in accordance with the notation defined in Chapter 2. Clearly, the remaining longitudinal response transfer functions can be obtained by applying Cramer's rule to equation (5.21) for each of the remaining motion variables. A comprehensive review of aeroplane dynamics based on transfer function analysis is contained in Chapters 6 and 7.

The complexity of this example is such that, although tedious, the entire computation is easily undertaken manually to produce a result of acceptable accuracy. Alternatively, transfer function (5.23) can be calculated merely by substituting the values of the derivative and other data into the appropriate polynomial expressions given in Appendix 2.

5.4 Response to controls

Time histories for the aircraft response to controls are readily obtained by finding the inverse Laplace transform of the appropriate transfer function expression. For example, the roll rate response to aileron is given by equation (5.5) as

$$p(s) = \frac{N_\xi^p(s)}{\Delta(s)}\xi(s) \tag{5.25}$$

assuming that the aeroplane is initially in trimmed flight. The numerator polynomial $N_\xi^p(s)$ and denominator polynomial $\Delta(s)$ are given in Appendix 2. The aileron input $\xi(s)$ is simply the Laplace transform of the required input function. For example, two commonly used inputs are the impulse and step functions where

Impulse of magnitude k is given by $\xi(s) = k$

Step of magnitude k is given by $\xi(s) = k/s$

Other useful input functions include the *ramp*, *pulse* (or step) of finite length, *doublet* and *sinusoid*. However, the Laplace transform of these functions is not quite so straightforward to obtain. Fortunately, most computer programs for handling transfer function problems have the most commonly used functions 'built-in'.

To continue with the example, the roll rate response to an aileron step input of magnitude k is therefore given by

$$p(t) = \mathrm{L}^{-1}\left\{\frac{k}{s}\frac{N_\xi^p(s)}{\Delta(s)}\right\} \tag{5.26}$$

Solution of equation (5.26) to obtain the time response involves finding the inverse Laplace transform of the expression on the right-hand side, which may be accomplished manually with the aid of a table of standard transforms. However, this calculation is painlessly achieved with the aid of an appropriate computer software package such as *MATLAB* or *Program CC*, for example. However, it is instructive to review the mathematical procedure since this provides valuable insight to aid the correct interpretation of a computer solution and this is most easily achieved by example, as follows.

EXAMPLE 5.3

We will obtain the pitch response of the F-104 aircraft to a unit step elevator input at the flight condition evaluated in Example 5.2. Assuming the unit step input to be in degree units, then from equation (5.24)

$$\theta(t) = \mathrm{L}^{-1}\left\{\frac{-4.664(s+0.135)(s+0.267)}{s(s^2+0.033s+0.022)(s^2+0.893s+4.884)}\right\}\text{deg} \tag{5.27}$$

Before the inverse Laplace transform of the expression in braces can be found it is first necessary to reduce it to partial fractions. Thus, writing

$$\frac{-4.664(s^2+0.402s+0.036)}{s(s^2+0.033s+0.022)(s^2+0.893s+4.884)} = -4.664\left(\frac{A}{s}+\frac{Bs+C}{(s^2+0.033s+0.022)}+\frac{Ds+E}{(s^2+0.893s+4.884)}\right) \tag{5.28}$$

To determine the values for A, B, C, D and E multiply out the fractions on the right-hand side and equate the numerator coefficients from both sides of the equation for like powers of s to obtain

$$\begin{aligned} 0 &= (A + B + D)s^4 \\ 0 &= (0.925A + 0.893B + C + 0.033D + E)s^3 \\ s^2 &= (4.935A + 4.884B + 0.893C + 0.022D + 0.033E)s^2 \\ 0.402s &= (0.182A + 4.884C + 0.022E)s \\ 0.036 &= 0.108A \end{aligned}$$

These simultaneous linear algebraic equations are easily solved using Cramer's rule if they are first written in matrix form

$$\begin{bmatrix} 1 & 1 & 0 & 1 & 0 \\ 0.925 & 0.893 & 1 & 0.033 & 1 \\ 4.935 & 4.884 & 0.893 & 0.022 & 0.033 \\ 0.182 & 0 & 4.884 & 0 & 0.022 \\ 0.108 & 0 & 0 & 0 & 0 \end{bmatrix} \begin{bmatrix} A \\ B \\ C \\ D \\ E \end{bmatrix} = \begin{bmatrix} 0 \\ 0 \\ 1 \\ 0.402 \\ 0.036 \end{bmatrix} \tag{5.29}$$

Thus, $A = 0.333$, $B = -0.143$, $C = 0.071$, $D = -0.191$ and $E = -0.246$. Thus, equation (5.27) may be written

$$\theta(t) = \mathrm{L}^{-1}\left\{-4.664\left(\frac{0.333}{s} - \frac{(0.143s - 0.071)}{(s^2 + 0.033s + 0.022)} - \frac{(0.191s + 0.246)}{(s^2 + 0.893s + 4.884)}\right)\right\} \text{deg} \tag{5.30}$$

A very short table of Laplace transforms relevant to this problem is given in Appendix 4. Inspection of the table of transforms determines that equation (5.30) needs some rearrangement before its inverse transform can be found. When solving problems of this type it is useful to appreciate that the solution will contain terms describing damped harmonic motion; the required form of the terms in equation (5.30) is then more easily established. With reference to Appendix 4, transform pairs 1, 5 and 6 would appear to be most applicable. Therefore, rearranging equation (5.30) to suit

$$\theta(t) = \mathrm{L}^{-1}\left\{-4.664\left(\frac{0.333}{s} - \left(\frac{0.143(s + 0.017)}{(s + 0.017)^2 + 0.148^2} - \frac{0.496(0.148)}{(s + 0.017)^2 + 0.148^2}\right) - \left(\frac{0.191(s + 0.447)}{(s + 0.447)^2 + 2.164^2} + \frac{0.074(2.164)}{(s + 0.447)^2 + 2.164^2}\right)\right)\right\} \text{deg} \tag{5.31}$$

Using transform pairs 1, 5 and 6, equation (5.31) may be evaluated to give the time response

$$\begin{aligned} \theta(t) = &-1.553 + 0.667\mathrm{e}^{-0.017t}(\cos 0.148t - 3.469 \sin 0.148t) \\ &+ 0.891\mathrm{e}^{-0.447t}(\cos 2.164t + 0.389 \sin 2.164t) \text{ deg} \end{aligned} \tag{5.32}$$

The solution given by equation (5.32) comprises three terms which may be interpreted as follows.

(i) The first term, −1.553°, is the constant steady state pitch attitude (gain) of the aeroplane.

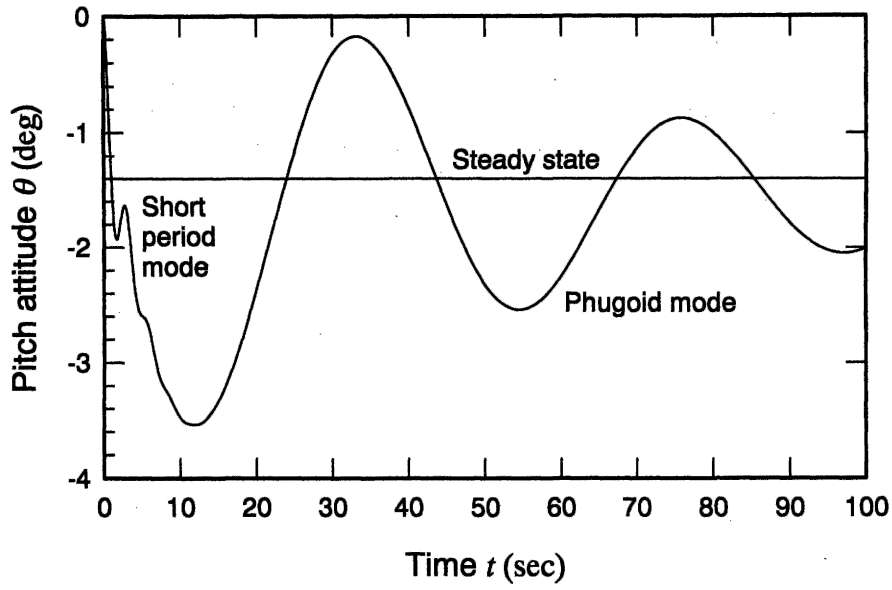

Fig. 5.2 Pitch attitude response of the F-104 to a 1° step of elevator

(ii) The second term describes the contribution made by the phugoid dynamics, the undamped natural frequency $\omega_p = 0.148$ rad/s and since $\zeta_p\omega_p = 0.017$ rad/s the damping ratio is $\zeta_p = 0.115$.

(iii) The third term describes the contribution made by the short period pitching oscillation dynamics, the undamped natural frequency $\omega_s = 2.164$ rad/s and since $\zeta_s\omega_s = 0.447$ rad/s the damping ratio is $\zeta_s = 0.207$.

The time response described by equation (5.32) is shown in Fig. 5.2 and the two dynamic modes are clearly visible. It is also clear that the pitch attitude eventually settles to the steady state value predicted above.

Example 5.3 illustrates that it is not necessary to obtain a complete time response solution merely to obtain the characteristics of the dynamic modes. The principal mode characteristics, damping ratio and natural frequency, are directly obtainable on inspection of the characteristic polynomial $\Delta(s)$ in any aircraft transfer function. The steady state gain is also readily established by application of the *Final Value Theorem* which states that

$$f(t)_{t\to\infty} = \lim_{s\to 0}(sf(s)) \tag{5.33}$$

The corresponding *Initial Value Theorem* is also a valuable tool and states that

$$f(t)_{t\to 0} = \lim_{s\to\infty}(sf(s)) \tag{5.34}$$

A complete discussion of these theorems may be found in most books on control theory, for example in Shinners (1980).

EXAMPLE 5.4

Apply the initial value and final value theorems to find the initial and steady values of the pitch attitude response of the F-104 of the previous examples. From equation (5.27) the Laplace transform of the unit step response is given by

$$\theta(s) = \frac{-4.664(s+0.135)(s+0.267)}{s(s^2+0.033s+0.022)(s^2+0.893s+4.884)} \text{ deg} \tag{5.35}$$

Applying the final value theorem to obtain

$$\theta(t)_{t\to\infty} = \lim_{s\to 0}\left(\frac{-4.664(s+0.135)(s+0.267)}{(s^2+0.033s+0.022)(s^2+0.893s+4.884)}\right) \text{deg} = -1.565^\circ \tag{5.36}$$

and applying the initial value theorem to obtain

$$\theta(t)_{t\to 0} = \lim_{s\to\infty}\left(\frac{-4.664(s+0.135)(s+0.267)}{(s^2+0.033s+0.022)(s^2+0.893s+4.884)}\right) \text{deg} = 0^\circ \tag{5.37}$$

Clearly, the values given by equations (5.36) and (5.37) correlate reasonably well with the known pitch attitude response calculated in Example 5.3. Bear in mind that, in all the calculations, numbers have been rounded to three decimal places for convenience.

5.5 Acceleration response transfer functions

Acceleration response transfer functions are frequently required but are not given directly by the solution of the equations of motion described above. Expressions for the components of inertial acceleration are given in equations (4.9) and, clearly, they comprise a number of motion variable contributions. Assuming small perturbation motion such that the usual simplifications can be made, equations (4.9) may be restated

$$\left.\begin{aligned} a_x &= \dot{u} - rV_e + qW_e - y\dot{r} + z\dot{q} \\ a_y &= \dot{v} - pW_e + rU_e + x\dot{r} - z\dot{p} \\ a_z &= \dot{w} - qU_e + pV_e - x\dot{q} + y\dot{p} \end{aligned}\right\} \tag{5.38}$$

Now if, for example, the normal acceleration response to an elevator referred to the *cg* is required ($x = y = z = 0$) and if fully decoupled motion is assumed ($pV_e = 0$) then the equation for normal acceleration simplifies to

$$a_z = \dot{w} - qU_e \tag{5.39}$$

The Laplace transform of equation (5.39), assuming zero initial conditions, may be written

$$a_z(s) = sw(s) - s\theta(s)U_e \tag{5.40}$$

Or, expressing equation (5.40) in terms of elevator response transfer functions

$$a_z(s) = s\frac{N_\eta^w(s)}{\Delta(s)}\eta(s) - sU_e\frac{N_\eta^\theta(s)}{\Delta(s)}\eta(s) = \frac{s(N_\eta^w(s) - U_eN_\eta^\theta(s))\eta(s)}{\Delta(s)} \tag{5.41}$$

whence the required normal acceleration response transfer function may be written

$$\frac{N_\eta^{a_z}(s)}{\Delta(s)} \equiv \frac{a_z(s)}{\eta(s)} = \frac{s(N_\eta^w(s) - U_eN_\eta^\theta(s))}{\Delta(s)} \tag{5.42}$$

Transfer functions for the remaining acceleration response components may be derived in a similar manner.

Another useful transfer function which is often required in handling qualities studies gives the normal acceleration response to an elevator measured at the pilot's seat. In this special case, x in equations (5.38) represents the distance measured from the *cg* to the pilot's seat and the normal acceleration is therefore given by

$$a_z = \dot{w} - qU_e - x\dot{q} \tag{5.43}$$

As before, the transfer function is easily derived

$$\frac{N_\eta^{a_z}(s)}{\Delta(s)_{\text{pilot}}} = \frac{s(N_\eta^w(s) - (U_e + xs)N_\eta^\theta(s))}{\Delta(s)} \tag{5.44}$$

EXAMPLE 5.5

We will calculate the normal acceleration response to elevator at the *cg* for the F-104 Starfighter aeroplane at the flight condition defined in Example 5.2. At the flight condition in question the steady axial velocity component $U_e = 305$ ft/s and the pitch attitude and normal velocity transfer functions describing response to elevator are given by

$$\frac{N_\eta^\theta(s)}{\Delta(s)} = \frac{-4.664(s + 0.135)(s + 0.267)}{(s^2 + 0.033s + 0.022)(s^2 + 0.893s + 4.884)} \text{ rad/rad} \tag{5.45}$$

and

$$\frac{N_\eta^w(s)}{\Delta(s)} = \frac{-22.147(s^2 + 0.035s + 0.022)(s + 64.675)}{(s^2 + 0.033s + 0.022)(s^2 + 0.893s + 4.884)} \text{ ft/s/rad} \tag{5.46}$$

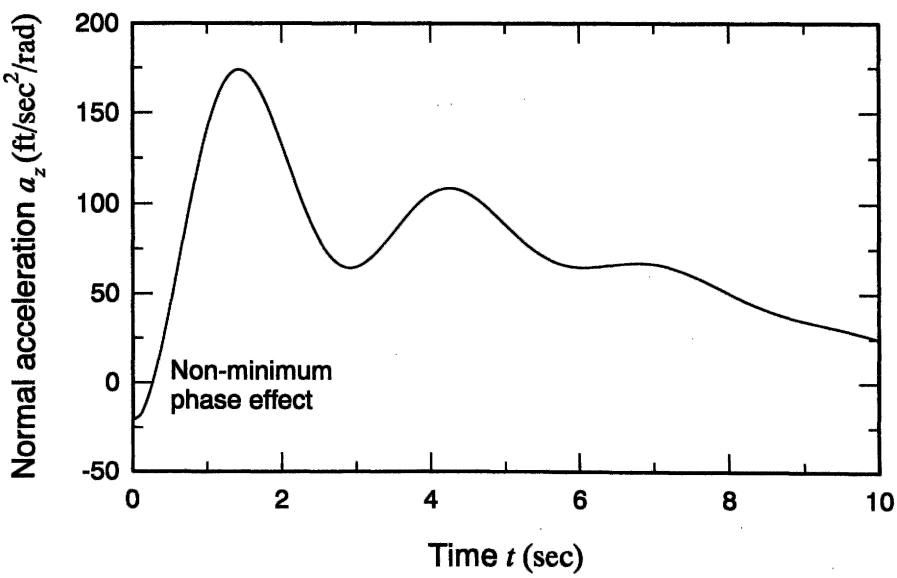

Fig. 5.3 Normal acceleration response at the *cg* to an elevator unit step input

Substitute equations (5.45) and (5.46) together with U_e into equation (5.42), pay particular attention to the units, multiply out the numerator and factorize the result to obtain the required transfer function

$$\frac{N_\eta^{a_z}(s)}{\Delta(s)} = \frac{-22.147s(s+0.037)(s-4.673)(s+5.081)}{(s^2+0.033s+0.022)(s^2+0.893s+4.884)} \text{ ft/s}^2/\text{rad} \tag{5.47}$$

Note that since the numerator and denominator are of the same order the acceleration transfer function (5.47) is an *improper* transfer function. The positive numerator root, or *zero*, implies that the transfer function is *non-minimum phase*, which is typical of aircraft acceleration transfer functions. The non-minimum phase effect is illustrated in the unit (1 rad) step response time history shown in Fig. 5.3 and causes the initial response to be in the wrong sense. The first few seconds of the response only are shown and, as may be determined by application of the final value theorem, the steady state acceleration is zero.

5.6 The state space method

The use of the state space method greatly facilitates the solution of the small perturbation equations of motion of aircraft. Since the computational mechanism is based on the use of matrix algebra it is most conveniently handled by a digital computer and, as already indicated, many suitable software packages are available. Most commercial software is intended for application to problems in modern control and some care is needed to ensure that the aircraft equations of motion are correctly assembled before a solution is computed using these tools. However, the available tools are generally very powerful and their use for the solution of the equations of motion of aircraft is a particularly simple application.

5.6.1 THE TRANSFER FUNCTION MATRIX

The general state equations (4.60) and (4.61), describing a linear dynamic system, may be written

$$\left.\begin{aligned} \dot{\mathbf{x}}(t) &= \mathbf{A}\mathbf{x}(t) + \mathbf{B}\mathbf{u}(t) \\ \mathbf{y}(t) &= \mathbf{C}\mathbf{x}(t) + \mathbf{D}\mathbf{u}(t) \end{aligned}\right\} \tag{5.48}$$

and the assembly of the equations of motion in this form, for the particular application to aircraft, is explained in Section 4.4.2. Since **A**, **B**, **C** and **D** are matrices of constant coefficients, the Laplace transform of equations (5.48), assuming zero initial conditions, is

$$\left.\begin{aligned} s\mathbf{x}(s) &= \mathbf{A}\mathbf{x}(s) + \mathbf{B}\mathbf{u}(s) \\ \mathbf{y}(s) &= \mathbf{C}\mathbf{x}(s) + \mathbf{D}\mathbf{u}(s) \end{aligned}\right\} \tag{5.49}$$

The state equation may be rearranged and written

$$\mathbf{x}(s) = [s\mathbf{I} - \mathbf{A}]^{-1}\mathbf{B}\mathbf{u}(s) \tag{5.50}$$

where **I** is the identity matrix and is the same order as **A**. Thus, eliminating $\mathbf{x}(s)$, the state

vector, by combining the output equation and equation (5.50), the output vector $\mathbf{y}(s)$ is given by

$$\mathbf{y}(s) = [\mathbf{C}[s\mathbf{I} - \mathbf{A}]^{-1}\mathbf{B} + \mathbf{D}]\mathbf{u}(s) = \mathbf{G}(s)\mathbf{u}(s) \tag{5.51}$$

where $\mathbf{G}(s)$ is called the *transfer function matrix*. In general the transfer function matrix has the form

$$\mathbf{G}(s) = \frac{1}{\Delta(s)}\mathbf{N}(s) \tag{5.52}$$

and $\mathbf{N}(s)$ is a polynomial matrix whose elements are all of the response transfer function numerators. The denominator $\Delta(s)$ is the characteristic polynomial and is common to all transfer functions. Thus, the application of the state space method to the solution of the equations of motion of an aeroplane enables all of the response transfer functions to be obtained in a single computation.

Now, as explained in Section 4.4.2, when dealing with the solution of the equations of motion it is usually required that $\mathbf{y}(s) = \mathbf{x}(s)$, i.e. the output vector and state vector are the same. In this case, equation (5.51) may be simplified since $\mathbf{C} = \mathbf{I}$ and $\mathbf{D} = 0$, therefore

$$\mathbf{G}(s) = [s\mathbf{I} - \mathbf{A}]^{-1}\mathbf{B} = \frac{\text{Adj}[s\mathbf{I} - \mathbf{A}]\mathbf{B}}{|s\mathbf{I} - \mathbf{A}|} \tag{5.53}$$

and equation (5.53) is equivalent to the multi-variable application of Cramer's rule as discussed in Section 5.3 above.

5.6.2 *THE LONGITUDINAL TRANSFER FUNCTION MATRIX*

The concise longitudinal state equations are given by equations (4.67) and (4.68). Thus, substituting for **A**, **B** and **I** into equation (5.53) the longitudinal transfer function matrix is given by

$$\mathbf{G}(s) = \begin{bmatrix} s - x_u & -x_w & -x_q & -x_\theta \\ -z_u & s - z_w & -z_q & -z_\theta \\ -m_u & -m_w & s - m_q & -m_\theta \\ 0 & 0 & -1 & s \end{bmatrix}^{-1} \begin{bmatrix} x_\eta & x_\tau \\ z_\eta & z_\tau \\ m_\eta & m_\tau \\ 0 & 0 \end{bmatrix} \tag{5.54}$$

Algebraic manipulation of equation (5.54) leads to

$$\mathbf{G}(s) = \frac{1}{\Delta(s)} \begin{bmatrix} N_\eta^u(s) & N_\tau^u(s) \\ N_\eta^w(s) & N_\tau^w(s) \\ N_\eta^q(s) & N_\tau^q(s) \\ N_\eta^\theta(s) & N_\tau^\theta(s) \end{bmatrix} \tag{5.55}$$

In this case the numerator and denominator polynomials are expressed in terms of the concise derivatives. A complete listing of the longitudinal algebraic transfer functions in this form is given in Appendix 2.

5.6.3 *THE LATERAL TRANSFER FUNCTION MATRIX*

The lateral state equation is given in terms of normalized derivatives by equation

(4.69). Thus, substituting for **A**, **B** and **I** into equation (5.53) the lateral transfer function matrix is given by

$$\mathbf{G}(s) = \begin{bmatrix} s-y_v & -y_p & -y_r & -y_\phi & -y_\psi \\ -l_v & s-l_p & -l_r & -l_\phi & -l_\psi \\ -n_v & -n_p & s-n_r & -n_\phi & -n_\psi \\ 0 & -1 & 0 & s & 0 \\ 0 & 0 & -1 & 0 & s \end{bmatrix}^{-1} \begin{bmatrix} y_\xi & y_\zeta \\ l_\xi & l_\zeta \\ n_\xi & n_\zeta \\ 0 & 0 \\ 0 & 0 \end{bmatrix} \tag{5.56}$$

and, as for the longitudinal solution, the lateral transfer function matrix may be written

$$\mathbf{G}(s) = \frac{1}{\Delta(s)} \begin{bmatrix} N_\xi^v(s) & N_\zeta^v(s) \\ N_\xi^p(s) & N_\zeta^p(s) \\ N_\xi^r(s) & N_\zeta^r(s) \\ N_\xi^\phi(s) & N_\zeta^\phi(s) \\ N_\xi^\psi(s) & N_\zeta^\psi(s) \end{bmatrix} \tag{5.57}$$

Again the numerator and denominator polynomials are expressed in terms of the normalized derivatives. A complete listing of the lateral algebraic transfer functions in this form is given in Appendix 2.

EXAMPLE 5.6

To illustrate the use of the state space method for obtaining the lateral transfer function matrix, data for the Lockheed C-5A were obtained from Heffley and Jewell (1972). The data relate to a flight condition at an altitude of 20 000 ft and Mach number 0.6 and are referred to aircraft body axes. Although the data are given in American Imperial units, here they are converted to SI units simply for illustration. The normalized derivatives were derived from the data, great care being exercised to ensure the correct units. The derivatives are listed below and, as in previous examples, missing derivatives were assumed to be insignificant and made equal to zero.

$y_v = -0.1060\,1/\text{s}$	$l_v = -0.0070\,1/\text{m/s}$	$n_v = 0.0023\,1/\text{m/s}$
$y_p = 0$	$l_p = -0.9880\,1/\text{s}$	$n_p = -0.0921\,1/\text{s}$
$y_r = -189.586\,\text{m/s}$	$l_r = 0.2820\,1/\text{s}$	$n_r = -0.2030\,1/\text{s}$
$y_\phi = 9.8073\,\text{m/s}^2$	$l_\phi = 0$	$n_\phi = 0$
$y_\psi = 0.3768\,\text{m/s}^2$	$l_\psi = 0$	$n_\psi = 0$
$y_\xi = -0.0178\,\text{m/s}^2$	$l_\xi = 0.4340\,1/\text{s}^2$	$n_\xi = 0.0343\,1/\text{s}^2$
$y_\zeta = 3.3936\,\text{m/s}^2$	$l_\zeta = 0.1870\,1/\text{s}^2$	$n_\zeta = -0.5220\,1/\text{s}^2$

The lateral state equation is obtained by substituting the derivative values into equation (4.69)

$$\begin{bmatrix} \dot{v} \\ \dot{p} \\ \dot{r} \\ \dot{\phi} \\ \dot{\psi} \end{bmatrix} = \begin{bmatrix} -0.106 & 0 & -189.586 & 9.8073 & 0.3768 \\ -0.007 & -0.988 & 0.282 & 0 & 0 \\ 0.0023 & -0.0921 & -0.203 & 0 & 0 \\ 0 & 1 & 0 & 0 & 0 \\ 0 & 0 & 1 & 0 & 0 \end{bmatrix} \begin{bmatrix} v \\ p \\ r \\ \phi \\ \psi \end{bmatrix} + \begin{bmatrix} -0.0178 & 3.3936 \\ 0.434 & 0.187 \\ 0.0343 & -0.522 \\ 0 & 0 \\ 0 & 0 \end{bmatrix} \begin{bmatrix} \xi \\ \zeta \end{bmatrix} \tag{5.58}$$

and the output equation, written out in full, is

$$\begin{bmatrix} v \\ p \\ r \\ \phi \\ \psi \end{bmatrix} = \begin{bmatrix} 1 & 0 & 0 & 0 & 0 \\ 0 & 1 & 0 & 0 & 0 \\ 0 & 0 & 1 & 0 & 0 \\ 0 & 0 & 0 & 1 & 0 \\ 0 & 0 & 0 & 0 & 1 \end{bmatrix} \begin{bmatrix} v \\ p \\ r \\ \phi \\ \psi \end{bmatrix} + \begin{bmatrix} 0 & 0 \\ 0 & 0 \\ 0 & 0 \\ 0 & 0 \\ 0 & 0 \end{bmatrix} \begin{bmatrix} \xi \\ \zeta \end{bmatrix} \tag{5.59}$$

The transfer function matrix was calculated using *Program CC*. The matrices **A**, **B**, **C** and **D** are input to the program and the command for finding the transfer function matrix is invoked. A print-out of the result produced the following

$$\mathbf{G}(s) = \frac{1}{\Delta(s)}\mathbf{N}(s) \tag{5.60}$$

where equation (5.60) is the shorthand version of equation (5.57) and

$$\mathbf{N}(s) = \begin{bmatrix} -0.018s(s+0.15)(s-0.98)(s+367.35) & 3.394s(s-0.012)(s+1.05)(s+2.31) \\ 0.434s(s-0.002)(s^2+0.33s+0.57) & 0.187s(s-0.002)(s+1.55)(s-2.16) \\ 0.343s(s+0.69)(s^2-0.77s+0.51) & -0.522s(s+1.08)(s^2+0.031s+0.056) \\ 0.434(s-0.002)(s^2+0.33s+0.57) & 0.187(s-0.002)(s+1.55)(s-2.16) \\ 0.343(s+0.69)(s^2-0.77s+0.51) & -0.522(s+1.08)(s^2+0.031s+0.056) \end{bmatrix} \tag{5.61}$$

and the common denominator, the lateral characteristic polynomial, is given by

$$\Delta(s) = s(s+0.01)(s+1.11)(s^2+0.18s+0.58) \tag{5.62}$$

The lateral characteristic polynomial factorizes into three real roots and a complex pair of roots. The roots, or poles, of the lateral characteristic polynomial provide a complete description of the lateral-directional stability characteristics of the aeroplane. The zero root indicates *neutral stability* in yaw, the first non-zero real root describes the *spiral mode*, the second real root describes the *roll subsidence mode* and the complex pair of roots describes the *oscillatory dutch roll mode*.

It is very important to remember the units of the transfer functions comprising the transfer function matrix, which are

$$\text{units of } \mathbf{G}(s) = \frac{1}{\Delta(s)} \begin{bmatrix} N_\xi^v(s) & N_\zeta^v(s) \\ N_\xi^p(s) & N_\zeta^p(s) \\ N_\xi^r(s) & N_\zeta^r(s) \\ N_\xi^\phi(s) & N_\zeta^\phi(s) \\ N_\xi^\psi(s) & N_\zeta^\psi(s) \end{bmatrix} = \begin{bmatrix} \text{m/s/rad} & \text{m/s/rad} \\ \text{rad/s/rad} & \text{rad/s/rad} \\ \text{rad/s/rad} & \text{rad/s/rad} \\ \text{rad/rad} & \text{rad/rad} \\ \text{rad/rad} & \text{rad/rad} \end{bmatrix} \tag{5.63}$$

Thus, the transfer functions of interest can be obtained from inspection of equation (5.61) together with equation (5.62). For example, the transfer function describing sideslip velocity response to rudder is given by

$$\frac{v(s)}{\zeta(s)} = \frac{N_\zeta^v(s)}{\Delta(s)} = \frac{3.394(s-0.012)(s+1.05)(s+29.31)}{(s+0.01)(s+1.11)(s^2+0.18s+0.58)} \text{ m/s/rad} \tag{5.64}$$

Comparison of these results with those of the original source material in Heffley and Jewell (1972) reveals a number of small numerical discrepancies. This is due, in part, to the numerical rounding employed to keep this illustration to a reasonable size and in part to the differences in the computational algorithms used to obtain the solutions. However, in both cases the accuracy is adequate for most practical purposes.

It is worth noting that many matrix inversion algorithms introduce numerical errors which accumulate rapidly with increasing matrix order and it is possible to obtain seriously inaccurate results with some poorly conditioned matrices. The typical aircraft state matrix has a tendency to fall into this category so it is advisable to check the result of a transfer function matrix computation for reasonableness when the accuracy is in doubt. This may be done, for example, by making a test calculation using the expressions given in Appendix 2. For this reason *Program CC* includes two different algorithms for calculating the transfer function matrix. In Example 5.6 it was found that the *Generalized Eigenvalue Problem* algorithm gave obviously incorrect values for some transfer function numerators, whereas the *Fadeeva* algorithm gave entirely the correct solution. Thus, when using computer tools for handling aircraft stability and control problems it is advisable to input the aircraft derivative and other data at the accuracy given.

5.6.4 RESPONSE IN TERMS OF STATE DESCRIPTION

The main reasons for the adoption of state space modelling tools are the extreme power and convenience of machine solution of the equations of motion and that the solution is obtained in a form that readily lends itself to further analysis in the context of flight control. Thus, the solution process is usually completely hidden from the investigator. However, it is important to be aware of the mathematical procedures implemented in the software algorithms for the reasons mentioned above. A description of the methods of solution of the state equations describing a general system may be found in many books on modern control or system theory. For example, descriptions may be found in Barnett (1975), Shinners (1980) and Owens (1981). The following description is a summary of the solution of the aircraft state equations and only includes those aspects of the process that are most relevant to the aircraft application. For a more comprehensive review the reader should consult the references.

The Laplace transform of the state equations (5.49) may be restated for the general case in which non-zero initial conditions are assumed

$$\begin{aligned} s\mathbf{x}(s) - \mathbf{x}(0) &= \mathbf{A}\mathbf{x}(s) + \mathbf{B}\mathbf{u}(s) \\ \mathbf{y}(s) &= \mathbf{C}\mathbf{x}(s) + \mathbf{D}\mathbf{u}(s) \end{aligned} \tag{5.65}$$

whence, the state equation may be written

$$\mathbf{x}(s) = [s\mathbf{I} - \mathbf{A}]^{-1}\mathbf{x}(0) + [s\mathbf{I} - \mathbf{A}]^{-1}\mathbf{B}\mathbf{u}(s) \tag{5.66}$$

or

$$\mathbf{x}(s) = \mathbf{\Phi}(s)\mathbf{x}(0) + \mathbf{\Phi}(s)\mathbf{B}\mathbf{u}(s) \tag{5.67}$$

where $\Phi(s)$ is called the *resolvent* of **A**. The most general expression for the state vector $\mathbf{x}(t)$ is determined by finding the inverse Laplace transform of equation (5.67), and is written

$$\mathbf{x}(t) = \Phi(t - t_0)\mathbf{x}(t_0) + \int_{t_0}^{t} \Phi(t - \tau)\mathbf{B}\mathbf{u}(\tau)\,d\tau \tag{5.68}$$

The *state transition matrix* $\Phi(t - t_0)$ is defined

$$\Phi(t - t_0) = L^{-1}\{[s\mathbf{I} - \mathbf{A}]^{-1}\} = e^{\mathbf{A}(t-t_0)} \tag{5.69}$$

it is equivalent to the *matrix exponential* and describes the transition in the state response $x(t)$ from time t_0 to time t. The state transition matrix has the following special properties

$$\left.\begin{aligned} \Phi(0) &= e^{\mathbf{A}t}_{t=0} = \mathbf{I} \\ \Phi(\infty) &= e^{\mathbf{A}t}_{t=\infty} = \mathbf{0} \\ \Phi(t+\tau) &= \Phi(t)\Phi(\tau) = e^{\mathbf{A}t}e^{\mathbf{A}\tau} \\ \Phi(t_2 - t_0) &= \Phi(t_2 - t_1)\Phi(t_1 - t_0) = e^{\mathbf{A}(t_2-t_1)}e^{\mathbf{A}(t_1-t_0)} \\ \Phi^{-1}(t) &= \Phi(-t) = e^{-\mathbf{A}t} \end{aligned}\right\} \tag{5.70}$$

The integral term in equation (5.68) is a *convolution integral* whose properties are well known and are discussed in most texts on linear systems theory. A very accessible explanation of the role of the convolution integral in determining system response may be found in Auslander *et al.* (1974).

For aircraft applications it is usual to measure time from $t_0 = 0$ and equation (5.68) may be written

$$\begin{aligned} \mathbf{x}(t) &= \Phi(t)\mathbf{x}(0) + \int_0^t \Phi(t - \tau)\mathbf{B}\mathbf{u}(\tau)\,d\tau \\ &= e^{\mathbf{A}t}\mathbf{x}(0) + \int_0^t e^{\mathbf{A}(t-\tau)}\mathbf{B}\mathbf{u}(\tau)\,d\tau \end{aligned} \tag{5.71}$$

The output response vector $\mathbf{y}(t)$ is determined by substituting the state vector $\mathbf{x}(t)$, obtained from equation (5.71), into the output equation

$$\begin{aligned} \mathbf{y}(t) &= \mathbf{C}\mathbf{x}(t) + \mathbf{D}\mathbf{u}(t) \\ &= \mathbf{C}e^{\mathbf{A}t}\mathbf{x}(0) + \mathbf{C}\int_0^t e^{\mathbf{A}(t-\tau)}\mathbf{B}\mathbf{u}(\tau)\,d\tau + \mathbf{D}\mathbf{u}(t) \end{aligned} \tag{5.72}$$

Analytical solution of the state equation (5.71) is only possible when the form of the input vector $\mathbf{u}(t)$ is known, therefore further limited progress can only be made for specified applications. Three solutions are of particular interest in aircraft applications: the *unforced* or *homogeneous* response, the *impulse* response and the *step* response.

5.6.4.1 Eigenvalues and eigenvectors

The characteristic equation is given by equating the characteristic polynomial to zero

$$\Delta(s) = |s\mathbf{I} - \mathbf{A}| = 0 \tag{5.73}$$

The roots or *zeros* of equation (5.73), denoted λ_i, are the *eigenvalues* of the state matrix **A**. An eigenvalue λ_i and its corresponding non-zero *eigenvector* $\mathbf{v}_i$ are such that

$$\mathbf{A}\mathbf{v}_i = \lambda_i \mathbf{v}_i \tag{5.74}$$

whence

$$[\lambda_i \mathbf{I} - \mathbf{A}]\mathbf{v}_i = 0 \tag{5.75}$$

Since $\mathbf{v}_i \neq 0$ then $[\lambda_i \mathbf{I} - \mathbf{A}]$ is singular. The eigenvectors $\mathbf{v}_i$ are always linearly independent provided the eigenvalues λ_i are *distinct*, i.e. the characteristic equation (5.73) has no repeated roots. When an eigenvalue is complex its corresponding eigenvector is also complex and the complex conjugate λ_i^* corresponds to the complex conjugate $\mathbf{v}_i^*$.

The *eigenvector* or *modal matrix* comprises all of the eigenvectors and is defined

$$\mathbf{V} = [\mathbf{v}_1 \quad \mathbf{v}_2 \quad \cdots \quad \mathbf{v}_m] \tag{5.76}$$

It follows directly from equation (5.74) that

$$\mathbf{AV} = \mathbf{V}\begin{bmatrix} \lambda_2 & & & \\ & \lambda_2 & \mathbf{0} & \\ & & \ddots & \\ & \mathbf{0} & & \ddots \\ & & & \lambda_m \end{bmatrix} \equiv \mathbf{V}\Lambda \tag{5.77}$$

where Λ is the diagonal *eigenvalue matrix*. Thus

$$\mathbf{V}^{-1}\mathbf{AV} = \Lambda \tag{5.78}$$

and **A** is said to be *similar* to the diagonal eigenvalue matrix Λ. The mathematical operation on the state matrix **A** described by equation (5.78) is referred to as a *similarity transform*. Similar matrices possess the special property that their eigenvalues are the same. When the state equations are transformed to a similar form such that the state matrix **A** is replaced by the diagonal eigenvalue matrix Λ their solution is greatly facilitated. Presented in this form the state equations are said to be in *modal form*.

Eigenvectors may be determined as follows. Now by definition

$$[\lambda_i \mathbf{I} - \mathbf{A}]^{-1} = \frac{\text{Adj}[\lambda_i \mathbf{I} - \mathbf{A}]}{|\lambda_i \mathbf{I} - \mathbf{A}|} \tag{5.79}$$

and since, for any eigenvalue λ_i, $|\lambda_i \mathbf{I} - \mathbf{A}| = \mathbf{0}$, equation (5.79) may be rearranged and written

$$[\lambda_i \mathbf{I} - \mathbf{A}]\text{Adj}[\lambda_i \mathbf{I} - \mathbf{A}] = |\lambda_i \mathbf{I} - \mathbf{A}|\mathbf{I} = \mathbf{0} \tag{5.80}$$

Comparing equation (5.80) with equation (5.75) the eigenvector $\mathbf{v}_i$ corresponding to the eigenvalue λ_i is defined

$$\mathbf{v}_i = \text{Adj}[\lambda_i \mathbf{I} - \mathbf{A}] \tag{5.81}$$

Any non-zero column of the adjoint matrix is an eigenvector and if there is more than one column they differ only by a constant factor. Eigenvectors are therefore unique in direction only and not in magnitude. However, the dynamic characteristics of a system determine the unique relationship between each of its eigenvectors.

5.6.4.2 The modal equations

Define the transform

$$\mathbf{x}(t) = \mathbf{V}\mathbf{z}(t) \equiv \mathbf{v}_1 z_1(t) + \mathbf{v}_2 z_2(t) + \ldots + \mathbf{v}_m z_m(t) = \sum_{i=1}^{i=m} \mathbf{v}_i z_i(t) \tag{5.82}$$

then the state equations (5.48) may be rewritten in modal form

$$\left.\begin{aligned} \dot{\mathbf{z}}(t) &= \boldsymbol{\Lambda}\mathbf{z}(t) + \mathbf{V}^{-1}\mathbf{B}\mathbf{u}(t) \\ \mathbf{y}(t) &= \mathbf{C}\mathbf{V}\mathbf{z}(t) + \mathbf{D}\mathbf{u}(t) \end{aligned}\right\} \tag{5.83}$$

5.6.4.3 Unforced response

With reference to equation (5.71) the solution to the state equation in modal form, equation (5.83), is given by

$$\mathbf{z}(t) = \mathrm{e}^{\boldsymbol{\Lambda}t}\mathbf{z}(0) + \int_0^t \mathrm{e}^{\boldsymbol{\Lambda}(t-\tau)}\mathbf{V}^{-1}\mathbf{B}\mathbf{u}(\tau)\,\mathrm{d}\tau \tag{5.84}$$

The *matrix exponential* $\mathrm{e}^{\boldsymbol{\Lambda}t}$ in diagonal form is defined

$$\mathrm{e}^{\boldsymbol{\Lambda}t} = \begin{bmatrix} \mathrm{e}^{\lambda_1 t} & & & \\ & \mathrm{e}^{\lambda_2 t} & \mathbf{0} & \\ & & \ddots & \\ & \mathbf{0} & & \ddots \\ & & & \mathrm{e}^{\lambda_m t} \end{bmatrix} \tag{5.85}$$

and since it is diagonal the solutions for the transformed state variables $z_i(t)$ given by equation (5.84) are uncoupled, the principal advantage of the transform, whence

$$z_i(t) = \mathrm{e}^{\lambda_i t} z_i(0) + \int_0^t \mathrm{e}^{\lambda_i(t-\tau)}\mathbf{V}^{-1}\mathbf{B}u_i(\tau)\,\mathrm{d}\tau \tag{5.86}$$

The unforced response is given by equation (5.84) when $u(t) = 0$, whence

$$\mathbf{z}(t) = \mathrm{e}^{\boldsymbol{\Lambda}t}\mathbf{z}(0) \tag{5.87}$$

Or, substituting equation (5.87) into equation (5.82), the unforced state trajectory $\mathbf{x}(t)$ may be derived

$$\mathbf{x}(t) = \mathbf{V}\mathrm{e}^{\boldsymbol{\Lambda}t}\mathbf{z}(0) = \sum_{i=1}^{i=m} \mathbf{v}_i \mathrm{e}^{\lambda_i t} z_i(0) = \sum_{i=1}^{i=m} \mathbf{v}_i \mathrm{e}^{\lambda_i t}\mathbf{V}^{-1} x_i(0) \tag{5.88}$$

or

$$\mathbf{x}(t) = \mathbf{V}\mathrm{e}^{\boldsymbol{\Lambda}t}\mathbf{V}^{-1}\mathbf{x}(0) \equiv \mathrm{e}^{\mathbf{A}t}\mathbf{x}(0) \tag{5.89}$$

and from equation (5.72) the output response follows

$$\mathbf{y}(t) = \mathbf{C}\mathbf{x}(t) = \mathbf{C}\mathbf{V}\mathrm{e}^{\boldsymbol{\Lambda}t}\mathbf{V}^{-1}\mathbf{x}(0) \equiv \mathbf{C}\mathrm{e}^{\mathbf{A}t}\mathbf{x}(0) \tag{5.90}$$

Clearly the system behaviour is governed by the *system modes* $\mathrm{e}^{\lambda_i t}$, the *eigenfunctions* $\mathbf{v}_i\mathrm{e}^{\lambda_i t}$ and by the *initial state* $\mathbf{z}(0) = \mathbf{V}^{-1}\mathbf{x}(0)$.

5.6.4.4 Impulse response

The *unit impulse function* or *Dirac delta function*, denoted $\delta(t)$, is usually taken to mean a rectangular pulse of unit area, and in the limit the width of the pulse tends to zero whilst its magnitude tends to infinity. Thus, the special property of the unit impulse function is

$$\int_{-\infty}^{+\infty} \delta(t - t_0)\,dt = 1 \tag{5.91}$$

where t_0 is the time at which the impulse commences.

The solution of the modal state equation in response to a unit impulse follows from equation (5.84)

$$\mathbf{z}(t) = e^{\lambda t}\mathbf{z}(0) + \int_0^t e^{\Lambda(t-\tau)}\mathbf{V}^{-1}\mathbf{B}\mathbf{u}_\delta(\tau)\,d\tau \tag{5.92}$$

where $\mathbf{u}_\delta(\tau)$ is a unit impulse vector. The property of the unit impulse function enables the convolution integral to be solved and

$$\mathbf{z}(t) = e^{\Lambda t}\mathbf{z}(0) + e^{\Lambda t}\mathbf{V}^{-1}\mathbf{B} = e^{\Lambda t}[\mathbf{z}(0) + \mathbf{V}^{-1}\mathbf{B}] \tag{5.93}$$

Thus the transform, equation (5.82), enables the state vector to be determined

$$\mathbf{x}(t) = \mathbf{V}e^{\Lambda t}\mathbf{V}^{-1}[\mathbf{x}(0) + \mathbf{B}] \equiv e^{\Lambda t}[\mathbf{x}(0) + \mathbf{B}] \tag{5.94}$$

and the corresponding output response vector is given by

$$\begin{aligned}\mathbf{y}(t) &= \mathbf{C}\mathbf{V}e^{\Lambda t}\mathbf{V}^{-1}[\mathbf{x}(0) + \mathbf{B}] + \mathbf{D}u_\delta(t)\\ &\equiv \mathbf{C}e^{\Lambda t}[\mathbf{x}(0) + \mathbf{B}] + \mathbf{D}u_\delta(t)\end{aligned} \tag{5.95}$$

Now for application to aeroplanes it has already been established in Section 4.4.2 that the direct matrix **D** is zero. Comparing equations (5.95) and (5.90) it is seen that the impulse response is the same as the unforced response with initial condition $[\mathbf{x}(0) + \mathbf{B}]$.

5.6.4.5 Step response

When the vector input to the system is a step of constant magnitude, denoted $\mathbf{u}_k$, applied at time $t_0 = 0$ then the state equation (5.84) may be written

$$\mathbf{z}(t) = e^{\Lambda t}\mathbf{z}(0) + \int_0^t e^{\Lambda(t-\tau)}\mathbf{V}^{-1}\mathbf{B}\mathbf{u}_k\,d\tau \tag{5.96}$$

Since the input is constant the convolution integral is easily evaluated and

$$\mathbf{z}(t) = e^{\Lambda t}\mathbf{z}(0) + \Lambda^{-1}[e^{\Lambda t} - \mathbf{I}]\mathbf{V}^{-1}\mathbf{B}\mathbf{u}_k \tag{5.97}$$

Thus the transform, equation (5.82), enables the state vector to be determined

$$\begin{aligned}\mathbf{x}(t) &= \mathbf{V}e^{\Lambda t}[\mathbf{V}^{-1}\mathbf{x}(0) + \Lambda^{-1}\mathbf{V}^{-1}\mathbf{B}\mathbf{u}_k] - \mathbf{A}^{-1}\mathbf{B}\mathbf{u}_k\\ &\equiv e^{\mathbf{A}t}[\mathbf{x}(0) + \mathbf{A}^{-1}\mathbf{B}\mathbf{u}_k] - \mathbf{A}^{-1}\mathbf{B}\mathbf{u}_k\end{aligned} \tag{5.98}$$

The derivation of equation (5.98) makes use of the following property of the matrix exponential

$$\mathbf{A}^{-1}e^{\Lambda t} \equiv e^{\mathbf{A}t}\mathbf{A}^{-1} \tag{5.99}$$

and the similarity transform

$$\mathbf{A}^{-1} = \mathbf{V}\mathbf{\Lambda}^{-1}\mathbf{V}^{-1} \tag{5.100}$$

Again, the output response is obtained by substituting the state vector $\mathbf{x}(t)$, equation (5.98), into the output equation to give

$$\begin{aligned}\mathbf{y}(t) &= \mathbf{C}\mathbf{V}e^{\mathbf{\Lambda}t}[\mathbf{V}^{-1}\mathbf{x}(0) + \mathbf{\Lambda}^{-1}\mathbf{V}^{-1}\mathbf{B}\mathbf{u}_k] - [\mathbf{C}\mathbf{A}^{-1}\mathbf{B} - \mathbf{D}]\mathbf{u}_k \\ &\equiv \mathbf{C}e^{\mathbf{A}t}[\mathbf{x}(0) + \mathbf{A}^{-1}\mathbf{B}\mathbf{u}_k] - [\mathbf{C}\mathbf{A}^{-1}\mathbf{B} - \mathbf{D}]\mathbf{u}_k \end{aligned} \tag{5.101}$$

Since the direct matrix $\mathbf{D}$ is zero for aeroplanes, comparing equations (5.101) and (5.95) it is seen that the step response is the same as the impulse response with initial condition $[\mathbf{x}(0) + \mathbf{A}^{-1}\mathbf{B}\mathbf{u}_k]$ superimposed on the constant output $-\mathbf{C}\mathbf{A}^{-1}\mathbf{B}\mathbf{u}_k$.

5.6.4.6 Response shapes

With reference to equations (5.90), (5.95) and (5.101) it is clear that, irrespective of the input, the transient output response shapes are governed by the system eigenfunctions $\mathbf{V}e^{\mathbf{\Lambda}t}$, or alternatively, by the eigenvectors and eigenvalues. Most computer solutions of the state equations produce an output response in the form of time history data together with the eigenvalues and eigenvectors. Thus, in aircraft response analysis the system modes and eigenfunctions may be calculated if required. The value of this facility is that it provides a very effective means for gaining insight into the key physical properties governing the response. In particular, it enables the mode content in any response variable to be assessed merely by inspection of the corresponding eigenvectors.

The output response to other input functions may also be calculated algebraically provided the input function can be expressed in a suitable analytic form. Typical examples include the ramp function and various sinusoidal functions. Computer software packages intended for analysing system response always include a number of common input functions and usually have provision for creating other functions. However, in aircraft response analysis, input functions other than those discussed in detail above are generally of less interest.

EXAMPLE 5.7

The longitudinal equations of motion for the Lockheed F-104 Starfighter aircraft given in Example 5.2 may be written in state form as described in Section 4.4.2. Whence

$$\begin{bmatrix} 746 & 0 & 0 & 0 \\ 0 & 746 & 0 & 0 \\ 0 & 36.4 & 65\,000 & 0 \\ 0 & 0 & 0 & 1 \end{bmatrix} \begin{bmatrix} \dot{u} \\ \dot{w} \\ \dot{q} \\ \dot{\theta} \end{bmatrix}$$

$$= \begin{bmatrix} -26.26 & 79.82 & 0 & -24\,021.2 \\ -159.64 & -328.64 & 227\,530 & 0 \\ 0 & -1014 & -18\,135 & 0 \\ 0 & 0 & 1 & 0 \end{bmatrix} \begin{bmatrix} u \\ w \\ q \\ \theta \end{bmatrix} + \begin{bmatrix} 0 \\ -16\,502 \\ -303\,575 \\ 0 \end{bmatrix} \eta \tag{5.102}$$

Premultiplying this equation by the inverse of the mass matrix results in the usual form of the state equation in terms of the concise derivatives

$$\begin{bmatrix} \dot{u} \\ \dot{w} \\ \dot{q} \\ \dot{\theta} \end{bmatrix} = \begin{bmatrix} -0.0352 & 0.1070 & 0 & -32.2 \\ -0.2140 & -0.4400 & 305 & 0 \\ 1.198 \times 10^{-4} & -0.0154 & -0.4498 & 0 \\ 0 & 0 & 1 & 0 \end{bmatrix} \begin{bmatrix} u \\ w \\ q \\ \theta \end{bmatrix} + \begin{bmatrix} 0 \\ -22.1206 \\ -4.6580 \\ 0 \end{bmatrix} \eta \tag{5.103}$$

or, in algebraic form,

$$\dot{\mathbf{x}}(t) = \mathbf{A}\mathbf{x}(t) + \mathbf{B}\mathbf{u}(t) \tag{5.104}$$

which defines the matrices **A** and **B** and the vectors $\mathbf{x}(t)$ and $\mathbf{u}(t)$. Using the computer software package *PC MATLAB* interactively the diagonal eigenvalue matrix is calculated

$$\begin{aligned} \mathbf{\Lambda} &= \begin{bmatrix} -0.4459 + 2.1644\text{j} & 0 & 0 & 0 \\ 0 & -0.4459 - 2.1644\text{j} & 0 & 0 \\ 0 & 0 & -0.0166 + 0.1474\text{j} & 0 \\ 0 & 0 & 0 & -0.0166 - 0.1474\text{j} \end{bmatrix} \\ &\equiv \begin{bmatrix} \lambda_s & 0 & 0 & 0 \\ 0 & \lambda_s^* & 0 & 0 \\ 0 & 0 & \lambda_p & 0 \\ 0 & 0 & 0 & \lambda_p^* \end{bmatrix} \end{aligned} \tag{5.105}$$

and the corresponding eigenvector matrix is calculated

$$\mathbf{V} = \begin{bmatrix} 0.0071 - 0.0067\text{j} & 0.0071 + 0.0067\text{j} & -0.9242 - 0.3816\text{j} & -0.9242 + 0.3816\text{j} \\ 0.9556 - 0.2944\text{j} & 0.9556 + 0.2944\text{j} & 0.0085 + 0.0102\text{j} & 0.0085 - 0.0102\text{j} \\ 0.0021 + 0.0068\text{j} & 0.0021 - 0.0068\text{j} & -0.0006 - 0.0002\text{j} & -0.0006 + 0.0002\text{j} \\ 0.0028 - 0.0015\text{j} & 0.0028 + 0.0015\text{j} & -0.0012 + 0.0045\text{j} & -0.0012 - 0.0045\text{j} \end{bmatrix} \tag{5.106}$$

λ_s, λ_p and their complex conjugates λ_s^*, λ_p^* are the eigenvalues corresponding to the short period pitching oscillation and the phugoid respectively. The corresponding matrix exponential is given by

$$e^{\mathbf{\Lambda}t} = \begin{bmatrix} e^{(-0.4459+2.1644\text{j})t} & 0 & 0 & 0 \\ 0 & e^{(-0.4459-2.1644\text{j})t} & 0 & 0 \\ 0 & 0 & e^{(-0.0166+0.1474\text{j})t} & 0 \\ 0 & 0 & 0 & e^{(-0.0166-0.1474\text{j})t} \end{bmatrix} \tag{5.107}$$

The eigenfunction matrix $\mathbf{V}e^{\mathbf{\Lambda}t}$ therefore has complex non-zero elements and each row describes the dynamic content of the state variable to which it relates. For example, the *first row* describes the dynamic content of the velocity perturbation u and comprises the following four elements

$$\left.\begin{aligned} &(0.0071 - 0.0067\text{j})e^{(-0.4459+2.1644\text{j})t} \\ &(0.0071 + 0.0067\text{j})e^{(-0.4459-2.1644\text{j})t} \\ &(-0.9242 - 0.3816\text{j})e^{(-0.0166+0.1474\text{j})t} \\ &(-0.9242 + 0.3816\text{j})e^{(-0.0166-0.1474\text{j})t} \end{aligned}\right\} \tag{5.108}$$

The first two elements in (5.108) describe the short period pitching oscillation

content in a velocity perturbation and the second two elements describe the phugoid content. The relative *magnitude* of the eigenvectors, the terms in parentheses, associated with the phugoid dynamics is the largest and clearly indicate that the phugoid dynamics is dominant in a velocity perturbation. The short period pitching oscillation, on the other hand, is barely visible. Obviously, this kind of observation can be made for all the state variables simply by inspection of the eigenvector and eigenvalue matrices only. This is a very useful facility for investigating the response properties of an aeroplane, especially when the behaviour is not conventional, when stability modes are obscured or when a significant degree of mode coupling is present.

When it is recalled that

$$e^{j\pi t} = \cos \pi t + j \sin \pi t \tag{5.109}$$

where π represents an arbitrary scalar variable, the velocity eigenfunctions (5.108) may be written alternatively

$$\left.\begin{aligned}
&(0.0071 - 0.0067j)e^{-0.4459t}(\cos 2.1644t + j \sin 2.1644t)\\
&(0.0071 + 0.0067j)e^{-0.4459t}(\cos 2.1644t - j \sin 2.1644t)\\
&(-0.9242 - 0.3816j)e^{-0.0166t}(\cos 0.1474t + j \sin 0.1474t)\\
&(-0.9242 + 0.3816j)e^{-0.0166t}(\cos 0.1474t - j \sin 0.1474t)
\end{aligned}\right\} \tag{5.110}$$

Since the elements in (5.110) include sine and cosine functions of time, the origins of the oscillatory response characteristics in the overall solution of the equations of motion are identified.

As described in Examples 5.2 and 5.3 the damping ratio and undamped natural frequency characterize the stability modes. This information comprises the eigenvalues, included in the matrix equation (5.105), and is interpreted as follows

(i) For the short period pitching oscillation, the higher frequency mode

$$\text{undamped natural frequency } \omega_s = 2.1644 \text{ rad/s}$$
$$\zeta_s\omega_s = 0.4459 \text{ rad/s}$$
$$\text{damping ratio } \zeta_s = 0.206$$

(ii) For the phugoid oscillation, the lower frequency mode

$$\text{undamped natural frequency } \omega_p = 0.1474 \text{ rad/s}$$
$$\zeta_p\omega_p = 0.0166 \text{ rad/s}$$
$$\text{damping ratio } \zeta_p = 0.1126$$

It is instructive to calculate the pitch attitude response to a unit elevator step input using the state space method for comparison with the method described in Example 5.3. The step response is given by equation (5.101) which, for zero initial conditions, a zero direct matrix **D** and output matrix **C** replaced with the identity matrix **I**, reduces to

$$\begin{aligned}
\mathbf{y}(t) &= \mathbf{I}\mathbf{V}e^{\Lambda t}\Lambda^{-1}\mathbf{V}^{-1}\mathbf{B}\mathbf{u}_k - \mathbf{I}\mathbf{A}^{-1}\mathbf{B}\mathbf{u}_k\\
&= \mathbf{V}e^{\Lambda t}\Lambda^{-1}\mathbf{V}^{-1}\mathbf{b} - \mathbf{A}^{-1}\mathbf{b}
\end{aligned} \tag{5.111}$$

since the single elevator input is a unit step $\mathbf{u}_k = 1$ and the input matrix **B** becomes the column matrix **b**. The expression on the right-hand side of equation (5.111) is a (4 × 1) column matrix the elements of which describe u, w, q and θ responses to the input. With the aid of *PC MATLAB* the following were calculated

$$\mathbf{\Lambda}^{-1}\mathbf{V}^{-1}\mathbf{b} = \begin{bmatrix} 147.36 + 19.07\mathrm{j} \\ 147.36 - 19.07\mathrm{j} \\ 223.33 - 133.29\mathrm{j} \\ 223.33 + 133.29\mathrm{j} \end{bmatrix} \qquad \mathbf{A}^{-1}\mathbf{b} = \begin{bmatrix} -512.2005 \\ 299.3836 \\ 0 \\ 1.5548 \end{bmatrix} \tag{5.112}$$

The remainder of the calculation of the first term on the right-hand side of equation (5.111) was completed by hand, an exercise which is definitely not recommended! Pitch attitude response is given by the fourth row of the resulting column matrix $\mathbf{y}(t)$ and is

$$\begin{aligned} \theta(t) = {} & 0.664\mathrm{e}^{-0.017t}(\cos 0.147t - 3.510 \sin 0.147t) \\ & + 0.882\mathrm{e}^{-0.446t}(\cos 2.164t + 0.380 \sin 2.164t) - 1.5548 \,\mathrm{deg} \end{aligned} \tag{5.113}$$

This equation compares very favourably with equation (5.32) and may be interpreted in exactly the same way.

This example is intended to illustrate the role of the various elements contributing to the solution and as such would not normally be undertaken on a routine basis. Machine computation simply produces the result in the most accessible form, which is usually graphical although the investigator can obtain additional information in much the same way as shown in this example.

5.7 State space model augmentation

It is frequently necessary to obtain response characteristics for variables that are not included in the equations of motion of the aeroplane. Provided that the variables of interest can be expressed as functions of the basic aeroplane motion variables then response transfer functions can be derived in the same way as the acceleration response transfer functions described in Section 5.5 above. However, when the additional transfer functions of interest are strictly proper they can also be obtained by extending, or *augmenting*, the state description of the aeroplane and solving in the usual way as described above. This latter course of action is extremely convenient as it extends the usefulness of the aeroplane state space model and requires little additional effort on behalf of the investigator.

For some additional variables, such as height, it is necessary to create a new state variable and to augment the state equation accordingly, whereas for others, such as flight path angle, which may be expressed as the simple sum of basic aeroplane state variables, it is only necessary to create an additional output variable and to augment the output equation accordingly. It is also a straightforward matter to augment the state description to include the additional dynamics of components such as engines and control surface actuators. In this case, all of the response transfer functions obtained in the solution of the equations of motion implicitly include the effects of the additional dynamics.

5.7.1 HEIGHT RESPONSE TRANSFER FUNCTION

An expression for height rate is given by equation (2.17) which, for small perturbations, may be written

$$\dot{h} = U\theta - V\phi - W \tag{5.114}$$

Substitute for (U, V, W) from equation (2.1) and note that for symmetric flight $V_e = 0$. Since the products of small quantities are insignificantly small they may be ignored and equation (5.114) may be written

$$\dot{h} = U_e\theta - W_e - w \tag{5.115}$$

With reference to Fig. 2.4, assuming α_e to be small then $U_e \cong V_0$, $W_e \cong 0$ and to a good approximation equation (5.114) may be written

$$\dot{h} = V_0\theta - w \tag{5.116}$$

The decoupled longitudinal state equation in concise form, equation (4.67), may be augmented to include the height variable by the inclusion of equation (5.116)

$$\begin{bmatrix} \dot{u} \\ \dot{w} \\ \dot{q} \\ \dot{\theta} \\ \dot{h} \end{bmatrix} = \begin{bmatrix} x_u & x_w & x_q & x_\theta & 0 \\ z_u & z_w & z_q & z_\theta & 0 \\ m_u & m_w & m_q & m_\theta & 0 \\ 0 & 0 & 1 & 0 & 0 \\ 0 & -w & 0 & V_0 & 0 \end{bmatrix} \begin{bmatrix} u \\ w \\ q \\ \theta \\ h \end{bmatrix} + \begin{bmatrix} x_\eta & x_\tau \\ z_\eta & z_\tau \\ m_\eta & m_\tau \\ 0 & 0 \\ 0 & 0 \end{bmatrix} \begin{bmatrix} \eta \\ \tau \end{bmatrix} \tag{5.117}$$

Alternatively, this may be written in a more compact form

$$\begin{bmatrix} \dot{\mathbf{x}}(t) \\ \cdots\cdots \\ \dot{h}(t) \end{bmatrix} = \left[\begin{array}{ccc:c} & \mathbf{A} & & \mathbf{0} \\ \hdashline 0 & -w & 0 & V_0 \quad 0 \end{array}\right] \begin{bmatrix} \mathbf{x}(t) \\ \cdots\cdots \\ h(t) \end{bmatrix} + \begin{bmatrix} \mathbf{B} \\ \cdots\cdots \\ 0 \quad 0 \end{bmatrix} \mathbf{u}(t) \tag{5.118}$$

where $\mathbf{x}(t)$ and $\mathbf{u}(t)$ are the state and input vectors respectively, and $\mathbf{A}$ and $\mathbf{B}$ are the state and input matrices respectively of the basic aircraft state equation (4.67). Solution of equation (5.118) to obtain the longitudinal response transfer functions will now result in two additional transfer functions describing the height response to an elevator perturbation and the height response to a thrust perturbation.

5.7.2 INCIDENCE AND SIDESLIP RESPONSE TRANSFER FUNCTIONS

We deal with the inclusion of incidence angle in the longitudinal decoupled equations of motion first. It follows from equation (2.5) that for small perturbation motion incidence α is given by

$$\alpha \cong \tan\alpha = \frac{w}{V_0} \tag{5.119}$$

since $U_e \to V_0$ as the perturbation tends to zero. Thus, incidence α is equivalent to normal velocity w divided by the steady free stream velocity. Incidence can be included in the longitudinal state equations in two ways. Either incidence can be added to the output vector $\mathbf{y}(t)$ without changing the state vector, or it can replace normal velocity w in the state vector. When the output equation is augmented the longitudinal state equations (4.67) and (4.68) are written

$$\dot{\mathbf{x}}(t) = \mathbf{A}\mathbf{x}(t) + \mathbf{B}\mathbf{u}(t)$$

$$\mathbf{y}(t) = \begin{bmatrix} u \\ w \\ q \\ \theta \\ \alpha \end{bmatrix} = \begin{bmatrix} 1 & 0 & 0 & 0 \\ 0 & 1 & 0 & 0 \\ 0 & 0 & 1 & 0 \\ 0 & 0 & 0 & 1 \\ 0 & 1/V_0 & 0 & 0 \end{bmatrix} \begin{bmatrix} u \\ w \\ q \\ \theta \end{bmatrix} = \begin{bmatrix} \mathbf{I} \\ \cdots\cdots\cdots\cdots \\ 0 \quad 1/V_0 \quad 0 \quad 0 \end{bmatrix} \mathbf{x}(t) \tag{5.120}$$

When normal velocity replaces incidence, it is first necessary to note that equation (5.119) may be differentiated to give $\dot{\alpha} = \dot{w}/V_0$. Thus, the longitudinal state equation (4.67) may be rewritten

$$\begin{bmatrix} \dot{u} \\ \dot{\alpha} \\ \dot{q} \\ \dot{\theta} \end{bmatrix} = \begin{bmatrix} x_u & x_w V_0 & x_q & x_\theta \\ z_u/V_0 & z_w & z_q/V_0 & z_\theta/V_0 \\ m_u & m_w V_0 & m_q & m_\theta \\ 0 & 0 & 1 & 0 \end{bmatrix} \begin{bmatrix} u \\ \alpha \\ q \\ \theta \end{bmatrix} + \begin{bmatrix} x_\eta & x_\tau \\ z_\eta/V_0 & z_\tau/V_0 \\ m_\eta & m_\tau \\ 0 & 0 \end{bmatrix} \begin{bmatrix} \eta \\ \tau \end{bmatrix} \tag{5.121}$$

The output equation (4.68) remains unchanged except that the output vector $\mathbf{y}(t)$ now includes α instead of w thus

$$\mathbf{y}^{\mathrm{T}}(t) = [u \quad \alpha \quad q \quad \theta] \tag{5.122}$$

In a similar way it is easily shown that in a lateral perturbation the sideslip angle β is given by

$$\beta \cong \tan\beta = \frac{v}{V_0} \tag{5.123}$$

and the lateral small perturbation equations can be modified in the same way as the longitudinal equations in order to incorporate sideslip angle β in the output equation or, alternatively, it may replace lateral velocity v in the state equation. When the output equation is augmented, the lateral state equations may be written

$$\dot{\mathbf{x}}(t) = \mathbf{A}\mathbf{x}(t) + \mathbf{B}\mathbf{u}(t)$$

$$\mathbf{y}(t) = \begin{bmatrix} v \\ p \\ r \\ \phi \\ \beta \end{bmatrix} = \begin{bmatrix} 1 & 0 & 0 & 0 \\ 0 & 1 & 0 & 0 \\ 0 & 0 & 1 & 0 \\ 0 & 0 & 0 & 1 \\ 1/V_0 & 0 & 0 & 0 \end{bmatrix} \begin{bmatrix} v \\ p \\ r \\ \phi \end{bmatrix} = \begin{bmatrix} \mathbf{I} \\ \cdots\cdots\cdots\cdots \\ 1/V_0 \quad 0 \quad 0 \quad 0 \end{bmatrix} \mathbf{x}(t) \tag{5.124}$$

where the lateral state equation is given by equation (4.70). When sideslip angle β replaces lateral velocity v in the lateral state equation (4.70), it is then written

$$\begin{bmatrix} \dot{\beta} \\ \dot{p} \\ \dot{r} \\ \dot{\phi} \end{bmatrix} = \begin{bmatrix} y_v & y_p/V_0 & y_r/V_0 & y_\phi/V_0 \\ l_v V_0 & l_p & l_r & l_\phi \\ n_v V_0 & n_p & n_r & n_\phi \\ 0 & 1 & 0 & 0 \end{bmatrix} \begin{bmatrix} \beta \\ p \\ r \\ \phi \end{bmatrix} + \begin{bmatrix} y_\xi/V_0 & y_\zeta/V_0 \\ l_\xi & l_\zeta \\ n_\xi & n_\zeta \\ 0 & 0 \end{bmatrix} \begin{bmatrix} \xi \\ \zeta \end{bmatrix} \tag{5.125}$$

Again, for this alternative, the lateral output vector $\mathbf{y}(t)$ remains unchanged except that sideslip angle β replaces lateral velocity v thus

$$\mathbf{y}^{\mathrm{T}}(t) = [\beta \quad p \quad r \quad \phi] \tag{5.126}$$

Solution of the longitudinal or lateral state equations will produce the transfer function matrix in the usual way. In every case, transfer functions will be calculated to correspond to the particular set of variables comprising the output vector.

5.7.3 FLIGHT PATH ANGLE RESPONSE TRANSFER FUNCTION

Sometimes flight path angle γ response to controls is required, especially when handling qualities in the approach flight condition are under consideration. Perturbations in flight path angle γ may be expressed in terms of perturbations in pitch attitude θ and incidence α, as indicated for the steady state case by equation (2.2), whence

$$\gamma = \theta - \alpha \cong \theta - \frac{w}{V_0} \tag{5.127}$$

Thus, the longitudinal output equation (4.68) may be augmented to include flight path angle as an additional output variable. The form of the longitudinal state equations is then similar to equations (5.120) and

$$\dot{\mathbf{x}}(t) = \mathbf{A}\mathbf{x}(t) + \mathbf{B}\mathbf{u}(t)$$

$$\mathbf{y}(t) = \begin{bmatrix} u \\ w \\ q \\ \theta \\ \gamma \end{bmatrix} = \left[\begin{array}{cccc} & & \mathbf{I} & \\ \hdashline 0 & -1/V_0 & 0 & 1 \end{array}\right] \mathbf{x}(t) \tag{5.128}$$

where the state vector $\mathbf{x}(t)$ remains unchanged

$$\mathbf{x}^{\mathrm{T}}(t) = [u \quad w \quad q \quad \theta] \tag{5.129}$$

5.7.4 ADDITION OF ENGINE DYNAMICS

Provided that the thrust producing devices can be modelled by a linear transfer function then, in general, it can be integrated into the aircraft state description. This then enables the combined engine and airframe dynamics to be modelled by the overall system response transfer functions. A very simple engine thrust model is described by equation (2.34), with transfer function

$$\frac{\tau(s)}{\varepsilon(s)} = \frac{k_\tau}{(1 + sT_\tau)} \tag{5.130}$$

where $\tau(t)$ is the thrust perturbation in response to a perturbation in throttle lever angle $\varepsilon(t)$. The transfer function equation (5.130) may be rearranged thus

$$s\tau(s) = \frac{k_\tau}{T_\tau}\varepsilon(s) - \frac{1}{T_\tau}\tau(s) \tag{5.131}$$

and this is the Laplace transform, assuming zero initial conditions, of the following time domain equation

$$\dot{\tau}(t) = \frac{k_\tau}{T_\tau}\varepsilon(t) - \frac{1}{T_\tau}\tau(t) \tag{5.132}$$

The longitudinal state equation (4.67) may be augmented to include the engine dynamics described by equation (5.132) which, after some rearrangement, may be written

$$\begin{bmatrix} \dot{u} \\ \dot{w} \\ \dot{q} \\ \dot{\theta} \\ \dot{\tau} \end{bmatrix} = \begin{bmatrix} x_u & x_w & x_q & x_\theta & x_\tau \\ z_u & z_w & z_q & z_\theta & z_\tau \\ m_u & m_w & m_q & m_\theta & m_\tau \\ 0 & 0 & 1 & 0 & 0 \\ 0 & 0 & 0 & 0 & -1/T_\tau \end{bmatrix} \begin{bmatrix} u \\ w \\ q \\ \theta \\ \tau \end{bmatrix} + \begin{bmatrix} x_\eta & 0 \\ z_\eta & 0 \\ m_\eta & 0 \\ 0 & 0 \\ 0 & k_\tau/T_\tau \end{bmatrix} \begin{bmatrix} \eta \\ \varepsilon \end{bmatrix} \tag{5.133}$$

Thus, the longitudinal state equation has been augmented to include thrust as an additional state and the second input variable is now throttle lever angle ε. The output equation (4.68) remains unchanged except that the **C** matrix is increased in order, to the (5 × 5) identity matrix **I**, in order to provide the additional output variable corresponding to the extra state variable τ.

The procedure described above in which a transfer function model of engine dynamics is converted to a form suitable for augmenting the state equation is known as *system realization*. More generally, relatively complex higher order transfer functions can be *realized* as state equations, although the procedure for so doing is rather more involved than that illustrated here for a particularly simple example. The mathematical methods required are described in most books on modern control theory. The advantage and power of this relatively straightforward procedure is very considerable since it literally enables the state equation describing a very complex system, such as an aircraft with advanced flight controls, to be built by repeated augmentation. The state descriptions of the various system components are simply added to the matrix state equation until the overall system dynamics is fully represented. Typically, this might mean, for example, that the basic longitudinal or lateral (4 × 4) airframe state matrix might be augmented to a much higher order of perhaps (12 × 12) or more, depending on the complexity of the engine model, control system, surface actuators and so on. However, whatever the result the equations are easily solved using the tools described above.

EXAMPLE 5.8

To illustrate the procedure for augmenting an aeroplane state model, let the longitudinal model for the Lockheed F-104 Starfighter of Example 5.2 be augmented to include height h and flight path angle γ and to replace normal velocity w with incidence α. The longitudinal state equation expressed in terms of concise derivatives is given by equation (5.103) and this is modified in accordance with equation (5.121) to replace normal velocity w with incidence α

$$\begin{bmatrix} \dot{u} \\ \dot{\alpha} \\ \dot{q} \\ \dot{\theta} \end{bmatrix} = \begin{bmatrix} -0.0352 & 32.6342 & 0 & -32.2 \\ -7.016 \times 10^{-4} & -0.4400 & 1 & 0 \\ 1.198 \times 10^{-4} & -4.6829 & -0.4498 & 0 \\ 0 & 0 & 1 & 0 \end{bmatrix} \begin{bmatrix} u \\ \alpha \\ q \\ \theta \end{bmatrix} + \begin{bmatrix} 0 \\ -0.0725 \\ -4.6580 \\ 0 \end{bmatrix} \eta \tag{5.134}$$

Equation (5.134) is now augmented by the addition of equation (5.104), the height equation expressed in terms of incidence α and pitch attitude θ

$$\dot{h} = V_0(\theta - \alpha) = 305\theta - 305\alpha \tag{5.135}$$

whence, the augmented state equation is written

$$\begin{bmatrix} \dot{u} \\ \dot{\alpha} \\ \dot{q} \\ \dot{\theta} \\ \dot{h} \end{bmatrix} = \begin{bmatrix} -0.0352 & 32.6342 & 0 & -32.2 & 0 \\ -7.016 \times 10^{-4} & -0.4400 & 1 & 0 & 0 \\ 1.198 \times 10^{-4} & -4.6829 & -0.4498 & 0 & 0 \\ 0 & 0 & 1 & 0 & 0 \\ 0 & -305 & 0 & 305 & 0 \end{bmatrix} \begin{bmatrix} u \\ \alpha \\ q \\ \theta \\ h \end{bmatrix} + \begin{bmatrix} 0 \\ -0.0725 \\ -4.6580 \\ 0 \\ 0 \end{bmatrix} \eta \tag{5.136}$$

The corresponding output equation is augmented to included flight path angle γ as given by equation (5.116) and is then written

$$\begin{bmatrix} u \\ \alpha \\ q \\ \theta \\ h \\ \gamma \end{bmatrix} = \begin{bmatrix} 1 & 0 & 0 & 0 & 0 \\ 0 & 1 & 0 & 0 & 0 \\ 0 & 0 & 1 & 0 & 0 \\ 0 & 0 & 0 & 1 & 0 \\ 0 & 0 & 0 & 0 & 1 \\ 0 & -1 & 0 & 1 & 0 \end{bmatrix} \begin{bmatrix} u \\ \alpha \\ q \\ \theta \\ h \end{bmatrix} \tag{5.137}$$

This, of course, assumes the direct matrix **D** to be zero as discussed above. Equations (5.136) and (5.137) together provide the complete state description of the Lockheed F-104 as required. Solving these equations with the aid of *Program CC* results in the six transfer functions describing the response to elevator.

(i) The common denominator polynomial (the characteristic polynomial) is given by

$$\Delta(s) = s(s^2 + 0.033s + 0.022)(s^2 + 0.892s + 4.883) \tag{5.138}$$

(ii) The numerator polynomials are given by

$$\begin{aligned} N_\eta^u(s) &= -2.367s(s - 4.215)(s + 5.519)\,\text{ft/s/rad} \\ N_\eta^\alpha(s) &= -0.073s(s + 64.675)(s^2 + 0.035s + 0.023)\,\text{rad/rad} \\ N_\eta^q(s) &= -4.658s^2(s + 0.134)(s + 0.269)\,\text{rad/s/rad} \\ N_\eta^\theta(s) &= -4.658s(s + 0.134)(s + 0.269)\,\text{rad/rad} \\ N_\eta^h(s) &= 22.121(s + 0.036)(s - 4.636)(s + 5.085)\,\text{ft/rad} \\ N_\eta^\gamma(s) &= 0.073s(s + 0.036)(s - 4.636)(s + 5.085)\,\text{rad/rad} \end{aligned} \tag{5.139}$$

Note that the additional zero pole in the denominator is due to the increase in order of the state equation from four to five and represents the *height integration*. This is easily interpreted since an elevator step input will cause the aeroplane to climb or descend steadily after the transient has died away when the response becomes similar to that of a simple integrator. Note also that the denominator zero cancels with a zero in all numerator polynomials except that describing the height response. Thus, the response transfer functions describing the basic aircraft motion variables u, α, q and θ are identically the same as those obtained from the basic fourth order state equations. The reason for the similarity between the height and flight path angle response numerators becomes obvious if the expression for the height equation (5.135) is compared with the expression for flight path angle, equation (5.116).

References

Auslander, D. M., Takahashi, Y. and Rabins, M. J. 1974: *Introducing Systems and Control.* McGraw-Hill Kogakusha Ltd, Tokyo.

Barnett, S. 1975: *Introduction to Mathematical Control Theory.* Clarendon Press, Oxford.

Duncan, W. J. 1959: *The Principles of the Control and Stability of Aircraft.* Cambridge University Press, Cambridge.

Goult, R. J., Hoskins, R. F., Milner, J. A. and Pratt, M. J. 1974: *Computational Methods in Linear Algebra.* Stanley Thornes (Publishers) Ltd, London.

Heffley, R. K. and Jewell, W. F. 1972: *Aircraft Handling Qualities Data.* NASA Contractor Report, NASA CR-2144.

Owens, D.H. 1981: *Multivariable and Optimal Systems.* Academic Press, London.

Shinners, S. M. 1980: *Modern Control System Theory and Application.* Addison-Wesley Publishing Co, Reading, Massachusetts.

Teper, G. L. 1969: *Aircraft Stability and Control Data.* Systems Technology, Inc, STI Technical Report 176-1.

6

Longitudinal Dynamics

6.1 Response to controls

The solution of the longitudinal equations of motion by, for example, the methods described in Chapter 5 enables the response transfer functions to be obtained. These completely describe the linear dynamic response to a control input in the plane of symmetry. Implicit in the response are the dynamic properties determined by the stability characteristics of the aeroplane. The transfer functions and the response variables described by them are linear since the entire modelling process is based on the assumption that the motion is constrained to small disturbances about an equilibrium trim state. However, it is common practice to assume that the response to controls is valid when the magnitude of the response can hardly be described as 'a small perturbation'. For many conventional aeroplanes the error incurred by so doing is generally acceptably small, as such aeroplanes tend to have substantially linear aerodynamic characteristics over their flight envelopes. For aeroplanes with very large flight envelopes, significant aerodynamic non-linearity and/or dependence on sophisticated flight control systems, it is advisable not to use the linearized equations of motion for analysis of response other than that which can justifiably be described as being of small magnitude.

It is convenient to review the longitudinal response to elevator about a trim state in which the thrust is held constant. The longitudinal state equation (4.67) may then be written

$$\begin{bmatrix} \dot{u} \\ \dot{w} \\ \dot{q} \\ \dot{\theta} \end{bmatrix} = \begin{bmatrix} x_u & x_w & x_q & x_\theta \\ z_u & z_w & z_q & z_\theta \\ m_u & m_w & m_q & m_\theta \\ 0 & 0 & 1 & 0 \end{bmatrix} \begin{bmatrix} u \\ w \\ q \\ \theta \end{bmatrix} + \begin{bmatrix} x_\eta \\ z_\eta \\ m_\eta \\ 0 \end{bmatrix} \eta \tag{6.1}$$

The four response transfer functions obtained in the solution of equation (6.1) may conveniently be written

$$\frac{u(s)}{\eta(s)} \equiv \frac{N_\eta^u(s)}{\Delta(s)} = \frac{k_u(s + 1/T_u)(s^2 + 2\zeta_u\omega_u s + \omega_u^2)}{(s^2 + 2\zeta_p\omega_p s + \omega_p^2)(s^2 + 2\zeta_s\omega_s s + \omega_s^2)} \tag{6.2}$$

$$\frac{w(s)}{\eta(s)} \equiv \frac{N_\eta^w(s)}{\Delta(s)} = \frac{k_w(s+1/T_\alpha)(s^2+2\zeta_\alpha\omega_\alpha s+\omega_\alpha^2)}{(s^2+2\zeta_p\omega_p s+\omega_p^2)(s^2+2\zeta_s\omega_s+\omega_s^2)} \tag{6.3}$$

$$\frac{q(s)}{\eta(s)} \equiv \frac{N_\eta^q(s)}{\Delta(s)} = \frac{k_q s(s+1/T_{\theta_1})(s+1/T_{\theta_2})}{(s^2+2\zeta_p\omega_p s+\omega_p^2)(s^2+2\zeta_s\omega_s s+\omega_s^2)} \tag{6.4}$$

$$\frac{\theta(s)}{\eta(s)} \equiv \frac{N_\eta^\theta(s)}{\Delta(s)} = \frac{k_\theta(s+1/T_{\theta_1})(s+1/T_{\theta_2})}{(s^2+2\zeta_p\omega_p s+\omega_p^2)(s^2+2\zeta_s\omega_s s+\omega_s^2)} \tag{6.5}$$

The solution of the equations of motion results in polynomial descriptions of the transfer function numerators and common denominator as set out in Appendix 2. The polynomials factorize into real and complex pairs of roots which are most explicitly quoted in the style of equations (6.2) to (6.5) above. Since the roots are interpreted as time constants, damping ratios and natural frequencies, the above style of writing makes the essential information instantly available. It should also be noted that the numerator and denominator factors are typical for a conventional aeroplane. Sometimes complex pairs of roots may become two real roots and vice versa. However, this does not usually mean that the dynamic reponse characteristics of the aeroplane become dramatically different. Differences in the interpretation of response may be evident but will not necessarily be large.

As has already been indicated, the common denominator of the transfer functions describes the characteristic polynomial which, in turn, describes the stability characteristics of the aeroplane. Thus, the response of all variables to an elevator input is dominated by the denominator parameters, namely, damping ratios and natural frequencies. The differences between the individual responses are entirely determined by their respective numerators. It is therefore important to appreciate fully the role of the numerator in determining response dynamics. The *response shapes* of the individual variables are determined by the common denominator and 'coloured' by their respective numerators. The numerator plays no part in determining stability in a linear system which is how the aeroplane is modelled here.

EXAMPLE 6.1

The equations of motion and aerodynamic data for the Ling-Temco-Vought A-7A Corsair II aircraft were obtained from Teper (1969). The flight condition corresponds to level cruising flight at an altitude of 15 000 ft at Mach 0.3. The equations of motion, referred to a body axis system, arranged in state space format are

$$\begin{bmatrix} \dot{u} \\ \dot{w} \\ \dot{q} \\ \dot{\theta} \end{bmatrix} = \begin{bmatrix} 0.00501 & 0.00464 & -72.90000 & -31.34000 \\ -0.08570 & -0.54500 & 309.00000 & -7.40000 \\ 0.00185 & -0.00767 & -0.39500 & 0.00132 \\ 0 & 0 & 1 & 0 \end{bmatrix} \begin{bmatrix} u \\ w \\ q \\ \theta \end{bmatrix} + \begin{bmatrix} 5.63000 \\ -23.80000 \\ -4.51576 \\ 0 \end{bmatrix} \eta \tag{6.6}$$

Since incidence α and flight path angle γ are useful variables in the evaluation of handling qualities, it is convenient to augment the corresponding output equation, as described in Section 5.7, in order to obtain their response transfer functions in the solution of the equations of motion. The output equation is therefore

$$\begin{bmatrix} u \\ w \\ q \\ \theta \\ \alpha \\ \gamma \end{bmatrix} = \begin{bmatrix} 1 & 0 & 0 & 0 \\ 0 & 1 & 0 & 0 \\ 0 & 0 & 1 & 0 \\ 0 & 0 & 0 & 1 \\ 0 & 0.00316 & 0 & 0 \\ 0 & -0.00316 & 0 & 1 \end{bmatrix} \begin{bmatrix} u \\ w \\ q \\ \theta \end{bmatrix} + \begin{bmatrix} 0 \\ 0 \\ 0 \\ 0 \\ 0 \\ 0 \end{bmatrix} \eta \tag{6.7}$$

Note that all elements in the matrices in equations (6.6) and (6.7) have been rounded to five decimal places simply to keep the equations to a reasonable physical size. This should not be done with the equations used in the actual computation.

Solution of the equations of motion using *Program CC* determines the following response transfer functions

$$\begin{aligned}
\frac{u(s)}{\eta(s)} &= \frac{5.63(s+0.369)(s+0.587)(s+58.437)}{(s^2+0.033s+0.020)(s^2+0.902s+2.666)} \text{ ft/s/rad} \\
\frac{w(s)}{\eta(s)} &= \frac{-23.8(s^2-0.0088s+0.0098)(s+59.048)}{(s^2+0.033s+0.020)(s^2+0.902s+2.666)} \text{ ft/s/rad} \\
\frac{q(s)}{\eta(s)} &= \frac{-4.516s(s-0.008)(s+0.506)}{(s^2+0.033s+0.020)(s^2+0.902s+2.666)} \text{ rad/s/rad(deg/s/deg)} \\
\frac{\theta(s)}{\eta(s)} &= \frac{-4.516(s-0.008)(s+0.506)}{(s^2+0.033s+0.020)(s^2+0.902s+2.666)} \text{ rad/rad(deg/deg)} \\
\frac{\alpha(s)}{\eta(s)} &= \frac{-0.075(s^2-0.0088s+0.0098)(s+59.048)}{(s^2+0.033s+0.020)(s^2+0.902s+2.666)} \text{ rad/rad(deg/deg)} \\
\frac{\gamma(s)}{\eta(s)} &= \frac{0.075(s-0.027)(s+5.004)(s-6.084)}{(s^2+0.033s+0.020)(s^2+0.902s+2.666)} \text{ rad/rad(deg/deg)}
\end{aligned} \tag{6.8}$$

All coefficients have again been rounded to a convenient number of decimal places and the above caution should be noted.

The characteristic equation is given by equating the common denominator polynomial to zero

$$\Delta(s) = (s^2+0.033s+0.020)(s^2+0.902s+2.666) = 0$$

The first pair of complex roots describes the phugoid stability mode with characteristics

$$\text{damping ratio } \zeta_p = 0.11$$
$$\text{undamped natural frequency } \omega_p = 0.14 \text{ rad/s}$$

The second pair of complex roots describes the short period pitching oscillation, or short period stability mode, with characteristics

$$\text{damping ratio } \zeta_s = 0.28$$
$$\text{undamped natural frequency } \omega_s = 1.63 \text{ rad/s}$$

These mode characteristics indicate that the airframe is aerodynamically stable although it will be shown later that the short period mode damping ratio is unacceptably low.

The response of the aircraft to a unit step (1°) elevator input is shown in Fig. 6.1.

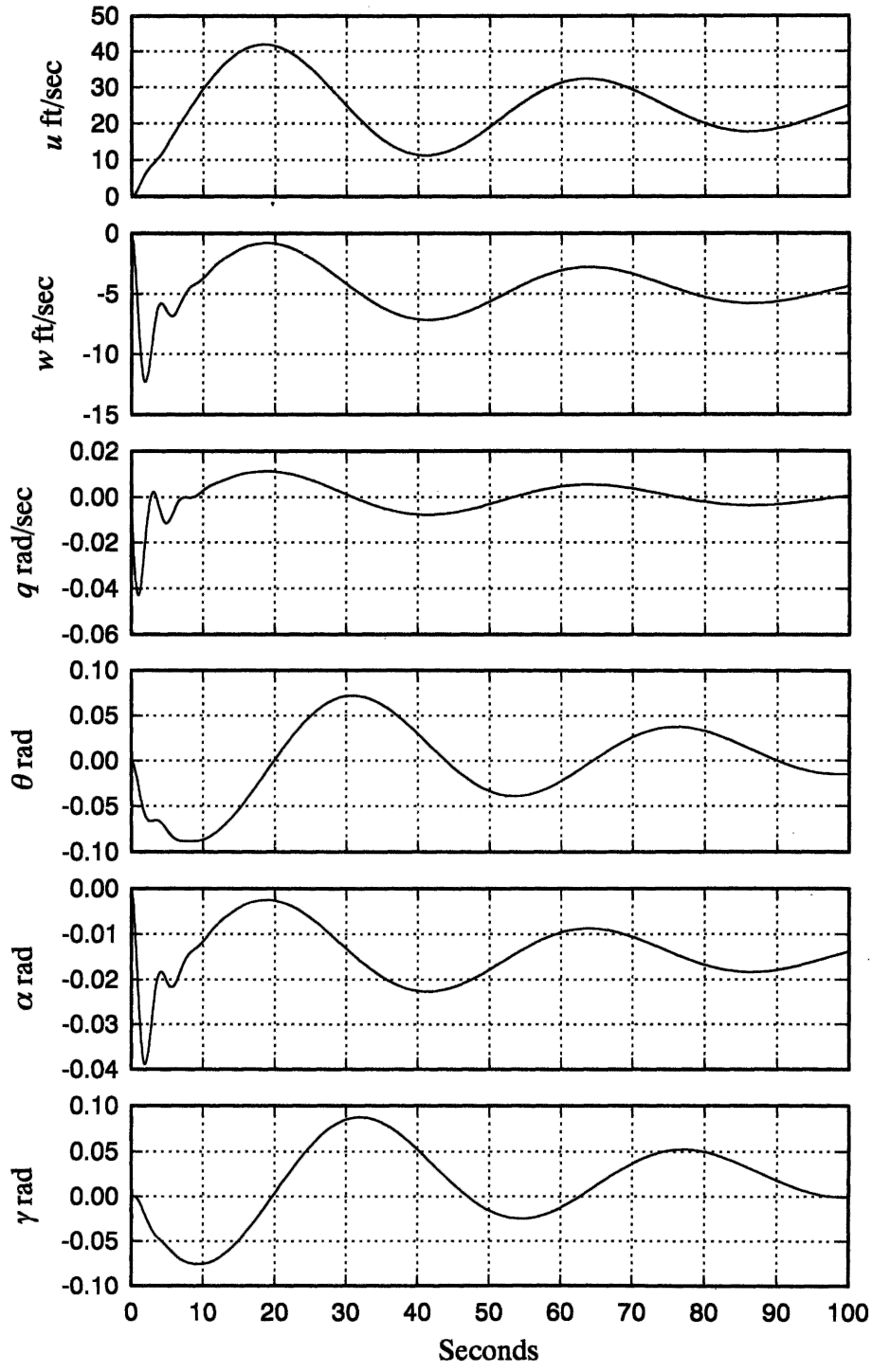

Fig. 6.1 Aircraft response to 1° elevator step input

All of the variables in the solution of the equations of motion are shown, the responses being characterized by the transfer functions, equations (6.8).

The responses clearly show both dynamic stability modes, the short period pitching oscillation and the phugoid. However, the magnitude of each stability mode differs in each response variable. For example, the short period pitching oscillation is most visible as the initial transient in the variables w, q and α, whereas the phugoid mode is visible in all variables although the relative magnitudes vary considerably. Clearly, the stability of the responses is the same, as determined by the common denominator of the transfer functions, equations (6.8), but the differences between each of the response variables are determined by the unique numerator of each response transfer function.

The mode content in each of the motion variables is given most precisely by the eigenvectors. The analytical procedure described in Example 5.7 is applied to the equations of motion for the A-7A. With the aid of *PC MATLAB* the eigenvector matrix $\mathbf{V}$ is determined as follows

$$\mathbf{V} = \begin{matrix} \text{short period mode} & & \text{phugoid mode} & \\ \end{matrix}$$

$$\begin{bmatrix} -0.1682 - 0.1302\text{j} & -0.1682 + 0.1302\text{j} & 0.1467 + 0.9677\text{j} & 0.1467 - 0.9677\text{j} \\ 0.2993 + 0.9301\text{j} & 0.2993 - 0.9301\text{j} & 0.0410 + 0.2008\text{j} & 0.0410 - 0.2008\text{j} \\ -0.0046 + 0.0018\text{j} & -0.0046 - 0.0018\text{j} & 0.0001 + 0.0006\text{j} & 0.0001 - 0.0006\text{j} \\ 0.00019 + 0.0024\text{j} & 0.0019 - 0.0024\text{j} & 0.0041 - 0.0013\text{j} & 0.0041 + 0.0013\text{j} \end{bmatrix} \begin{matrix} : u \\ : w \\ : q \\ : \theta \end{matrix} \tag{6.9}$$

To facilitate interpretation of the eigenvector matrix, the magnitude of each component eigenvector is calculated as follows

$$\begin{bmatrix} 0.213 & 0.213 & 0.979 & 0.979 \\ 0.977 & 0.977 & 0.204 & 0.204 \\ 0.0049 & 0.0049 & 0.0006 & 0.0006 \\ 0.0036 & 0.0036 & 0.0043 & 0.0043 \end{bmatrix} \begin{matrix} : u \\ : w \\ : q \\ : \theta \end{matrix}$$

Clearly, the phugoid mode is dominant in u since $0.979 \gg 0.213$, the short period mode is dominant in w since $0.977 \gg 0.204$, the short period mode is dominant in q since $0.0049 \gg 0.0006$ and the short period and phugoid modes content in θ are of similar order. These observations accord very well with the responses shown in Fig. 6.1.

The steady state values of the variables following a unit step (1°) elevator input may be determined by application of the final value theorem, equation (5.33). The transfer functions, equations (6.8), assume a unit elevator displacement to mean 1 rad and this has transfer function

$$\eta(s) = \frac{1}{s} \text{ rad}$$

For a unit step input of 1° the transfer function becomes

$$\eta(s) = \frac{1}{57.3s} = \frac{0.0175}{s} \text{ rad}$$

Thus, for example, the Laplace transform of the speed response to a 1° elevator step input is given by

$$u(s) = \frac{5.63(s + 0.369)(s + 0.587)(s + 58.437)}{(s^2 + 0.033s + 0.020)(s^2 + 0.902s + 2.666)} \frac{0.0175}{s} \text{ ft/s}$$

Applying the final value theorem, equation (5.33)

$$u(t)|_{ss} = \lim_{s\to 0}\left(s\frac{5.63(s+0.369)(s+0.587)(s+58.437)}{(s^2+0.033s+0.020)(s^2+0.902s+2.666)}\frac{0.0175}{s}\right)\text{ft/s} = 23.39\,\text{ft/s}$$

Since the step input is positive in the nose down sense the response eventually settles to the small steady increase in speed indicated.

In a similar way, the steady state response of all the motion variables may be calculated to give

$$\begin{bmatrix} u \\ w \\ q \\ \theta \\ \alpha \\ \gamma \end{bmatrix}_{\text{steady state}} = \begin{bmatrix} 23.39\,\text{ft/s} \\ -4.53\,\text{ft/s} \\ 0 \\ 0.34\,\text{deg} \\ -0.81\,\text{deg} \\ 1.15\,\text{deg} \end{bmatrix} \tag{6.10}$$

It is important to remember that the steady state values given in equation (6.10) represent the *changes* with respect to the initial equilibrium trim state following the 1° elevator step input. Although the initial response is applied in the nose down sense, inspection of equation (6.10) indicates that after the mode transients have damped out the aircraft is left with a small reduction in incidence, a small increase in pitch attitude and is climbing steadily at a flight path angle of 1.15°. This apparent anomaly is due to the fact that at the chosen flight condition the aircraft is operating close to the stall boundary on the *back side* of the drag-speed curve, i.e. below the minimum drag speed. Thus, the disturbance results in a significant decrease in drag leaving the aircraft with sufficient excess power enabling it to climb gently. It is for the same reason that a number of the transfer functions, equations (6.8), have non-minimum phase numerator terms where these would not normally be expected.

6.1.1 THE CHARACTERISTIC EQUATION

The longitudinal characteristic polynomial for a classical aeroplane is fourth order, it determines the common denominator in the longitudinal response transfer functions and, when equated to zero, defines the characteristic equation which may be written

$$As^4 + Bs^3 + Cs^2 + Ds + E = 0 \tag{6.11}$$

The characteristic equation (6.11) most commonly factorizes into two pairs of complex roots which are most conveniently written

$$(s^2 + 2\zeta_p\omega_p s + \omega_p^2)(s^2 + 2\zeta_s\omega_s s + \omega_s^2) = 0 \tag{6.12}$$

As already explained, the second order characteristics in equation (6.12) describe the phugoid and short period stability modes respectively. The stability modes comprising equation (6.12) provide a *complete description* of the longitudinal stability properties of the aeroplane subject to the constraint of small perturbation motion. Interpretation of the characteristic equation written in this way is most readily accomplished if reference is first made to the properties of the classical mechanical mass–spring–damper system, which are summarized in Appendix 5.

Thus, the longitudinal dynamics of the aeroplane may be likened to a pair of loosely

coupled mass–spring–damper systems, and the interpretation of the motion of the aeroplane following a disturbance from equilibrium may be made by direct comparison with the behaviour of the mechanical mass–spring–damper. However, the damping and frequency characteristics of the aeroplane are obviously not mechanical in origin; they derive entirely from the aerodynamic properties of the airframe. The connection between the observed dynamics of the aeroplane and its aerodynamic characteristics is made by comparing equation (6.12) with equation (6.11) and then referring to Appendix 2 for the definitions of the coefficients in equation (6.11) in terms of aerodynamic stability derivatives. Clearly, the relationships between the damping ratios and undamped frequencies of equation (6.12) and their aerodynamic *drivers* is neither obvious nor simple. Means for dealing with this difficulty are described below in which simplifying approximations are made based on the observation and understanding of the physical behaviour of aeroplane dynamics.

6.2 The dynamic stability modes

Both longitudinal dynamic stability modes are excited whenever the aeroplane is disturbed from its equilibrium trim state. A disturbance may be initiated by pilot control inputs, a change in power setting, airframe configuration changes such as flap deployment and by external atmospheric influences such as gusts and turbulence.

6.2.1 THE SHORT PERIOD PITCHING OSCILLATION

The short period mode is typically a damped oscillation in pitch about the oy axis. Whenever an aircraft is disturbed from its pitch equilibrium state the mode is excited and manifests itself as a classical second order oscillation in which the principal variables are incidence $\alpha(w)$, pitch rate q and pitch attitude θ. This observation is easily confirmed by reference to the eigenvectors in the solution of the equations of motion; this may be seen in Example 6.1 and also in Fig. 6.1. Typically, the undamped natural frequency of the mode is in the range 1 rad/s to 10 rad/s and the damping is usually stabilizing although the damping ratio is often lower than desired. A significant feature of the mode is that the speed remains approximately constant ($u = 0$) during a disturbance. As the period of the mode is short, inertia and momentum effects ensure that speed response in the time scale of the mode is negligible.

The physical situation applying can be interpreted by comparison with a torsional mass–spring–damper system. The aircraft behaves as if it were restrained by a torsional spring about the oy axis as indicated in Fig. 6.2. A pitch disturbance from trim equilibrium causes the 'spring' to produce a restoring moment thereby giving rise to an oscillation in pitch. The oscillation is damped and this can be interpreted as a viscous damper as suggested in Fig. 6.2. Of course the spring and viscous damping effects are not mechanical. In reality they are produced entirely by aerodynamic mechanisms with contributions from all parts of the airframe, not all of which are necessarily stabilizing in effect. However, in the interests of promoting understanding, the stiffness and damping effects are assumed to be dominated by the aerodynamics of the tailplane.

The spring stiffness arises from the natural *weathercock* tendency of the tailplane to align with the incident flow. The damping arises from the motion of the tailplane during the oscillation when, clearly, it behaves as a kind of viscous paddle damper. The total observed mode dynamics depends not only on the tailplane contribution, but also on the

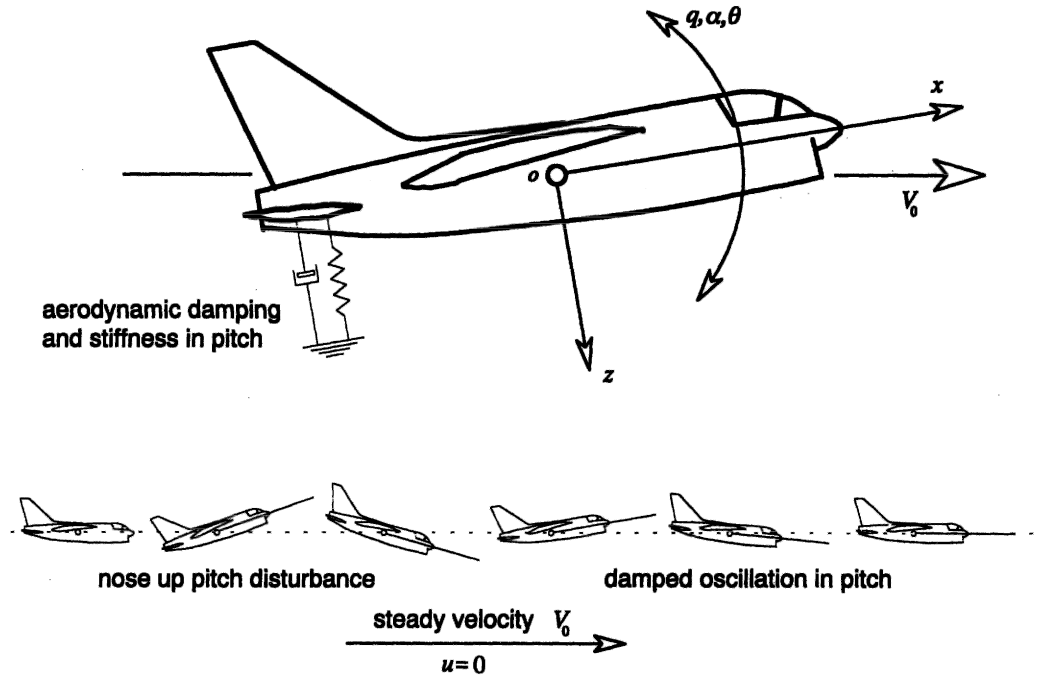

Fig. 6.2 A stable short period pitching oscillation

magnitudes of the additional contributions from other parts of the airframe. When the overall stability is marginal it is implied that the additional contributions are also significant and it becomes much more difficult to identify and quantify the principal aerodynamic mode drivers.

6.2.2 THE PHUGOID

The phugoid mode is most commonly a lightly damped low frequency oscillation in speed u which couples into pitch attitude θ and height h. A significant feature of this mode is that the incidence $\alpha(w)$ remains substantially constant during a disturbance. Again, these observations are easily confirmed by reference to the eigenvectors in the solution of the equations of motion; this may be seen in Example 6.1 and also in Fig.

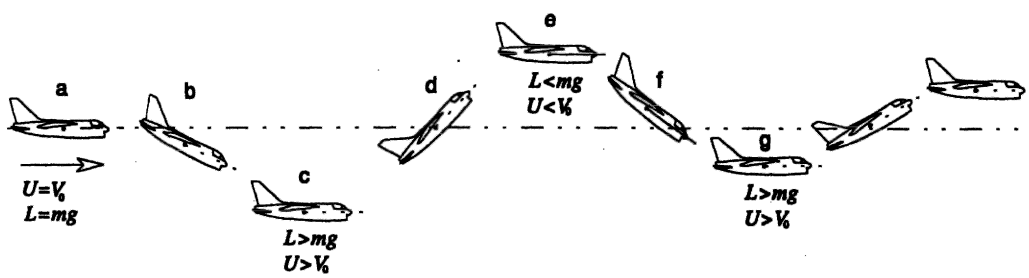

Fig. 6.3 The development of a stable phugoid

6.1. However, it is clear that the phugoid appears, to a greater or lesser extent, in all of the longitudinal motion variables, but the relative magnitudes of the phugoid components in incidence $\alpha(w)$ and in pitch rate q are very small. Typically, the undamped natural frequency of the phugoid is in the range 0.1 rad/s to 1 rad/s and the damping ratio is very low. However, the apparent damping characteristics of the mode may be substantially influenced by power effects in some aeroplanes.

Consider the development of classical phugoid motion following a small disturbance in speed as illustrated on Fig. 6.3. Initially, the aeroplane is in trimmed level equilibrium flight with steady velocity V_0 such that the lift L and weight mg are equal. Let the aeroplane be disturbed at (a) such that the velocity is reduced by a small amount u. Since the incidence remains substantially constant this results in a small reduction in lift such that the aeroplane is no longer in vertical equilibrium. It therefore starts to lose height and since it is flying 'down hill' it starts to accelerate as at (b). The speed continues to build up to a value in excess of V_0, which is accompanied by a build up in lift which eventually exceeds the weight by a significant margin. The build up in speed and lift cause the aircraft to pitch up steadily until at (c) it starts to climb. Since it now has an excess of kinetic energy, inertia and momentum effects cause it to fly up through the nominal trimmed height datum at (d) losing speed and lift as it goes, as it is now flying 'up hill'. As it decelerates, it pitches down steadily until at (e) its lift is significantly less than the weight and the accelerating descent starts again. Inertia and momentum effects cause the aeroplane to continue flying down through the nominal trimmed height datum (f) and as the speed and lift continue to build up so it pitches up steadily until at (g) it starts climbing again to commence the next cycle of oscillation. As the motion progresses the effects of drag cause the motion variable maxima and minima at each peak to reduce gradually in magnitude until the motion eventually damps out.

Thus, the phugoid is classical damped harmonic motion resulting in the aircraft flying a gentle sinusoidal flight path about the nominal trimmed height datum. As large inertia and momentum effects are involved, the motion is necessarily relatively slow such that the angular accelerations, $\dot{q}$ and $\dot{\alpha}(\dot{w})$, are insignificantly small. Consequently, the natural frequency of the mode is low and since drag is designed to be low so the damping is also low. Typically, once excited, many cycles of the phugoid may be visible before it eventually damps out. Since the rate of loss of energy is low, a consequence of low drag damping effects, the motion is often approximated by undamped harmonic motion in which potential and kinetic energy are exchanged as the aircraft flies the sinusoidal flight path. This, in fact, was the basis on which Lanchester (1908) first successfully analysed the motion.

6.3 Reduced order models

Thus far, the emphasis has been on the exact solution of the longitudinal equations of motion, which results in an exact description of the stability and response characteristics of the aircraft. Although this is usually the object of a flight dynamics investigation it has two disadvantages. Firstly, a computational facility is required if a very tedious manual solution is to be avoided and, secondly, it is difficult, if not impossible, to establish the relationships between the stability characteristics and their aerodynamic drivers. Both of these disadvantages can be avoided by seeking approximate solutions, which can also provide considerable insight into the physical phenomena governing the dynamic behaviour of the aircraft.

For example, an approximate solution of the longitudinal characteristic equation (6.11) is based on the fact that the coefficients A, B, C, D and E have relative values which do not change very much for conventional aeroplanes. Generally, A, B and C are significantly larger than D and E such that the quartic has the following approximate factors

$$A\left(s^2+\frac{(CD-BE)}{C^2}s+\frac{E}{C}\right)\left(s^2+\frac{B}{A}s+\frac{C}{A}\right)=0 \tag{6.13}$$

Equation (6.13) is in fact the first step in the classical manual iterative solution of the quartic, the first pair of complex roots describes the phugoid and the second pair describes the short period mode. Algebraic expressions, in terms of aerodynamic derivatives, mass and inertia parameters, etc, for the coefficients A, B, C, D and E are given in Appendix 1. Since these expressions are relatively complex, further physical insight is not particularly revealing unless simplifying assumptions are made. However, the approximate solution given by equation (6.13) is often useful for preliminary mode evaluations, or as a check of computer solutions, when the numerical values of the coefficients A, B, C, D and E are known. For conventional aeroplanes, the approximate solution is often surprisingly close to the exact solution of the characteristic equation.

6.3.1 THE SHORT PERIOD MODE APPROXIMATION

The short term response characteristics of an aircraft are of particular importance in flying and handling qualities considerations, for the reasons stated in Section 6.5. Since short term behaviour is dominated by the short period mode it is convenient to obtain the *reduced order* equations of motion in which the phugoid is suppressed or omitted. By observing the nature of the short period pitching oscillation, sometimes called the *rapid incidence adjustment*, it is possible to simplify the longitudinal equations of motion to describe short term dynamics only. The terms remaining in the reduced order equations of motion are therefore the terms that dominate short term dynamics, thereby providing insight into the important aerodynamic drivers governing physical behaviour.

It has already been established that the short period pitching oscillation is almost exclusively an oscillation in which the principal variables are pitch rate q and incidence α, the speed remaining essentially constant, thus $u=0$. Therefore, the speed equation and the speed-dependent terms may be removed from the longitudinal equations of motion (6.1) since they are all approximately zero in short term motion, and the revised equations may be written

$$\begin{bmatrix}\dot{w}\\ \dot{q}\\ \dot{\theta}\end{bmatrix}=\begin{bmatrix}z_w & z_q & z_\theta\\ m_w & m_q & m_\theta\\ 0 & 1 & 1\end{bmatrix}\begin{bmatrix}w\\ q\\ \theta\end{bmatrix}+\begin{bmatrix}z_\eta\\ m_\eta\\ 0\end{bmatrix}\eta \tag{6.14}$$

Further, assuming the equations of motion are referred to aircraft wind axes and that the aircraft is initially in steady level flight then

$$\theta_e \equiv \alpha_e = 0 \quad \text{and} \quad U_e = V_0$$

and, with reference to Appendix 1, it follows that

$$z_\theta = m_\theta = 0$$

Equation (6.14) then reduces to its simplest possible form

$$\begin{bmatrix} \dot{w} \\ \dot{q} \end{bmatrix} = \begin{bmatrix} z_w & z_q \\ m_w & m_q \end{bmatrix} \begin{bmatrix} w \\ q \end{bmatrix} + \begin{bmatrix} z_\eta \\ m_\eta \end{bmatrix} \eta \tag{6.15}$$

where, now, the derivatives are referred to a wind axes system. Equation (6.15) is sufficiently simple that the transfer function matrix may be calculated manually by the application of equation (5.53)

$$\mathbf{G}(s) = \frac{\mathbf{N}(s)}{\Delta(s)} = \frac{\begin{bmatrix} s - m_q & z_q \\ m_w & s - z_w \end{bmatrix} \begin{bmatrix} z_\eta \\ m_\eta \end{bmatrix}}{\begin{vmatrix} s - z_w & -z_q \\ -m_w & s - m_q \end{vmatrix}} = \frac{\begin{bmatrix} z_\eta \left(s - \left(m_q - z_q \frac{m_\eta}{z_\eta} \right) \right) \\ m_\eta \left(s + \left(m_w \frac{z_\eta}{m_\eta} - z_w \right) \right) \end{bmatrix}}{(s^2 - (m_q + z_w)s + (m_q z_w - m_w z_q))} \tag{6.16}$$

The transfer functions may be further simplified by noting that

$$\left| z_q \frac{m_\eta}{z_\eta} \right| \gg |m_q| \quad \text{and} \quad |z_w| \gg \left| m_w \frac{z_\eta}{m_\eta} \right|$$

and with reference to Appendix 1

$$z_q = \frac{\overset{\circ}{Z}_q + mU_e}{m - \overset{\circ}{Z}_{\dot{w}}} \cong U_e$$

since

$$\overset{\circ}{Z}_q \ll mU_e \quad \text{and} \quad m \gg \overset{\circ}{Z}_{\dot{w}}$$

Thus, the two short term transfer functions describing the response to elevator may be written

$$\frac{w(s)}{\eta(s)} = \frac{z_\eta \left(s + U_e \frac{m_\eta}{z_\eta} \right)}{(s^2 - (m_q + z_w)s + (m_q z_w - m_w U_e))} \equiv \frac{k_w(s + 1/T_\alpha)}{(s^2 + 2\zeta_s \omega_s s + \omega_s^2)} \tag{6.17}$$

$$\frac{q(s)}{\eta(s)} = \frac{m_\eta(s - z_w)}{(s^2 - (m_q + z_w)s + (m_q z_w - m_w U_e))} \equiv \frac{k_q(s + 1/T_{\theta_2})}{(s^2 + 2\zeta_s \omega_s s + \omega_s^2)} \tag{6.18}$$

where now it is understood that k_w, k_q, T_α, T_{θ_2}, ζ_s and ω_s represent approximate values. Clearly it is now very much easier to relate the most important parameters describing longitudinal short term transient dynamics of the aircraft to the aerodynamic properties of the airframe, represented in equations (6.17) and (6.18) by the concise derivatives.

The reduced order characteristic equation may be written down on inspection of equation (6.17) or (6.18)

$$\Delta(s) = s^2 + 2\zeta_s \omega_s s + \omega_s^2 = s^2 - (m_q + z_w)s + (m_q z_w - m_w U_e) = 0 \tag{6.19}$$

and, by analogy with the classical mass–spring–damper system described in Appendix 5, the damping and natural frequency of the short period mode are given, to a good approximation, by

$$\left.\begin{aligned} 2\zeta_s \omega_s &= -(m_q + z_w) \\ \omega_s &= \sqrt{m_q z_w - m_w U_e} \end{aligned}\right\} \tag{6.20}$$

It is instructive to write the damping and natural frequency expressions (6.20) in terms of the dimensional derivatives. The appropriate conversions are obtained from Appendix 1 and the assumptions made above are applied to give

$$\left.\begin{aligned} 2\zeta_s\omega_s &= -\left(\frac{\mathring{M}_q}{I_y} + \frac{\mathring{Z}_w}{m} + \frac{\mathring{M}_w U_e}{I_y}\right) \\ \omega_s &= \sqrt{\frac{\mathring{M}_q}{I_y}\frac{\mathring{Z}_w}{m} - \frac{\mathring{M}_w U_e}{I_y}} \end{aligned}\right\} \tag{6.21}$$

Note that the terms on the right-hand side of expressions (6.21) comprise aerodynamic derivatives divided either by mass or moment of inertia in pitch. These terms may be interpreted in exactly the same way as those of the classical mass–spring–damper. Thus, it becomes apparent that the aerodynamic derivatives are providing stiffness and viscous damping in pitch although there is more than one term contributing to damping and to natural frequency. Therefore, the aerodynamic origins of the short period dynamics are a little more complex than those of the classical mass–spring–damper and the various contributions do not always act in the most advantageous way. However, for conventional aeroplanes the overall dynamic characteristics usually describe a stable short period mode.

For a typical conventional aeroplane, the relative magnitudes of the aerodynamic derivatives are such that, to a crude approximation

$$\left.\begin{aligned} 2\zeta_s\omega_s &= \frac{-\mathring{M}_q}{I_y} \\ \omega_s &= \sqrt{\frac{-\mathring{M}_w U_e}{I_y}} \end{aligned}\right\} \tag{6.22}$$

which serves only to indicate what are usually regarded as the dominant terms governing the short period mode. Normally the derivative $\mathring{Z}_w$, which is dependent on the lift curve slope of the wing, and the derivative $\mathring{M}_q$, which is determined largely by the viscous 'paddle' damping properties of the tailplane, are both negative numbers. The derivative $\mathring{M}_w$ is a measure of the aerodynamic stiffness in pitch and is also dominated by the aerodynamics of the tailplane. The sign of $\mathring{M}_w$ depends on the position of the *cg*, becoming increasingly negative as the *cg* moves forward in the airframe. Thus, the short period mode will be stable if the *cg* is far enough forward in the airframe. The *cg* position in the airframe where $\mathring{M}_w$ changes sign is called the *controls fixed neutral point* and $\mathring{M}_w$ is therefore also a measure of the *controls fixed stability margin* of the aircraft. With reference to equation (6.19) and expressions (6.20), the corresponding *cg* position where $(m_q z_w - m_w U_e)$ changes sign is called the *controls fixed manoeuvre point* and $(m_q z_w - m_w U_e)$ is a measure of the *controls fixed manoeuvre margin* of the aircraft. The subject of manoeuvrability is discussed in Chapter 8.

6.3.2 THE PHUGOID MODE APPROXIMATION

A reduced order model of the aircraft retaining only the phugoid dynamics is very rarely required in flight dynamics studies. However, the greatest usefulness of such a model is

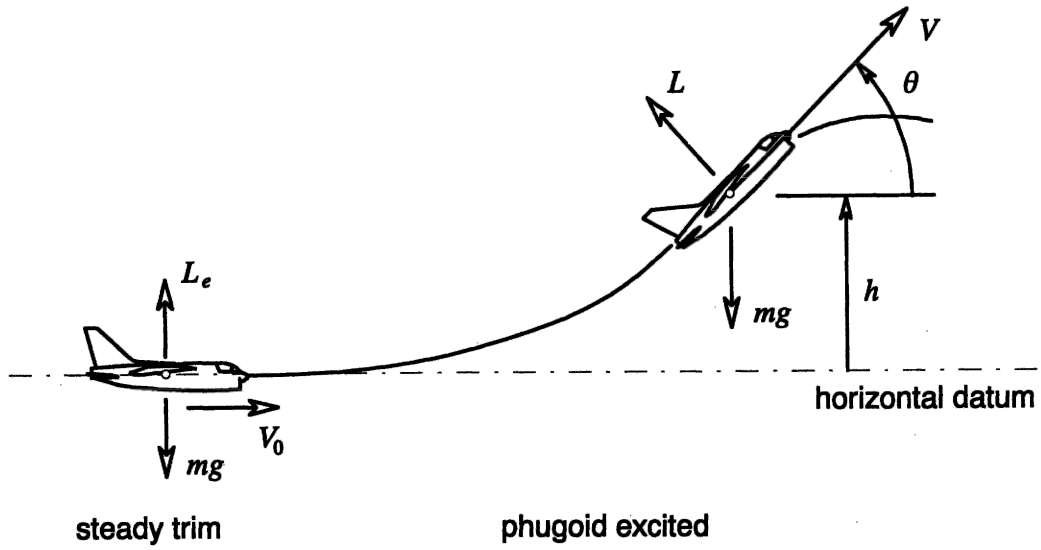

Fig. 6.4 The phugoid oscillation

to identify those aerodynamic properties of the airframe governing the characteristics of the mode.

6.3.2.1 The Lanchester model

Probably the first successful analysis of aeroplane dynamics was made by Lanchester (1908) who devised a mathematical model to describe phugoid motion based on his observations of the behaviour of gliding model aeroplanes. His analysis gives an excellent insight to the physical nature of the mode and may be applied to the modern aeroplane by interpreting and restating his original assumptions as follows.

(i) The aircraft is initially in steady level flight.
(ii) The total energy of the aircraft remains constant.
(iii) The incidence α remains constant at its initial trim value.
(iv) The thrust τ balances the drag D.
(v) The motion is sufficiently slow that pitch rate q effects may be ignored.

Referring to Fig. 6.4 the aircraft is initially in trimmed straight level flight with velocity V_0. Following a disturbance in speed which excites the phugoid mode, the disturbed speed, pitch attitude and height are denoted V, θ and h respectively. Then based on assumption (ii)

$$\frac{1}{2}mV_0^2 = \frac{1}{2}mV^2 + mgh = \text{constant}$$

whence

$$V^2 = V_0^2 - 2gh \tag{6.23}$$

which describes the exchange of kinetic and potential energy as the aeroplane flies the sinusoidal flight path.

In the initial steady trim state the lift and weight are in balance thus

$$L_e = \frac{1}{2}\rho V_0^2 S C_L = mg \tag{6.24}$$

and in disturbed flight the lift is given by

$$L = \frac{1}{2}\rho V^2 S C_L \tag{6.25}$$

As a consequence of assumption (iii) the lift coefficient C_L also remains constant and equations (6.23), (6.24) and (6.25) may be combined to give

$$L = mg - \rho g h S C_L \tag{6.26}$$

Since simple undamped oscillatory motion is assumed, a consequence of assumption (ii), the single degree of freedom equation of motion in height may be written

$$m\ddot{h} = L\cos\theta - mg \cong L - mg \tag{6.27}$$

since, by definition, θ is a small angle. Substituting for lift L from equation (6.26) into equation (6.27)

$$\ddot{h} + \left(\frac{\rho g S C_L}{m}\right)h = \ddot{h} + \omega_p^2 h = 0 \tag{6.28}$$

Thus, approximately, the frequency of the phugoid mode is given by

$$\omega_p = \sqrt{\frac{\rho g S C_L}{m}} = \frac{g\sqrt{2}}{V_0} \tag{6.29}$$

when equation (6.24) is used to eliminate the mass.

Thus, to a reasonable approximation, Lanchester's model shows that the phugoid frequency is inversely proportional to the steady trimmed speed about which the mode oscillates and that its damping is zero.

6.3.2.2 A reduced order model

A more detailed approximate model of the phugoid mode may be derived from the equations of motion by making simplifications based on assumptions about the nature of the motion. Following a disturbance, the variables $w(\alpha)$ and q respond in the time scale associated with the short period mode; thus, it is reasonable to assume that $w(\alpha)$ and q are quasi-steady in the longer time scale associated with the phugoid. Hence, it follows that

$$\dot{w} = \dot{q} = 0$$

Once again, it is assumed that the equations of motion are referred to aircraft wind axes and, since the disturbance takes place about steady level flight, then

$$\theta_e \equiv \alpha_e = 0 \quad \text{and} \quad U_e = V_0$$

and, with reference to Appendix 1, it follows that

$$x_\theta = -g \quad \text{and} \quad z_\theta = m_\theta = 0$$

Also, as for the reduced order short period model and with reference to Appendix 1

$$z_q = \frac{\mathring{Z}_q + mU_e}{m - \mathring{Z}_{\dot{w}}} \cong U_e$$

since

$$\mathring{Z}_q \ll mU_e \quad \text{and} \quad m \gg \mathring{Z}_{\dot{w}}$$

Additionally, it is usually assumed that the aerodynamic derivative x_q is insignificantly small. Thus the equations of motion (equations 6.1) may be simplified accordingly

$$\begin{bmatrix} \dot{u} \\ 0 \\ 0 \\ \dot{\theta} \end{bmatrix} = \begin{bmatrix} x_u & x_w & 0 & -g \\ z_u & z_w & U_e & 0 \\ m_u & m_w & m_q & 0 \\ 0 & 0 & 1 & 0 \end{bmatrix} \begin{bmatrix} u \\ w \\ q \\ \theta \end{bmatrix} + \begin{bmatrix} x_\eta \\ z_\eta \\ m_\eta \\ 0 \end{bmatrix} \eta \tag{6.30}$$

The second and third rows of equation (6.30) may be written

$$\left.\begin{aligned} z_u u + z_w w + U_e q + z_\eta \eta = 0 \\ m_u u + m_w w + m_q q + m_\eta \eta = 0 \end{aligned}\right\} \tag{6.31}$$

Equations (6.31) may be solved algebraically to obtain expressions for w and q in terms of u and η

$$\left.\begin{aligned} w &= \left(\frac{m_u U_e - m_q z_u}{m_q z_w - m_w U_e}\right) u + \left(\frac{m_\eta U_e - m_q z_\eta}{m_q z_w - m_w U_e}\right) \eta \\ q &= \left(\frac{m_w z_u - m_u z_w}{m_q z_w - m_w U_e}\right) u + \left(\frac{m_w z_\eta - m_\eta z_w}{m_q z_w - m_w U_e}\right) \eta \end{aligned}\right\} \tag{6.32}$$

The expressions for w and q are substituted into the first and third rows of equation (6.30) and following some rearrangement the reduced order state equation is obtained

$$\begin{bmatrix} \dot{u} \\ \dot{\theta} \end{bmatrix} = \left[\begin{array}{c|c} x_u - x_w\left(\dfrac{m_u U_e - m_q z_u}{m_w U_e - m_q z_w}\right) & -g \\ \hline \left(\dfrac{m_u z_w - m_w z_u}{m_w U_e - m_q z_w}\right) & 0 \end{array}\right] \begin{bmatrix} u \\ \theta \end{bmatrix} + \left[\begin{array}{c} x_\eta - \left(\dfrac{m_\eta U_e - m_q z_\eta}{m_w U_e - m_q z_w}\right) \\ \left(\dfrac{m_\eta z_w - m_w z_\eta}{m_w U_e - m_q z_w}\right) \end{array}\right] \eta \tag{6.33}$$

or

$$\dot{\mathbf{x}} = \mathbf{A}_p \mathbf{x} + \mathbf{B}_p \mathbf{u} \tag{6.34}$$

Equation (6.33) may be solved algebraically to obtain the reponse transfer functions for the phugoid variables u and θ. However, it is not very meaningful to analyse a long term dynamic response to elevator in this way. The characteristic equation describing the reduced order phugoid dynamics is considerably more useful and is given by

$$\Delta(s) = \det[s\mathbf{I} - \mathbf{A}_p] = 0$$

whence

$$\begin{aligned}\Delta(s) &= s^2 + 2\zeta_p\omega_p s + \omega_p^2 \\ &= s^2 - \left(x_u - x_w\left(\frac{m_u U_e - m_q z_u}{m_w U_e - m_q z_w}\right)\right)s + g\left(\frac{m_u z_w - m_w z_u}{m_w U_e - m_q z_w}\right)\end{aligned} \tag{6.35}$$

Thus, the approximate damping and natural frequency of the phugoid mode are given in terms of a limited number of aerodynamic derivatives. More explicit, but rather more approximate, insight into the aerodynamic properties of the aeroplane dominating the mode characteristics may be obtained by making some further assumptions. Typically, for conventional aeroplanes in subsonic flight

$$m_u \to 0, \quad |m_u z_w| \ll |m_w z_u| \quad \text{and} \quad |m_w U_e| \gg |m_q z_w|$$

then the corresponding expressions for the damping and natural frequency become

$$\left.\begin{aligned} 2\zeta_p\omega_p &= -x_u \\ \omega_p &= \sqrt{\frac{-gz_u}{U_e}} \end{aligned}\right\} \tag{6.36}$$

Now, with reference to Appendix 1

$$x_u \cong \frac{\overset{\circ}{X}_u}{m} = \frac{\rho V_0 S X_u}{2m} \quad \text{and} \quad z_u \cong \frac{\overset{\circ}{Z}_u}{m} = \frac{\rho V_0 S Z_u}{2m} \tag{6.37}$$

since $\overset{\circ}{X}_{\dot{w}}$ is negligibly small and $m \gg \overset{\circ}{Z}_{\dot{w}}$. Expressions for the dimensionless aerodynamic derivatives are given in Appendix 6 and may be approximated as shown in expressions (6.38) when the basic aerodynamic properties are assumed to be independent of speed. This follows from the assumption that the prevailing flight condition is subsonic such that the aerodynamic properties of the airframe are not influenced by compressibility effects

$$\left.\begin{aligned} X_u &= -2C_D - V_0\frac{\partial C_D}{\partial V} + \left(\frac{1}{\frac{1}{2}\rho V_0 S}\right)\frac{\partial \tau}{\partial V} \cong -2C_D \\ Z_u &= -2C_L - V_0\frac{\partial C_L}{\partial V} \cong -2C_L \end{aligned}\right\} \tag{6.38}$$

Expressions (6.36) may therefore be restated in terms of aerodynamic parameters, assuming again that the trimmed lift is equal to the aircraft weight, to obtain

$$\left.\begin{aligned} \zeta_p\omega_p &= \frac{gC_D}{C_L V_0} \\ \omega_p &= \sqrt{\frac{2g^2}{U_e V_0}} \equiv \frac{g\sqrt{2}}{V_0} \end{aligned}\right\} \tag{6.39}$$

and a simplified approximate expression for the damping ratio follows

$$\zeta_p \cong \frac{1}{\sqrt{2}}\left(\frac{C_D}{C_L}\right) \tag{6.40}$$

These expressions for damping ratio and natural frequency of the phugoid mode are obviously very approximate since they are the result of many simplifying assumptions. Note that the expression for ω_p is the same as that derived by Lanchester, equation

(6.29), which indicates that the natural frequency of the phugoid mode is approximately inversely proportional to the trimmed speed. It is also interesting and important to note that the damping ratio of the phugoid mode is approximately inversely proportional to the *lift to drag* ratio of the aeroplane, equation (6.40). Since one of the main objectives of aeroplane design is to achieve a high lift to drag ratio it is easy to see why the damping of the phugoid mode is usually very low.

EXAMPLE 6.2

To illustrate the use of reduced order models, consider the A-7A Corsair II aircraft of Example 6.1 and at the same flight condition. Now the equations of motion in Example 6.1 are referred to a body axis system and the use of the reduced order models described above requires the equations of motion referred to a wind or stability axis system. Thus, using the axis transformation relationships given in Appendices 7 and 8, the stability and control derivatives and inertia parameters referred to wind axes were calculated from the original values, which are of course referred to body axes. The longitudinal state equation was then recalculated to give

$$\begin{bmatrix} \dot{u} \\ \dot{w} \\ \dot{q} \\ \dot{\theta} \end{bmatrix} = \begin{bmatrix} -0.04225 & -0.11421 & 0 & -32.2 \\ -0.20455 & -0.49774 & 317.48 & 0 \\ 0.00003 & -0.00790 & -0.39499 & 0 \\ 0 & 0 & 1 & 0 \end{bmatrix} \begin{bmatrix} u \\ w \\ q \\ \theta \end{bmatrix} + \begin{bmatrix} 0.00381 \\ -24.4568 \\ -4.51576 \\ 0 \end{bmatrix} \eta \tag{6.41}$$

The reduced order model corresponding to the short period approximation, as given by equation (6.15), is simply taken out of equation (6.41) and is written

$$\begin{bmatrix} \dot{w} \\ \dot{q} \end{bmatrix} = \begin{bmatrix} -0.49774 & 317.48 \\ -0.00790 & -0.39499 \end{bmatrix} \begin{bmatrix} w \\ q \end{bmatrix} + \begin{bmatrix} -24.4568 \\ -4.51576 \end{bmatrix} \eta \tag{6.42}$$

Solution of the equations of motion (6.42) using *Program CC* determines the following reduced order response transfer functions

$$\begin{aligned} \frac{w(s)}{\eta(s)} &= \frac{-24.457(s+59.015)}{(s^2+0.893s+2.704)} \text{ ft/s/rad} \\ \frac{q(s)}{\eta(s)} &= \frac{-4.516(s+0.455)}{(s^2+0.893s+2.704)} \text{ rad/s/rad (deg/s/deg)} \\ \frac{\alpha(s)}{\eta(s)} &= \frac{-0.077(s+59.015)}{(s^2+0.893s+2.704)} \text{ rad/rad (deg/deg)} \end{aligned} \tag{6.43}$$

It is important to remember that these transfer functions describe, approximately, the short term response of those variables which are dominant in short period motion. The corresponding short term pitch attitude response transfer function follows since, for small perturbation motion,

$$\frac{\theta(s)}{\eta(s)} = \frac{1}{s}\frac{q(s)}{\eta(s)} = \frac{-4.516(s+0.455)}{s(s^2+0.893s+2.704)} \text{ rad/rad (deg/deg)} \tag{6.44}$$

From the pitch rate response transfer function in equations (6.43) it is readily determined that the steady state pitch rate following a positive unit step elevator input is −0.76 rad/s, which implies that the aircraft pitches continuously until the input is

removed. The pitch attitude response transfer function confirms this since, after the short period transient has damped out, the aircraft behaves like a perfect integrator in pitch. This is indicated by the presence of the s term in the denominator of equation (6.44). In reality the phugoid dynamics usually prevents this situation developing unless the input is very large and accompanied by a thrust increase, which results in a vertical loop manoeuvre. The model described here would be most inappropriate for the analysis of such large amplitude motion.

The common denominator of transfer functions (6.43) represents the approximate reduced order short period characteristic polynomial, equation (6.19). Thus, approximate values of the damping ratio and undamped natural frequency of the short period mode are easily calculated and are

$$\text{damping ratio } \zeta_s = 0.27$$
$$\text{undamped natural frequency } \omega_s = 1.64 \text{ rad/s}$$

It will be seen that these values compare very favourably with the exact values given in Example 6.1.

Interpretation of the reduced order model is probably best illustrated by observing short term response to an elevator input. The responses to a 1° elevator step input of the variables given in equations (6.43) are shown on Fig. 6.5. Also shown on the same plots are the corresponding responses of the full aircraft model derived from equation (6.41). It is clear that the responses diverge with time, as expected, as no phugoid

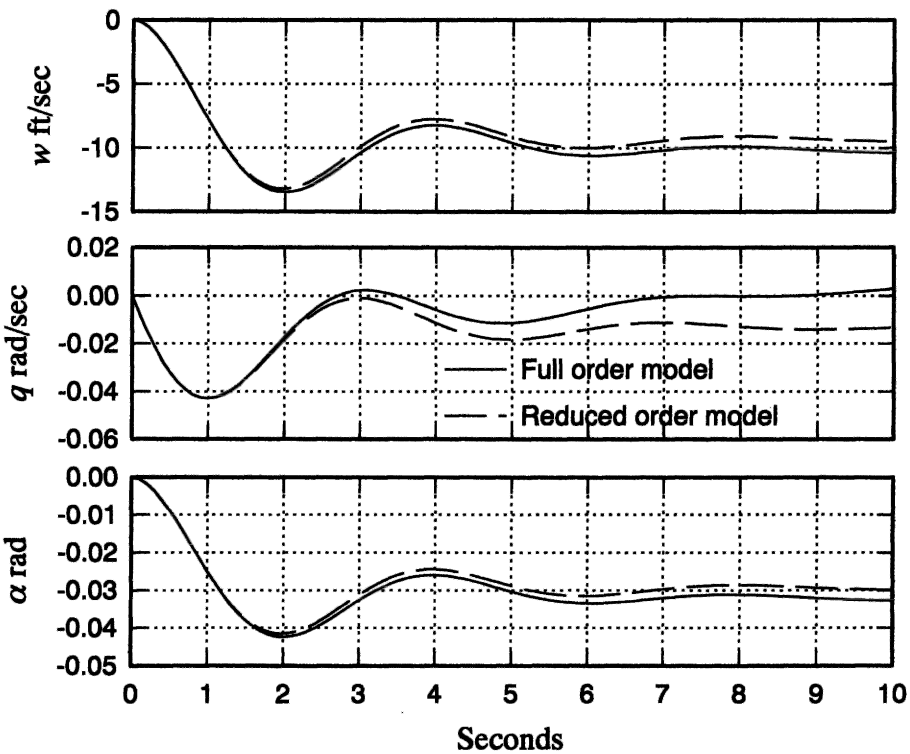

Fig. 6.5 Reduced order longitudinal response to 1° elevator step input

dynamics is present in the reduced order model. However, for the first ten seconds or so, the comparison is favourable indicating that the reduced order model is acceptable for most short term response studies.

Turning now to the approximate reduced order phugoid mode characteristics, from the state equation referred to wind axes, equation (6.41), the required numerical parameters are

$$x_u = -0.04225 \text{ l/s}$$
$$z_u = -0.20455 \text{ l/s}$$
$$m_u = -0.00003 \text{ rad/ft}$$
$$U_e \equiv V_0 = 317.48 \text{ ft/s}$$

The simple Lanchester model determines that the damping of the phugoid is zero and that the undamped natural frequency is given by equation (6.29). Thus the approximate characteristics of the phugoid mode calculated according to this model are

$$\text{damping ratio } \zeta_p = 0$$
$$\text{undamped natural frequency } \omega_p = 0.143 \text{ rad/s}$$

The approximate phugoid mode characteristics determined according to the rather more detailed reduced order model are given by equation (6.36). Since the chosen flight condition is genuinely subsonic, the derivative m_u is very small indeed which matches the constraints of the model well. The approximate characteristics of the phugoid mode calculated according to this model are

$$\text{damping ratio } \zeta_p = 0.147$$
$$\text{undamped natural frequency } \omega_p = 0.144 \text{ rad/s}$$

Again, comparing these approximate values of the phugoid mode characteristics with the exact values in Example 6.1 indicates good agreement, especially for the undamped natural frequency. Since the phugoid damping ratio is always small (near to zero) it is very sensitive to computational rounding errors and to the approximating assumptions, which makes a really good approximate match difficult to achieve. The goodness of the match here is enhanced by the very subsonic flight condition which correlates well with assumptions made in the derivation of the approximate models.

6.4 Frequency response

For the vast majority of flight dynamics investigations time domain analysis is usually adequate, especially when the subject is the classical unaugmented aeroplane. The principal graphical tool used in time domain analysis is, of course, the time history plot showing the response of the aeroplane to controls or to some external disturbance. However, when the subject aeroplane is an advanced modern aeroplane fitted with a flight control system, flight dynamics analysis in the frequency domain can provide additional valuable insight into its behaviour. In recent years, frequency domain analysis has made an important contribution to the understanding of the sometimes unconventional handling qualities of aeroplanes whose flying qualities are largely shaped

by a flight control system. It is for this reason that a brief review of simple frequency response ideas is considered here. Since frequency response analysis tools are fundamental to classical control engineering, their description can be found in almost every book on the subject: very accessible material can be found in Shinners (1980) and Friedland (1987) for example.

Consider the hypothetical situation when the elevator of an otherwise trimmed aeroplane is operated sinusoidally with constant amplitude k and variable frequency ω; the longitudinal input to the aeroplane may therefore be expressed

$$\eta(t) = k \sin \omega t \tag{6.45}$$

It is reasonable to expect that each of the output variables describing aircraft motion will respond sinusoidally to the input. However, the amplitudes of the output variables will not necessarily be the same and they will not necessarily be in phase with one another or with the input. Thus, the general expression describing any output response variable may be written

$$y(t) = K \sin(\omega t + \phi) \tag{6.46}$$

where both the output amplitude K and phase shift ϕ are functions of the exciting frequency ω. As the exciting frequency ω is increased from zero so, initially, at low frequencies, the sinusoidal response will be clearly visible in all output variables. As the exciting frequency is increased further so the sinusoidal response will start to diminish in magnitude and will eventually become imperceptible in the outputs. Simultaneously, the phase shift ϕ will indicate an increasingly large lag between the input and output. The reason for these observations is that at sufficiently high frequencies the mass and inertia properties of the aeroplane simply prevent it responding quickly enough to follow the input.

The limiting frequency at which the response commences to diminish rapidly is referred to as the *bandwidth* of the aeroplane with respect to the output variable of interest. A more precise definition of bandwidth is given below. Since aeroplanes only respond to frequencies below the bandwidth frequency they have the frequency response properties of a *low pass system*. At exciting frequencies corresponding to the damped natural frequencies of the phugoid and the short period mode, peaks in output magnitude K will be seen together with significant changes in phase shift ϕ. The mode frequencies are described as *resonant frequencies* and the magnitudes of the output parameters K and ϕ at *resonance* are determined by the damping ratios of the modes. The system (or aeroplane) *gain* in any particular response variable is defined

$$\text{system gain} = \left| \frac{K(\omega)}{k} \right| \tag{6.47}$$

where, in normal control system applications, it is usually assumed that the input and output variables have the same units. This is often not the case in aircraft applications and care must be exercised in the interpretation of gain.

A number of graphical tools have been developed for the frequency response analysis of linear systems and include the Nyquist diagram, the Nichols chart and the Bode diagram. All are intended to simplify analytical procedures, the mathematical calculation of which is tedious without a computer, and all plot input–output gain and phase as functions of frequency. Perhaps the simplest of the graphical tools to use and

interpret is the Bode diagram, although the amount of information it is capable of providing is limited. However, today it is used extensively for flight dynamics analysis, especially in advanced handling qualities studies.

6.4.1 THE BODE DIAGRAM

The intention here is not to describe the method for constructing a Bode diagram but to describe its application to the aeroplane and to explain its correct interpretation. For an explanation of the method for constructing a Bode diagram the reader should consult a suitable control engineering text, such as either of those referenced above.

To illustrate the application of the Bode diagram to a typical classical aeroplane consider the pitch attitude response to the elevator transfer function as given by equation (6.5)

$$\frac{\theta(s)}{\eta(s)} = \frac{k_\theta(s + 1/T_{\theta_1})(s + 1/T_{\theta_2})}{(s^2 + 2\zeta_p\omega_p s + \omega_p^2)(s^2 + 2\zeta_s\omega_s s + \omega_s^2)} \tag{6.48}$$

This response transfer function is of particular relevance to longitudinal handling studies and it has the simplifying advantage that both the input and output variables have the same units. Typically, in frequency response calculations it is usual to assume a sinusoidal input signal of unit magnitude. It is also important to note that whenever the response transfer function is negative, which is often the case in aircraft applications, a negative input is assumed, which ensures the correct computation of phase. Therefore, in this particular application, since k_θ is usually a negative number, a sinusoidal elevator input of unit magnitude, $\eta(t) = -1 \sin \omega t$, is assumed. The pitch attitude frequency response is calculated by writing $s = j\omega$ in equation (6.48); the right-hand side then becomes a complex number whose magnitude and phase can be evaluated for a suitable range of frequency ω. Since the input magnitude is unity the *system gain*, equation (6.47), is given simply by the absolute value of the magnitude of the complex number representing the right-hand side of equation (6.48) and is, of course, a function of frequency ω.

Since the calculation of gain and phase involves the products of several complex numbers it is preferred to work in terms of the logarithm of the complex number representing the transfer function. The total gain and phase then become the simple sums of the gain and phase of each factor in the transfer function. For example, each factor in parentheses on the right-hand side of equation (6.48) may have its gain and phase characteristics calculated separately as a function of frequency; the total gain and phase is then given by summing the contributions from each factor. However, the system gain is now expressed as a logarithmic function of the gain ratio, equation (6.47), and is defined

$$\text{logarithmic gain} = 20 \log_{10} \left| \frac{K(\omega)}{k} \right| \text{dB} \tag{6.49}$$

and has units of *decibels*, denoted dB. Fortunately it is no longer necessary to calculate frequency response by hand since many computer software packages, such as *PC MATLAB*, have this facility and can also provide the desired graphical output. However, as always, some knowledge of the analytical procedure for obtaining frequency response is essential in order that the computer output may be correctly interpreted.

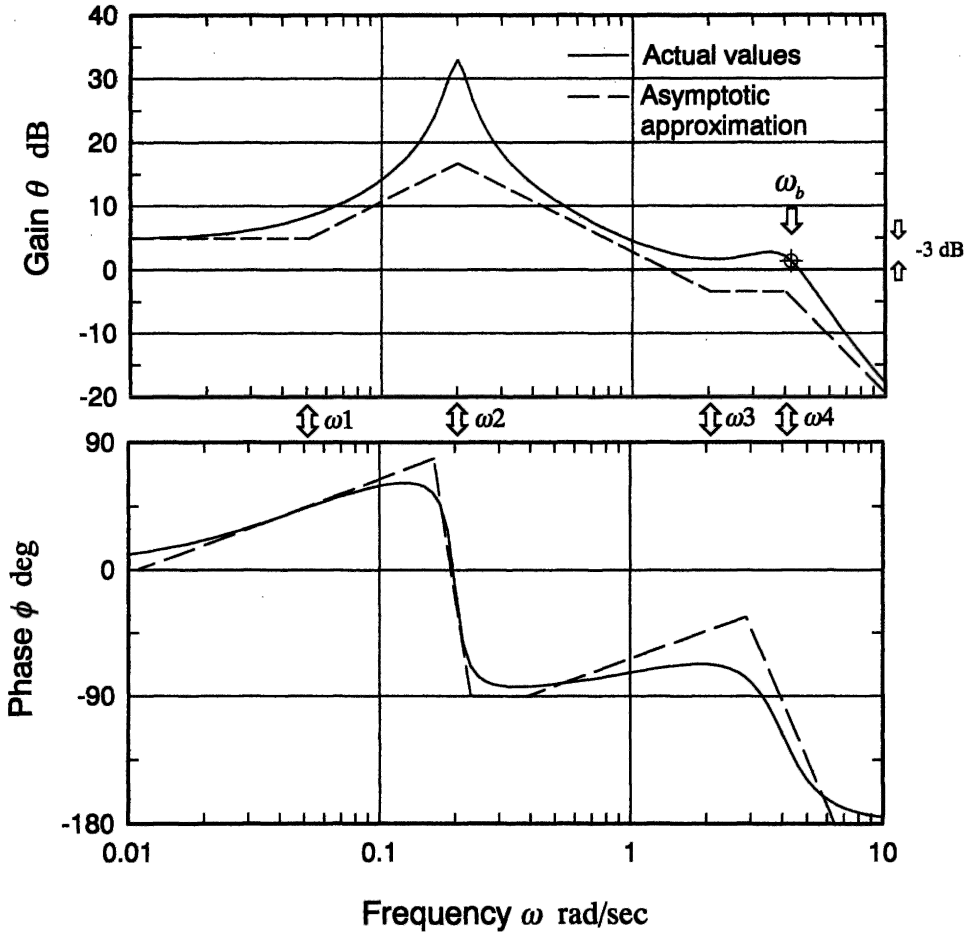

Fig. 6.6 Bode diagram showing classical pitch attitude frequency response

The Bode diagram comprises two corresponding plots, the *gain plot* and the *phase plot*. The gain plot shows the logarithmic gain, in dB, plotted against $\log_{10}(\omega)$ and the phase plot shows the phase, in degrees, also plotted against $\log_{10}(\omega)$. To facilitate interpretation the two plots are often superimposed on a common frequency axis. The Bode diagram showing the typical pitch attitude frequency response, as given by transfer function (6.48), is shown on Fig. 6.6.

Also shown in Fig. 6.6 are the asymptotic approximations to the actual gain and phase plots as functions of frequency. The asymptotes can be drawn in simply from inspection of the transfer function, equation (6.48), and serve as an aid to interpretation. Quite often the asymptotic approximation is sufficient for the evaluation in hand, thereby dispensing with the need to compute the actual frequency response entirely.

The shape of the gain plot is characterized by the *break frequencies* $\omega 1$ to $\omega 4$ which determine the locations of the discontinuities in the asymptotic gain plot. Each break frequency is defined by a key frequency parameter in the transfer function, namely

$$\omega 1 = \frac{1}{T_{\theta_1}} \quad \text{with first order phase lead} \quad (+45°)$$

$$\omega 2 = \omega_p \quad \text{with second order phase lag} \quad (-90°)$$

$$\omega 3 = \frac{1}{T_{\theta_2}} \quad \text{with first order phase lead} \quad (+45°)$$

$$\omega 4 = \omega_s \quad \text{with second order phase lag} \quad (-90°)$$

Since the transfer function is classical minimum phase, the corresponding phase shift at each break frequency is a *lead* if it arises from a numerator term or a *lag* if it arises from a denominator term. If, as is often the case in aircraft studies, non-minimum phase terms appear in the transfer function, then their frequency response properties are unchanged except that the sign of the phase is reversed. Further, a first order term gives rise to a total phase shift of 90° and a second order term gives rise to a total phase shift of 180°. The characteristic phase response is such that half the total phase shift associated with any particular transfer function factor occurs at the corresponding break frequency. Armed with this limited information, a modest interpretation of the pitch attitude frequency response of the aeroplane is possible. The frequency response of the other motion variables may be dealt with in a similar way.

6.4.2 *INTERPRETATION OF THE BODE DIAGRAM*

With reference to Fig. 6.6 it is seen that at very low frequencies, $\omega < 0.01$ rad/s, there is no phase shift between the input and output and the gain remains constant, at a little below 5 dB in this illustration. In other words, the pitch attitude will follow the stick movement more-or-less precisely. As the input frequency is increased through $\omega 1$ so the pitch response leads the input in phase, the output magnitude increases rapidly and the aeroplane appears to behave like an *amplifier*. At the phugoid frequency the output reaches a substantial peak, consistent with the low damping, and thereafter the gain drops rapidly, accompanied by a rapid increase in phase lag. As the input frequency is increased further so the gain continues to reduce gently and the phase settles at −90° until the influence of break frequency $\omega 3$ comes into play. The reduction in gain is arrested and the effect of the phase lead may be seen clearly. However, when the input frequency reaches the short period break frequency a small peak in gain is seen, consistent with the higher damping ratio, and at higher frequencies the gain continues to reduce steadily. Meanwhile, the phase lag associated with the short period mode results in a constant total phase lag of −180° at higher frequencies.

Once the output–input gain ratio drops below unity, or 0 dB, the aeroplane appears to behave like an *attenuator*. The frequency at which the gain becomes sufficiently small that the magnitude of the output response becomes insignificant is called the *bandwidth frequency*, denoted ω_b. There are various definitions of bandwidth, but the definition used here is probably the most common and defines the bandwidth frequency as the frequency at which the gain first drops to −3 dB below the zero frequency, or steady state, gain. The bandwidth frequency is indicated in Fig. 6.6 and it is commonly a little higher than the short period frequency. A gain of −3 dB corresponds to a gain ratio of $1/\sqrt{2} = 0.707$. Thus, by definition, the gain at the bandwidth frequency is 0.707 times the steady state gain. Since the pitch attitude bandwidth frequency is close to the short

period frequency, the latter may sometimes be substituted for the bandwidth frequency, which is often good enough for most practical purposes.

The peaks in the gain plot are determined by the characteristics of the stability modes. A very pronounced peak indicates low mode damping and vice versa, an infinite peak corresponding to zero damping. The magnitude of the changes in gain and phase occurring in the vicinity of a peak indicates the significance of the mode in the response variable in question. The illustration in Fig. 6.6 indicates the magnitude of the phugoid to be much greater than the magnitude of the short period mode in the pitch response of the aeroplane. This would, in fact, be confirmed by response time histories and inspection of the corresponding eigenvectors.

In the classical application of the Bode diagram, as used by the control engineer, inspection of the gain and phase properties in the vicinity of the bandwidth frequency enables conclusions about the stability of the system to be made. Typically, frequency is quantified in terms of *gain margin* and *phase margin*. However, such evaluations are only appropriate when the system transfer function is *minimum phase*. Since aircraft transfer functions that are non-minimum phase are frequently encountered, and many also have the added complication that they are negative, it is not usual for aircraft stability to be assessed on the Bode diagram. It is worth noting that, for aircraft augmented with flight control systems, the behaviour of the phase plot in the vicinity of the bandwidth frequency is now known to be linked to the susceptibility of the aircraft to *pilot-induced oscillations*, a particularly nasty handling deficiency.

Now, the foregoing summary interpretation of frequency response assumes a sinusoidal elevator input to the aircraft. Clearly, this is never likely to occur as a result of normal pilot action. However, normal pilot actions may be interpreted to comprise a mix of many different frequency components. For example, in gentle manoeuvring the frequency content of the input would generally be low, whilst in aggressive or high workload situations the frequency content would be higher and might even exceed the bandwidth of the aeroplane. In such a limiting condition the pilot would certainly be aware that the aeroplane could not follow his demands quickly enough and, depending in detail on the gain and phase response properties of the aeroplane, he could well encounter hazardous handling problems. Thus, bandwidth is a measure of the *quickness of response* achievable in a given aeroplane. As a general rule, it is desirable that flight control system designers should seek the highest response bandwidth consistent with the dynamic capabilities of the airframe.

EXAMPLE 6.3

The longitudinal frequency response of the A-7A Corsair II aircraft is evaluated for the same flight condition as Examples 6.1 and 6.2. However, the longitudinal response transfer functions used for the evaluations are referred to wind axes and were obtained in the solution of the full order state equation (6.41). The transfer functions of primary interest are

$$\frac{u(s)}{\eta(s)} = \frac{0.00381(s+0.214)(s+135.93)(s+598.3)}{(s^2+0.033s+0.02)(s^2+0.902s+2.666)} \text{ ft/s/rad}$$

$$\frac{\theta(s)}{\eta(s)} = \frac{-4.516(s-0.008)(s+0.506)}{(s^2+0.033s+0.02)(s^2+0.902s+2.666)} \text{ rad/rad} \qquad (6.50)$$

$$\frac{\alpha(s)}{\eta(s)} = \frac{-0.077(s^2+0.042s+0.02)(s+59.016)}{(s^2+0.033s+0.02)(s^2+0.902s+2.666)} \text{ rad/rad}$$

It will be noticed that the values of the various numerator terms in the velocity and incidence transfer functions differ significantly from the values in the corresponding transfer functions in Example 6.1, equations (6.8). This is due to the different reference axes used and to the fact that the angular difference between body and wind axes is a significant body incidence angle of 13.3°. Such a large angle is consistent with the very low speed flight condition. The frequency response of each transfer function was calculated with the aid of *Program CC* and the Bode diagrams are shown in Figs 6.7 to 6.9 respectively. Interpretation of the Bode diagrams for the three variables is

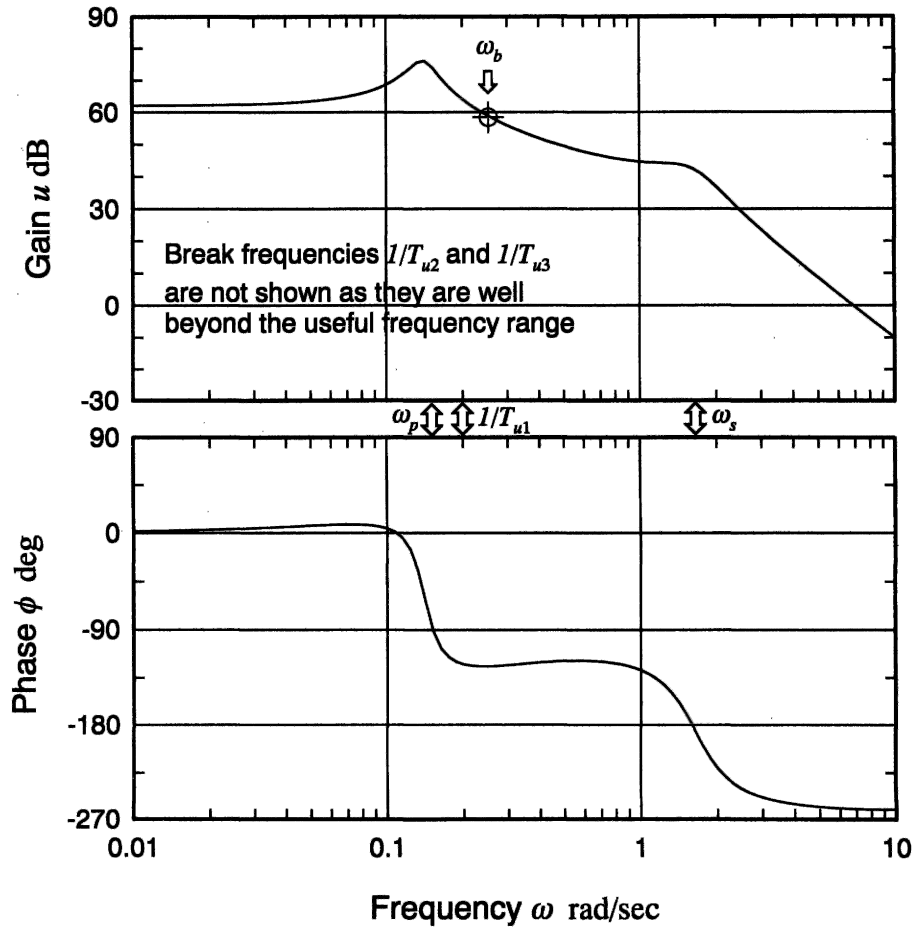

Fig. 6.7 A-7A velocity frequency response

straightforward and follows the general interpretation discussed above. However, important or significant differences are commented on as follows.

The frequency response of axial velocity u to elevator input η is shown in Fig. 6.7 and it is clear, as might be expected, that it is dominated by the phugoid. The very large low frequency gain values are due entirely to the transfer function units which are ft/s/rad, and a unit radian elevator input is of course unrealistically large! The peak gain of 75 dB at the phugoid frequency corresponds to a gain ratio of approximately 5600 ft/s/rad. However, since the aircraft model is linear, this very large gain ratio may be interpreted equivalently as approximately 98 ft/s/deg, which is much easier to appreciate physically. Since the gain drops away rapidly as the frequency increases beyond the phugoid frequency, the velocity bandwidth frequency is only a little higher than the phugoid frequency. This accords well with practical observation; velocity perturbations at frequencies in the vicinity of the short period mode are usually insignificantly small. The phase plot indicates that there is no appreciable phase shift between input and output until the frequency exceeds the phugoid frequency when there is a rapid increase in phase lag. This means that

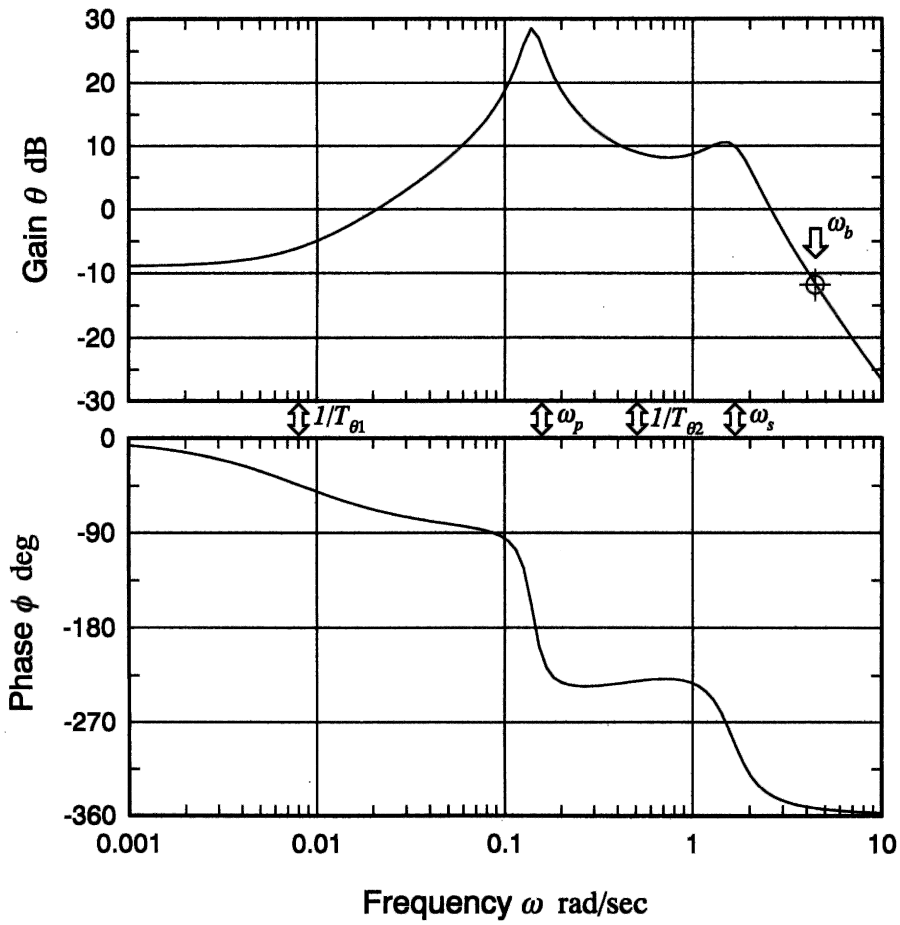

Fig. 6.8 A-7A pitch attitude frequency response

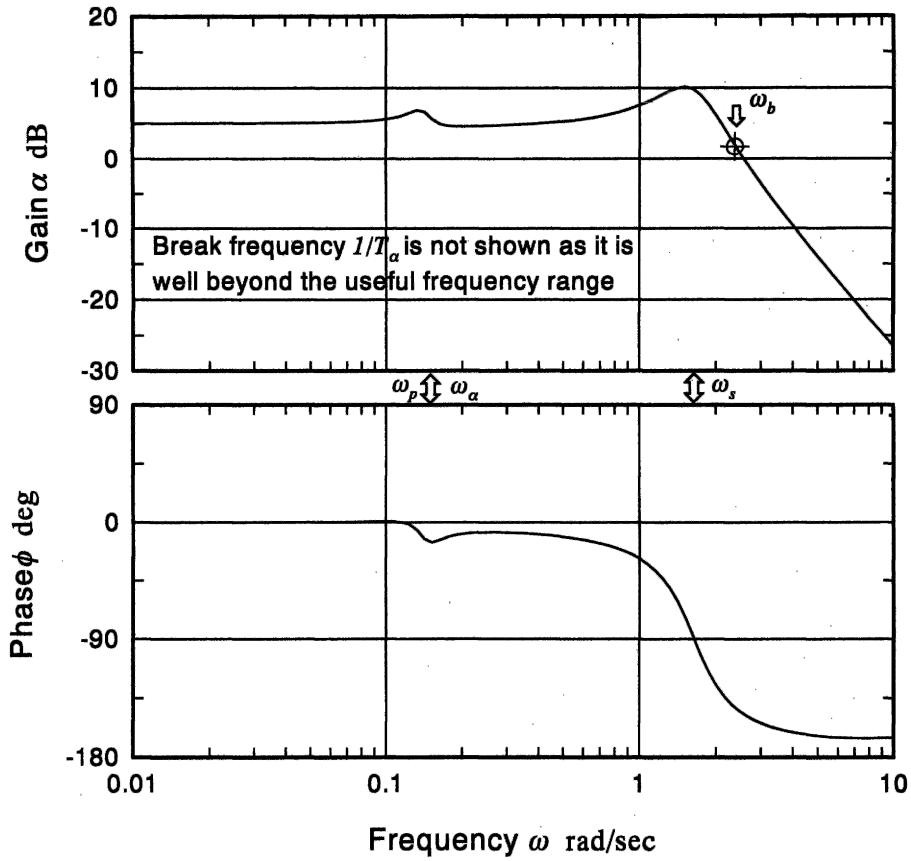

Fig. 6.9 A-7A body incidence frequency response

for all practical purposes speed changes demanded by the pilot will follow the stick in the usable frequency band.

The pitch attitude θ frequency response to elevator input η is shown in Fig. 6.8. Its general interpretation follows the discussion of Fig. 6.6 above and is not repeated here. However, there are some significant differences which must not be overlooked. The differences are due to the fact that the transfer function is non-minimum phase, a consequence of selecting a very low speed flight condition for the example. Referring to equations (6.50), this means that the numerator zero $1/T_{\theta_1}$ is negative, and the reasons for this are discussed in Example 6.1. The non-minimum phase effects do not influence the gain plot in any significant way, so its interpretation is quite straightforward. However, the effect of the non-minimum phase numerator zero is to introduce phase lag at very low frequencies rather than the usual phase lead. It is likely that in manoeuvring at this flight condition the pilot would be aware of the pitch attitude lag in response to his stick input.

The body incidence α frequency response to elevator input η is shown in Fig. 6.9 and it is clear that, as might be expected, this is dominated by the short period mode. For all practical purposes the influence of the phugoid on both the gain and phase frequency responses is insignificant. This may be confirmed by reference to the

appropriate transfer function in equations (6.50), where it will be seen that the second order numerator term very nearly cancels the phugoid term in the denominator. This is an important observation since it is quite usual to cancel approximately equal numerator and denominator terms in any response transfer function to simplify it. Simplified transfer functions often provide adequate response models in both the time and frequency domains, and can be extremely useful for explaining and interpreting aircraft dynamic behaviour. In modern control parlance the phugoid dynamics would be said to be *not observable* in this illustration. The frequency response in both gain and phase is more-or-less flat at frequencies up to the short period frequency, or for most of the usable frequency range. In practical terms this means that incidence will follow the stick at constant gain and without appreciable phase lag, which is obviously a desirable state of affairs.

6.5 Flying and handling qualities

The longitudinal stability modes play an absolutely fundamental part in determining the longitudinal flying and handling qualities of an aircraft and it is essential that their characteristics must be 'correct' if the aircraft is to be flown by a human pilot. A simplistic view of the human pilot suggests that he behaves like an adaptive dynamic system and will adapt his dynamics to harmonize with that of the controlled vehicle. Since his dynamics interacts and couples with that of the aircraft he will adapt, within human limits, to produce the best *closed loop* system dynamics compatible with the piloting task. His adaptability enables him to cope well with aircraft with less than desirable flying qualities. However, the problems of coupling between incompatible dynamic systems can be disastrous and it is this latter aspect of the piloting task which has attracted much attention in recent years. Every time the aircraft is disturbed in response to control commands so the stability modes are excited, and it is not difficult to appreciate why their characteristics are so important. Similarly, the stability modes are equally important in determining *ride quality* when the main concern is response to atmospheric disturbances. In military combat aircraft ride quality determines the effectiveness of the airframe as a weapons platform and in civil transport aircraft it determines the comfort of passengers.

In general, it is essential that the short period mode, which has a natural frequency close to human pilot natural frequency, is adequately damped. Otherwise, dynamic coupling with the pilot may occur under certain conditions leading to severe, or even catastrophic, handling problems. On the other hand, as the phugoid mode is much lower in frequency its impact on the piloting task is much less demanding. The average human pilot can easily control the aircraft even when the phugoid is mildly unstable. The phugoid mode can, typically, manifest itself as a minor trimming problem when poorly damped. Although not in itself hazardous, it can lead to increased pilot workload and, for this reason, it is desirable to ensure adequate phugoid damping. It is also important that the natural frequencies of the stability modes should be well separated in order to avoid interaction, or coupling, between the modes. Mode coupling may give rise to unusual handling characteristics and is generally regarded as an undesirable feature in longitudinal dynamics. The subject of aircraft handling qualities is discussed in rather more detail in Chapter 10.

6.6 Mode excitation

Since the longitudinal stability modes are usually well separated in frequency, it is possible to excite the modes more-or-less independently for the purposes of demonstration or measurement. Indeed, it is a general flying qualities requirement that the modes be well separated in frequency in order to avoid handling problems arising from dynamic mode coupling. The modes may be excited selectively by the application of a sympathetic elevator input to the trimmed aircraft. The methods developed for in-flight mode excitation reflect an intimate understanding of the dynamics involved and are generally easily adapted to the analytical environment. Because the longitudinal modes are usually well separated in frequency the form of the input disturbance is not, in practice, very critical. However, some consistency in the flight test or analytical procedures adopted is desirable if meaningful comparative studies are to be made.

The short period pitching oscillation may be excited by applying a short duration

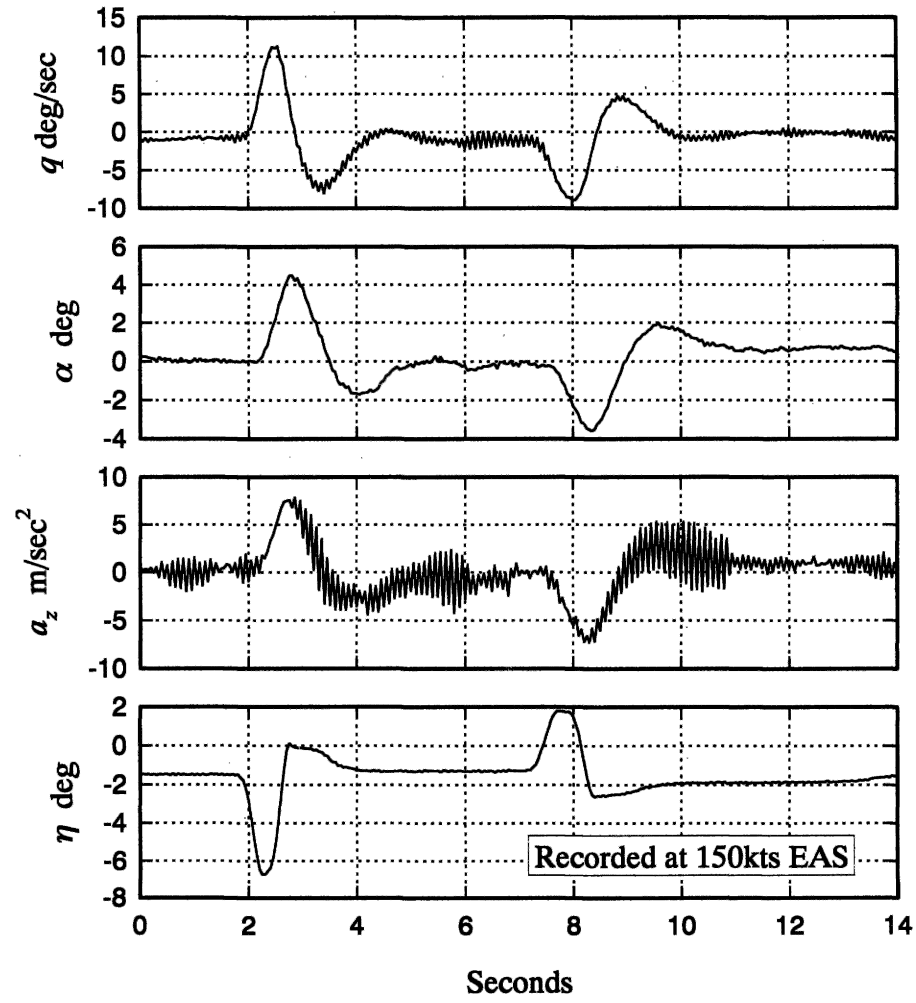

Fig. 6.10 Flight recording of the short period pitching oscillation

disturbance in pitch to the trimmed aircraft. This is best achieved with an elevator pulse having a duration of a second or less. Analytically this is adequately approximated by a unit impulse applied to the elevator. The essential feature of the disturbance is that it must be sufficiently short so as not to excite the phugoid significantly. However, as the phugoid damping is usually very low it is almost impossible not to excite the phugoid at the same time, but it does not usually develop fast enough to obscure observation of the short period mode. An example of a short period response recorded during a flight test exercise in a Handley Page Jetstream aircraft is shown in Fig. 6.10. In fact, two excitations are shown, the first in the nose up sense and the second in the nose down sense. The pilot input 'impulse' is clearly visible and represents his best attempt at achieving a clean impulse like input; some practice is required before consistently good results are obtained. Immediately following the input the pilot released the controls to obtain the controls free dynamic response, which explains why the elevator angle does not recover its equilibrium trim value until the short period transient has settled. During this short elevator free period its motion is driven by oscillatory aerodynamic loading and is also coloured by the control circuit dynamics, which can be noticeably intrusive. Otherwise the response is typical of a well-damped aeroplane.

The phugoid mode may be excited by applying a small speed disturbance to the aircraft in trimmed flight. This is best achieved by applying a small step input to the elevator, which will cause the aircraft to fly up, or down, according to the sign of the input. If the power is left at its trimmed setting then the speed will decrease, or increase, accordingly. When the speed has diverged from its steady trimmed value by about 5% or so, the elevator is returned to its trim setting. This provides the disturbance and a stable aircraft will then execute a phugoid oscillation as it recovers its trim equilibrium. Analytically, the input is equivalent to an elevator pulse of several seconds' duration. The magnitude and length of the pulse would normally be established by trial and error since its effect will be very aircraft dependent. However, it should be remembered that for proper interpretation of the resulting response the disturbance should be small in magnitude since a small perturbation model is implied.

An example of a phugoid response recorded during a flight test exercise in a Handley Page Jetstream aircraft is shown in Fig. 6.11. The pilot input 'pulse' is clearly visible and, as for the short period mode, some practice is required before consistently good results are obtained. Again, the controls are released following the input to obtain the controls free dynamic response and the subsequent elevator motion is caused by the sinusoidal aerodynamic loading on the surface itself. The leading and trailing edge steps of the input elevator pulse may excite the short period mode. However, the short period mode transient would normally decay to zero well before the phugoid has properly developed and would not therefore obscure the observation of interest.

It is clear from an inspection of Fig. 6.11 that the phugoid damping is significantly higher than might be expected from the previous discussion of the mode characteristics. What is in fact shown is the aerodynamic, or basic airframe, phugoid modified by the inseparable effects of power. The Astazou engines of the Jetstream are governed to run at constant rpm and thrust changes are achieved by varying the propeller blade pitch. Thus, as the aircraft flies the sinusoidal flight path during a phugoid disturbance, the sinusoidal propeller loading causes the engine automatically to adjust its power to maintain constant propeller rpm. This very effectively increases the apparent damping of the phugoid. It is possible to operate the aircraft at a constant power condition when the 'power damping' effect is suppressed. Under these circumstances it is found that the

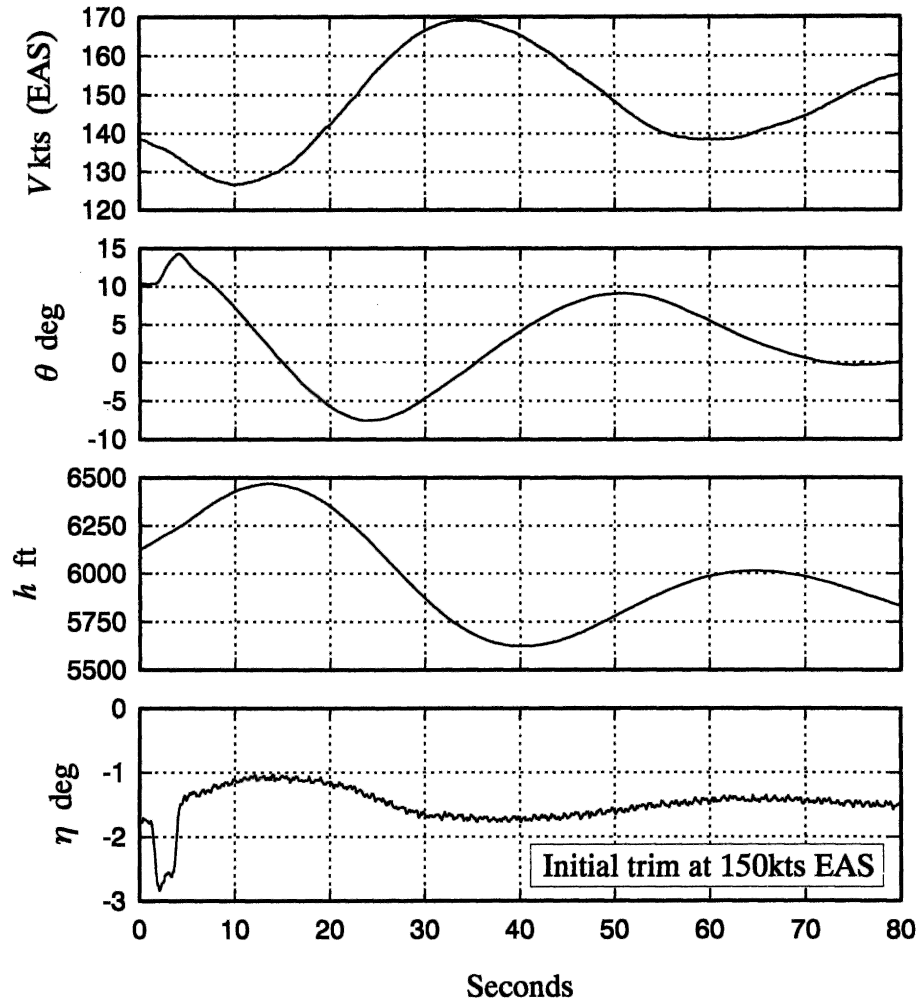

Fig. 6.11 Flight recording of the phugoid

aerodynamic phugoid is much less stable, as predicted by the simple theoretical model, and at some flight conditions it is unstable.

The above flight recording of the longitudinal stability modes illustrates the *controls free* dynamic stability characteristics. The same exercise could of course be repeated with the controls held fixed following the disturbing input. In this event the *controls fixed* dynamic stability characteristics would be observed. In general the differences between the responses would be small and not too significant. Now a controls free dynamic response is only possible in aeroplanes with reversible controls, which includes most small classical aeroplanes. Virtually all larger modern aircraft have powered controls, driven by electronic flight control systems, which are effectively irreversible and which means that they are only capable of exhibiting controls fixed dynamic response. Thus, today, most theoretical modelling and analysis is concerned with controls fixed dynamics only, as is the case throughout this book. However, a discussion of the differences between controls fixed and controls free aeroplane dynamics may be found in Hancock (1995).

When it is required to analyse the dynamics of a single mode in isolation, the best approach is to emulate flight test practice as far as that is possible. It is necessary to choose the most appropriate transfer functions to show the dominant response variables in the mode of interest. For example, as illustrated in Figs 6.10 and 6.11 the short period mode is best observed in the dominant response variables q and $w(\alpha)$, whereas the phugoid is best observed in its dominant response variables u, h and θ. It is necessary to apply a control input disturbance sympathetic to the mode dynamics and it is necessary to observe the response for an appropriate period of time. For example, Fig. 6.1 shows both longitudinal modes but the time scale of the illustration reveals the phugoid in much greater detail than the short period mode, whereas the time scale of Fig. 6.5 was chosen to reveal the short period mode in detail since that is the mode of interest. The form of the control input is not usually difficult to arrange in analytical work since most software packages have built-in impulse, step and pulse functions, whilst more esoteric functions can usually be programmed by the user. This kind of informed approach to the analysis is required if the best possible visualization of the longitudinal modes and their associated dynamics is to be obtained.

References

Friedland, B. 1987: *Control System Design.* McGraw-Hill Book Company, New York.

Hancock, G. J. 1995: *An Introduction to the Flight Dynamics of Rigid Aeroplanes.* Ellis Horwood Ltd, Hemel Hempstead.

Lanchester, F. W. 1908: *Aerodonetics.* Macmillan and Co, London.

Shinners, S. M. 1980: *Modern Control System Theory and Application.* Addison-Wesley Publishing Co, Reading, Massachusetts.

Teper, G. L. 1969: *Aircraft Stability and Control Data.* Systems Technology, Inc, STI Technical Report 176-1.

7

Lateral-directional Dynamics

7.1 Response to controls

The procedures for investigating and interpreting the lateral-directional dynamics of an aeroplane are much the same as those used to deal with the longitudinal dynamics and are not repeated at the same level of detail in this chapter. However, some aspects of lateral-directional dynamics, and their interpretation, differ significantly from the longitudinal dynamics and the procedures for interpreting the differences are dealt with appropriately. The lateral-directional response transfer functions are obtained in the solution of the lateral equations of motion using, for example, the methods described in Chapter 5.

The transfer functions completely describe the linear dynamic asymmetric response in sideslip, roll and yaw to aileron and rudder inputs. As in the longitudinal solution, implicit in the response are the dynamic properties determined by the lateral-directional stability characteristics of the aeroplane. As before, the transfer functions and the response variables described by them are linear since the entire modelling process is based on the assumption that the motion is constrained to small disturbances about an equilibrium trim state. The equilibrium trim state is assumed to mean steady level flight in the first instance and the previously stated caution concerning the magnitude of a small lateral-directional perturbation applies.

The most obvious difference between the solution of the longitudinal equations of motion and the lateral equations of motion is that there is more algebra to deal with. Since two aerodynamic inputs are involved, the ailerons and the rudder, two sets of input–output response transfer functions are produced in the solution of the equations of motion. However, these are no more difficult to deal with than a single input–output set of transfer functions, there are just more of them! The most significant difference between the longitudinal and lateral-directional dynamics of the aeroplane concerns the interpretation. In general, the lateral-directional stability modes are not so distinct and tend to exhibit dynamic coupling to a greater extent. Thus, some care is needed in the choice of assumptions made to facilitate their interpretation. A mitigating observation is that, unlike the longitudinal dynamics, the lateral-directional dynamics does not change very much with flight condition since most aeroplanes possess aerodynamic symmetry by design.

The lateral-directional equations of motion describing small perturbations about an

equilibrium trim condition and referred to wind axes are given by the state equation (4.70) as follows

$$\begin{bmatrix} \dot{v} \\ \dot{p} \\ \dot{r} \\ \dot{\phi} \end{bmatrix} = \begin{bmatrix} y_v & y_p & y_r & y_\phi \\ l_v & l_p & l_r & l_\phi \\ n_v & n_p & n_r & n_\phi \\ 0 & 1 & 0 & 0 \end{bmatrix} \begin{bmatrix} v \\ p \\ r \\ \phi \end{bmatrix} + \begin{bmatrix} y_\xi & y_\zeta \\ l_\xi & l_\zeta \\ n_\xi & n_\zeta \\ 0 & 0 \end{bmatrix} \begin{bmatrix} \xi \\ \zeta \end{bmatrix} \tag{7.1}$$

The solution of equation (7.1) produces two sets of four response transfer functions, one set describing motion in response to aileron input and a second set describing response to rudder input. As for the longitudinal response transfer functions, it is convenient to adopt a shorthand style of writing the transfer functions. The transfer functions describing response to aileron are conveniently written

$$\frac{v(s)}{\xi(s)} \equiv \frac{N_\xi^v(s)}{\Delta(s)} = \frac{k_v(s+1/T_{\beta_1})(s+1/T_{\beta_2})}{(s+1/T_s)(s+1/T_r)(s^2+2\zeta_d\omega_d s+\omega_d^2)} \tag{7.2}$$

$$\frac{p(s)}{\xi(s)} \equiv \frac{N_\xi^p(s)}{\Delta(s)} = \frac{k_{ps}(s^2+2\zeta_\phi\omega_\phi s+\omega_\phi^2)}{(s+1/T_s)(s+1/T_r)(s^2+2\zeta_d\omega_d s+\omega_d^2)} \tag{7.3}$$

$$\frac{r(s)}{\xi(s)} \equiv \frac{N_\xi^r(s)}{\Delta(s)} = \frac{k_r(s+1/T_\psi)(s^2+2\zeta_\psi\omega_\psi s+\omega_\psi^2)}{(s+1/T_s)(s+1/T_r)(s^2+2\zeta_d\omega_d s+\omega_d^2)} \tag{7.4}$$

$$\frac{\phi(s)}{\xi(s)} \equiv \frac{N_\xi^\phi(s)}{\Delta(s)} = \frac{k_\phi(s^2+2\zeta_\phi\omega_\phi s+\omega_\phi^2)}{(s+1/T_s)(s+1/T_r)(s^2+2\zeta_d\omega_d s+\omega_d^2)} \tag{7.5}$$

and the transfer functions describing response to rudder are conveniently written

$$\frac{v(s)}{\zeta(s)} \equiv \frac{N_\zeta^v(s)}{\Delta(s)} = \frac{k_v(s+1/T_{\beta_1})(s+1/T_{\beta_2})(s+1/T_{\beta_3})}{(s+1/T_s)(s+1/T_r)(s^2+2\zeta_d\omega_d s+\omega_d^2)} \tag{7.6}$$

$$\frac{p(s)}{\zeta(s)} \equiv \frac{N_\zeta^p(s)}{\Delta(s)} = \frac{k_p s(s+1/T_{\phi_1})(s+1/T_{\phi_2})}{(s+1/T_s)(s+1/T_r)(s^2+2\zeta_d\omega_d s+\omega_d^2)} \tag{7.7}$$

$$\frac{r(s)}{\zeta(s)} \equiv \frac{N_\zeta^r(s)}{\Delta(s)} = \frac{k_r(s+1/T_\psi)(s^2+2\zeta_\psi\omega_\psi s+\omega_\psi^2)}{(s+1/T_s)(s+1/T_r)(s^2+2\zeta_d\omega_d s+\omega_d^2)} \tag{7.8}$$

$$\frac{\phi(s)}{\zeta(s)} \equiv \frac{N_\zeta^\phi(s)}{\Delta(s)} = \frac{k_\phi(s+1/T_{\phi_1})(s+1/T_{\phi_2})}{(s+1/T_s)(s+1/T_r)(s^2+2\zeta_d\omega_d s+\omega_d^2)} \tag{7.9}$$

The solution of the equations of motion results in polynomial descriptions of the transfer function numerators and common denominator as set out in Appendix 2. The polynomials factorize into real and pairs of complex roots which are most explicitly quoted in the style of equations (7.2) to (7.9) above. Since the roots are interpreted as time constants, damping ratios and natural frequencies, the above style of writing makes the essential information instantly available. It should also be noted that the numerator and denominator factors are typical for a conventional aeroplane. Sometimes pairs of complex roots may be replaced with two real roots and vice versa. However, this does not usually mean that the dynamic response characteristics of the aeroplane become dramatically different. Differences in the interpretation of response may be evident but will not necessarily be large.

Transfer functions (7.2) to (7.9) each describe uniquely different, but related, variables

in the motion of the aeroplane in response to a control input. However, it will be observed that the notation adopted indicates similar values for some numerator terms in both aileron and rudder response transfer functions, for example k_r, T_ψ, ζ_ψ and ω_ψ appear in both $N^r_\xi(s)$ and $N^r_\zeta(s)$. It must be understood that the numerator parameters are context dependent and usually have a numerical value which is unique to the transfer function in question. To repeat the comment made above, the notation is a convenience for allocating particular numerator terms and serves only to identify the role of each term as a gain, time constant, damping ratio or frequency.

As before, the denominator of the transfer functions describes the characteristic polynomial which, in turn, describes the lateral-directional stability characteristics of the aeroplane. The transfer function denominator is therefore common to all response transfer functions. Thus, the response of all variables to an aileron or to a rudder input is dominated by the denominator parameters, namely time constants, damping ratio and natural frequency. The differences between the individual responses are entirely determined by their respective numerators and the *response shapes* of the individual variables are determined by the common denominator and 'coloured' by their respective numerators.

EXAMPLE 7.1

The equations of motion and aerodynamic data for the Douglas DC-8 aircraft were obtained from Teper (1969). At the flight condition of interest the aircraft has a total weight of 190 000 lb and is flying at Mach 0.44 at an altitude of 15 000 ft. The source data are referenced to aircraft body axes and for the purposes of this illustration they have been converted to a wind axes reference using the transformations given in Appendices 7 and 8. The equations of motion, referred to wind axes and quoted in terms of concise derivatives are, in state space format,

$$\begin{bmatrix} \dot{v} \\ \dot{p} \\ \dot{r} \\ \dot{\phi} \end{bmatrix} = \begin{bmatrix} -0.1008 & 0 & -468.2 & 32.2 \\ -0.00579 & -1.232 & 0.397 & 0 \\ 0.00278 & -0.0346 & -0.257 & 0 \\ 0 & 1 & 0 & 0 \end{bmatrix} \begin{bmatrix} v \\ p \\ r \\ \phi \end{bmatrix} + \begin{bmatrix} 0 & 13.48416 \\ -1.62 & 0.392 \\ -0.01875 & -0.864 \\ 0 & 0 \end{bmatrix} \begin{bmatrix} \xi \\ \zeta \end{bmatrix} \tag{7.10}$$

Since it is useful to have the transfer function describing sideslip angle β as well as sideslip velocity v, the output equation is augmented as described in Section 5.7. Thus, the output equation is

$$\begin{bmatrix} v \\ p \\ r \\ \phi \\ \beta \end{bmatrix} = \begin{bmatrix} 1 & 0 & 0 & 0 \\ 0 & 1 & 0 & 0 \\ 0 & 0 & 1 & 0 \\ 0 & 0 & 0 & 1 \\ 0.00214 & 0 & 0 & 0 \end{bmatrix} \begin{bmatrix} v \\ p \\ r \\ \phi \end{bmatrix} \tag{7.11}$$

Again, the numerical values of the matrix elements in equations (7.10) and (7.11) have been rounded to five decimal places in order to keep the equations to a reasonable written size. This should not be done with the equations used in the actual computation.

Solution of the equations of motion using *Program CC* produced the following two sets of transfer functions. First, the transfer functions describing response to aileron

$$\frac{v(s)}{\xi(s)} = \frac{8.779(s+0.197)(s-7.896)}{(s+0.0065)(s+1.329)(s^2+0.254s+1.433)} \text{ ft/s/rad}$$

$$\frac{p(s)}{\xi(s)} = \frac{-1.62s(s^2+0.362s+1.359)}{(s+0.0065)(s+1.329)(s^2+0.254s+1.433)} \text{ rad/s/rad (deg/s/deg)}$$

$$\frac{r(s)}{\xi(s)} = \frac{-0.0188(s+1.59)(s^2-3.246s+4.982)}{(s+0.0065)(s+1.329)(s^2+0.254s+1.433)} \text{ rad/s/rad (deg/s/deg)} \qquad (7.12)$$

$$\frac{\phi(s)}{\xi(s)} = \frac{-1.62(s^2+0.362s+1.359)}{(s+0.0065)(s+1.329)(s^2+0.254s+1.433)} \text{ rad/rad (deg/deg)}$$

$$\frac{\beta(s)}{\xi(s)} = \frac{0.0188(s+0.197)(s-7.896)}{(s+0.0065)(s+1.329)(s^2+0.254s+1.433)} \text{ rad/rad (deg/deg)}$$

and second, the transfer functions describing response to rudder

$$\frac{v(s)}{\zeta(s)} = \frac{13.484(s-0.0148)(s+1.297)(s+30.207)}{(s+0.0065)(s+1.329)(s^2+0.254s+1.433)} \text{ ft/s/rad}$$

$$\frac{p(s)}{\zeta(s)} = \frac{0.392s(s+1.85)(s-2.566)}{(s+0.0065)(s+1.329)(s^2+0.254s+1.433)} \text{ rad/s/rad (deg/s/deg)}$$

$$\frac{r(s)}{\zeta(s)} = \frac{-0.864(s+1.335)(s^2-0.03s+0.109)}{(s+0.0065)(s+1.329)(s^2+0.254s+1.433)} \text{ rad/s/rad(deg/s/deg)} \qquad (7.13)$$

$$\frac{\phi(s)}{\zeta(s)} = \frac{0.392s(s+1.85)(s-2.566)}{(s+0.0065)(s+1.329)(s^2+0.254s+1.433)} \text{ rad/rad (deg/deg)}$$

$$\frac{\beta(s)}{\zeta(s)} = \frac{0.029(s-0.0148)(s+1.297)(s+30.207)}{(s+0.0065)(s+1.329)(s^2+0.254s+1.433)} \text{ rad/rad (deg/deg)}$$

The characteristic equation is given by equating the denominator to zero

$$\Delta(s) = (s+0.0065)(s+1.329)(s^2+0.254s+1.433) = 0 \qquad (7.14)$$

The first real root describes the *spiral mode* with time constant

$$T_s = \frac{1}{0.0065} \cong 154\,\text{s}$$

the second real root describes the *roll subsidence* mode with time constant

$$T_r = \frac{1}{1.329} = 0.75\,\text{s}$$

and the pair of complex roots describe the oscillatory *dutch roll mode* with characteristics

$$\text{damping ratio } \zeta_d = 0.11$$

$$\text{undamped natural frequency } \omega_d = 1.2 \text{ rad/s}$$

Since both real roots are negative and the pair of complex roots have negative real parts then the mode characteristics indicate the airframe to be aerodynamically stable.

The response of the aeroplane to a unit (1°) aileron pulse, held on for two seconds

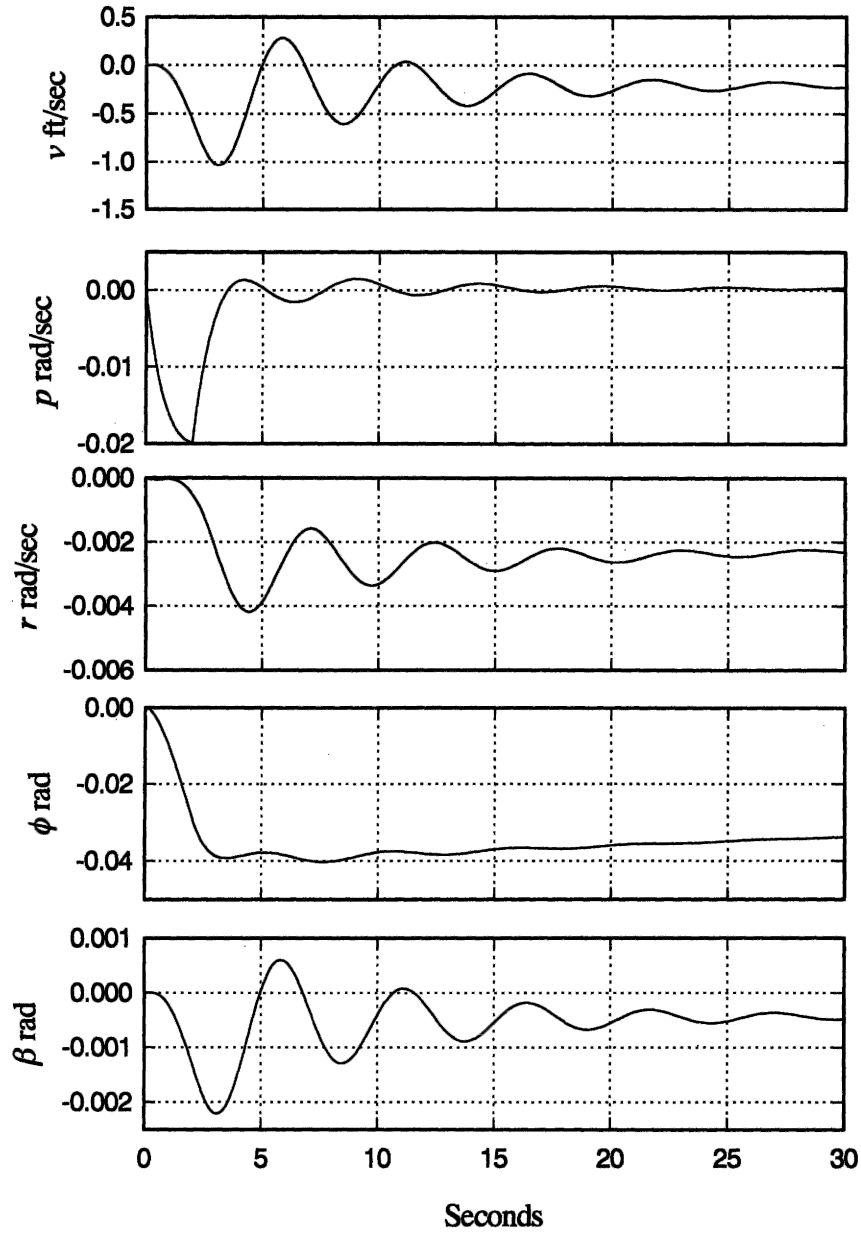

Fig. 7.1 Aircraft response to 1°–2 s aileron pulse input

and then returned to zero, is shown in Fig. 7.1. All of the variables obtained in the solution of the equations of motion are shown, the individual responses being characterized by the transfer functions, equations (7.12).

The dynamics associated with the three stability modes is visible in the responses although, at first glance, the dynamics would appear to be dominated by the oscillatory dutch roll mode since its damping is relatively low. Since the non-oscillatory spiral and roll modes are not so distinct, and since the dynamic

coupling between modes is significant, it is rather more difficult to expose the modes analytically unless some care is taken in their graphical presentation. This subject is discussed in greater detail in Section 7.6 below. Both the roll and spiral modes appear as exponentially convergent characteristics since they are both stable in this example. The roll mode converges relatively quickly with a time constant of 0.75 s, whereas the spiral mode converges very slowly indeed with a time constant of 154 s. The roll mode is most clearly seen in the roll rate response p

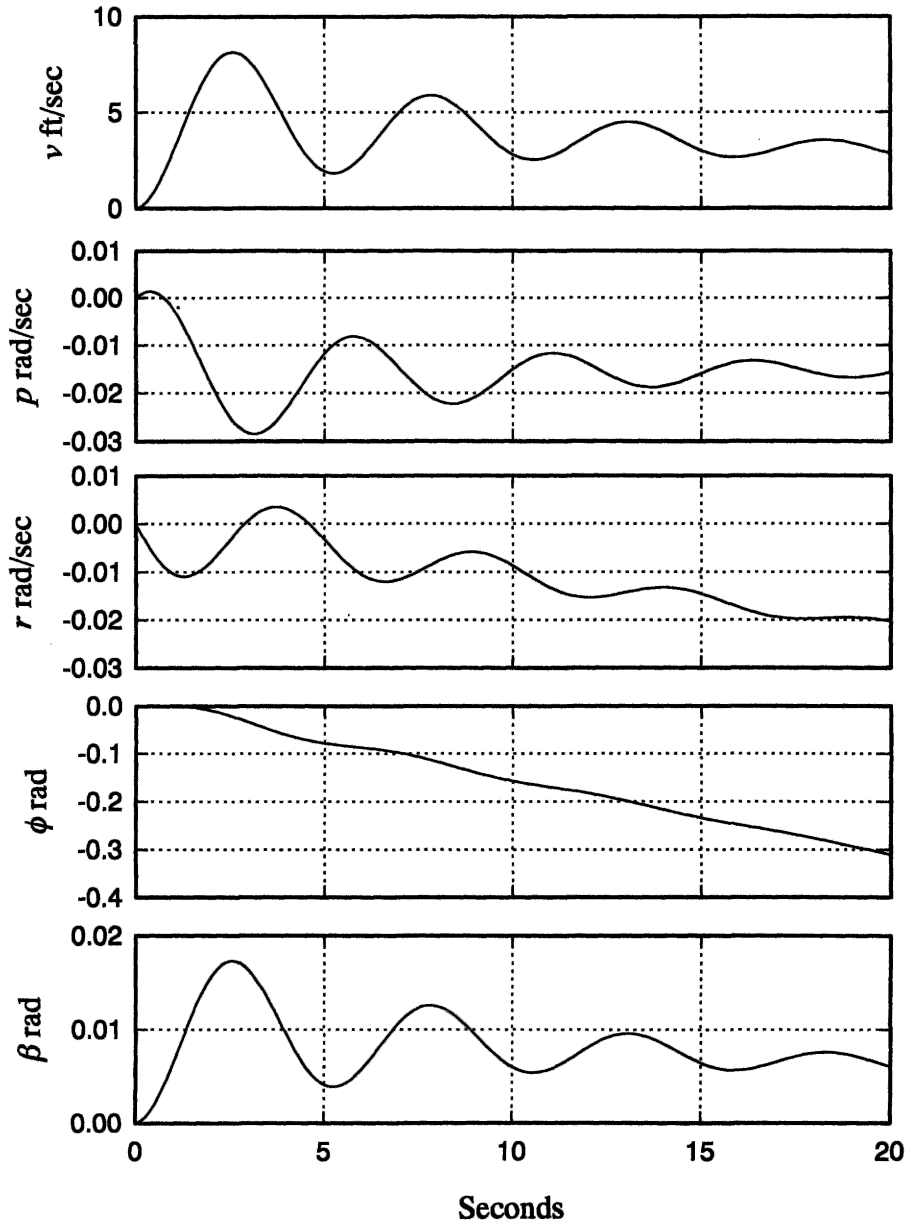

Fig. 7.2 Aircraft response to 1° rudder step input

where it determines the exponential rise at zero seconds and the exponential recovery when the pulse is removed at 2 s.

The spiral mode characteristic is rather more subtle and is most easily seen in the roll attitude response ϕ where it determines the longer term convergence to zero and is fully established at 30 s. Once again, all of the response shapes are determined by the common stability mode dynamics and the obvious differences between them are due to the unique numerators in each transfer function. All of the response variables shown in Fig. 7.1 eventually decay to zero in the time scale of the spiral mode (about 200 s) since the aircraft is stable.

The response of the aeroplane to a unit (1°) rudder step input is shown in Fig. 7.2. All of the variables obtained in the solution of the equations of motion are shown, the individual responses being characterized by the transfer functions, equations (7.13).

Again, it is very clear that the response is dominated by the oscillatory dutch roll mode. However, unlike the previous illustration, the roll and spiral modes are not discernible in the response. This is due to the fact that a step was chosen as the input which simply causes the aircraft to diverge from its initial equilibrium. This motion, together with the dutch roll oscillation, effectively masks the two non-oscillatory modes. Now it is possible to observe another interesting phenomenon in the response. Inspection of the transfer functions, equations (7.12) and (7.13), reveals that a number possess non-minimum phase numerator terms. The effect of these non-minimum phase terms would seem to be insignificantly small since they are not detectable in the responses shown in Fig. 7.1 and Fig. 7.2, with one exception. The roll rate response p to rudder, shown in Fig. 7.2, exhibits a sign reversal for the first second or so of its response and this is the manifestation of the non-minimum phase effect. In aeronautical parlance it is referred to as *adverse roll* in response to rudder.

A positive rudder step input is assumed and this will cause the aircraft to turn to the left, which is a negative response in accordance with the notation. Once the turn is established this results in negative yaw and yaw rate together with negative roll and roll rate induced by yaw–roll coupling. These general effects are correctly portrayed in the responses shown in Fig. 7.2. However, when the rudder is deflected initially, a substantial sideforce is generated at the centre of pressure of the fin which in turn generates the yawing moment causing the aircraft to turn. However, the sideforce acts at some distance above the roll axis and also generates a rolling moment which causes the aircraft to roll in the opposite sense to that induced by the yawing motion. Since inertia in roll is somewhat lower than inertia in yaw the aircraft responds quicker in roll and starts to roll in the 'wrong' direction, but as the yawing motion becomes established the aerodynamically induced rolling moment eventually overcomes the adverse rolling moment and the aircraft then rolls in the 'correct' sense. This behaviour is clearly visible in Fig. 7.2 and is a characteristic found in most aircraft. The magnitude of the effect is aircraft dependent and, if not carefully controlled by design, can lead to unpleasant handling characteristics.

A similar characteristic, *adverse yaw* in response to aileron, is caused by the differential drag effects associated with aileron deflection giving rise to an adverse yawing moment. This characteristic is also commonly observed in many aircraft: reference to equations (7.12) indicates that it is present in the DC-8 but is insignificantly small at the chosen flight condition.

The mode content in each of the motion variables is given most precisely by the eigenvectors. The relevance of eigenvectors is discussed in Section 5.6 and the

analytical procedure for obtaining them is illustrated in Example 5.7. With the aid of *PC MATLAB* the eigenvector matrix **V** was obtained from the state matrix in equation (7.10)

$$\mathbf{V} = \begin{array}{c} \begin{matrix} \multicolumn{2}{c}{\text{dutch roll mode}} & \text{roll mode} & \text{spiral mode} \end{matrix} \\ \begin{bmatrix} -0.845+0.5291\text{j} & -0.845-0.5291\text{j} & -0.9970 & 0.9864 \\ 0.0012-0.0033\text{j} & 0.0012+0.0033\text{j} & -0.0619 & -0.0011 \\ 0.0011+0.0021\text{j} & 0.0011-0.0021\text{j} & 0.0006 & 0.0111 \\ -0.0029-0.0007\text{j} & -0.0029+0.0007\text{j} & 0.0466 & 0.1641 \end{bmatrix} \end{array} \begin{matrix} :v \\ :p \\ :r \\ :\phi \end{matrix} \tag{7.15}$$

To facilitate interpretation of the eigenvector matrix, the magnitude of each component eigenvector is calculated as follows

$$|\mathbf{V}| = \begin{bmatrix} 0.9970 & 0.9970 & 0.9970 & 0.9864 \\ 0.0035 & 0.0035 & 0.0619 & 0.0011 \\ 0.0024 & 0.0024 & 0.0006 & 0.0111 \\ 0.0030 & 0.0030 & 0.0466 & 0.1641 \end{bmatrix} \begin{matrix} :v \\ :p \\ :r \\ :\phi \end{matrix}$$

Clearly, the content of all three modes in sideslip velocity v, and hence in β, is of similar order, the roll mode is dominant in roll rate p and the spiral mode is dominant in roll attitude response ϕ. These observations correlate well with the responses shown in Figs 7.1 and 7.2 although the low dutch roll damping obscures the observation in some response variables. Although not the case in this example, eigenvector analysis can be particularly useful for interpreting lateral-directional response in aircraft where mode coupling is rather more pronounced and the modes are not so distinct.

The steady state values of the motion variables following a unit step (1°) aileron or rudder input may be determined by the application of the final value theorem, equation (5.33), to the transfer functions, equations (7.12) and (7.13). The calculation procedure is illustrated in Example 6.1 and is not repeated here. Thus, the steady state response of all the motion variables to an aileron step input is

$$\begin{bmatrix} v \\ p \\ r \\ \phi \\ \beta \end{bmatrix}_{\text{steady state}} = \begin{bmatrix} -19.24 \text{ ft/s} \\ 0 \\ -11.99 \text{ deg/s} \\ -177.84 \text{ deg} \\ -2.35 \text{ deg} \end{bmatrix}_{\text{aileron}} \tag{7.16}$$

and the steady state response to a rudder step input is

$$\begin{bmatrix} v \\ p \\ r \\ \phi \\ \beta \end{bmatrix}_{\text{steady state}} = \begin{bmatrix} -11.00 \text{ ft/s} \\ 0 \\ -10.18 \text{ deg/s} \\ -150.36 \text{ deg} \\ -1.35 \text{ deg} \end{bmatrix}_{\text{rudder}} \tag{7.17}$$

It must be realized that the steady state values given in equations (7.16) and (7.17) serve only to give an indication of the control sensitivity of the aeroplane. At such large roll attitudes the small perturbation model ceases to apply and in practice significant changes in the aerodynamic operating conditions would accompany the response. The actual steady state values would undoubtedly be somewhat different and could only be ascertained with a full non-linear simulation model. This illustration indicates the

limiting nature of a small perturbation model for the analysis of lateral-directional dynamics and the need to exercise care in its interpretation.

7.1.1 THE CHARACTERISTIC EQUATION

The lateral-directional characteristic polynomial for a classical aeroplane is fourth order, it determines the common denominator of the lateral and directional response transfer functions and, when equated to zero, defines the characteristic equation which may be written

$$As^4 + Bs^3 + Cs^2 + Ds + E = 0 \tag{7.18}$$

The characteristic equation (7.18) most commonly factorizes into two real roots and a pair of complex roots which are most conveniently written

$$(1 + 1/T_s)(1 + 1/T_r)(s^2 + 2\zeta_d\omega_d s + \omega_d^2) = 0 \tag{7.19}$$

As indicated previously, the first real root in equation (7.19) describes the non-oscillatory spiral mode, the second real root describes the non-oscillatory roll subsidence mode and the pair of complex roots describe the oscillatory dutch roll mode. Now, since the equations of motion from which the characteristic equation is derived are referred to a wind axes reference, the stability modes, comprising equation (7.19), provide a complete description of the lateral-directional stability properties of the aeroplane with respect to the total steady velocity vector and subject to the constraints of small perturbation motion.

When the equations of motion are referred to a body axes system, the state equation (4.69) is fifth order and the characteristic equation is also of fifth order. The solution of the characteristic equation then has the following factors

$$s(1 + 1/T_s)(1 + 1/T_r)(s^2 + 2\zeta_d\omega_d s + \omega_d^2) = 0 \tag{7.20}$$

The modes are unchanged except for the addition of a zero root which indicates neutral stability. The zero root results from the addition of yaw angle to the state equation and indicates neutral stability in yaw, or heading. Interpretation of lateral-directional dynamics is unchanged and the additional information indicates the aeroplane to have an indeterminate yaw or heading angle. In other words, lateral-directional dynamics is evaluated about the steady total velocity vector which assumes an arbitrary direction in azimuth, yaw or heading. Interpretation of the non-zero roots of the characteristic equation is most easily accomplished if reference is first made to the properties of the classical mass–spring–damper system, which are summarized in Appendix 5.

Unlike the longitudinal dynamics, interpretation of the lateral-directional dynamics is not quite so straightforward; as the stability modes are not so distinct, there usually exists a significantly greater degree of mode coupling or interaction. This tends to make the necessary simplifying assumptions less appropriate with a consequent reduction of confidence in the observations. However, an assortment of well-tried procedures for interpreting the dynamic characteristics of the well-behaved aeroplane exist and these will be discussed below. The principal objective, of course, is to identify the aerodynamic drivers for each of the stability modes.

The connection between the observed dynamics of the aeroplane and its aerodynamic

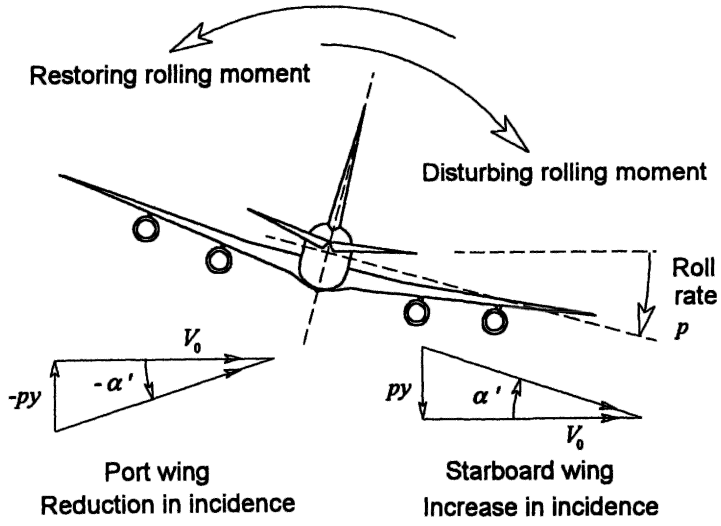

Fig. 7.3 The roll subsidence mode

characteristics is made by comparing equation (7.18) with either of equations (7.19) or (7.20), and then referring to Appendix 2 for the definitions of the coefficients in equation (7.18) in terms of aerodynamic stability derivatives. It will be appreciated immediately that further analytical progress is impossibly difficult unless some gross simplifying assumptions are made. Means for dealing with this difficulty require the derivation of reduced order models as described in Section 7.3 below.

7.2 The dynamic stability modes

As for the longitudinal stability modes, whenever the aeroplane is disturbed from its equilibrium trim state the lateral-directional stability modes will also be excited. Again, the disturbance may be initiated by pilot control action, a change in power setting, airframe configuration changes, such as flap deployment, and by external influences such as gusts and turbulence.

7.2.1 THE ROLL SUBSIDENCE MODE

The *roll subsidence mode*, or simply the *roll mode*, is a non-oscillatory lateral characteristic which is usually substantially decoupled from the spiral and dutch roll modes. Since it is non-oscillatory, it is described by a single real root of the characteristic polynomial, and it manifests itself as an exponential lag characteristic in rolling motion. The aeromechanical principles governing the behaviour of the mode are illustrated in Fig. 7.3.

With reference to Fig. 7.3, the aircraft is viewed from the rear so the indicated motion is shown in the same sense as it would be experienced by the pilot. Assume that the aircraft is constrained to one degree of freedom motion in roll about the *ox* axis only, and that it is initially in trimmed wings level flight. If, then, the aeroplane experiences a positive disturbing rolling moment it will commence to roll with an angular acceleration in accordance with Newton's second law of motion.

In rolling motion the wing experiences a component of velocity normal to the wing py, where y is the spanwise coordinate measured from the roll axis ox. As indicated in Fig. 7.3 this results in a small increase in incidence on the down-going starboard wing and a small decrease in incidence on the up-going port wing. The resulting differential lift gives rise to a restoring rolling moment as indicated. The corresponding resulting differential induced drag would also give rise to a yawing moment, but this is usually sufficiently small that it is ignored. Thus, following a disturbance, the roll rate builds up exponentially until the restoring moment balances the disturbing moment and a steady roll rate is established.

In practice, of course, this kind of behaviour would be transient rather than continuous as implied in this illustration. The physical behaviour explained is simple 'paddle' damping and is stabilizing in effect in all aeroplanes operating in normal, aerodynamically linear, flight regimes. For this reason, the stability mode is sometimes referred to as the *damping in roll.*

In some modern combat aeroplanes, which are designed to operate in seriously non-linear aerodynamic conditions, for example at angles of attack approaching 90°, it is possible for the physical conditions governing the roll mode to break down completely. The consequent loss of roll stability can result in rapid roll departure followed by complex lateral-directional motion of a hazardous nature. However, in a conventional aeroplane the roll mode appears to the pilot as a lag in roll response to controls. The lag time constant is largely dependent on the moment of inertia in roll and the aerodynamic properties of the wing, and is typically around one second or less.

7.2.2 THE SPIRAL MODE

The *spiral mode* is also non-oscillatory and is determined by the other real root in the characteristic polynomial. When excited, the mode dynamics is usually slow to develop

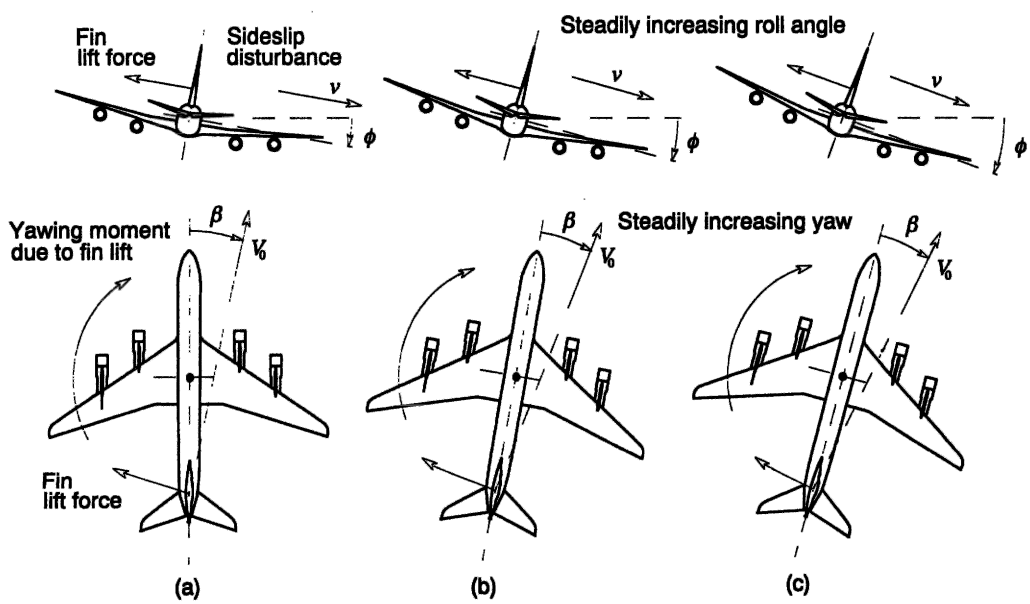

Fig. 7.4 The spiral mode development

and involves complex coupled motion in roll, yaw and sideslip. The dominant aero-mechanical principles governing the mode dynamics are illustrated in Fig. 7.4. The mode characteristics are very dependent on the lateral static stability and on the directional static stability of the aeroplane and these topics are discussed in Sections 3.4 and 3.5.

The mode is usually excited by a disturbance in sideslip which typically follows a disturbance in roll causing a wing to drop. Assume that the aircraft is initially in trimmed wings level flight and that a disturbance causes a small positive roll angle ϕ to develop; left unchecked this results in a small positive sideslip velocity v as indicated at (a) in Fig. 7.4. The sideslip puts the fin at incidence β which produces lift, and which in turn generates a yawing moment to turn the aircraft into the direction of the sideslip. The yawing motion produces differential lift across the wing-span which, in turn, results in a rolling moment causing the starboard wing to drop further, thereby exacerbating the situation. This developing divergence is indicated at (b) and (c) in Fig. 7.4. Simultaneously, the dihedral effect of the wing generates a negative restoring rolling moment due to sideslip, which acts to return the wing to a level attitude. Some additional restoring rolling moment is also generated by the fin lift force when it acts at a point above the roll axis ox, which is usual.

Therefore, the situation is one in which the fin effect, or directional static stability, and the dihedral effect, or lateral static stability, act in opposition to create this interesting dynamic condition. Typically, the requirements for lateral and directional static stability are such that the opposing effects are very nearly equal. When the dihedral effect is greater the spiral mode is stable, and hence convergent, and when the fin effect is greater the spiral mode is unstable, and hence divergent. Since these effects are nearly equal the spiral mode will be nearly neutrally stable, and sometimes it may even be neutrally stable, i.e. it will be neither convergent nor divergent. Since the mode is non-oscillatory it manifests itself as a classical exponential convergence or divergence and, since it is nearly neutral, the time constant is very large, typically 100 s or more. This means that when the mode is stable the wing is slow to recover a level attitude following a disturbance and when it is unstable the rate at which it diverges is also very slow. When it is neutral the aircraft simply flies a turn at constant roll attitude.

Now, it is the unstable condition which attracts most attention for obvious reasons. Once the mode is excited the aircraft flies a slowly diverging path in both roll and yaw and since the vertical forces are no longer in equilibrium the aircraft will also lose height. Thus, the unstable flight path is a spiral descent which left unchecked will end when the aircraft hits the ground! However, since the rate at which the mode diverges is usually very slow most pilots can cope with it. Consequently, an unstable spiral mode is permitted provided its time constant is sufficiently large. Because the mode is very slow to develop, the accelerations in the resulting motion are insignificantly small and the motion cues available to the pilot are almost imperceptible. In a spiral departure the visual cues become the most important cues to the pilot. It is also important to appreciate that a spiral departure is not the same as a spin. Spinning motion is a fully stalled flight condition whereas, in a spiral descent, the wing continues to fly in the usual sense.

7.2.3 THE DUTCH ROLL MODE

The *dutch roll* mode is a classical damped oscillation in yaw, about the oz axis of the aircraft, which couples into roll and, to a lesser extent, into sideslip. The motion

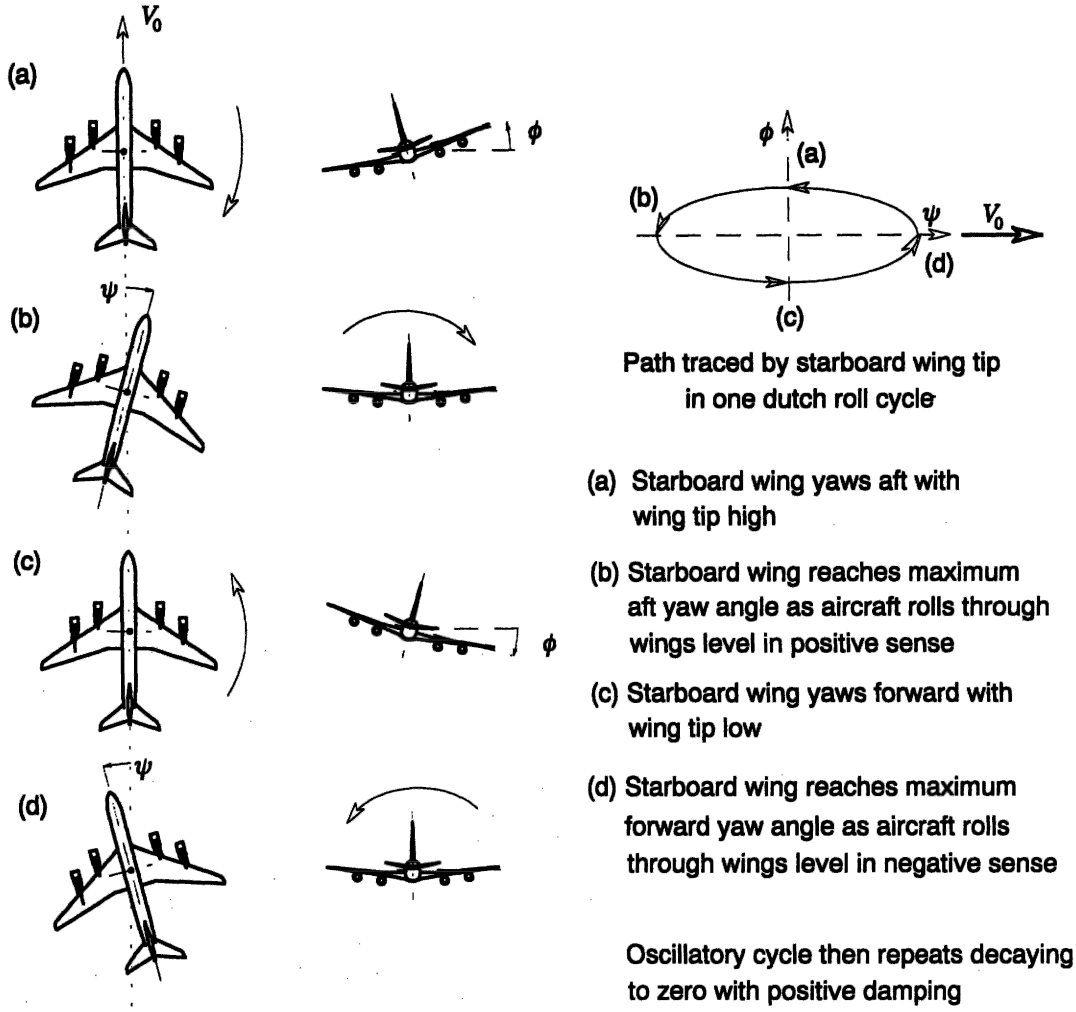

Fig. 7.5 The oscillatory dutch roll mode

described by the dutch roll mode is therefore a complex interaction between all three lateral-directional degrees of freedom. Its characteristics are described by the pair of complex roots in the characteristic polynomial. Fundamentally, the dutch roll mode is the lateral-directional equivalent of the longitudinal short period mode. Since the moments of inertia in pitch and yaw are of similar magnitude, the frequency of the dutch roll mode and the longitudinal short period mode are of similar order. However, the fin is generally less effective than the tailplane as a damper and the damping of the dutch roll mode is often inadequate. The dutch roll mode is so called since the motion of the aeroplane following its excitation is said to resemble the rhythmical flowing motion of a dutch skater on a frozen canal. One cycle of typical dutch rolling motion is shown in Fig. 7.5.

The physical situation applying can be appreciated by imagining that the aircraft is restrained in yaw by a torsional spring acting about the yaw axis *oz*, the spring stiffness being aerodynamic and determined largely by the fin. Thus, when in straight, level

trimmed equilibrium flight a disturbance in yaw causes the 'aerodynamic spring' to produce a restoring yawing moment which results in classical oscillatory motion. However, once the yaw oscillation is established the relative velocity of the air over the port and starboard wing also varies in an oscillatory manner giving rise to oscillatory differential lift and drag perturbations. This aerodynamic coupling gives rise in turn to an oscillation in roll which lags the oscillation in yaw by approximately 90°. This phase difference between yawing and rolling motion means that the forward going wing panel is low and the aft going wing panel is high, as indicated in Fig. 7.5. Consequently, the classical manifestation of the dutch roll mode is given by the path described by the wing tips relative to the horizon and which is usually elliptical, also shown in Fig. 7.5.

The peak roll to peak yaw ratio is usually less than one, as indicated, and is usually associated with a stable dutch roll mode. However, when the peak roll to peak yaw ratio is greater than one an unstable dutch roll mode is more likely.

Whenever the wing is disturbed from level trim, left to its own devices the aeroplane starts to slip sideways in the direction of the low wing. Thus, the oscillatory rolling motion leads to some oscillatory sideslipping motion in dutch rolling motion although the sideslip velocity is generally small. Thus, it is fairly easy to build up a visual picture of the complex interactions involved in the dutch roll mode. In fact, the motion experienced in a dutch rolling aircraft would seem to be analogous to that of a ball bearing dropped into an inclined channel having a semi-circular cross section. The ball bearing rolls down the inclined channel whilst oscillating from side to side on the circular surface.

Both the damping and stiffness in yaw, which determine the characteristics of the mode, are largely determined by the aerodynamic properties of the fin, a large fin being desirable for a well-behaved stable dutch roll mode. Unfortunately this contradicts the requirement for a stable spiral mode. The resulting aerodynamic design compromise usually results in aeroplanes with a mildly unstable spiral mode and a poorly damped dutch roll mode. Of course, the complexity of the dynamics associated with the dutch roll mode suggests that there must be other aerodynamic contributions to the mode characteristics in addition to the fin. This is generally the case and it is quite possible for the additional aerodynamic effects to be as significant as the aerodynamic properties of the fin if not more so. However, one thing is quite certain: it is very difficult to quantify all the aerodynamic contributions to the dutch roll mode characteristics with any degree of confidence.

7.3 Reduced order models

Unlike the longitudinal equations of motion it is more difficult to solve the lateral-directional equations of motion approximately. Because of the motion coupling present, to a greater or lesser extent, in all three mode dynamics, the modes are not so distinct and simplifying approximations are less relevant with the consequent loss of accuracy. Response transfer functions derived from reduced order models based on simplified approximate equations of motion are generally insufficiently accurate to be of any real use other than as a means for providing enhanced understanding of the aeromechanics of lateral-directional motion.

The simplest, and most approximate, solution of the characteristic equation provides an initial estimate for the two real roots only. This approximate solution of the lateral-directional characteristic equation (7.18) is based on the observation that conventional

aeroplanes give rise to coefficients A, B, C, D and E that have relative values which do not change very much with flight condition. Typically, A and B are relatively large whilst D and E are relatively small; in fact E is very often close to zero. Further, it is observed that $B \gg A$ and $E \ll D$, suggesting the following real roots as approximate solutions of the characteristic equation

$$\begin{aligned}(s + 1/T_r) &\cong (s + B/A)\\ (s + 1/T_s) &\cong (s + E/D)\end{aligned} \tag{7.21}$$

No such simple approximation for the pair of complex roots describing the dutch roll mode may be determined. Further insight into the aerodynamic drivers governing the characteristics of the roll and spiral modes may be made, with some difficulty, by applying assumptions based on the observed behaviour of the modes to the polynomial expressions for A, B, D and E given in Appendix 2. Fortunately, the same information may be deduced by a rather more orderly process involving a reduction in order of the equations of motion. The approximate solutions for the non-oscillatory modes as given by equations (7.21) are only useful for preliminary mode evaluations, or as a check of computer solutions, when the numerical values of the coefficients in the characteristic equation are known.

7.3.1 THE ROLL MODE APPROXIMATION

Provided the perturbation is small, the roll subsidence mode is observed to involve almost pure rolling motion with little coupling into sideslip or yaw. Thus, a reduced order model of the lateral-directional dynamics retaining only the roll mode follows by removing the sideforce and yawing moment equations from the lateral-directional state equation (7.1) to give

$$\begin{bmatrix}\dot{p}\\ \dot{\phi}\end{bmatrix} = \begin{bmatrix}l_p & l_\phi\\ 1 & 0\end{bmatrix}\begin{bmatrix}p\\ \phi\end{bmatrix} + \begin{bmatrix}l_\xi & l_\zeta\\ 0 & 0\end{bmatrix}\begin{bmatrix}\xi\\ \zeta\end{bmatrix} \tag{7.22}$$

Further, if aircraft wind axes are assumed then $l_\phi = 0$ and equation (7.22) reduces to the single degree of freedom rolling moment equation

$$\dot{p} = l_p p + l_\xi \xi + l_\zeta \zeta \tag{7.23}$$

The roll response to aileron transfer function is easily derived from equations (7.23). Taking the Laplace transform of equation (7.23), assuming zero initial conditions and assuming that the rudder is held fixed, $\zeta = 0$, then

$$sp(s) = l_p p(s) + l_\xi \xi(s) \tag{7.24}$$

which on rearranging may be written

$$\frac{p(s)}{\xi(s)} = \frac{l_\xi}{(s - l_p)} \equiv \frac{k_p}{(s + 1/T_r)} \tag{7.25}$$

The transfer function given by equation (7.25) is the approximate reduced order equivalent to the transfer function given by equation (7.3) and is the transfer function of a simple first order lag with time constant T_r. For small perturbation motion, equation (7.25) describes the first second or two of roll response to aileron with a reasonable degree of accuracy and is especially valuable as a means for identifying the dominant

physical properties of the airframe which determine the roll mode time constant. With reference to the definitions of the concise aerodynamic stability derivatives in Appendix 1, the roll mode time constant is determined approximately by

$$T_r \cong \frac{1}{l_p} = -\frac{(I_x I_z - I_{xz}^2)}{(I_z \mathring{L}_p + I_{xz} \mathring{N}_p)} \tag{7.26}$$

Since $I_x \gg I_{xz}$ and $I_z \gg I_{xz}$ then equation (7.26) may be further simplified to give the classical approximate expression for the roll mode time constant

$$T_r \cong -\frac{I_x}{\mathring{L}_p} \tag{7.27}$$

where I_x is the moment of inertia in roll and $\mathring{L}_p$ is the dimensional derivative describing the aerodynamic damping in roll.

7.3.2 *THE SPIRAL MODE APPROXIMATION*

Since the spiral mode is very slow to develop following a disturbance, it is usual to assume that the motion variables v, p and r are quasi-steady relative to the time scale of the mode. Hence $\dot{v} = \dot{p} = \dot{r} = 0$ and the lateral-directional state equation (7.1) may be written

$$\begin{bmatrix} 0 \\ 0 \\ 0 \\ \dot{\phi} \end{bmatrix} = \begin{bmatrix} y_v & y_p & y_r & y_\phi \\ l_v & l_p & l_r & l_\phi \\ n_v & n_p & n_r & n_\phi \\ 0 & 1 & 0 & 0 \end{bmatrix} \begin{bmatrix} v \\ p \\ r \\ \phi \end{bmatrix} + \begin{bmatrix} y_\xi & y_\zeta \\ l_\xi & l_\zeta \\ n_\xi & n_\zeta \\ 0 & 0 \end{bmatrix} \begin{bmatrix} \xi \\ \zeta \end{bmatrix} \tag{7.28}$$

Further, if aircraft wind axes are assumed $l_\phi = n_\phi = 0$ and if the controls are assumed fixed such that unforced motion only is considered $\xi = \zeta = 0$, then equation (7.28) simplifies to

$$\begin{bmatrix} 0 \\ 0 \\ 0 \\ \dot{\phi} \end{bmatrix} = \begin{bmatrix} y_v & y_p & y_r & y_\phi \\ l_v & l_p & l_r & 0 \\ n_v & n_p & n_r & 0 \\ 0 & 1 & 0 & 0 \end{bmatrix} \begin{bmatrix} v \\ p \\ r \\ \phi \end{bmatrix} \tag{7.29}$$

The first three rows in equation (7.29) may be rearranged to eliminate the variables v and r to give a reduced order equation in which the variables are roll rate p and roll angle ϕ only

$$\begin{bmatrix} 0 \\ \dot{\phi} \end{bmatrix} = \begin{bmatrix} y_v \dfrac{(l_p n_r - l_r n_p)}{(l_r n_v - l_v n_r)} + y_p + y_r \dfrac{(l_v n_p - l_p n_v)}{(l_r n_v - l_v n_r)} & y_\phi \\ 1 & 0 \end{bmatrix} \begin{bmatrix} p \\ \phi \end{bmatrix} \tag{7.30}$$

The first element of the first row of the reduced order state matrix in equation (7.30) may be simplified since the terms involving y_v and y_p are assumed to be insignificantly small compared with the term involving y_r. Thus, equation (7.30) may be rewritten

$$\begin{bmatrix} 0 \\ \dot{\phi} \end{bmatrix} = \begin{bmatrix} y_r \dfrac{(l_v n_p - l_p n_v)}{(l_r n_v - l_v n_r)} & y_\phi \\ 1 & 0 \end{bmatrix} \begin{bmatrix} p \\ \phi \end{bmatrix} \tag{7.31}$$

Since $\dot{\phi} = p$, equation (7.31) may be reduced to the single degree of freedom equation describing, approximately, the unforced rolling motion involved in the spiral mode

$$\dot{\phi} + \left(\frac{y_\phi(l_r n_v - l_v n_r)}{y_r(l_v n_p - l_p n_v)}\right)\phi = 0 \tag{7.32}$$

The Laplace transform of equation (7.32), assuming zero initial conditions, is

$$\phi(s)\left(s + \left(\frac{y_\phi(l_r n_v - l_v n_r)}{y_r(l_v n_p - l_p n_v)}\right)\right) \equiv \phi(s)(s + 1/T_s) = 0 \tag{7.33}$$

It should be noted that equation (7.33) is the reduced order lateral-directional characteristic equation retaining a very approximate description of the spiral mode characteristics only. Hence, an approximate expression for the time constant of the spiral mode is defined

$$T_s \cong \frac{y_r(l_v n_p - l_p n_v)}{y_\phi(l_r n_v - l_v n_r)} \tag{7.34}$$

The spiral mode time constant (equation 7.34) may be expressed conveniently in terms of the dimensional or dimensionless aerodynamic stability derivatives to provide a more direct link with the aerodynamic mode drivers. With reference to Appendix 1 and noting that $\mathring{Y}_r \ll mU_e$, so $y_r \cong U_e \equiv V_0$, and that $y_\phi = g$ since aircraft wind axes are assumed, then equation (7.34) may be restated

$$T_s \cong -\frac{U_e(\mathring{L}_v \mathring{N}_p - \mathring{L}_p \mathring{N}_v)}{g(\mathring{L}_r \mathring{N}_v - \mathring{L}_v \mathring{N}_r)} \equiv -\frac{V_0(L_v N_p - L_p N_v)}{g(L_r N_v - L_v N_r)} \tag{7.35}$$

Now a stable spiral mode requires that the time constant T_s is positive. Typically for most aeroplanes, especially in subsonic flight,

$$(L_v N_p - L_p N_v) > 0$$

and the condition for the mode to be stable simplifies to the approximate classical requirement that

$$L_v N_r > L_r N_v \tag{7.36}$$

Further analysis of this requirement is only possible if the derivatives in equation (7.36) are expressed in terms of the aerodynamic properties of the airframe. This means that L_v, dihedral effect, and N_r, damping in yaw, should be large whilst N_v, the yaw stiffness, should be small. Rolling moment due to yaw rate, L_r, is usually significant in magnitude and positive. In very simple terms aeroplanes with small fins and reasonable dihedral are more likely to have a stable spiral mode.

7.3.3 THE DUTCH ROLL MODE APPROXIMATION

For the purpose of creating a reduced order model to describe the dutch roll mode it is usual to make the rather gross assumption that dutch rolling motion involves no rolling motion at all. Clearly this is contradictory, but it is based on the fact that the mode is firstly a yawing oscillation and aerodynamic coupling causes rolling motion as a secondary effect. It is probably true that for most aeroplanes the roll to yaw ratio in dutch rolling motion is less than one, and in some cases may be much less than one,

which gives the assumption some small credibility. Hence, the lateral-directional state equation (7.1) may be simplified by writing

$$\dot{p} = p = \dot{\phi} = \phi = 0$$

As before, if aircraft wind axes are assumed $l_\phi = n_\phi = 0$ and if the controls are assumed fixed such that unforced motion only is considered, $\xi = \zeta = 0$, then equation (7.1) simplifies to

$$\begin{bmatrix} \dot{v} \\ \dot{r} \end{bmatrix} = \begin{bmatrix} y_v & y_r \\ n_v & n_r \end{bmatrix} \begin{bmatrix} v \\ r \end{bmatrix} \tag{7.37}$$

If equation (7.37) is written

$$\dot{\mathbf{x}}_d = \mathbf{A}_d \mathbf{x}_d$$

then the reduced order characteristic equation describing the approximate dynamic characteristics of the dutch roll mode is given by

$$\Delta_d(s) = \det[s\mathbf{I} - \mathbf{A}_d] = \begin{vmatrix} s - y_v & -y_r \\ -n_v & s - n_r \end{vmatrix} = 0$$

or

$$\Delta_d(s) = s^2 - (n_r + y_v)s + (n_r y_v - n_v y_r) = 0 \tag{7.38}$$

Therefore, the damping and frequency properties of the mode are given approximately by

$$\left.\begin{aligned} 2\zeta_d \omega_d &\cong -(n_r + y_v) \\ \omega_d^2 &\cong (n_r y_v - n_v y_r) \end{aligned}\right\} \tag{7.39}$$

With reference to Appendix 1, the expressions given by equations (7.39) can be restated in terms of dimensional aerodynamic stability derivatives. Further approximating simplifications are made by assuming $\mathring{Y}_r \ll mU_e$, so that $y_r \cong U_e \equiv V_0$, and by assuming, quite correctly, that both I_x and I_z are usually much greater than I_{xz}. It then follows that

$$\left.\begin{aligned} 2\zeta_d \omega_d &\cong -\left(\frac{\mathring{N}_r}{I_z} + \frac{\mathring{Y}_v}{m}\right) \\ \omega_d^2 &\cong \left(\frac{\mathring{N}_r}{I_z}\frac{\mathring{Y}_v}{m} - V_0\frac{\mathring{N}_v}{I_z}\right) \cong -V_0\frac{\mathring{N}_v}{I_z} \end{aligned}\right\} \tag{7.40}$$

Comparing the damping and frequency terms in the expressions in equations (7.40) with those of the mass–spring–damper in Appendix 5 it is easy to identify the roles of those aerodynamic stability derivatives which are dominant in determining the characteristics of the dutch roll mode. For example, $\mathring{N}_r$ is referred to as the yaw damping derivative and $\mathring{N}_v$ is referred to as the yaw stiffness derivative, and both are very dependent on the aerodynamic design of the fin and the fin volume ratio.

Although the dutch roll mode approximation gives a rather poor impression of the real thing, it is useful as means for gaining insight into the physical behaviour of the mode and its governing aerodynamics.

EXAMPLE 7.2

It has been stated that the principal use of the lateral-directional reduced order models is for providing insight into the aerodynamic mode drivers. With the exception of the transfer function describing roll rate response to aileron, transfer functions derived from the reduced order models are not commonly used in analytical work as their accuracy is generally poor. However, it is instructive to compare the values of the mode characteristics obtained from reduced order models with those obtained in the solution of the full order equations of motion.

Consider the Douglas DC-8 aircraft of Example 7.1. The equations of motion referred to wind axes are given by equation (7.10) and the solution gives the characteristic equation (7.14). The unfactorized characteristic equation is

$$\Delta(s) = s^4 + 1.5898s^3 + 1.7820s^2 + 1.9200s + 0.0125 = 0 \tag{7.41}$$

In accordance with the expression given in equations (7.21), approximate values for the roll mode and spiral mode time constants are given by

$$\left.\begin{aligned} T_r &\cong \frac{A}{B} = \frac{1}{1.5898} = 0.629\,\text{s} \\ T_s &\cong \frac{D}{E} = \frac{1.9200}{0.0125} = 153.6\,\text{s} \end{aligned}\right\} \tag{7.42}$$

The approximate roll mode time constant does not compare particularly well with the exact value of 0.75 s, whereas the spiral mode time constant compares extremely well with the exact value of 154 s.

The approximate roll rate response to aileron transfer function, given by equation (7.25), may be evaluated by obtaining the values for the concise derivatives l_p and l_ξ from equation (7.10) whence

$$\frac{p(s)}{\xi(s)} = \frac{-1.62}{(s + 1.232)}\,\text{deg/s/deg} \tag{7.43}$$

With reference to equation (7.25), an approximate value for the roll mode time constant is given by

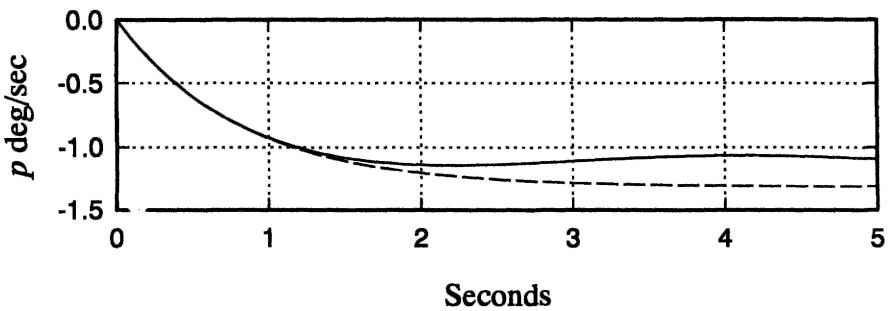

Fig. 7.6 Roll rate response to 1° aileron step input

$$T_r \cong \frac{1}{1.232} = 0.812\,\text{s} \tag{7.44}$$

and this value compares rather more favourably with the exact value. The short term roll rate response of the DC-8 to a 1° aileron step input as given by equation (7.43) is shown in Fig. 7.6 where it is compared with the exact response of the full order model as given by equations (7.12).

Clearly, for the first two seconds or so, the match is extremely good, which confirms the assumptions made about the mode to be valid provided the period of observation of roll behaviour is limited to the time scale of the roll mode. The approximate roll mode time constant calculated by substituting the appropriate derivative and roll inertia values, given in the aircraft data, into the expression given by equation (7.27) results in a value almost the same as that given by equation (7.44). This simply serves to confirm the validity of the assumptions made about the roll mode.

With reference to equations (7.34) and (7.35) the approximate spiral mode time constant may be written in terms of concise derivatives as

$$T_s \cong -\frac{U_e(l_v n_p - l_p n_v)}{g(l_r n_v - l_v n_r)} \tag{7.45}$$

Substituting values for the concise derivatives obtained from equation (7.10), the velocity U_e and g then

$$T_s \cong -\frac{468.2(0.0002 + 0.00343)}{32.2(0.0011 - 0.00149)} = 135.34\,\text{s} \tag{7.46}$$

Clearly this approximate value of the spiral mode time constant does not compare so well with the exact value of 154 s. However, this is not so important since the mode is very *slow* in the context of normal piloted manoeuvring activity. The classical requirement for spiral mode stability given by the inequality condition of equation (7.36) is satisfied since

$$0.00149 > 0.0011$$

Notice how close the values of the two numbers are, suggesting the mode to be close to neutrally stable in the time scale of normal transient response. This observation is quite typical of a conventional aeroplane like the DC-8.

Approximate values for the dutch roll mode damping ratio and undamped natural frequency are obtained by substituting the relevant values for the concise derivatives, obtained from equation (7.10), into the expressions given by equations (7.39). Thus, approximately

$$\omega_d \cong 1.152\ \text{rad/s}$$
$$\zeta_d \cong 0.135$$

These approximate values compare reasonably well with the exact values which are: a natural frequency of 1.2 rad/s and a damping ratio of 0.11. Such a good comparison is not always achieved and merely emphasizes, once more, the validity of the assumptions about the dutch roll mode in this particular application. The implication is that at the flight condition of interest the roll to yaw ratio of the dutch roll mode in the DC-8 is significantly less than one and, indeed, this may be inferred from either Fig. 7.1 or Fig. 7.2.

7.4 Frequency response

It is useful, and sometimes necessary, to investigate the lateral-directional response properties of an aeroplane in the frequency domain. The reasons why such an investigation might be made are much the same as those given for the longitudinal case in Section 6.4. Again, the Bode diagram is the most commonly used graphical tool for lateral-directional frequency response analysis. The method of construction of the Bode diagram and its interpretation follow the general principles described in Section 6.4 and are not repeated here. Since it is difficult to generalize, a typical illustration of lateral-directional frequency response analysis is given in the following example.

EXAMPLE 7.3

The lateral-directional frequency reponse of the Douglas DC-8 aircraft is evaluated for the same flight condition as Examples 7.1 and 7.2. The total number of transfer functions that could be evaluated on a Bode diagram is ten, given by equations (7.12) and (7.13), and to create ten Bode diagrams would be prohibitively lengthy in the present context. Since the essential frequency response information can be obtained from a much smaller number of transfer functions, the present example is limited to four transfer functions only. The chosen transfer functions were selected from equations (7.12) and (7.13), all are referred to aircraft wind axes and are repeated here for convenience

$$\begin{aligned}
\frac{\phi(s)}{\xi(s)} &= \frac{-1.62(s^2+0.362s+1.359)}{(s+0.0065)(s+1.329)(s^2+0.254s+1.433)} \text{ rad/rad (deg/deg)} \\
\frac{\beta(s)}{\xi(s)} &= \frac{0.0188(s+0.197)(s-7.896)}{(s+0.0065)(s+1.329)(s^2+0.254s+1.433)} \text{ rad/rad (deg/deg)} \\
\frac{r(s)}{\zeta(s)} &= \frac{-0.864(s+1.335)(s^2-0.03s+0.109)}{(s+0.0065)(s+1.329)(s^2+0.254s+1.433)} \text{ rad/s/rad (deg/s/deg)} \\
\frac{p(s)}{\zeta(s)} &= \frac{0.392s(s+1.85)(s-2.566)}{(s+0.0065)(s+1.329)(s^2+0.254s+1.433)} \text{ rad/s/rad (deg/s/deg)}
\end{aligned} \tag{7.47}$$

The first two transfer functions in equations (7.47) describe lateral response to the lateral command (aileron) variable, the third transfer function describes directional response to the directional command (rudder) variable, the last transfer function was chosen to illustrate cross-coupling and describes lateral response to the directional command variable. Now consider the frequency response of each transfer function in turn.

The frequency response of roll attitude ϕ to aileron input ξ is shown in Fig. 7.7. The most obvious features of the Bode diagram are the very high steady state gain, 45 dB, and the very small peak at the dutch roll frequency. The *roll-off* in phase behaves quite conventionally in accordance with the transfer function properties. The high zero frequency gain corresponds to a gain ratio of approximately 180. This means that following a 1° aileron step input the aeroplane will settle at a roll attitude of −180°, in other words inverted! Clearly, this is most inappropriate for a large civil transport aeroplane and serves as yet another illustration of the limitations of linear system modelling. Such a large amplitude excursion is definitely not a small perturbation and should not be regarded as such. However, the high zero frequency, or

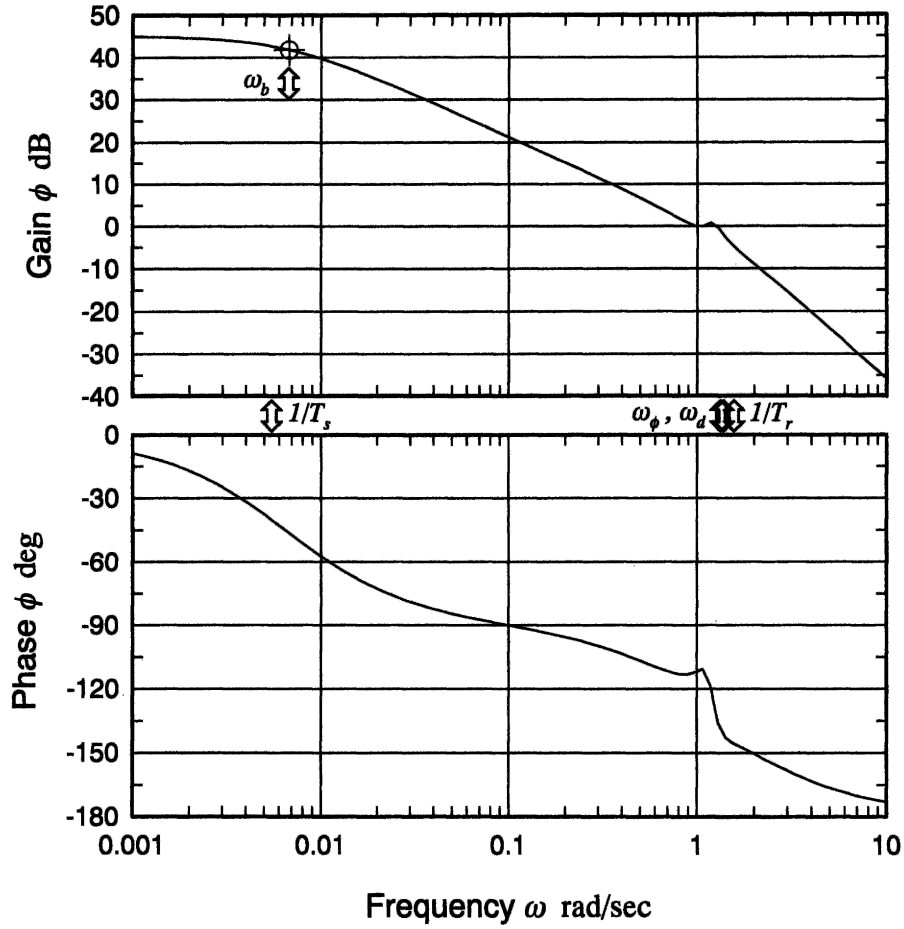

Fig. 7.7 DC-8 roll attitude frequency response to aileron

steady state, gain provides a good indication of the roll control sensitivity. As the control input frequency is increased the attitude response attenuates steadily with increasing phase lag, the useful bandwidth being a little above the spiral mode break frequency $1/T_s$. However, at all frequencies up to that corresponding to the roll subsidence mode break frequency, $1/T_r$, the aeroplane will respond to aileron since the gain is always greater than 0 dB, and it is the steady reduction in control sensitivity that will be noticed by the pilot.

Since the dutch roll damping ratio is relatively low at 0.11, an obvious peak might be expected in the gain plot at the dutch roll frequency. Clearly this is not the case. Inspection of the relevant transfer function in equations (7.47) shows that the second order numerator factor very nearly cancels the dutch roll roots in the denominator. This means that the dutch roll dynamics will not be very obvious in the roll attitude response to aileron in accordance with the observation. This conclusion is also confirmed by the time history response shown in Fig. 7.1. In fact the dutch roll cancellation is sufficiently close that it is permissible to write the transfer function in approximate form

$$\frac{\phi(s)}{\xi(s)} = \frac{-1.62}{(s+0.0065)(s+1.329)} \text{ rad/rad(deg/deg)} \tag{7.48}$$

with little loss of meaning. The time response plot and the Bode diagram derived from this approximate transfer function correspond closely with those derived from the full transfer function and may be interpreted to achieve the same conclusions for all practical purposes.

The frequency response of sideslip angle β to aileron input ξ is shown in Fig. 7.8 and corresponds to the second transfer function given in equations (7.47). Again, there are no real surprises here. The transfer function is non-minimum phase since the numerator term $1/T_{\beta_2}$ is negative, which introduces 90° of phase lag at the corresponding break frequency. In this response variable the dutch roll gain peak is clearly visible although at the dutch roll frequency the gain is attenuated by about −20 dB which means that the pilot would see no significant oscillatory sideslip behaviour. Again, it is established that the usable bandwidth is a little higher than the spiral mode break frequency $1/T_s$.

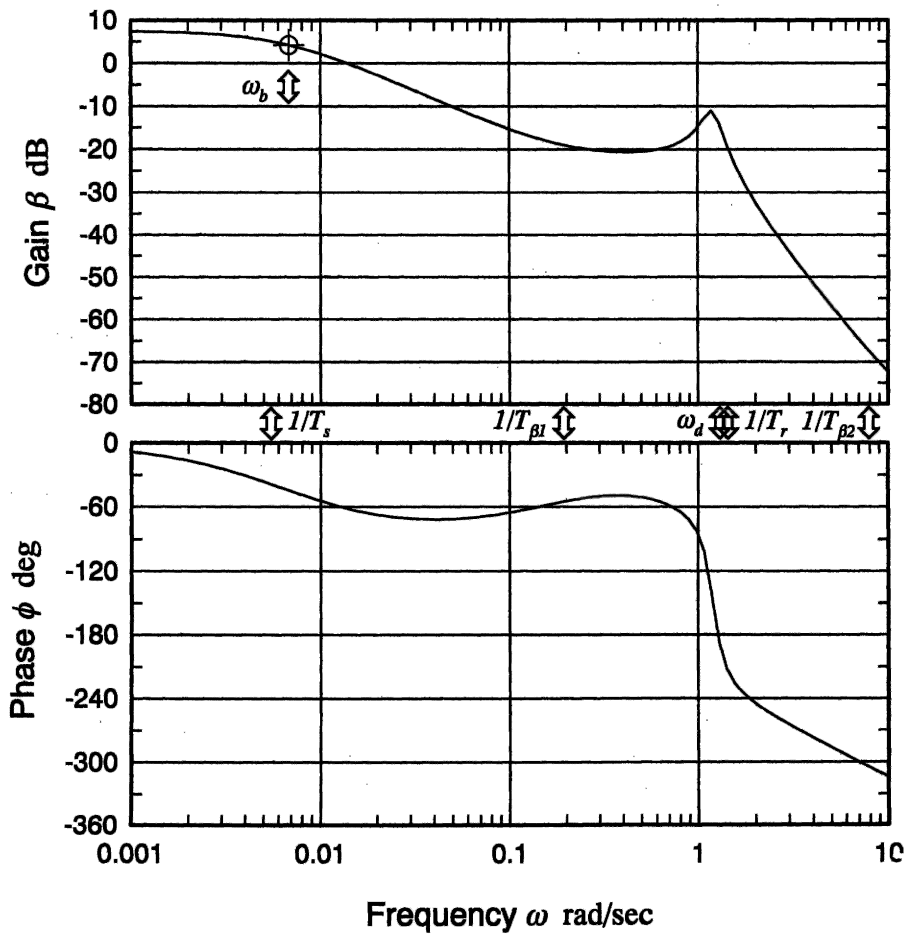

Fig. 7.8 DC-8 sideslip angle frequency response to aileron

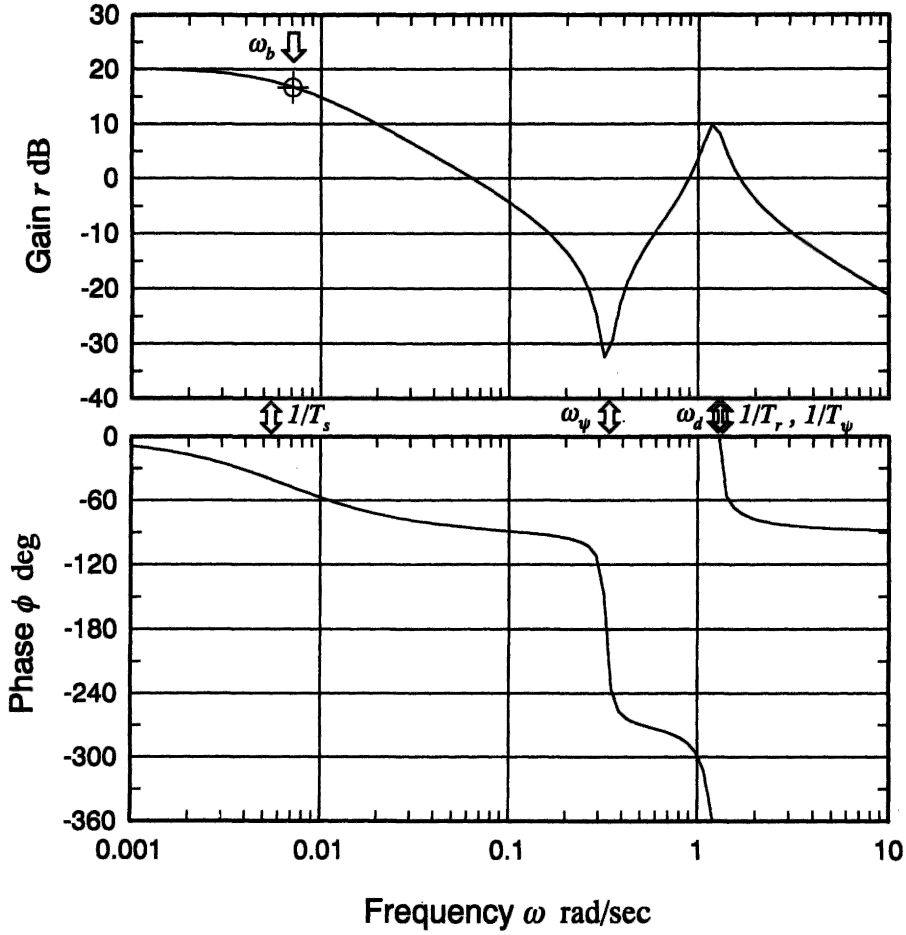

Fig. 7.9 DC-8 yaw rate frequency response to rudder

The frequency response of yaw rate r to rudder input ζ is shown in Fig. 7.9. This transfer function describes the typical classical directional response to control and the frequency response, shown in Fig. 7.9, has some interesting features. The gain plot shows a steady but significant attenuation with increasing frequency to reach a minimum of about −30 dB at ω_ψ, the resonant frequency of the second order numerator factor. The gain rises rapidly with a further increase in frequency to reach a maximum of 10 dB at the dutch roll frequency only to decrease rapidly thereafter. At very low input frequencies the phase lag increases gently in accordance with the spiral mode dynamics until the effect of the second order numerator term becomes apparent. The rate of change of phase is then very dramatic since the effective damping ratio of the second order numerator term is very small and negative. At the dutch roll frequency, approximately, the phase reaches −360° and the response appears to be in phase again only to roll off smartly at higher frequency. Again, the effective bandwidth is a little higher than the spiral mode break frequency $1/T_s$. These unusual frequency response characteristics are easily appreciated in a flight demonstration.

If the pilot approximates a sinusoidal rudder input by pedalling gently on the rudder

pedals then, at very low frequencies approaching the steady state, the yaw rate response will follow the input easily and obviously, since the gain is approximately 20 dB, and with very little phase lag. As the pilot increases the frequency of his pedalling the response will lag the input and the magnitude of the response will reduce very quickly until there is no significant observable response. If he increases the frequency of his forcing yet further, then the aircraft will spring into life again as the dutch roll frequency (resonance) is reached when the yaw rate response will be approximately in phase with the input. At higher frequencies still the response will rapidly attenuate for good.

The substantial dip in both gain and phase response with frequency, caused by the second order numerator factor, effectively isolates the dutch roll mode to a small window in the frequency band. This then makes it very easy for the pilot to identify and excite the dutch roll mode by rudder pedalling. This is very good for flight demonstration but may not be so good for handling if the dutch roll damping is low and the second order numerator factor is not too close in frequency to that of the dutch roll mode.

The frequency response of roll rate p to rudder input ζ is shown in Fig. 7.10. This

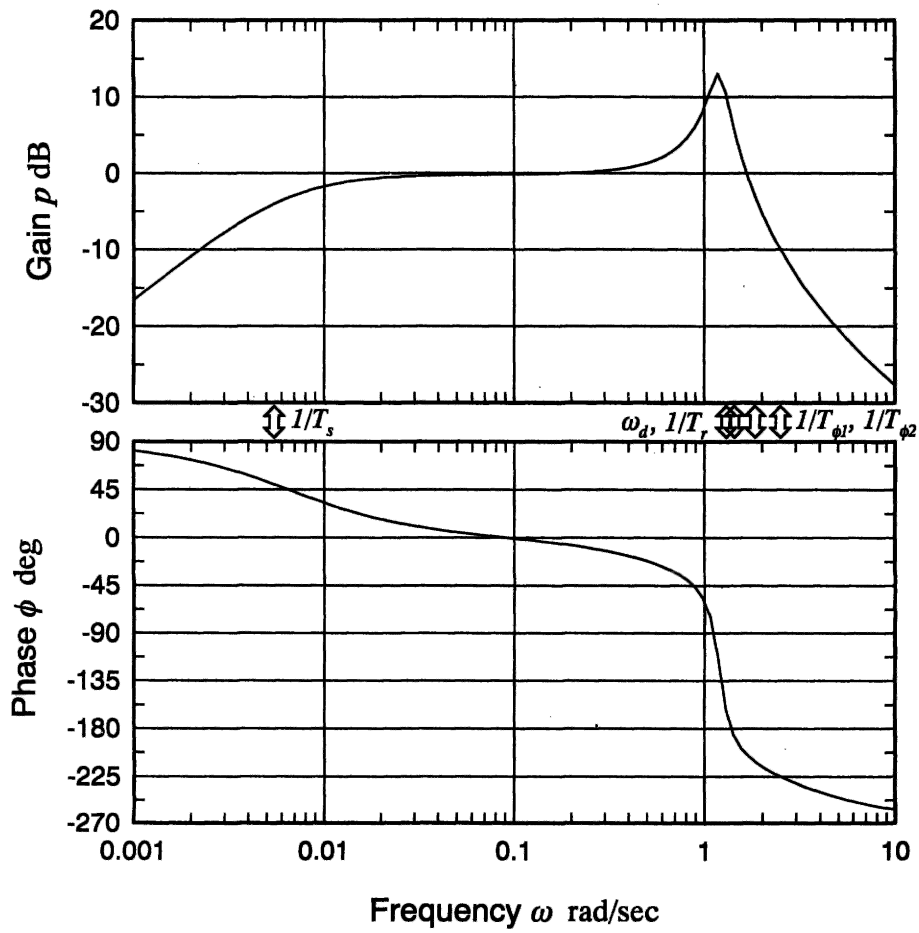

Fig. 7.10 DC-8 roll rate frequency response to rudder

frequency response example is interesting since it represents a cross-coupling case. In the steady state, or equivalently at zero frequency, roll rate in response to a rudder input would not be expected. This is clearly evident on the gain plot where the gain is $-\infty$ dB at zero frequency. This observation is driven by the zero in the numerator which also introduces 90° of phase lead at the very lowest frequencies. This zero also very nearly cancels with the spiral mode denominator root such that at input frequencies above the spiral mode break frequency $1/T_s$ the response in both gain and phase is essentially *flat* until the effects of the remaining numerator and denominator roots come into play, all at frequencies around the dutch roll frequency. The dutch roll resonant peak in gain and the subsequent roll-off in both gain and phase is absolutely classical and is easily interpreted. These frequency response observations correspond well with the response time history shown in Fig. 7.2, where the effects of the roll subsidence mode and the dutch roll mode are clearly visible, whilst the longer term convergence associated with the spiral mode is not visible at all. In this example, bandwidth tends to lose its meaning. However, it would not be unrealistic to suggest that the usable bandwidth is a little higher than the dutch roll mode frequency, provided the effects at very low frequency are ignored. This then assumes that the zero numerator factor cancels with the spiral mode denominator factor to give the approximate transfer function

$$\frac{p(s)}{\zeta(s)} = \frac{0.392(s+1.85)(s-2.566)}{(s+1.329)(s^2+0.254s+1.433)} \text{ rad/s/rad(deg/s/deg)} \tag{7.49}$$

As before, this approximate transfer function may be interpreted both in the time domain and in the frequency domain with little loss of meaning over the usable frequency band.

7.5 Flying and handling qualities

As with longitudinal stability the lateral-directional stability characteristics of the aeroplane are critically important in the determination of its flying and handling qualities and there is no doubt that they must be correct. Traditionally the emphasis on lateral-directional flying and handling qualities has been much less than the emphasis on the longitudinal flying and handling qualities. Unlike the longitudinal flying and handling qualities the lateral-directional flying and handling qualities do not usually change significantly with flight condition, especially in the context of small perturbation modelling. So once they have been fixed by the aerodynamic design of the airframe they tend to remain more-or-less constant irrespective of flight condition. Any major lateral-directional departures from nominally small perturbations about trim are likely to be transient, under full pilot control and, consequently, unlikely to give rise to serious handling problems. However, this is not necessarily a safe assumption to make when considering highly augmented aircraft, a topic which is beyond the scope of the present discussion.

It is a recurrent theme in handling qualities work that short term dynamics is properly controlled by design. The typical frequencies involved in short term dynamics are similar to human pilot frequencies and their inadvertent mismatch is a sure recipe for potential handling problems. So for reasons similar to those discussed in greater detail in Section 6.5 referring to longitudinal dynamics, it is equally important that the

lateral-directional short period stability modes be properly controlled. This may be interpreted to mean that the damping of both the roll subsidence mode and the dutch roll mode should be adequate.

The roll subsidence mode appears to the pilot as a lag in the response to control and, clearly, if the time constant should become too large, roll response to control would become too sluggish. A large roll mode time constant is the direct result of low roll stability although the mode is usually stable as discussed in Section 7.2.1. Generally, acceptable levels of roll mode stability result in a time constant or roll response lag which is almost imperceptible to the pilot. However, it is quite common to find aircraft in which the roll mode damping is inadequate, but it is unusual to find over-damped aircraft.

The spiral mode, being a long period mode, does not usually influence short term handling significantly. When it is stable and its time constant is sufficiently long it has little or no impact on flying and handling qualities. However, when it is unstable it manifests itself as a trimming problem since the aeroplane will continually attempt to diverge laterally. When the time constant of the mode is short it is more unstable and the rate of divergence becomes faster with a corresponding increase in pilot workload. Since the mode is generally so slow to develop, the motion cues associated with it may well be imperceptible to the pilot. Thus, a hazardous situation may easily arise if the external visual cues available to the pilot are poor or absent altogether, such as in IMC flight conditions. It is not unknown for inexperienced pilots to become disorientated in such circumstances with the inevitable outcome! Therefore, the general requirement is that the spiral mode should preferably be stable but, since this is difficult to achieve in many aeroplanes, when it is unstable the time constant should be greater than a defined minimum.

Since the dutch roll mode is a short period mode and is the directional equivalent of the longitudinal short period mode, its importance to handling is similarly critical. Generally, it is essential that the dutch roll mode is stable and that its damping is greater than a defined minimum. Similarly tight constraints are placed on the permitted range of combinations of frequency and damping. However, a level of damping lower than that of the longitudinal short period mode is permitted. This is perhaps convenient but is more likely to result from the design conflict with the spiral mode, which must not have more than a limited degree of instability.

7.6 Mode excitation

Unlike the longitudinal stability modes the lateral-directional stability modes usually exhibit a significant level of dynamic coupling and, as a result, it is more difficult to excite the modes independently for the purposes of demonstration or measurement. However, the lateral-directional stability modes may be excited selectively by the careful application of a sympathetic aileron or rudder input to the trimmed aircraft. Again, the methods developed for in-flight mode excitation reflect an intimate understanding of the dynamics involved and are generally easily adapted to the analytical environment. Because the lateral-directional stability modes usually exhibit a degree of dynamic coupling, the choice and shape of the disturbing input is critical to the mode under investigation. As always, standard experimental procedures have been developed in order to achieve consistency in the flight test or analytical process so that meaningful comparative studies may be made.

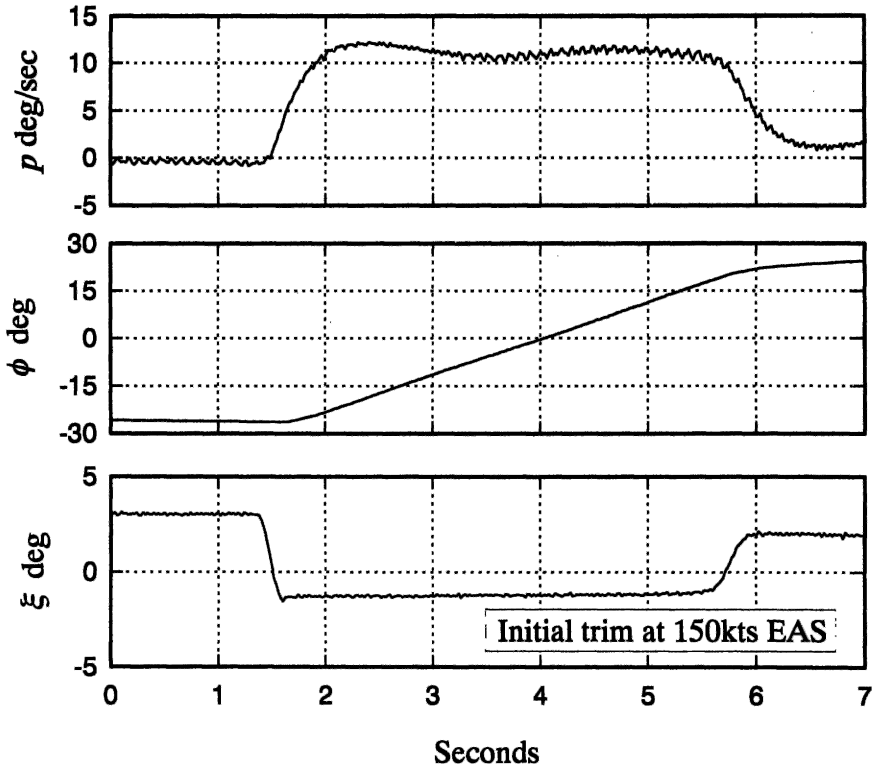

Fig. 7.11 Flight recording of the roll subsidence mode

The roll subsidence mode may be excited by applying a short duration square pulse to the aileron, the other controls remaining fixed at their trim settings. The magnitude and duration of the pulse must be carefully chosen if the aeroplane is not to roll too rapidly through a large attitude change and thereby exceed the limit of small perturbation motion. Since the mode involves almost pure rolling motion only no significant motion coupling will be seen in the relatively short time scale of the mode. Therefore, to see the classical characteristics of the roll subsidence mode it is only necessary to observe roll response for a few seconds.

An example of a roll response showing the roll subsidence mode recorded during a flight test exercise in a Handley Page Jetstream aircraft is shown in Fig. 7.11. The input aileron pulse is clearly seen and has a magnitude of about 4° and a duration of about 4 s. The shape of this input will have been established by the pilot by trial and error since the ideal input is very much aircraft dependent. The effect of the roll mode time constant is clearly visible since it governs the exponential rise in roll rate p as the response attempts to follow the leading edge of the input ξ. The same effect is seen again in reverse when the input is returned to its datum at the end of the pulse. The barely perceptible oscillation in roll rate during the 'steady part' of the response is, in fact, due to a small degree of coupling with the dutch roll mode.

In order to conduct the flight experiment without large excursions in roll attitude ϕ it is usual first to establish the aircraft in a steady turn with, in this illustration, $-30°$ of roll attitude. On application of the input pulse the aircraft rolls steadily through to

+30° of roll attitude when the motion is terminated by returning the aileron to datum. This is also clearly visible in Fig. 7.11. The effect of the roll mode time constant on the roll attitude response is to smooth the entry to, and exit from, the steady part of the response. Since the roll mode time constant is small, around 0.4 s for the Jetstream, its effect is only just visible in the roll attitude response. It is interesting to observe that the steady part of the roll response is achieved when the moment due to the damping in roll becomes established at a value equal and opposite to the disturbing moment in roll caused by the aileron deflection. Clearly, therefore, the roll subsidence mode governs the transient entry to, and exit from, all rolling motion.

The spiral mode may be excited by applying a small step input to rudder ζ, the remaining controls being held at their trim settings. The aeroplane responds by starting to turn, the wing on the inside of the turn starts to drop and sideslip develops in the direction of the turn. When the roll attitude has reached about 20° the rudder is gently returned to datum and the aeroplane left to its own devices. When the spiral mode is

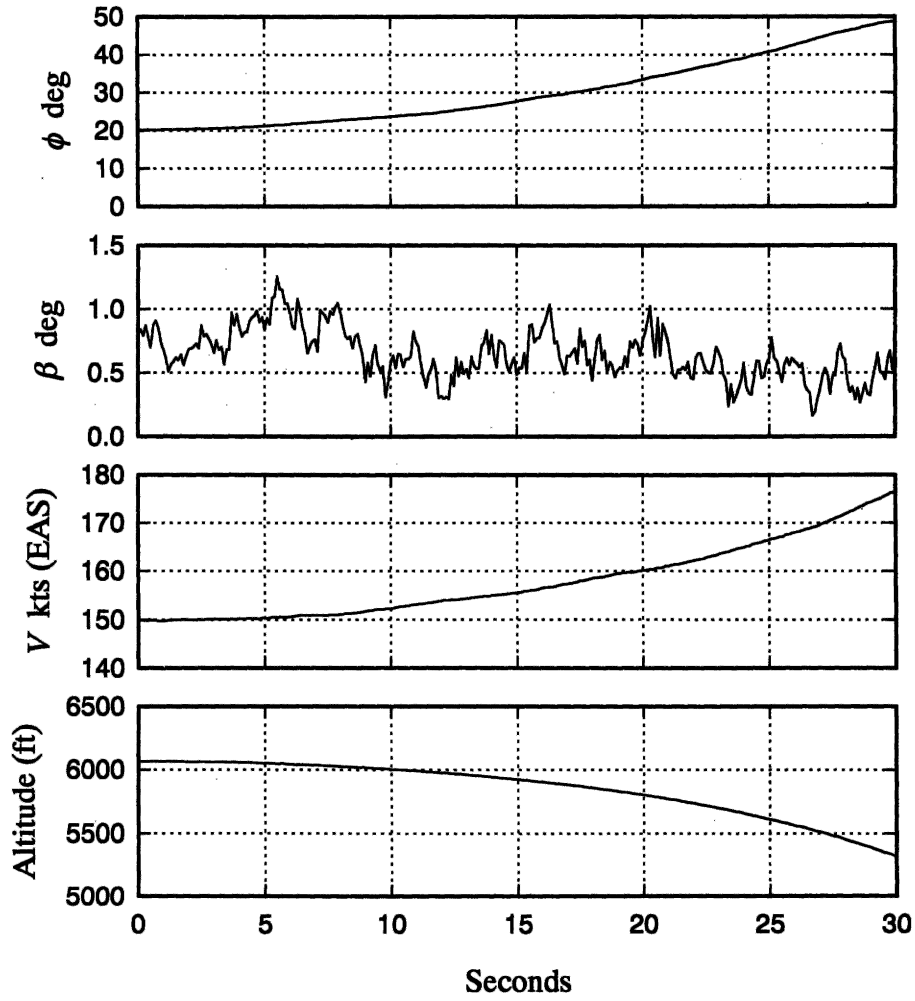

Fig. 7.12 Flight recording of the spiral mode departure

stable the aeroplane will slowly recover wings level flight, the recovery being exponential with spiral mode time constant. When the mode is unstable the coupled roll–yaw–sideslip departure will continue to develop exponentially with spiral mode time constant. An example of an unstable spiral mode, captured from the time the disturbing rudder input is returned gently to datum, and recorded during a flight test exercise in a Handley Page Jetstream aircraft, is shown in Fig. 7.12. The slow exponential divergence is clearly visible in all recorded variables, with the possible exception of sideslip angle β which is rather noisy. In any event the magnitude of sideslip would normally be limited to a small value by the weathercock effect of the fin.

Although speed and altitude play no part in determining the characteristic of the mode, the exponential departure in these variables is a classical, and very visible, consequence of an unstable spiral mode. Once excited, since the aircraft is no longer in wings level flight, lift is insufficient to maintain altitude and so an accelerating descent follows and the spiral flight path is determined by the aeromechanics of the mode. The first 30 s of the descent is shown in Fig. 7.12. Obviously, the departure must be terminated after a short time if the safety of the aeroplane and its occupants is not to be jeopardized.

Ideally, the dutch roll mode may be excited by applying a doublet to the rudder pedals with a period matched to that of the mode, all other controls remaining at their trim settings. In practice, the pilot pedals continuously and cyclically on the rudder pedal and by adjusting the frequency it is easy to find the resonant condition. See the related comments in Example 7.3 and note that the dutch roll frequency is comfortably within the human bandwidth. In this manner a forced oscillation may easily be sustained. On ceasing the forcing input the free transient characteristics of the dutch roll mode may be seen. This free response is shown in the flight recording in Fig. 7.13 which was made in a Handley Page Jetstream aircraft. The rudder input ζ shows the final doublet before ceasing the forcing at about 5 s; the obvious oscillatory rudder motion after 5 s is due to the cyclic aerodynamic load on the free rudder. The classical damped oscillatory motion is clearly visible in the variables shown: yaw rate r, roll rate p and sideslip angle β. The motion would also be clearly evident in both roll and yaw attitude variables which are not shown. Note the relative magnitudes of, and the phase shift between, yaw rate r and roll rate p, observations which are consistent with the classical physical explanation of the mode dynamics.

As for the longitudinal modes discussed in Section 6.6 the above flight recordings of the lateral-directional stability modes illustrate the *controls free* dynamic stability characteristics. The same exercise could be repeated with the controls held fixed following the disturbing input. Obviously, in this event the *controls fixed* dynamic stability characteristics would be observed and, in general, the differences between the responses would be small. To reiterate the important comments made in Section 6.6, controls free dynamic response is only possible in aeroplanes with reversible controls, which includes most small classical aeroplanes. Virtually all larger modern aircraft have powered controls, driven by electronic flight control systems, which are effectively irreversible and which means that they are only capable of exhibiting controls fixed dynamic response. Thus, today, most theoretical modelling and analysis is concerned with controls fixed dynamics only, as is the case throughout this book. However, a discussion of the differences between controls fixed and controls free aeroplane dynamics may be found in Hancock (1995).

When it is required to investigate the dynamics of a single mode in isolation

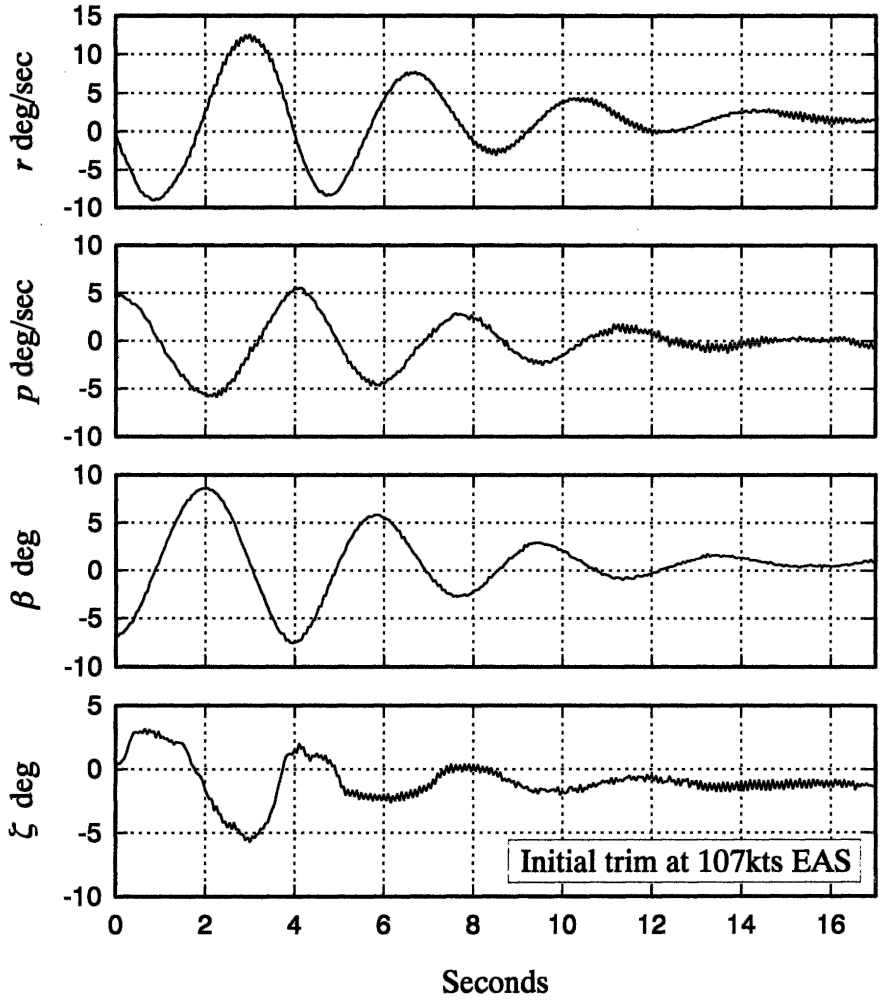

Fig. 7.13 Flight recording of the dutch roll mode

analytically, the best approach is to emulate flight test practice as far as that is possible. It is necessary to choose the most appropriate transfer functions to show the dominant response variables in the mode of interest. For example, the roll subsidence mode may only be observed sensibly in the dominant response variable p and, to a lesser extent, in ϕ. Similarly, for the spiral and dutch roll modes, it is important to observe the motion in those variables which are dominant, and hence most visible in the mode dynamics. It is also essential to apply a control input disturbance sympathetic to the mode dynamics and it is essential to observe the response for an appropriate period of time. Otherwise the dynamics of interest will inevitably be obscured by motion coupling effects. For example, Fig. 7.11 shows both the roll subsidence mode and the dutch roll mode, but the excitation, choice of output variables and time scale were chosen to optimize the recording of the roll subsidence mode. The form of the control input is not usually difficult to arrange in analytical work since most software packages have built-in impulse, step and pulse functions, whilst more esoteric functions can usually be

programmed by the user. For the analysis of the lateral-directional mode dynamics in particular, this kind of informed approach is critically important if the best possible visualization of the modes and their associated dynamics are to be obtained.

References

Hancock, G. J. 1995: *An Introduction to the Flight Dynamics of Rigid Aeroplanes.* Ellis Horwood Ltd, Hemel Hempstead.

Teper, G. L. 1969: *Aircraft Stability and Control Data.* Systems Technology, Inc, STI Technical Report 176-1.

8

Manoeuvrability

8.1 Introduction

8.1.1 MANOEUVRING FLIGHT

What is a manoeuvre? An aeroplane executing aerobatics in a vast blue sky or aeroplanes engaged in aerial combat are the kind of images associated with manoeuvring flight. By their very nature such manoeuvres are difficult to quantify, especially when it is required to describe manoeuvrability in an analytical framework. In reality most manoeuvres are comparatively mundane and simply involve changing from one trimmed flight condition to another.

When a pilot wishes to manoeuvre away from the current flight condition he applies control inputs which upset the equilibrium trim state by producing forces and moments to manoeuvre the aeroplane toward the desired flight condition. The temporary out-of-trim forces and moments cause the aeroplane to *accelerate* in a sense determined by the combined action of the control inputs. Thus, manoeuvring flight is sometimes called *accelerated flight* and is defined as the condition when the airframe is subject to temporary, or transient, out-of-trim linear and angular accelerations resulting from the displacement of the controls relative to their trim settings. In analytical terms, the manoeuvre is regarded as an increment in steady motion, over and above the initial trim state, in response to an increment in control angle.

The main aerodynamic force producing device in an aeroplane is the wing, and wing lift acts normal to the direction of flight in the plane of symmetry. Normal manoeuvring involves rotating the airframe in roll, pitch and yaw to point the lift vector in the desired direction and the simultaneous adjustment of both angle of attack and speed enables the lift force to generate the acceleration to manoeuvre. For example, in turning flight the aeroplane is rolled to the desired bank angle when the horizontal component of lift causes the aeroplane to turn in the desired direction. Simultaneous aft displacement of the pitch stick is required to generate pitch rate, which in turn generates an increase in angle of attack to produce more lift such that the vertical component is sufficient to balance the weight of the aeroplane, and hence to maintain level flight. The requirements for simple turning flight are illustrated in Example 2.3. Thus, manoeuvrability is mainly concerned with the ability to rotate about aircraft axes, the modulation of the normal or lift force and the modulation of the axial or thrust force.

The use of lateral sideforce to manoeuvre is not common in conventional aeroplanes

since it is aerodynamically inefficient and it is both unnatural and uncomfortable for the pilot. The principal aerodynamic manoeuvring force is therefore lift, which acts in the plane of symmetry of the aeroplane, and this is controlled by operating the control column in the pitch sense. When the pilot pulls back on the pitch stick the aeroplane pitches up to generate an increased lift force and since this results in out-of-trim normal acceleration he senses, and is very sensitive to, the change in acceleration. The pilot senses what appears to be an increase in the earth's gravitational acceleration g and is said to be *pulling g*.

8.1.2 STABILITY

Aircraft stability is generally concerned with the requirement that trimmed equilibrium flight may be achieved and that small transient upsets from equilibrium shall decay to zero. However, in manoeuvring flight the *transient upset* is the deliberate result following a control input, it may not be small and may well be prolonged. In the manoeuvre the aerodynamic forces and moments may be significantly different from the steady trim values and it is essential that the changes do not impair the stability of the aeroplane. In other words, there must be no tendency for the aeroplane to diverge in manoeuvring flight.

The classical theory of manoeuvrability is generally attributed to Gates and Lyon (1944) and various interpretations of that original work may be found in most books on aircraft stability and control. Perhaps one of the most comprehensive and accessible summaries of the theory is included in Babister (1961). In this chapter the subject is introduced at the most basic level in order to provide an understanding of the concepts involved since they are critically important in the broader considerations of flying and handling qualities. The original work makes provision for the effects of compressibility. In the following analysis subsonic flight only is considered in the interests of simplicity and hence in the promotion of understanding.

The traditional analysis of *manoeuvre stability* is based on the concept of the steady manoeuvre in which the aeroplane is subject to a steady normal acceleration in response to a pitch control input. Although rather contrived, this approach does enable the manoeuvre stability of an aeroplane to be explained analytically. The only realistic manoeuvres which can be flown at constant normal acceleration are the inside or outside loop and the steady banked turn. For the purpose of analysis the loop is simplified to a pull-up, or push-over, which is just a small segment of the circular flight path. Whichever manoeuvre is analysed, the resulting conditions for stability are the same.

Since the steady acceleration is constrained to the plane of symmetry the problem simplifies to the analysis of *longitudinal manoeuvre stability* and, since the motion is steady, the analysis is a simple extension of that applied to *longitudinal static stability* as described in Chapter 3. Consequently, the analysis leads to the concept of the *longitudinal manoeuvre margin*, the stability margin in manoeuvring flight, which in turn gives rise to the corresponding control parameters: *stick displacement per g* and *stick force per g*.

8.1.3 AIRCRAFT HANDLING

It is not difficult to appreciate that the manoeuvrability of an airframe is a critical factor in its overall flying and handling qualities. Too much manoeuvre stability means that

large control displacements and forces are needed to encourage the development of the normal acceleration vital to effective manoeuvring. On the other hand, too little manoeuvre stability implies that an enthusiastic pilot could over-stress the airframe by the application of excessive levels of normal acceleration. Clearly, the difficult balance between control power, manoeuvre stability, static stability and dynamic stability must be correctly controlled over the entire flight envelope of the aeroplane.

Today, considerations of manoeuvrability in the context of aircraft handling have moved on from the simple analysis of normal acceleration response to controls alone. Important additional considerations concern the accompanying roll, pitch and yaw rates and accelerations that may be achieved from control inputs since these determine how quickly a manoeuvre can become established. Manoeuvre entry is also *coloured* by transients associated with the short term dynamic stability modes. The aggressiveness with which a pilot may fly a manoeuvre and the motion cues available to him also contribute to his perception of the overall handling characteristics of the aeroplane. The 'picture' therefore becomes very complex, and it is further complicated by the introduction of flight control systems to the aeroplane. The subject of *aircraft agility* is a relatively new and exciting topic of research which embraces the ideas mentioned above and which is, unfortunately, beyond the scope of the present book.

8.1.4 THE STEADY SYMMETRIC MANOEUVRE

The analysis of longitudinal manoeuvre stability is based on steady motion which results in constant additional normal acceleration and, as mentioned above, the simplest such manoeuvre to analyse is the pull-up. In symmetric flight inertial normal acceleration, referred to the *cg*, is given by equation (5.39)

$$a_z = \dot{w} - qU_e \tag{8.1}$$

Since the manoeuvre is steady, $\dot{w} = 0$ and the aeroplane must fly a steady pitch rate in order to generate the normal acceleration required to manoeuvre. A steady turn enables this condition to be maintained *ad infinitum* in flight but is less straightforward to analyse. In symmetric flight, a short duration pull-up can be used to represent the lower segment of a continuous circular flight path in the vertical plane since a continuous loop is not practical for many aeroplanes.

It is worth noting that many modern combat aeroplanes and some advanced civil transport aeroplanes have flight control systems which feature *direct lift control* (DLC). In such aeroplanes, pitch rate is not an essential prerequisite to the generation of normal acceleration since the wing is fitted with a system of flaps for producing lift directly. However, in some applications it is common to mix the DLC flap control with conventional elevator control in order to improve manoeuvrability, manoeuvre entry in particular. The manoeuvrability of aeroplanes fitted with DLC systems may be significantly enhanced although its analysis may become rather more complex.

8.2 The steady pull-up manoeuvre

An aeroplane flying initially in steady level flight at speed V_0 is subject to a small elevator input $\delta\eta$ which causes it to pull up with steady pitch rate q. Consider the situation when the aircraft is at the lowest point of the vertical circle flight path as shown in Fig. 8.1.

In order to sustain flight in the vertical circle it is necessary that the lift L balances

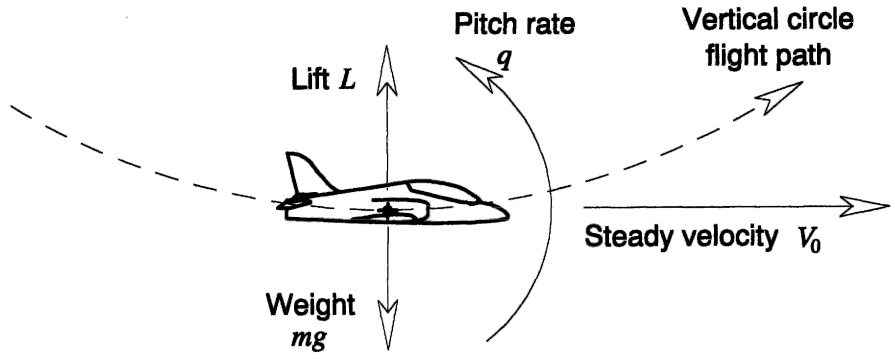

Fig. 8.1 A symmetric pull-up manoeuvre

not only the weight mg but the centrifugal force also, thus the lift is greater than the weight and

$$L = nmg \tag{8.2}$$

where n is the normal load factor. Thus, the normal load factor quantifies the total lift necessary to maintain the manoeuvre, and in steady level flight $n = 1$. The centrifugal force balance is therefore given by

$$L - mg = mV_0q \tag{8.3}$$

and the incremental normal load factor may be derived directly

$$\delta n = (n - 1) = \frac{V_0 q}{g} \tag{8.4}$$

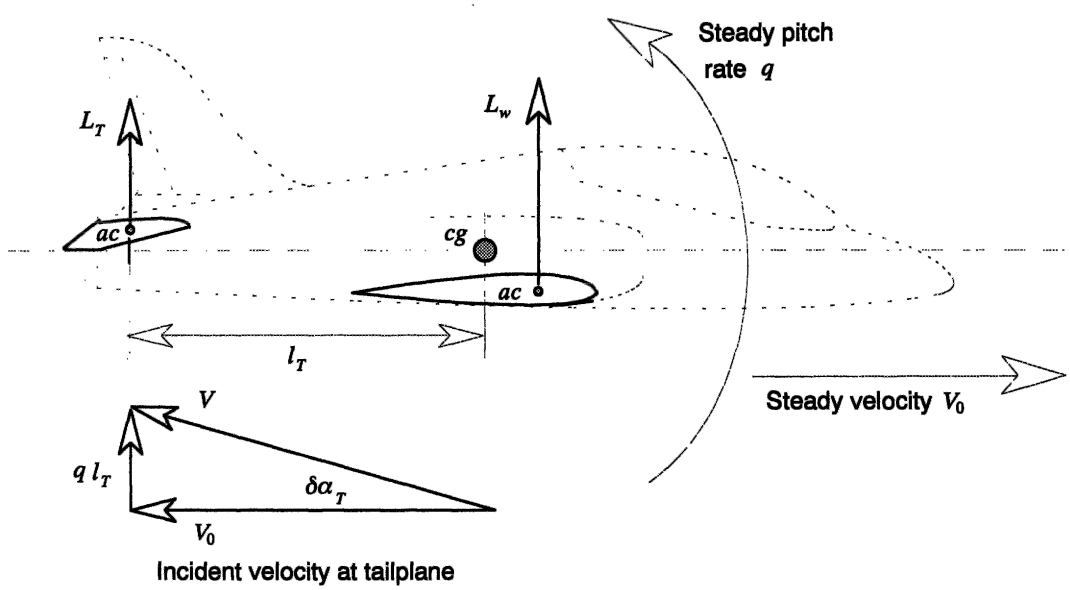

Fig. 8.2 Incremental tailplane incidence in pull-up manoeuvre

Now, as the aircraft is pitching up steadily the tailplane experiences an increase in incidence $\delta\alpha_T$ due to the pitch manoeuvre as indicated in Fig. 8.2.

Since small perturbation motion is assumed, the increase in tailplane incidence is given by

$$\delta\alpha_T \cong \tan \delta\alpha_T = \frac{ql_T}{V_0} \tag{8.5}$$

where l_T is the moment arm of the aerodynamic centre of the tailplane with respect to the centre of rotation in pitch, the *cg*. Eliminating pitch rate q from equations (8.4) and (8.5)

$$\delta\alpha_T = \frac{(n-1)gl_T}{V_0^2} \tag{8.6}$$

Now, in the steady level flight condition about which the manoeuvre is executed the lift and weight are equal, whence

$$V_0^2 = \frac{2mg}{\rho S C_{L_w}} \tag{8.7}$$

where C_{L_w} is the steady level flight value of the wing–body lift coefficient.

Thus, from equations (8.6) and (8.7)

$$\delta\alpha_T = \frac{(n-1)\rho S C_{L_w} l_T}{2m} = \frac{(n-1)C_{L_w} l_T}{\mu_1 \bar{\bar{c}}} \equiv \frac{\delta C_{L_w} l_T}{\mu_1 \bar{\bar{c}}} \tag{8.8}$$

where μ_1 is the *longitudinal relative density parameter* and is defined

$$\mu_1 = \frac{m}{\frac{1}{2}\rho S \bar{\bar{c}}} \tag{8.9}$$

and the increment in lift coefficient, alternatively referred to as incremental 'g', necessary to sustain the steady manoeuvre is given by

$$\delta C_{L_w} = (n-1)C_{L_w} \tag{8.10}$$

Care should be exercised when using the longitudinal relative density parameter since various definitions are in common use.

8.3 The pitching moment equation

Subject to the same assumptions about thrust, drag, speed effects and so on, in the steady symmetric manoeuvre the pitching moment equation in coefficient form given by equation (3.7) applies and may be written

$$C'_m = C_{m_0} + C'_{L_w}(h - h_0) - C'_{L_T}\bar{V}_T \tag{8.11}$$

where a dash indicates the manoeuvring value of the coefficient and

$$C'_m = C_m + \delta C_m$$
$$C'_{L_w} = C_{L_w} + \delta C_{L_w} \equiv nC_{L_w}$$
$$C'_{L_T} = C_{L_T} + \delta C_{L_T}$$

where C_m, C_{L_w} and C_{L_T} denote the steady trim values of the coefficients and δC_m, δC_{L_w} and δC_{L_T} denote the increments in the coefficients required to manoeuvre. The corresponding expression for the tailplane lift coefficient is given by equation (3.8) which, for manoeuvring flight, may be written

$$C'_{L_T} = a_1\alpha'_T + a_2\eta' + \alpha_3\beta_\eta \tag{8.12}$$

It is assumed that the tailplane has a symmetric aerofoil section, $a_0 = 0$, and that the tab angle is held at the constant steady trim value, β_η, throughout the manoeuvre. In other words, the manoeuvre is the result of elevator input only. Thus, using the above notation

$$\alpha'_T = \alpha_T + \delta\alpha_T$$
$$\eta' = \eta + \delta\eta$$

Tailplane incidence is given by equation (3.11) and in the manoeuvre this may be written

$$\alpha_T = \frac{C'_{L_w}}{a}\left(1 - \frac{d\varepsilon}{d\alpha}\right) + \eta_T \tag{8.13}$$

Total tailplane incidence in the manoeuvre is therefore given by the sum of equations (8.8) and (8.13)

$$\alpha'_T = \frac{C'_{L_w}}{a}\left(1 - \frac{d\varepsilon}{d\alpha}\right) + \eta_T + \frac{\delta C_{L_w} l_T}{\mu_1 \bar{\bar{c}}} \tag{8.14}$$

Substituting for α'_T in equation (8.12) the expression for tailplane lift coefficient in the manoeuvre may be written

$$C'_{L_T} = \frac{C'_{L_w} a_1}{a}\left(1 - \frac{d\varepsilon}{d\alpha}\right) + a_1\eta_T + \frac{\delta C_{L_w} a_1 l_T}{\mu_1 \bar{\bar{c}}} + a_2\eta' + a_3\beta_\eta \tag{8.15}$$

Substitute the expression for tailplane lift coefficient, equation (8.15), into equation (8.11), and after some rearrangement the pitching moment equation may be written

$$C'_m = C_{m_0} + C'_{L_w}(h - h_0) - \bar{V}_T\left(\frac{C'_{L_w} a_1}{a}\left(1 - \frac{d\varepsilon}{d\alpha}\right) + a_1\eta_T + \frac{\delta C_{L_w} a_1 l_T}{\mu_1 \bar{\bar{c}}} + a_2\eta' + a_3\beta_\eta\right) \tag{8.16}$$

Equation (8.16) describes the total pitching moment in the manoeuvre. To obtain the incremental pitching moment equation which describes the manoeuvre effects only, it is first necessary to replace the 'dashed' variables and coefficients in equation (8.16) with their equivalent expressions. Then, after some rearrangement, equation (8.16) may be written

$$\begin{aligned} C_m + \delta C_m = &\left\{C_{m_0} + C_{L_w}(h - h_0) - \bar{V}_T\left(\frac{C_{L_w} a_1}{a}\left(1 - \frac{d\varepsilon}{d\alpha}\right) + a_1\eta_T + a_2\eta + a_3\beta_\eta\right)\right\} \\ &+ \left\{\delta C_{L_w}(h - h_0) - \bar{V}_T\left(\frac{\delta C_{L_w} a_1}{a}\left(1 - \frac{d\varepsilon}{d\alpha}\right) + \frac{\delta C_{L_w} a_1 l_T}{\mu_1 \bar{\bar{c}}} + a_2\delta\eta\right)\right\} \end{aligned} \tag{8.17}$$

Now in the steady equilibrium flight condition about which the manoeuvre is executed the pitching moment is zero, therefore

$$C_m = C_{m_0} + C_{L_w}(h - h_0) - \bar{V}_T\left(\frac{C_{L_w} a_1}{a}\left(1 - \frac{d\varepsilon}{d\alpha}\right) + a_1\eta_T + a_2\eta + a_3\beta_\eta\right) = 0 \tag{8.18}$$

and equation (8.17) simplifies to that describing the incremental pitching moment coefficient

$$\delta C_m = \delta C_{L_w}(h - h_0) - \bar{V}_T\left(\frac{\delta C_{L_w} a_1}{a}\left(1 - \frac{d\varepsilon}{d\alpha}\right) + \frac{\delta C_{L_w} a_1 l_T}{\mu_1 \bar{\bar{c}}} + a_2\delta\eta\right) \tag{8.19}$$

8.4 Longitudinal manoeuvre stability

As for longitudinal static stability, discussed in Chapter 3, in order to achieve a stable manoeuvre the following condition must be satisfied

$$\frac{dC'_m}{dC'_{L_w}} < 0 \tag{8.20}$$

and for the manoeuvre to remain steady then

$$C'_m = 0 \tag{8.21}$$

Analysis and interpretation of these conditions leads to the definition of *controls fixed manoeuvre stability* and *controls free manoeuvre stability*, which correspond to the parallel concepts derived in the analysis of longitudinal static stability.

8.4.1 CONTROLS FIXED STABILITY

The total pitching moment equation (8.16) may be written

$$C'_m = C_{m_0} + C'_{L_w}(h - h_0) - \bar{V}_T\left(\frac{C'_{L_w}a_1}{a}\left(1 - \frac{d\varepsilon}{d\alpha}\right) + a_1\eta_T + \frac{(C'_{L_w} - C_{L_w})}{\mu_1\bar{\bar{c}}} + a_2\eta' + a_3\beta_\eta\right) \tag{8.22}$$

and since, by definition, the controls are held fixed in the manoeuvre

$$\frac{d\eta'}{dC'_{L_w}} = 0$$

Applying the condition for stability, equation (8.20), to equation (8.22) and noting that C_{L_w} and β_η are constant at their steady level flight values and that η_T is also a constant of the aircraft configuration then

$$\frac{dC'_m}{dC'_{L_w}} = (h - h_0) - \bar{V}_T\left(\frac{a_1}{a}\left(1 - \frac{d\varepsilon}{d\alpha}\right) + \frac{a_1 l_T}{\mu_1\bar{\bar{c}}}\right) \tag{8.23}$$

Or, writing

$$H_m = -\frac{dC'_m}{dC'_{L_w}} = h_m - h \tag{8.24}$$

where H_m is the *controls fixed manoeuvre margin* and the location of the *controls fixed manoeuvre point* h_m on the mean aerodynamic chord $\bar{\bar{c}}$ is given by

$$h_m = h_0 + \bar{V}_T\left(\frac{a_1}{a}\left(1 - \frac{d\varepsilon}{d\alpha}\right) + \frac{a_1 l_T}{\mu_1\bar{\bar{c}}}\right) = h_n + \frac{\bar{V}_T a_1 l_T}{\mu_1\bar{\bar{c}}} \tag{8.25}$$

Clearly, for controls fixed manoeuvre stability the manoeuvre margin H_m must be positive and, with reference to equation (8.24), this implies that the *cg* must be ahead of the manoeuvre point. Equation (8.25) indicates that the controls fixed manoeuvre point is aft of the corresponding neutral point by an amount depending on the aerodynamic properties of the tailplane. It therefore follows that

$$H_m = K_n + \frac{\bar{V}_T a_1 l_T}{\mu_1\bar{\bar{c}}} \tag{8.26}$$

which indicates that the controls fixed manoeuvre stability is greater than the controls

fixed static stability. With reference to Appendix 6, equation (8.26) may be restated in terms of aerodynamic stability derivatives

$$H_m = -\frac{M_w}{a} - \frac{M_q}{\mu_1} \tag{8.27}$$

A most important conclusion is then that additional stability in manoeuvring flight is provided by the aerodynamic pitch damping properties of the tailplane. However, caution is advised since this conclusion may not apply to all aeroplanes in large amplitude manoeuvring, or to manoeuvring in conditions where the assumptions do not apply.

As for controls fixed static stability, the meaning of controls fixed manoeuvre stability is easily interpreted by considering the pilot action required to establish a steady symmetric manoeuvre from an initial trimmed level flight condition. Since the steady (fixed) incremental elevator angle needed to induce the manoeuvre is of interest the incremental pitching moment, equation (8.19), is applicable. In a stable steady, and hence by definition, non-divergent manoeuvre, the incremental pitching moment δC_m is zero. Whence, equation (8.19) may be rearranged to give

$$\frac{\delta\eta}{\delta C_{L_w}} = \frac{1}{\bar{V}_T a_2}\left\{(h - h_0) - \bar{V}_T\left(\frac{a_1}{a}\left(1 - \frac{d\varepsilon}{d\alpha}\right) + \frac{a_1 l_T}{\mu_1 \bar{c}}\right)\right\} = \frac{-H_m}{\bar{V}_T a_2} \tag{8.28}$$

Or, in terms of aerodynamic stability derivatives,

$$\frac{\delta\eta}{\delta C_{L_w}} = \frac{-H_m}{M_\eta} = \frac{1}{M_\eta}\left(\frac{M_w}{a} + \frac{M_q}{\mu_1}\right) \tag{8.29}$$

Referring to equation (8.10)

$$\delta C_{L_w} = (n-1)C_{L_w}$$

which describes the incremental aerodynamic load acting on the aeroplane causing it to execute the manoeuvre, expressed in coefficient form, and measured in units of '*g*'. Thus, both equation (8.28) and equation (8.29) express the *elevator displacement per g* capability of the aeroplane, which is proportional to the controls fixed manoeuvre margin and inversely proportional to the elevator control power, quantified by the aerodynamic control derivative M_η. Since elevator angle and pitch control stick angle are directly related by the control gearing then the very important *stick displacement per g* control characteristic follows directly and is also proportional to the controls fixed manoeuvre margin. This latter control characteristic is critically important in the determination of longitudinal handling qualities.

Measurements of elevator angle and normal acceleration in steady manoeuvres for a range of values of normal load factor provide an effective means for determining controls fixed manoeuvre stability from flight experiments. However, in such experiments it is not always possible to ensure that one can adhere to all of the assumptions.

8.4.2 CONTROLS FREE STABILITY

The controls free manoeuvre is not a practical way of controlling an aeroplane. It does, of course, imply that the elevator angle required to achieve the manoeuvre is obtained by adjustment of the tab angle. As in the case of controls free static stability, this equates to the control force required to achieve the manoeuvre which is a most significant

control characteristic. Control force derives from elevator hinge moment in a conventional aeroplane and the elevator hinge moment coefficient in manoeuvring flight is given by equation (3.21) and may be restated as

$$C'_H = C_H + \delta C_H = b_1\alpha'_T + b_2\eta' + b_3\beta_\eta \tag{8.30}$$

Since the elevator angle in a controls free manoeuvre is indeterminate it is convenient to express η' in terms of hinge moment coefficient by rearranging equation (8.30)

$$\eta' = \frac{1}{b_2}C'_H - \frac{b_1}{b_2}\alpha'_T - \frac{b_3}{b_2}\beta_\eta \tag{8.31}$$

Substitute the expression for α'_T, equation (8.14), into equation (8.31) to obtain

$$\eta' = \frac{1}{b_2}C'_H - \frac{b_1}{ab_2}\left(1 - \frac{d\varepsilon}{d\alpha}\right)C'_{L_w} - \frac{b_1}{b_2}\eta_T - \frac{b_1 l_T}{b_2\mu_1\bar{\bar{c}}}\delta C_{L_w} - \frac{b_3}{b_2}\beta_\eta \tag{8.32}$$

Equation (8.32) may be substituted into the manoeuvring pitching moment equation (8.16) in order to replace the indeterminate elevator angle by hinge moment coefficient. After some algebraic rearrangement the manoeuvring pitching moment may be expressed in the same format as equation (8.22)

$$C'_m = C_{m_0} + C'_{L_w}(h - h_0) - \bar{V}_T\left(\begin{array}{l} C'_{L_w}\dfrac{a_1}{a}\left(1 - \dfrac{d\varepsilon}{d\alpha}\right)\left(1 - \dfrac{a_2b_1}{a_1b_2}\right) + a_1\eta_T + C'_H\dfrac{a_2}{b_2} \\ +(C'_{L_w} - C_{L_w})\dfrac{a_1 l_T}{\mu_1\bar{\bar{c}}}\left(1 - \dfrac{a_2b_1}{a_1b_2}\right) + \beta_\eta\left(1 - \dfrac{a_2b_3}{a_3b_2}\right) \end{array}\right) \tag{8.33}$$

and since, by definition, the controls are free in the manoeuvre then

$$C'_H = 0$$

Applying the condition for stability, equation (8.20), to equation (8.33) and noting that, as before, C_{L_w} and β_η are constant at their steady level flight values and that η_T is also a constant of the aircraft configuration, then

$$\frac{dC'_m}{dC'_{L_w}} = (h - h_0) - \bar{V}_T\left(\frac{a_1}{a}\left(1 - \frac{d\varepsilon}{d\alpha}\right) + \frac{a_1 l_T}{\mu_1\bar{\bar{c}}}\right)\left(1 - \frac{a_2b_1}{a_1b_2}\right) \tag{8.34}$$

Or, writing

$$H'_m = -\frac{dC'_m}{dC'_{L_w}} = h'_m - h \tag{8.35}$$

where H'_m is the *controls free manoeuvre margin* and the location of the *controls free manoeuvre point* h'_m on the mean aerodynamic chord $\bar{\bar{c}}$ is given by

$$\begin{aligned} h'_m &= h_0 + \bar{V}_T\left(\frac{a_1}{a}\left(1 - \frac{d\varepsilon}{d\alpha}\right) + \frac{a_1 l_T}{\mu_1\bar{\bar{c}}}\right)\left(1 - \frac{a_2b_1}{a_1b_2}\right) \\ &= h'_n + \bar{V}_T\frac{a_1 l_T}{\mu_1\bar{\bar{c}}}\left(1 - \frac{a_2b_1}{a_1b_2}\right) \end{aligned} \tag{8.36}$$

Clearly, for controls free manoeuvre stability the manoeuvre margin H'_m must be positive and, with reference to equation (8.35), this implies that the *cg* must be ahead of the manoeuvre point. Equation (8.36) indicates that the controls fixed manoeuvre point is

aft of the corresponding neutral point by an amount again depending on the aerodynamic damping properties of the tailplane. It therefore follows that

$$H'_m = K'_n + \bar{V}_T \frac{a_1 l_T}{\mu_1 \bar{\bar{c}}} \left(1 - \frac{a_2 b_1}{a_1 b_2}\right) \equiv K'_n + \frac{M_q}{\mu_1} \left(1 - \frac{a_2 b_1}{a_1 b_2}\right) \tag{8.37}$$

which indicates that the controls fixed manoeuvre stability is greater than the controls fixed static stability when

$$\left(1 - \frac{a_2 b_1}{a_1 b_2}\right) > 0 \tag{8.38}$$

Since a_1 and a_2 are both positive the degree of controls free manoeuvre stability, over and above the controls free static stability, is controlled by the signs of the hinge moment parameters b_1 and b_2. This, in turn, depends on the aerodynamic design of the elevator control surface.

As for controls free static stability the meaning of controls free manoeuvre stability is easily interpreted by considering the pilot action required to establish a steady symmetric manoeuvre from an initial trimmed level flight condition. Since the controls are 'free' this equates to a steady tab angle increment or, more appropriately, a steady control force increment in order to cause the aeroplane to manoeuvre. Equation (8.33) may be rewritten in terms of the steady and incremental contributions to the total controls free manoeuvring pitching moment in the same way as equation (8.17)

$$\begin{aligned} C_m + \delta C_m = &\left\{ C_{m_0} + C_{L_w}(h - h_0) - \bar{V}_T \left(\begin{array}{l} C_{L_w} \dfrac{a_1}{a} \left(1 - \dfrac{d\varepsilon}{d\alpha}\right)\left(1 - \dfrac{a_2 b_1}{a_1 b_2}\right) \\ + a_1 \eta_T + C_H \dfrac{a_2}{b_2} + \beta_\eta \left(1 - \dfrac{a_2 b_3}{a_3 b_2}\right) \end{array} \right) \right\} \\ &+ \left\{ \delta C_{L_w}(h - h_0) - \bar{V}_T \left(\begin{array}{l} \delta C_{L_w} \dfrac{a_1}{a} \left(1 - \dfrac{d\varepsilon}{d\alpha}\right)\left(1 - \dfrac{a_2 b_1}{a_1 b_2}\right) \\ + \delta C_H \dfrac{a_2}{b_2} + \delta C_{L_w} \dfrac{a_1 l_T}{\mu_1 \bar{\bar{c}}} \left(1 - \dfrac{a_2 b_1}{a_1 b_2}\right) \end{array} \right) \right\} \end{aligned} \tag{8.39}$$

Now in the steady equilibrium flight condition about which the manoeuvre is executed the pitching moment is zero, thus

$$C_m = C_{m_0} + C_{L_w}(h - h_0) - \bar{V}_T \left(\begin{array}{l} C_{L_w} \dfrac{a_1}{a} \left(1 - \dfrac{d\varepsilon}{d\alpha}\right)\left(1 - \dfrac{a_2 b_1}{a_1 b_2}\right) \\ + a_1 \eta_T + C_H \dfrac{a_2}{b_2} + \beta_\eta \left(1 - \dfrac{a_2 b_3}{a_3 b_2}\right) \end{array} \right) = 0 \tag{8.40}$$

and equation (8.39) simplifies to that describing the incremental controls free pitching moment coefficient

$$\delta C_m = \delta C_{L_w}(h - h_0) - \bar{V}_T \left(\begin{array}{l} \delta C_{L_w} \dfrac{a_1}{a} \left(1 - \dfrac{d\varepsilon}{d\alpha}\right)\left(1 - \dfrac{a_2 b_1}{a_1 b_2}\right) \\ + \delta C_H \dfrac{a_2}{b_2} + \delta C_{L_w} \dfrac{a_1 l_T}{\mu_1 \bar{\bar{c}}} \left(1 - \dfrac{a_2 b_1}{a_1 b_2}\right) \end{array} \right) \tag{8.41}$$

Now, in the steady manoeuvre the incremental pitching moment δC_m is zero and equation (8.41) may be rearranged to give

$$\frac{\delta C_H}{\delta C_{L_w}} = \frac{b_2}{a_2 \bar{V}_T}\left\{(h - h_0) - \bar{V}_T\left(\frac{a_1}{a}\left(1 - \frac{d\varepsilon}{d\alpha}\right) + \frac{a_1 l_T}{\mu_1 \bar{c}}\right)\left(1 - \frac{a_2 b_1}{a_1 b_2}\right)\right\} = -\frac{b_2 H'_m}{a_2 \bar{V}_T} \qquad (8.42)$$

In a conventional aeroplane the hinge moment coefficient relates directly to the control stick force, see equation (3.32). Equation (8.42) therefore indicates the very important result that the *stick force per g* control characteristic is proportional to the controls free manoeuvre margin. This control characteristic is critically important in the determination of longitudinal handling qualities and it must have the correct value. In other words, the controls free manoeuvre margin must lie between precisely defined upper and lower bounds. As stated above, in an aerodynamically controlled aeroplane this control characteristic can be adjusted independently of the other stability characteristics by selective design of the values of the hinge moment parameters b_1 and b_2.

The controls free manoeuvre stability is critically dependent on the ratio b_1/b_2, which controls the magnitude and sign of expression (8.38). For conventional aeroplanes fitted with a plain flap type elevator control both b_1 and b_2 are usually negative and, see equation (8.37), the controls free manoeuvre stability would be less than the controls free static stability. Adjustment of b_1 and b_2 is normally achieved by aeromechanical means which are designed to modify the elevator hinge moment characteristics. Typically, this involves carefully tailoring the aerodynamic balance of the elevator by means such as: set back hinge line, horn balances, spring tabs, servo tabs and so on. Excellent descriptions of these devices may be found in Dickinson (1968) and in Babister (1961).

The measurement of stick force per g is easily undertaken in flight. The aeroplane is flown in steady manoeuvring flight, the turn probably being the simplest way of achieving a steady normal acceleration for a period long enough to enable good quality measurements to be made. Measurements of stick force and normal acceleration enable estimates to be made of the controls free manoeuvre margin and the location of the controls free manoeuvre point. With greater experimental difficulty, stick force per g can also be measured in steady pull-ups and in steady push-overs. However the experiment is done it must be remembered that it is not always possible to ensure that all of the assumptions can be adhered to.

8.5 Aircraft dynamics and manoeuvrability

The preceding analysis shows how the stability of an aeroplane in manoeuvring flight is dependent on the manoeuvre margins and, further, that the magnitude of the manoeuvre margins determines the critical handling characteristics, stick displacement per g and stick force per g. However, the manoeuvre margins of the aeroplane are also instrumental in determining some of the dynamic response characteristics of the aeroplane. This fact further reinforces the statement made elsewhere that the static, manoeuvre and dynamic stability and control characteristics of an aeroplane are really very much interrelated and should not be treated entirely as isolated topics.

In Chapter 6, reduced order models of an aircraft are discussed and, from the longitudinal model representing short term dynamic stability and response, an approximate expression for the short period mode undamped natural frequency is derived, equation (6.21), in terms of dimensional aerodynamic stability derivatives. With reference to Appendix 1, this expression may be restated in terms of dimensionless derivatives

$$\omega_s^2 = \frac{\frac{1}{2}\rho V_0^2 S\bar{c}}{I_y}\left(\frac{\frac{1}{2}\rho S\bar{c}}{m} M_q Z_w + M_w\right) = \frac{\frac{1}{2}\rho V_0^2 S\bar{c}}{I_y}\left(\frac{M_q Z_w}{\mu_1} + M_w\right) \tag{8.43}$$

where μ_1 is the longitudinal relative density factor defined in equation (8.9).

Now with reference to Appendix 6 an approximate expression for Z_w is given as

$$Z_w \cong -C_D - \frac{\partial C_L}{\partial \alpha} = -C_D - a \tag{8.44}$$

for small perturbation motion in subsonic flight. Since $a \gg C_D$ equation (8.44) may be approximated further, and substituting for Z_w in equation (8.43) gives

$$\omega_s^2 = \frac{\frac{1}{2}\rho V_0^2 S\bar{c}a}{I_y}\left(-\frac{M_q}{\mu_1} - \frac{M_w}{a}\right) = kH_m \equiv k\left(K_n - \frac{M_q}{\mu_1}\right) \tag{8.45}$$

where k is a constant at the given flight condition. Equation (8.45) therefore shows that the undamped natural frequency of the longitudinal short period mode is directly dependent on the controls fixed manoeuvre margin. Alternatively, this may be interpreted as a dependency on the controls fixed static margin and pitch damping. Clearly, since the controls fixed manoeuvre margin must lie between carefully defined boundaries if satisfactory handling is to be ensured, this implies that the longitudinal short period mode must also be constrained to a corresponding frequency band. Flying qualities requirements have been developed from this kind of understanding and are discussed in Chapter 10.

In many modern aeroplanes the link between the aerodynamic properties of the control surface and the stick force is broken by a servo-actuator and other flight control system components. In this case the control forces are provided artificially and may not interrelate with other stability and control characteristics in the classical way. However, it is obviously important that the pilot's perception of the handling qualities of his aeroplane look like those of an aeroplane with acceptable aerodynamic manoeuvre margins. Since many of the subtle aerodynamic interrelationships do not exist in aeroplanes employing sophisticated flight control systems, it is critically important to be fully aware of the handling qualities implications at all stages of a control system design.

References

Babister, A. W. 1961: *Aircraft Stability and Control.* Pergamon Press, London.

Dickinson, B. 1968: *Aircraft Stability and Control for Pilots and Engineers.* Pitman, London.

Gates, S. B. and Lyon, H. M. 1944: *A Continuation of Longitudinal Stability and Control Analysis; Part 1, General Theory.* Aeronautical Research Council, Reports and Memoranda No: 2027.

9
Stability

9.1 Introduction

Stability is referred to frequently in the foregoing chapters without a formal definition so it is perhaps useful to revisit the subject in a little more detail in this chapter. Having established the implications of both static and dynamic stability in the context of aircraft response to controls it is convenient to develop some simple analytical and graphical tools to help in the interpretation of aircraft stability.

9.1.1 A DEFINITION OF STABILITY

There are many different definitions of stability, which are dependent on the kind of system to which they are applied. Fortunately, in the present context the aircraft model is linearized by limiting its motion to small perturbations. The definition of the stability of a linear system is the simplest and most commonly encountered, and is adopted here for application to the aeroplane. The definition of the stability of a linear system may be found in many texts in applied mathematics, in system analysis and in control theory. A typical definition of the stability of a linear system with particular reference to the aeroplane may be stated as follows.

> A system (aeroplane) which is initially in a state of static equilibrium is said to be stable if, after a disturbance of finite amplitude and duration, the response ultimately becomes vanishingly small.

Stability is therefore concerned with the nature of the free motion of the system following a disturbance. When the system is linear the nature of the response, and hence its stability, is independent of the nature of the disturbing input. The small perturbation equations of motion of an aircraft are linear since, by definition, the perturbations are small. Consequently, it is implied that the disturbing input must also be small in order to preserve that linearity. When, as is often the case, input disturbances which are not really small are applied to the linear small perturbation equations of motion of an aircraft, some degradation in the interpretation of stability from the observed response must be anticipated. However, for most applications this does not give rise to major difficulties since the linearity of the aircraft model usually degrades relatively slowly with

increasing perturbation amplitude. Thus, it is considered reasonable to use linear system stability theory for general aircraft applications.

9.1.2 NON-LINEAR SYSTEMS

Many modern aircraft, especially combat aircraft which depend on flight control systems for their normal flying qualities, can, under certain conditions, demonstrate substantial non-linearity in their behaviour. This may be due, for example, to large amplitude manoeuvring at the extremes of the flight envelope where the aerodynamic properties of the airframe are decidedly non-linear. A rather more common source of non-linearity, often found in an otherwise nominally linear aeroplane and often overlooked, arises from the characteristics of common flight control system components. For example, control surface actuators all demonstrate static friction, hysteresis, amplitude and rate limiting to a greater or lesser extent. The non-linear response associated with these characteristics is not normally intrusive unless the demands on the actuator are limiting, such as might be found in the fly-by-wire control system of a high performance aircraft. The mathematical models describing such non-linear behaviour are much more difficult to create and the applicable stability criteria are rather more sophisticated and, in any event, beyond the scope of the present discussion. Non-linear system theory, more popularly known as *chaotic system theory* today, is developing rapidly to provide the mathematical tools, understanding and stability criteria for dealing with the kind of problems posed by modern highly augmented aircraft.

9.1.3 STATIC AND DYNAMIC STABILITY

Any discussion of stability must consider the total stability of the aeroplane at the flight condition of interest. However, it is usual and convenient to discuss static stability and dynamic stability separately since the related dependent characteristics can be identified explicitly in aircraft behaviour. In reality, static and dynamic stability are inseparable and must be considered as an entity. An introductory discussion of static and dynamic stability is contained in Section 3.1 and their simple definitions are reiterated here. The static stability of an aeroplane is commonly interpreted to describe its tendency to converge on the initial equilibrium condition following a small disturbance from trim. Dynamic stability describes the transient motion involved in the process of recovering equilibrium following the disturbance. It is very important that an aeroplane possesses both static and dynamic stability in order that it shall be safe. However, the degree of stability is also very important since this determines the effectiveness of the controls of the aeroplane.

9.1.4 CONTROL

By definition, a stable aeroplane is resistant to disturbance, in other words it will attempt to remain at its trimmed equilibrium flight condition. The 'strength' of the resistance to disturbance is determined by the degree of stability possessed by the aeroplane. It follows then that a stable aeroplane is reluctant to respond when a disturbance is deliberately introduced as the result of pilot control action. Thus, the degree of stability is critically important to aircraft handling. An aircraft which is very stable requires a greater pilot control action in order to manoeuvre about the trim state and, clearly, too

much stability may limit the controllability, and hence the manoeuvrability, of the aeroplane. On the other hand, too little stability in an otherwise stable aeroplane may give rise to an over-responsive aeroplane with the resultant pilot tendency to over-control. Therefore, too much stability can be as hazardous as too little stability and it is essential to place upper and lower bounds on the acceptable degree of stability in an aeroplane in order that it shall remain completely controllable in all flight conditions. By reducing the total stability to static and dynamic components, which are further reduced to the individual dynamic modes, it becomes relatively easy to assign the appropriate degree of stability to each mode in order to achieve a safe controllable aeroplane in total.

9.2 The characteristic equation

It has been shown in previous chapters that the denominator of every aircraft response transfer function defines the characteristic polynomial, the roots of which determine the stability modes of the aeroplane. Equating the characteristic polynomial to zero defines the classical characteristic equation and thus far two such equations have been identified. Since decoupled motion only is considered, the solution of the equations of motion of the aeroplane results in two fourth order characteristic equations, one relating to longitudinal symmetric motion and one relating to lateral-directional asymmetric motion. In the event that the decoupled equations of motion provide an inadequate aircraft model, such as is often the case for the helicopter, then a single characteristic equation, typically of eighth order, describes the stability characteristics of the aircraft for fully coupled longitudinal–lateral motion. For aircraft with significant stability augmentation, the flight control system introduces additional dynamics resulting in a higher order characteristic equation. For advanced combat aircraft the longitudinal characteristic equation, for example, can be of order 30 or more! Interpretation of *high order* characteristic equations can be something of a challenge for the flight dynamicist.

The characteristic equation of a general system of order n may be expressed in the familiar format as a function of the Laplace operator s

$$\Delta(s) = a_n s^n + a_{n-1}s^{n-1} + a_{n-2}s^{n-2} + a_{n-3}s^{n-3} + \ldots + a_1 s + a_0 = 0 \qquad (9.1)$$

and the stability of the system is determined by the n roots of equation (9.1). Provided that the constant coefficients in equation (9.1) are real then the roots may be real, complex pairs or a combination of the two. Thus, the roots may be written in the general form

(i) $s = -\sigma_1$ with time solution $k_1 e^{-\sigma_1 t}$

(ii) $s = -\sigma_2 \pm j\gamma_2$ with time solution $k_2 e^{-\sigma_2 t}\sin(\gamma_2 t + \phi_2)$
or, more familiarly, $s^2 + 2\sigma_2 s + (\sigma_2^2 + \gamma_2^2) = 0$

where σ is the real part, γ is the imaginary part, ϕ is the phase angle and k is a gain constant. When all the roots have negative real parts the transient component of the response to a disturbance decays to zero as $t \to \infty$ and the system is said to be stable. The system is unstable when any root has a positive real part and neutrally stable when any root has a zero real part. Thus, the stability and dynamic behaviour of any linear system is governed by the sum of the dynamics associated with each root of its characteristic equation. The interpretation of the stability and dynamics of a linear system is summarized in Appendix 5.

9.3 The Routh–Hurwitz stability criterion

The development of a criterion for testing the stability of linear systems is generally attributed to Routh. Application of the criterion involves an analysis of the characteristic equation and methods for interpreting and applying the criterion are very widely known and used, especially in control systems analysis. A similar analytical procedure for testing the stability of a system by analysis of the characteristic equation was developed simultaneously, and quite independently, by Hurwitz. As a result both authors share the credit and the procedure is commonly known to control engineers as the Routh–Hurwitz criterion. The criterion provides an analytical means for testing the stability of a linear system of any order without having to obtain the roots of the characteristic equation.

With reference to the typical characteristic equation (9.1), if any coefficient is zero or if any coefficient is negative, then at least one root has a zero or positive real part indicating the system to be unstable, or at best neutrally stable. However, it is a necessary but not sufficient condition for stability that all coefficients in equation (9.1) are non-zero and of the same sign. When this condition exists the stability of the system described by the characteristic equation may be tested as follows.

An array, commonly known as the Routh Array, is constructed from the coefficients of the characteristic equation arranged in descending powers of s as follows

$$\begin{array}{c|ccccc} s^n & a_n & a_{n-2} & a_{n-4} & a_{n-6} & \cdots \\ s^{n-1} & a_{n-1} & a_{n-3} & a_{n-5} & a_{n-7} & \cdots \\ s^{n-2} & u_1 & u_2 & u_3 & u_4 & \cdot \\ s^{n-3} & v_1 & v_2 & v_3 & \cdot & \\ \cdot & \cdot & \cdot & \cdot & & \\ \cdot & \cdot & \cdot & & & \\ \cdot & \cdot & & & & \\ s^1 & y & & & & \\ s^0 & z & & & & \end{array} \tag{9.2}$$

The first row of the array is written to include alternate coefficients starting with the highest power term and the second row includes the remaining alternate coefficients starting with the second highest power term as indicated. The third row is constructed as follows

$$u_1 = \frac{a_{n-1}a_{n-2} - a_n a_{n-3}}{a_{n-1}} \qquad u_2 = \frac{a_{n-1}a_{n-4} - a_n a_{n-5}}{a_{n-1}} \qquad u_3 = \frac{a_{n-1}a_{n-6} - a_n a_{n-7}}{a_{n-1}}$$

and so on until all remaining u are zero. The fourth row is constructed similarly from coefficients in the two rows immediately above as follows

$$v_1 = \frac{u_1 a_{n-3} - u_2 a_{n-1}}{u_1} \qquad v_2 = \frac{u_1 a_{n-5} - u_3 a_{n-1}}{u_1} \qquad v_3 = \frac{u_1 a_{n-7} - u_2 a_{n-1}}{u_1}$$

and so on until all remaining v are zero. This process is repeated until all remaining rows of the array are completed. The array is triangular as indicated and the last two rows comprise only one term each, y and z respectively.

The Routh–Hurwitz criterion states:

> The number of roots of the characteristic equation with positive real parts (unstable) is equal to the number of changes of sign of the coefficients in the first column of the array.

Thus, for the system to be stable all the coefficients in the first column of the array must have the same sign.

EXAMPLE 9.1

The lateral-directional characteristic equation for the Douglas DC-8 aircraft in a low altitude cruise flight condition, obtained from Teper (1969), is

$$\Delta(s) = s^4 + 1.326s^3 + 1.219s^2 + 1.096s - 0.015 = 0 \tag{9.3}$$

Inspection of the characteristic equation (9.3) indicates an unstable aeroplane since the last coefficient has a negative sign. The number of unstable roots may be determined by constructing the array as described above

s^4	1	1.219	−0.015
s^3	1.326	1.096	0
s^2	0.393	−0.015	0
s^1	1.045	0	0
s^0	−0.015	0	0

(9.4)

Working down the first column of the array there is one sign change, from 1.045 to −0.015, which indicates the characteristic equation to have one unstable root. This is verified by obtaining the exact roots of the characteristic equation (9.3)

$$\left.\begin{aligned} s &= -0.109 \pm 0.99\mathrm{j} \\ s &= -1.21 \\ s &= +0.013 \end{aligned}\right\} \tag{9.5}$$

The pair of complex roots with negative real parts describe the stable dutch roll, the real root with negative real part describes the stable roll subsidence mode and the real root with positive real part describes the unstable spiral mode—a typical solution for a classical aeroplane.

9.3.1 *SPECIAL CASES*

Two special cases, which may arise in the application of the Routh–Hurwitz criterion, need to be considered although they are unlikely to occur in aircraft applications. The first case occurs when, in the routine calculation of the array, a coefficient in the first column is zero. The second case occurs when, in the routine calculation of the array, all coefficients in a row are zero. In either case no further progress is possible and an alternative procedure is required. The methods for dealing with these cases are best illustrated by example.

EXAMPLE 9.2

Consider the arbitrary characteristic equation

$$\Delta(s) = s^4 + s^3 + 6s^2 + 6s + 7 = 0 \tag{9.6}$$

The array for this equation is constructed in the usual way

$$\begin{array}{c|ccc} s^4 & 1 & 6 & 7 \\ s^3 & 1 & 6 & 0 \\ s^2 & \varepsilon & 7 & 0 \\ s^1 & \left(\dfrac{6\varepsilon - 7}{\varepsilon}\right) & 0 & 0 \\ s^0 & 7 & 0 & 0 \end{array} \tag{9.7}$$

Normal progress cannot be made beyond the third row since the first coefficient is zero. In order to proceed the zero is replaced with a small positive number, denoted ε. The array can be completed as at equation (9.7) and as $\varepsilon \to 0$ so the first coefficient in the fourth row tends to a large negative value. The signs of the coefficients in the first column of the array (9.7) are then easily determined

$$\begin{array}{c|c} s^4 & + \\ s^3 & + \\ s^2 & + \\ s^1 & - \\ s^0 & + \end{array} \tag{9.8}$$

There are two changes of sign, from the third row to the fourth row and from the fourth row to the fifth row. Therefore, the characteristic equation (9.6) has two roots with positive real parts and this is verified by the exact solution

$$\left.\begin{array}{l} s = -0.6454 \pm 0.9965\mathrm{j} \\ s = +0.1454 \pm 2.224\mathrm{j} \end{array}\right\} \tag{9.9}$$

EXAMPLE 9.3

To illustrate the required procedure when all the coefficients in a row of the array are zero consider the arbitrary characteristic equation

$$\Delta(s) = s^5 + 2s^4 + 4s^3 + 8s^2 + 3s + 6 = 0 \tag{9.10}$$

Constructing the array in the usual way

$$\begin{array}{c|ccc} s^5 & 1 & 4 & 3 \\ s^4 & 2 & 8 & 6 \\ s^3 & 0 & 0 & \end{array} \tag{9.11}$$

no further progress is possible since the third row comprises all zeros. In order to proceed, the zero row, the third row in this example, is replaced by an auxiliary function

derived from the preceding non-zero row. Thus, the function is created from the row commencing with the coefficient of s to the power of four as follows

$$2s^4 + 8s^2 + 6 = 0 \quad \text{or, equivalently,} \quad s^4 + 4s^2 + 3 = 0 \tag{9.12}$$

Only terms in alternate powers of s are included in the auxiliary function (9.12) commencing with the highest power term determined from the row of the array from which it is derived. The auxiliary function is differentiated with respect to s and the resulting polynomial is used to replace the zero row in the array. Equation (9.12) is differentiated to obtain

$$4s^3 + 8s = 0 \quad \text{or, equivalently,} \quad s^3 + 2s = 0 \tag{9.13}$$

Substituting equation (9.13) into the third row of the array (9.11), it may then be completed in the usual way

s^5	1	4	3
s^4	2	8	6
s^3	1	2	0
s^2	4	6	0
s^1	0.5	0	0
s^0	6	0	0

(9.14)

Inspection of the first column of the array (9.14) indicates that all roots of the characteristic equation (9.10) have negative real parts. However, the fact that in the derivation of the array one row comprises zero coefficients suggests that something is different. The exact solution of equation (9.10) confirms this suspicion

$$\left.\begin{aligned} s &= 0 \pm 1.732\text{j} \\ s &= 0 \pm 1.0\text{j} \\ s &= -2.0 \end{aligned}\right\} \tag{9.15}$$

Clearly the system is neutrally stable since the two pairs of complex roots both have zero real parts.

9.4 The stability quartic

Since both the longitudinal and lateral-directional characteristic equations derived from the small perturbation equations of motion of an aircraft are fourth order, considerable emphasis has always been placed on the solution of a fourth order polynomial, sometimes referred to as the *stability quartic*. A general quartic equation applicable to either longitudinal or lateral-directional motion may be written

$$As^4 + Bs^3 + Cs^2 + Ds + E = 0 \tag{9.16}$$

When all of the coefficients in equation (9.16) are positive, as is often the case, then no conclusions may be drawn concerning stability unless the roots are found or the Routh–Hurwitz array is constructed. Constructing the Routh–Hurwitz array as described in Section 9.3 above

$$\begin{array}{c|cc} s^4 & A & C \quad E \\ s^3 & B & D \\ s^2 & \left(\dfrac{BC-AD}{B}\right) & E \\ s^1 & \left(\dfrac{D(BC-AD)-B^2E}{BC-AD}\right) & \\ s^0 & E & \end{array} \tag{9.17}$$

Assuming that all of the coefficients in the characteristic equation (9.16) are positive and that B and C are large compared with D and E, as is usually the case, then the coefficients in the first column of array (9.17) are also positive with the possible exception of the coefficient in the fourth row. Writing

$$R = D(BC - AD) - B^2E \tag{9.18}$$

R is called *Routh's Discriminant* and since $(BC - AD)$ is positive, the outstanding condition for stability is

$$R > 0$$

For most classical aircraft operating within the constraints of small perturbation motion, the only coefficient in the characteristic equation (9.16) likely to be negative is E. Thus, typically the necessary and sufficient conditions for an aeroplane to be stable are

$$R > 0 \quad \text{and} \quad E > 0$$

When an aeroplane is unstable some conclusions about the nature of the instability can be made simply by observing the values of R and E.

9.4.1 INTERPRETATION OF CONDITIONAL INSTABILITY

(i) When $R < 0$ and $E > 0$

Observation of the signs of the coefficients in the first column of the array (9.17) indicates that two roots of the characteristic equation (9.16) have positive real parts. For longitudinal motion this implies a pair of complex roots and in most cases this means an unstable phugoid mode since its stability margin is usually smallest. For lateral-directional motion the implication is that either the two real roots, or the pair of complex roots, have positive real parts. This means either that the spiral and roll subsidence modes are unstable or that the dutch roll mode is unstable. Within the limitations of small perturbation modelling an unstable roll subsidence mode is not possible. Therefore, the instability must be determined by the pair of complex roots describing the dutch roll mode.

(ii) When $R < 0$ and $E < 0$

For this case, observation of the signs of the coefficients in the first column of the array (9.17) indicates that one root only of the characteristic equation (9.16) has a positive real part. Clearly, the 'unstable' root can only be a real root. For longitudinal motion this may be interpreted to mean that the phugoid mode has changed such that it is no longer oscillatory and is therefore described by a pair of real roots, one of which has a positive

real part. The 'stable' real root typically describes an exponential *heave mode*, whereas the 'unstable' root describes an exponentially divergent *speed mode*. For lateral-directional motion the interpretation is similar and in this case the only 'unstable' real root must be that describing the spiral mode. This, of course, is a commonly encountered condition in lateral-directional dynamics.

(iii) When $R > 0$ and $E < 0$

As for the previous case, observation of the signs of the coefficients in the first column of the array (9.17) indicates that one root only of the characteristic equation (9.16) has a positive real part. Again, the 'unstable' root can only be a real root. Interpretation of the stability characteristics corresponding to this particular condition is exactly the same as described in (ii) above.

When all the coefficients in the characteristic equation (9.16) are positive and R is negative the instability can only be described by a pair of complex roots, the interpretation of which is described in (i) above. Since the unstable motion is oscillatory the condition $R > 0$ is sometimes referred to as the criterion for dynamic stability. Alternatively, the most common unstable condition arises when the coefficients in the characteristic equation (9.16) are positive with the exception of E. In this case the instability can only be described by a single real root, the interpretation of which is described in (iii) above. Now the instability is clearly identified as a longitudinal speed divergence or as the divergent lateral-directional spiral mode, both of which are dynamic characteristics. However, the aerodynamic contribution to E is substantially dependent on static stability effects and when $E < 0$ the cause is usually static instability. Consequently, the condition $E > 0$ is sometimes referred to as the criterion for static stability. This simple analysis emphasizes the role of the characteristic equation in describing the total stability of the aeroplane and reinforces the reason why, in reality, static and dynamic stability are inseparable, and why one should not be considered without reference to the other.

9.4.2 INTERPRETATION OF THE COEFFICIENT E

Assuming the longitudinal equations of motion to be referred to aircraft wind axes, then the coefficient E in the longitudinal characteristic equation may be obtained directly from Appendix 2

$$E = mg(\mathring{M}_w\mathring{Z}_u - \mathring{M}_u\mathring{Z}_w) \tag{9.19}$$

and the longitudinal static stability criterion may be expressed in terms of dimensionless derivatives

$$M_wZ_u > M_uZ_w \tag{9.20}$$

For most aeroplanes the derivatives in equation (9.20) have negative values so that the terms on either side of the inequality are usually both positive. M_w is a measure of the controls fixed longitudinal static stability margin, Z_u is largely dependent on lift coefficient, Z_w is dominated by lift curve slope and M_u only assumes significant values at high Mach number. Thus, provided the aeroplane possesses a sufficient margin of controls fixed longitudinal static stability M_w will be sufficiently large to ensure that the inequality (9.20) is satisfied. At higher Mach numbers when M_u becomes larger the inequality is generally maintained since the associated aerodynamic changes also cause M_w to increase.

Similarly, the coefficient E in the lateral-directional characteristic equation may be obtained directly from Appendix 2

$$E = mg(\mathring{L}_v\mathring{N}_r - \mathring{L}_r\mathring{N}_v) \tag{9.21}$$

and the lateral-directional static stability criterion may be expressed in terms of dimensionless derivatives

$$L_vN_r > L_rN_v \tag{9.22}$$

For most aeroplanes the derivatives L_v and N_r are both negative, the derivative L_r is usually positive and the derivative N_v is always positive. Thus, the terms on either side of the inequality (9.22) are usually both positive. Satisfaction of the inequality is usually determined by the relative magnitudes of the derivatives L_v and N_v. Now L_v and N_v are the derivatives describing the lateral and directional controls fixed static stability of the aeroplane respectively, as discussed in Sections 3.4 and 3.5. The magnitude of the derivative L_v is determined by the *lateral dihedral effect* and the magnitude of the derivative N_v is determined by the *directional weathercock effect*. The inequality (9.22) also determines the condition for a stable spiral mode as described in Section 7.3.2 and, once again, the inseparability of static and dynamic stability is illustrated.

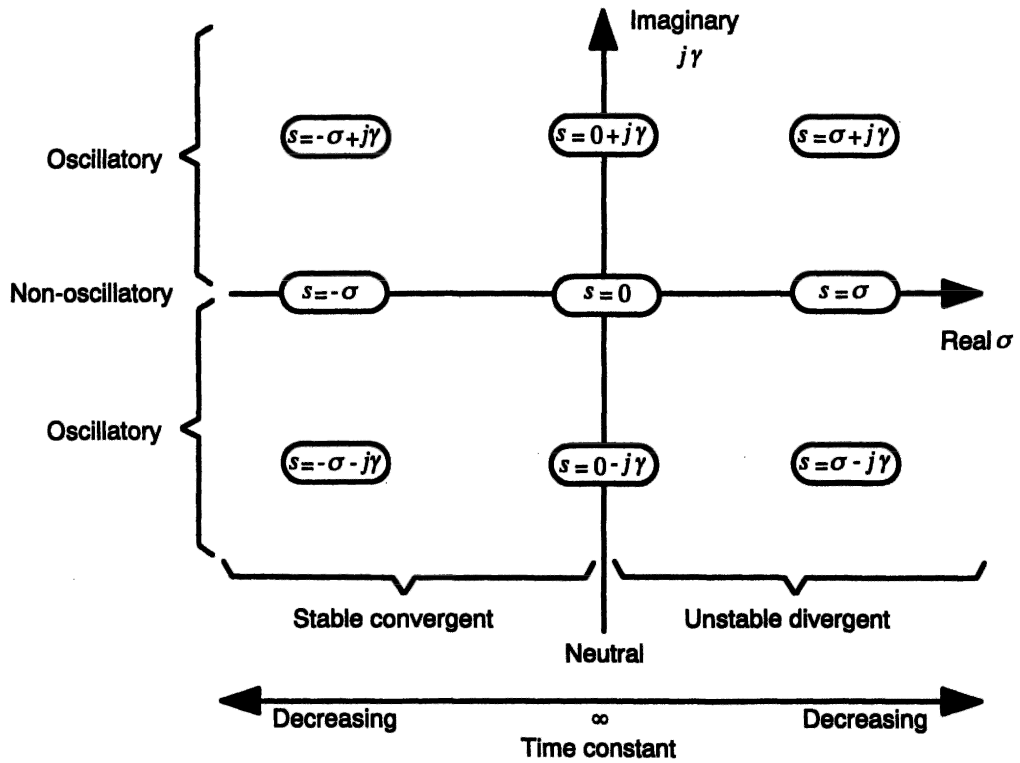

Fig. 9.1 Roots on the *s*-plane

9.5 Graphical interpretation of stability

Today, the foregoing analysis of stability is of limited practical value since all of the critical information is normally obtained in the process of solving the equations of motion exactly and directly using suitable computer software tools as described elsewhere. However, its greatest value is in the understanding and interpretation of stability that it provides. Of much greater practical value are the graphical tools much favoured by the control engineer for the interpretation of stability on the *s-plane*.

9.5.1 ROOT MAPPING ON THE S-PLANE

The roots of the characteristic equation are either real or complex pairs as stated in Section 9.2. The possible forms of the roots may be mapped on to the *s*-plane as shown in Fig. 9.1. Since the roots describe various dynamic and stability characteristics possessed by the system to which they relate the location of the roots on the *s*-plane also conveys the same information in a highly accessible form. 'Stable' roots have negative real parts and lie on the left half of the *s*-plane, 'unstable' roots have positive real parts and lie on the right half of the *s*-plane and roots describing neutral stability have zero real parts and lie on the imaginary axis. Complex roots lie in the upper half of the *s*-plane, their conjugates lie in the lower half of the *s*-plane and since their locations are mirrored in the real axis it is usual to show the upper half of the plane only.

Complex roots describe oscillatory motion, so all roots lying in the plane and not on the real axis describe such characteristics. Roots lying on the real axis describe non-oscillatory motions, the time constants of which are given by $T = 1/\sigma$. A root lying at the origin, therefore, is neutrally stable and has an infinite time constant. As real roots move away from the origin so their time constants decrease, in the stable sense, on the left half plane and in the unstable sense on the right half plane.

Consider the interpretation of a pair of complex roots on the *s*-plane in rather greater detail. As stated in Section 9.2, the typical pair of complex roots may be written

$$(s + \sigma + j\gamma)(s + \sigma - j\gamma) = s^2 + 2\sigma s + (\sigma^2 + \gamma^2) = 0 \tag{9.23}$$

which is equivalent to the familiar expression

$$s^2 + 2\zeta\omega s + \omega^2 = 0 \tag{9.24}$$

whence

$$\left.\begin{aligned} \zeta\omega &= \sigma \\ \omega^2 &= \sigma^2 + \gamma^2 \\ \zeta = \cos\phi &= \frac{\sigma}{\sqrt{\sigma^2 + \gamma^2}} \end{aligned}\right\} \tag{9.25}$$

where ϕ is referred to as the *damping angle*. This information is readily interpreted on the *s*-plane as shown in Fig. 9.2. The complex roots of equation (9.23) are plotted at p, the upper half of the *s*-plane only being shown since the lower half containing the complex conjugate root is a *mirror image* in the real axis. With reference to equations (9.24) and (9.25), it is evident that undamped natural frequency is given by the magnitude of the line joining the origin and the point p. Thus, lines of constant frequency are circles concentric with the origin provided that both axes have the same scales. Care should be exercised when the scales are dissimilar, which is often the case,

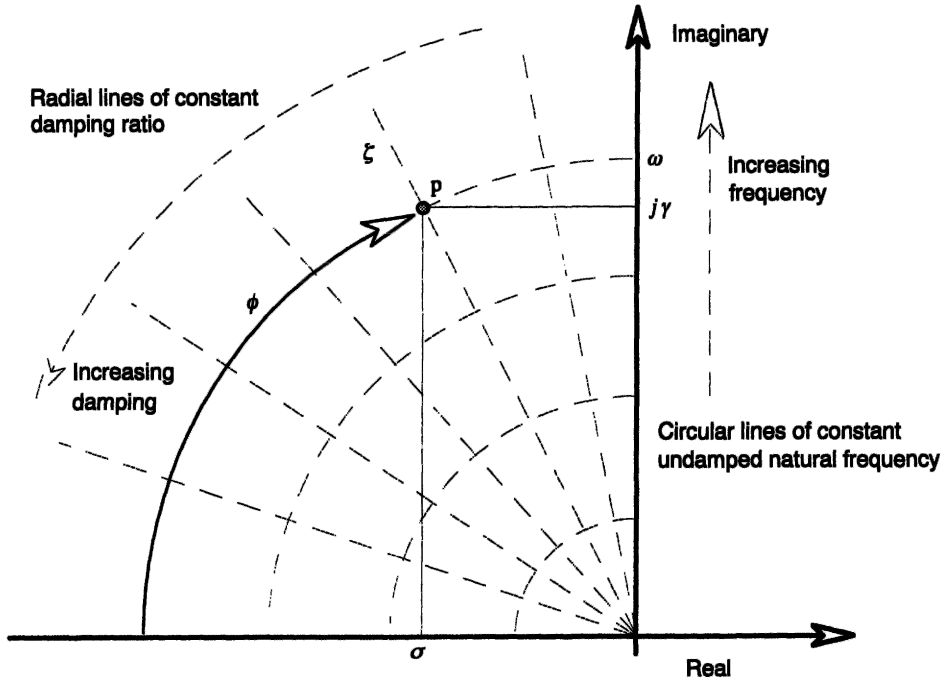

Fig. 9.2 Typical complex roots on the *s*-plane

as the lines of constant frequency then become ellipses. Thus, clearly, roots indicating low frequency dynamics are near to the origin and vice versa.

Whenever possible, it is good practice to draw *s*-plane plots and *root locus plots* on axes having the same scales to facilitate the easy interpretation of frequency. With reference to equations (9.25), it is evident that radial lines drawn through the origin are lines of constant damping. The imaginary axis then becomes a line of zero damping and the real axis becomes a line of *critical damping* where the damping ratio is unity and the roots become real. The upper left quadrant of the *s*-plane shown in Fig. 9.2 contains the stable region of positive damping ratio in the range $0 \leqslant \zeta \leqslant 1$ and is therefore the region of critical interest in most practical applications. Thus, roots indicating stable well-damped dynamics are seen toward the left of the region and vice versa. Thus, information about the dynamic behaviour of a system is instantly available on inspection of the roots of its characteristic equation on the *s*-plane. The interpretation of the stability of an aeroplane on the *s*-plane becomes especially useful for the assessment of stability augmentation systems on the *root locus plot* as described in Chapter 11.

EXAMPLE 9.4

The Boeing B-747 is typical of a large classical transport aircraft and the following characteristics were obtained from Heffley and Jewell (1972). The flight case chosen is representative of typical cruising flight at Mach 0.65 at an altitude of 20000 ft. The longitudinal characteristic equation is

$$\Delta(s)_{\text{long}} = s^4 + 1.1955s^3 + 1.5960s^2 + 0.0106s + 0.00676 \tag{9.26}$$

with roots

$$\left.\begin{aligned} s &= -0.001725 \pm 0.0653\text{j} \\ s &= -0.596 \pm 1.1101\text{j} \end{aligned}\right\} \tag{9.27}$$

describing stability mode characteristics

$$\left.\begin{aligned} \omega_p &= 0.065 \text{ rad/s} \quad & \zeta_p &= 0.0264 \\ \omega_s &= 1.260 \text{ rad/s} \quad & \zeta_s &= 0.4730 \end{aligned}\right\} \tag{9.28}$$

The corresponding lateral characteristic equation is

$$\Delta(s)_{\text{long}} = s^4 + 1.0999s^3 + 1.3175s^2 + 1.0594s + 0.01129 \tag{9.29}$$

with roots

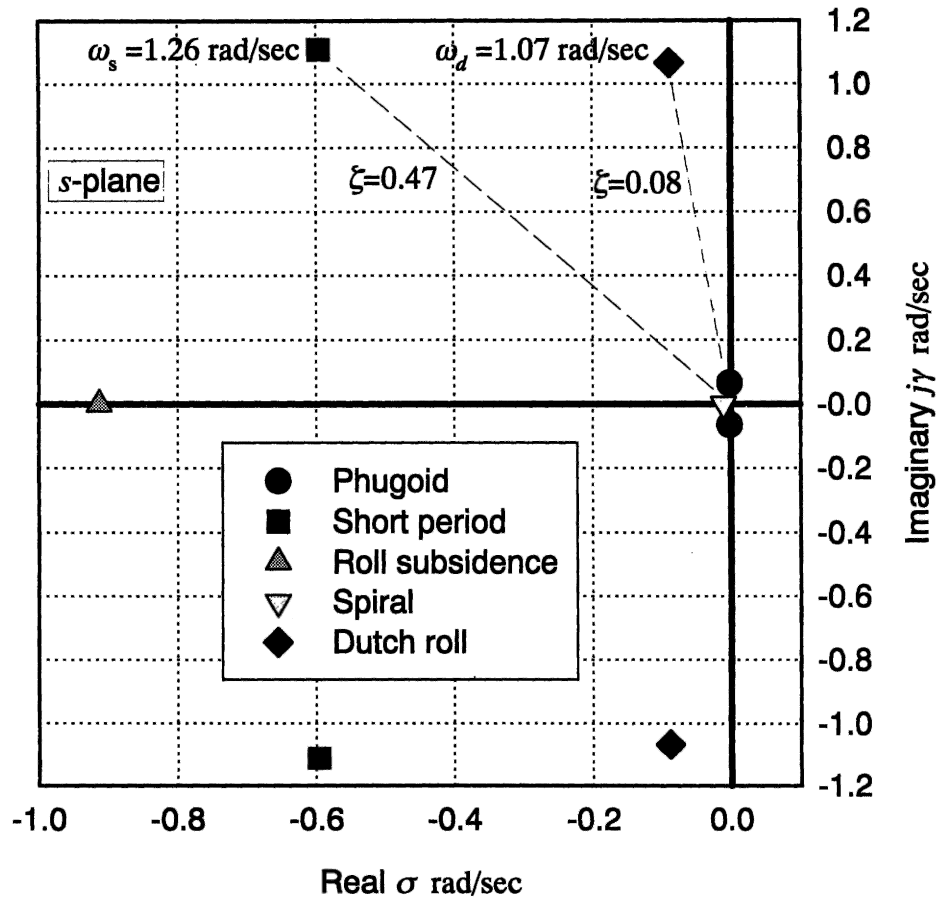

Fig. 9.3 Boeing B-747 stability modes on the *s*-plane

$$\left.\begin{aligned} s &= -0.0108 \\ s &= -0.9130 \\ s &= -0.0881 \pm 1.0664\text{j} \end{aligned}\right\} \tag{9.30}$$

describing stability mode characteristics

$$\left.\begin{aligned} T_s &= 92.6\,\text{s} \\ T_r &= 1.10\,\text{s} \\ \omega_d &= 1.070\ \text{rad/s} \qquad \zeta_d = 0.082 \end{aligned}\right\} \tag{9.31}$$

The longitudinal roots given by equation (9.27) and the lateral roots given by equation (9.30) are mapped on to the s-plane as shown in Fig. 9.3. The plot is absolutely typical for a large number of aeroplanes and shows the *stability modes*, represented by their corresponding roots, on regions of the s-plane normally associated with the modes. For example, the *slow modes*, the phugoid and spiral mode, are clustered around the origin whereas the *faster modes* are further out in the plane. Since the vast majority of aeroplanes have longitudinal and lateral-directional control bandwidths of less than 10 rad/s, then the scales of the s-plane plot would normally lie in the range $-10\,\text{rad/s} < \text{real} < 0\,\text{rad/s}$ and $-10\,\text{rad/s} < \text{imaginary} < 10\,\text{rad/s}$. Clearly, the control bandwidth of the B-747 at the chosen flight condition is a little over 1 rad/s as might be expected for such a large aeroplane. The important observation to be made from this illustration is the relative locations of the stability mode roots on the s-plane since they are quite typical of many aeroplanes.

References

Heffley, R. K. and Jewell, W. F. 1972: *Aircraft Handling Qualities Data*. NASA Contractor Report, NASA CR-2144.

Teper, G. L. 1969: *Aircraft Stability and Control Data*. Systems Technology, Inc, STI Technical Report 176-1.

10

Flying and Handling Qualities

10.1 Introduction

Some general concepts describing the meaning of *flying and handling qualities* of aeroplanes were introduced in Chapter 1 and are not repeated in full here. However, it is useful to recall that the flying and handling qualities of an aeroplane are those properties which govern the ease and precision with which it responds to pilot commands in the execution of the flight task. Although these rather intangible properties are described qualitatively and are formulated in terms of *pilot opinion*, it becomes necessary to find alternative quantitative descriptions for more formal analytical purposes. Now, as described previously, the flying and handling qualities of an aeroplane are, in part, intimately dependent on its stability and control characteristics, including the effects of a flight control system when one is installed. It has been shown in previous chapters how the stability and control parameters of an aeroplane may be quantified, and these are commonly used as indicators and measures of the flying and handling qualities. So, the object here is to introduce, at an introductory level, the way in which stability and control parameters are used to quantify the flying and handling qualities of an aeroplane.

10.1.1 STABILITY

A stable aeroplane is an aeroplane that can be established in an equilibrium flight condition where it will remain, showing no tendency to diverge. Therefore, a stable aeroplane is, in general, a safe aeroplane. However, it has already been established that too much stability can be as hazardous as too little stability. The degree of stability determines the magnitude of the control action, measured in terms of control displacement and force, required to manoeuvre about a given flight path. Thus, *controllability* is concerned with the correct *harmonization* of control power with the degrees of static, manoeuvre and dynamic stability of the airframe. Because of the inter-dependence of the various aspects of stability and control, the provision of well-harmonized control characteristics by entirely aerodynamic means over the entire flight envelope of an aeroplane may well be difficult, if not impossible, to achieve. This is especially so in many modern aeroplanes that are required to operate over extended flight envelopes and in aerodynamically difficult flight regimes. The solution to this

problem is found in the installation of a *control and stability augmentation system* (CSAS) where the object is to restore good flying qualities by *artificial* non-aerodynamic means.

Aircraft handling is generally concerned with two relatively distinct aspects of response to controls, the short term, or transient, response and the rather longer term response. Short term handling is very much concerned with the short period dynamic modes and their critical influence on manoeuvrability. The ability of a pilot to handle the short term dynamics of an aeroplane satisfactorily is critically dependent on the speed and stability of response. In other words, the bandwidth of the human pilot and the control bandwidth of the aeroplane must be compatible and the stability margins of the dynamic modes must be adequate. An aeroplane with poor, or inadequate, short term dynamic stability and control characteristics is simply not acceptable. Thus, the provision of good short term handling tends to be the main consideration in studies of flying and handling qualities.

Longer term handling is concerned with the establishment and maintenance of a steady flight condition, or trimmed equilibrium, which is determined by static stability in particular and is influenced by the long period dynamic modes. The dynamic modes associated with long term handling tend to be slow and the frequencies involved are relatively low. Thus, their control is well within the bandwidth and capabilities of the average human pilot even when the modes are marginally unstable. As a result, the requirements for the stability of the low frequency dynamics are more relaxed. However, those aspects of control which are dependent on static and manoeuvre stability parameters are very important and result in well-defined boundaries for the static and manoeuvre margins.

10.2 Short term dynamic models

As explained above, the critical aspects of aircraft handling qualities are mainly concerned with the dynamics of the initial, or transient, response to controls. Thus, since the short term dynamics is of greatest interest it is common practice to conduct handling qualities studies using reduced order dynamic models derived from the full order equations of motion. The advantage of this approach is that it gives maximum *functional visibility* to the motion drivers of greatest significance. It is therefore easier to interpret and understand the role of the fundamental aerodynamic and dynamic properties of the aeroplane in the determination of its handling qualities. It also goes without saying that the reduced order models are much easier to work with as they are algebraically simpler.

10.2.1 CONTROLLED MOTION AND MOTION CUES

Reduced to the simplest interpretation, when a pilot applies a control input to his aeroplane he is simply commanding a change in flight path. The change might be temporary, such as manoeuvring about the flight path to return to the original flight path on completion of the manoeuvre. Alternatively, the change might be permanent, such as manoeuvring to effect a change in trim state involving a change of flight path direction. Whatever the ultimate objective the method of control is much the same.

Normal manoeuvring involves rotating the airframe in roll, pitch and yaw to point the lift vector in the desired direction and, by operating the pitch control, the angle of

attack is adjusted to produce the lift force required to generate the acceleration to manoeuvre. Thus, the pilot's perception of the handling qualities of his aeroplane is concerned with the precise way in which it responds to his commands, sensed predominantly as the change in normal acceleration. Indeed, the human pilot is extremely sensitive to even the smallest changes in acceleration in all three axes. Clearly then, short term normal acceleration dynamics provides a vitally important cue in aircraft handling qualities considerations and is most easily modelled with the reduced order equations of motion. Obviously, other motion cues are equally important to the pilot such as attitude, angular rate and angular acceleration, although these variables have not, in the past, been regarded with the same level of importance as normal acceleration. Thus, in the analysis of aircraft handling qualities, by far the greatest emphasis is placed on the longitudinal short term dynamic response to controls.

10.2.2 THE LONGITUDINAL REDUCED ORDER MODEL

The reduced order longitudinal state equation describing short term dynamics only is given by equation (6.1) in terms of concise derivatives and may be written

$$\begin{bmatrix} \dot{\alpha} \\ \dot{q} \end{bmatrix} = \begin{bmatrix} z_w & 1 \\ m_w & m_q \end{bmatrix} \begin{bmatrix} \alpha \\ q \end{bmatrix} + \begin{bmatrix} \dfrac{z_\eta}{U_e} \\ m_\eta \end{bmatrix} \eta \tag{10.1}$$

since $z_q \cong U_e$ and w is replaced by α. Solution of equation (10.1) gives the two short term response transfer functions

$$\frac{\alpha(s)}{\eta(s)} = \frac{\dfrac{z_\eta}{U_e}\left(s + U_e \dfrac{m_\eta}{z_\eta}\right)}{(s^2 - (m_q + z_w)s + (m_q z_w - m_w U_e))} \equiv \frac{k_\alpha(s + 1/T_\alpha)}{(s^2 + 2\zeta_s\omega_s s + \omega_s^2)} \tag{10.2}$$

$$\frac{q(s)}{\eta(s)} = \frac{m_\eta(s - z_w)}{(s^2 - (m_q + z_w)s + (m_q z_w - m_w U_e))} \equiv \frac{k_q(s + 1/T_{\theta_2})}{(s^2 + 2\zeta_s\omega_s s + \omega_s^2)} \tag{10.3}$$

Equations (10.2) and (10.3) compare directly with equations (6.17) and (6.18) respectively. The short term response transfer function describing pitch attitude response to elevator follows directly from equation (10.3)

$$\frac{\theta(s)}{\eta(s)} = \frac{k_q(s + 1/T_{\theta_2})}{s(s^2 + 2\zeta_s\omega_s s + \omega_s^2)} \tag{10.4}$$

With reference to Section 5.5 the short term response transfer function describing, approximately, the normal acceleration response to elevator may be derived from equations (10.2) and (10.3)

$$\frac{a_z(s)}{\eta(s)} = \frac{m_\eta z_w U_e}{(s^2 - (m_q + z_w)s + (m_q z_w - m_w U_e))} \equiv \frac{k_{a_z}}{(s^2 + 2\zeta_s\omega_s s + \omega_s^2)} \tag{10.5}$$

In the derivation it is assumed that z_η/U_e is insignificantly small. With reference to Section 5.7.3 the short term response transfer function describing flight path angle response to elevator is also readily derived from equations (10.2) and (10.4)

$$\frac{\gamma(s)}{\eta(s)} = \frac{-m_\eta z_w}{s(s^2 - (m_q + z_w)s + (m_q z_w - m_w U_e))} \equiv \frac{k_\gamma}{s(s^2 + 2\zeta_s\omega_s s + \omega_s^2)} \tag{10.6}$$

and again, it is assumed that z_η/U_e is insignificantly small. By dividing equation (10.6) by equation (10.4) it may be shown that

$$\frac{\gamma(s)}{\theta(s)} = \frac{1}{(1+sT_{\theta_2})} \tag{10.7}$$

which gives the important result that, in the short term, flight path angle response lags pitch attitude response by T_{θ_2}, sometimes referred to as *incidence lag*.

For the purpose of longitudinal short term handling analysis the responsiveness or manoeuvrability of the aeroplane is quantified by the derivative parameter *normal load factor per unit angle of attack*, denoted n_α. Since this parameter relates to the aerodynamic lift generated per unit angle of attack at a given flight condition it is proportional to the lift curve slope and the square of the velocity. An expression for n_α is easily derived from the above short term transfer functions. Assuming a unit step input to the elevator such that $\eta(s) = 1/s$ then the Laplace transform of the incidence response follows from equation (10.2)

$$\alpha(s) = \frac{\frac{z_\eta}{U_e}\left(s + U_e\frac{m_\eta}{z_\eta}\right)}{(s^2 - (m_q + z_w)s + (m_q z_w - m_w U_e))}\frac{1}{s} \tag{10.8}$$

Applying the final value theorem, equation (5.33), to equation (10.8) the resultant steady value of incidence may be obtained

$$\alpha(t)|_{ss} = \frac{m_\eta}{(m_q z_w - m_w U_e)} \tag{10.9}$$

In a similar way the corresponding resultant steady value of normal acceleration may be derived from equation (10.5)

$$a_z(t)|_{ss} = \frac{m_\eta z_w U_e}{(m_q z_w - m_w U_e)} \tag{10.10}$$

Now the normal load factor per unit angle of attack is given by

$$n_\alpha = \left.\frac{n_z(t)}{\alpha(t)}\right|_{ss} \equiv -\left.\frac{1}{g}\frac{a_z(t)}{\alpha(t)}\right|_{ss} \tag{10.11}$$

Thus, substituting equations (10.9) and (10.10) into equation (10.11) the important result is obtained

$$n_\alpha = -\frac{z_w U_e}{g} \equiv \frac{U_e}{gT_{\theta_2}} \tag{10.12}$$

since, approximately, $T_{\theta_2} = -1/z_w$.

The transfer functions given by equations (10.2) to (10.7) above describe the classical longitudinal short term response to elevator and represent the foundation on which most modern handling qualities ideas are based, see, for example, Gibson (1995). For the classical aeroplane the response characteristics are determined by the aerodynamic properties of the airframe, which are usually linear, bounded and predictable. It is also clear that the short term dynamics is that of a linear second order system and aeroplanes which possess similar dynamic behaviour are said to have *second-order-like* response characteristics. The response properties of all real aeroplanes diverge from these very simple and rather idealized models to some extent. Actual response is coloured by longer

term dynamics, non-linear aerodynamic airframe characteristics and, of course, the influence of a stability augmentation system when fitted. However, whatever the degree of complexity of the aeroplane and its operating conditions a sound design objective would be to achieve second-order-like dynamic response properties.

EXAMPLE 10.1

The classical second-order-like response characteristics are most easily seen in simple light aircraft having a limited subsonic flight envelope and whose flying qualities are determined entirely by aerodynamic design. Such an aeroplane is the Navion Aircraft Corporation, Navion/H and the equations of motion for the aeroplane were obtained from Teper (1969). The flight condition corresponds to a cruising speed of 176 ft/s at sea level. The longitudinal reduced order state equation is

$$\begin{bmatrix}\dot{\alpha}\\ \dot{q}\end{bmatrix}=\begin{bmatrix}-0.0115 & 1\\ -0.0395 & -2.9857\end{bmatrix}\begin{bmatrix}\alpha\\ q\end{bmatrix}+\begin{bmatrix}-0.1601\\ -11.0437\end{bmatrix}\eta \tag{10.13}$$

and the reduced order longitudinal response transfer functions are

$$\frac{\alpha(s)}{\eta(s)}=\frac{-0.1601(s+71.9844)}{(s^2+5.0101s+12.9988)} \tag{10.14}$$

$$\frac{q(s)}{\eta(s)}=\frac{-11.0437(s+1.9236)}{(s^2+5.0101s+12.9988)}\ 1/s \tag{10.15}$$

$$\frac{\theta(s)}{\eta(s)}=\frac{-11.0437(s+1.9236)}{s(s^2+5.0101s+12.9988)} \tag{10.16}$$

$$\frac{a_z(s)}{\eta(s)}=\frac{-28.1700(s-10.1241)(s+13.1099)}{(s^2+5.0101s+12.9988)}\ \text{ft/s}^2/\text{rad} \tag{10.17}$$

$$\frac{\gamma(s)}{\eta(s)}=\frac{0.1601(s-10.1241)(s+13.1099)}{s(s^2+5.0101s+12.9988)} \tag{10.18}$$

The first five seconds of the longitudinal response of the Navion to a 1° elevator step input, as defined by equations (10.14) to (10.18), is shown in Fig. 10.1. The response plots shown are absolutely typical of the second-order-like characteristics of a classical aeroplane.

The key parameters defining the general response shapes are

the short period undamped natural frequency $\omega_s = 3.61$ rad/s

the short period damping ratio $\zeta_s = 0.7$

and the incidence lag $T_{\theta_2} = \dfrac{1}{1.9236} = 0.52\,\text{s}$

These parameters may be obtained directly from inspection of the appropriate transfer functions above.

It will be observed that the normal acceleration response transfer functions given by equations (10.5) and (10.17) have different numerators, and similarly for the flight path angle response transfer functions given by equations (10.6) and (10.18). This is due to the fact that the algebraic forms are based on a number of simplifying approximations, whereas the numerical forms were obtained from an exact solution of the state equation (10.8) without approximation. However, with reference to Fig.

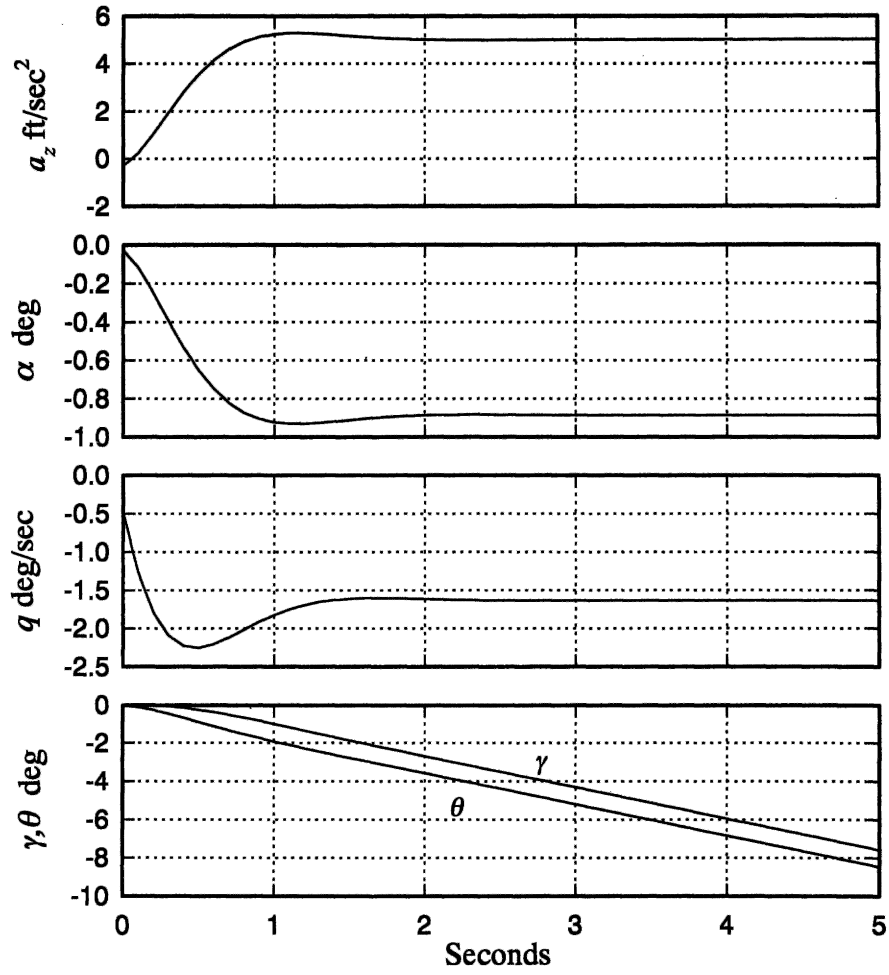

Fig. 10.1 Longitudinal short term response to elevator step input

10.1 both equation (10.17) and equation (10.18) may be approximated by transfer functions having constant numerators in the style of equations (10.5) and (10.6) respectively, and in both cases the response shapes are essentially identical. Equations (10.17) and (10.18) may be approximated by

$$\frac{a_z(s)}{\eta(s)} = \frac{3738.89}{(s^2 + 5.0101s + 12.9988)} \text{ ft/s}^2/\text{rad} \tag{10.19}$$

$$\frac{\gamma(s)}{\eta(s)} = \frac{-1.6347}{s(s^2 + 5.0101s + 12.9988)} \tag{10.20}$$

With reference to Fig. 10.1 it is clear that following a steady step elevator input the short term response, after the short period transient has damped out, results in steady normal acceleration a_z, steady incidence α and steady pitch rate q. The corresponding pitch attitude θ and flight path angle γ responses increase linearly with time, the aeroplane behaving like a simple integrator in this respect. It is evident from the latter response plots that flight path angle γ lags pitch attitude θ by about 0.5 s, see equation

(10.7), which corresponds to the exact value of T_{θ_2} very well. These response characteristics are quite typical and do not change significantly with flight condition since the Navion has a very limited flight envelope.

Now, operation of the elevator causes tailplane camber change which results in instantaneous change in tailplane lift. This in turn generates a pitching moment causing the aeroplane to respond in pitch. Thus, as a result of his control action, the pilot sees a change in pitch attitude as the primary response. Or, for a steady step input the response is a steady pitch rate, at least for the first few seconds. For this reason the nature of control is referred to as a *rate command* characteristic, which is typical of all three control axes since the aerodynamic mechanism of control is similar.

With reference to Fig. 10.1, the pitch rate response couples with forward speed to produce the incidence response, which in turn results in the normal acceleration response. This explains why a steady pitch rate is accompanied by steady incidence and normal acceleration responses. In an actual aeroplane these simple relationships are modified by the influence of the longer term phugoid dynamics. In particular, the pitch rate and normal acceleration response tend to decay with the damped phugoid motion. However, incidence tends to remain more nearly constant at its trim value throughout. Thus, viewed more broadly the nature of longitudinal control is sometimes referred to alternatively as an *incidence command* characteristic. These ideas may be more easily appreciated by referring to Examples 6.1 and 6.2.

Since the traditional longitudinal motion cue has always focused on normal acceleration, and since in the short term approximation this is represented by a transfer function with a constant numerator, equation (10.19), the only parameters defining the response shape are short period mode damping ratio and undamped natural frequency. Similarly, it is evident that incidence dynamics is governed by the same parameters. Pitch rate response is similar in shape to both normal acceleration and incidence responses with the exception of the peak overshoot, which is governed by the value of the numerator term $1/T_{\theta_2}$. However, T_{θ_2} is determined largely by the value of the wing lift curve slope which, for a simple aeroplane like the Navion, is essentially constant throughout the flight envelope. So, for a classical aeroplane with second-order-like response characteristics it is concluded that the short term dynamics is predictable and that the transient is governed predominantly by short period mode dynamics. It is not surprising, therefore, that the main emphasis in the specification of the flying qualities of aeroplanes has been on the correct design of the damping and frequency of the short term stability modes, in particular the longitudinal short period mode.

10.2.3 THE 'THUMB PRINT' CRITERION

For the reasons outlined above, the traditional indicators of the short term longitudinal handling qualities of an aeroplane were securely linked to the damping ratio and undamped natural frequency of the short period mode. As experience grew over the years of evolutionary development of aeroplanes so the short period dynamics, which resulted in good handling characteristics, became established fact. A tradition of experimental flight tests using variable stability aeroplanes was established in the early years after the Second World War for the specific purpose of investigating flying and handling qualities. In particular, much of this early experimental work was concerned

with longitudinal short term handling qualities. This research has enabled the definition of many *handling qualities criteria* and the production of *flying qualities specification* documents. The tradition of experimental flight tests for handling qualities research is still continued today, mainly in the USA.

One of the earliest flying qualities criteria, the so-called longitudinal short period *thumb print* criterion, became an established tool in the 1950s, see, for example, Chalk (1958). The thumb print criterion provides guidance for the use of aeroplane designers and evaluators concerning the best combinations of longitudinal short period mode damping and frequency to give good handling qualities. However, it must be remembered that the information provided is empirical and is based entirely on pilot opinion. The common form of presentation of the criterion is shown in Fig. 10.2, and the example shown relates to typical classical aeroplanes in which the undamped short period mode frequency is around 3 rad/s.

Although the criterion is still most applicable to the modern aeroplane, as has been suggested above, the achievement of excellent short period mode dynamics does not necessarily guarantee excellent longitudinal handling qualities. Indeed, many other factors play an important part and some of these are discussed in the following sections.

10.2.4 INCIDENCE LAG

The incidence lag, T_{θ_2}, plays a critically important part in the determination of the longitudinal handling characteristics of an aeroplane. For classical subsonic aeroplanes

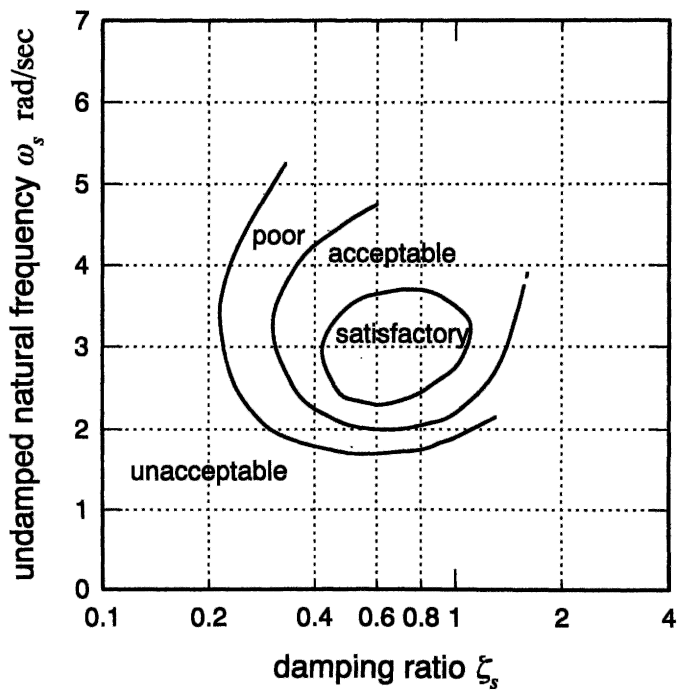

Fig. 10.2 Longitudinal short period pilot opinion contours—the thumb print criterion

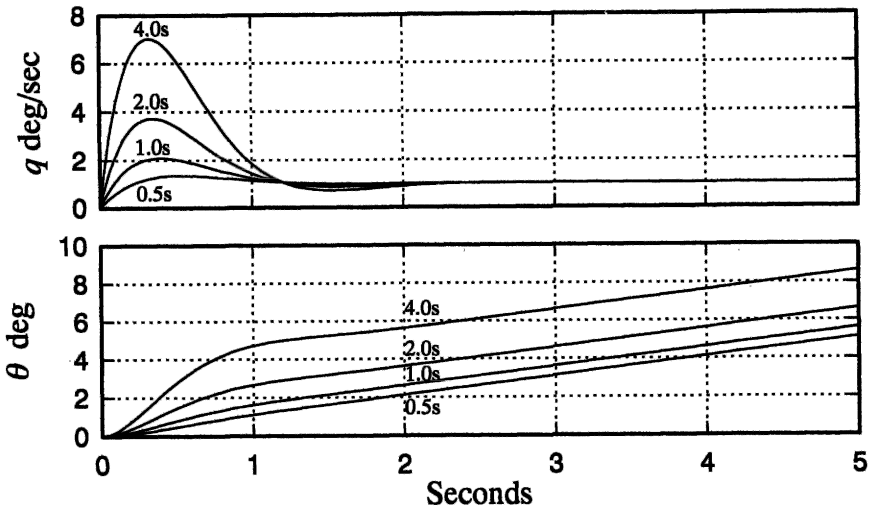

Fig. 10.3 The effect of variation in incidence lag on pitch response

T_{θ_2} remains near constant over the flight envelope and, consequently, the short term pitch dynamics also remains near constant for a given short period mode damping and frequency. Therefore, the overall longitudinal handling qualities tend to remain nicely consistent over the flight envelope. For this reason incidence lag has not been accorded a great deal of attention in the past. However, as aeroplanes have become larger and their operating altitude and Mach number envelopes have been greatly extended, so the variation in lift curve slope has become significant. The result of this is that the variation in T_{θ_2} over the flight envelope of typical modern high performance aeroplanes can no longer be ignored. Incidence lag has therefore become as important as short period mode damping and frequency in the determination of longitudinal short term handling.

Gibson (1995) suggests that, typically, T_{θ_2} may vary from less than 0.5 s at high speed at sea level to greater than 4.0 s at low speed at high altitude. Other significant changes might be introduced by camber control or by direct lift control as frequently found in advanced modern aircraft of all types. To illustrate the effect of incidence lag on short term pitch response consider the following transfer functions which are based nominally on those of Example 10.1.

$$\left.\begin{aligned}\frac{q(s)}{\eta(s)} &= \frac{-13(1+0.5s)}{(s^2+5s+13)}\ \text{1/s}\\ \frac{\theta(s)}{\eta(s)} &= \frac{-13(1+0.5s)}{s(s^2+5s+13)}\end{aligned}\right\} \tag{10.21}$$

and clearly, $\omega_s = 3.6\,\text{rad/s}$, $\zeta_s = 0.69$ and $T_{\theta_2} = 0.5\,\text{s}$. The response to a stick pull equivalent to a 1° elevator step input is shown in Fig. 10.3. Also shown are the responses for an incidence lag of 1, 2 and 4 s, the short period mode parameters being held constant throughout. In accordance with the models given by equations (10.2), (10.5) and (10.6) the corresponding incidence, normal acceleration and flight path angle responses would remain unchanged. However, the pitch motion cue to the pilot may well suggest a reduction in damping in view of the significant increase in pitch rate overshoot at larger values of T_{θ_2}. This is, of course, not the case since the short period mode

damping is 0.69 throughout. The pilot would also become aware of the increase in lag between the pitch attitude response and acquisition of the desired flight path.

10.3 Flying qualities requirements

Most countries involved in aviation have national agencies to oversee aeronautical activity in their territories. In the UK the Civil Aviation Authority (CAA) regulates all non-military aviation and the Ministry of Defence (MoD) oversees all military aeronautical activity. Additionally, a group of European countries has agreed to cooperate in the development of Joint Aviation Requirements (JAR) and, where relevant, these requirements supersede the British Civil Airworthiness Requirements (BCAR). The Joint Aviation Authority which administers this activity comprises the Aviation Authorities from the participating countries. Thus, for example, in the UK the JAR documents are issued by the CAA. In the USA the corresponding agencies are the Federal Aviation Administration (FAA) and the Department of Defense (DoD) respectively. All of these agencies issue extensive documentation specifying the minimum acceptable standards for construction, performance, operation and safety of all air vehicles operated under their jurisdiction. In more recent years, the emphasis has been on the adoption of common standards, for obvious reasons. In the absence of their own standards many countries adopt those of the American, British or joint European agencies, which is obviously constructively helpful in achieving very high standards of aviation safety worldwide.

All of the above-mentioned agencies issue documents which specify the minimum acceptable standard of flying qualities in some detail, more commonly known as *flying qualities requirements*. Some examples of the relevant documents are listed in the references at the end of this chapter. In very general terms the flying qualities requirements for civil aircraft issued by the CAA and FAA are primarily concerned with safety, and specific requirements relating to stability, control and handling are relatively relaxed. On the other hand, the flying qualities requirements issued by the MoD and DoD are specified in much greater detail in every respect. It is the responsibility of the aircraft manufacturer, or supplier, to demonstrate that their aircraft *complies* with the appropriate specification prior to acceptance by the operator. Thus, *demonstration of compliance* with the specification is the principal interest of the regulating agencies.

Since the military flying qualities requirements in particular are relatively complex, their correct interpretation may not always be obvious. To alleviate this difficulty the documents also include advisory information on *acceptable means of compliance* to help the user to apply the requirements to his particular aeroplane. The extensive programme of flight tests which most new aeroplanes undergo prior to entry into service is, in part, used to demonstrate compliance with the flying qualities requirements. However, it is unlikely that an aeroplane will satisfy the flying qualities requirements completely unless it has been designed to do so from the outset. Therefore, the flying qualities requirements documents are also vitally important to the aircraft designer and to the flight control system designer. In this context, the specifications define the *rules* to which stability, control and handling must be designed and evaluated.

The formal specification of flying and handling qualities is intended to 'assure flying qualities that provide adequate mission performance and flight safety'. Since the most comprehensive, and hence demanding, requirements are included in the military documents it is these on which the material in the following sections is based. As the

military use all kinds of aeroplanes including small light trainers, large transports and high performance combat aircraft, then flying qualities requirements applicable to all types are quantified in the specification documents. Further, an aeroplane designed to meet the military flying and handling qualities requirements would undoubtedly also meet the civil requirements. Since most of the requirements are quantified in terms of stability and control parameters they are most readily applied in the current analytical context.

The object here, then, is to provide a summary, or overview, of the flying qualities requirements as set out in the military specification documents. Liberal reference has been made to the British Defence Standard DEF-STAN 00-970 and to the American Military Specification MIL-F-8785C, which are very similar in style and which both convey much the same information. This is not surprising since the former was deliberately modelled on the latter in the interests of uniformity. Using an amalgam of material from both sources no attempt is made to reproduce the requirements with great accuracy or in great detail; for a complete appreciation the reader should consult the references. Rather, the emphasis is on a limited review of the material relevant to the fundamental stability and control properties of the aeroplane, as described in earlier chapters.

Now, it is important to appreciate that the requirements in both DEF-STAN 00-970 and MIL-F-8785C are based on the dynamics of classical aeroplanes whose short term response is essentially second-order-like. This is simply due to the fact that the requirements are empirical and have evolved to capitalize on many years of accumulated experience and pilot opinion. Although attempts have been made to revise the requirements to allow for aeroplanes with stability augmentation this has only had limited success. Aeroplanes with simple stability augmentation which behave essentially like classical unaugmented aeroplanes are generally adequately catered for. However, in recent years it has become increasingly obvious that the requirements in both DEF-STAN 00-970 and MIL-F-8785C are unable to cope with aeroplanes whose flying qualities are substantially dependent on a flight control system. For example, evidence exists to suggest that some advanced-technology aeroplanes have been designed to meet the flying qualities requirements very well only to attract adverse pilot opinion concerning their handling qualities. With the advent of the fly-by-wire (FBW) aeroplane it became necessary to seek additional or alternative methods for quantifying and specifying flying qualities requirements.

The obvious deficiencies of the earlier flying qualities requirements documents for dealing with highly augmented aeroplanes spawned a considerable amount of research activity from the late 1960s onward. As a result all kinds of handling qualities criteria have emerged, a few of which have enjoyed enduring, but limited, success. Nevertheless, understanding has improved considerably and the first serious attempt at producing a flying qualities requirements document suitable for application to highly augmented aeroplanes resulted in the proposal reported by Hoh *et al.* (1982). This report eventually evolved into the formal American Military Standard MIL-STD-1797A, which is not available in the public domain. However, the report by Hoh *et al.* (1982) is a useful alternative and it contains some supporting explanatory material. These newer flying qualities requirements still include much of the classical flying qualities material derived from the earlier specifications but with the addition of material relating to the influence of command and stability augmentation systems on handling. Although Hoh *et al.* (1982) and MIL-STD-1797A provide a very useful progression from DEF-STAN 00-970

and MIL-F-8785C, the material relating to highly augmented aeroplanes takes the subject well beyond the scope of the present book. The interested reader will find an excellent overview of the ideas relating to the handling qualities of advanced-technology aeroplanes in Gibson (1995).

10.4 Aircraft role

It is essential that the characteristics of any dynamic system, which is subject to direct human control, are bounded, and outside these bounds the system would not be capable of human control. However, the human is particularly adaptable such that the variation in acceptable dynamic characteristics within the performance boundary of the system is considerable. In terms of aeroplane dynamics this means that wide variation in stability and control characteristics can be tolerated within the bounds of acceptable flying qualities. However, it is important that the flying qualities are appropriate to the type of aeroplane in question and to the task it is carrying out. For example, the dynamic handling qualities appropriate to a fighter aircraft in an air combat situation are quite inappropriate to a large civil transport aircraft on final approach. Thus, it is easy to appreciate that the stability and control characteristics which comprise the flying qualities requirements of an aeroplane are bounded by the limitations of the human pilot, but within those bounds the characteristics are defined in a way that is most appropriate to the prevailing flight condition.

Thus, flying qualities requirements are formulated to allow for the type, or *class*, of aeroplane and for the flight task, or *flight phase*, in question. Further, the degree of excellence of flying qualities is described as the *level of flying qualities*. Thus, prior to referring to the appropriate flying qualities requirements the aeroplane must be classified and its flight phase defined. A designer would then design to achieve the highest level of flying qualities, whereas an evaluator would seek to establish that the aeroplane achieved the highest level of flying qualities in all normal operating states.

10.4.1 AIRCRAFT CLASSIFICATION

Aeroplane types are classified broadly according to size and weight as follows

Class I Small light aeroplanes.

Class II Medium weight, low to medium manoeuvrability aeroplanes.

Class III Large, heavy, low to medium manoeuvrability aeroplanes.

Class IV High manoeuvrability aeroplanes.

10.4.2 FLIGHT PHASE

A sortie or mission may be completely defined as a sequence of piloting tasks. Alternatively, a mission may be described as a succession of flight phases. Flight phases are grouped into three categories and each category comprises a variety of tasks requiring similar flying qualities for their successful execution. The tasks are separately defined in terms of *flight envelopes*. The flight phase categories are defined as follows.

Category A Non-terminal flight phases that require rapid manoeuvring, precision tracking, or precise flight path control.

Category B Non-terminal flight phases that require gradual manoeuvring, less precise tracking and accurate flight path control.

Category C Terminal flight phases that require gradual manoeuvring and precision flight path control.

10.4.3 LEVELS OF FLYING QUALITIES

The levels of flying qualities quantify the degree of acceptability of an aeroplane in terms of its ability to complete the mission for which it is designed. The three levels of flying qualities seek to indicate the severity of the *pilot workload* in the execution of a mission flight phase and are defined as follows.

Level 1 Flying qualities clearly adequate for the mission flight phase.

Level 2 Flying qualities adequate to accomplish the mission flight phase, but with an increase in pilot workload and/or degradation in mission effectiveness.

Level 3 Degraded flying qualities, but such that the aeroplane can be controlled, inadequate mission effectiveness and high, or limiting, pilot workload.

Level 1 flying qualities implies a fully functional aeroplane which is 100% capable of achieving its mission with acceptable pilot workload at all times. Therefore, it follows that any fault or failure occurring in the airframe, engines or systems may well degrade the level of flying qualities. Consequently, the *probability* of such a situation arising during a mission becomes an important issue. Thus, the levels of flying qualities are very much dependent on the aircraft failure state which, in turn, is dependent on the reliability of the critical functional components of the aeroplane. The development of this aspect of flying qualities assessment is a subject in its own right and is beyond the scope of the present book.

10.4.4 FLIGHT ENVELOPES

The operating boundaries of altitude, Mach number and normal load factor define the *flight envelope* for an aeroplane. Flight envelopes are used to describe the absolute 'never exceed' limits of the airframe and also to define the operating limits required for the execution of a particular mission or flight phase.

10.4.4.1 Permissible flight envelope

The permissible flight envelopes are the limiting boundaries of flight conditions to which an aeroplane may be flown and safely recovered without exceptional pilot skill.

10.4.4.2 Service flight envelope

The service flight envelopes define the boundaries of altitude, Mach number and normal load factor which encompass all operational mission requirements. The service flight envelopes denote the limits to which an aeroplane may normally be flown without risk of exceeding the permissible flight envelopes.

Table 10.1 Operational flight envelopes

Flight phase category	Flight phase
A	Air-to-air combat Ground attack Weapon delivery/launch Reconnaissance In-flight refuel (receiver) Terrain following Maritime search Aerobatics Close formation flying
B	Climb Cruise Loiter In-flight refuel (tanker) Descent Aerial delivery
C	Take-off Approach Overshoot Landing

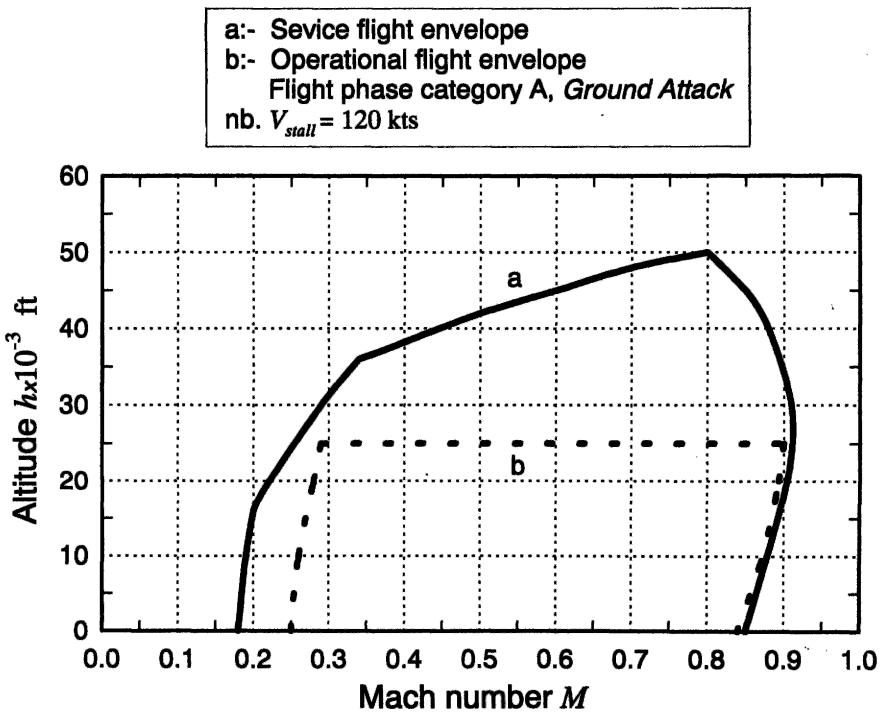

Fig. 10.4 Flight envelopes for the McDonnell-Douglas A4-D Skyhawk

10.4.4.3 Operational flight envelope

The operational flight envelopes lie within the service flight envelopes and define the boundaries of altitude, Mach number and normal load factor for each flight phase. It is a requirement that the aeroplane must be capable of operation to the limits of the appropriate operational flight envelopes in the execution of its mission. The operational flight envelopes defined in DEF-STAN 00-970 are listed in Table 10.1.

When assessing the flying qualities of an aeroplane Table 10.1 may be used to determine which flight phase category is appropriate for the flight condition in question.

EXAMPLE 10.2

To illustrate the altitude–Mach number flight envelopes consider the McDonnell-Douglas A4-D Skyhawk and its possible deployment in a *ground attack* role. The service flight envelope for the aircraft was obtained from Teper (1969) and is shown in Fig. 10.4. Assuming this aircraft were to be procured by the Royal Air Force then it would have to meet the operational flight envelope requirement for the ground attack role as defined in DEF-STAN 00-970. The altitude–speed requirements for this role are given as follows

Minimum operational speed $V_{0_{min}} = 1.4V_{stall}$
Maximum operational speed $V_{0_{max}} = 1.4V_{MAT}$
Minimum operational altitude $h_{0_{min}}$ = Mean sea level (MSL)
Maximum operational altitude $h_{0_{max}} = 25\,000$ ft

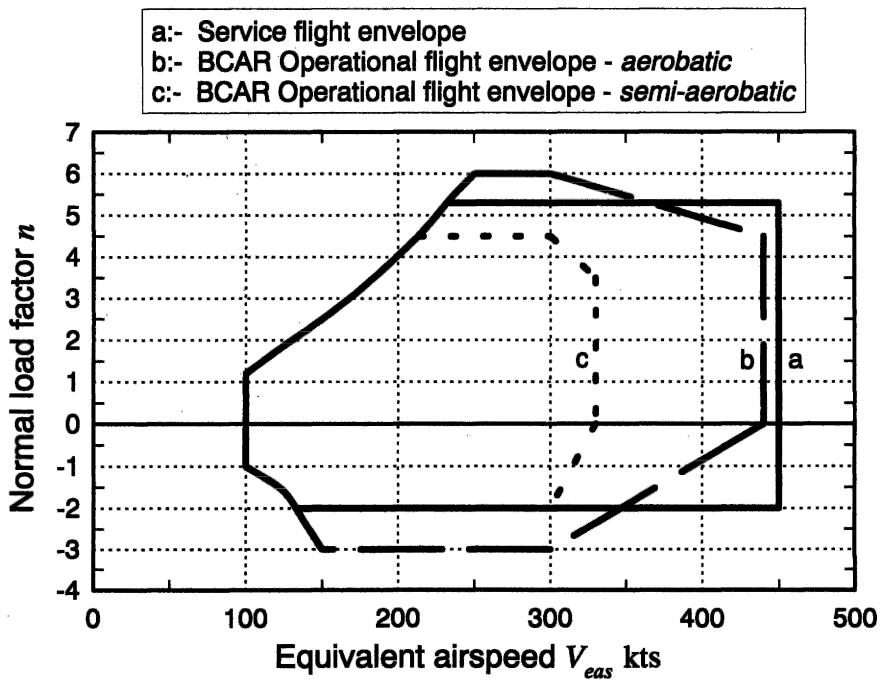

Fig. 10.5 Flight envelopes for the Morane Saulnier MS-760 Paris

where V_{MAT} is the maximum speed at *maximum augmented thrust* in level flight. The operational flight envelope for the ground attack role is superimposed on the service flight envelope for the aircraft as shown in Fig. 10.4 and the implications of these limits are self-evident for the role in question.

EXAMPLE 10.3

To illustrate the normal load factor–speed flight envelopes consider the Morane Saulnier MS-760 Paris aircraft as registered by the CAA for operation in the UK. The Paris is a small four-seat twin-jet fast liaison aircraft which first flew in the late 1950s. The aircraft is a classical 'aerodynamic' machine, it has an unswept wing, a T-tail and is typical of the small jet trainers of the period. The manoeuvring flight envelopes for this aircraft were obtained from *Notes for Technical Observers* (1965) and are reproduced in Fig. 10.5. Clearly the service flight envelope fully embraces the BCAR operational flight envelope for *semi-aerobatic* aircraft, whereas some parts of the BCAR operational flight envelope for fully *aerobatic* aircraft are excluded. Consequently the aircraft is registered in the semi-aerobatic category and certain aerobatic manoeuvres

Table 10.2 The Cooper–Harper handling qualities rating scale

Adequacy for selected task	Aircraft characteristic	Demands on pilot (workload)	Pilot rating
Satisfactory	Excellent	Very low	1
Satisfactory	Good	Low	2
Satisfactory	Fair	Minimal pilot compensation required	3
Unsatisfactory—warrants improvements	Minor deficiencies	Moderate pilot compensation required	4
Unsatisfactory—warrants improvements	Moderate deficiencies	Considerable pilot compensation required	5
Unsatisfactory—warrants improvements	Tolerable deficiencies	Extensive pilot compensation required	6
Unacceptable—requires improvements	Major deficiencies	Adequate performance not attainable	7
Unacceptable—requires improvements	Major deficiencies	Considerable pilot compensation required for control	8
Unacceptable—requires improvements	Major deficiencies	Intense pilot compensation required for control	9
Catastrophic—improvement mandatory	Major deficiencies	Loss of control likely	10

Table 10.3 Equivalence of Cooper–Harper rating scale with levels of flying qualities

Level of flying qualities	Level 1			Level 2			Level 3		Below Level 3	
Cooper–Harper rating scale	1	2	3	4	5	6	7	8	9	10

are prohibited. It is clear from this illustration that the Paris was designed with structural normal load factor limits of $+5.2g$, $-2g$ which are inadequate for fully aerobatic manoeuvring.

10.5 Pilot opinion rating

Pilot opinion rating scales have been in use for a considerable time and provide a formal procedure for the qualitative assessment of aircraft flying qualities by experimental means. Since qualitative flying qualities assessment is very subjective, the development of a formal method for the interpretation of pilot opinion has turned a rather 'imprecise art' into a useful tool which is routinely used in flight test programmes. The current pilot opinion rating scale was developed by Cooper and Harper (1969) and is universally known as the *Cooper–Harper rating scale.*

The Cooper–Harper rating scale is used to assess the flying qualities, or more specifically the handling qualities, of an aeroplane in a given flight phase. The procedure for conducting the flight test evaluation and the method for post flight reduction and interpretation of pilot comments are defined. The result of the assessment is a *pilot rating* between 1 and 10. A rating of 1 suggests excellent handling qualities and low pilot workload whereas a rating of 10 suggests an aircraft with many handling qualities deficiencies. The adoption of a common procedure for rating handling qualities enables pilots to state clearly their assessment without ambiguity or the use of misleading terminology. A summary of the Cooper–Harper handling qualities rating scale is shown in Table 10.2.

It is usual and convenient to define an equivalence between the qualitative Cooper–Harper handling qualities rating scale and the quantitative levels of flying qualities. This permits easy and meaningful interpretation of flying qualities between both the piloting and analytical domains. The equivalence is summarized in Table 10.3.

10.6 Longitudinal flying qualities requirements

10.6.1 LONGITUDINAL STATIC STABILITY

It has been shown in Chapter 3 that longitudinal static stability determines the pitch control displacement and force to trim. Clearly this must be of the correct magnitude if effective control of the aeroplane is to be maintained at all flight conditions. For this to be so the controls fixed and controls free static margins must not be too large or too small.

In piloting terms a change of trim is seen as a change in airspeed, or Mach number, and involves a forward stick push to increase speed and an aft stick pull to decrease speed when the aeroplane possesses a normal level of static stability. The requirement states that the variation in pitch control position and force with speed is to be smooth and the gradients at the nominal trim speed are to be stable or, at worst, neutrally stable. In other words the static margins are to be greater than or equal to zero. The maximum acceptable degree of static stability is not specified. However, this will be limited by the available control power and the need to be able to lift the nose wheel at rotation for take-off at a reasonable airspeed. Abrupt changes in gradient with airspeed are not acceptable. Typical stable gradients are

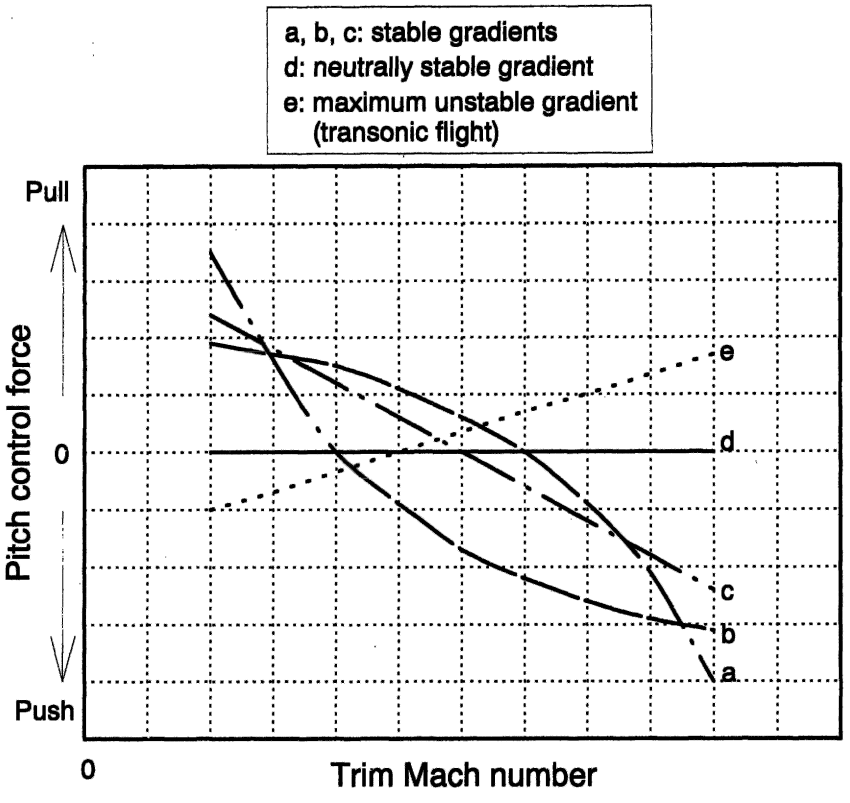

Fig. 10.6 Typical pitch control force gradients

shown in Fig. 10.6 where it is indicated that the control characteristics do not necessarily have to be linear but the changes in gradient must be smooth. Clearly, the minimum acceptable control characteristics correspond to neutral static stability.

In the transonic flight regime in particular, the static stability margins can change significantly such that the aeroplane may become unstable for some part of its speed envelope. The requirements recognize such conditions and permit mildly unstable pitch control force gradients in transonic flight provided that the flight condition is transitory. Maximum allowable unstable gradients are quantified and a typical boundary is indicated by plot e in Fig. 10.6. Aeroplanes which may be required to operate for prolonged periods in transonic flight conditions are not permitted to have unstable control force gradients.

10.6.2 LONGITUDINAL DYNAMIC STABILITY

10.6.2.1 Short period pitching oscillation

For the reasons explained in Section 10.2 the very important normal acceleration motion cue and the short period dynamics are totally interdependent. The controls fixed manoeuvre margin H_m and the short period frequency ω_s are also interdependent as explained in Section 8.5. Thus, the requirements for short period mode frequency reflect

these relationships and are relatively complex; a typical illustration is shown in Fig. 10.7.

Three similar charts are given, one for each flight phase category, and that for category A is shown in Fig. 10.7. The boundaries shown in Fig. 10.7 are equivalent to lines of constant *Control Anticipation Parameter* (CAP) which is proportional to the controls fixed manoeuvre margin. The boundaries therefore implicitly specify the constraint on manoeuvrability, quantified in terms of short period mode undamped natural frequency. The meaning of CAP is explained in Section 10.7. Now the derivative parameter n_α quantifies the normal load factor per unit angle of attack, or incidence, as defined by equation (10.11). As its value increases with speed, the lower values of n_α correlate with the lower speed characteristics of the aeroplane and vice versa. Now as speed increases so the aerodynamic pitch stiffness of the aeroplane also increases, which in turn results in an increase in short period mode frequency. This natural phenomenon is reflected in the requirements as the boundaries allow for increasing frequency with increasing n_α.

Acceptable limits on the stability of the short period mode are quantified in terms of maximum and minimum values of the damping ratio as a function of flight phase category and level of flying qualities as set out in Table 10.4.

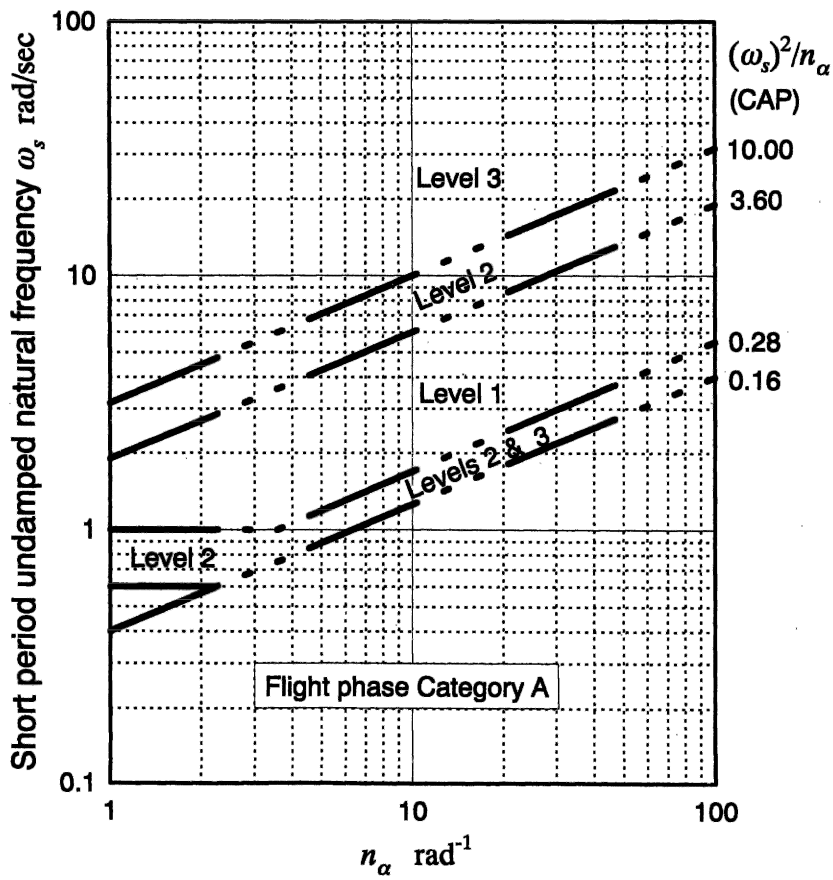

Fig. 10.7 Typical short period mode frequency requirements

Table 10.4 Short period mode damping

	Level 1		Level 2		Level 3
Flight phase	ζ_s min	ζ_s max	ζ_s min	ζ_s max	ζ_s min
CAT A	0.35	1.30	0.25	2.00	0.10
CAT B	0.30	2.00	0.20	2.00	0.10
CAT C	0.50	1.30	0.35	2.00	0.25

The maximum values of short period mode damping ratio obviously imply that a stable non-oscillatory mode is acceptable.

10.6.2.2 Phugoid

Upper and lower values for phugoid frequency are not quantified. However, it is recommended that the phugoid and short period mode frequencies are well separated. It is suggested that handling difficulties may become obtrusive if the frequency ratio of the modes $\omega_p/\omega_s > 0.1$. Generally, the phugoid dynamics is acceptable provided the mode is stable and damping ratio limits are quantified as shown in Table 10.5.

10.6.3 LONGITUDINAL MANOEUVRABILITY

The requirements for longitudinal manoeuvrability are largely concerned with manoeuvring control force, or *stick force per g*. It is important that the value of this control characteristic is not too large or too small. In other words, the controls free manoeuvre margin must be constrained to an acceptable and appropriate range. If the control force is too *light* there is a danger that the pilot may inadvertently apply too much normal acceleration to the aircraft with the consequent possibility of structural failure. On the other hand, if the control force is too *heavy* then the pilot may not be strong enough to utilize fully the manoeuvring flight envelope of the aircraft.

Thus, the requirements define the permitted upper and lower limits for controls free manoeuvre margin expressed in terms of the pitch control manoeuvring force gradient since this is the quantifiable parameter seen by the pilot. Further, the limits are functions of the type of control inceptor, a single stick or wheel type, and the limiting normal load factor appropriate to the airframe in question. The rather complex requirements are tabulated and their interpretation for an aircraft with a single stick controller, and having a limiting normal load factor of $n_L = 7.0$, is shown in Fig. 10.8. Again, the limits on stick force per g are expressed as a function of the flight condition parameter n_α.

Table 10.5 Phugoid damping ratio

Level of flying qualities	Minimum ζ_p
1	0.04
2	0
3	Unstable, period $T_p > 55$ s

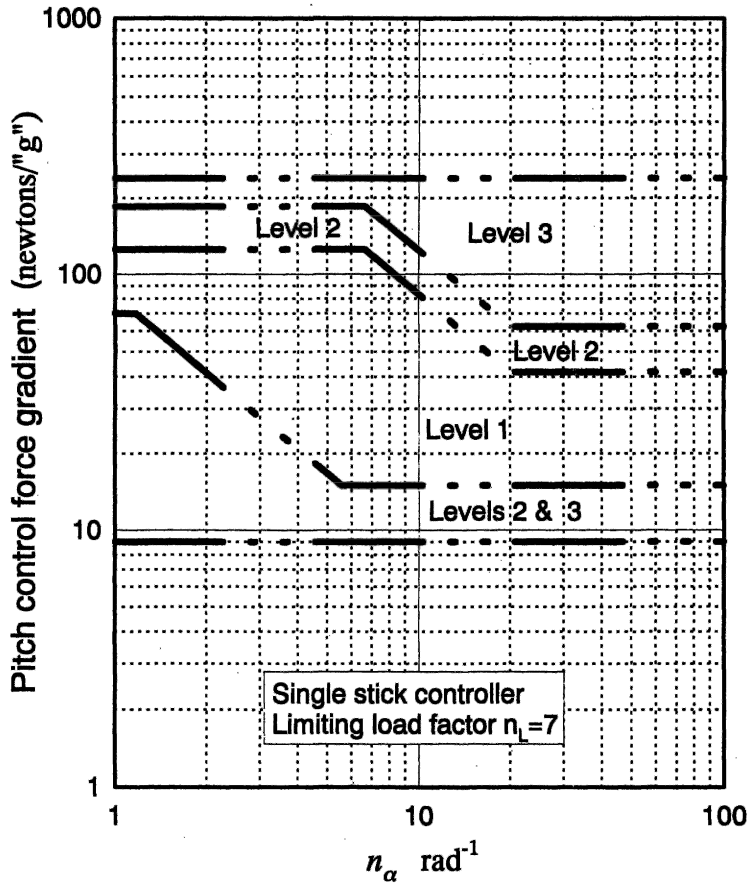

Fig. 10.8 Typical pitch control manoeuvring force gradients

10.7 Control anticipation parameter

It has been reported by Birhle (1966) that, 'in order to make precise adjustments to the flight path, the pilot must be able to anticipate the ultimate response of the airplane and that angular pitching acceleration is used for this purpose'. Now aeroplanes that have good second-order-like short term longitudinal response properties generally provide the pilot with good anticipatory handling cues. Clearly, this depends on the damping and frequency of the short period pitching mode in particular. However, Birhle (1966) reports pilot observation that, 'for airplanes having high inertia or low static stability the angular pitching acceleration accompanying small adjustments to flight path may fall below the threshold of perception'. In other words, the anticipatory nature of the response cues may become insignificant, thereby giving rise to poor handling qualities. To deal with such cases he defines a quantifiable measure of the anticipatory nature of the response which he called *Control Anticipation Parameter* (CAP). The formal definition of CAP is

> the amount of instantaneous angular pitching acceleration per unit of steady state normal acceleration.

Now the steady normal acceleration response to a pitch control input is determined by the aerodynamic properties of the aeroplane, the wing and tailplane in particular. However, the transient peak magnitude of angular pitching acceleration immediately following the control input is largely determined by the short period dynamics which, in turn, is dependent on the longitudinal static stability and moment of inertia in pitch. Thus, CAP effectively quantifies acceptable short period mode characteristics appropriate to the aerodynamic properties and operating condition of the aeroplane.

A simple expression for CAP is easily derived from the longitudinal short term transfer functions described in Section 10.2.2.

The angular pitch acceleration transfer function is obtained from equation (10.3)

$$\frac{\dot{q}(s)}{\eta(s)} = \frac{m_\eta s(s - z_w)}{(s^2 - (m_q + z_w)s + (m_q z_w - m_w U_e))} \tag{10.22}$$

The initial pitch acceleration may be derived by assuming a unit elevator step input and applying the initial value theorem, equation (5.34), to equation (10.22). Whence

$$\dot{q}(0) = \lim_{s\to\infty}\left(s\frac{m_\eta s(s - z_w)}{(s^2 - (m_q + z_w)s + (m_q z_w - m_w U_e))}\frac{1}{s}\right) = m_\eta \tag{10.23}$$

Similarly, the steady state normal acceleration may be derived by assuming a unit elevator input and applying the final value theorem, equation (5.33), to equation (10.5). Whence

$$a_z(\infty) = \lim_{s\to 0}\left(s\frac{m_\eta z_w U_e}{(s^2 - 2\zeta_s\omega_s s + \omega_s^2)}\frac{1}{s}\right) = \frac{m_\eta z_w U_e}{\omega_s^2} \tag{10.24}$$

The dimensionless normal acceleration, or load factor, is given by

$$n_z(\infty) = -\frac{a_z(\infty)}{g} = -\frac{m_\eta z_w U_e}{g\omega_s^2} \tag{10.25}$$

and CAP is given by

$$\text{CAP} = \frac{\dot{q}(0)}{n_z(\infty)} = -\frac{g\omega_s^2}{z_w U_e} = \frac{g\omega_s^2 T_{\theta_2}}{U_e} \tag{10.26}$$

since, approximately, $T_{\theta_2} = -1/z_w$. With reference to equation (10.12) an alternative and more commonly used expression for CAP follows

$$\text{CAP} = \frac{\omega_s^2}{n_\alpha} \tag{10.27}$$

and this is the boundary parameter shown in Fig. 10.7.

Now equation (8.45) states that

$$\omega_s^2 = \frac{\frac{1}{2}\rho V_0^2 S\bar{c}a}{I_y} H_m \tag{10.28}$$

With reference to Appendix 1 it may be shown that

$$z_w \cong \frac{\overset{\circ}{Z}_w}{m} = \frac{\frac{1}{2}\rho V_0 S Z_w}{m} \tag{10.29}$$

assuming, as is usually the case, that $\mathring{Z}_{\dot{w}} \ll m$. With reference to Appendix 6 it may be determined that

$$Z_w \cong -\frac{\partial C_L}{\partial \alpha} \equiv -a \tag{10.30}$$

the lift curve slope. Thus, substituting equations (10.28), (10.29) and (10.30) into equation (10.26) the expression for CAP reduces to the important result

$$\text{CAP} = \frac{mg\bar{\bar{c}}}{I_y} H_m = \frac{g\bar{\bar{c}}}{k^2} H_m \tag{10.31}$$

where here k denotes the *longitudinal radius of gyration*. Since aircraft axes are assumed to be wind axes throughout then $U_e \equiv V_0$. Thus, it is shown that CAP is directly proportional to the controls fixed manoeuvre margin H_m and that the constant of proportionality is dependent on aircraft geometry and mass distribution.

10.8 Lateral-directional flying qualities requirements

10.8.1 STEADY LATERAL-DIRECTIONAL CONTROL

Unlike the longitudinal flying qualities requirements, the lateral-directional requirements do not address static stability in quite the same way. In general, the lateral-directional static stability is independent of *cg* position and flight condition and, once set by the aerodynamic design of the aeroplane, does not change significantly. The main concerns centre on the provision of adequate control power for maintaining control in steady asymmetric flight conditions, or in otherwise potentially limiting conditions in symmetric flight. Further, it is essential that the control forces required to cope with such conditions do not exceed the physical capabilities of the average human pilot.

General normal lateral-directional control requirements specify limits for the roll stick and rudder pedal forces and require that the force gradients have the correct sense and do not exceed the prescribed limits. The control requirement for trim is addressed as is the requirement for roll–yaw control coupling which must be correctly harmonized. In particular, it is important that the pilot can fly properly coordinated turns with similar and acceptable degrees of control effort in both roll and yaw control.

The lateral-directional requirements relating to asymmetric, or otherwise potentially difficult, control conditions are concerned with steady sideslip, flight in crosswind conditions, steep dives and engine out conditions resulting in asymmetric thrust. For each condition the requirements specify the maximum permissible roll and yaw control forces necessary to maintain controlled flight up to relatively severe adverse conditions. Since the specified conditions interrelate and also have to take into account the aircraft class, flight phase and level of flying qualities, many tables of quantitative limits are needed to embrace all eventualities. Thus, the flying qualities requirements relating to steady lateral-directional flight are comprehensive and of necessity substantial.

10.8.2 LATERAL-DIRECTIONAL DYNAMIC STABILITY

10.8.2.1 Roll subsidence mode

Since the roll subsidence mode describes short term lateral dynamics it is critically important in the determination of lateral handling qualities. For this reason the

Table 10.6 Roll subsidence mode time constant

		Maximum value of T_r (s)		
Aircraft class	Flight phase category	Level 1	Level 2	Level 3
I, IV	A, C	1.0	1.4	–
II, III	A, C	1.4	3.0	–
I, II, III, IV	B	1.4	3.0	–

limiting acceptable values of its time constant are specified precisely as listed in Table 10.6.

It seems that no common agreement exists as to a suitable maximum value of the time constant for level 3 flying qualities. It is suggested in DEF-STAN 00-970 that a suitable value would appear to be in the range $6 < T_r < 8$ s whereas MIL-F-8785C quotes a value of 10 s.

10.8.2.2 Spiral mode

A stable spiral mode is acceptable irrespective of its time constant. However, since its time constant is dependent on lateral static stability (dihedral effect) the maximum level of stability is determined by the maximum acceptable roll control force. Because the mode gives rise to very slow dynamic behaviour it is not too critical to handling unless it is very unstable. For this reason minimum acceptable degrees of instability are quantified in terms of time to double bank angle T_2 in an uncontrolled departure from straight and level flight. The limiting values are shown in Table 10.7.

For analytical work it is sometimes more convenient to express the spiral mode requirement in terms of time constant T_s rather than time to double bank angle. If it is assumed that the unstable mode characteristic gives rise to a purely exponential divergence in roll then it is easily shown that the time constant and the time to double bank angle are related by the following expression

$$T_s = \frac{T_2}{\log_e 2} \tag{10.32}$$

Thus, alternatively the requirement may be quantified as listed in Table 10.8.

10.8.2.3 Dutch roll mode

Since the dutch roll mode is a short period mode it has an important influence on lateral-directional handling and, as a consequence, its damping and frequency requirements are specified in some detail. It is approximately the lateral-directional

Table 10.7 Spiral mode time to double bank angle

	Minimum value of T_2 (s)		
Flight phase category	Level 1	Level 2	Level 3
A, C	12	8	5
B	20	8	5

Table 10.8 Spiral mode time constant

	Minimum value of T_s (s)		
Flight phase category	Level 1	Level 2	Level 3
A, C	17.3	11.5	7.2
B	28.9	11.5	7.2

equivalent of the longitudinal short period mode and has frequency of the same order since pitch and yaw inertias are usually similar in magnitude. However, yaw damping is frequently low as a result of the design conflict with the need to constrain spiral mode instability with dihedral. Although the longitudinal short period mode and the dutch roll mode are similar in bandwidth, the latter is not as critical to handling. In fact, a poorly damped dutch roll is seen more as a handling irritation rather than a serious problem.

The acceptable minima for damping ratio, undamped natural frequency and damping ratio–frequency product are specified for various combinations of aircraft class and flight phase category, as shown in Table 10.9.

10.8.3 LATERAL-DIRECTIONAL MANOEUVRABILITY AND RESPONSE

The lateral-directional manoeuvrability requirements are largely concerned with limiting roll oscillations, sideslip excursions and roll and yaw control forces to acceptable levels during rolling and turning manoeuvres.

Oscillation in roll response to controls will occur whenever the dutch roll is intrusive and poorly damped. Thus, limiting the magnitude and characteristics of oscillation in roll is effectively imposing additional constraints on the dutch roll mode when it is intrusive. Oscillation is also possible in cases when the roll and spiral modes couple to form a second pair of complex roots in the lateral-directional characteristic equation. However, the influence of this characteristic on handling is not well understood and it is recommended that the condition should be avoided.

Sideslip excursions during lateral-directional manoeuvring are normal and expected, especially in entry and exit to turning manoeuvres. It is required that the rudder control displacement and force increase approximately linearly with increase in sideslip response

Table 10.9 Dutch roll frequency and damping

		Minimum values							
		Level 1			Level 2			Level 3	
Aircraft class	Flight phase	ζ_d	$\zeta_d\omega_d$	ω_d	ζ_d	$\zeta_d\omega_d$	ω_d	ζ_d	ω_d
I, IV	CAT A	0.19	0.35	1.0	0.02	0.05	0.5	0	0.4
II, III	CAT A	0.19	0.35	0.5	0.02	0.05	0.5	0	0.4
All	CAT B	0.08	0.15	0.5	0.02	0.05	0.5	0	0.4
I, IV	CAT C	0.08	0.15	1.0	0.02	0.05	0.5	0	0.4
II, III	CAT C	0.08	0.10	0.5	0.02	0.05	0.5	0	0.4

for sideslip of modest magnitude. It is also required that the effect of dihedral shall not be too great otherwise excessive roll control displacement and force may be needed to manoeuvre. Remember that too much stability can be as hazardous as too little stability! It would seem that the main emphasis is on the provision of acceptable levels of roll and yaw control displacement with particular concern for entry and exit to turning manoeuvres, which, after all, is lateral-directional manoeuvring flight.

10.9 Flying qualities requirements on the *s*-plane

In Chapter 9, the way in which the roots of the characteristic equation may be mapped on to the *s*-plane was illustrated in order to facilitate the interpretation of aircraft stability graphically. By superimposing boundaries defined by the appropriate flying qualities requirements on to the same *s*-plane plots the stability characteristics of an aeroplane may be assessed directly with respect to those requirements. This graphical approach to the assessment of aircraft flying qualities is particularly useful for analysis and design and is used extensively in flight control system design.

10.9.1 LONGITUDINAL MODES

Typical boundaries describing the limits on longitudinal mode frequency and damping on the *s*-plane are shown in Fig. 10.9. It is not usually necessary to show more than the upper

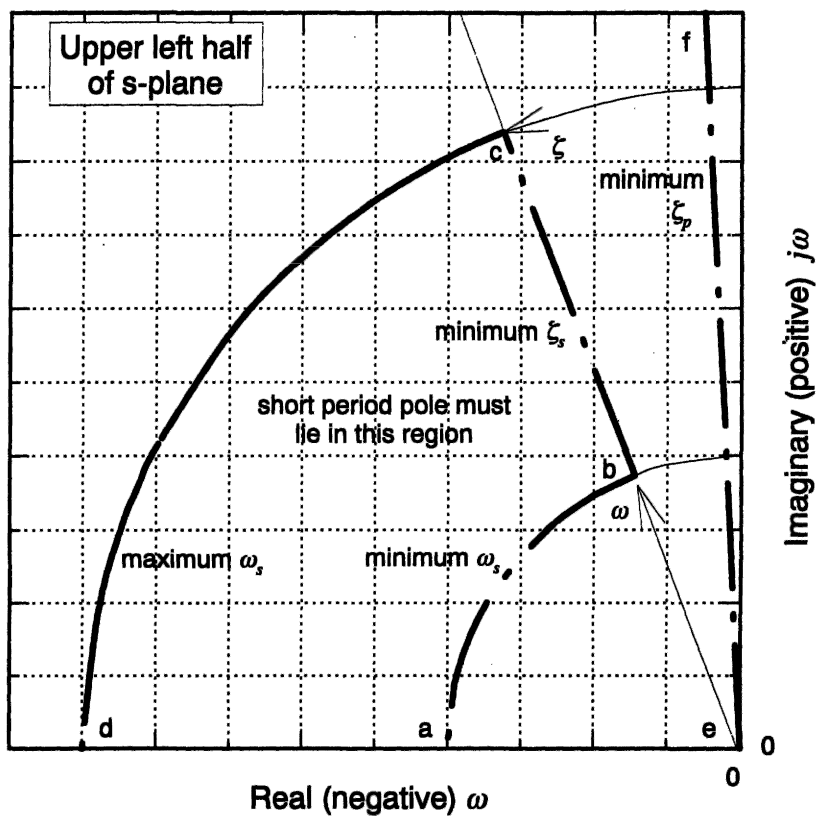

Fig. 10.9 Longitudinal flying qualities requirements on the *s*-plane

left half of the *s*-plane since stable characteristics only are of primary interest and the lower half of the *s*-plane is simply the mirror image of the upper half of the *s*-plane reflected in the real axis.

The upper and lower short period mode frequency boundaries are described by arcs cd and ab respectively. The frequency limits are determined from charts like Fig. 10.7 and depend on the operating flight condition, which is determined by n_α. Alternatively, the boundaries may be determined from a consideration of the limiting CAP values, also given on charts like Fig. 10.7, at the flight condition of interest. Note that when the *s*-plane is drawn to the same scale on both the *x* and *y* axes, the frequency boundaries become circular arcs about the origin. When the scales are not the same the arcs become ellipses, which can be more difficult to interpret.

The minimum short period mode damping ratio is obtained from Table 10.4 and maps on to the line bc radiating from the origin. The maximum permitted damping ratio is greater than one, which obviously means that the corresponding roots lie on the real axis. Thus, when the short period mode roots, or poles, are mapped on to the *s*-plane they must lie within the region bounded by abcd and its mirror image in the real axis. If the damping ratio is greater than one then the pair of roots must lie on the real axis in locations bounded by the permitted maximum value of damping ratio.

The minimum phugoid damping ratio is given in Table 10.5 and, for level 1 flying qualities, maps on to the *s*-plane as the boundary ef. Thus, when the phugoid roots, or poles, are mapped on to the *s*-plane they must lie to the left of the line ef in order to meet level 1 flying qualities requirements. The level 3 requirement on phugoid damping obviously allows for the case when the poles become real, one of which may be unstable, thereby giving rise to divergent motion. In this case the limit implicitly defines a minimum acceptable value for the corresponding time constant. This is mapped on to the *s*-plane in exactly the same way as the lateral-directional spiral mode boundary as described below.

10.9.2 LATERAL-DIRECTIONAL MODES

Typical boundaries describing the limits on lateral-directional mode frequency and damping on the *s*-plane are shown in Fig. 10.10. Again, the upper left half of the *s*-plane is shown but with a small extension into the upper right half of the *s*-plane to include the region appropriate to the unstable spiral mode. As for the longitudinal case, interpretation implicitly includes the lower half of the *s*-plane, which is the mirror image of the upper half of the *s*-plane in the real axis.

The maximum permitted value of the roll subsidence mode time constant is given in Table 10.6 and this maps into the boundary e since the corresponding real root is given by the inverse of the time constant T_r. Further, since the mode must always be stable it will always lie on the negative real axis. The precise location of the boundary e is determined by the aircraft class, the flight phase category and the required level of flying qualities. However, at the appropriate operating flight condition the pole describing the roll subsidence mode must lie on the real axis to the left of the boundary e.

The location of the spiral mode boundary f is established in the same way. Since the required limits only apply to the mode when it is unstable then the corresponding boundary lies on the right half of the *s*-plane. The precise location of the boundary may be determined from the minimum acceptable value of the time constant T_s, given in Table 10.8, and, again, this depends on aircraft class and the required level of flying

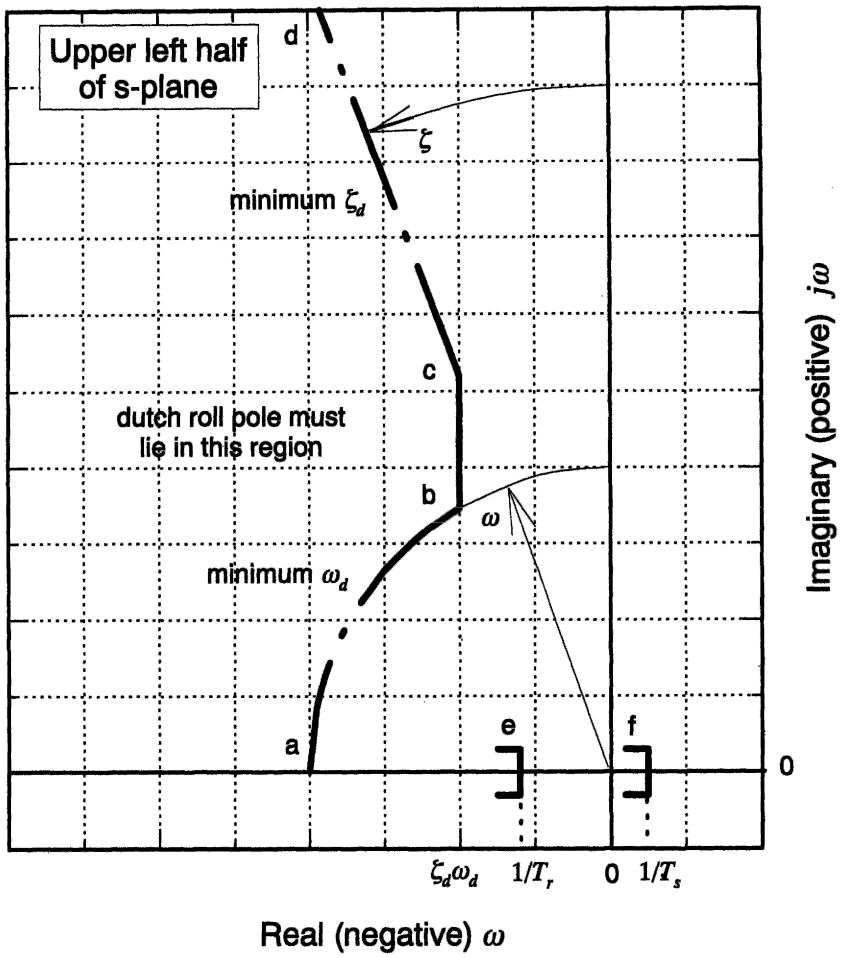

Fig. 10.10 Lateral-directional flying qualities requirements on the *s*-plane

qualities. Thus, the spiral mode pole must always lie on the real axis to the left of the boundary f.

The limiting frequency and damping requirements for the dutch roll mode are given in Table 10.9 and are interpreted in much the same way as the requirements for the longitudinal short period mode. The minimum permitted frequency boundary is described by the arc ab and the minimum permitted damping ratio boundary by the line cd. The minimum permitted value of $\zeta_d\omega_d$ maps into the line bc to complete the dutch roll mode boundary and, as before, the boundary has its mirror image in the lower half of the *s*-plane. Thus, the dutch roll mode roots, or poles, must always lie to the left of the boundary abcd at the flight condition of interest. Clearly, the precise location of the boundary is determined by the appropriate combination of aircraft class, flight phase category and required level of flying qualities.

EXAMPLE 10.4

To illustrate the application of the flying qualities requirements consider the McDonnell F-4 Phantom, the following data for which were obtained from Heffley and Jewell

(1972). Since the available data are limited to the equations of motion and some supporting material the flying qualities assessment is limited to consideration of basic stability and control characteristics only.

For the case selected the general flight condition parameters given are

Altitude	h	35 000 ft
Mach number	M	1.2
Weight	mg	38 925 lb
Trim airspeed	V_0	1167 ft/s
Trim body incidence	α_e	1.6°
Flight path angle	γ_e	0
Normal load factor derivative	n_α	22.4 g/rad
Control anticipation parameter	CAP	1.31 1/s^2
'Elevator' angle per g	η/g	3.64 deg/g

Clearly the Phantom is a high performance combat aircraft; thus, for the purposes of flying qualities assessment, it is described as a *Class IV* aircraft. The flight task to which the data relate is not stated. Therefore, it may be assumed that either the aircraft is in steady cruising flight, flight phase category B, or it is manoeuvring about the given condition in which case flight phase category A applies. For this illustration *flight phase category A* is assumed since it determines the most demanding flying qualities requirements. It is interesting to note that the parameter *'elevator' angle per g* is given which is, of course, a measure of the controls fixed manoeuvre margin.

Considering the longitudinal stability and control characteristics first, sufficient information about the stability characteristics of the basic airframe is given by the pitch attitude response to 'elevator' transfer function, which for the chosen flight condition is

$$\frac{\theta(s)}{\eta(s)} \equiv \frac{N_\eta^\theta(s)}{\Delta(s)} = \frac{-20.6(s+0.0131)(s+0.618)}{(s^2+0.0171s+0.00203)(s^2+1.759s+29.49)} \tag{10.33}$$

The essential longitudinal stability and control parameters may be obtained on inspection of transfer function (10.33) as follows

Phugoid damping ratio	$\zeta_p = 0.19$
Phugoid undamped natural frequency	$\omega_p = 0.045$ rad/s
Short period damping ratio	$\zeta_s = 0.162$
Short period undamped natural frequency	$\omega_s = 5.43$ rad/s
Numerator time constant	$T_{\theta_1} = 1/0.0131 = 76.34$ s
Numerator time constant (incidence lag)	$T_{\theta_2} = 1/0.618 = 1.62$ s

Since the Phantom is an American aeroplane it would seem appropriate to assess its basic stability characteristics against the requirements of MIL-F-8785C. However, in practice, it would be assessed against the requirements document specified by the procuring agency.

With reference to Table 10.5, which is directly applicable, the phugoid damping ratio is greater than 0.04 and since $\omega_p/\omega_s < 0.1$ the phugoid achieves level 1 flying qualities and is unlikely to give rise to handling difficulties at this flight condition.

With reference to the short period mode frequency chart for flight phase category A, which is the same as Fig. 10.7, at $n_\alpha = 22.4g$/rad and for level 1 flying qualities it is required that

$$2.6 \text{ rad/s} \leqslant \omega_s \leqslant 9.0 \text{ rad/s}$$

or, equivalently,

$$0.281/\text{s}^2 \leqslant \omega_s^2/n_\alpha \text{ (CAP)} \leqslant 3.61/\text{s}^2$$

Clearly, the short period undamped natural frequency achieves level 1 flying qualities.

Unfortunately, the short period mode damping ratio is less than desirable. A table similar to Table 10.4 indicates that the damping only achieves level 3 flying qualities and to achieve level 1 it would need to be in the range $0.35 \leqslant \zeta_s \leqslant 1.3$.

Considering now the lateral-directional stability and control characteristics, sufficient information about the stability characteristics of the basic airframe is given, for example, by the roll rate response to aileron transfer function, which for the chosen flight condition is

$$\frac{p(s)}{\xi(s)} \equiv \frac{N_\xi^p(s)}{\Delta(s)} = \frac{-10.9s(s^2 + 0.572s + 13.177)}{(s + 0.00187)(s + 1.4)(s^2 + 0.519s + 12.745)} \tag{10.34}$$

The essential lateral-directional stability and control parameters may be obtained on inspection of transfer function (10.34) as follows

Roll mode time constant	$T_r = 1/1.4 = 0.714\,\text{s}$
Spiral mode time constant	$T_s = 1/0.00187 = 535\,\text{s}$
Dutch roll damping ratio	$\zeta_d = 0.0727$
Dutch roll undamped natural frequency	$\omega_d = 3.57\,\text{rad/s}$
Dutch roll damping ratio–frequency product	$\zeta_d\omega_d = 0.26\,\text{rad/s}$

Clearly, at this flight condition the spiral mode is stable with a very long time constant. In fact it is approaching neutral stability for all practical considerations. Since the mode is stable it achieves level 1 flying qualities and is most unlikely to give rise to handling difficulties.

A table similar to Table 10.6 indicates that the roll subsidence mode damping ratio achieves level 1 flying qualities since $T_r < 1.0\,\text{s}$.

The dutch roll mode characteristics are less than desirable since their damping is very low. A table similar to Table 10.9 indicates that the damping ratio only achieves level 2 flying qualities. In order to achieve the desirable level 1 flying qualities the mode characteristics would need to meet

Dutch roll damping ratio	$\zeta_d \geqslant 0.19$
Dutch roll undamped natural frequency	$\omega_d \geqslant 1.0\,\text{rad/s}$
Dutch roll damping ratio–frequency product	$\zeta_d\omega_d \geqslant 0.35\,\text{rad/s}$

It is therefore concluded that both the longitudinal short period mode and the lateral-directional dutch roll mode damping ratios are too low at the flight condition evaluated. In all other respects the aeroplane achieves level 1 flying qualities. The deficient aerodynamic damping of the Phantom, in common with many other aeroplanes, is augmented artificially by the introduction of a feedback control system.

It must be emphasized that this illustration is limited to an assessment of the basic stability properties of the airframe only. This determines the need, or otherwise, for stability augmentation. Once the stability has been satisfactorily augmented by an appropriate control system then further and more far reaching assessments of the control and handling characteristics of the augmented aeroplane would be made. The

scope of this kind of evaluation may be appreciated by reference to the specification documents discussed above. In any event, analytical assessment would need the addition of a simulation model developed from the linearized equations of motion in order to investigate properly some of the dynamic control and response properties.

References

Anon: *British Civil Airworthiness Requirements—Section K—Light Aeroplanes.* Civil Aviation Authority.

Anon: *Federal Aviation Regulations—Part 25, Subpart B—Flight.* Federal Aviation Administration, United States Department of Transportation.

Anon. 1965: Morane Saulnier M.S.760—*Notes for Technical Observers.* The College of Aeronautics, Cranfield.

Anon. 1980: *Military Specification—Flying Qualities of Piloted Airplanes.* MIL-F-8785C. Department of Defense, USA.

Anon. 1983: *Design and Airworthiness Requirements for Service Aircraft.* Defence Standard 00-970/Issue 1, Volume 1, Book 2, Part 6—*Aerodynamics, Flying Qualities and Performance.* Ministry of Defence, UK.

Anon. 1987: *Military Standard—Flying Qualities of Piloted Airplanes.* MIL-STD-1797A (USAF). Department of Defense, USA.

Anon. 1994: *Joint Aviation Requirements-JAR 25-Large Aeroplanes, Section 1—Requirements, Subpart B—Flight.* Joint Aviation Authority.

Bihrle, W. 1966: *A Handling Qualities Theory for Precise Flight Path Control.* Air Force Flight Dynamics Laboratory, Technical Report AFFDL-TR-65-198.

Chalk, C. R. 1958: *Additional Flight Evaluations of Various Longitudinal Handling Qualities in a Variable-Stability Jet Fighter.* Wright Air Development Center Technical Report, WADC TR 57-719.

Cooper, G. E. and Harper, R. P. 1969: *The Use of Pilot Rating in the Evaluation of Aircraft Handling Qualities.* AGARD Report 567.

Gibson, J. C. 1995: *The Definition, Understanding and Design of Aircraft Handling Qualities.* Delft University of Technology, Faculty of Aerospace Engineering, Report LR-756.

Heffley, R. K. and Jewell, W. F. 1972: *Aircraft Handling Qualities Data.* NASA Contractor Report, NASA CR-2144.

Hoh, R. H., Mitchell, D. G., Ashkenas, I. L., Klein, R. H., Heffley, R. K. and Hodgkinson, J. 1982: *Proposed MIL Standard and Handbook—Flying Qualities of Air Vehicles, Volume II: Proposed MIL Handbook.* Air Force Wright Aeronautical Laboratory, Technical Report AFWAL-TR-82-3081, Vol. II.

Teper, G. L. 1969: *Aircraft Stability and Control Data.* Systems Technology, Inc, STI Technical Report 176-1.

11

Stability Augmentation

11.1 Introduction

In the previous chapter it is shown how the stability and control characteristics of an aeroplane may be assessed in the context of flying and handling qualities requirements. In the event that the aeroplane fails to meet the requirements in some way, then it is necessary to consider remedial action. For all except perhaps the most trivial of problems it is not usually practical to modify the aerodynamic design of the aeroplane once its design has been finalized. Quite often the deficiencies occur simply as a result of the requirement for the aeroplane to operate over an extended flight envelope and not necessarily as a result of an aerodynamic design oversight. Alternatively, this might be explained as the effects of aerodynamic non-linearity.

The preferred solution is, therefore, to modify artificially, or *augment*, the apparent stability characteristics of the airframe. This is most conveniently achieved by the introduction of *negative feedback* in which the output signals from motion sensors are processed in some way and used to drive the appropriate control surfaces via actuators. The resultant *closed loop control system* is similar in many respects to the classical servo-mechanism familiar to the control engineer.

A significant advantage of this approach is that the analysis of the augmented, or closed loop, aircraft makes full use of the well-established tools of the control engineer. The *systems* approach to flight dynamics analysis has already been introduced in earlier chapters where, for example, control engineering tools have been utilized for solving the equations of motion.

A functional block diagram of a typical *flight control system* (FCS) is shown in Fig. 11.1. It is assumed that the primary flying controls are mechanical such that pilot commands drive the control surfaces via control actuators, which augment the available power to levels sufficient to overcome the aerodynamic loads on the surfaces. The *electronic flight control system* (EFCS) comprises two feedback loops, both of which derive their control signals from motion sensors appropriate to the requirements of the *control laws*. The outputs from the inner and outer loop controllers are electronically summed and the resultant signal controls the aircraft via a small servo actuator. Typically, the servo actuator is an electro-hydraulic device which converts low power electrical signals to mechanical signals at a power level compatible with those originating at the pilot to which they are mechanically summed.

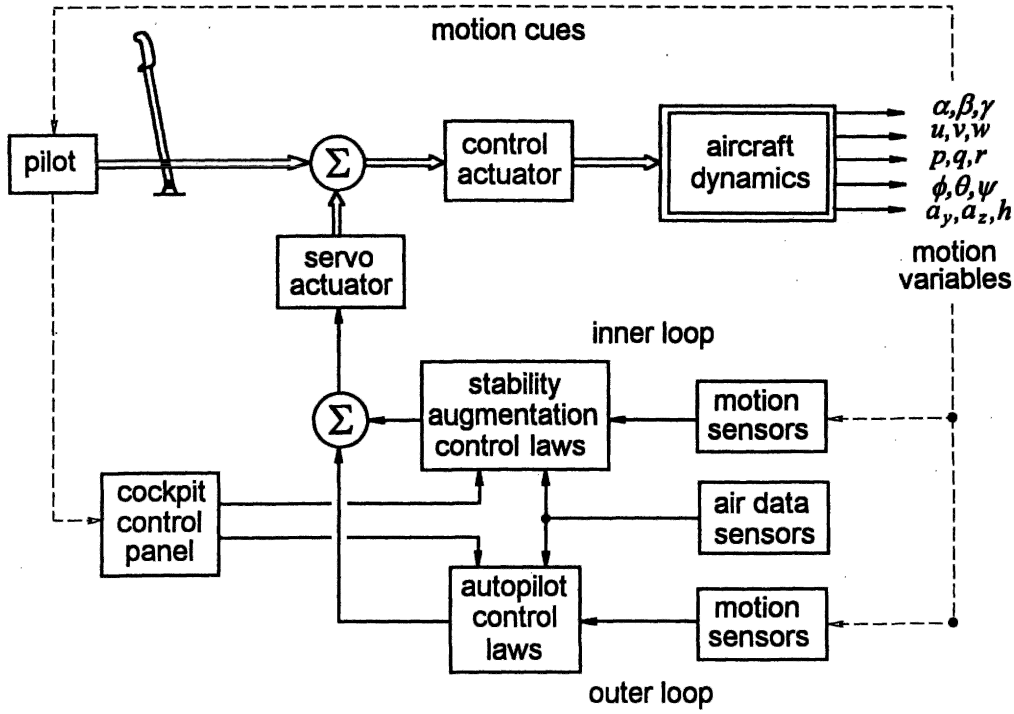

Fig. 11.1 A typical flight control system

Although only a single control axis is indicated in Fig. 11.1, it is important to appreciate that the FCS will, in general, include closed loop controllers operating on the roll, pitch and yaw control axes of the aircraft simultaneously and may even extend to include closed loop engine control as well. Thus, multi-variable feedback involving many separate control loops is implied, which is typical of many modern FCSs.

The *inner loop* provides stability augmentation and is usually regarded as essential for continued proper operation of the aircraft. The inner loop control system alone comprises the *stability augmentation system* (SAS), it is usually the first part of the FCS to be designed and, together with the airframe, comprises the *augmented aircraft*.

The *outer loop* provides the *autopilot* which, as its name suggests, enables the pilot to fly various manoeuvres under automatic control. Although necessary for operational reasons, an autopilot is not essential for the provision of a safe well-behaved aircraft. The *autopilot control modes* are designed to function with the augmented aircraft and may be selectively engaged as required to automate the piloting task. Their use is intended to release the pilot from the monotony of flying steady conditions manually and to fly precision manoeuvres in adverse conditions which may be at, or beyond, the limits of human capability. Autopilot control modes vary from the very simple, for example *height hold*, to the very complex, for example *automatic landing*.

Since, typically, for most aircraft the *control law gains* required to effect good stability, control and handling vary with operating condition, it is necessary to make provision for their continuous adjustment. The variations often arise as a result of variations in the aerodynamic properties of the airframe over the flight envelope. For example, at low speed the aerodynamic effectiveness of the control surfaces is generally less than at high

speed. This means that higher *control gains* are required at low speeds and vice versa. It is, therefore, common practice to vary, or *schedule*, gains as a function of flight condition.

Commonly used flight condition variables are dynamic pressure, Mach number, altitude and so on, information which is grouped under the description of *air data*. Generally, air data information would be available to all control laws in an FCS as indicated in Fig. 11.1.

A control panel is provided in the cockpit to enable the pilot to control and monitor the operation of the FCS. SAS controls are usually minimal and enable the pilot to monitor the system for correct, and hence safe, operation. In some cases he may also be provided with means for selectively isolating parts of the SAS. On the other hand, the autopilot control panel is rather more substantial. Controls are provided to enable the pilot to set up, engage and disengage the various autopilot mode functions. The control panel also enables him to monitor progress during the automated manoeuvre selected.

In piloted phases of flight the autopilot would normally be disengaged and, as indicated in Fig. 11.1, the pilot would derive his perception of flying and handling qualities from the motion cues provided by the augmented aircraft. Thus, the inner loop control system provides the means by which all aspects of stability, control and handling may be tailored in order to improve the characteristics of the basic aircraft.

11.1.1 THE CONTROL LAW

The control law is a mathematical expression which describes the function implemented by an augmentation or autopilot controller. For example, a very simple and very commonly used control law describing an inner loop control system for augmenting yaw damping is

$$\zeta(s) = K_\zeta \delta_\zeta(s) - K_r\left(\frac{s}{1+sT}\right)r(s) \tag{11.1}$$

Equation (11.1) simply states that the control signal applied to the rudder $\zeta(s)$ comprises the sum of the pilot command $\delta_\zeta(s)$ and yaw rate feedback $r(s)$. The gain K_ζ is the mechanical gearing between rudder pedals and rudder and the gain K_r is the all-important feedback gain chosen by design to optimize the damping in yaw. The second term in equation (11.1) is negative since negative feedback is required to increase stability in yaw. The second term also, typically, includes a *washout*, or *high pass*, filter with a time constant of around one or two seconds. The filter is included to block yaw rate feedback in steady turning flight in order to prevent the feedback loop opposing the pilot command once the rudder pedals are returned to centre after manoeuvre initiation. However, the filter is effectively *transparent* during transient motion, thereby enabling the full effect of the feedback loop quickly to damp out the yaw oscillation.

11.1.2 SAFETY

In any aeroplane fitted with a flight control system safety is the most critical issue. Since the FCS has direct 'access' to the control surfaces, considerable care must be exercised in the design of the system to ensure that under no circumstances can a maximum instantaneous uncontrolled command be applied to any control surface. For example, a sensor failure might cause its output to *saturate* at its maximum possible value. This

signal, in turn, is *conditioned* by the control law to apply what could well be a demand of magnitude sufficient to cause a maximum control surface displacement. The resulting *failure transient* might well be some kind of hazardous divergent response. Clearly, steps must be taken in the design of the flight control system architecture to incorporate mechanisms to protect the aircraft from partial or total system malfunction.

The design of *safety critical* flight control system architectures, as opposed to the simpler problem of control law design, is a substantial subject in its own right. However, at an introductory level, it is sufficient to appreciate that the requirements for safety can sometimes override the requirements for control, especially when relatively large control system gains are necessary. For simple stability augmentation systems, of the kind exemplified by the control law, equation (11.1), the problem may be overcome by limiting the maximum values of the control signals, giving rise to what is referred to as a *limited authority* control system. In more complex FCSs, where authority limiting is not acceptable for control reasons, it may be necessary to employ control system *redundancy*. Redundant FCSs comprise two, or more, systems which are functionally similar and which normally operate in parallel. In the event of a system malfunction, the faulty equipment is isolated leaving the remaining *healthy* system components to continue the augmentation task. In such systems, automatic fault containment can reduce the failure transient to an imperceptible level. It is then necessary to provide the pilot with information enabling him to *monitor* continuously the state of health of the FCS on an appropriate cockpit display.

11.1.3 STABILITY AUGMENTATION SYSTEM ARCHITECTURE

The architecture of an inner loop stability augmentation system (SAS) is shown in Fig. 11.2. This classical system description assumes an aeroplane with mechanical flying

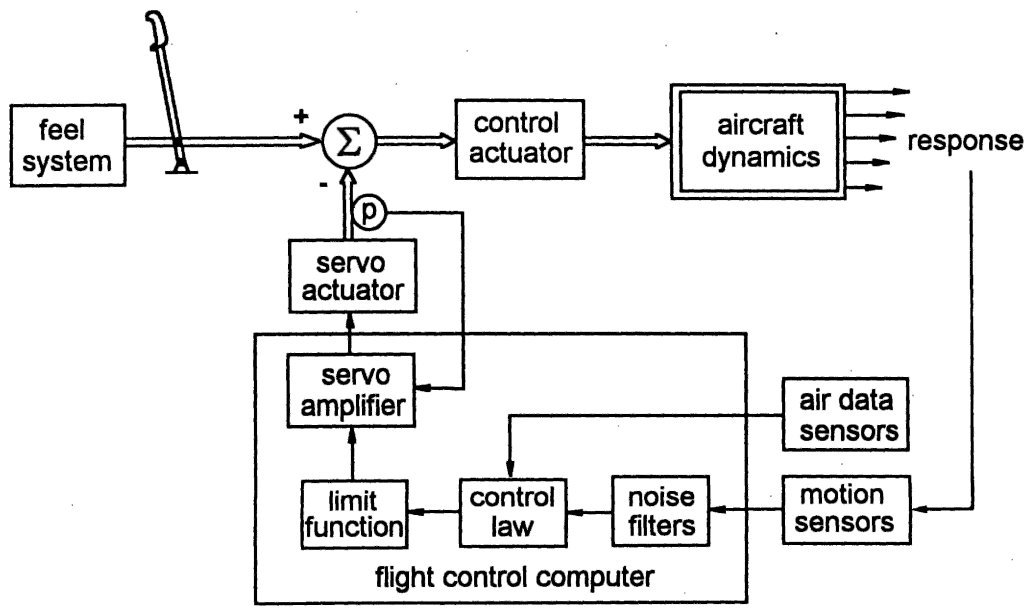

Fig. 11.2 A typical stability augmentation system

controls to which the EFCS connects via the servo actuator. The system is typical of those applied to many aeroplanes of the 1950s and 1960s. For the purpose of discussion one control axis only is shown in Fig. 11.2 but it applies equally well to the remaining axes.

As above, the essential element of the SAS is the control law; the remaining components of the system are the necessary by-products of its implementation. Noise filtering is often required to remove unwanted information from sensor outputs. At best noise can cause unnecessary actuator activity and, at worst, may even give rise to unwanted aircraft motion. Sometimes, when the sensor is located in a region of significant structural flexibility the 'noise' may be due to normal structure distortion; the control demand may then exacerbate the structure bending to result in structural divergence. Thus, an unwanted unstable structural feedback loop can be inadvertently created. The cure usually involves narrow band filtering to remove information from the sensor output signal at sensitive structural bending mode frequencies.

The fundamental role of the SAS is to minimize response transients following an upset from equilibrium. Therefore, when the system is working correctly in non-manoeuvring flight the response variables will have values at, or near, zero since the action of the negative feedback loop is to drive the *error* to zero. Thus, an SAS does not normally require large authority control and the limit function would typically limit the amplitude of the control demand to, say, $\pm 10\%$ of the total surface deflection. The limiter may also incorporate a rate limit function to contain transient response by imposing a maximum actuator slew rate demand. It is important to realize that whenever the control demand exceeds the limit the system saturates, becomes temporarily open loop, and the dynamics of the aircraft reverts to that of the unaugmented airframe. This is not usually considered to be a problem as saturation is most likely to occur during manoeuvring flight when the pilot has very 'tight' manual control of the aeroplane and effectively replaces the SAS control function.

The servo amplifier, together with the servo actuator, provide the interface between the flight control system and the mechanical flying controls. These two elements comprise a classical position servo mechanism as indicated by the electrical feedback from a position sensor on the servo actuator output. Mechanical amplitude limiting may well be applied to the servo actuator as well as, or instead of, the electronic limits programmed into the flight control computer.

Since the main power control actuator, also a classical mechanical servo mechanism, breaks the direct mechanical link between the pilot's controller and the control surface, the control feel may bear little resemblance to the aerodynamic surface loads. The feedback loop around the control actuator would normally be mechanical since it may well need to function with the SAS inoperative. It is therefore necessary to augment the controller feel characteristics as well. The feel system may be a simple non-linear spring but is more commonly an electro-hydraulic device, often referred to as a *Q-feel system* since its characteristics are scheduled with dynamic pressure Q. Careful design of the feel system enables the apparent controls free manoeuvre margin of the aircraft to be adjusted independently of the other interrelated stability parameters.

When the mechanical flying controls are dispensed with altogether and replaced by an electrical or electronic link the resultant stability augmentation system is described as a fly-by-wire (FBW) system. When the FCS shown in Fig. 11.2 is implemented as an FBW system its functional structure is changed to that shown in Fig. 11.3. The SAS inner control loop remains unchanged; the only changes relate to the primary control path and the actuation systems.

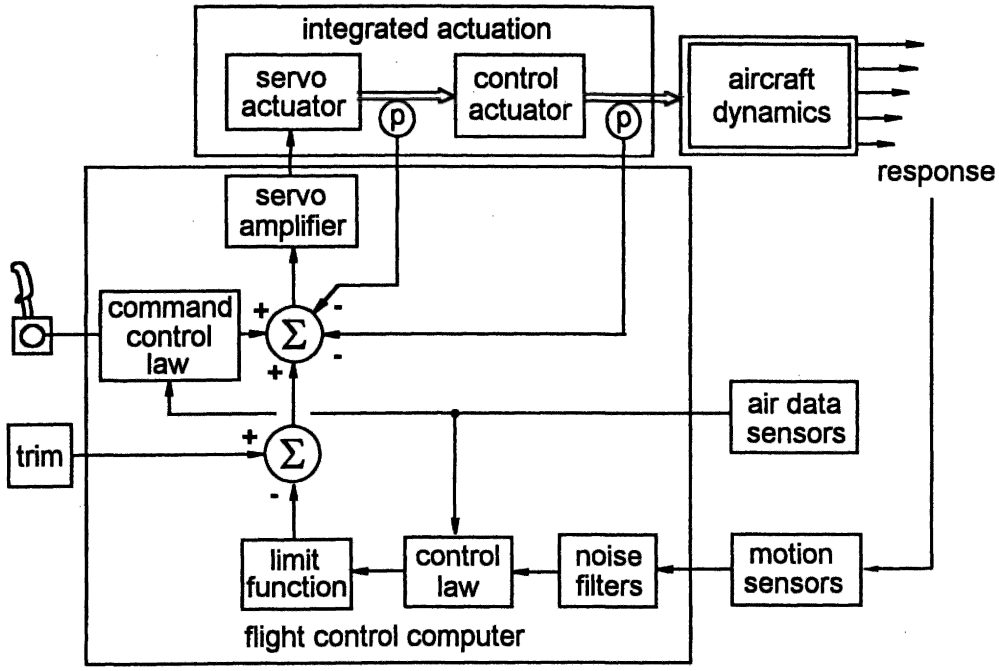

Fig. 11.3 A typical fly-by-wire command and stability augmentation system

Since the only mechanical elements in the FCS are the links between the control actuator and the surfaces it is usual for the servo actuator and the control actuator to be combined into one unit. Its input is then the electrical control demand from the flight control computer and its output is the control surface deflection. An advantage of an integrated actuation system is the facility for mechanical simplification since the feedback loops may be closed electrically rather than by a combination of electrical and mechanical feedbacks. Mechanical feedback is an unnecessary complication since in the event of a flight control computer failure the aeroplane would be uncontrollable. Clearly, this puts a rather more demanding emphasis on the safety of the flight control system.

Primary control originates at the pilot's control inceptors which, since they are not constrained by mechanical control linkages, may now take alternative forms, for example a *side-stick controller*. The control command signal is conditioned by a command control law which determines the control and response characteristics of the augmented aircraft. Since the command control law is effectively *shaping* the command signal in order to achieve acceptable response characteristics, its design is a means for augmenting handling qualities independently of stability augmentation. For this reason, an FCS with the addition of command path augmentation is known as a command and stability augmentation system (CSAS).

Provision is shown in Fig. 11.3 for an electrical trim function since not all aircraft with advanced-technology FCSs employ mechanical trimmers. The role of the trim function is to set the datum control signal value, and hence the control surface angle, to that required to maintain the chosen equilibrium flight condition. The precise trim function utilized would be application dependent and in some cases an entirely automatic trim system might be implemented. In this latter case no pilot trimming facility is required.

Since the pilot must have full authority control over the aircraft at all times it is implied that the actuation system must also have full authority control. The implications for safety following a failure in any component in the primary control path are obviously critical. As for the simple SAS the feedback control signal may be authority limited prior to summing with the primary control commands and this will protect the system against failures within the stability augmentation function. However, this solution cannot be used in the primary control path. Consequently, FBW systems must have reliability of a very high order and this usually means significant levels of redundancy in the control system architecture together with sophisticated mechanisms for identifying and containing the worst effects of system malfunction.

In the above brief description of an FBW system it is assumed that all control signals are electrical and transmitted by normal electrical cables. However, since most modern flight control computers are digital the transmission of control signals also involves digital technology. Digital signals can also be transmitted optically with some advantage, especially in the demanding environment within aircraft.

Today it is common for optical signal transmission to be used in flight control systems if for no other reason than to maintain electrical isolation between redundant components within the system. There is no reason why optical signalling should not be used for primary flight control and there are a small number of systems currently flying which are optically signalled. Such a control system is referred to as a fly-by-light (FBL) system and the control function is essentially the same as that of the FBW system or the simple stability augmentation system it replaces. It fact, it is most important to recognize that, for a given aeroplane, the stability augmentation function required of the flight control system is the same irrespective of the architecture adopted for its implementation. In the context of stability augmentation there is nothing special or different in an FBW or FBL system solution.

11.1.4 SCOPE

In the preceding sections an attempt has been made to introduce and review some of the important issues concerning flight control system design in general. In particular, the role of the SAS or CSAS and the possible limitation of the control function imposed by the broader concerns of system structure have been emphasized. The temptation now is to embark on a discussion of FCS design but, unfortunately, such a vast subject is beyond the scope of the present book.

Rather, the remainder of this chapter is concerned with the very fundamental, and sometimes subtle, way in which feedback may be used to augment the dynamics of the basic aircraft. It is very important that the flight dynamicist understands the way in which his chosen control system design augments the stability and control properties of the airframe. It is not good enough to treat the aircraft like an arbitrary *plant* and to design a *controller* to meet a predefined set of performance requirements, an approach much favoured by control system designers. It is vital that the flight control system designer retains a complete understanding of the implications of his design decisions throughout the design process. In the interests of *functional visibility*, and hence of safety, it is important that flight control systems are made as simple as possible. This is often only achievable when the designer has a complete and intimate understanding of the design process.

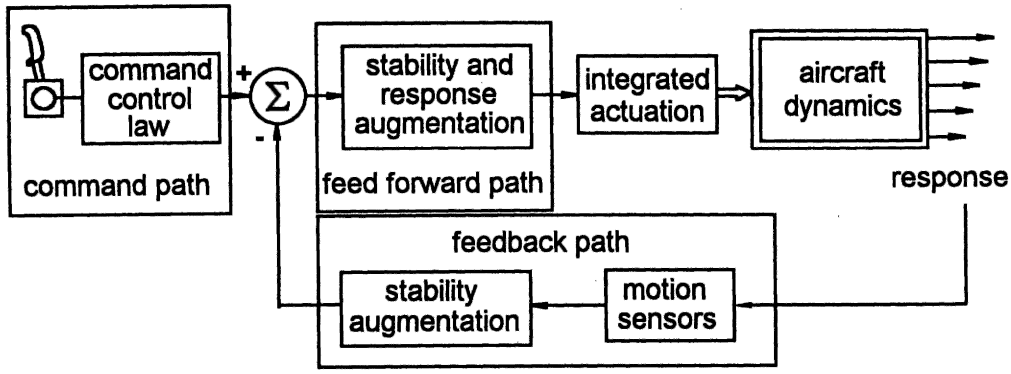

Fig. 11.4 Inner loop control functions

11.2 Augmentation system design

The most critical aspect of flight control system design is concerned with the design of the inner loop control law, the design objective being to endow the aircraft with good stability, control and handling characteristics throughout its flight envelope. Today, an FBW system gives the designer the greatest freedom of choice as to how he might allocate the control law functions for 'optimum' performance. The main CSAS control functions are indicated in the rather over-simplified representation shown in Fig. 11.4. The problem confronting the FCS designer is to design suitable functions for the command, feed-forward and feedback paths of the CSAS and, obviously, it is necessary to appreciate the role of each path in the overall context of aircraft stability augmentation.

The *feedback path* comprises the classical inner loop stability augmentation system whose primary role is to augment static and dynamic stability. It generally improves flying and handling qualities but may not necessarily lead to ideal handling qualities since it has insufficient direct control over *response shaping*.

The *feed-forward path* is also within the closed loop and its function augments stability in exactly the same way as the feedback path. However, it has a direct influence on command signals as well and, by careful design, its function may also be used to exercise some degree of response shaping. Its use in this role is limited since the stability augmentation function must take priority.

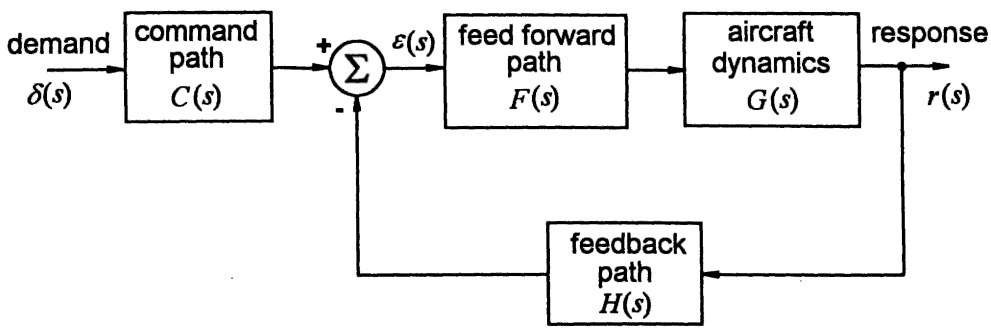

Fig. 11.5 Inner loop transfer function representation

The *command path* control function provides the principal means for response shaping – it has no influence on stability since it is outside the closed loop. This assumes, of course, that the augmented aircraft may be represented as a *linear* system. The command path indicated in Fig. 11.4 assumes entirely electronic signalling as appropriate to an FBW system. However, there is no reason why the command and feed-forward paths should not comprise a combination of parallel electrical and mechanical paths, an architecture commonly employed in aircraft of the 1960s and 1970s. In such systems it is only really practical to incorporate all, other than very simple, signal shaping into the electrical signal paths.

Further analysis of the simple CSAS structure may be made if it is represented by its transfer function equivalent as shown in Fig. 11.5.

With reference to Fig. 11.5 the *control error* signal $\varepsilon(s)$ is given by

$$\varepsilon(s) = C(s)\delta(s) - H(s)r(s) \tag{11.2}$$

where $\delta(s)$ and $r(s)$ are the command and response signals respectively, and $C(s)$ and $H(s)$ are the command path and feedback path transfer functions respectively. The output response $r(s)$ is given by

$$r(s) = F(s)G(s)\varepsilon(s) \tag{11.3}$$

where $F(s)$ is the feed-forward path transfer function and $G(s)$ is the all important transfer function representing the basic airframe. Combining equations (11.2) and (11.3) to eliminate the error signal, the closed loop transfer function is obtained

$$\frac{r(s)}{\delta(s)} = C(s)\left(\frac{F(s)G(s)}{1 + F(s)G(s)H(s)}\right) \tag{11.4}$$

Thus, the transfer function given by equation (11.4) is that of the augmented aircraft and replaces that of the unaugmented aircraft $G(s)$. Clearly, by appropriate choice of $C(s)$, $F(s)$ and $H(s)$ the flight control system designer has considerable scope for tailoring the stability, control and handling characteristics of the augmented aircraft. The characteristic equation of the augmented aircraft is given by

$$\Delta(s)_{\text{aug}} = 1 + F(s)G(s)H(s) = 0 \tag{11.5}$$

Note that the command path transfer function $C(s)$ does not appear in the characteristic equation, therefore, as noted above, it cannot influence stability in any way.

Let the aircraft transfer function be denoted by its numerator and denominator in the usual way

$$G(s) = \frac{N(s)}{\Delta(s)} \tag{11.6}$$

Let the feed-forward transfer function be a simple proportional gain

$$F(s) = K \tag{11.7}$$

and let the feedback transfer function be represented by a typical lead–lag function

$$H(s) = \left(\frac{1 + sT_1}{1 + sT_2}\right) \tag{11.8}$$

Then the transfer function of the augmented aircraft, equation (11.4), may be written

$$\frac{r(s)}{\delta(s)} = C(s)\left(\frac{KN(s)(1+sT_2)}{\Delta(s)(1+sT_2)+KN(s)(1+sT_1)}\right) \tag{11.9}$$

Now let the roles of $F(s)$ and $H(s)$ be reversed, whence

$$F(s) = \left(\frac{1+sT_1}{1+sT_2}\right) \qquad H(s) = K \tag{11.10}$$

In this case the transfer function of the augmented aircraft, equation (11.4), may be written

$$\frac{r(s)}{\delta(s)} = C(s)\left(\frac{KN(s)(1+sT_1)}{\Delta(s)(1+sT_2)+KN(s)(1+sT_1)}\right) \tag{11.11}$$

Comparing the closed loop transfer functions, equations (11.9) and (11.11), it is clear that the stability of the augmented aircraft is unchanged since the denominators are the same. However, the numerators are different, implying a difference in the response to control and this difference can be exploited to some advantage in some FCS applications.

Now, if the gains in the control system transfer functions $F(s)$ and $H(s)$ are deliberately made large such that at all frequencies over the bandwidth of the aeroplane

$$F(s)G(s)H(s) \gg 1 \tag{11.12}$$

then the closed loop transfer function, equation (11.4), is given approximately by

$$\frac{r(s)}{\delta(s)} \cong \frac{C(s)}{H(s)} \tag{11.13}$$

This demonstrates the important result that in highly augmented aircraft the stability and control characteristics may become substantially independent of the dynamics of the basic airframe. In other words, the stability, control and handling characteristics are largely determined by the design of the CSAS, in particular the design of the transfer functions $C(s)$ and $H(s)$. In practice, this situation is only likely to be encountered when the basic airframe is significantly unstable. This illustration implies that augmentation would be provided by an FBW system and ignores the often intrusive effects of the dynamics of the FCS components.

11.3 Closed loop system analysis

For the purpose of illustrating how motion feedback augments basic airframe stability consider the very simple example in which pitch attitude is fed back to elevator. The most basic essential features of the control system are shown in Fig. 11.6. In this example the controller comprises a simple gain constant K_θ in the feedback path.

The control law is given by

$$\eta(t) = \delta_\eta(t) - K_\theta\theta(t) \tag{11.14}$$

and the appropriate aircraft transfer function is

$$\frac{\theta(s)}{\eta(s)} = G(s) = \frac{N_\eta^\theta(s)}{\Delta(s)} \tag{11.15}$$

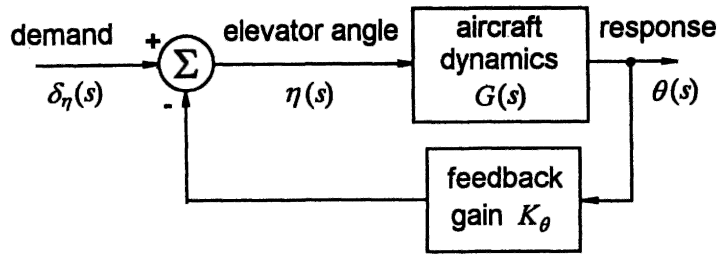

Fig. 11.6 A simple pitch attitude feedback system

Therefore, the closed loop transfer function of the augmented aircraft is

$$\frac{\theta(s)}{\delta_\eta(s)} = \frac{N_\eta^\theta(s)}{\Delta(s) + K_\theta N_\eta^\theta(s)} \tag{11.16}$$

and the augmented characteristic equation is

$$\Delta(s)_{\text{aug}} = \Delta(s) + K_\theta N_\eta^\theta(s) = 0 \tag{11.17}$$

Thus, for a given aircraft transfer function, its stability may be augmented by selecting a suitable value of feedback gain K_θ. Clearly, when K_θ is zero there is no feedback, the aircraft is said to be *open loop* and its stability characteristics are unmodified. As the value of K_θ is increased so the degree of augmentation is increased and the stability modes increasingly diverge from those of the open loop aircraft. Note that the open and closed loop transfer function numerators, equations (11.15) and (11.16), are the same in accordance with the findings of Section 11.2.

Alternatively, the closed loop equations of motion may be obtained by incorporating the control law into the open loop equations of motion. The open loop equations of motion in state space form and referred to a body axis system are given by equation (4.67)

$$\begin{bmatrix} \dot{u} \\ \dot{w} \\ \dot{q} \\ \dot{\theta} \end{bmatrix} = \begin{bmatrix} x_u & x_w & x_q & x_\theta \\ z_u & z_w & z_q & z_\theta \\ m_u & m_w & m_q & m_\theta \\ 0 & 0 & 1 & 0 \end{bmatrix} \begin{bmatrix} u \\ w \\ q \\ \theta \end{bmatrix} + \begin{bmatrix} x_\eta & x_\tau \\ z_\eta & z_\tau \\ m_\eta & m_\tau \\ 0 & 0 \end{bmatrix} \begin{bmatrix} \eta \\ \tau \end{bmatrix} \tag{11.18}$$

Substitute the control law expression for η, equation (11.14), into equation (11.18) and rearrange to obtain the closed loop state equation

$$\begin{bmatrix} \dot{u} \\ \dot{w} \\ \dot{q} \\ \dot{\theta} \end{bmatrix} = \begin{bmatrix} x_u & x_w & x_q & x_\theta - K_\theta x_\eta \\ z_u & z_w & z_q & z_\theta - K_\theta z_\eta \\ m_u & m_w & m_q & m_\theta - K_\theta m_\eta \\ 0 & 0 & 1 & 0 \end{bmatrix} \begin{bmatrix} u \\ w \\ q \\ \theta \end{bmatrix} + \begin{bmatrix} x_\eta & x_\tau \\ z_\eta & z_\tau \\ m_\eta & m_\tau \\ 0 & 0 \end{bmatrix} \begin{bmatrix} \delta_\eta \\ \tau \end{bmatrix} \tag{11.19}$$

Clearly, the effect of θ feedback is to modify, or augment, the derivatives x_θ, z_θ and m_θ. For a given value of the feedback gain K_θ, equation (11.19) may be solved in the usual way to obtain all of the closed loop longitudinal response transfer functions

$$\frac{u(s)}{\delta_\eta(s)} = \frac{N_\eta^u(s)}{\Delta_\eta(s)_{\text{aug}}} \qquad \frac{w(s)}{\delta_\eta(s)} = \frac{N_\eta^w(s)}{\Delta(s)_{\text{aug}}} \qquad \frac{q(s)}{\delta_\eta(s)} = \frac{N_\eta^q(s)}{\Delta(s)_{\text{aug}}} \qquad \frac{\theta(s)}{\delta_\eta(s)} = \frac{N_\eta^\theta(s)}{\Delta(s)_{\text{aug}}}$$

and

$$\frac{u(s)}{\tau(s)} = \frac{N_\tau^u(s)}{\Delta(s)_{\text{aug}}} \qquad \frac{w(s)}{\tau(s)} = \frac{N_\tau^w(s)}{\Delta(s)_{\text{aug}}} \qquad \frac{q(s)}{\tau(s)} = \frac{N_\tau^q(s)}{\Delta(s)_{\text{aug}}} \qquad \frac{\theta(s)}{\tau(s)} = \frac{N_\tau^\theta(s)}{\Delta(s)_{\text{aug}}}$$

where $\Delta(s)_{\text{aug}}$ is given by equation (11.17).

An obvious problem with this analytical approach is the need to solve equation (11.19) repetitively for a range of values of K_θ in order to determine the value which gives the desired stability characteristics. Fortunately, the *root locus plot* provides an extremely effective graphical tool for the determination of feedback gain without the need for repetitive computation.

EXAMPLE 11.1

The pitch attitude response to elevator transfer function for the Lockheed F-104 Starfighter in a take-off configuration was obtained from Teper (1969) and may be written in factorized form

$$\frac{\theta(s)}{\eta(s)} = \frac{-4.66(s+0.133)(s+0.269)}{(s^2+0.015s+0.021)(s^2+0.911s+4.884)} \tag{11.20}$$

Inspection of the denominator of equation (11.20) enables the stability mode characteristics to be written down

$$\text{phugoid damping ratio } \zeta_p = 0.0532$$
$$\text{phugoid undamped natural frequency } \omega_p = 0.145 \text{ rad/s}$$
$$\text{short period damping ratio } \zeta_s = 0.206$$
$$\text{short period undamped natural frequency } \omega_s = 2.21 \text{ rad/s}$$

The values of these characteristics suggest that the short period mode damping ratio is unacceptably low, the remainder being acceptable. Therefore, stability augmentation is required to increase the short period damping ratio.

In the first instance, assume a stability augmentation system in which pitch attitude is fed back to elevator through a gain constant K_θ in the feedback path. The SAS is then exactly the same as that shown in Fig. 11.6 and, as before, the control law is given by equation (11.14). However, since the aircraft transfer function, equation (11.20), is negative, a negative feedback loop effectively results in overall positive feedback which is, of course, destabilizing. This situation arises frequently in aircraft control and, whenever a negative open loop transfer function is encountered, it is necessary to assume a positive feedback loop, or equivalently a negative value of the feedback gain constant, in order to obtain a stabilizing control system. *Care must always be exercised in this context.* Therefore, in this particular example, when the negative sign of the open loop transfer function is taken into account the closed loop transfer function, equation (11.16), of the augmented aircraft may be written

$$\frac{\theta(s)}{\delta_\eta(s)} = \frac{N_\eta^\theta(s)}{\Delta(s) - K_\theta N_\eta^\theta(s)} \tag{11.21}$$

Substitute the open loop numerator and denominator polynomials from equation (11.20) into equation (11.21) and rearrange to obtain the closed loop transfer function

$$\frac{\theta(s)}{\delta_\eta(s)} = \frac{-4.66(s+0.133)(s+0.269)}{s^4+0.926s^2+(4.919+4.66K_\theta)s^2+(0.095+1.873K_\theta)s+(0.103+0.167K_\theta)} \tag{11.22}$$

Thus, the augmented characteristic equation is

$$\Delta(s)_{aug} = s^4+0.927s^3+(4.919+4.66K_\theta)s^2+(0.095+1.873K_\theta)s+(0.103+0.167K_\theta)=0 \tag{11.23}$$

The effect of the feedback gain K_θ on the longitudinal stability modes of the F-104 can only be established by repeatedly solving equation (11.23) for a range of suitable gain values. However, a reasonable appreciation of the effect of K_θ on the stability modes can be obtained from the approximate solution of equation (11.23). Writing equation (11.23)

$$As^4+Bs^3+Cs^2+Ds+E=0 \tag{11.24}$$

then an approximate solution is given by equation (6.13).

Thus, the characteristics of the short period mode are given approximately by

$$s^2+\frac{B}{A}s+\frac{C}{A}=s^2+0.927s+(4.919+4.66K_\theta)=0 \tag{11.25}$$

Whence

$$\left.\begin{aligned}\omega_s &= \sqrt{(4.919+4.66K_\theta)}\\ 2\zeta_s\omega_s &= 0.927\,\text{rad/s}\end{aligned}\right\} \tag{11.26}$$

It is therefore easy to see how the mode characteristics change as the feedback gain is increased from zero to a large value. Or, more generally, as $K_\theta \to \infty$ so

$$\left.\begin{aligned}\omega_s &\to \infty\\ \zeta_s &\to 0\end{aligned}\right\} \tag{11.27}$$

Similarly, with reference to equation (6.13), the characteristics of the phugoid mode are given approximately by

$$s^2+\frac{(CD-BE)}{C^2}s+\frac{E}{C}=s^2+\left(\frac{8.728K_\theta^2+9.499K_\theta+0.369}{21.716K_\theta^2+45.845K_\theta+24.197}\right)s+\left(\frac{0.103+0.167K_\theta}{4.919+4.66K_\theta}\right)=0 \tag{11.28}$$

Thus, again, as $K_\theta \to \infty$ so

$$\left.\begin{aligned}\omega_p &\to \sqrt{\frac{0.167}{4.66}} = 0.184\,\text{rad/s}\\ 2\zeta_p\omega_p &\to \frac{8.728}{21.716} = 0.402\,\text{rad/s}\end{aligned}\right\} \tag{11.29}$$

and allowing for rounding errors

$$\zeta_p \to 1.0 \tag{11.30}$$

The conclusion is then that negative pitch attitude feedback to elevator tends to destabilize the short period mode and increase its frequency, whereas its effect on the phugoid mode is more beneficial. The phugoid stability is increased whilst its frequency also tends to increase a little but is bounded by an acceptable maximum value. For all practical purposes the frequency is assumed to be approximately constant. This result is, perhaps, not too surprising since pitch attitude is a dominant motion variable in phugoid dynamics and is less significant in short period pitching motion. It is quite clear that pitch attitude feedback to elevator is not the correct way to augment the longitudinal stability of the F-104.

What this approximate analysis does not show is the relative sensitivity of each mode to the feedback gain. This can only be evaluated by solving the characteristic equation repeatedly for a range of values of K_θ from zero to a suitably large value. A typical practical range of values might be $0 \leqslant K_\theta \leqslant 2$ rad/rad, for example. This kind of analysis is most conveniently achieved with the aid of a *root locus plot.*

11.4 The root locus plot

The *root locus plot* is a relatively simple tool for determining, by graphical means, detailed information about the stability of a closed loop system knowing only the open loop transfer function. The plot shows the roots, or *poles*, of the closed loop system characteristic equation for every value of a single loop variable, typically the feedback gain. It is therefore not necessary to calculate the roots of the closed loop characteristic equation for every single value of the chosen loop variable. As its name implies, the root locus plot shows loci on the s-plane of all the roots of the closed loop transfer function denominator as a function of the single loop gain variable.

The root locus plot was proposed by Evans (1954) and from its first appearance rapidly gained in importance as an essential control systems design tool. Consequently, it is described in most books concerned with linear control systems theory, for example it is described by Friedland (1987). Because of the relative mathematical complexity of the underlying theory, Evans' (1954) main contribution was the development of an approximate asymptotic procedure for manually 'sketching' closed loop root loci on the s-plane without recourse to extensive calculation. This was achieved with the aid of a set of 'rules' which resulted in a plot of sufficient accuracy for most design purposes. It was therefore essential that control system designers were familiar with the rules. Today, the root locus plot is universally produced by computational means. It is no longer necessary for the designer to know the rules although he must still know how to interpret the plot correctly and, of course, he must know its limitations.

In aeronautical applications it is vital to understand the correct interpretation of the root locus plot. This is especially so when it is being used to evaluate augmentation schemes for the precise control of the stability characteristics of an aircraft over the flight envelope. In the opinion of the author, this can only be done from the position of strength which comes with a secure knowledge of the rules for plotting a root locus by hand. For this reason the rules are set out in Appendix 9. However, it is not advocated that root locus plots should be drawn by hand—this is unnecessary when computational tools such as *CODAS*, *PC MATLAB* and *Program CC* are readily available. The processes involved in the construction of a root locus plot are best illustrated by example as follows.

EXAMPLE 11.2

Consider the use of the root locus plot to evaluate the effect of pitch attitude feedback to elevator on the F-104 aircraft at the same flight condition as discussed in Example 11.1. The closed loop system block diagram applying is that shown in Fig. 11.6. The open loop system transfer function is, from equation (11.20),

$$\frac{\theta(s)}{\eta(s)} = \frac{-4.66K_\theta(s+0.133)(s+0.269)}{(s^2+0.015s+0.021)(s^2+0.911s+4.884)} \tag{11.31}$$

with poles and zeros

$$p_1 = -0.0077 + 0.1448\text{j}$$
$$p_2 = -0.0077 - 0.1448\text{j}$$
$$p_3 = -0.4553 + 2.1626\text{j}$$
$$p_4 = -0.4553 - 2.1626\text{j}$$
$$z_1 = -0.133$$
$$z_2 = -0.269$$

whence number of poles $n_p = 4$, number of zeros $n_z = 2$

The open loop poles and zeros are mapped on to the s-plane as shown in Fig. 11.7.

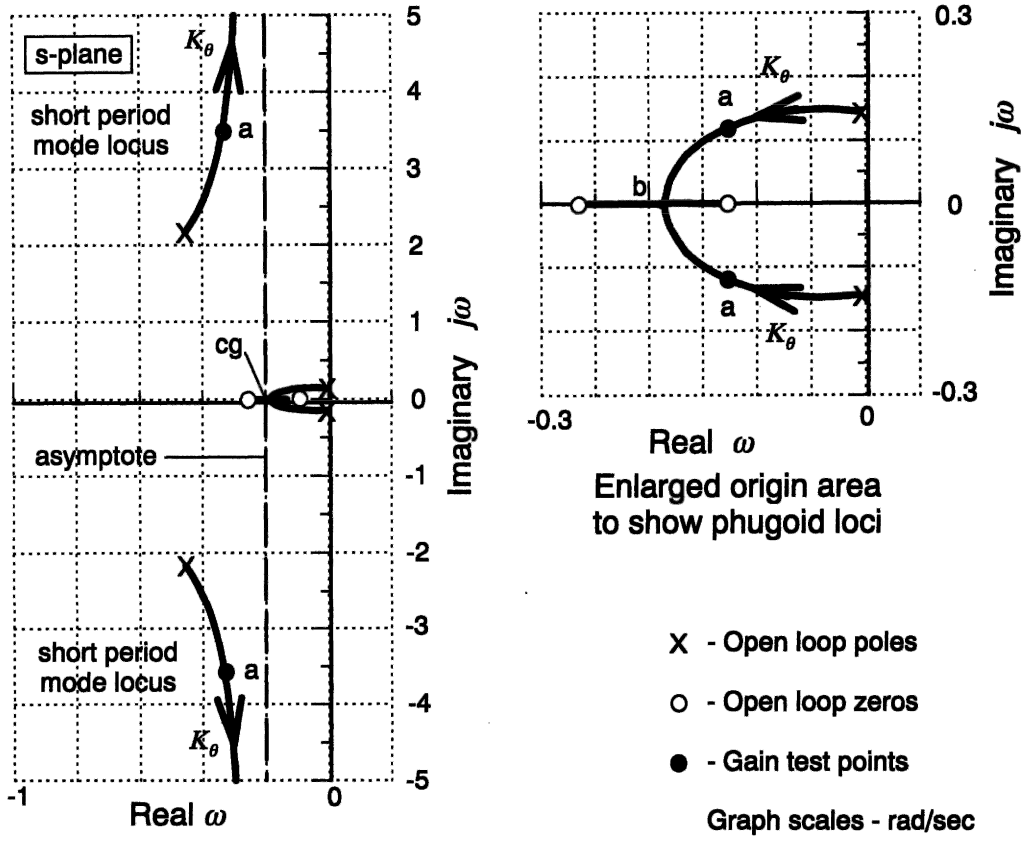

Fig. 11.7 Example of root locus plot construction

The loci of the closed loop poles are then plotted as the feedback gain K_θ is allowed to increase from zero to a large value. In this example the loci were obtained computationally and are discussed in the context of the *rules* set out in Appendix 9.

Rule 1 locates the poles and zeros on the s-plane and determines that, since there are two more poles than zeros, four loci commence at the poles, two of which terminate at the zeros and two of which go off to infinity as $K_\theta \to \infty$.

Rule 2 determines that the real axis between the two zeros is part of a locus.

Rule 3 determines that the two loci which go off to infinity do so asymptotically to lines at 90° and at 270° to the real axis.

Rule 4 determines that the asymptotes radiate from the *cg* of the plot located at −0.262 on the real axis.

Rule 5 determines the point on the real axis at which two loci break in to the locus between the two zeros. Method 1, the approximate method, determines the break-in point at −0.2. Method 2, the exact method, determines the break-in point at −0.186. Either value is satisfactory for all practical purposes.

Rule 6 simply states that the two loci branching in to the real axis do so at ±90° to the real axis.

Rule 7 determines the angle of departure of the loci from the poles and the angles of arrival at the zeros. This is rather more difficult to calculate by hand and, to do so, the entire s-plane plot is required. The angles given by the computer program used to plot the loci are as follows

angle of departure from p_1, 194°

angle of departure from p_2, −194°

angle of departure from p_3, 280°

angle of departure from p_4, −280°

angle of arrival at z_1, 180°

angle of arrival at z_2, 0°

Note that these values compare well with those calculated by hand from measurements made on the s-plane using a protractor.

Rule 8 enables the total loop gain to be evaluated at any point on the loci. To do this by hand is particularly tedious, it requires a plot showing the entire s-plane and it is not always very accurate, especially if the plot is drawn to a small scale. However, since this is the primary reason for plotting root loci in the first instance all computer programs designed to plot root loci provide a means for obtaining values of the feedback gain at test points on the loci. Not all root locus plotting programs provide the information given by rules 4, 5 and 7. In this example the feedback gain at test point a is $K_\theta = -1.6$ and at test point b, the break-in point, $K_\theta = -12.2$. Note that, in this example, the feedback gain has units deg/deg or, equivalently, rad/rad. When all test points of interest have been investigated the root locus plot is complete.

One of the more powerful features of the root locus plot is that it gives explicit information about the relative sensitivity of the stability modes to the feedback in question. In this example, the open loop aircraft stability characteristics are

phugoid damping ratio $\zeta_p = 0.0532$

phugoid undamped natural frequency $\omega_p = 0.145$ rad/s

short period damping ratio $\zeta_s = 0.206$

short period undamped natural frequency $\omega_s = 2.21$ rad/s

and at test point a, where $K_\theta = -1.6$, the closed loop stability characteristics are

phugoid damping ratio $\zeta_p = 0.72$

phugoid undamped natural frequency $\omega_p = 0.17$ rad/s

short period damping ratio $\zeta_s = 0.10$

short period undamped natural frequency $\omega_s = 3.49$ rad/s

Thus, the phugoid damping is increased by about 14 times and its frequency remains nearly constant. In fact, the oscillatory phugoid frequency can never exceed 0.186 rad/s. The short period mode damping is approximately halved whilst its frequency is increased by about 50%. Obviously the phugoid damping is the parameter which is most sensitive to the feedback gain by a substantial margin. A modest feedback gain of, say, $K_\theta = -0.1$ rad/rad would result in a very useful increase in phugoid damping whilst causing only very small changes in the other stability parameters. However, the fact remains that pitch attitude feedback to elevator destabilizes the short period mode by reducing the damping ratio from its open loop value. This, then, is not the cure for the poor short period mode stability exhibited by the open loop F-104 aircraft at this flight condition. All of these conclusions support the findings of Example 11.1 but, clearly, very much greater analytical detail is directly available from inspection of the root locus plot.

Additional important points relating to the application of the root locus plot to aircraft stability augmentation include the following.

- Since the plot is symmetric about the real axis it is not necessary to show the lower half of the s-plane, unless the plot is constructed by hand. All of the relevant information provided by the plot is available in the upper half of the s-plane.
- At typical scales it is frequently necessary to obtain a plot of the origin area at enlarged scale in order to resolve the essential detail. This is usually very easy to achieve with most computational tools.
- As has been mentioned previously, it is essential to be aware of the sign of the open loop aircraft transfer function. Most root locus plotting computer programs assume the standard positive transfer function with negative feedback. A negative transfer function will result in an incorrect locus. The easy solution to this problem is to enter the transfer function with a positive sign and to change the sign of the feedback gains given by the program. However, it is important to remember the changes made when assessing the result of the investigation.

EXAMPLE 11.3

In Examples 11.1 and 11.2 it is shown that pitch attitude feedback to elevator is not the most appropriate means for augmenting the deficient short period mode damping of the F-104. The correct solution is to augment pitch damping by implementing pitch

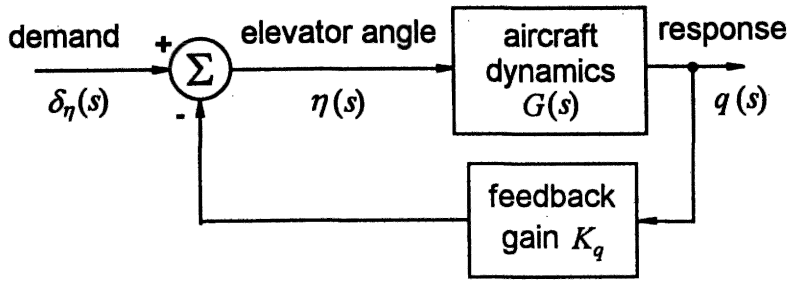

Fig. 11.8 A simple pitch rate feedback system

rate feedback to elevator—velocity feedback in servomechanism terms. The control system functional block diagram is shown in Fig. 11.8.

For the same flight condition, a take-off configuration, as in the previous examples, the pitch rate response to elevator transfer function for the Lockheed F-104 Starfighter was obtained from Teper (1969) and may be written in factorized form

$$\frac{q(s)}{\eta(s)} = \frac{-4.66s(s+0.133)(s+0.269)}{(s^2+0.015s+0.021)(s^2+0.911s+4.884)} \text{ rad/s/rad} \tag{11.32}$$

As before, the stability modes of the open loop aircraft are

phugoid damping ratio $\zeta_p = 0.0532$

phugoid undamped natural frequency $\omega_p = 0.145$ rad/s

short period damping ratio $\zeta_s = 0.206$

short period undamped natural frequency $\omega_s = 2.21$ rad/s

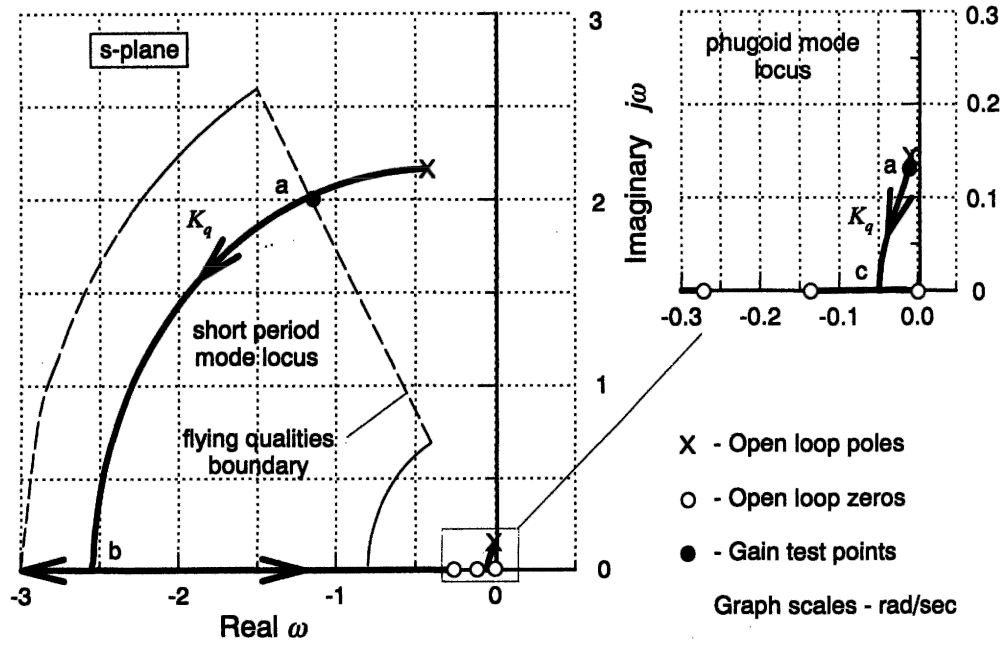

Fig. 11.9 Root locus plot for pitch rate feedback to elevator

With reference to MIL-F-8785C (1980), defining the F-104 as a class IV aircraft, operating in flight phase category C and assuming level 1 flying qualities are desired, the following constraints on the stability modes may be determined

$$\text{phugoid damping ratio } \zeta_p \geqslant 0.04$$
$$\text{short period damping ratio } \zeta_s \geqslant 0.5$$
$$\text{short period undamped natural frequency } 0.8 \leqslant \omega_s \leqslant 3.0 \text{ rad/s}$$

The upper limit on the short period mode damping ratio is ignored since it is greater than one. Additionally, the closed loop phugoid frequency should ideally conform to $\omega_p \leqslant 1.1\omega_s$ where ω_s here is the closed loop short period mode frequency. Clearly, the unaugmented aircraft meets these flying qualities requirements with the exception of the short period mode damping ratio, which is much too low.

The root locus plot constructed from the transfer function, equation (11.32), is shown in Fig. 11.9. Also shown on the same s-plane plot are the flying qualities short period mode boundaries according to the limits determined from MIL-F-8785C and quoted above.

Clearly, pitch rate feedback to elevator is ideal since it causes the damping of both the phugoid and short period modes to be increased, although the short period mode is most sensitive to feedback gain. Further, the frequency of the short period mode remains more-or-less constant through the usable range of values of feedback gain K_θ. For the same range of feedback gains the frequency of the phugoid mode is reduced, thereby increasing the separation between the frequencies of the two modes. At test point a, $K_q = -1.3$ rad/rad/s, which is the smallest feedback gain required to bring the closed loop short period mode into agreement with the flying qualities boundaries. Allowing for a reasonable margin of error and uncertainty, a practical choice of feedback gain might be $K_q = -0.5$ rad/rad/s. The stability augmentation control law would then be

$$\eta = \delta_\eta + 0.5q \tag{11.33}$$

This augmentation system is the classical *pitch damper* used on many aeroplanes from the same period as the Lockheed F-104 and typical feedback gains would be in the range $-0.1 \leqslant K_q \leqslant -1.0$ rad/rad/s. It is not known what value of feedback gain is used in the F-104 at this flight condition but the published description of the longitudinal augmentation system structure is the same as that shown in Fig. 11.8.

Substituting the control law, equation (11.33), into the open loop longitudinal equations of motion, as described in Section 11.3, enables the closed loop equations of motion to be derived. Solution of the equations in the usual way gives the response transfer functions for the augmented aircraft. Solution of the closed loop characteristic equation determines that at $K_q = -1.5$ rad/rad/s the longitudinal modes have the following characteristics

$$\text{phugoid damping ratio } \zeta_p = 0.079$$
$$\text{phugoid undamped natural frequency } \omega_p = 0.133 \text{ rad/s}$$
$$\text{short period damping ratio } \zeta_s = 0.68$$
$$\text{short period undamped natural frequency } \omega_s = 2.41 \text{ rad/s}$$

Clearly, at this value of feedback gain the flying qualities requirements are met

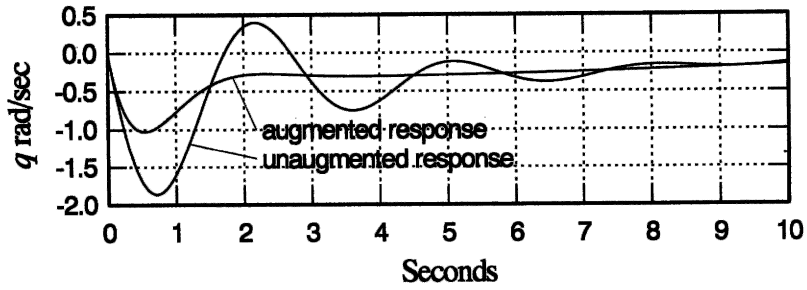

Fig. 11.10 Pitch rate response to a unit elevator step input

completely with margins sufficient to allow for uncertainty. The closed loop system thus defined provides the basis for further analytical studies concerning the implementation architecture and safety issues. The pitch rate response of the aircraft before and after the addition of the augmentation loop is illustrated in Fig. 11.10. The first ten seconds of the response to a unit elevator step input are shown to emphasize the considerable improvement in short period mode stability. The longer term response is not shown since this is not changed significantly by the augmentation and, in any event, the phugoid dynamics are acceptable.

11.5 Longitudinal stability augmentation

In Examples 11.2 and 11.3 it has been shown how negative feedback using a single variable can be used to augment selectively the stability characteristics of an aeroplane. It has also been shown how the effect of single variable feedback may readily be evaluated with the aid of a root locus plot. Now, clearly, the choice of feedback variable is important in determining the nature of the change in the stability characteristics of the aeroplane since each variable results in a unique combination of changes. Provided that the aircraft is equipped with the appropriate motion sensors various feedback control schemes are possible and it then becomes necessary to choose the feedback variable(s) best suited to augment the deficiencies of the basic airframe. It is also useful to appreciate what effect each feedback variable has on the stability modes when

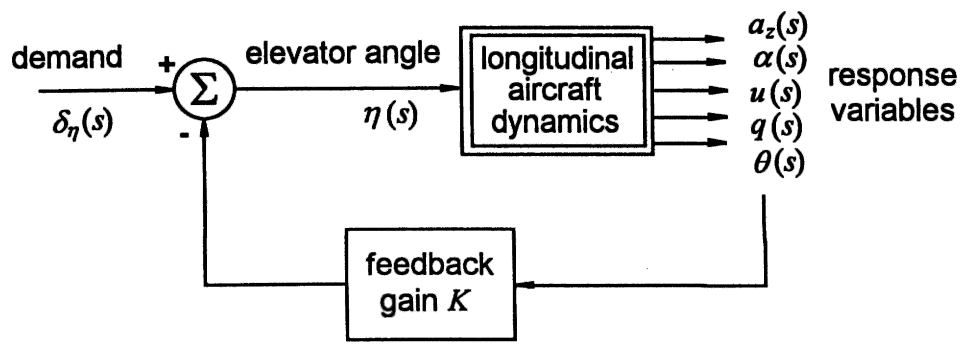

Fig. 11.11 Longitudinal feedback options

assessing a flight control system design. However complex the functional structure of the system, the basic augmentation effect of each feedback variable does not change. Feedback is also used for reasons other than stability augmentation; for example, in autopilot functions. In such cases augmentation will also occur and it may not be desirable, in which case a thorough understanding of the effects of the most commonly used feedback variables is invaluable.

In order to evaluate the effect of feedback utilizing a particular response variable it is instructive to conduct a survey of all the single loop feedback options. In every case the feedback loop is reduced to a simple gain component only. By this means the possible intrusive effects of other loop components, such as noise filters, phase compensation filters, sensor and actuator dynamics, are prevented from masking the true augmentation effects. The longitudinal stability augmentation options are summarized in Fig. 11.11, in which it is implied that a negative feedback loop may be closed between any of the motion variables and the elevator. Other loops could, of course, be closed between the motion variables and alternative longitudinal control motivators, or engine thrust control, for example, but these are not considered here.

The survey is conducted by taking each motion variable in turn and evaluating its influence on the closed loop stability characteristics as a function of the loop gain K. The root locus plot is an especially useful tool for this purpose since it enables the relative influence on, and the relative sensitivity of, each of the stability modes to be assessed simultaneously. As the detailed effect of feedback depends on the aircraft and flight condition of interest it is not easy to generalize and is best illustrated by example. Consequently, the following survey (Example 11.4) is based on a typical aircraft operating at a typical flight condition and the observations may be applied loosely to the longitudinal stability augmentation of most aircraft.

EXAMPLE 11.4

Transfer function data for the McDonnell-Douglas A-4D Skyhawk aircraft were obtained from Teper (1969). The flight condition chosen corresponds to an all up weight of 17578 lb at an altitude of 35000 ft at Mach 0.6. In factorized form the longitudinal characteristic equation is

$$\Delta(s) = (s^2 + 0.014s + 0.0068)(s^2 + 1.009s + 5.56) = 0 \tag{11.34}$$

and the longitudinal stability mode characteristics are

$$\text{phugoid damping ratio } \zeta_p = 0.086$$
$$\text{phugoid undamped natural frequency } \omega_p = 0.082 \text{ rad/s}$$
$$\text{short period damping ratio } \zeta_s = 0.214$$
$$\text{short period undamped natural frequency } \omega_s = 2.358 \text{ rad/s}$$

These stability mode characteristics would normally be considered acceptable with the exception of the short period mode damping ratio, which is too low. The Skyhawk is typical of combat aeroplanes of the 1960s in which modest degrees of augmentation only are required to rectify the stability deficiencies of the basic airframe. This, in turn, implies that modest feedback gains only are required in the range say, typically, $0 \leqslant K \leqslant 2.0$. In modern FBW aircraft having unstable airframes rather larger gain values would be required to achieve the same levels of augmentation. In general, the

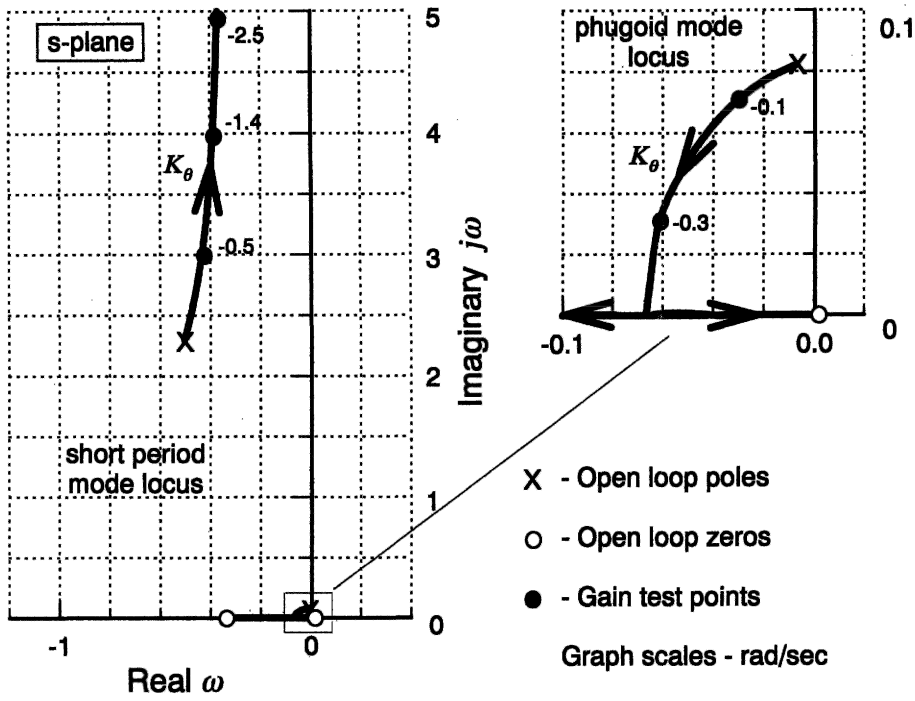

Fig. 11.12 Root locus plot—pitch attitude feedback to elevator

greater the required change in the stability characteristics the greater the feedback gains needed to effect the change. In the following catalogue of root locus plots each plot illustrates the effect of a single feedback loop closure as a function of increasing feedback gain K.

(i) *Pitch attitude feedback to elevator*
The open loop aircraft transfer function is

$$\frac{\theta(s)}{\eta(s)} \equiv \frac{N_\eta^\theta(s)}{\Delta(s)} = \frac{-8.096(s-0.0006)(s+0.3591)}{(s^2+0.014s+0.0068)(s^2+1.009s+5.56)} \text{ rad/rad} \tag{11.35}$$

and the corresponding root locus plot is shown in Fig. 11.12.

As K_θ is increased the phugoid damping increases rapidly whilst the frequency remains nearly constant, whereas as K_θ is increased the short period mode frequency increases whilst the damping decreases, both characteristics changing relatively slowly. Thus, as might be expected, since pitch attitude is a dominant variable in the phugoid mode, this mode is considerably more sensitive to the loop gain than the short period mode. Since this feedback option further destabilizes the short period mode its usefulness in an SAS is very limited indeed. However, it does improve phugoid stability, the mode becoming critically damped at a gain of $K_\theta = -0.37$ rad/rad. A practical gain value might be $K_\theta = -0.1$ rad/rad which would result in a good level of closed loop phugoid stability without reducing the short period mode stability too much. These observations are, of course, in good agreement with the findings of Example 11.2.

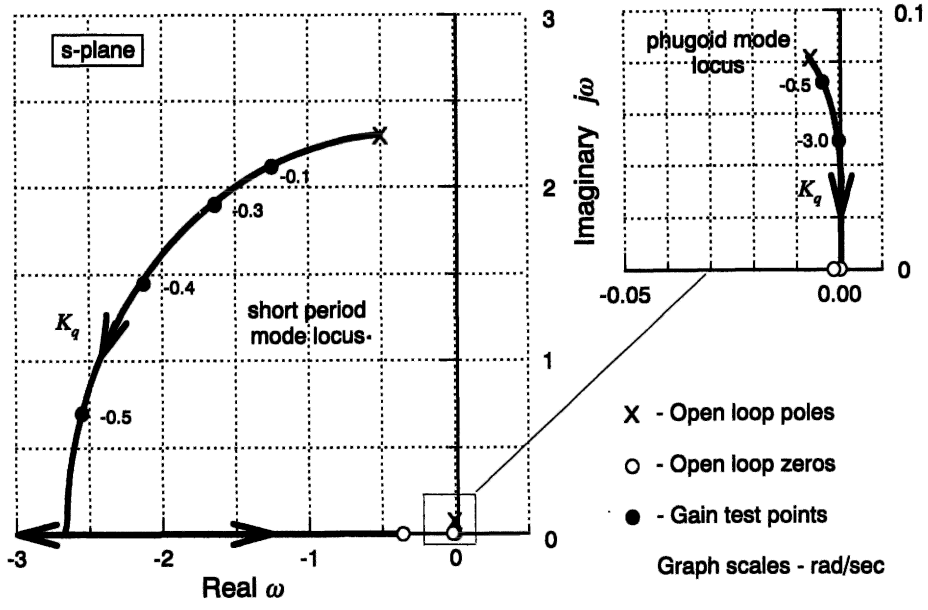

Fig. 11.13 Root locus plot—pitch rate feedback to elevator

(ii) *Pitch rate feedback to elevator*
The open loop aircraft transfer function is

$$\frac{q(s)}{\eta(s)} \equiv \frac{N_\eta^q(s)}{\Delta(s)} = \frac{-8.096s(s-0.0006)(s+0.3591)}{(s^2+0.014s+0.0068)(s^2+1.009s+5.56)} \text{ rad/s/rad} \qquad (11.36)$$

and the corresponding root locus plot is shown in Fig. 11.13.

As K_q is increased the short period mode damping increases rapidly whilst the frequency remains nearly constant, whereas as K_q is increased the phugoid frequency and damping decrease relatively slowly. More typically, a slow increase in phugoid damping would be seen. Thus, as might be expected, since pitch rate is a dominant variable in the short period mode, this mode is considerably more sensitive to the loop gain than the short period mode. As discussed in Example 11.3, this feedback option describes the classical pitch damper and is found on many aeroplanes. It also exactly describes the longitudinal stability augmentation solution used on the Skyhawk. Its dominant effect is to increase artificially the magnitude of the derivative m_q; it also increases the magnitude of the derivatives x_q and z_q but to a lesser degree. The short period mode becomes critically damped at a gain of $K_q = -0.53$ rad/rad/s. A practical gain value might be $K_q = -0.3$ rad/rad/s which would result in an adequate level of closed loop short period mode stability whilst simultaneously increasing the frequency separation between the two modes. However, at this value of feedback gain the changes in the phugoid characteristics would be almost insignificant. As before, these observations are in good agreement with the findings of Example 11.3.

(iii) *Velocity feedback to elevator*
The open loop aircraft transfer function is

$$\frac{u(s)}{\eta(s)} \equiv \frac{N_\eta^u(s)}{\Delta(s)} = \frac{6.293(s^2+0.615s+0.129)(s+115.28)}{(s^2+0.014s+0.0068)(s^2+1.009s+5.56)} \text{ ft/s/rad} \qquad (11.37)$$

and the corresponding root locus plot is shown in Fig. 11.14.

As K_u is increased the short period mode frequency increases quite rapidly whilst, initially, the damping decreases. However, at very large gain values the damping commences to increase again to become eventually critical, whereas as K_u is increased both the frequency and damping of the phugoid mode increase relatively rapidly. Thus, at this flight condition, both modes appear to have similar sensitivity to feedback gain. The stabilizing influence on the phugoid mode is much as might be expected since velocity is the dominant variable in the mode dynamics. The dominant effect of the feedback is therefore to increase artificially the magnitude of the derivative m_u, and since m_u is usually small it is not surprising that even modest values of feedback gain have a significant effect on phugoid stability. It also increases the magnitude of the derivatives x_u and z_u but to a lesser degree. A practical gain value might be $K_u = 0.001$ rad/ft/s which would result in a significant improvement in closed loop phugoid mode stability whilst simultaneously decreasing the stability of the short period mode by a small amount. However, such values of feedback gain are quite impractically small and, in any event, this feedback option would not find much useful application in a conventional longitudinal SAS.

(iv) *Incidence angle feedback to elevator*

The open loop aircraft transfer function is

$$\frac{\alpha(s)}{\eta(s)} \equiv \frac{N_\eta^\alpha(s)}{\Delta(s)} = \frac{-0.04(s^2-0.0027s+0.0031)(s+203.34)}{(s^2+0.014s+0.0068)(s^2+1.009s+5.56)} \text{ rad/rad} \qquad (11.38)$$

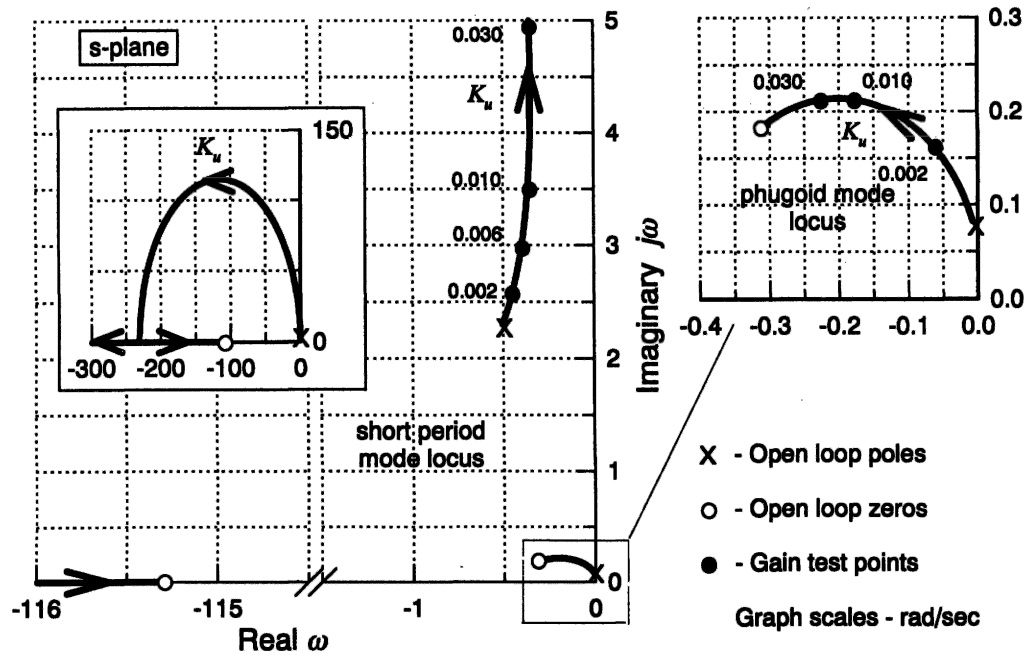

Fig. 11.14 Root locus plot—velocity feedback to elevator

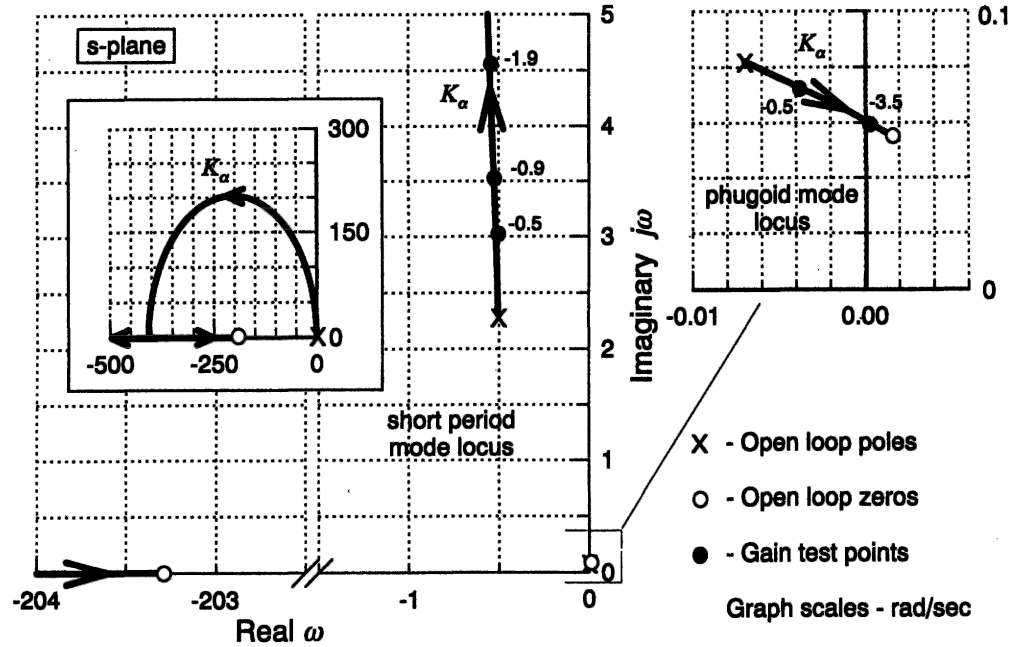

Fig. 11.15 Root locus plot—incidence feedback to elevator

and the corresponding root locus plot is shown in Fig. 11.15.

As K_α is increased the short period mode frequency increases very rapidly whilst, initially, the damping decreases slowly. However, as the gain increases further, the damping slowly starts to increase eventually to become critical at an impractically large value of feedback gain. At all practical gain values the damping remains more-or-less constant. As K_α is increased both the frequency and damping of the phugoid are reduced, the mode becoming unstable at a gain of $K_\alpha = -3.5$ rad/rad in this example. Incidence feedback to elevator is a powerful method for augmenting the longitudinal static stability of an aeroplane and finds extensive application in unstable FBW aircraft. The effect of the feedback is equivalent to increasing the pitch stiffness of the aircraft which artificially increases the magnitude of the derivative $m_w(\partial C_m/\partial\alpha)$ and to a lesser degree it also increases the magnitude of the derivatives x_w and z_w. Thus, the increase in short period mode frequency together with the less significant influence on damping is entirely consistent with the augmentation option. Since phugoid dynamics is typically very nearly incidence constant, the expected effect of the feedback on the mode is negligible. This is not the case in this example, probably due to aerodynamic effects at the relatively high subsonic Mach number. This is confirmed by the fact that the phugoid roots do not even approximately cancel with the complex pair of numerator roots, which might normally be expected. It would therefore be expected to see some incidence variation in the phugoid dynamics.

(v) *Normal acceleration feedback to elevator*

The open loop aircraft transfer function is

$$\frac{a_z(s)}{\eta(s)} \equiv \frac{N_\eta^{a_z}(s)}{\Delta(s)} = \frac{-23.037(s-0.018)(s-0.0003)(s+8.717)(s-8.203)}{(s^2+0.014s+0.0068)(s^2+1.009s+5.56)} \text{ ft/s}^2/\text{rad} \tag{11.39}$$

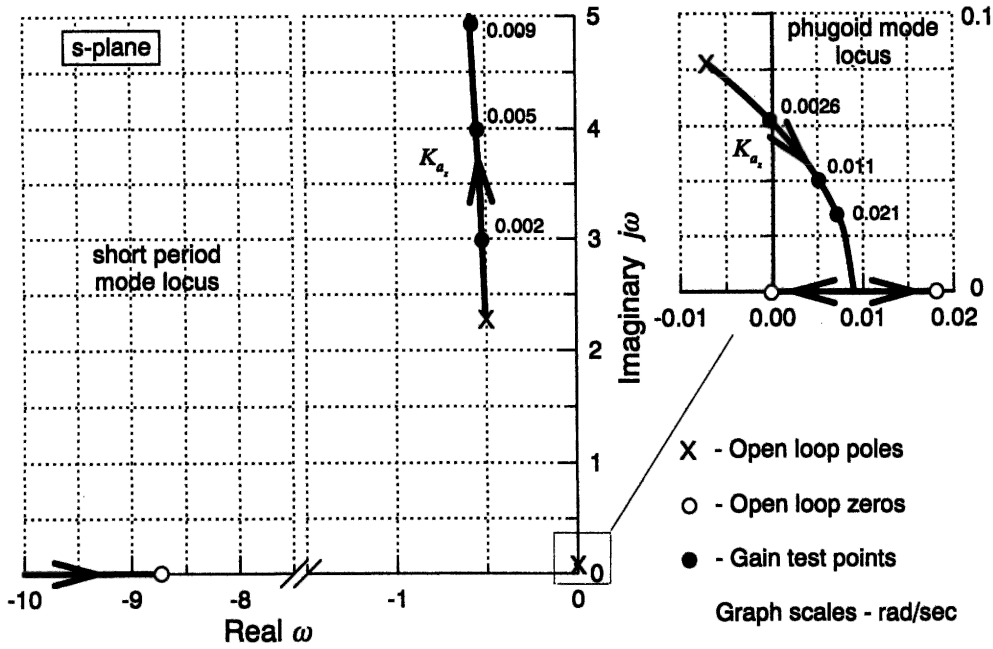

Fig. 11.16 Root locus plot—normal acceleration feedback to elevator

and the corresponding root locus plot is shown in Fig. 11.16. Since the transfer function is *not proper*, care must be exercised in the production of the root locus plot and in its interpretation. However, at typically small values of feedback gain its interpretation seems quite straightforward.

Since an accelerometer is rather more robust than an incidence sensor, normal acceleration feedback to elevator is commonly used instead of, or to complement, incidence feedback. Both feedback variables have a similar effect on the phugoid and short period stability mode at practical values of feedback gain. However, both modes are rather more sensitive to feedback gain since very small values result in significant changes to the mode characteristics. As K_{a_z} is increased the short period mode frequency increases very rapidly whilst, initially, the damping decreases slowly. However, as the gain increases further the damping slowly starts to increase eventually to become critical at an impractically large value of feedback gain. At all practical gain values the damping remains more-or-less constant. The full short period mode branch of the locus is not shown in Fig. 11.16 since the gain range required exceeded the capability of the computational software used to produce the plots. As K_{a_z} is increased both the frequency and damping of the phugoid are reduced, the mode becoming unstable at a gain of $K_{a_z} = 0.0026\,\text{rad/ft/s}^2$ in this example. Since the normal acceleration variable comprises a mix of incidence, velocity and pitch rate, see Section 5.5, then the augmentation it provides in a feedback control system may be regarded as equivalent to the sum of the effects of feedback of the separate variables. Thus, at moderate gains the increase in pitch stiffness is significant and results in a rapid increase in short period mode frequency. The corresponding increase in short period mode damping is rather greater than that achieved with incidence feedback alone due to the effect of implicit pitch rate

feedback. Since the incidence-dependent term dominates the determination of normal acceleration, it is not surprising that normal acceleration feedback behaves like incidence feedback. It is approximately equivalent to artificially increasing the magnitude of the derivative m_w and to a lesser degree it also increases the magnitude of the derivatives x_w and z_w.

11.6 Lateral-directional stability augmentation

As for the longitudinal stability augmentation options described in Section 11.5, it is also instructive to conduct a survey of all the lateral-directional single loop feedback options. The lateral-directional stability augmentation options are summarized in Fig. 11.17 in which it is implied that a negative feedback loop may be closed between any of the motion variables and either the ailerons or rudder. Other loops could be closed between the motion variables and alternative lateral-directional control motivators but, again, these are not considered here.

As before, the survey is conducted by taking each motion variable in turn and evaluating its influence on the closed loop stability characteristics as a function of the loop gain K. The detailed effects of the lateral-directional feedback options are much more dependent on the aircraft and flight condition than the longitudinal feedback options. Therefore, it is more difficult, and probably less appropriate, to generalize and the effects are also best illustrated by example. The following survey, Example 11.5, is based on a typical aircraft operating at a typical flight condition and the observations may be interpreted as being applicable to the lateral-directional stability augmentation of most aircraft. However, care must be exercised when applying the observations to other aircraft and every new application should be evaluated in its own right.

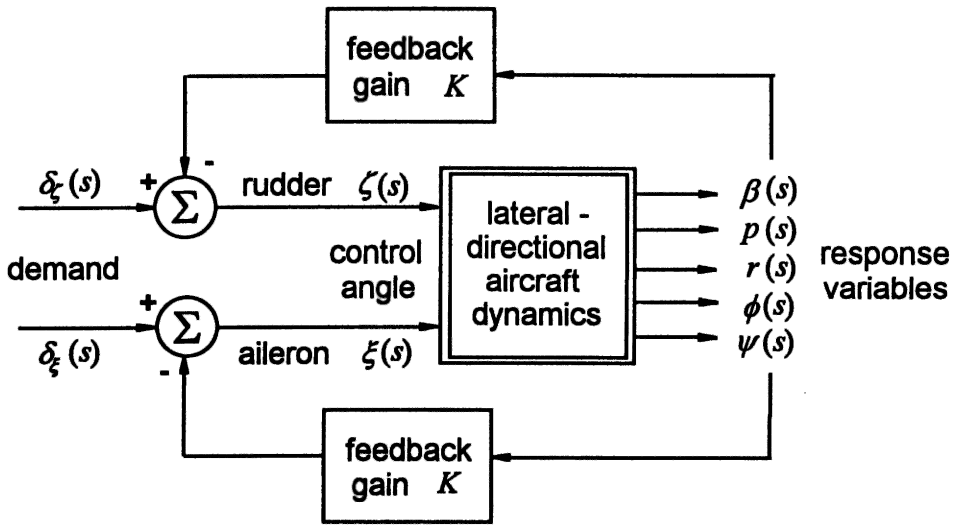

Fig. 11.17 Lateral-directional feedback options

EXAMPLE 11.5

Transfer function data for the Northrop T-38 Talon aircraft were also obtained from Teper (1969). The flight condition chosen corresponds to an all up weight of 10 000 lb at Mach 0.8 at sea level. In factorized form the lateral-directional characteristic equation is

$$\Delta(s) = (s - 0.0014)(s + 4.145)(s^2 + 1.649s + 38.44) = 0 \tag{11.40}$$

and the lateral-directional stability mode characteristics are

spiral mode time constant $T_s = -714$ s

roll mode time constant $T_r = 0.24$ s

dutch roll damping ratio $\zeta_d = 0.133$

dutch roll undamped natural frequency $\omega_d = 6.2$ rad/s

Clearly, the spiral mode is unstable, which is quite typical, and the time constant is sufficiently large that it is most unlikely to give rise to handling problems. In fact, all of the stability characteristics are better than the minimum acceptable for level 1 flying qualities. However, the aircraft is fitted with a simple yaw damper to improve the lateral-directional flying and handling qualities at all flight conditions, including some where the minimum standards are not met. In the following catalogue of root locus plots each plot illustrates the effect of a single feedback loop closure as a function of increasing feedback gain K. It should be noted that, in the original data source, the sign convention for aileron angle is opposite to that adopted in this book. In the following illustrations the aileron sign convention is changed to be consistent with the British notation.

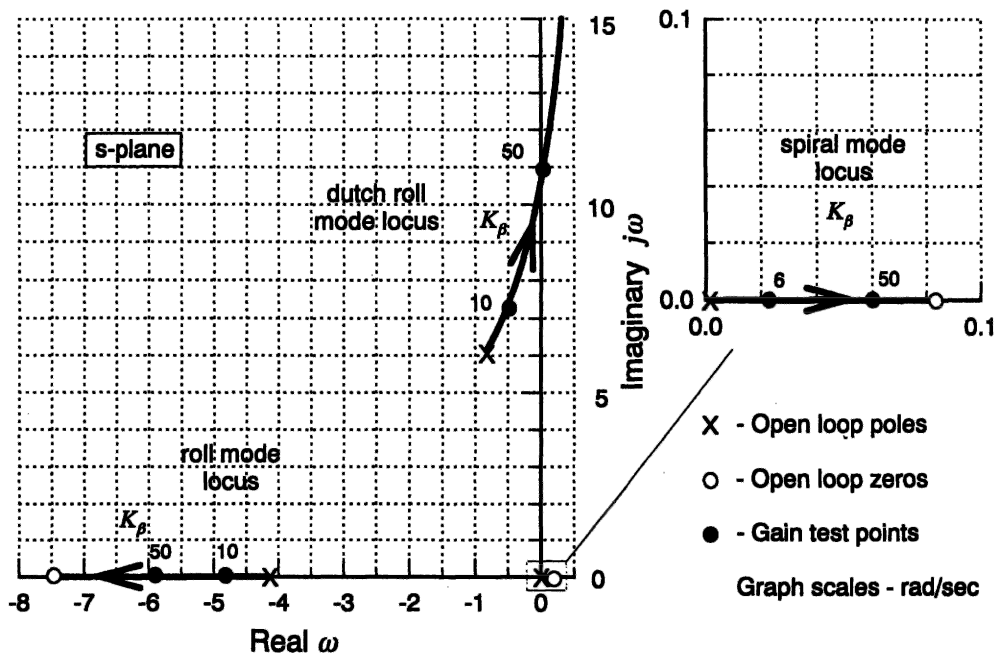

Fig. 11.18 Root locus plot—sideslip angle feedback to aileron

(i) *Sideslip angle feedback to aileron*
The open loop transfer function is

$$\frac{\beta(s)}{\xi(s)} \equiv \frac{N_\xi^\beta(s)}{\Delta(s)} = \frac{1.3235(s-0.0832)(s+7.43)}{(s-0.0014)(s+4.145)(s^2+1.649s+38.44)} \text{ rad/rad} \tag{11.41}$$

and the corresponding root locus plot is shown in Fig. 11.18.

As K_β is increased so the spiral mode pole moves further to the right on the s-plane and its instability is worsened as its time constant is reduced. The roll mode stability is increased as the gain K_β is increased since its pole moves to the left on the s-plane. As K_β is increased the dutch roll frequency is increased whilst its damping is decreased and it eventually becomes unstable at a gain of approximately $K_\beta = 50$ rad/rad. All three modes are relatively insensitive to the feedback since large gains are required to achieve modest changes in the mode characteristics, although the spiral mode is the most sensitive. Negative feedback of sideslip angle to aileron is equivalent to an increase in dihedral effect. In particular, for this example, it augments the magnitude of the stability derivatives l_v and n_v and the degree of augmentation of each derivative depends on the value of K_β and the aileron control derivatives l_ξ and n_ξ respectively. Clearly, the effect is to increase artificially the lateral stiffness of the aeroplane resulting in an increase in dutch roll frequency and a corresponding increase in roll damping. It is unlikely that sideslip angle feedback to aileron alone would find much use in stability augmentation systems.

(ii) *Roll rate feedback to aileron*
The open loop transfer function is

$$\frac{p(s)}{\xi(s)} \equiv \frac{N_\xi^p(s)}{\Delta(s)} = \frac{-27.75(s-0.0005)(s^2+1.55s+41.91)}{(s-0.0014)(s+4.145)(s^2+1.649s+38.44)} \text{ rad/s/rad} \tag{11.42}$$

and the corresponding root locus plot is shown in Fig. 11.19. Note that both the spiral mode pole and the dutch roll poles are approximately cancelled by the numerator zeros. This means that both modes are insensitive to this feedback option.

As K_p is increased so the spiral mode pole moves to the left on the s-plane and its instability is reduced as its time constant is increased. However, the spiral mode remains unstable at all values of K_p although roll rate feedback to aileron generally improves the handling qualities associated with the spiral mode. The roll mode stability increases rapidly as the gain K_p is increased since its pole moves to the left on the s-plane. The roll mode is most sensitive to this feedback option and, in fact, roll rate feedback to aileron describes the classical roll damper and is used in many aeroplanes. Whatever the value of K_p the effect on the stability characteristics of the dutch roll mode is insignificant as stated above. At all levels of feedback gain the dutch roll mode poles remain in a very small localized area on the s-plane. Negative roll rate feedback to aileron is equivalent to an increase in the roll damping properties of the wing. In particular, it augments the magnitude of the stability derivative l_p and, to a lesser extent, n_p. As before, the degree of augmentation of each derivative depends on the value of K_p and the aileron control derivatives l_ξ and n_ξ respectively.

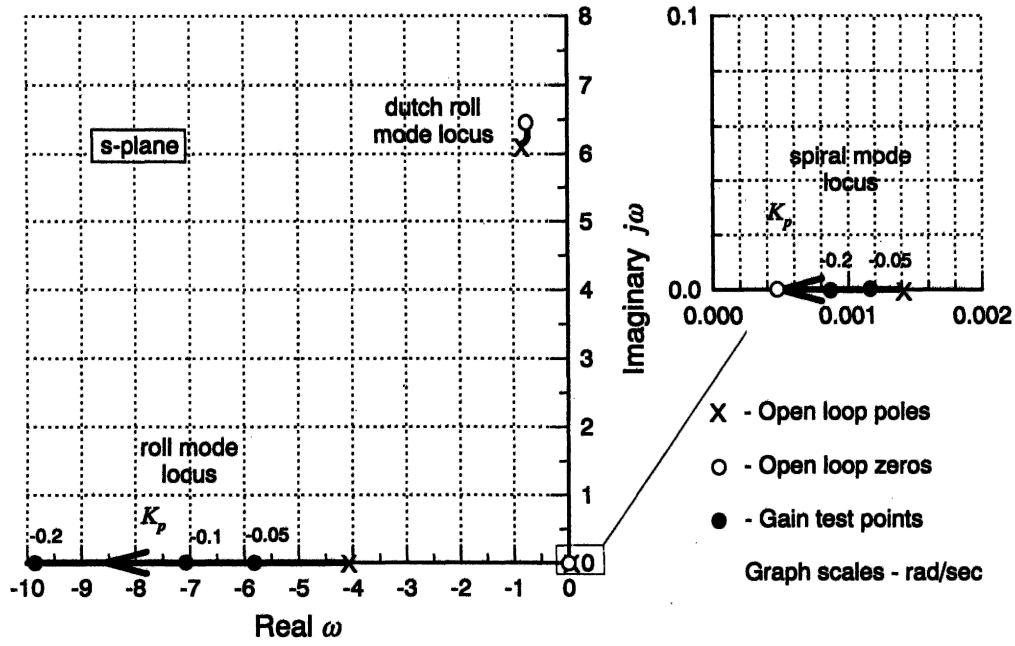

Fig. 11.19 Root locus plot—roll rate feedback to aileron

(iii) *Yaw rate feedback to aileron*
The open loop transfer function is

$$\frac{r(s)}{\xi(s)} \equiv \frac{N_\xi^r(s)}{\Delta(s)} = \frac{-1.712(s+5.405)(s^2+1.788s+4.465)}{(s-0.0014)(s+4.145)(s^2+1.649s+38.44)} \text{ rad/s/rad} \qquad (11.43)$$

and the corresponding root locus plot is shown in Fig. 11.20.

As K_r is increased so the spiral mode pole moves to the left on the s-plane to become stable at a small value of gain. At a gain of approximately $K_r = 6$ rad/rad/s, which is somewhat greater than a practical value, the spiral and roll modes couple to form a low frequency oscillatory characteristic. The roll mode stability decreases as the gain K_r is increased since its pole moves to the right on the s-plane before coupling with the spiral mode. The dutch roll mode is the most sensitive mode and as K_r is increased the damping increases rapidly whilst the frequency increases rather more slowly. At practical levels of feedback gain the most useful improvements would be to stabilize the spiral mode and to improve dutch roll damping whilst degrading roll mode stability only slightly. However, yaw rate feedback to aileron cross-couples both the roll and yaw control axes of the aeroplane and is not so desirable for safety reasons. The feedback is equivalent to an increase in the yaw damping properties of the wing. In particular, it augments the magnitude of the stability derivatives l_r and n_r.

(iv) *Roll attitude feedback to aileron*
The open loop transfer function is

$$\frac{\phi(s)}{\xi(s)} \equiv \frac{N_\xi^\phi(s)}{\Delta(s)} = \frac{-27.75(s^2+1.55s+41.91)}{(s-0.0014)(s+4.145)(s^2+1.649s+38.44)} \text{ rad/rad} \qquad (11.44)$$

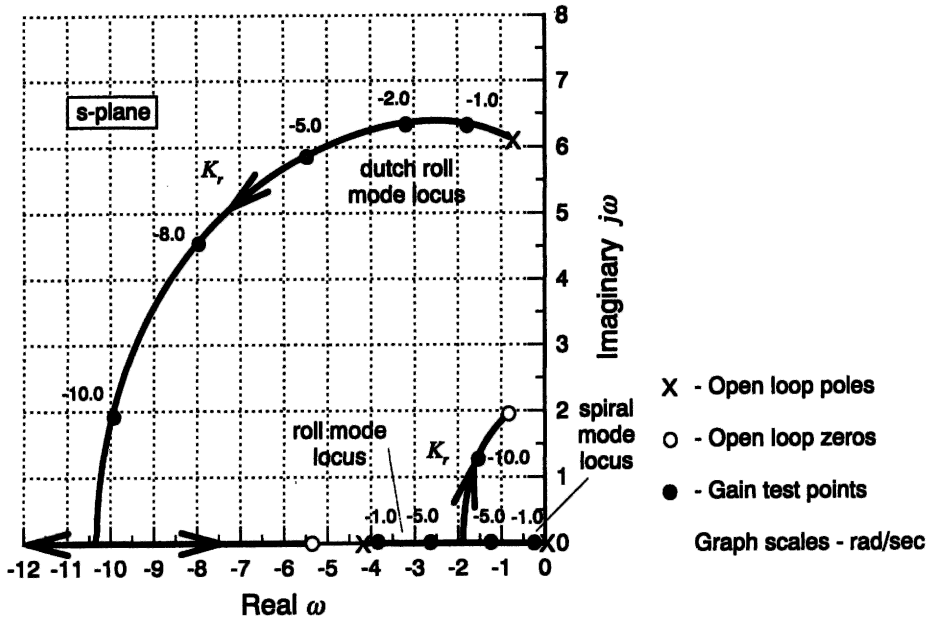

Fig. 11.20 Root locus plot—yaw rate feedback to aileron

and the corresponding root locus plot is shown in Fig. 11.21. Note that the dutch roll poles are approximately cancelled by the numerator zeros, which implies that the mode is insensitive to this feedback option.

As K_ϕ is increased the spiral mode pole moves to the left on the s-plane and its stability increases very rapidly, a very small value of gain being sufficient to place the

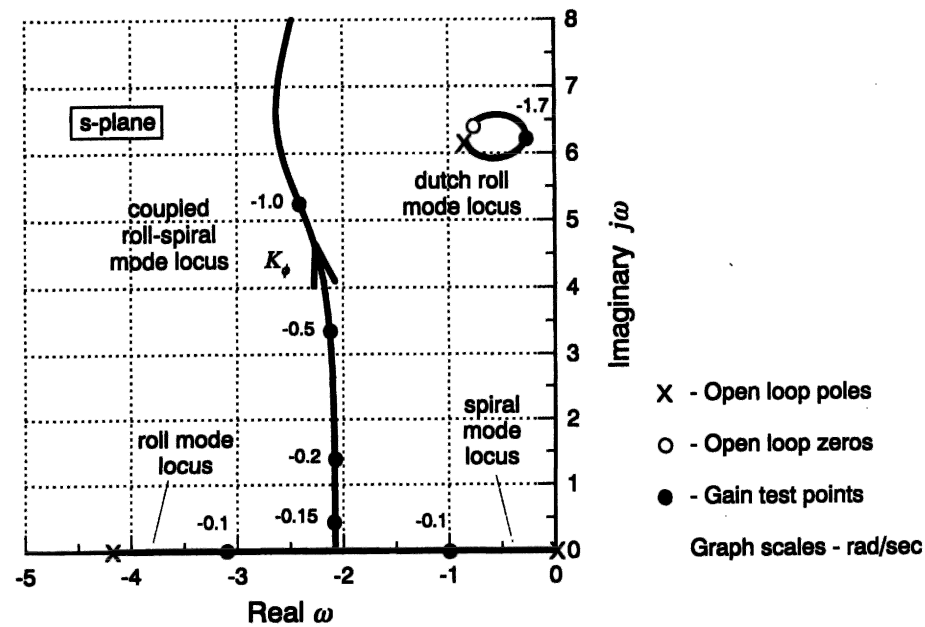

Fig. 11.21 Root locus plot—roll attitude feedback to aileron

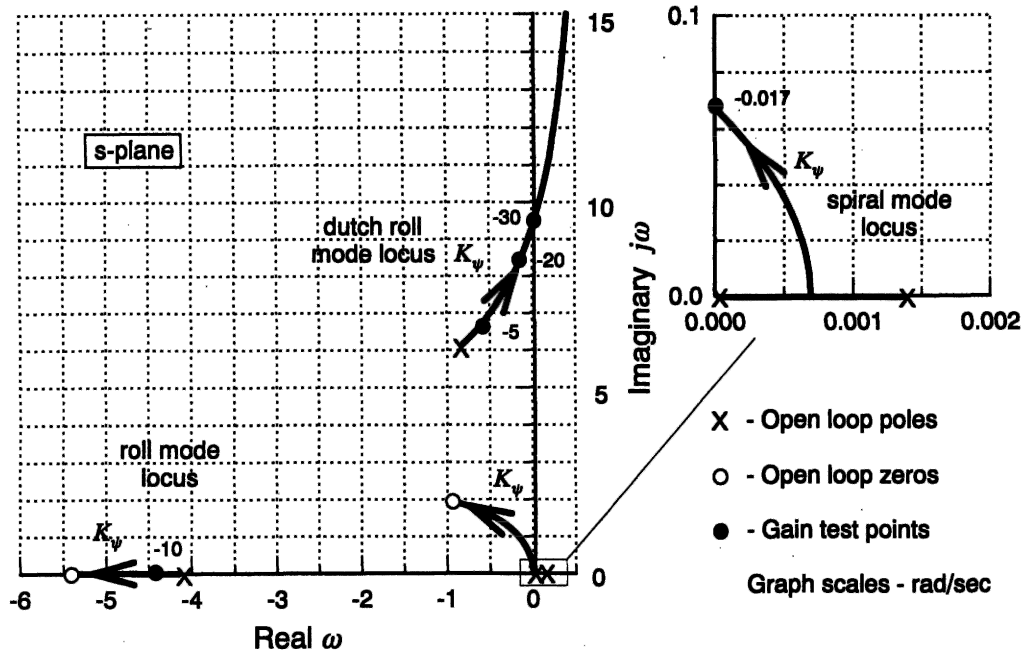

Fig. 11.22 Root locus plot—yaw attitude feedback to aileron

pole on the left half of the s-plane. At a slightly larger value of gain, $K_\phi = -0.14$ rad/rad, the spiral and roll modes couple to form a low frequency oscillatory characteristic as in the previous illustration. Therefore, roll mode stability decreases rapidly as the gain K_ϕ is increased until its pole couples with that of the spiral mode. Clearly, both the roll and spiral modes are most sensitive to this feedback option. As expected, for all values of K_ϕ the effect on the stability characteristics of the dutch roll mode is insignificant. At all levels of feedback gain the dutch roll mode poles remain in a very small localized area on the s-plane and the minimum damping corresponds to a feedback gain of $K_\phi = -1.7$ rad/rad. Negative roll attitude feedback to aileron is, very approximately, equivalent to an increase in roll stiffness and at quite small feedback gain values manifests itself as the coupled roll–spiral oscillatory mode, which may be regarded as a kind of lateral pendulum mode.

(v) *Yaw attitude feedback to aileron*
The open loop transfer function is

$$\frac{\psi(s)}{\xi(s)} \equiv \frac{N_\xi^\psi(s)}{\Delta(s)} = \frac{-1.712(s+5.405)(s^2+1.788s+4.465)}{s(s-0.0014)(s+4.145)(s^2+1.649s+38.44)} \text{ rad/rad} \qquad (11.45)$$

and the corresponding root locus plot is shown in Fig. 11.22.

As K_ψ is increased the spiral mode pole moves to the left on the s-plane, towards the pole at the origin, to which it couples at a very small value of gain indeed to form a low frequency unstable oscillatory characteristic. At a gain of approximately $K_\psi = -0.017$ rad/rad the low frequency oscillatory characteristic becomes stable. The roll mode stability increases very slowly as the gain K_ψ is increased since its pole moves to the left on the s-plane towards the zero at -5.404. As K_ψ is increased the dutch roll

mode frequency increases whilst the damping decreases, both characteristics changing rather slowly. The dutch roll mode eventually becomes unstable at a gain of approximately $K_\psi = -30$ rad/rad. At practical levels of feedback gain the effect on the roll and dutch roll modes is almost insignificant. On the other hand the effect of the feedback on the spiral mode is most significant, even at very low values of gain. As in (iii), yaw attitude feedback to aileron cross-couples both the roll and yaw control axes of the aeroplane and is not so desirable for safety reasons. The feedback is equivalent to an increase in the yaw stiffness properties of the wing.

(vi) *Sideslip angle feedback to rudder*
The open loop transfer function is

$$\frac{\beta(s)}{\zeta(s)} \equiv \frac{N_\zeta^\beta(s)}{\Delta(s)} = \frac{0.10(s-0.0015)(s+4.07)(s+113.4)}{(s-0.0014)(s+4.145)(s^2+1.649s+38.44)} \text{ rad/rad} \qquad (11.46)$$

and the corresponding root locus plot is shown in Fig. 11.23. Note that both the spiral and roll mode poles are very nearly cancelled by numerator zeros. It may therefore be expected that negative sideslip angle feedback to rudder will only significantly augment the dutch roll mode.

As expected, as K_β is increased, both the spiral mode pole and the roll mode pole move to the right on the s-plane but the reduction in stability really is insignificant. As K_β is increased both the dutch roll frequency and damping are increased, the mode eventually becoming critically damped at the absurdly high frequency of $\omega_d = 226$ rad/s at a gain of approximately $K_\beta = 4500$ rad/rad! Negative feedback of sideslip angle to rudder is equivalent to an increase in the weathercock effect of the fin, or yaw stiffness. In particular, for this example, it very effectively augments the magnitude of the stability

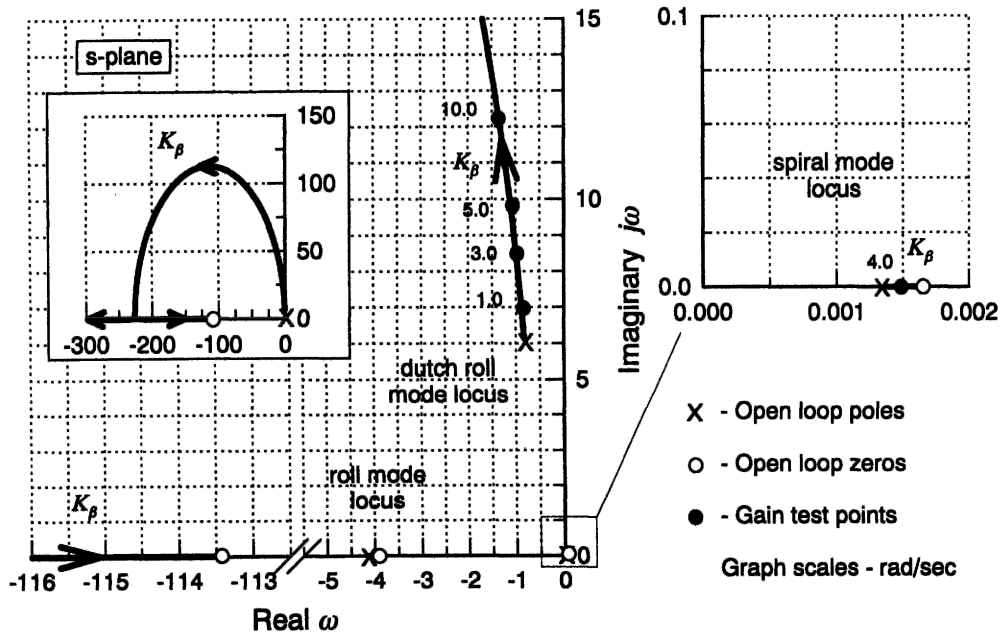

Fig. 11.23 Root locus plot—sideslip angle feedback to rudder

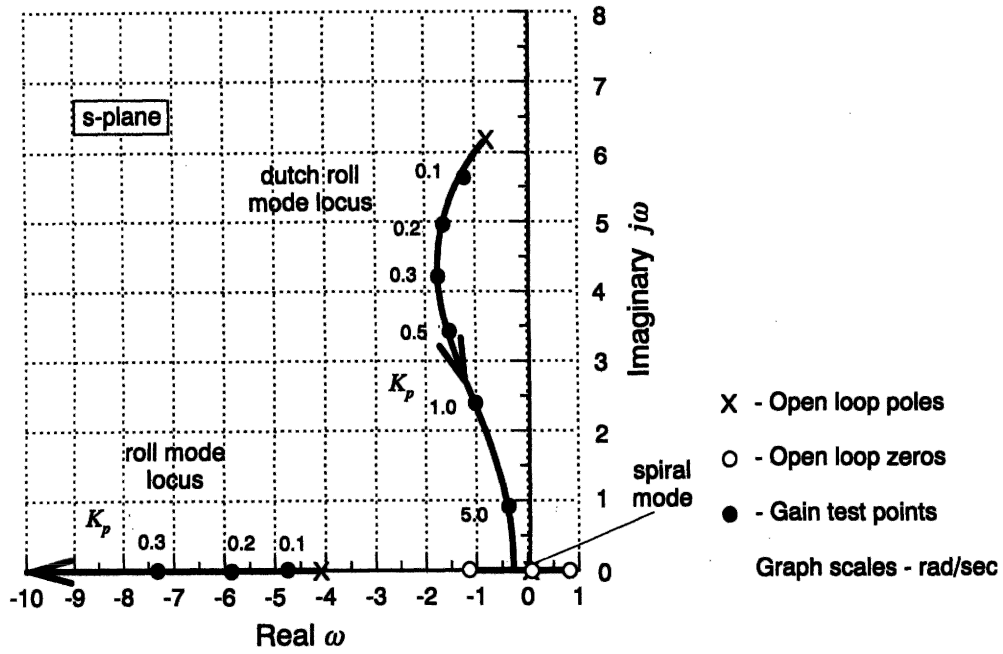

Fig. 11.24 Root locus plot—roll rate feedback to rudder

derivative n_v and to a lesser extent l_v. The degree of augmentation of each derivative depends on the value of K_β and the rudder control derivatives n_ζ and l_ζ respectively. Clearly, the effect is artificially to increase the directional stiffness of the aeroplane resulting in an increase in dutch roll frequency and a corresponding, but much slower, increase in roll damping. At all practical values of feedback gain the dutch roll damping remains more-or-less constant at its open loop value.

(vii) *Roll rate feedback to rudder*
The open loop transfer function is

$$\frac{p(s)}{\zeta(s)} \equiv \frac{N_\zeta^p(s)}{\Delta(s)} = \frac{16.65(s-0.0006)(s-0.79)(s+1.09)}{(s-0.0014)(s+4.145)(s^2+1.649s+38.44)} \text{ rad/s/rad} \qquad (11.47)$$

and the corresponding root locus plot is shown in Fig. 11.24. Note that the spiral mode pole is very approximately cancelled by a numerator zero. It is therefore expected that the spiral mode will be insensitive to this feedback option.

As expected, the effect on the spiral mode of this feedback option is insignificant. The roll mode stability increases rapidly as the gain K_p is increased since its pole moves to the left on the s-plane. The roll mode is quite sensitive to this feedback option, which is not surprising since roll rate is the dominant motion variable in the aircraft dynamics associated with the mode. The dutch roll mode is also very sensitive to this feedback option. As K_p is increased the dutch roll damping increases rapidly whilst the frequency is reduced. For values of the feedback gain $K_p \geqslant 8.9$ rad/rad/s the dutch roll mode is critically damped and is therefore non-oscillatory. Negative roll rate feedback to rudder is equivalent to an increase in the yaw damping properties of the wing. In particular, it augments the magnitude of the stability derivative n_p and, to a lesser extent, l_p. As before, the degree of augmentation

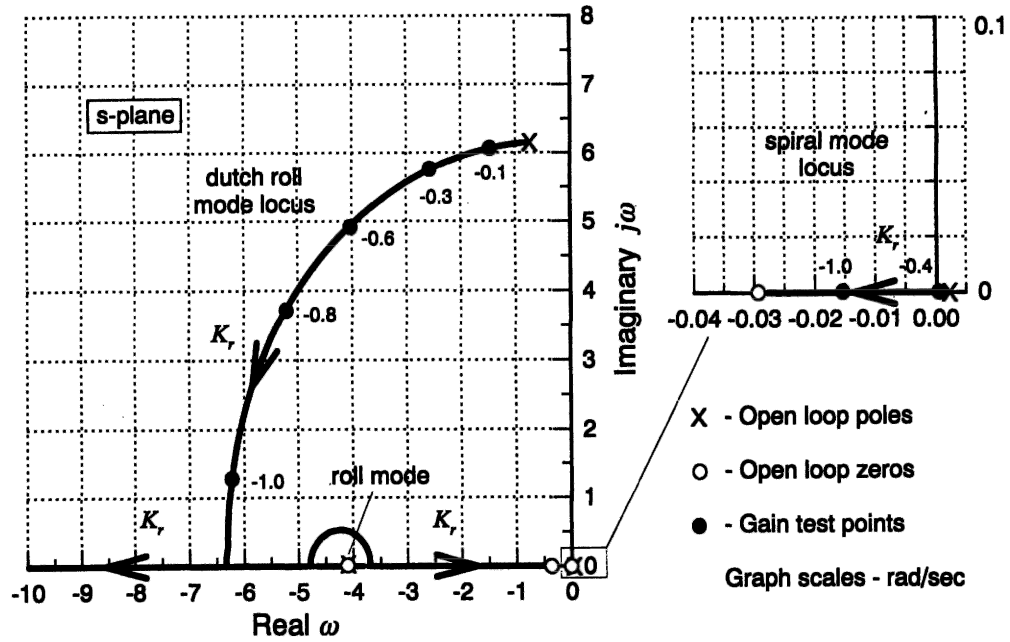

Fig. 11.25 Root locus plot—yaw rate feedback to rudder

of each derivative depends on the value of K_p and the rudder control derivatives n_ζ and l_ζ respectively.

(viii) *Yaw rate feedback to rudder*
The open loop transfer function is

$$\frac{r(s)}{\zeta(s)} \equiv \frac{N_\zeta^r(s)}{\Delta(s)} = \frac{-11.01(s+0.302)(s+0.366)(s+4.11)}{(s-0.0014)(s+4.145)(s^2+1.649s+38.44)} \text{ rad/s/rad} \qquad (11.48)$$

and the corresponding root locus plot is shown in Fig. 11.25. Note that the roll mode pole is almost exactly cancelled by a numerator zero. It is therefore expected that the roll mode will be insensitive to this feedback option.

The spiral mode stability increases rapidly as the gain K_r is increased since its pole moves to the left on the s-plane. The spiral mode is very sensitive to this feedback option and becomes stable at a gain of $K_r = -0.4$ rad/rad/s. As expected, the effect of this feedback option on the roll mode is insignificant. The branching of the loci around the roll mode simply indicates that the pole–zero cancellation is not exact. The dutch roll mode is also very sensitive to this feedback option. As K_r is increased the dutch roll damping increases rapidly whilst the frequency remains almost constant. For values of the feedback gain $K_r \leqslant -1.2$ rad/rad/s the dutch roll mode becomes critically damped. Practical values of feedback gain would, typically, be in the range $0 \geqslant K_r \geqslant -0.7$ rad/rad/s. The dutch roll mode damping is most sensitive to this feedback option, and yaw rate feedback to rudder describes the classical yaw damper, which is probably the most common augmentation system. However, its use brings a bonus since it also improves the spiral mode stability significantly. Negative yaw rate feedback to rudder is equivalent to an increase in the yaw damping properties of the aeroplane, or to an increase in the effectiveness of the fin as a damper. In particular, it augments the magnitude of the stability derivative n_r and, to a lesser extent, l_r.

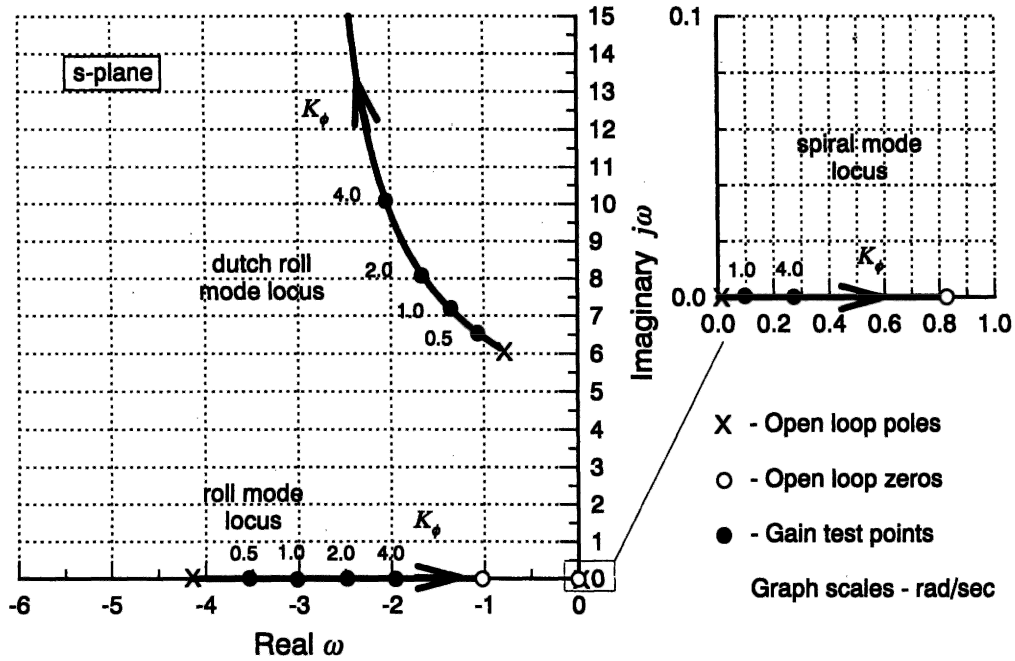

Fig. 11.26 Root locus plot—roll attitude feedback to rudder

(ix) *Roll attitude feedback to rudder*
The open loop transfer function is

$$\frac{\phi(s)}{\zeta(s)} \equiv \frac{N_\zeta^\phi(s)}{\Delta(s)} = \frac{16.5(s-0.825)(s+1.08)}{(s-0.0014)(s+4.145)(s^2+1.649s+38.44)} \text{ rad/rad} \qquad (11.49)$$

and the corresponding root locus plot is shown in Fig. 11.26.

As K_ϕ is increased the spiral mode pole moves to the right on the s-plane and its stability decreases slowly. The roll mode stability also decreases slowly as the gain K_ϕ is increased, a gain of $K_\phi \cong 4.0$ rad/rad being required to double the time constant, for example. As K_ϕ is increased the dutch roll mode frequency increases relatively quickly. The damping ratio also increases a little initially but, as the gain is increased further, the damping decreases steadily to zero at infinite feedback gain. Negative roll attitude feedback to rudder is, very approximately, equivalent to an increase in directional stiffness and is not commonly used in autostabilization systems since it introduces cross-coupling between the roll and yaw control axes.

(x) *Yaw attitude feedback to rudder*
The open loop transfer function is

$$\frac{\psi(s)}{\zeta(s)} \equiv \frac{N_\zeta^\psi(s)}{\Delta(s)} = \frac{-11.01(s+0.0302)(s+0.367)(s+4.11)}{s(s-0.0014)(s+4.145)(s^2+1.649s+38.44)} \text{ rad/rad} \qquad (11.50)$$

and the corresponding root locus plot is shown in Fig. 11.27. Note that the roll mode pole is almost exactly cancelled by a numerator zero indicating that the mode is not sensitive to this feedback option.

As K_ψ is increased, the spiral mode pole moves to the left on the s-plane, towards

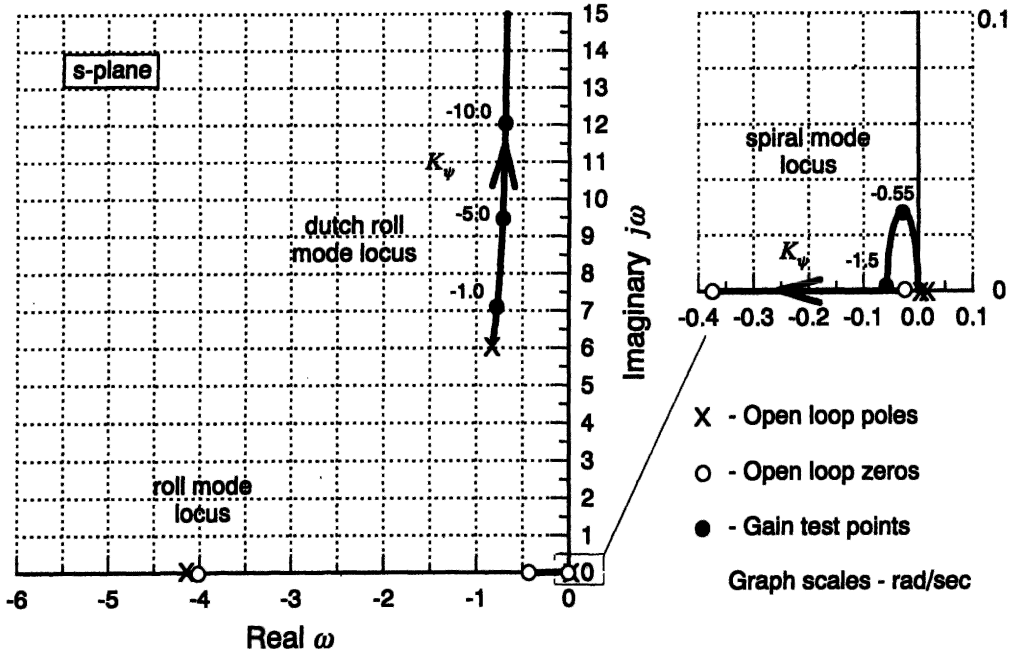

Fig. 11.27 Root locus plot—yaw attitude feedback to rudder

the pole at the origin, to which it couples at a very small value of gain to form a stable low frequency oscillatory characteristic at all practical small values of gain. At a gain of approximately $K_\psi = -1.5$ rad/rad the low frequency oscillatory characteristic becomes critically damped. Since the frequency of this mode is so low, and when stable it is reasonably well damped, it is unlikely to give rise to handling problems. As expected, the roll mode stability remains effectively unchanged by this feedback option. As K_ψ is increased, the dutch roll mode frequency increases whilst the damping decreases, both characteristics changing relatively slowly. The dutch roll mode eventually becomes neutrally stable at infinite feedback gain. At practical levels of feedback gain the effect on the dutch roll mode is to increase the frequency with only a very small reduction in damping. Negative yaw attitude feedback to rudder is equivalent to an increase in directional stiffness and is not commonly used in autostabilization systems.

11.7 The pole placement method

An alternative and very powerful method for designing feedback gains for autostabilization systems is the *pole placement method.* The method is based on the manipulation of the equations of motion in state space form and makes full use of the appropriate computational tools in the analytical process. Practical application of the method to aeroplanes is limited since it assumes that all state, or motion, variables are available for use in an augmentation system, which is not usually the case. However, regardless of the limitations of the method, it can be very useful to the FCS designer in the initial stages of assessment of augmentation system structure.

The state and output matrix equations describing the unaugmented, or open loop, aircraft, equations (5.48), are written

$$\left.\begin{aligned}\dot{\mathbf{x}}(t) &= \mathbf{A}\mathbf{x}(t) + \mathbf{B}\mathbf{u}(t)\\ \mathbf{y}(t) &= \mathbf{C}\mathbf{x}(t) + \mathbf{D}\mathbf{u}(t)\end{aligned}\right\} \tag{11.51}$$

Assuming that augmentation is achieved by negative feedback of the state vector $\mathbf{x}(t)$ to the input vector $\mathbf{u}(t)$ then the control law may be written

$$\mathbf{u}(t) = \mathbf{v}(t) - \mathbf{K}\mathbf{x}(t) \tag{11.52}$$

where $\mathbf{v}(t)$ is a vector of input demand variables and $\mathbf{K}$ is a matrix of feedback gains. Note that equation (11.52) is the general multi-variable equivalent of equation (11.14). The closed loop state and output equations describing the augmented aircraft are obtained by substituting equation (11.52) into equations (11.51)

$$\left.\begin{aligned}\dot{\mathbf{x}}(t) &= [\mathbf{A} - \mathbf{B}\mathbf{K}]\mathbf{x}(t) + \mathbf{B}\mathbf{v}(t)\\ \mathbf{y}(t) &= [\mathbf{C} - \mathbf{D}\mathbf{K}]\mathbf{x}(t) + \mathbf{D}\mathbf{v}(t)\end{aligned}\right\} \tag{11.53}$$

or, more simply,

$$\left.\begin{aligned}\dot{\mathbf{x}}(t) &= \mathbf{A}_{aug}\mathbf{x}(t) + \mathbf{B}\mathbf{v}(t)\\ \mathbf{y}(t) &= \mathbf{C}_{aug}\mathbf{x}(t) + \mathbf{D}\mathbf{v}(t)\end{aligned}\right\} \tag{11.54}$$

Equations (11.54) are solved in exactly the same way as those of the open loop aircraft, equations (11.51), to obtain the response transfer functions for the augmented aircraft. Note that, as discussed in Section 5.6, for typical aircraft applications the direct matrix $\mathbf{D} = 0$, the output matrix $\mathbf{C} = \mathbf{I}$, the identity matrix, and equations (11.51) to (11.54) simplify accordingly.

Now the characteristic equation of the augmented aircraft is given by

$$\Delta_{aug}(s) = |s\mathbf{I} - \mathbf{A}_{aug}| \equiv |s\mathbf{I} - \mathbf{A} + \mathbf{B}\mathbf{K}| = 0 \tag{11.55}$$

and the roots of equation (11.55), or equivalently the eigenvalues of $\mathbf{A}_{aug}$, describe the stability characteristics of the augmented aircraft.

Subject to the constraint that the open loop state equation (11.51) describes a *controllable system*, which an aircraft is, then a feedback matrix $\mathbf{K}$ exists such that the eigenvalues of the closed loop system may be completely specified. Thus, if the required stability and control characteristics of the augmented aircraft are specified, the roots of equation (11.55) may be calculated and, knowing the open loop state and input matrices, $\mathbf{A}$ and $\mathbf{B}$ respectively, then equation (11.55) may be solved to find $\mathbf{K}$. Thus, this method enables the stability characteristics of the augmented aircraft to be designed completely and exactly as required. Equivalently, this therefore means that the poles of the closed loop aircraft may be *placed* on the s-plane exactly as required. However, full state feedback is essential if all of the closed loop poles are to be placed on the s-plane as required.

When the controlled system is *single input* then the feedback matrix $\mathbf{K}$ is unique and only one set of feedback gains will provide the required stability characteristics. When the controlled system is *multi-input* then an infinite number of gain matrices $\mathbf{K}$ may be found which will provide the required stability characteristics. Consequently, most control system design problems involving the use of the pole placement method are

solved by arranging the open loop system as a single input system. This is most easily done when dealing with aircraft stability augmentation since the inputs naturally separate into elevator, ailerons, rudder and thrust at the most basic level. It is a simple matter to arrange the state equation to include only one input variable and then to apply the pole placement method to design an augmentation system feedback structure.

EXAMPLE 11.6

The longitudinal equations of motion for the McDonnell Douglas F-4C Phantom aircraft were obtained from Heffley and Jewell (1972). At the chosen flight condition the weight is 38 925 lb and the aircraft is flying at Mach 1.1 at sea level. The state equations (11.51) were derived for the unaugmented aircraft from the data provided, to give

$$\mathbf{A} = \begin{bmatrix} -0.068 & -0.011 & 0 & -9.81 \\ 0.023 & -2.10 & 375 & 0 \\ 0.011 & -0.160 & -2.20 & 0 \\ 0 & 0 & 1 & 0 \end{bmatrix} \qquad \mathbf{B} = \begin{bmatrix} -0.41 & 1.00 \\ -77.0 & -0.09 \\ -61.0 & -0.11 \\ 0 & 0 \end{bmatrix}$$

with state vector $\mathbf{x}^{\mathrm{T}} = [u \quad w \quad q \quad \theta]$ and input vector $\mathbf{u}^{\mathrm{T}} = [\eta \quad \tau]$. Note that two input variables are given in the model: elevator angle η and thrust τ. Using *Program CC* the equations of motion were solved and the open loop characteristic polynomial was found

$$\Delta(s) = (s^2 + 4.3s + 64.6)(s^2 + 0.07s + 0.003) \tag{11.56}$$

and the corresponding longitudinal stability mode characteristics are

$$\begin{aligned} \text{phugoid damping ratio } \zeta_{\mathrm{p}} &= 0.646 \\ \text{phugoid undamped natural frequency } \omega_{\mathrm{p}} &= 0.054 \text{ rad/s} \\ \text{short period damping ratio } \zeta_{\mathrm{s}} &= 0.267 \\ \text{short period undamped natural frequency } \omega_{\mathrm{s}} &= 8.038 \text{ rad/s} \end{aligned}$$

Referring to the flying qualities requirements in MIL-F-8785C (1980) it was found that for a class IV aeroplane in the most demanding category A flight phase, the Phantom comfortably meets level 1 requirements with the exception of short period mode damping, which is too low. Clearly, some augmentation is required to improve the pitch damping in particular.

The design decision was made to increase the short period mode damping ratio to 0.7 whilst retaining the remaining stability characteristics at the nominal values of the basic unaugmented airframe. A short period mode damping ratio of 0.7 was chosen since this gives a good margin of stability and results in the shortest mode settling time after a disturbance. However, the exact value chosen is not important provided that the margin of stability is adequate to allow for uncertainty in the modelling. Therefore, the pole placement method is to be used to give the augmented aircraft the following longitudinal stability characteristics

phugoid damping ratio $\zeta_p = 0.065$

phugoid undamped natural frequency $\omega_p = 0.054$ rad/s

short period damping ratio $\zeta_s = 0.7$

short period undamped natural frequency $\omega_s = 8.0$ rad/s

Thus, the required closed loop characteristic polynomial is

$$\Delta_{aug}(s) = (s^2 + 11.2s + 64.0)(s^2 + 0.07s + 0.003) \tag{11.57}$$

Since a single input control system is required, the input being elevator angle, the open loop state equation is modified accordingly, simply by removing the thrust terms. The open loop state equation may then be written

$$\begin{bmatrix} \dot{u} \\ \dot{w} \\ \dot{q} \\ \dot{\theta} \end{bmatrix} = \begin{bmatrix} -0.068 & -0.011 & 0 & -9.81 \\ 0.023 & -2.10 & 375 & 0 \\ 0.011 & -0.160 & -2.20 & 0 \\ 0 & 0 & 1 & 0 \end{bmatrix} \begin{bmatrix} u \\ w \\ q \\ \theta \end{bmatrix} + \begin{bmatrix} -0.41 \\ -77.0 \\ -61.0 \\ 0 \end{bmatrix} \eta \tag{11.58}$$

With the aid of the pole placement tool in *Program CC* the feedback gain matrix required to give the augmented aircraft the characteristic polynomial, equation (11.57), was determined

$$\mathbf{K} = [K_u \quad K_w \quad K_q \quad K_\theta] = [-7.7 \times 10^{-6} \quad 5.99 \times 10^{-4} \quad -0.114 \quad -1.96 \times 10^{-4}] \tag{11.59}$$

Care is required in order to maintain the correct units of the elements in the feedback matrix. The stability augmentation system control law is obtained by substituting for $\mathbf{K}$ in equation (11.52) whence

$$\eta = \delta_\eta - K_u u - K_w w - K_q q - K_\theta \theta \tag{11.60}$$

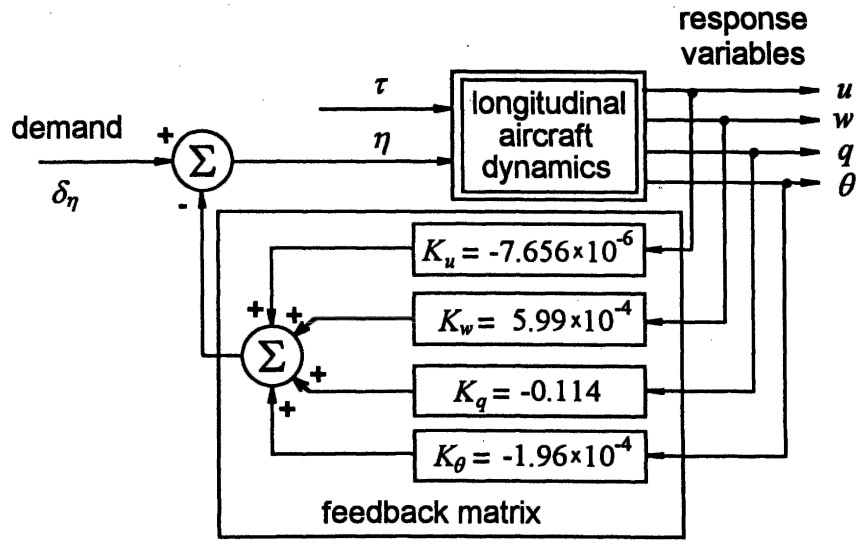

Fig. 11.28 Stability augmentation system with full state feedback

The corresponding closed loop control system structure follows and is shown in Fig. 11.28.

Now, clearly, the choice of closed loop stability characteristics has resulted in a gain matrix in which the gains K_u, K_w and K_θ are impractically and insignificantly small. This is simply due to the fact that the only significant change between the open and closed loop stability characteristics is the increase in short period mode damping and, as has already been established in Examples 11.3 and 11.4, the pole placement method confirms that this can be achieved with pitch rate feedback to elevator alone. If additional changes in the stability characteristics were required then the gains K_u, K_w and K_θ would, of course, not necessarily be insignificant. Let the feedback gain matrix be simplified to include only practical gain values, and equation (11.59) may be written

$$\mathbf{K} = [0 \quad 0 \quad -0.12 \quad 0] \tag{11.61}$$

The closed loop state equation (equation 11.53) may then be calculated by writing

$$\mathbf{K} = \begin{bmatrix} 0 & 0 & -0.12 & 0 \\ 0 & 0 & 0 & 0 \end{bmatrix} \tag{11.62}$$

where the second row describes the feedback to the second, thrust, input, which is not used in this example for the reason given above. $[\mathbf{A} - \mathbf{BK}]$ is easily calculated with the aid of *Program CC* for example and the closed loop state equation, written to include both input variables, is

$$\begin{bmatrix} \dot{u} \\ \dot{w} \\ \dot{q} \\ \dot{\theta} \end{bmatrix} = \begin{bmatrix} -0.068 & -0.011 & -0.049 & -9.81 \\ 0.023 & -2.10 & 366 & 0 \\ 0.011 & -0.160 & -9.52 & 0 \\ 0 & 0 & 1 & 0 \end{bmatrix} \begin{bmatrix} u \\ w \\ q \\ \theta \end{bmatrix} + \begin{bmatrix} -0.41 & 1.00 \\ -77.0 & -0.09 \\ -61.0 & -0.11 \\ 0 & 0 \end{bmatrix} \begin{bmatrix} \eta \\ \tau \end{bmatrix} \tag{11.63}$$

Comparison of the open loop equation (11.58) and the closed loop equation (11.63) indicates, as expected, that the only changes occur in the third column of the state matrix, the column associated with the variable q. The augmented state equation (11.63) is readily solved to obtain the closed loop transfer function matrix

$$\begin{bmatrix} u(s) \\ w(s) \\ q(s) \\ \theta(s) \end{bmatrix} = \mathbf{G}(s) \begin{bmatrix} \eta(s) \\ \tau(s) \end{bmatrix} = \frac{\mathbf{N}(s)}{\Delta_{aug}(s)} \begin{bmatrix} \eta(s) \\ \tau(s) \end{bmatrix} \tag{11.64}$$

where the numerator matrix is given by

$$\mathbf{N}(s) = \begin{bmatrix} -0.41(s+1.36)(s-44.45)(s+45.31) & 1.0(s+0.027)(s^2+11.60s+79.75) \\ -77.0(s-0.003)(s+0.071)(s+299.3) & -0.09(s+0.008)(s-0.044)(s+456.4) \\ -61.0s(s+0.068)(s+1.90) & -0.11s(s-0.022)(s+1.96) \\ -61.0(s+0.068)(s+1.90) & -0.11(s-0.022)(s+1.96) \end{bmatrix} \tag{11.65}$$

and the closed loop characteristic polynomial is

$$\Delta_{aug}(s) = (s^2 + 11.62s + 78.49)(s^2 + 0.07s + 0.002) \tag{11.66}$$

The corresponding longitudinal stability mode characteristics are

$$\text{phugoid damping ratio } \zeta_p = 0.71$$
$$\text{phugoid undamped natural frequency } \omega_p = 0.049 \text{ rad/s}$$
$$\text{short period damping ratio } \zeta_s = 0.656$$
$$\text{short period undamped natural frequency } \omega_s = 8.86 \text{ rad/s}$$

Thus, by simplifying the feedback gain matrix to an approximate equivalent it is not surprising that the specified stability characteristics, defined by equation (11.57), have also only been achieved approximately. However, the differences are small and are quite acceptable. The main objective, to increase the short period mode damping to a reasonable level, has been achieved comfortably. The changes in the stability characteristics caused by the feedback are in complete agreement with the observations made in Examples 11.3 and 11.4.

Note that the numerators of the closed loop transfer functions describing response to elevator, given in the first column of the numerator matrix in equation (11.65), are unchanged by the feedback, which is also in accordance with earlier findings concerning the effect of feedback. However, the numerators of the closed loop transfer functions describing response to thrust, given in the second column of the numerator matrix in equation (11.65), include some changes. The numerators $N_\tau^u(s)$ and $N_\tau^w(s)$ are both changed a little by the effect of feedback, whereas the numerators $N_\tau^q(s)$ and $N_\tau^\theta(s)$ remain unchanged.

It will be noted that the longitudinal stability augmentation for the F-4A could just as easily have been 'designed' with the aid of a single-input single-output root locus plot as described in Example 11.3. However, the subsequent calculation of the closed loop response transfer functions would have been rather more laborious. The pole placement method is undoubtedly a very powerful design tool, especially for the preliminary assessment of the feedback gains needed to achieve a specified level of closed loop stability. Once the gains required to achieve a given set of augmented stability characteristics have been determined their values will not be significantly changed by subsequent increases in flight control system complexity. The main disadvantage of the method, especially in aircraft applications, is that it assumes all motion variables are sensed and are available for use in a control system. This is not often the case. Then it is necessary to simplify the feedback structure, making use of the understanding provided by Examples 11.4 and 11.5, to achieve a reasonable performance compromise—much as illustrated by this example.

It is also good practice to minimize the demands on the augmentation system by limiting the required changes to the stability characteristics. Remember that small changes result in small feedback gains, again, much as illustrated by this example.

References

Anon. 1980: *Military Specification—Flying Qualities of Piloted Airplanes.* MIL-F-8785C. Department of Defense, USA.

Evans, W. R. 1954: *Control-System Dynamics.* McGraw-Hill Book Company, New York.

Friedland, B. 1987: *Control System Design.* McGraw-Hill Book Company, New York.

Heffley, R. K. and Jewell, W. F. 1972: *Aircraft Handling Qualities Data.* NASA Contractor Report, NASA CR-2144.

Teper, G. L. 1969: *Aircraft Stability and Control Data.* Systems Technology, Inc, STI Technical Report 176-1.

12

Aerodynamic Modelling

12.1 Introduction

Probably the most difficult task confronting the flight dynamicist is the identification and quantification of the aerodynamic description of the aeroplane for use in the equations of motion. *Aerodynamic modelling* is concerned with the development of mathematical models to describe the aerodynamic forces and moments acting on the airframe. As the flow conditions around the airframe are generally complex any attempt to describe the aerodynamic phenomena mathematically must result in compromise. Obviously, the most desirable objective is to devise the most accurate mathematical description of the airframe aerodynamics as can possibly be achieved. Unfortunately, even if accurate mathematical models can be devised they are often difficult to handle in an analytical context and do not, in general, lend themselves to application to the linearized equations of motion. Therefore, the solution to the problem is to seek simpler approximate aerodynamic models which can be used in the equations of motion and which represent the aerodynamic properties of the airframe with an acceptable degree of accuracy. A consequence of this is that the aerodynamic models are only valid for a small range of operating conditions and, therefore, the solution of the equations of motion is also only valid for the same limited range of conditions. By repeating this procedure at many points within the flight envelope of the aeroplane an acceptable 'picture' of its dynamic properties can be built up, subject of course to the limitations of the modelling techniques used.

In the present context *aerodynamic stability and control derivatives* are used to model the aerodynamic properties of the aeroplane. The concept of the aerodynamic derivative as a means for describing aerodynamic force and moment characteristics is introduced and described in Chapter 4, Section 4.2. The use of the aerodynamic derivative as a means for explaining the dependence of the more important dynamic characteristics of the aeroplane on its dominant aerodynamic properties follows in subsequent chapters, in particular Chapters 6 and 7.

In the illustrations, only those derivatives associated with the dominant aerodynamic effects have been discussed. Clearly, if the most important aerodynamic properties ascribed to every derivative are known then a more subtle and expansive interpretation of aircraft dynamics may be made in the analysis of the response transfer functions. Thus, a good understanding of the origin, meaning and limitation of the aerodynamic

derivatives provides the means by which the flight dynamicist may achieve very considerable insight into the subtleties of aircraft dynamics and into the aircraft's flying and handling qualities. In the author's opinion, this knowledge is also essential for the designer of stability augmentation systems for the reasons illustrated in Chapter 11.

Thus, this chapter is concerned with a preliminary review of, and introduction to, aerodynamic stability and control derivatives at the simplest level consistent with the foregoing material. However, it must be remembered that alternative methods for aerodynamic modelling are commonly in use when rather greater detail is required in the equations of motion. For example, in continuous simulation models, the equations of motion may well be non-linear and the aerodynamic models are correspondingly rather more complex. Or, today, it is common practice to investigate analytically the dynamic behaviour of combat aircraft at very high angles of incidence, conditions which may be grossly non-linear and for which the aerodynamic derivative would be incapable of providing an adequate description of the aerodynamics. For such applications, experimental or semi-empirical sources of aerodynamic information would be more appropriate. Whatever the source of the aerodynamic models, simple or complex, the best that can be achieved is an *estimate* of the aerodynamic properties. This immediately prompts the question, *how good is the estimate*? This question is not easy to answer and depends ultimately on the confidence in the aerodynamic modelling process and the fidelity of the aircraft dynamics derived from the aerodynamic model.

12.2 Quasi-static derivatives

In order to appreciate the 'meaning' of the aerodynamic derivative consider, for example, the derivative which quantifies *normal force due to rate of pitch*, denoted

$$\mathring{Z}_q = \frac{\partial Z}{\partial q} \tag{12.1}$$

The component of normal force experienced by the aircraft resulting from a pitch velocity perturbation is therefore given by

$$Z = \mathring{Z}_q q \tag{12.2}$$

Now, in general, the disturbance giving rise to the pitch rate perturbation will also include perturbations in the other motion variables which will give rise to additional components of normal force, as indicated by the appropriate terms in the aerodynamic normal force model included in equations (4.37). However, when considering the derivative $\mathring{Z}_q$ it is usual to consider its effect in isolation, as if the perturbation comprised only pitch rate. Similarly, the effects of all the other derivatives are also considered in isolation by assuming the perturbation to comprise only the motion appropriate to the derivative in question.

By definition, the equations of motion, equations (4.37), in which the derivatives appear, describe small perturbation motion about a steady trimmed equilibrium flight condition. Thus, for example, in the undisturbed state the component of normal force Z given by equation (12.2) will be zero since the perturbation variable q is zero. Similarly, all the aerodynamic force and moment components in all of the small perturbation equations of motion will be zero at the trim condition. The point of this perhaps obvious statement is to emphasize that, in the present context, the aerodynamic derivatives only play a part in determining the motion of the aeroplane when it is in a state of 'dynamic

upset' with respect to its initial trim condition. As described in earlier chapters, the state of dynamic upset is referred to equivalently as a perturbation about the equilibrium condition and is usually transient in nature. Thus, to be strictly applicable to the dynamic conditions they describe, the derivatives should be expressed in terms of the non-steady aerodynamic conditions they attempt to quantify—clearly a difficult demand!

Since the motion of interest is limited, by definition, to small perturbations about equilibrium, then in the limit the perturbations tend to zero and the dynamic condition becomes coincident with the equilibrium flight condition. It is therefore common practice to evaluate the aerodynamic derivatives at the steady equilibrium condition and to assume that they are applicable to the small perturbation motion about that equilibrium. This procedure gives rise to the so-called *quasi-static aerodynamic derivatives*: quantities based on, and derived from, static aerodynamic conditions but which are used in the description of dynamically varying aerodynamic conditions.

Aerodynamic derivatives obtained by this means seem to be quite adequate for studies of small perturbation dynamics but, not surprisingly, become increasingly inappropriate as the magnitude of the perturbation is increased. As suggested above, studies of large amplitude dynamics require rather more sophisticated methods of aerodynamic modelling.

To illustrate the concept of the quasi-static derivative, consider the contribution of aerodynamic drag D to the axial force X acting on the aircraft in a disturbance. Assuming that the aircraft axes are wind axes then

$$X = -D \tag{12.3}$$

A typical aerodynamic drag–velocity plot is shown in Fig. 12.1. Let the steady equilibrium velocity be V_0 at the flight condition of interest, which defines the operating

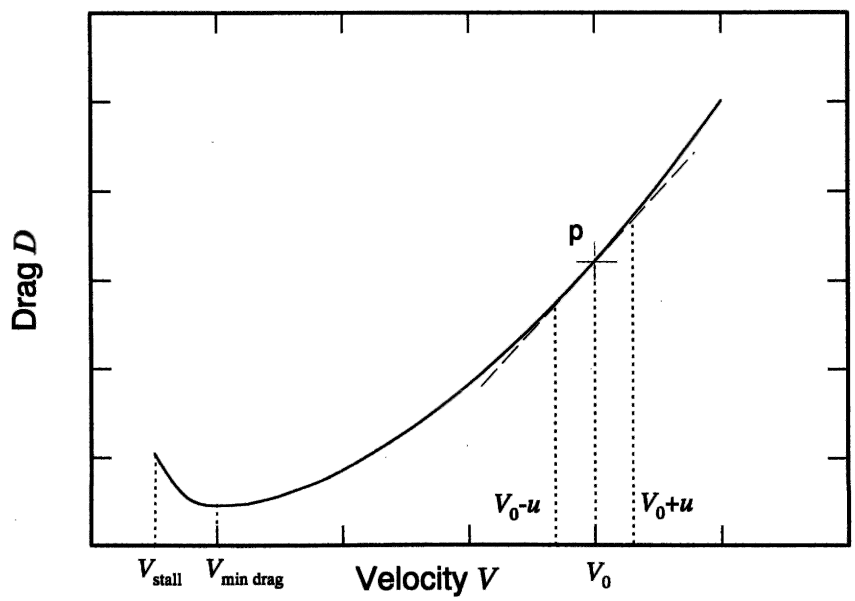

Fig. 12.1 A typical aerodynamic drag–velocity characteristic

point p on the plot. Now let the aeroplane be subjected to a disturbance giving rise to a small velocity perturbation $\pm u$ about the operating point as indicated. The derivative *axial force due to velocity* is defined

$$\mathring{X}_u = \frac{\partial X}{\partial U} \equiv \frac{\partial X}{\partial V} \tag{12.4}$$

where the total perturbation velocity component along the x axis is given by

$$U = U_e + u \equiv V_0 + u \equiv V \tag{12.5}$$

whence

$$\mathring{X}_u = -\frac{\partial D}{\partial V} \tag{12.6}$$

and the slope of the drag–velocity plot at p gives the quasi-static value of the derivative $\mathring{X}_u$ at the flight condition corresponding to the trimmed velocity V_0. Some further simple analysis is possible since the drag is given by

$$D = \frac{1}{2}\rho V^2 S C_D \tag{12.7}$$

and assuming the air density ρ remains constant, since the perturbation is small, then

$$\frac{\partial D}{\partial V} = \tfrac{1}{2}\rho V S\left(2C_D + V\frac{\partial C_D}{\partial V}\right) \tag{12.8}$$

To define the derivative $\mathring{X}_u$ at the flight condition of interest, let the perturbation become vanishingly small such that $u \to 0$ and hence $V \to V_0$. Then, from equations (12.6) and (12.8)

$$\mathring{X}_u = -\tfrac{1}{2}\rho V_0 S\left(2C_D + V_0\frac{\partial C_D}{\partial V}\right) \tag{12.9}$$

where C_D and $\partial C_D/\partial V$ are evaluated at velocity V_0. Thus, in order to evaluate the derivative, the governing aerodynamic properties are *linearized about the operating point* of interest, which is a direct consequence of the assumption that the perturbation is small. A similar procedure enables all of the aerodynamic stability and control derivatives to be evaluated, although the governing aerodynamic properties may not always lend themselves to such simple interpretation.

It is important to note that in the above illustration the derivative $\mathring{X}_u$ varies with velocity. In general, most derivatives vary with velocity, or Mach number, altitude and incidence. In fact many derivatives demonstrate significant and sometimes abrupt changes over the flight envelope, especially in the transonic region.

12.3 Derivative estimation

A number of methods are used to evaluate the aerodynamic derivatives. However, whichever method is used the resulting evaluations can, at best, only be regarded as *estimates* of the exact values. The degree of confidence associated with the derivative estimates is dependent on the quality of the aerodynamic source material and the method of evaluation used. It is generally possible to obtain estimates of the longitudinal aerodynamic derivatives with a greater degree of confidence than can usually be ascribed to estimates of the lateral-directional aerodynamic derivatives.

12.3.1 CALCULATION

The calculation of derivatives from first principles using approximate mathematical models of the aerodynamic properties of the airframe is probably the simplest and least accurate method of estimation. In particular, it can provide estimates of questionable validity, especially for the lateral-directional derivatives. However, since the approximate aerodynamic models used are based on an understanding of the physical phenomena involved, simple calculation confers significant advantage as a means for gaining insight into the dominant aerodynamic properties driving the airframe dynamics. Hence, an appreciation of the theoretical methods of estimating aerodynamic derivatives provides a sound foundation on which to build most analytical flight dynamics studies.

In order to improve on the often poor derivative estimates obtained by calculation, *semi-empirical* methods of estimation have evolved in the light of experience gained from the earliest days of aviation to the present. Semi-empirical methods are based on simple theoretical calculation, modified with the addition of generalized aerodynamic data obtained from experimental sources and accumulated over many years. Semi-empirical methods are generally made available in various series of reference documents and, today, many are also available as interactive computer programs. In the UK the Engineering Sciences Data Unit (ESDU) publishes a number of volumes on aerodynamics of which some are specifically concerned with aerodynamic derivative estimation. Similar source material is also published in the USA (DATCOM) and elsewhere.

Use of the semi-empirical data items requires some limited information about the geometry and aerodynamics of the subject aeroplane at the outset. The investigator then works through the estimation process, which involves calculation and frequent reference to graphical data and nomograms, to arrive at an estimate of the value of the derivative at the flight condition of interest. Such is the state of development of these methods that it is now possible to obtain derivative estimates of good accuracy, at least for aeroplanes having conventional configurations.

Because of the recurring need to estimate aircraft stability and control derivatives a number of authors have written computer programs to calculate derivatives with varying degrees of success. Indeed, a number of the ESDU data items are now available as computer software. The program by Mitchell (1973) and its subsequent modification by Ross and Benger (1975) has enjoyed some popularity, especially for preliminary estimates of the stability and control characteristics of new aircraft configurations. The text by Smetana (1984) also includes listings for a number of useful computer programs concerned with aircraft performance and stability.

12.3.2 WIND TUNNEL MEASUREMENT

The classical wind tunnel test is one in which a reduced scale model of the aircraft is attached to a balance and the six components of force and moment are measured for various combinations of wind velocity, incidence angle, sideslip angle and control surface angle. The essential feature of such tests is that the conditions are *static* when the measurements are made. Provided the experiments are carefully designed and executed wind tunnel tests can give good estimates of the force–velocity and moment–velocity derivatives in particular. Scale effects can give rise to accuracy problems,

especially when difficult full scale flight conditions are simulated, and although some derivatives can be estimated with good accuracy it may be very difficult to devise experiments to measure other derivatives adequately. However, despite the limitations of the experimental methods, measurements are made for real aerodynamic flow conditions and, in principle, it is possible to obtain derivative estimates of greater fidelity than is likely by calculation.

Dynamic, or non-stationary, experiments can be conducted from which estimates for the force-rotary and moment-rotary derivatives can be made. The simplest of these requires a special rig in which to mount the model and which enables the model to undergo a single degree of freedom free or forced oscillation in either roll, pitch or yaw. Analysis of the oscillatory time response obtained in such an experiment enables estimates to be made of the relevant damping and stiffness derivatives. For example, an oscillatory pitch experiment enables estimates to be made of $\mathring{M}_q$ and $\mathring{M}_w$. More complex multi-degree of freedom test rigs become necessary when it is intended to measure the motion coupling derivatives, for example derivatives like yawing moment due to roll rate $\mathring{N}_p$. As the experimental complexity is increased so the complexity of the analysis required to calculate the derivative estimates from the measurements is also increased and, consequently, it becomes more difficult to guarantee the accuracy of the derivatives thus obtained.

12.3.3 FLIGHT TEST MEASUREMENT

The estimation of aerodynamic derivatives from flight test measurements is an established and well-developed experimental process. However, derivative estimates are usually obtained indirectly since it is not possible to measure the aerodynamic components of force and moment acting on the airframe directly. Also, since the aircraft has six degrees of freedom it is not always possible to perturb the single motion variable of interest without perturbing some, or all, of the others as well. However, as in wind tunnel testing, some derivatives are easily estimated from the flight test experiment with a good degree of confidence, whereas others can be notoriously difficult to estimate.

Although it is relatively easy to set up approximately steady conditions in flight from which direct estimates of some derivatives can be made, for example a steady sideslip for the estimation of $\mathring{Y}_v$, $\mathring{L}_v$ and $\mathring{N}_v$, the technique often produces results of indifferent accuracy and has limited usefulness. Today *parameter identification* techniques are commonly used in which measurements are made following the deliberate excitation of multi-variable dynamic conditions. Complex multi-variable response analysis then follows from which it is possible to derive a complete estimate of the mathematical model of the aircraft corresponding to the flight condition at which the measurements were made.

Parameter identification is an analytical process in which full use is made of state space computational tools in order to estimate the aircraft state description that best matches the input–output response measured in flight. It is essentially a multi-variable curve fitting procedure and the computational output is the coefficients in the aircraft state equation from which estimates of the aerodynamic stability and control derivatives may be obtained. The method is complex and success depends, to a considerable extent, on the correct choice of computational algorithm appropriate to the experiment.

A simple diagram containing the essential functions of the parameter identification procedure is shown in Fig. 12.2. A flight test exercise is flown in the fully instrumented

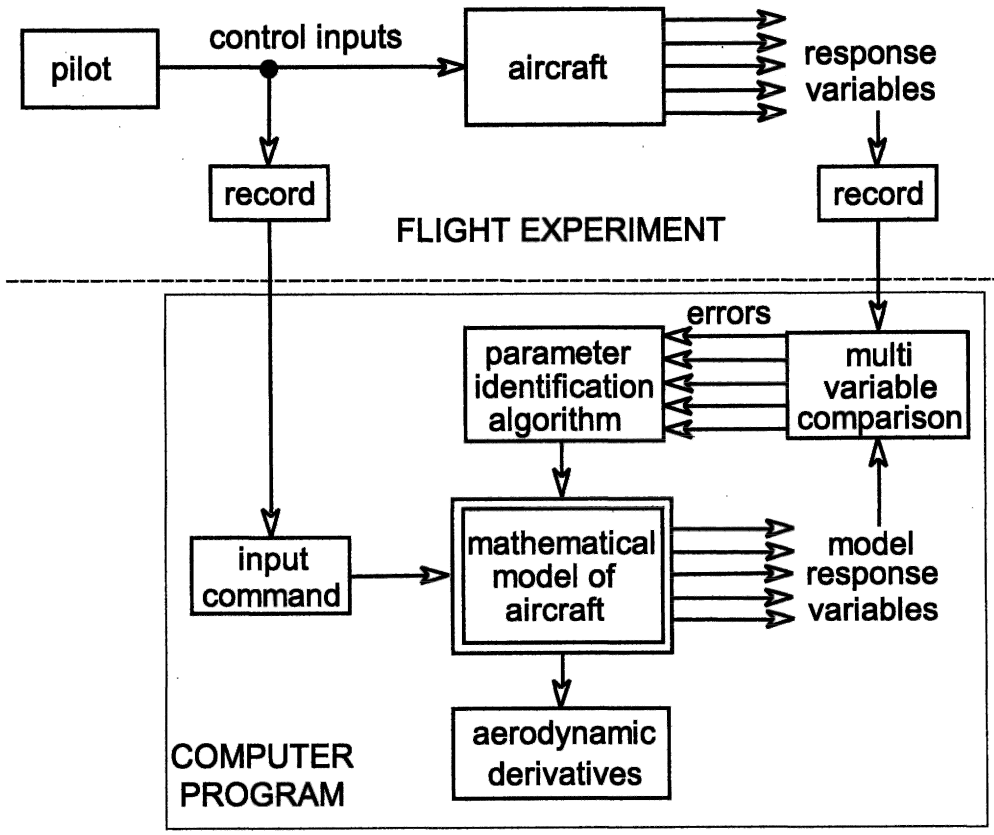

Fig. 12.2 The parameter identification process

subject aircraft and the pilot applies control inputs designed to excite the dynamic response of interest. The control inputs and the full complement of dynamic response variables are recorded *in situ* or may be telemetered directly to a ground station for on-line analysis.

The parameter identification process is entirely computational and is based on a mathematical model of the aeroplane that is deliberately structured to include the terms appropriate to the flight experiment. The object then is to identify the coefficients in the aircraft model that give the best match with the dynamics of the experimental response.

The recorded control inputs are applied to the model of the aircraft and its multi-variable response is compared with the recorded response made in the flight experiment. Response matching errors are then used to adjust the coefficients in the aircraft model according to the parameter identification algorithm and the process is repeated iteratively until the response matching errors are minimized.

All of the recorded signals contain noise, measurement errors and uncertainties of various kinds to a greater or lesser extent. The complexity of the identification process is therefore magnified considerably since statistical analysis methods play an essential part in all modern algorithms. For example, Kalman filtering techniques are frequently used to obtain consistent, and essentially error free, estimates of the state variables for

subsequent use in the identification process. Typical commonly encountered parameter identification algorithms include the *Equation Error* method, the *Maximum Likelihood* method and various methods based on *Statistical Regression* techniques. The development of parameter identification methods for application to aeronautical problems has been the subject of considerable research over the last 25 years or so and a vast wealth of published material is available. A more detailed discussion of the subject is well beyond the scope of this book.

Few, if any, books have been published which are entirely concerned with aircraft parameter identification. Most of the available material appears to be contained in research papers. However, the interested reader will find a useful collection of aircraft related papers in AGARD (1979). It is rare to find published listings of parameter identification computer programs, which makes the work by Ross and Foster (1976) especially useful, if somewhat dated. Probably two of the more useful sources of information on current developments in aircraft parameter identification are the proceedings of the AIAA annual Flight Mechanics and bi-annual Flight Test conferences.

The main disadvantages of parameter identification methods include the requirement for substantial computational 'power' and the essential need for recorded flight data of the very highest quality. Despite these constraints, the process is now used routinely by many of the leading flight test organizations. Given adequate resources the advantages of parameter identification methods are significant. All of the aerodynamic stability and control derivatives can be estimated in one pass and the dynamic conditions to which they relate do not necessarily have to be linear. For example, it is now routinely possible to identify aircraft models in extreme manoeuvring conditions such as the stall, the spin and at very high angles of attack when the aerodynamics are substantially non-linear. It is interesting to note that the method can also be used for estimating aerodynamic derivatives from 'dynamic' wind tunnel experiments.

12.4 The effects of compressibility

The onset of compressible flow conditions gives rise to changes in the aerodynamic properties of the aeroplane which, in general, leads to corresponding changes in the stability and control characteristics. Clearly this means a change in the flying and handling qualities of the aeroplane as the Mach number envelope is traversed. Typically, compressibility effects begin to become apparent at a Mach number of approximately 0.3, although changes in the stability and control characteristics may not become significant until the Mach number reaches 0.6 or more. As Mach number is increased the changes due to compressibility are continuous and gradual. However, in the transonic flow regime changes can be dramatic and abrupt. When appropriate, it is therefore important that the aerodynamic changes arising from the effects of compressibility are allowed for in even the simplest and most approximate aerodynamic derivative estimation procedure.

An interesting chapter on the effects of compressibility on aircraft stability, control and handling may be found in Hilton (1952). However, it must be remembered that at the time the book was written the problems were very clearly recognized but the mathematical models used to describe the phenomena were, in most cases, at an early stage of development. Today, sophisticated computational tools are commonly used to deal with the problems of modelling compressible aerodynamics. However, the simpler

models described by Hilton (1952) are still applicable, as will be shown in the following pages, provided their limitations are appreciated.

12.4.1 SOME USEFUL DEFINITIONS

Mach number M is defined as the ratio of the local flow velocity V to the local speed of sound a, whence

$$M = \frac{V}{a} \tag{12.10}$$

Subsonic flight commonly refers to local aerodynamic flow conditions where $M < 1.0$. Practically, this means that the free stream Mach number is less than approximately 0.8.

Transonic flight usually refers to generally subsonic flight but where the local flow Mach number $M \geqslant 1.0$. Practically, transonic flight conditions are assumed when the free stream Mach number lies in the range $0.8 < M_0 < 1.2$. The greatest degree of aerodynamic unpredictability is associated with this Mach number range.

Supersonic flight commonly refers to aerodynamic flow conditions when $M > 1.0$ everywhere in the local flow field. Practically, supersonic flow conditions are assumed when the free stream Mach number is greater than approximately 1.2.

The *critical Mach number* M_{crit} is the free stream Mach number at which the local flow Mach number just reaches unity at some point on the airframe. In general, $M_{crit} < 1.0$ and is typically of the order of 0.9.

A *shock wave* is a compression wavefront which occurs in the supersonic flow field around an airframe. A shock wave originating at a point on the airframe, such as the nose of the aeroplane, is initially a plane wavefront normal to the direction of the flow. As the flow Mach number is increased, so the shock wave becomes a conical wavefront, or *Mach cone*, the apex angle of which decreases with increasing Mach number. As the air flow traverses the shock wave it experiences an abrupt increase in pressure, density and temperature and the energy associated with these changes is extracted from the total flow energy to result in reduced velocity behind the wavefront. Collectively, these changes are seen as an abrupt increase in drag in particular and may be accompanied by significant changes in trim and in the stability and control characteristics of the aeroplane.

The *shock stall* is sometimes used to describe the abrupt aerodynamic changes experienced when an aeroplane accelerating through the transonic flight regime first reaches the critical Mach number. At the critical Mach number, shock waves begin to form at various places on the airframe and are accompanied by abrupt reduction in local lift, abrupt increase in local drag and some associated change in pitching moment. Since the effect of these aerodynamic changes is not unlike that of the classical low speed stall it is referred to as the shock stall. However, unlike the classical low speed stall, the aeroplane continues to fly through the condition.

12.4.2 AERODYNAMIC MODELS

Because of the aerodynamic complexity of the conditions applying to an aeroplane in a compressible flow field it is difficult to derive other than the very simplest mathematical models to describe those conditions. Thus, for analytical application, as required in

aerodynamic derivative estimation, mathematical modelling is usually limited to an approximate description of the effects of compressibility on the lifting surfaces of the aeroplane only. In particular, the ease with which the aerodynamic properties of a wing in compressible flow can be estimated is dependent, to a large extent, on the leading edge flow conditions.

As flow Mach number is increased to unity a shock wave forms a small distance ahead of the leading edge of a typical wing and the shock wave is said to be detached. As the Mach number is increased further so the shock wave moves nearer to the leading edge of the wing and eventually moves on to the wing, when it is said to be *attached.* Since the flow velocity behind the shock wave is lower than the free stream value, when the shock wave is detached the leading edge of the wing would typically be in subsonic flow. In this condition the pressure distribution on the wing, in particular the leading edge suction peak, would be subsonic in nature and the aerodynamic characteristics of the wing would be quite straightforward to estimate. However, when the shock wave is attached, the leading edge of the wing would typically be in supersonic flow conditions and the aerodynamic properties, in particular the drag rise, would be much less straightforward to estimate.

Since the incident flow velocity direction is always considered perpendicular to the leading edge of the wing, it will always be lower on a swept wing as it is equivalent to the free stream velocity resolved through the leading edge sweep angle. Further, since wing sweep will bring more, or more likely all, of the wing within the Mach cone the high drag associated with a supersonic leading edge will be reduced or avoided altogether for a larger range of supersonic Mach number.

12.4.3 SUBSONIC LIFT, DRAG AND PITCHING MOMENT

The theoretical maximum value of lift curve slope for a rectangular flat plate wing of infinite span in incompressible flow is given by

$$a_\infty = 2\pi \cos \Lambda_{le} \text{ rad}^{-1} \tag{12.11}$$

where Λ_{le} is the leading edge sweep angle. For a wing of finite thickness this value of lift curve slope is reduced and Houghton and Carpenter (1993) give an approximate empirical expression which is a function of geometric thickness to chord ratio t/c such that equation (12.11) becomes

$$a_\infty = 1.8\pi\left(1 + 0.8\frac{t}{c}\right) \cos \Lambda_{le} \text{ rad}^{-1} \tag{12.12}$$

For a wing of finite span the lift curve slope is reduced further as a function of aspect ratio A and is given by the expression

$$a = \frac{a_\infty}{\left(1 + \frac{a_\infty}{\pi A}\right)} \tag{12.13}$$

For Mach numbers below M_{crit}, but when the effects of compressibility are evident, the *Prandtl–Glauert rule* provides a means for estimating the lifting properties of a wing. For an infinite span wing with leading edge sweep angle Λ_{le} the lift curve slope a_{∞_c} in the presence of compressibility effects is given by

$$a_{\infty_c} = \frac{a_{\infty_i}}{\sqrt{1 - M^2 \cos^2 \Lambda_{le}}} \tag{12.14}$$

where a_{∞_i} is the corresponding incompressible lift curve slope given, for example, by equation (12.12). An equivalent expression for a wing of finite span and having an aspect ratio A is quoted in Babister (1961) and is given by

$$a_c = \frac{(A + 2\cos \Lambda_{le}) a_{\infty_i}}{2\cos \Lambda_{le} + A\sqrt{1 - M^2 \cos^2 \Lambda_{le}}} \tag{12.15}$$

For Mach numbers below M_{crit} the zero lift drag coefficient C_{D_0} remains at its nominal incompressible value and the changes in drag due to the effects of compressibility are due mainly to the induced drag contribution. Thus, the classical expression for the drag coefficient applies

$$C_{D_c} = C_{D_0} + kC_{L_c}^2 = C_{D_0} + ka_c^2\alpha^2 \tag{12.16}$$

In general, the effect of compressibility on pitching moment coefficient in subsonic flight is small and is often disregarded. However, in common with lift and drag coefficients, such changes in pitching moment coefficient as may be evident increase as the Mach number approaches unity. Further, the changes in pitching moment coefficient are more pronounced in aircraft with a large wing sweep angle and result from a progressive aft shift in aerodynamic centre. Since the effect is dependent on the inverse of $\sqrt{1 - M^2 \cos^2 \Lambda_{le}}$, or its equivalent for a wing of finite span, it does not become significant until, approximately, $M \geqslant 0.6$.

It is important to appreciate that the Prandtl–Glauert rule only applies to subsonic flight in the presence of the effects of compressibility. The models given above become increasingly inaccurate at Mach numbers approaching and exceeding unity. In other words, the Prandtl–Glauert rule is not applicable to transonic flight conditions.

12.4.4 SUPERSONIC LIFT, DRAG AND PITCHING MOMENT

The derivation of simple approximate aerodynamic models to describe lift, drag and pitching moment characteristics in supersonic flow conditions is very much more difficult. Such models as are available are dependent on the location of the shocks on the principal lifting surfaces and, in particular, on whether the leading edge of the wing is subsonic or supersonic. In every case, the aerodynamic models require a reasonable knowledge of the geometry of the wing including the aerofoil section.

The three commonly used theoretical tools are, in order of increasing complexity, the linearized *Ackeret theory*, the second order *Busemann theory* and the *shock expansion* method. A full discussion of the theories is not appropriate here and only the simplest linear models are summarized below. The material is included in most aerodynamics texts, for example in Bertin and Smith (1989) and in Houghton and Carpenter (1993).

The lift curve slope of an infinite span swept wing in supersonic flow, which implies a supersonic leading edge condition, is given by

$$a_{\infty_c} = \frac{4\cos \Lambda_{le}}{\sqrt{M^2 \cos^2 \Lambda_{le} - 1}} \tag{12.17}$$

Clearly, the expression given by equation (12.17) is only valid for Mach numbers $M > \sec \Lambda_{le}$; at lower Mach numbers the leading edge is subsonic since it is within the

Mach cone. For a wing of finite span the expression given by equation (12.17) is 'corrected' for aspect ratio

$$a_c = a_{\infty_c}\left(1 - \frac{1}{2A\sqrt{M^2\cos^2\Lambda_{le} - 1}}\right) \tag{12.18}$$

and the parameter $A\sqrt{M^2\cos^2\Lambda_{le} - 1}$ is termed the *effective aspect ratio* by Liepmann and Roshko (1957).

The drag of an aeroplane in supersonic flight is probably one of the most difficult aerodynamic parameters to estimate with any degree of accuracy. The drag of a wing with a supersonic leading edge comprises three components: the *drag due to lift*, *wave drag* and *skin friction drag*. The drag due to lift, sometimes known as *wave drag due to lift*, is equivalent to the induced drag in subsonic flight. Wave drag, also known as *form drag* or *pressure drag*, only occurs in compressible flow conditions and is a function of aerofoil section geometry. Skin friction drag is the same as the familiar zero lift drag in subsonic flight, which is a function of wetted surface area.

A simple approximate expression for the drag coefficient of an infinite span swept wing in supersonic flight is given by

$$C_{D_\infty} = \frac{4\alpha^2\cos\Lambda_{le}}{\sqrt{M^2\cos^2\Lambda_{le} - 1}} + \frac{k\left(\frac{t}{c}\right)^2\cos^3\Lambda_{le}}{\sqrt{M^2\cos^2\Lambda_{le} - 1}} + C_{D_0} \tag{12.19}$$

where the first term is the drag coefficient due to lift, the second term is the wave drag coefficient and the third term is the zero lift drag coefficient. Here, in the interests of simplicity, the wave drag is shown to be dependent on the aerofoil section thickness to chord ratio t/c only, which implies that the section is symmetrical. When the section has camber, the wave drag includes a second term which is dependent on the square of the local angle of attack with respect to the mean camber line. The camber term is not included in equation (12.19) since many practical supersonic aerofoils are symmetric or near symmetric. The constant k is also a function of the aerofoil section geometry and is 2/3 for bi-convex or typical modified double wedge sections, both of which are symmetric.

For a finite span wing with aspect ratio A, the drag coefficient is given very approximately by

$$C_{D_\infty} = \left(\frac{4\alpha^2\cos\Lambda_{le}}{\sqrt{M^2\cos^2\Lambda_{le} - 1}} + \frac{k\left(\frac{t}{c}\right)^2\cos^3\Lambda_{le}}{\sqrt{M^2\cos^2\Lambda_{le} - 1}}\right)\left(1 - \frac{1}{2A\sqrt{M^2\cos^2\Lambda_{le} - 1}}\right) + C_{D_0} \tag{12.20}$$

It is assumed that the wing to which equation (12.20) relates is of constant thickness with span and that it has a rectangular planform, which is most unlikely for a real practical wing. Alternative and rather more complex expressions can be derived which are specifically dependent on wing geometry to a much greater extent. However, there is no guarantee that the estimated drag coefficient will be more accurate since it remains necessary to make significant assumptions about the aerodynamic operating conditions of the wing.

It is also difficult to obtain a simple and meaningful expression for pitching moment coefficient in supersonic flight conditions. However, it is relatively straightforward to show that for an infinite span flat plate wing the aerodynamic centre moves aft to the

half chord point in supersonic flow. This results in an increase in nose down pitching moment together with an increase in the longitudinal static stability margins with corresponding changes in the longitudinal trim, stability and control characteristics of the aeroplane. An increase in thickness and a reduction in aspect ratio of the wing causes the aerodynamic centre to move forward from the half chord point with a corresponding reduction in stability margins. Theoretical prediction of these changes for anything other than a simple rectangular wing is not generally practical.

12.4.5 SUMMARY

It is most important to realize that the aerodynamic models outlined in Sections 12.4.3 and 12.4.4 describe, approximately, the properties of the main lifting wing of the aeroplane only. Since the wing provides most of the lift, with perhaps smaller contributions from the fuselage and tailplane, or fore plane, then it is expected that equations (12.15) and (12.18) would give a reasonable indication of the lift curve slope of a complete aeroplane. However, this would not necessarily be expected of the drag estimates given by equations (12.16) and (12.20). The drag contributions from the fuselage and tailplane, or fore plane, may well be a large fraction of the total. Therefore, estimates obtained with equations (12.16) and (12.20) should be treated accordingly.

It is suggested that the main usefulness of the material given in Sections 12.4.3 and 12.4.4 is to provide an appreciation of the main aerodynamic effects of compressibility as they relate to stability and control and to provide a means for checking the plausibility of estimates obtained by other means, especially computational means. Little mention has been made of the transonic flight regime for the simple reason that analytical models suitable for the estimation of aerodynamic stability and control properties at the present level of interest are just not available. Considerable research has been undertaken in recent years into transonic aerodynamics but the analysis remains complex and has found greatest use in computational methods for flow prediction. When estimates of the aerodynamic properties of a complete aeroplane configuration in compressible flow conditions are required it is preferable to refer to source material such as the ESDU data items.

Today, increasing use is made of computational methods for the estimation of the aerodynamic properties of complete aeroplane configurations and at all flight conditions. Provided the geometry of the airframe can be described in sufficient detail then computational methods, such as the *vortex lattice method* or the *panel method*, can be used to obtain estimates of aerodynamic characteristics at acceptable levels of accuracy. By such means aerodynamic information can be obtained for conditions which would otherwise be impossible using analytical methods.

EXAMPLE 12.1

A substantial database comprising aerodynamic, stability and control parameters for the McDonnell-Douglas F-4C Phantom aircraft is given in Heffley and Jewell (1972). Data are given for altitudes from sea level to 55 000 ft and for Mach numbers from 0.2 to 2.2 and the aircraft shows most of the classical effects of translation from subsonic to supersonic flight. Some limited additional information was obtained from Jane's (1969–1970 see Taylor, 1970). The main geometric parameters of the aircraft used in the example are

wing area (reference area)	$S = 530\,\text{ft}^2$
wing-span	$b = 38.67\,\text{ft}$
mean geometric chord (reference chord)	$\bar{c} = 16.04\,\text{ft}$
average thickness–chord ratio	$t/c = 0.051$
aspect ratio	$A = 2.82$
leading edge sweep angle	$\Lambda_{le} = 50°$
centre of gravity position	$h = 0.289$

The lift, drag and pitching moment characteristics are summarized in Fig. 12.3 as a function of Mach number for two altitudes, 15 000 ft and 35 000 ft, since the data for these two altitudes extend over the entire Mach number envelope.

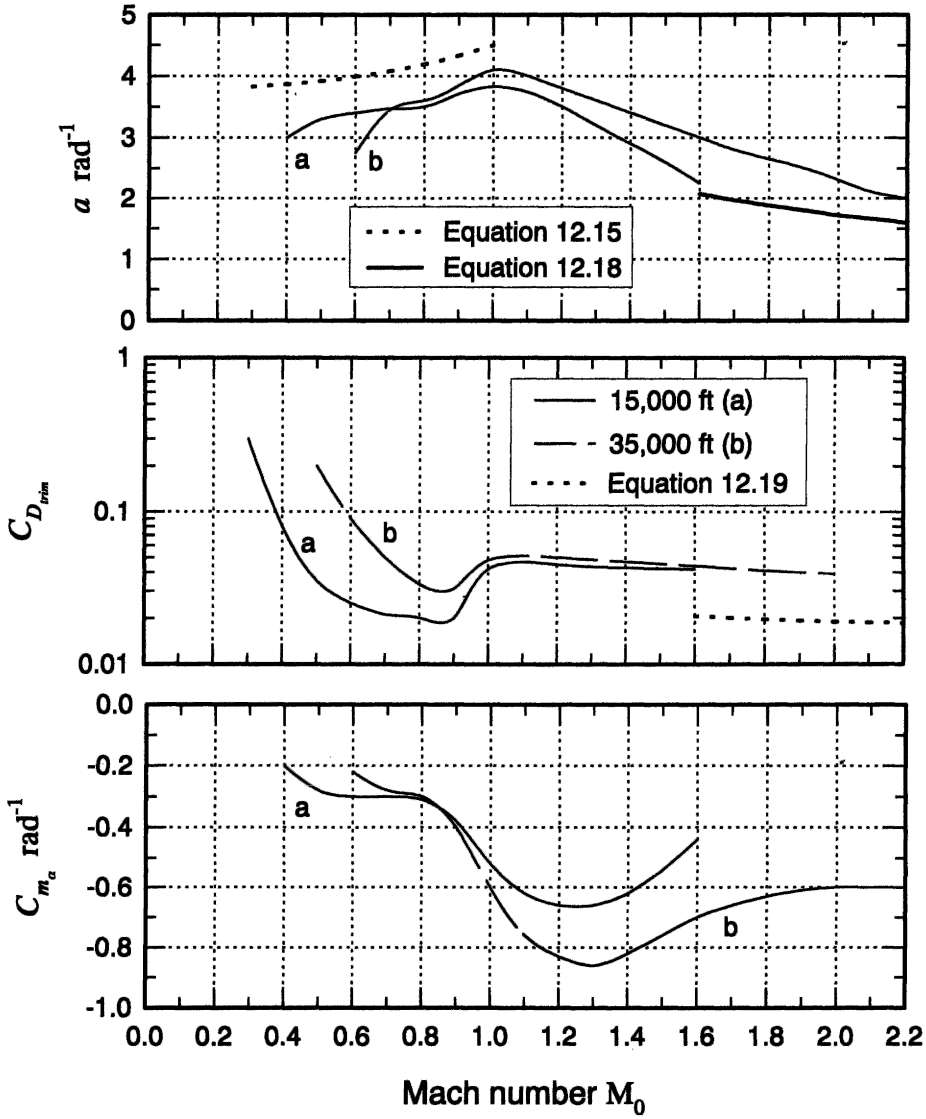

Fig. 12.3 Lift, drag and pitching moment variation with Mach number

Lifting properties are represented by the plot of lift curve slope a as a function of Mach number. The effect of compressibility becomes obvious at Mach 0.8 at the onset of the transonic flow regime. The lift curve slope reaches a maximum at Mach 1.0 and its gentle reduction thereafter is almost linear with Mach number. The Prandtl–Glauert rule approximation, as given by equation (12.15) is shown for comparison in the subsonic Mach number range. The approximation assumes a two dimensional (2D) lift curve slope calculated according to equation (12.12) and shows the correct trend but gives an overestimate of total lift curve slope. The linear supersonic approximation for lift curve slope, as given by equation (12.18) is also shown for completeness. In this case the 2D lift curve slope was calculated using equation (12.17). Again, the trend matches reasonably well but the model gives a significant underestimate. It is prudent to recall at this juncture that both models describe the lift curve slope of a finite wing only, whereas the F-4C data describe the entire airframe characteristic.

The drag properties are represented by the trim drag coefficient, plotted on a logarithmic scale, as a function of Mach number. The use of a logarithmic scale helps to emphasize the abrupt drag rise at Mach 1.0. In the subsonic Mach number range the drag coefficient reduces with increasing Mach number, the classical characteristic, which implies that it is dominated by the induced drag contribution as might be expected. However, in supersonic flight the drag coefficient remains almost constant, the contribution due to lift will be small as both C_L and α are small and the main contributions will be due to wave drag and skin friction. Shown on the same plot is the supersonic drag coefficient calculated according to equation (12.19) and clearly, the match is poor. The trend is correct but the magnitude is about half the actual airframe value. Once again, it should be remembered that equation (12.19) relates to a finite wing and not to a complete airframe. It is reasonably easy to appreciate that the fuselage and tail surfaces will make a significant contribution to the overall drag of the aeroplane. Careful scrutiny of the aerodynamic data for 35 000 ft enabled the expression for the subsonic drag coefficient, equation (12.16), to be estimated as

$$C_D = C_{D_0} + kC_L^2 = 0.017 + 0.216C_L^2 \tag{12.21}$$

This expression gave a good fit to the actual data and the value of C_{D_0} was used in the evaluation of the supersonic drag coefficient, equation (12.19).

The final plot in Fig. 12.3 represents the effect of Mach number on pitching moment and shows the variation in the slope, denoted C_{m_α}, of the C_m–α curve as a function of Mach number. Since C_{m_α} is proportional to the controls fixed static margin it becomes more negative as the aerodynamic centre moves aft. This is clearly seen in the plot and the increase in stability margin commences at a Mach number of 0.8. Now, the relationship between controls fixed stability margin, neutral point and centre of gravity locations is given by equation (3.17)

$$K_n = h_n - h \tag{12.22}$$

With reference to Appendix 6 the expression for the derivative M_w is given by

$$M_w = \frac{\partial C_m}{\partial \alpha} = -aK_n \tag{12.23}$$

Thus, from equations (12.22) and (12.23) an expression for the location of the controls fixed neutral point is easily calculated

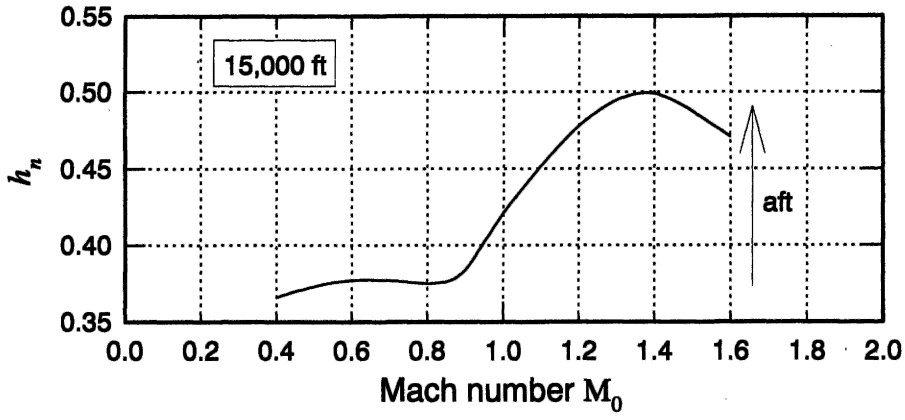

Fig. 12.4 Variation of controls fixed neutral point position with Mach number

$$h_n = h - \frac{1}{a}\frac{\partial C_m}{\partial \alpha} \equiv h - \frac{1}{a}C_{m_\alpha} \tag{12.24}$$

Using equation (12.24) with the F-4C data for an altitude of 15 000 ft the variation in neutral point position as a function of Mach number was calculated and the result is shown in Fig. 12.4.

Since the neutral point corresponds to the centre of pressure for the whole aeroplane its aft shift with Mach number agrees well with the predictions given by 'simple' aerofoil theory. Over the transonic Mach number range the neutral point moves back to the mid point of the mean aerodynamic chord and then moves forward a little at higher Mach numbers. It is interesting to note that at subsonic Mach numbers the neutral point remains more-or-less stationary at around $0.37\bar{c}$, which is quite typical for many aeroplanes.

12.5 Limitations of aerodynamic modelling

Simple expressions for the aerodynamic stability and control derivatives may be developed from first principles based on the analysis of the aerodynamic conditions following an upset from equilibrium. The cause of the upset may be external, as the result of a gust for example, or internal as the result of a pilot control action. It is important to appreciate that in either event the disturbance is of short duration and that the controls remain fixed at their initial settings for the duration of the response. As explained in Section 12.2, the derivatives are then evaluated by linearizing the aerodynamics about the nominal operating, or trim, condition. The aerodynamic models thus derived are limited in their application to small perturbation motion about the trim condition only. The simplest possible analytical models for the aerodynamic stability and control derivatives are developed, subject to the limitations outlined in this chapter, and described in Chapter 13.

References

AGARD, 1979: *Parameter Identification*. Lecture Series, AGARD-LS-104.

Anon. 1960: *USAF Stability and Control Handbook (DATCOM)*. McDonnell-Douglas Corp.

Babister, A. W. 1961: *Aircraft Stability and Control.* Pergamon Press, Oxford.

Bertin, J. J. and Smith, M. L. 1989: *Aerodynamics for Engineers.* Second edition. Prentice Hall, Englewood Cliffs, New Jersey.

ESDU: *Aerodynamics.* (Especially, *Volume 9—Stability of Aircraft.*) Engineering Sciences Data, ESDU International Ltd, London.

Heffley, R. K. and Jewell, W. F. 1972: *Aircraft Handling Qualities Data.* NASA Contractor Report, NASA CR-2144.

Hilton, W. F. 1952: *High Speed Aerodynamics.* Longmans, Green and Co, London.

Houghton, E. L. and Carpenter, P. W. 1993: *Aerodynamics for Engineering Students.* Fourth edition. Edward Arnold, London.

Liepmann, H. W. and Roshko, A. 1957: *Elements of Gas Dynamics.* John Wiley and Sons, Inc, New York.

Mitchell, C. G. B. 1973: *A Computer Programme to Predict the Stability and Control Characteristics of Subsonic Aircraft.* Royal Aircraft Establishment Technical Report, RAE TR-73079.

Ross, A. J. and Benger, N. J. 1975: *Modifications to a Computer Program for Predicting the Stability and Control Characteristics of Subsonic Aircraft (RAE Technical Report TR-73079).* Royal Aircraft Establishment Technical Memorandum, RAE Tech Memo FS 40.

Ross, A. J. and Foster, G. W. 1976: *FORTRAN Programs for the Determination of Aerodynamic Derivatives from Transient Longitudinal or Lateral Responses of Aircraft.* Aeronautical Research Council, Current Papers, ARC-CP 1344.

Smetana, F. O. 1984: *Computer Assisted Analysis of Aircraft Performance Stability and Control.* McGraw-Hill Book Co, New York.

Taylor, J. W. R. (Editor) 1970: *Jane's All The World's Aircraft 1969–70.* Jane's Yearbooks, Haymarket Publishing, London.

13

Aerodynamic Stability and Control Derivatives

13.1 Introduction

As is usual in aerodynamic analysis, for the purposes of obtaining simple expressions for the stability and control derivatives a wind axis reference system is assumed throughout. The choice of wind axes is convenient since it reduces the derivatives to their simplest possible description by retaining only the essential contributions and hence maximizes the *visibility* of the physical phenomena involved. It is therefore very important to remember that if the derivatives thus obtained are required for use in equations of motion referred to an alternative axis system then the appropriate axis transformation must be applied to the derivatives.

Some useful transformations are given in Appendices 7 and 8. In all cases analytical expressions are obtained for the derivatives assuming subsonic flight conditions: it is then relatively straightforward to develop the expressions further to allow for the effects of Mach number, as suggested in Section 12.4.

It has already been established that simple analytical expressions for the derivatives rarely give accurate estimates. Their usefulness is significantly more important as a means for explaining their physical origins, thereby providing the essential link between aircraft dynamics and airframe aerodynamics. The analytical procedure for obtaining simple derivative expressions has been well established for very many years and the approach commonly encountered in the UK today is comprehensively described by Babister (1961), and in less detail in Babister (1980). The following sections owe much to that work since it is unlikely that the treatment can be bettered. For the calculation of more reliable estimates of derivative values, reference to the ESDU data items is advised. The reader requiring a more detailed aerodynamic analysis of stability and control derivatives will find much useful material in Hancock (1995).

13.2 Longitudinal aerodynamic stability derivatives

For convenience, a summary of the derivative expressions derived in this section is included in Appendix 6.

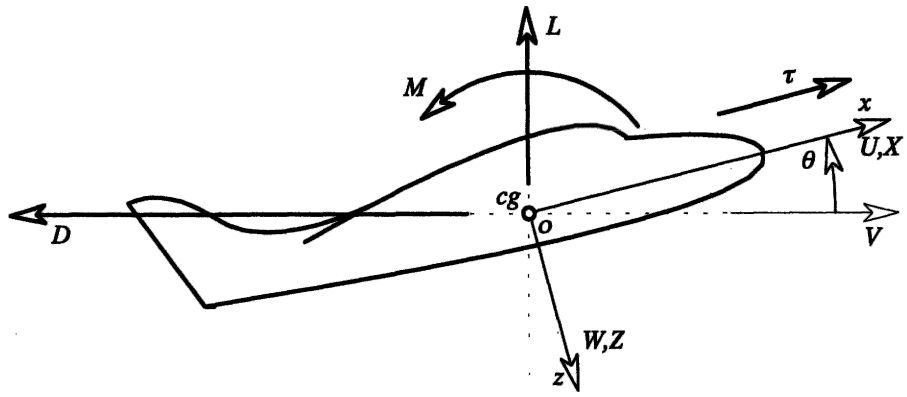

Fig. 13.1 Perturbed wind axes

13.2.1 PRELIMINARY CONSIDERATIONS

A number of expressions are required repeatedly in the derivative analysis, so it is convenient to assemble these expressions prior to embarking on the analysis. A longitudinal small perturbation is shown in Fig. 13.1 in which the aircraft axes are wind axes and the initial condition assumes steady symmetric level flight at velocity V_0. Although not strictly an aerodynamic force the thrust τ is shown since it may behave like an aerodynamic variable in a perturbation. As indicated, the thrust force is tied to the aircraft x axis and moves with it.

In the perturbation the total velocity becomes V with components U and W along the ox and oz axes respectively. Whence

$$V^2 = U^2 + W^2 \tag{13.1}$$

and

$$\left.\begin{aligned} U &= U_e + u = V\cos\theta \\ W &= W_e + w = V\sin\theta \end{aligned}\right\} \tag{13.2}$$

Since wind axes are assumed the pitch attitude perturbation θ and the incidence perturbation α are the same and are given by

$$\tan\theta \equiv \tan\alpha = \frac{W}{U} \tag{13.3}$$

Differentiate equation (13.1) with respect to U and W in turn to obtain the following partial derivatives

$$\frac{\partial V}{\partial U} = \frac{U}{V} \quad \text{and} \quad \frac{\partial V}{\partial W} = \frac{W}{V} \tag{13.4}$$

and substitute for U and W from equation (13.2) to obtain

$$\frac{\partial V}{\partial U} = \cos\theta \cong 1 \quad \text{and} \quad \frac{\partial V}{\partial W} = \sin\theta \cong 0 \tag{13.5}$$

since, by definition, θ is a small angle.

In a similar way, differentiate equation (13.3) with respect to U and W in turn and substitute for U and W from equation (13.2) to obtain

$$\left.\begin{aligned}\frac{\partial\theta}{\partial U} \equiv \frac{\partial\alpha}{\partial U} &= \frac{-\sin\theta}{V} \cong 0\\ \frac{\partial\theta}{\partial W} \equiv \frac{\partial\alpha}{\partial W} &= \frac{\cos\theta}{V} \cong \frac{1}{V}\end{aligned}\right\} \tag{13.6}$$

since again, by definition, θ is a small angle.

From equation (12.10)

$$\frac{\partial}{\partial V} = a\frac{\partial}{\partial \mathrm{M}} \tag{13.7}$$

which is useful for transforming from a velocity dependency to a Mach number dependency and where, here, a is the local speed of sound.

13.2.2 AERODYNAMIC FORCE AND MOMENT COMPONENTS

With reference to Fig. 13.1 the lift and drag forces may be resolved into the disturbed aircraft axes to give the following components of aerodynamic force. The perturbed axial force is

$$X = L\sin\theta - D\cos\theta + \tau = \frac{1}{2}\rho V^2 S(C_L\sin\theta - C_D\cos\theta) + \tau \tag{13.8}$$

and the perturbed normal force is

$$Z = -L\cos\theta - D\sin\theta = -\frac{1}{2}\rho V^2 S(C_L\cos\theta + C_D\sin\theta) \tag{13.9}$$

In the initial steady trim condition, by definition the pitching moment M is zero. However, in the perturbation the transient pitching moment is non-zero and is given by

$$M = \frac{1}{2}\rho V^2 S\bar{c}C_m \tag{13.10}$$

Note that considerable care is needed in order not to confuse pitching moment M and Mach number M.

13.2.3 FORCE DERIVATIVES DUE TO VELOCITY PERTURBATIONS

$\mathring{X}_u = \dfrac{\partial X}{\partial U}$ *Axial force due to axial velocity*

Differentiating equation (13.8) gives

$$\begin{aligned}\frac{\partial X}{\partial U} = \frac{1}{2}\rho V^2 S\left(\frac{\partial C_L}{\partial U}\sin\theta + C_L\cos\theta\frac{\partial\theta}{\partial U} - \frac{\partial C_D}{\partial U}\cos\theta + C_D\sin\theta\frac{\partial\theta}{\partial U}\right)\\ + \rho VS\frac{\partial V}{\partial U}(C_L\sin\theta - C_D\cos\theta) + \frac{\partial\tau}{\partial U}\end{aligned} \tag{13.11}$$

Substitute for $\partial V/\partial U$ from equation (13.5) and for $\partial\theta/\partial U$ from equation (13.6). As θ is a small angle, in the limit, $\cos\theta \cong 1$ and $\sin\theta \cong 0$ and equation (13.11) simplifies to

$$\frac{\partial X}{\partial U} = -\frac{1}{2}\rho V^2 S\frac{\partial C_D}{\partial U} - \rho VSC_D + \frac{\partial\tau}{\partial U} \tag{13.12}$$

Now

$$\frac{\partial C_D}{\partial U} = \frac{\partial C_D}{\partial V}\frac{\partial V}{\partial U} = \frac{\partial C_D}{\partial V} \tag{13.13}$$

and similarly

$$\frac{\partial \tau}{\partial U} = \frac{\partial \tau}{\partial V} \tag{13.14}$$

In the limit the total perturbation velocity tends to the equilibrium value and $V \cong V_0$. Hence equation (13.12) may be written

$$\mathring{X}_u = \frac{\partial X}{\partial U} = -\rho V_0 S C_D - \frac{1}{2}\rho V_0^2 S \frac{\partial C_D}{\partial V} + \frac{\partial \tau}{\partial V} \tag{13.15}$$

With reference to Appendix 1, the dimensionless form of the derivative is given by

$$X_u = \frac{\mathring{X}_u}{\frac{1}{2}\rho V_0 S} = -2C_D - V_0 \frac{\partial C_D}{\partial V} + \frac{1}{\frac{1}{2}\rho V_0 S}\frac{\partial \tau}{\partial V} \tag{13.16}$$

Alternatively, using equation (13.7), the dimensionless derivative may be expressed in terms of Mach number rather than velocity

$$X_u = -2C_D - \frac{1}{\mathrm{M}_0}\frac{\partial C_D}{\partial \mathrm{M}} + \frac{1}{\frac{1}{2}\rho \mathrm{M}_0 S}\frac{\partial \tau}{\partial \mathrm{M}} \tag{13.17}$$

Expressions for the remaining force–velocity derivatives are obtained in a similar way as follows

$\mathring{Z}_u = \dfrac{\partial Z}{\partial U}$ *Normal force due to axial velocity*

Thus, by differentiating equation (13.9) with respect to U it is easily shown that

$$\mathring{Z}_u = \frac{\partial Z}{\partial U} = -\rho V S C_L - \frac{1}{2}\rho V^2 S \frac{\partial C_L}{\partial U} \tag{13.18}$$

Now, in the manner of equation (13.13)

$$\frac{\partial C_L}{\partial U} = \frac{\partial C_L}{\partial V}\frac{\partial V}{\partial U} = \frac{\partial C_L}{\partial V} \tag{13.19}$$

Thus, in the limit $V \cong V_0$ and equation (13.18) may be written

$$\mathring{Z}_u = -\rho V_0 S C_L - \frac{1}{2}\rho V_0^2 S \frac{\partial C_L}{\partial V} \tag{13.20}$$

With reference to Appendix 1, the dimensionless form of the derivative is given by

$$Z_u = \frac{\mathring{Z}_u}{\frac{1}{2}\rho V_0 S} = -2C_L - V_0 \frac{\partial C_L}{\partial V} \tag{13.21}$$

or, alternatively, expressed in terms of Mach number rather than velocity

$$Z_u = -2C_L - \frac{1}{\mathrm{M}_0}\frac{\partial C_L}{\partial \mathrm{M}} \tag{13.22}$$

$\mathring{X}_w = \dfrac{\partial X}{\partial W}$ *Axial force due to normal velocity*

As before, it may be shown that by differentiating equation (13.8) with respect to W

$$\mathring{X}_w = \frac{\partial X}{\partial W} = \frac{1}{2}\rho V^2 S\left(\frac{1}{V}C_L - \frac{\partial C_D}{\partial W}\right) + \frac{\partial \tau}{\partial W} \tag{13.23}$$

Now, with reference to equation (13.6) and noting that $\alpha = \theta$

$$\frac{\partial C_D}{\partial W} = \frac{\partial C_D}{\partial \theta}\frac{\partial \theta}{\partial W} \equiv \frac{1}{V}\frac{\partial C_D}{\partial \alpha} \tag{13.24}$$

Similarly, it may be shown that

$$\frac{\partial \tau}{\partial W} \equiv \frac{1}{V}\frac{\partial \tau}{\partial \alpha} = 0 \tag{13.25}$$

since it is assumed that thrust variation resulting from small incidence perturbations is negligible. Thus, in the limit, equation (13.23) may be written

$$\mathring{X}_w = \frac{1}{2}\rho V_0 S\left(C_L - \frac{\partial C_D}{\partial \alpha}\right) \tag{13.26}$$

With reference to Appendix 1, the dimensionless form of the derivative is given by

$$X_w = \frac{\mathring{X}_w}{\frac{1}{2}\rho V_0 S} = \left(C_L - \frac{\partial C_D}{\partial \alpha}\right) \tag{13.27}$$

$\mathring{Z}_w = \dfrac{\partial Z}{\partial W}$ *Normal force due to normal velocity*

As before, by differentiating equation (13.9) with respect to W and with reference to equation (13.24) it may be shown that

$$\mathring{Z}_w = \frac{\partial Z}{\partial W} = -\frac{1}{2}\rho V^2 S\left(\frac{\partial C_L}{\partial W} + \frac{1}{V}C_D\right) = -\frac{1}{2}\rho V S\left(\frac{\partial C_L}{\partial \alpha} + C_D\right) \tag{13.28}$$

In the limit, equation (13.28) may be rewritten

$$\mathring{Z}_w = -\frac{1}{2}\rho V_0 S\left(\frac{\partial C_L}{\partial \alpha} + C_D\right) \tag{13.29}$$

With reference to Appendix 1, the dimensionless form of the derivative is given by

$$Z_w = \frac{\mathring{Z}_w}{\frac{1}{2}\rho V_0 S} = -\left(\frac{\partial C_L}{\partial \alpha} + C_D\right) \tag{13.30}$$

13.2.4 MOMENT DERIVATIVES DUE TO VELOCITY PERTURBATIONS

$\mathring{M}_u = \dfrac{\partial M}{\partial U}$ *Pitching moment due to axial velocity*

In a perturbation the pitching moment becomes non-zero and is given by equation (13.10). Differentiating equation (13.10) with respect to U

$$\frac{\partial M}{\partial U} = \frac{1}{2}\rho V^2 S\bar{\bar{c}}\frac{\partial C_m}{\partial U} + \rho V S\bar{\bar{c}} C_m \tag{13.31}$$

and with reference to equation (13.5)

$$\frac{\partial C_m}{\partial U} = \frac{\partial C_m}{\partial V}\frac{\partial V}{\partial U} = \frac{\partial C_m}{\partial V} \tag{13.32}$$

Now, in the limit, as the perturbation tends to zero, so the pitching moment coefficient C_m in the second term in equation (13.31) tends to the steady equilibrium value which is, of course, zero. Therefore, in the limit, equation (13.31) simplifies to

$$\mathring{M}_u = \frac{\partial M}{\partial U} = \frac{1}{2}\rho V_0^2 S\bar{\bar{c}}\frac{\partial C_m}{\partial V} \tag{13.33}$$

With reference to Appendix 1, the dimensionless form of the derivative is given by

$$M_u = \frac{\mathring{M}_u}{\frac{1}{2}\rho V_0 S\bar{\bar{c}}} = V_0\frac{\partial C_m}{\partial V} \tag{13.34}$$

Alternatively, using equation (13.7), the dimensionless derivative may be expressed in terms of Mach number rather than velocity

$$M_u = \frac{1}{\mathrm{M}_0}\frac{\partial C_m}{\partial \mathrm{M}} \tag{13.35}$$

In subsonic flight the pitching moment coefficient C_m is very nearly independent of velocity, or Mach number, whence the derivative M_u is often assumed to be negligibly small for those flight conditions.

$\mathring{M}_w = \dfrac{\partial M}{\partial W}$ *Pitching moment due to normal velocity*

As previously, differentiating equation (13.10) with respect to W and with reference to equation (13.24) it may be shown that

$$\mathring{M}_w = \frac{\partial M}{\partial W} = \frac{1}{2}\rho V^2 S\bar{\bar{c}}\frac{\partial C_m}{\partial W} = \frac{1}{2}\rho V S\bar{\bar{c}}\frac{\partial C_m}{\partial \alpha} \tag{13.36}$$

In the limit $V \cong V_0$ and equation (13.36) may be written

$$\mathring{M}_w = \frac{1}{2}\rho V_0 S\bar{\bar{c}}\frac{\partial C_m}{\partial \alpha} \tag{13.37}$$

and with reference to Appendix 1, the dimensionless form of the derivative is given by

$$M_w = \frac{\mathring{M}_w}{\frac{1}{2}\rho V_0 S\bar{\bar{c}}} = \frac{\partial C_m}{\partial \alpha} \tag{13.38}$$

Further, assuming that linear aerodynamic conditions apply, such as are typical of subsonic flight, then with reference to equation (3.17)

$$M_w = \frac{\mathrm{d}C_m}{\mathrm{d}\alpha} = \frac{\mathrm{d}C_L}{\mathrm{d}\alpha}\frac{\mathrm{d}C_m}{\mathrm{d}C_L} = -aK_n \tag{13.39}$$

where, here, a denotes the lift curve slope and K_n is the controls fixed static margin. As shown in Chapter 6 the derivative M_w is a measure of the *pitch stiffness* of the aeroplane and plays an important part in the determination of the longitudinal short term dynamics.

13.2.5 DERIVATIVES DUE TO A PITCH VELOCITY PERTURBATION

It is usually assumed that the longitudinal aerodynamic properties of an aeroplane are dominated by those of the wing and tailplane. However, when the disturbance is a small perturbation in pitch rate q it is assumed that the dominating aerodynamic properties are those of the tailplane. Thus, in the first instance the resulting aerodynamic changes contributing to the stability derivatives are assumed to arise entirely from tailplane effects. By so doing it is acknowledged that the wing contribution may not necessarily be small and that its omission will reduce the accuracy of the derivative estimates. However, experience has shown that the error incurred by adopting this assumption is usually acceptably small.

An aeroplane pitching through its equilibrium attitude with pitch rate perturbation q is shown in Fig. 13.2. Since the effect of the pitch rate is to cause the tailplane to experience a normal velocity component due to rotation about the *cg* the resultant effect is a change in the local incidence α_T of the tailplane. The total perturbation velocity is V and the tailplane incidence perturbation is given by

$$\alpha_T \cong \tan\alpha_T = \frac{ql_T}{V} \tag{13.40}$$

since, by definition, α_T is a small angle. It is important to appreciate that α_T is the change or increment in tailplane incidence relative to its equilibrium value and, like the pitch rate perturbation, is transient in nature. From equation (13.40) it follows that

$$\frac{\partial\alpha_T}{\partial q} = \frac{l_T}{V} \tag{13.41}$$

$\mathring{X}_q = \dfrac{\partial X}{\partial q}$ *Axial force due to pitch rate*

In this instance, for the reasons given above, it is assumed that the axial force perturbation arises from the tailplane drag perturbation only, thus

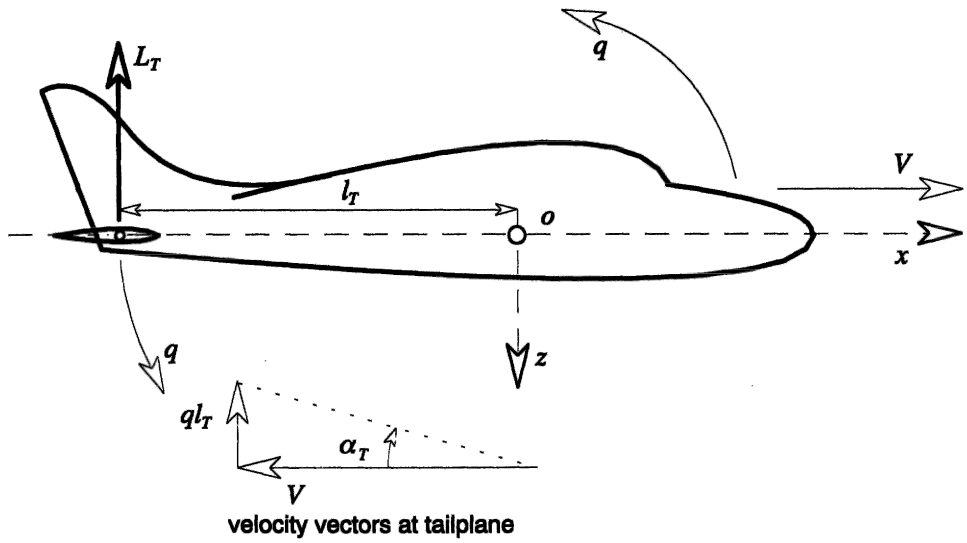

Fig. 13.2 Tailplane incidence due to pitch rate

$$X = -D_T = -\frac{1}{2}\rho V^2 S_T C_{D_T} \tag{13.42}$$

Assuming V to be independent of pitch rate q, differentiate equation (13.42) with respect to the perturbation variable q

$$\frac{\partial X}{\partial q} = -\frac{1}{2}\rho V^2 S_T \frac{\partial C_{D_T}}{\partial q} \tag{13.43}$$

Now, with reference to equation (13.41) write

$$\frac{\partial C_{D_T}}{\partial q} = \frac{\partial C_{D_T}}{\partial \alpha_T}\frac{\partial \alpha_T}{\partial q} = \frac{l_T}{V}\frac{\partial C_{D_T}}{\partial \alpha_T} \tag{13.44}$$

Substitute equation (13.44) into equation (13.43) then, in the limit, $V \cong V_0$ and equation (13.43) may be written

$$\mathring{X}_q = \frac{\partial X}{\partial q} = -\frac{1}{2}\rho V_0 S_T l_T \frac{\partial C_{D_T}}{\partial \alpha_T} \tag{13.45}$$

and with reference to Appendix 1, the dimensionless form of the derivative is given by

$$X_q = \frac{\mathring{X}_q}{\frac{1}{2}\rho V_0 S\bar{\bar{c}}} = -\bar{V}_T \frac{\partial C_{D_T}}{\partial \alpha_T} \tag{13.46}$$

where the *tail volume ratio* is given by

$$\bar{V}_T = \frac{S_T l_T}{S\bar{\bar{c}}} \tag{13.47}$$

Since the rate of change of tailplane drag with incidence is usually small it is customary to assume that the derivative X_q is insignificantly small and it is frequently ignored in aircraft stability and control analysis.

$\mathring{Z}_q = \dfrac{\partial Z}{\partial q}$ *Normal force due to pitch rate*

Similarly, it is assumed that in a pitch rate perturbation the change in normal force arises from tailplane lift only, thus

$$Z = -L_T = -\frac{1}{2}\rho V^2 S_T C_{L_T} \tag{13.48}$$

Differentiate equation (13.48) with respect to q and with reference to equation (13.44) then

$$\frac{\partial Z}{\partial q} = -\frac{1}{2}\rho V S_T l_T \frac{\partial C_{L_T}}{\partial \alpha_T} = -\frac{1}{2}\rho V S_T l_T a_1 \tag{13.49}$$

where, again, it is assumed that V is independent of pitch rate q and that, additionally, the tailplane lift coefficient is a function of incidence only with lift curve slope denoted a_1. Hence, in the limit, $V \cong V_0$ and equation (13.49) may be written

$$\mathring{Z}_q = \frac{\partial Z}{\partial q} = -\frac{1}{2}\rho V_0 S_T l_T a_1 \tag{13.50}$$

and with reference to Appendix 1, the dimensionless form of the derivative is given by

$$Z_q = \frac{\mathring{Z}_q}{\frac{1}{2}\rho V_0 S\bar{\bar{c}}} = -\bar{V}_T a_1 \tag{13.51}$$

$\mathring{M}_q = \dfrac{\partial M}{\partial q}$ *Pitching moment due to pitch rate*

Again, in a pitch rate perturbation q, the pitching moment is assumed to arise entirely from the moment of the tailplane normal force perturbation, given by equation (13.48) about the *cg*. Thus, in the perturbation

$$M = Zl_T = -\frac{1}{2}\rho V^2 S_T l_T C_{L_T} \tag{13.52}$$

Differentiate equation (13.52) with respect to q to obtain the relationship

$$\mathring{M}_q = \frac{\partial M}{\partial q} = l_T \frac{\partial Z}{\partial q} = l_T \mathring{Z}_q \tag{13.53}$$

It therefore follows that

$$\mathring{M}_q = -\frac{1}{2}\rho V_0 S_T l_T^2 a_1 \tag{13.54}$$

and with reference to Appendix 1, the dimensionless form of the derivative is given by

$$M_q = \frac{\mathring{M}_q}{\frac{1}{2}\rho V_0 S\bar{\bar{c}}^2} = -\bar{V}_T \frac{l_T}{\bar{\bar{c}}} a_1 \equiv \frac{l_T}{\bar{\bar{c}}} Z_q \tag{13.55}$$

It is shown in Chapter 6 that M_q is the all important pitch damping derivative. Although this simple model illustrates the importance of the tailplane in determining the pitch damping characteristics of the aeroplane, wing and body contributions may also be significant. Equation (13.55) should therefore be regarded as the first estimate rather than the definitive estimate of the derivative. However, it is often good enough for preliminary analysis of stability and control.

13.2.6 DERIVATIVES DUE TO ACCELERATION PERTURBATIONS

The derivatives due to the acceleration perturbations $\dot{u}$, $\dot{w}$ and $\dot{q}$ are not commonly encountered in the longitudinal equations of motion since their numerical values are usually insignificantly small. Their meaning is perhaps easier to appreciate when the longitudinal equations of motion are written in matrix form, equation (4.65), to include all of the acceleration derivatives. To recap, the state equation is given by

$$\mathbf{M}\dot{\mathbf{x}} = \mathbf{A}'\mathbf{x} + \mathbf{B}'\mathbf{u} \tag{13.56}$$

with state vector $\mathbf{x}^T = [u \quad w \quad q \quad \theta]$ and input vector $\mathbf{u}^T = [\eta \quad \tau]$. The state matrix $\mathbf{A}'$ and input matrix $\mathbf{B}'$ remain unchanged whereas the mass matrix $\mathbf{M}$ is modified to include all the additional acceleration derivatives

$$\mathbf{M} = \begin{bmatrix} (m - \overset{\circ}{X}_{\dot{u}}) & -\overset{\circ}{X}_{\dot{w}} & -\overset{\circ}{X}_{\dot{q}} & 0 \\ -\overset{\circ}{Z}_{\dot{u}} & (m - \overset{\circ}{Z}_{\dot{w}}) & -\overset{\circ}{Z}_{\dot{q}} & 0 \\ -\overset{\circ}{M}_{\dot{u}} & -\overset{\circ}{M}_{\dot{w}} & (I_y - \overset{\circ}{M}_{\dot{q}}) & 0 \\ 0 & 0 & 0 & 1 \end{bmatrix} \tag{13.57}$$

Since all of the acceleration derivatives appear in the mass matrix alongside the normal mass and inertia terms, their effect is to change (increase) the apparent mass and inertia properties of the aircraft. For this reason they are sometimes referred to as *apparent* or *virtual* mass and inertia terms. Whenever the aeroplane moves some of the surrounding displaced air mass is entrained and moves with the aircraft, and it is the mass and inertia of this air which modifies the apparent mass and inertia of the aeroplane. The acceleration derivatives quantify this effect. For most aircraft, since the mass of the displaced air is a small fraction of the mass of the aircraft, the acceleration derivatives are insignificantly small. An exception to this is the airship for which the apparent mass and inertia can be as much as 50% larger than the actual physical value. Other vehicles in which these effects may be non-negligible include balloons, parachutes and underwater vehicles which operate in a much denser fluid medium.

For many modern high performance aeroplanes the derivatives due to a rate of change of normal velocity perturbation $\dot{w}$ ($\dot{\alpha}$) may not be negligible. A rate of change of normal velocity perturbation causes a transient disturbance in the downwash field behind the wing which passes over the tailplane a short time later. The disturbance to the moving air mass in the vicinity of the wing is, in itself, insignificant for the reason given above. However, since the tailplane sees this as a transient in incidence, a short time later it responds accordingly and the effect on the airframe is not necessarily insignificant. This particular characteristic is known as the *downwash lag* effect.

An expression for the total incidence of the tailplane is given by equation (3.9) which, for the present application, may be written

$$\alpha_T(t) = \alpha_e + \eta_T - \varepsilon(t) \tag{13.58}$$

where α_e is the steady equilibrium incidence of the wing, η_T is the tailplane setting angle and $\varepsilon(t)$ is the downwash flow angle at the tailplane. Thus, any change in downwash angle at the tailplane in otherwise steady conditions gives rise to a change in tailplane incidence of equal magnitude and opposite sign. It is important to appreciate that the perturbation at the tailplane is observed at time t and is due to an event on the wing which took place some time earlier. For this reason the flow conditions on the wing at time t are assumed to have recovered their steady equilibrium state.

With reference to Fig. 13.3, the point a in the flow field around the wing arrives at point b in the flow field around the tailplane at a time l_T/V_0 later, referred to as the *downwash lag* and where, for convenience, the mean distance travelled is assumed to be equal to the tail moment arm l_T. Thus, a perturbation in $\dot{w}$ ($\dot{\alpha}$) causes a perturbation in the wing downwash field which arrives at the tailplane after the downwash lag time interval. Therefore, there is a short delay between cause and effect.

The downwash angle $\varepsilon(t)$ at the tailplane at time t is therefore a function of the incidence of the wing at time $t' = t - l_T/V_0$ and may be expressed

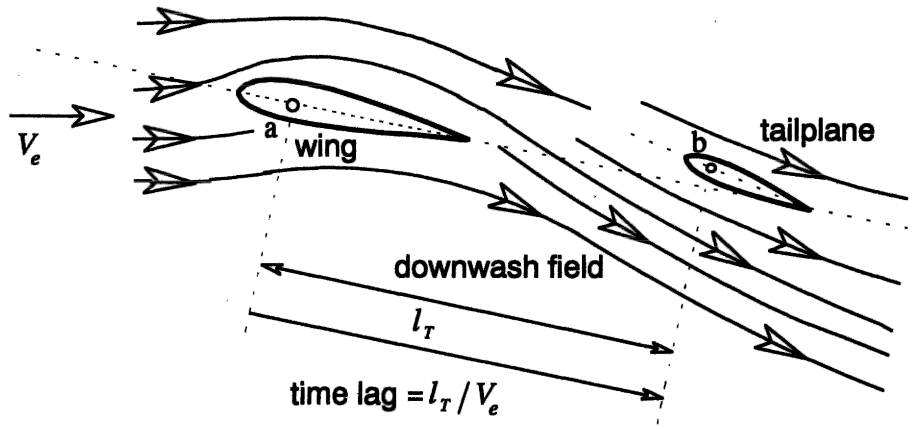

Fig. 13.3 A typical downwash field

$$\varepsilon(t) = \frac{d\varepsilon}{d\alpha}\alpha(t') = \frac{d\varepsilon}{d\alpha}\frac{d\alpha}{dt}\left(t - \frac{l_T}{V_0}\right)$$
$$= \frac{d\varepsilon}{d\alpha}\alpha_e - \frac{d\varepsilon}{d\alpha}\frac{\dot{w}l_T}{V_0^2} = \varepsilon_e - \frac{d\varepsilon}{d\alpha}\frac{\dot{w}l_T}{V_0^2} \tag{13.59}$$

since

$$\frac{d\alpha}{dt}t = \alpha(t) \equiv \alpha_e \tag{13.60}$$

and

$$\alpha \cong \tan\alpha = \frac{w}{V_0} \tag{13.61}$$

whence

$$\frac{d\alpha}{dt} = \frac{\dot{w}}{V_0} \tag{13.62}$$

Thus, with reference to equations (13.58) and (13.59) the total tailplane incidence during a downwash perturbation may be written

$$\alpha_{T_e} + \alpha_T(t) = \alpha_e + \eta_T - \varepsilon_e + \frac{d\varepsilon}{d\alpha}\frac{\dot{w}l_T}{V_0^2} \tag{13.63}$$

The perturbation in tailplane incidence due to the downwash lag effect is therefore given by

$$\alpha_T(t) = \frac{d\varepsilon}{d\alpha}\frac{\dot{w}l_T}{V_0^2} \tag{13.64}$$

$\mathring{X}_{\dot{w}} = \dfrac{\partial X}{\partial \dot{w}}$ *Axial force due to rate of change of normal velocity*

In this instance, it is assumed that the axial force perturbation arises from the perturbation in tailplane drag due solely to the perturbation in incidence, whence

$$X = -D_T = -\frac{1}{2}\rho V^2 S_T C_{D_T} = -\frac{1}{2}\rho V^2 S_T \frac{\partial C_{D_T}}{\partial \alpha_T}\alpha_T \tag{13.65}$$

Now, by definition

$$X = \mathring{X}_{\dot{w}}\dot{w} \tag{13.66}$$

and in the limit $V \cong V_0$. Thus, substitute equation (13.64) into (13.65) and apply equation (13.66) to obtain

$$\mathring{X}_{\dot{w}} = -\frac{1}{2}\rho S_T l_T \frac{\partial C_{D_T}}{\partial \alpha_T}\frac{d\varepsilon}{d\alpha} \tag{13.67}$$

and with reference to Appendix 1, the dimensionless form of the derivative is given by

$$X_{\dot{w}} = \frac{\mathring{X}_{\dot{w}}}{\frac{1}{2}\rho S\bar{c}} = -\bar{V}_T \frac{\partial C_{D_T}}{\partial \alpha_T}\frac{d\varepsilon}{d\alpha} \equiv X_q \frac{d\varepsilon}{d\alpha} \tag{13.68}$$

Since X_q is usually very small and $d\varepsilon/d\alpha < 1$ the derivative $X_{\dot{w}}$ is insignificantly small and is usually omitted from the equations of motion.

$\mathring{Z}_{\dot{w}} = \dfrac{\partial Z}{\partial \dot{w}}$ *Normal force due to rate of change of normal velocity*

Again, it is assumed that the normal force perturbation arises from the perturbation in tailplane lift due solely to the perturbation in incidence, whence

$$Z = -L_T = -\frac{1}{2}\rho V^2 S_T C_{L_T} = -\frac{1}{2}\rho V^2 S_T \frac{\partial C_{L_T}}{\partial \alpha_T}\alpha_T \tag{13.69}$$

Again, by definition

$$Z = \mathring{Z}_{\dot{w}}\dot{w} \tag{13.70}$$

and in the limit $V \cong V_0$. Thus, substitute equation (13.64) into (13.69) and apply equation (13.70) to obtain

$$\mathring{Z}_{\dot{w}} = -\frac{1}{2}\rho S_T l_T a_1 \frac{d\varepsilon}{d\alpha} \tag{13.71}$$

As in Section 13.2.4, it is assumed that the tailplane lift coefficient is a function of incidence only with lift curve slope denoted a_1. With reference to Appendix 1, the dimensionless form of the derivative is given by

$$Z_{\dot{w}} = \frac{\mathring{Z}_{\dot{w}}}{\frac{1}{2}\rho S\bar{c}} = -\bar{V}_T a_1 \frac{d\varepsilon}{d\alpha} \equiv Z_q \frac{d\varepsilon}{d\alpha} \tag{13.72}$$

Care should be exercised since $Z_{\dot{w}}$ is not always insignificant.

$\mathring{M}_{\dot{w}} = \dfrac{\partial M}{\partial \dot{w}}$ *Pitching moment due to rate of change of normal velocity*

In this instance the pitching moment is assumed to arise entirely from the moment of the tailplane normal force perturbation about the *cg* resulting from the perturbation in incidence, given by equation (13.64). Thus, in the perturbation

$$M = Zl_T = -\frac{1}{2}\rho V^2 S_T l_T \frac{\partial C_{L_T}}{\partial \alpha_T}\alpha_T \tag{13.73}$$

Again, by definition

$$M = \mathring{M}_{\dot{w}}\dot{w} \tag{13.74}$$

and in the limit $V \cong V_0$. Thus, substitute equation (13.64) into (13.73) and apply equation (13.74) to obtain

$$\mathring{M}_{\dot{w}} = -\frac{1}{2}\rho S_T l_T^2 a_1 \frac{d\varepsilon}{d\alpha} \tag{13.75}$$

and with reference to Appendix 1, the dimensionless form of the derivative is given by

$$M_{\dot{w}} = \frac{\mathring{M}_{\dot{w}}}{\frac{1}{2}\rho S\bar{\bar{c}}^2} = -\bar{V}_T \frac{l_T}{\bar{\bar{c}}} a_1 \frac{d\varepsilon}{d\alpha} \equiv M_q \frac{d\varepsilon}{d\alpha} \tag{13.76}$$

The derivative $M_{\dot{w}}$ is nearly always significant and makes an important contribution to the damping of the short period pitching oscillation, see equation (6.21).

13.3 Lateral-directional aerodynamic stability derivatives

For convenience, a summary of the derivative expressions derived in this section is also included in Appendix 6.

13.3.1 PRELIMINARY CONSIDERATIONS

Unlike the longitudinal aerodynamic stability derivatives the lateral-directional derivatives are much more difficult to estimate with any degree of confidence. The problem arises from the mutual aerodynamic interference between the lifting surfaces, fuselage, power plant, undercarriage, etc, in asymmetric flow conditions, which makes it difficult to identify the most significant contributions to a particular derivative with any degree of certainty. When a derivative cannot be estimated by the simplest analysis of the often complex aerodynamics, then the use of *strip theory* is resorted to which is a method of analysis which also tends to over-simplify the aerodynamic conditions in order that progress can be made. Either way, analytical estimates of the lateral-directional derivatives are often of poor accuracy and, for more reliable estimates, use of the ESDU data items is preferable. However, the simple theories used for the purpose do give a useful insight into the physical phenomena involved and, consequently, are a considerable asset to the proper understanding of aeroplane dynamics.

13.3.2 DERIVATIVES DUE TO SIDESLIP

As seen by the pilot (and consistent with the notation), a positive sideslip is to the right (starboard) and is defined by the small perturbation lateral velocity transient denoted v. The nature of a free positive sideslip disturbance is such that the right wing tends to drop and the nose tends to swing to the left of the incident *wind vector* as the aeroplane slips to the right. The reaction to the disturbance is stabilizing if the aerodynamic forces and moments produced in response to the sideslip velocity tend to restore the aeroplane to a wings level equilibrium state. The motions involved are discussed in greater detail

in the context of lateral static stability in Section 3.4, in the context of directional static stability in Section 3.5 and in the context of dynamic stability in Section 7.2.

$\mathring{Y}_v = \dfrac{\partial Y}{\partial V}$ *Sideforce due to sideslip*

Sideforce due to sideslip arises mainly from the fuselage, the fin, the wing, especially a wing with dihedral, and engine nacelles in aircraft with external engines. The derivative is notoriously difficult to estimate with any degree of confidence and simple analysis assumes the dominant contributions arise from the fuselage and fin only.

With reference to Fig. 13.4, the fuselage creates a sideforce Y_B in a sideslip, which may be regarded as *lateral drag* and which is given by

$$Y_B = \frac{1}{2}\rho V_0^2 S_B \beta y_B \tag{13.77}$$

where S_B is the projected fuselage side area and y_B is a dimensionless coefficient. Note that the product βy_B is equivalent to a *lateral drag coefficient* for the fuselage. Further, since the disturbance is small the sideslip angle β is given by

$$\beta \cong \tan\beta = \frac{v}{V_0} \tag{13.78}$$

In a sideslip the fin is at incidence β and produces lift as indicated in Fig. 13.4. The fin lift resolves into a sideforce Y_F given by

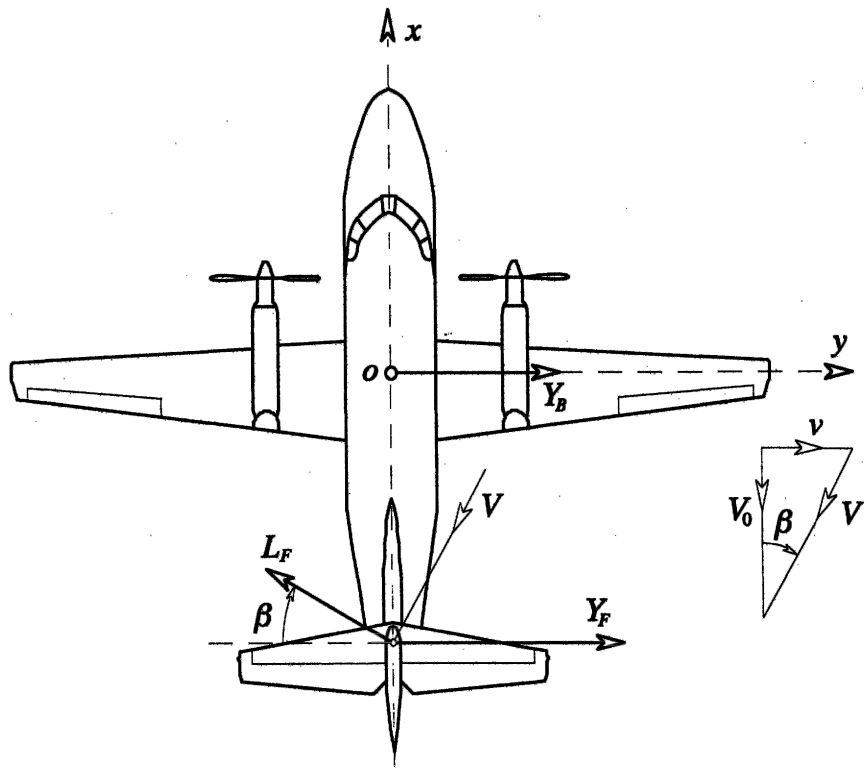

Fig. 13.4 Sideforce generation in a sideslip

$$Y_F = -\frac{1}{2}\rho V_0^2 S_F a_{1_F} \beta \cos\beta \cong -\frac{1}{2}\rho V_0^2 S_F a_{1_F} \beta \tag{13.79}$$

and since the sideslip angle β is small, $\cos\beta \cong 1$.

Let the total sideforce due to sideslip be denoted Y, then, by definition,

$$v\mathring{Y}_v = Y = Y_B + Y_F = \frac{1}{2}\rho V_0^2 (S_B y_B - S_F a_{1_F})\beta \tag{13.80}$$

Substitute the expression for β given by equation (13.78) into equation (13.80) to obtain an expression for the dimensional derivative

$$\mathring{Y}_v = \frac{1}{2}\rho V_0 (S_B y_B - S_F a_{1_F}) \tag{13.81}$$

and with reference to Appendix 1, the dimensionless form of the derivative is given by

$$Y_v = \frac{\mathring{Y}_v}{\frac{1}{2}\rho V_0 S} = \left(\frac{S_B}{S} y_B - \frac{S_F}{S} a_{1_F}\right) \tag{13.82}$$

$\mathring{L}_v = \dfrac{\partial L}{\partial V}$ *Rolling moment due to sideslip*

Rolling moment due to sideslip is one of the most important lateral stability derivatives since it quantifies the *lateral static stability* of the aeroplane, discussed in Section 3.4. It is one of the most difficult derivatives to estimate with any degree of confidence since it is numerically small and has many identifiable contributions. Preliminary estimates are based on the most significant contributions which are usually assumed to arise from wing dihedral, wing sweep, wing–fuselage geometry and the fin.

In many classical aeroplanes the wing dihedral makes the most significant contribution to the overall value of the derivative. Indeed, dihedral is one of the most important variables available to the aircraft designer with which to tailor the lateral static stability of the aeroplane. The derivative is therefore frequently referred to as the *dihedral effect* irrespective of the magnitude of the other contributions. Since the tendency is for the right wing to drop in a positive sideslip disturbance the associated disturbing rolling moment is also positive. A stabilizing aerodynamic reaction is one in which the rolling moment due to sideslip is negative since this will tend to oppose the disturbing rolling moment. The dihedral effect is particularly beneficial in this respect.

In a positive sideslip disturbance to the right, the effect of dihedral is to increase the incidence of the right wing panel indicated in Fig. 13.5. The left wing panel 'sees' a corresponding reduction in incidence. Thus, the rolling moment is generated by the differential lift across the wing-span.

Referring to Fig. 13.5, the component of sideslip velocity perpendicular to the plane of the wing panel is given by

$$v' = v\sin\Gamma \cong v\Gamma \tag{13.83}$$

since the dihedral angle Γ is usually small.

The velocity component v' gives rise to a small increment in incidence α' as shown where

$$\alpha' \cong \tan\alpha' = \frac{v'}{V_0} = \frac{v\Gamma}{V_0} \tag{13.84}$$

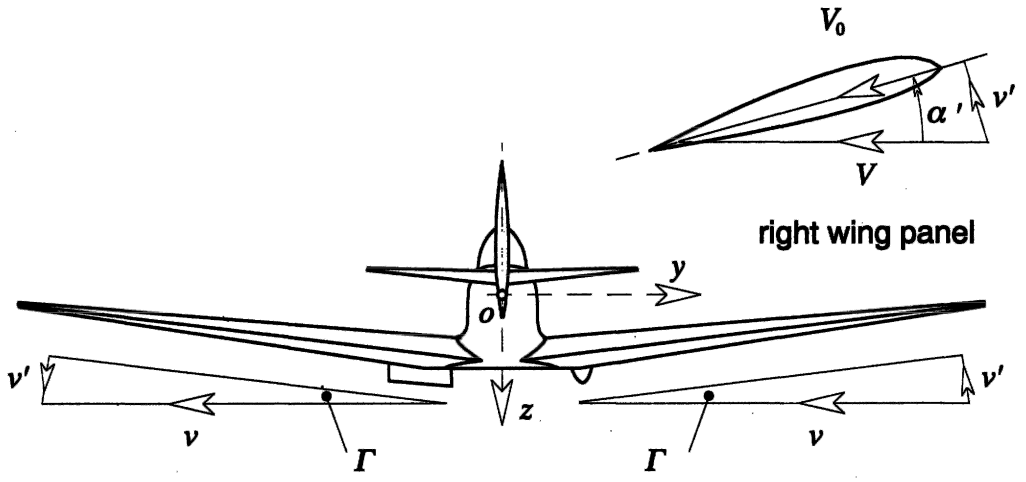

Fig. 13.5 Incidence due to sideslip on a wing with dihedral

Consider the lift due to the increment in incidence on the chordwise strip element on the right wing panel as shown in Fig. 13.6. The strip is at spanwise coordinate y measured from the ox axis, has elemental width dy and local chord c_y. The lift increment on the strip resolves into a normal force increment δZ given by

$$\delta Z_{\text{right}} = -\frac{1}{2}\rho V_0^2 c_y \mathrm{d}y a_y \alpha' \cos\Gamma \cong -\frac{1}{2}\rho V_0 c_y a_y v \Gamma \mathrm{d}y \tag{13.85}$$

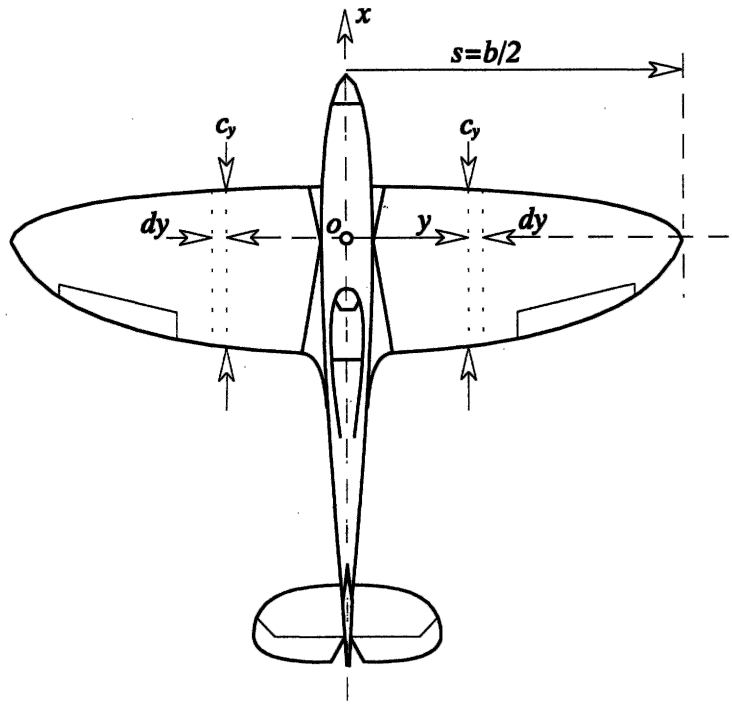

Fig. 13.6 A chordwise strip element on the right wing panel

where a_y is the local lift curve slope. The corresponding increment in rolling moment δL is given by

$$\delta L_{\text{right}} = \delta Z_{\text{right}} y = -\frac{1}{2}\rho V_0 c_y a_y v \Gamma y \mathrm{d}y \tag{13.86}$$

The total rolling moment due to the right wing panel may be obtained by integrating equation (13.86) from the root to the tip, whence

$$L_{\text{right}} = -\frac{1}{2}\rho V_0 v \int_0^s c_y a_y \Gamma y \mathrm{d}y \tag{13.87}$$

Similarly for the left-hand wing panel

$$\delta L_{\text{left}} = -\delta Z_{\text{left}} y = -y\left(\frac{1}{2}\rho V_0 c_y a_y v \Gamma \mathrm{d}y\right) \tag{13.88}$$

Note that the sign of the normal force increment is reversed on the left wing panel since the incidence is, in fact, a decrement, and that the sign of the moment arm is also reversed. Thus

$$L_{\text{left}} = -\frac{1}{2}\rho V_0 v \int_0^s c_y a_y \Gamma y \mathrm{d}y \tag{13.89}$$

By definition the total rolling moment in the sideslip disturbance is given by

$$v\mathring{L}_v = L_{\text{right}} + L_{\text{left}} = L_{\text{total}} = -\rho V_0 v \int_0^s c_y a_y \Gamma y \mathrm{d}y \tag{13.90}$$

Whence, the contribution to the dimensional derivative due to dihedral is

$$\mathring{L}_{v(\text{dihedral})} = -\rho V_0 \int_0^s c_y a_y \Gamma y \mathrm{d}y \tag{13.91}$$

and with reference to Appendix 1, the dimensionless form of the contribution is given by

$$L_{v(\text{dihedral})} = \frac{\mathring{L}_{v(\text{dihedral})}}{\frac{1}{2}\rho V_0 S b} = -\frac{1}{Ss}\int_0^s c_y a_y \Gamma y \mathrm{d}y \tag{13.92}$$

where $b = 2s$ is the wing-span. It is clear that for a wing with dihedral the expression given by equation (13.92) will always be negative and hence stabilizing. On the other hand, a wing with anhedral will be destabilizing.

Wing sweep also makes a significant contribution to L_v. The lift on a yawed wing is determined by the component of velocity normal to the quarter chord line in subsonic flight and normal to the leading edge in supersonic flight. A swept wing is therefore treated as a yawed wing. With reference to Fig. 13.7, consider an elemental chordwise strip on the right wing panel which is perpendicular to the quarter chord line. Subsonic flow conditions are therefore assumed and the flow direction is parallel to the chord line. The strip element is at spanwise distance h from the ox axis, measured along the quarter chord line, the local chord is c_h and the width of the strip is dh. In the steady equilibrium flight condition the chordwise component of velocity is given by

$$V_c = V_0 \cos \Lambda_{1/4} \tag{13.93}$$

and in the presence of a positive sideslip disturbance this becomes

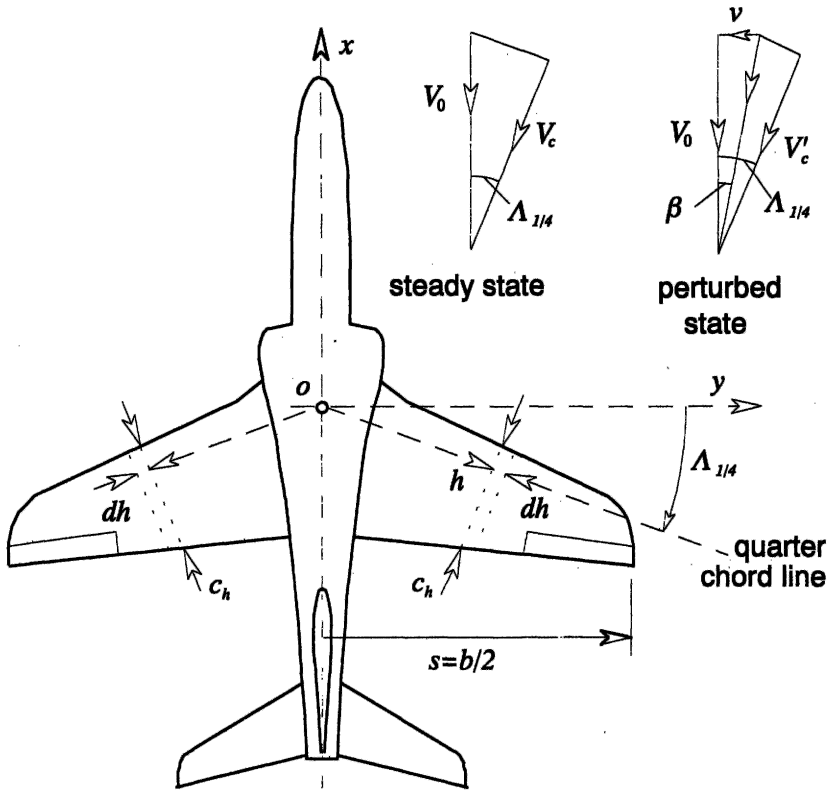

Fig. 13.7 A swept wing in sideslip

$$V_c' = \frac{V_0}{\cos\beta}\cos(\Lambda_{1/4} - \beta) \cong V_0\cos(\Lambda_{1/4} - \beta) \tag{13.94}$$

where β is the sideslip angle which is small by definition. The increment in normal force δZ on the chordwise strip due to the sideslip disturbance arises from the difference in lift between the steady flight condition and the perturbed condition and is given by

$$\delta Z_{\text{right}} = -\left(\frac{1}{2}\rho V_c'^2 c_h \mathrm{d}h a_h \alpha - \frac{1}{2}\rho V_c^2 c_h \mathrm{d}h a_h \alpha\right) = -\frac{1}{2}\rho(V_c'^2 - V_c^2)c_h \mathrm{d}h a_h \alpha \tag{13.95}$$

Substitute the velocity expressions, equations (13.93) and (13.94), into equation (13.95), rearrange and make small angle approximations where appropriate to obtain

$$\delta Z_{\text{right}} = -\frac{1}{2}\rho V_0^2(\beta^2 \sin^2\Lambda_{1/4} + 2\beta \sin\Lambda_{1/4}\cos\Lambda_{1/4})a_h \alpha c_h \mathrm{d}h \tag{13.96}$$

Thus, the resulting increment in rolling moment is

$$\begin{aligned}\delta L_{\text{right}} &= h\cos\Lambda_{1/4}\delta Z_{\text{right}} \\ &= -\frac{1}{2}\rho V_0^2\cos\Lambda_{1/4}(\beta^2 \sin^2\Lambda_{1/4} + 2\beta \sin\Lambda_{1/4}\cos\Lambda_{1/4})a_h \alpha c_h h \mathrm{d}h\end{aligned} \tag{13.97}$$

On the corresponding strip element on the left-hand wing panel the chordwise velocity in the sideslip disturbance is given by

$$V_c' = \frac{V_0}{\cos\beta}\cos(\Lambda_{1/4} + \beta) \cong V_0 \cos(\Lambda_{1/4} + \beta) \tag{13.98}$$

It therefore follows that the resulting increment in rolling moment arising from the left wing panel is

$$\begin{aligned}\delta L_{\text{left}} &= -h\cos\Lambda_{1/4}\delta Z_{\text{left}} \\ &= \frac{1}{2}\rho V_0^2 \cos\Lambda_{1/4}(\beta^2 \sin^2\Lambda_{1/4} - 2\beta \sin\Lambda_{1/4}\cos\Lambda_{1/4}) a_h \alpha c_h h dh\end{aligned} \tag{13.99}$$

The total increment in rolling moment is given by the sum of the right and left wing panel contributions, equations (13.97) and (13.99), and substituting for β from equation (13.78) then

$$\delta L_{\text{total}} = \delta L_{\text{right}} + \delta L_{\text{left}} = -2\rho V_0 v \sin\Lambda_{1/4}\cos^2\Lambda_{1/4} a_h \alpha c_h h dc \tag{13.100}$$

Thus, the total rolling moment due to the sideslip disturbance is given by integrating equation (13.100) along the quarter chord line from the root to the wing tip. By definition, the total rolling moment due to sweep is given by

$$v\mathring{L}_{v(\text{sweep})} = \int \delta L_{\text{total}} = -2\rho V_0 v \sin\Lambda_{1/4}\cos^2\Lambda_{1/4}\int_0^{s\sec\Lambda_{1/4}} a_h \alpha c_h h dh \tag{13.101}$$

or

$$\mathring{L}_{v(\text{sweep})} = -2\rho V_0 \sin\Lambda_{1/4}\cos^2\Lambda_{1/4}\int_0^{s\sec\Lambda_{1/4}} a_h \alpha c_h h dh \tag{13.102}$$

Now it is more convenient to express the geometric variables in equation (13.102) in terms of spanwise and chordwise parameters measured parallel to the oy and ox axes respectively. The geometry of the wing determines that $c_y = c_h \cos\Lambda_{1/4}$, $dy = dh\cos\Lambda_{1/4}$, $y = h\cos\Lambda_{1/4}$ and the integral limit $s\sec\Lambda_{1/4}$ becomes s. Equation (13.102) may then be written

$$\mathring{L}_{v(\text{sweep})} = -2\rho V_0 \tan\Lambda_{1/4}\int_0^s C_{L_y} c_y y dy \tag{13.103}$$

where $C_{L_y} = a_h\alpha$ is the local lift coefficient. However, in the interests of practicality the constant mean lift coefficient for the wing is often assumed and equation (13.103) then simplifies to

$$\mathring{L}_{v(\text{sweep})} = -2\rho V_0 C_L \tan\Lambda_{1/4}\int_0^s c_y y dy \tag{13.104}$$

and with reference to Appendix 1, the dimensionless form of the contribution is given by

$$\mathring{L}_{v(\text{sweep})} = \frac{\mathring{L}_{v(\text{sweep})}}{\frac{1}{2}\rho V_0 S b} = -\frac{2C_L \tan\Lambda_{1/4}}{Ss}\int_0^s c_y y dy \tag{13.105}$$

where $b = 2s$ is the wing-span. Again, it is clear that for a wing with aft sweep the expression given by equation (13.105) will always be negative and hence stabilizing. Thus, wing sweep is equivalent to dihedral as a mechanism for improving lateral stability. On the other hand, a wing with forward sweep will be laterally destabilizing.

The geometry of the wing and fuselage in combination may also make a significant contribution to dihedral effect since, in a sideslip condition, the lateral cross flow in the vicinity of the wing root gives rise to differential lift which, in turn, gives rise to rolling moment.

As shown in Fig. 13.8, in a positive sideslip perturbation the aeroplane 'sees' the lateral sideslip velocity component approaching from the right, it being implied that the right wing starts to drop at the onset of the disturbance. The lateral flow around the fuselage is approximately as indicated, thereby giving rise to small perturbations in upwash and downwash in the vicinity of the wing root. As a consequence of the flow condition the high wing configuration experiences a transient increase in incidence at the right wing root and a corresponding decrease in incidence at the left wing root. The differential lift thus created causes a negative rolling moment and, since this will tend to 'pick up' the right wing, the effect is stabilizing. Clearly, as indicated, a low wing

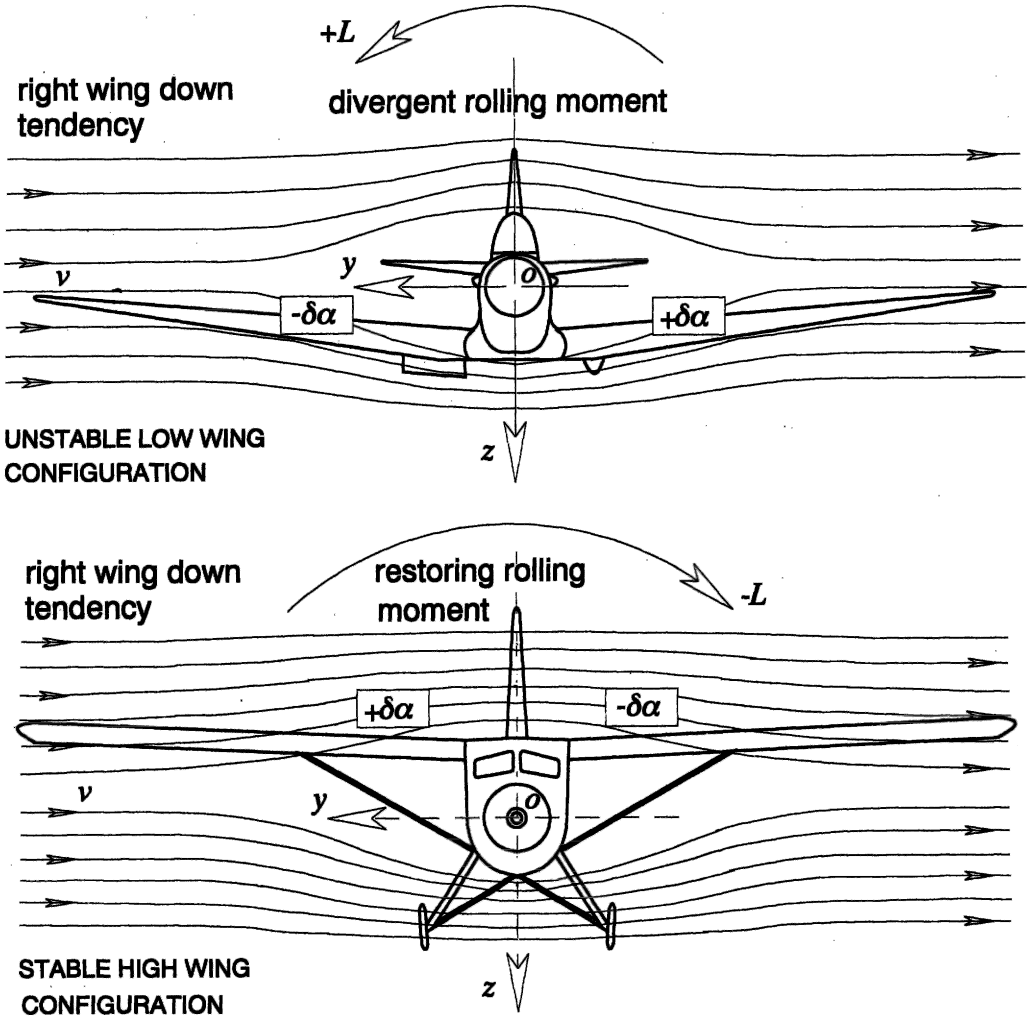

Fig. 13.8 Lateral cross flow in a sideslip

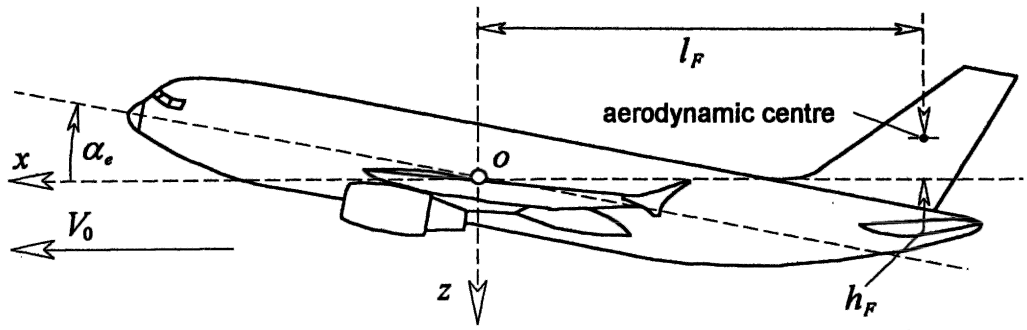

Fig. 13.9 Rolling moment due to fin lift in sideslip

configuration behaves in the opposite manner and the rolling moment due to sideslip is very definitely destabilizing. Thus, a high wing configuration enjoys an additional stabilizing contribution to dihedral effect whereas a low wing configuration makes a destabilizing contribution.

It is not generally possible to develop simple aerodynamic expressions to quantify the wing–fuselage geometry contribution to rolling moment due to sideslip. The aerodynamic phenomena involved are rather too complex to be modelled simply. It is known, for example, that the magnitude of the contribution is increased with an increase in fuselage width or depth and with an increase in aspect ratio. Reliable values for the contribution are best obtained by measurement or by reference to source documents such as ESDU data items.

The fin contribution to rolling moment due to sideslip arises from the way in which the lift developed on the fin in a sideslip perturbation acts on the airframe. The lift acts at the aerodynamic centre of the fin, which may be above or below the roll axis, thereby giving rise to a rolling moment. A typical situation is shown in Fig. 13.9.

The sideforce Y_F resulting from the lift developed by the fin in a sideslip perturbation is given by equation (13.79) and if the moment arm of the aerodynamic centre about the roll axis (ox axis) is denoted h_F then, in the perturbation, by definition

$$v\mathring{L}_{v(\text{fin})} = L = Y_F h_F = -\frac{1}{2}\rho V_0^2 S_F a_{1_F} \beta h_F \tag{13.106}$$

Substitute for β from equation (13.78) to obtain the following expression for the dimensional contribution to the derivative

$$\mathring{L}_{v(\text{fin})} = -\frac{1}{2}\rho V_0 S_F a_{1_F} h_F \tag{13.107}$$

and with reference to Appendix 1, the dimensionless form of the contribution is given by

$$L_{v(\text{fin})} = \frac{\mathring{L}_{v(\text{fin})}}{\frac{1}{2}\rho V_0 S b} = -\frac{S_F h_F}{Sb} a_{1_F} = -\bar{V}_F \frac{h_F}{l_F} a_{1_F} \tag{13.108}$$

where the *fin volume ratio* is given by

$$\bar{V}_F = \frac{S_F l_F}{Sb} \tag{13.109}$$

When the aerodynamic centre of the fin is above the roll axis, h_F is positive and the

expression given by equation (13.108) will be negative and hence stabilizing. However, it is evident that, depending on aircraft geometry, h_F may be small and may even change sign at extreme aircraft attitude. Thus, at certain flight conditions, the contribution to rolling moment due to sideslip arising from the fin may become positive and hence laterally destabilizing.

An estimate of the total value of the derivative L_v is obtained by summing the estimates of all the contributions for which a value can be obtained. Since the value of the derivative is usually small and negative, and hence stabilizing, even small inaccuracies in the estimated values of the contributions can lead to a very misleading conclusion. Since the derivative is so important in the determination of the lateral stability and control characteristics of an aeroplane the ESDU data items include a comprehensive procedure for estimating meaningful values of the significant contributions. Although, collectively, all the contributions probably embrace the most complex aerodynamics of all the derivatives it is, fortunately, relatively easy to measure in both a wind tunnel test and in a flight test.

$\mathring{N}_v = \dfrac{\partial N}{\partial V}$ *Yawing moment due to sideslip*

The *weathercock*, or directional static stability of an aircraft, is determined by the yawing moment due to sideslip derivative. It quantifies the tendency of the aeroplane to turn *into wind* in the presence of a sideslip disturbance. Directional static stability is also discussed in greater detail in Section 3.5. In a sideslip disturbance the resulting lift increments arising from wing dihedral, wing sweep, wing–fuselage geometry, etc, as described previously, also give rise to associated increments in induced drag. The differential drag effects across the wing-span give rise in turn to contributions to yawing moment due to sideslip. However, these contributions are often regarded as insignificant compared with that due to the fin, at least for preliminary estimates. Note that, in practice, the additional contributions may well be significant and that by ignoring them a degree of inaccuracy is implied in the derivative estimate.

With reference to Figs 13.4 and 13.9 consider only the fin contribution which arises from the turning moment in yaw caused by the fin sideforce resulting from the sideslip. By definition this may be quantified as follows

$$v\mathring{N}_{v(\text{fin})} = -l_F Y_F = \frac{1}{2}\rho V_0^2 S_F a_{1_F} \beta l_F \tag{13.110}$$

where the fin sideforce due to sideslip is given by equation (13.79). Substitute for β from equation (13.78) to obtain the expression for the dimensional derivative

$$\mathring{N}_{v(\text{fin})} = \frac{1}{2}\rho V_0 S_F a_{1_F} l_F \tag{13.111}$$

and with reference to Appendix 1, the dimensionless form of the derivative is given by

$$N_{v(\text{fin})} = \frac{\mathring{N}_{v(\text{fin})}}{\frac{1}{2}\rho V_0 S b} = \bar{V}_F a_{1_F} \tag{13.112}$$

Note that the sign of N_v is positive, which indicates that it is stabilizing in effect. In a positive sideslip the incident wind vector is offset to the right of the nose, see Fig. 13.4, and the stabilizing yawing moment due to sideslip results in a positive yaw response to

turn the aircraft to the right until the aircraft aligns directionally with the wind vector. The yawing effect of the sideslip is thus nullified. The contribution from the wing due to differential drag effects is also usually stabilizing and may well become the most significant contribution at high angles of attack since a large part of the fin may become immersed in the forebody wake, with the consequent reduction in its aerodynamic effectiveness. The contribution from the *lateral drag* effects on the gross side area ahead of and behind the *cg* may also be significant. However, it is commonly found that the yawing moment due to sideslip arising from the side area is often negative, and hence destabilizing. For certain classes of aircraft, such as large transport aeroplanes, this destabilizing contribution can be very significant and requires a very large fin to ensure a reasonable degree of aerodynamic directional stability.

13.3.3 DERIVATIVES DUE TO RATE OF ROLL

As seen by the pilot, positive roll is to the right, is consistent with a down going right wing and the small perturbation roll rate transient is denoted p. The nature of a free positive roll rate disturbance is such that as the right wing tends to drop it is accompanied by a tendency for the nose to turn to the right and for the aeroplane to sideslip to the right. The reaction to the roll rate disturbance is stabilizing if the aerodynamic forces and moments produced in response tend to restore the aeroplane to a wings level zero sideslip equilibrium state.

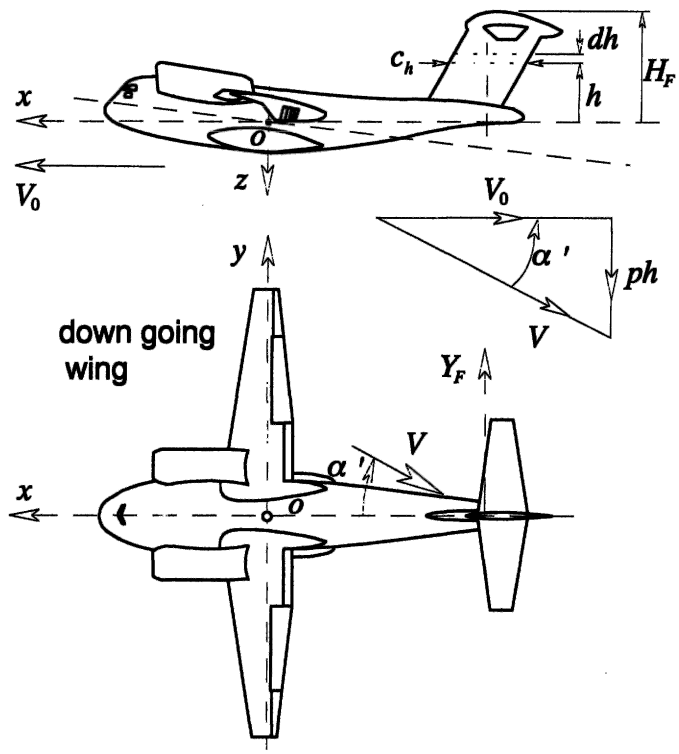

Fig. 13.10 Fin sideforce generation in rolling flight

$\mathring{Y}_p = \dfrac{\partial Y}{\partial p}$ *Sideforce due to roll rate*

The sideforce due to roll rate is usually considered to be negligible except for aircraft with a large high aspect ratio fin. Even then, the effect may well be small. Thus, the fin contribution is assumed to be the only significant contribution to the derivative and may be estimated as follows.

With reference to Fig. 13.10, consider the chordwise strip element on the fin of width dh and at coordinate h measured upwards from the ox axis. When the aeroplane experiences a positive roll rate disturbance p the strip element on the fin experiences a lateral velocity component ph. The resultant total velocity transient V is at incidence α' to the fin and, since the incidence transient is small by definition,

$$\alpha' \cong \tan\alpha' = \frac{ph}{V_0} \tag{13.113}$$

The incidence transient causes a fin lift transient, which resolves into a lateral force increment δY on the chordwise strip element and is given by

$$\delta Y = -\frac{1}{2}\rho V_0^2 c_h \mathrm{d}h a_h \alpha' = -\frac{1}{2}\rho V_0 p a_h c_h h \mathrm{d}h \tag{13.114}$$

where a_h is the local lift curve slope and c_h is the local chord. The total sideforce transient acting on the fin in the roll rate disturbance is given by integrating equation (13.114) from the root to the tip of the fin and by definition

$$p\mathring{Y}_{p(\mathrm{fin})} = Y_F = -\frac{1}{2}\rho V_0 p \int_0^{H_F} a_h c_h h \mathrm{d}h \tag{13.115}$$

where H_F is the fin span measured from the ox axis. The expression for the fin contribution to the dimensional derivative is therefore given by

$$\mathring{Y}_{p(\mathrm{fin})} = -\frac{1}{2}\rho V_0 \int_0^{H_F} a_h c_h h \mathrm{d}h \tag{13.116}$$

and with reference to Appendix 1, the dimensionless form of the derivative is given by

$$Y_{p(\mathrm{fin})} = \frac{\mathring{Y}_{p(\mathrm{fin})}}{\frac{1}{2}\rho V_0 S b} = -\frac{1}{Sb}\int_0^{H_F} a_h c_h h \mathrm{d}h \tag{13.117}$$

$\mathring{L}_p = \dfrac{\partial L}{\partial p}$ *Rolling moment due to roll rate*

Rolling moment due to roll rate arises largely from the wing with smaller contributions from the fuselage, tailplane and fin. This derivative is most important since it quantifies the damping in roll and is therefore significant in determining the dynamic characteristics of the roll subsidence mode, discussed in some detail in Section 7.2. The following analysis considers the wing contribution only.

With reference to Fig. 13.11, when the right wing panel experiences a positive perturbation in roll rate p, assuming the aircraft rolls about the ox axis, then the small increase in incidence α' at the chordwise strip element is given by

$$\alpha' \cong \tan\alpha' = \frac{py}{V_0} \tag{13.118}$$

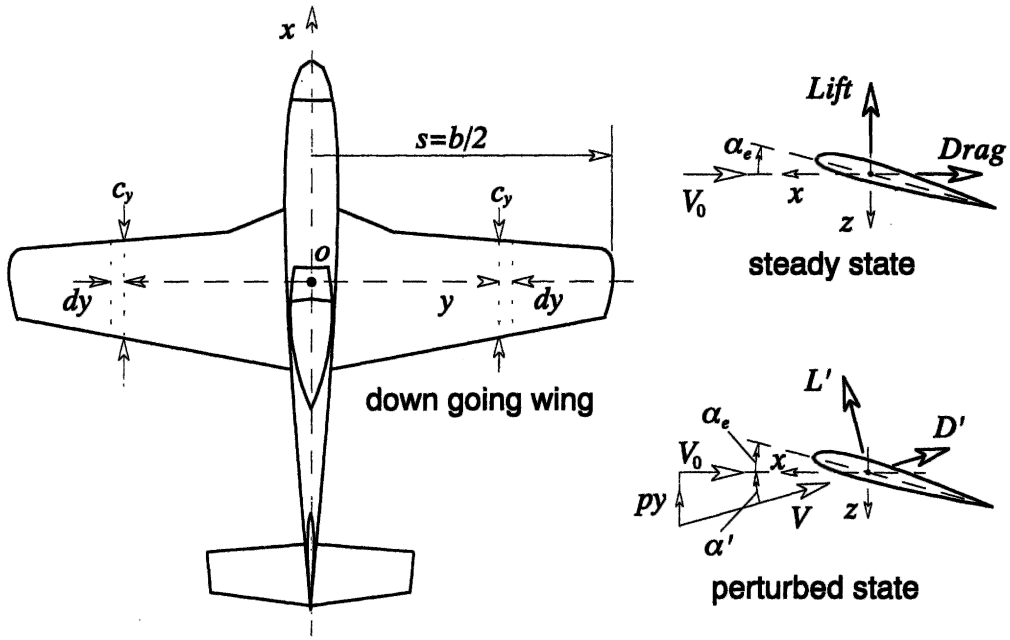

Fig. 13.11 Wing incidence in rolling flight

There is, of course, a reduction in incidence on the corresponding chordwise strip element on the left wing panel. Denoting the total lift and drag increments in the disturbance on the chordwise strip element on the right wing panel L' and D' respectively, then

$$L' = \frac{1}{2}\rho V_0^2 c_y \mathrm{d}y a_y(\alpha_e + \alpha') \tag{13.119}$$

and

$$D' = \frac{1}{2}\rho V_0^2 c_y \mathrm{d}y C_{D_y} \tag{13.120}$$

The normal force increment $\delta Z_{(\text{right})}$ acting at the chordwise strip element in the roll rate perturbation is given by

$$\delta Z_{(\text{right})} = -L' \cos\alpha' - D' \sin\alpha' \cong -L' - D'\alpha' \tag{13.121}$$

since α' is a small angle. Substitute for L', D' and α' from equations (13.119), (13.120) and (13.118) respectively to obtain

$$\delta Z_{(\text{right})} = -\frac{1}{2}\rho V_0^2 \left(a_y\alpha_e + (a_y + C_{D_y})\frac{py}{V_0}\right) c_y \mathrm{d}y \tag{13.122}$$

The resulting increment in rolling moment is then given by

$$\delta L_{(\text{right})} = y\delta Z_{(\text{right})} = -\frac{1}{2}\rho V_0^2 \left(a_y\alpha_e + (a_y + C_{D_y})\frac{py}{V_0}\right) c_y y \mathrm{d}y \tag{13.123}$$

and the corresponding increment in rolling moment arising from the left wing panel, where the incidence is reduced by α' since the panel is rising with respect to the incident air flow, is given by

$$\delta L_{(\text{left})} = -y\delta Z_{(\text{left})} = \frac{1}{2}\rho V_0^2\left(a_y\alpha_e - (a_y + C_{D_y})\frac{py}{V_0}\right)c_y y\mathrm{d}y \tag{13.124}$$

The total rolling moment due to roll rate is obtained by summing the increments from the right and left chordwise strips, given by equations (13.123) and (13.124) respectively, and integrating from the root to the tip of the wing

$$L_{\text{total}} = \int_{\text{span}} (\delta L_{(\text{left})} + \delta L_{(\text{right})}) = -\rho V_0 p \int_0^s (a_y + C_{D_y})c_y y^2\mathrm{d}y \tag{13.125}$$

and by definition

$$p\mathring{L}_p = L_{\text{total}} = -\rho V_0 p \int_0^s (a_y + C_{D_y})c_y y^2\mathrm{d}y \tag{13.126}$$

Whence, the dimensional derivative expression is given by

$$\mathring{L}_p = -\rho V_0 \int_0^s (a_y + C_{D_y})c_y y^2\mathrm{d}y \tag{13.127}$$

and with reference to Appendix 1, the dimensionless form of the derivative is given by

$$L_p = \frac{\mathring{L}_p}{\frac{1}{2}\rho V_0 S b^2} = -\frac{1}{2Ss^2}\int_0^s (a_y + C_{D_y})c_y y^2\mathrm{d}y \tag{13.128}$$

where $b = 2s$ is the wing-span.

$\mathring{N}_p = \dfrac{\partial N}{\partial p}$ *Yawing moment due to roll rate*

Yawing moment due to roll rate is almost entirely determined by the wing contribution, although in some aircraft a large fin may give rise to a significant additional contribution. Only the wing contribution is considered here.

It is shown in Fig. 13.11 that in a roll rate perturbation the chordwise strip element on the right (down going) wing experiences an incremental increase in lift and induced drag, given by equations (13.119) and (13.120), whilst there is an equal decrease in lift and induced drag on the corresponding strip on the left (up going) wing. The differential drag thereby produced gives rise to the yawing moment perturbation.

With reference to Fig. 13.11, the longitudinal axial force increment acting on the chordwise strip element on the right wing panel is given by

$$\delta X_{(\text{right})} = L' \sin\alpha' - D' \cos\alpha' \cong L'\alpha' - D' \tag{13.129}$$

Substitute for L' and D' from equations (13.119) and (13.120) respectively and write

$$C_{D_y} = \frac{\mathrm{d}C_D}{\mathrm{d}\alpha_y}(\alpha_e + \alpha') \tag{13.130}$$

to obtain

$$\delta X_{(\text{right})} = \frac{1}{2}\rho V_0^2\left(a_y\alpha' - \frac{\mathrm{d}C_D}{\mathrm{d}\alpha_y}\right)(\alpha_e + \alpha')c_y\mathrm{d}y \tag{13.131}$$

The incremental axial force gives rise to a negative increment in yawing moment given by

$$\delta N_{(\text{right})} = -y\delta X_{(\text{right})} = -\frac{1}{2}\rho V_0^2\left(a_y\alpha' - \frac{dC_D}{d\alpha_y}\right)(\alpha_e + \alpha')c_y y dy \tag{13.132}$$

The reduction in incidence due to roll rate on the corresponding chordwise strip element on the left wing panel gives rise to a positive increment in yawing moment and, in a similar way, it may be shown that

$$\delta N_{(\text{left})} = y\delta X_{(\text{left})} = -\frac{1}{2}\rho V_0^2\left(a_y\alpha' + \frac{dC_D}{d\alpha_y}\right)(\alpha_e - \alpha')c_y y dy \tag{13.133}$$

The total yawing moment increment due to roll rate is given by summing equations (13.132) and (13.133) and substituting for α' from equation (13.118)

$$\delta N_{\text{total}} = \delta N_{(\text{left})} + \delta N_{(\text{right})} = -\rho V_0 p\left(a_y\alpha_e - \frac{dC_D}{d\alpha_y}\right)c_y y^2 dy \tag{13.134}$$

By definition, the total yawing moment due to roll rate is given by

$$p\mathring{N}_p = N_{\text{total}} = \int_{\text{semispan}} \delta N_{\text{total}} = -\rho V_0 p \int_0^s \left(a_y\alpha_e - \frac{dC_D}{d\alpha_y}\right)c_y y^2 dy \tag{13.135}$$

Whence, the expression for the dimensional derivative

$$\mathring{N}_p = -\rho V_0 \int_0^s \left(C_{L_y} - \frac{dC_D}{d\alpha_y}\right)c_y y^2 dy \tag{13.136}$$

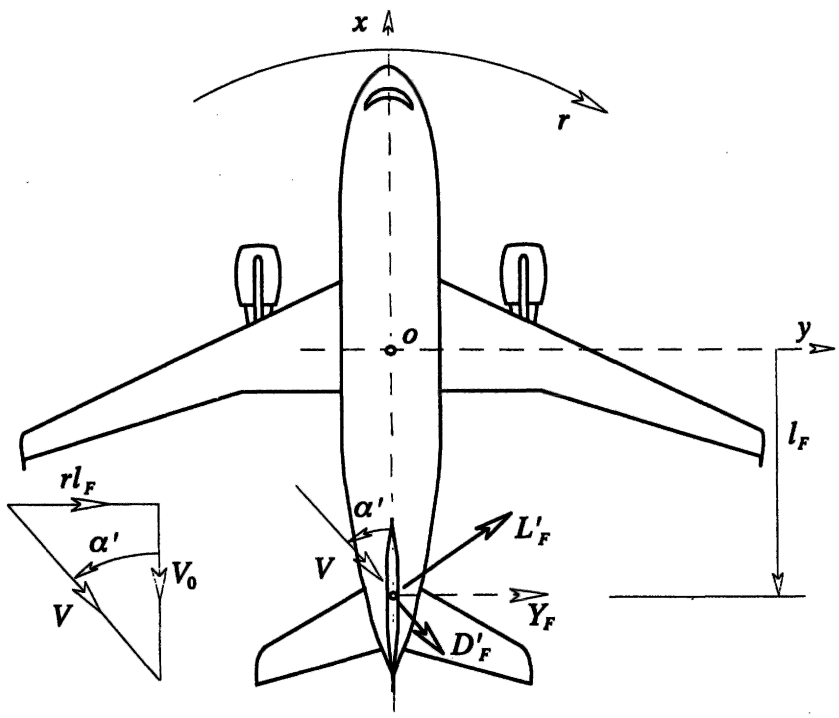

Fig. 13.12 Fin incidence due to yaw rate

where $C_{L_y} = a_y \alpha_e$ is the equilibrium local lift coefficient. With reference to Appendix 1, the dimensionless form of the derivative is given by

$$N_p = \frac{\mathring{N}_p}{\frac{1}{2}\rho V_0 S b^2} = -\frac{1}{2Ss^2}\int_0^s \left(C_{L_y} - \frac{dC_D}{d\alpha_y}\right) c_y y^2 dy \tag{13.137}$$

13.3.4 DERIVATIVES DUE TO RATE OF YAW

As seen by the pilot, a positive yaw rate is such that the nose of the aeroplane swings to the right and the small perturbation yaw rate transient is denoted r. The nature of a free positive yaw rate disturbance is such that as the nose swings to the right, the right wing tends to drop and the aeroplane sideslips to the right. The reaction to the yaw rate disturbance is stabilizing if the aerodynamic forces and moments produced in response tend to restore the aeroplane to a symmetric wings level equilibrium flight condition.

$\mathring{Y}_r = \dfrac{\partial Y}{\partial r}$ *Sideforce due to yaw rate*

For most conventional aeroplanes the sideforce due to yaw rate is insignificant unless the fin is relatively large. In such cases the fin lift generated by the yawing motion gives rise to a sideforce of significant magnitude.

Referring to Fig. 13.12, in a yaw rate perturbation the transient incidence of the fin may be written

$$\alpha' \cong \tan\alpha' = \frac{r l_F}{V_0} \tag{13.138}$$

where l_F is the moment arm of the fin aerodynamic centre about the centre of rotation in yaw, the *cg*, and by definition, the incidence transient is a small angle. The resultant transient fin lift L'_F gives rise to a sideforce Y_F

$$Y_F = L'_F \cos\alpha' \cong \frac{1}{2}\rho V_0^2 S_F a_{1_F} \alpha' = \frac{1}{2}\rho V_0 S_F l_F a_{1_F} r \tag{13.139}$$

By definition, the sideforce arising in a yaw rate disturbance is given by

$$r\mathring{Y}_r = Y_F = \frac{1}{2}\rho V_0 S_F l_F a_{1_F} r \tag{13.140}$$

Whence, the expression for the dimensional sideforce due to yaw rate derivative is given by

$$\mathring{Y}_r = \frac{1}{2}\rho V_0 S_F l_F a_{1_F} \tag{13.141}$$

and with reference to Appendix 1, the dimensionless form of the derivative is given by

$$Y_r = \frac{\mathring{Y}_r}{\frac{1}{2}\rho V_0 S b} = \bar{V}_F a_{1_F} \tag{13.142}$$

where the *fin volume ratio* $\bar{V}_F$ is given by equation (13.109). Clearly, the resolved component of the induced drag transient on the fin D'_F will also make a contribution to the total sideforce transient. However, this is usually considered to be insignificantly small compared with the lift contribution.

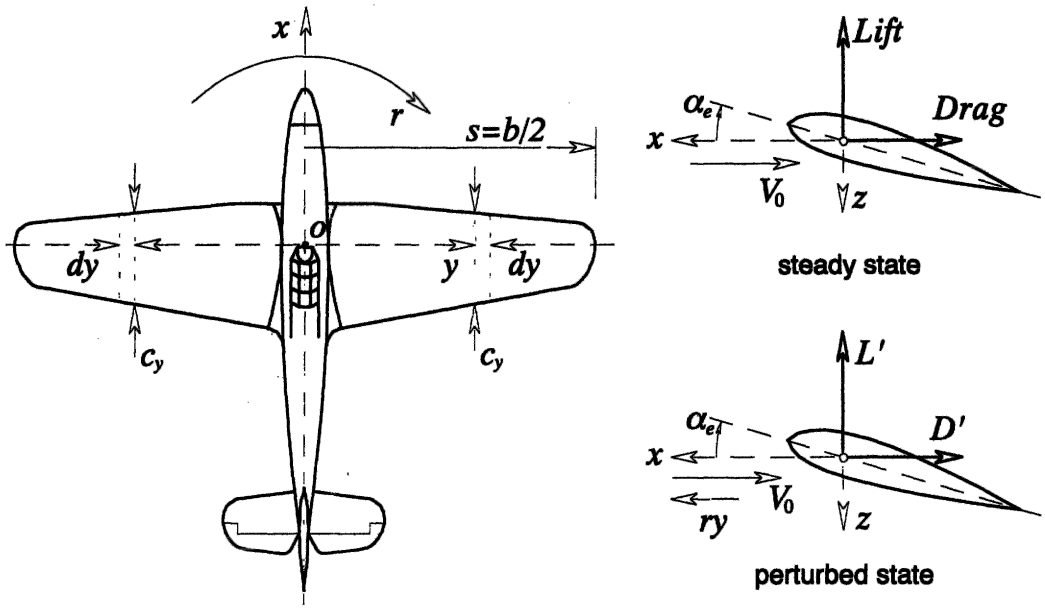

Fig. 13.13 Wing forces due to yaw rate

$\mathring{L}_r = \dfrac{\partial L}{\partial r}$ *Rolling moment due to yaw rate*

In positive yawing motion the relative velocity of the air flowing over the right wing panel is decreased whilst the velocity over the left wing panel is increased. This gives rise to an increase in lift and induced drag on the port wing with a corresponding decrease in lift and drag on the starboard wing. The force increments thus produced result in a rolling moment and a yawing moment about the *cg*. A contribution to rolling moment also arises due to the sideforce generated by the fin in yawing motion although it is generally smaller than the wing contribution.

With reference to Fig. 13.13, the velocity at the chordwise strip element on the right wing during a yaw rate perturbation is given by

$$V = V_0 - ry \tag{13.143}$$

and the total lift on the chordwise strip element during the perturbation is given by

$$\begin{aligned}\delta L'_{(\text{right})} &= \frac{1}{2}\rho V^2 c_y \mathrm{d}y C_{L_y} = \frac{1}{2}\rho(V_0 - ry)^2 c_y \mathrm{d}y C_{L_y} \\ &= \frac{1}{2}\rho(V_0^2 - 2ryV_0)c_y \mathrm{d}y C_{L_y}\end{aligned} \tag{13.144}$$

when products of small quantities are neglected. The rolling moment due to the lift on the chordwise strip element on the right wing is therefore given by

$$\delta L_{(\text{right})} = -\delta L'_{(\text{right})} y = -\frac{1}{2}\rho(V_0^2 - 2ryV_0)c_y y \mathrm{d}y C_{L_y} \tag{13.145}$$

Similarly, the rolling moment due to the lift on the chordwise strip element on the left wing is given by

$$\delta L_{(\text{left})} = \delta L'_{(\text{left})} y = \frac{1}{2}\rho(V_0^2 + 2ryV_0)c_y y\mathrm{d}yC_{L_y} \tag{13.146}$$

Thus, the total rolling moment due to yaw rate arising from the wing is given by integrating the sum of the components due to the chordwise strip elements, equations (13.145) and (13.146), over the semi-span

$$L_{\text{wing}} = \int_{\text{semispan}} (\delta L_{(\text{left})} + \delta L_{(\text{right})}) = 2\rho V_0 r \int_0^s C_{L_y} c_y y^2 \mathrm{d}y \tag{13.147}$$

By definition, the rolling moment due to wing lift in a yaw rate disturbance is given by

$$r\mathring{L}_{r(\text{wing})} = L_{\text{wing}} = 2\rho V_0 r \int_0^s C_{L_y} c_y y^2 \mathrm{d}y \tag{13.148}$$

Whence, the expression for the wing contribution to the dimensional rolling moment due to yaw rate derivative is

$$\mathring{L}_{r(\text{wing})} = 2\rho V_0 \int_0^s C_{L_y} c_y y^2 \mathrm{d}y \tag{13.149}$$

and with reference to Appendix 1, the dimensionless form of the derivative is given by

$$L_{r(\text{wing})} = \frac{\mathring{L}_{r(\text{wing})}}{\frac{1}{2}\rho V_0 S b^2} = \frac{1}{Ss^2}\int_0^s C_{L_y} c_y y^2 \mathrm{d}y \tag{13.150}$$

where $b = 2s$ is the wing-span.

Note that for a large aspect ratio rectangular wing it may be assumed that $C_{L_y} = C_L$,

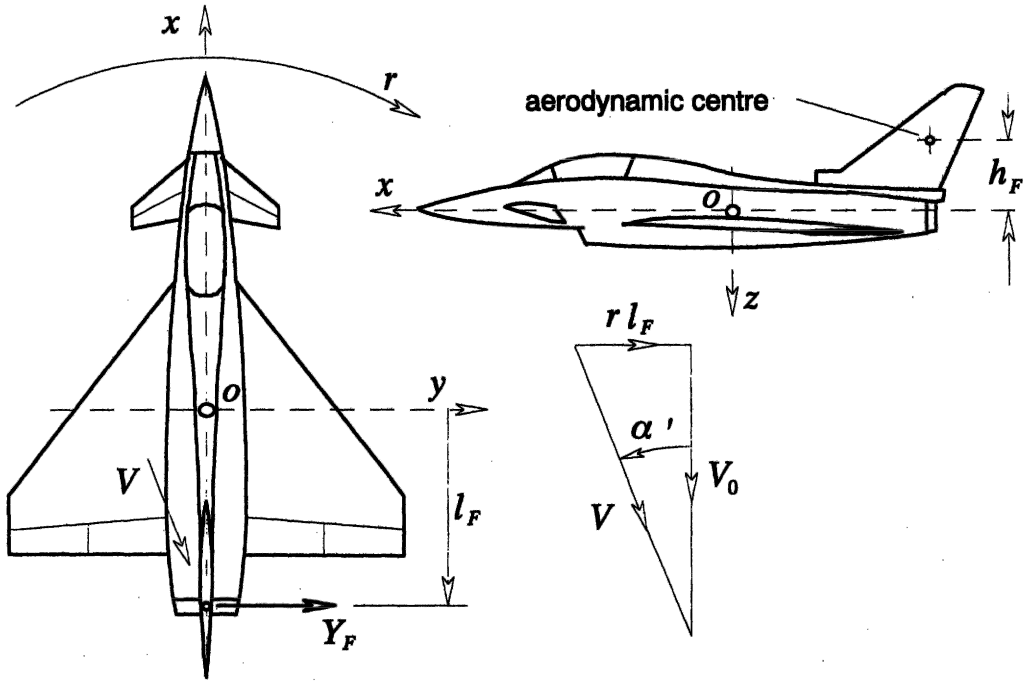

Fig. 13.14 Rolling moment due to yaw rate arising from the fin

the lift coefficient for the whole wing, and that $c_y = c$, the constant geometric chord of the wing. For this special case it is easily shown, from equation (13.150), that

$$L_r = \frac{1}{6} C_L \tag{13.151}$$

However, it should be appreciated that the assumption relating to constant lift coefficient across the span is rather crude and, consequently, the result given by equation (13.151) is very approximate although it can be useful as a guide for checking estimated values of the derivative.

The fin contribution to the rolling moment due to yaw rate derivative arises from the moment about the roll axis of the sideforce generated by the fin in yaw. The sideforce is generated by the mechanism illustrated in Fig. 13.12 and acts at the aerodynamic centre of the fin, which is usually above the roll axis, and hence gives rise to a negative rolling moment. The situation prevailing is illustrated in Fig. 13.14.

With reference to Fig. 13.14, a rolling moment is developed by the fin sideforce due to yaw rate Y_F, which is given by equation (13.139), acting at the aerodynamic centre which is located h_F above the roll axis. Whence, the rolling moment is given by

$$L_{fin} = Y_F h_F = \frac{1}{2} \rho V_0 S_F l_F a_{1_F} r h_F \tag{13.152}$$

By definition, the rolling moment due to fin sideforce in a yaw rate disturbance is given by

$$r\mathring{L}_{r(fin)} = L_{fin} = \frac{1}{2} \rho V_0 S_F l_F a_{1_F} r h_F \tag{13.153}$$

Hence, the fin contribution to the dimensional derivative is given by

$$\mathring{L}_{r(fin)} = \frac{1}{2} \rho V_0 S_F l_F a_{1_F} h_F \tag{13.154}$$

As before, and with reference to Appendix 1, the dimensionless form of the derivative is given by

$$L_{r(fin)} = \frac{\mathring{L}_{r(fin)}}{\frac{1}{2} \rho V_0 S b^2} = a_{1_F} \bar{V}_F \frac{h_F}{b} \equiv -L_{v(fin)} \frac{l_F}{b} \tag{13.155}$$

The total value of the rolling moment due to yaw rate derivative is then given by the sum of all the significant contributions.

$\mathring{N}_r = \dfrac{\partial N}{\partial r}$ *Yawing moment due to yaw rate*

The yawing moment due to yaw rate derivative is an important parameter in the determination of aircraft directional stability. In particular, it is a measure of the damping in yaw and is therefore dominant in determining the stability of the oscillatory dutch roll mode. The significance of this derivative to lateral-directional dynamics is discussed in detail in Section 7.2. The most easily identified contributions to yaw damping arise from the fin and from the wing. However, it is generally accepted that the most significant contribution arises from the fin, although in some aircraft the fin contribution may become significantly reduced at high angles of attack in which case the wing contribution becomes more important.

Considering the wing contribution first, this arises as a result of the differential drag effect in yawing motion as illustrated in Fig. 13.13. Referring to Fig. 13.13, the total drag on the chordwise strip element on the right wing subject to a steady yaw rate r is reduced for the same reason as the lift, given by equation (13.144), and may be written

$$\delta D'_{(\text{right})} = \frac{1}{2}\rho(V_0^2 - 2ryV_0)c_y \mathrm{d}y C_{D_y} \tag{13.156}$$

The yawing moment about the *cg* generated by the drag on the chordwise strip element is

$$\delta N_{(\text{right})} = \delta D'_{(\text{right})} y = \frac{1}{2}\rho(V_0^2 - 2ryV_0)c_y y \mathrm{d}y C_{D_y} \tag{13.157}$$

and similarly, for the yawing moment arising at the corresponding chordwise strip on the left wing

$$\delta N_{(\text{left})} = -\delta D'_{(\text{left})} y = -\frac{1}{2}\rho(V_0^2 + 2ryV_0)c_y y \mathrm{d}y C_{D_y} \tag{13.158}$$

Thus, the total yawing moment due to yaw rate arising from the wing is given by integrating the sum of the components due to the chordwise strip elements, equations (13.157) and (13.158), over the semi-span

$$N_{\text{wing}} = \int_{\text{semispan}} (\delta N_{(\text{right})} - \delta N_{(\text{left})}) = -2\rho V_0 r \int_0^s C_{D_y} c_y y^2 \mathrm{d}y \tag{13.159}$$

By definition, the yawing moment due to differential wing drag in a yaw rate perturbation is given by

$$r\mathring{N}_{r(\text{wing})} = N_{\text{wing}} = -2\rho V_0 r \int_0^s C_{D_y} c_y y^2 \mathrm{d}y \tag{13.160}$$

Hence, the expression for the wing contribution to the dimensional yawing moment due to yaw rate derivative is

$$\mathring{N}_{r(\text{wing})} = -2\rho V_0 \int_0^s C_{D_y} c_y y^2 \mathrm{d}y \tag{13.161}$$

and with reference to Appendix 1, the dimensionless form of the derivative is given by

$$N_{r(\text{wing})} = \frac{\mathring{N}_{r(\text{wing})}}{\frac{1}{2}\rho V_0 S b^2} = -\frac{1}{Ss^2}\int_0^s C_{D_y} c_y y^2 \mathrm{d}y \tag{13.162}$$

where $b = 2s$ is the wing-span.

As for the derivative L_r, for a large aspect ratio rectangular wing it may be assumed that $C_{D_y} = C_D$, the drag coefficient for the whole wing, and that $c_y = c$, the constant geometric chord of the wing. For this special case it is easily shown, from equation (13.162), that

$$N_{r(\text{wing})} = \frac{1}{6}C_D \tag{13.163}$$

Although the result given by equation (13.163) is rather approximate and subject to the assumptions made, it is useful as a guide for checking the value of an estimated contribution to the derivative.

The fin contribution to yawing moment due to yaw rate is generated by the yawing moment of the fin sideforce due to yaw rate. The mechanism for the generation of fin sideforce is illustrated in Fig. 13.12 and, with reference to that figure and to equation (13.139), the yawing moment thereby generated is given by

$$N_{\text{fin}} = -Y_F l_F = -\frac{1}{2}\rho V_0 S_F l_F^2 a_{1_F} r \tag{13.164}$$

By definition, the yawing moment due to the fin in a yaw rate perturbation is given by

$$r\mathring{N}_{r(\text{fin})} = N_{\text{fin}} = -\frac{1}{2}\rho V_0 S_F l_F^2 a_{1_F} r \tag{13.165}$$

Whence, the expression for the fin contribution to the dimensional yawing moment due to yaw rate derivative is

$$\mathring{N}_{r(\text{fin})} = -\frac{1}{2}\rho V_0 S_F l_F^2 a_{1_F} \tag{13.166}$$

As before, and with reference to Appendix 1, the dimensionless form of the derivative is given by

$$N_{r(\text{fin})} = \frac{\mathring{N}_{r(\text{fin})}}{\frac{1}{2}\rho V_0 S b^2} = -a_{1_F}\bar{V}_F \frac{l_F}{b} = -\frac{l_F}{b} N_{v(\text{fin})} \tag{13.167}$$

The fin volume ratio $\bar{V}_F$ is given by equation (13.109). The total value of the yawing moment due to yaw rate derivative is therefore given by the sum of all the significant contributions.

13.4 Aerodynamic control derivatives

Estimates may be made for the aerodynamic control derivatives provided that the controller in question is a simple flap-like device and provided that its aerodynamic properties can be modelled with a reasonable degree of confidence. However, estimates of the aileron and rudder control derivatives obtained from simple models are unlikely to be accurate since it is very difficult to describe the aerodynamic conditions applying in sufficient detail. Estimates for the lateral-directional aerodynamic control derivatives are best obtained from the appropriate ESDU data items or, preferably, by experimental measurement, although an approximate analysis is given in Babister (1961). For this reason, simple models for the aileron and rudder control derivatives are not given here, although crude estimates may be obtained by the same methods as used to estimate the elevator derivatives as described below.

13.4.1 DERIVATIVES DUE TO ELEVATOR

Typically, the lift coefficient for a tailplane with elevator control is given by

$$C_{L_T} = a_0 + a_1\alpha_T + a_2\eta \tag{13.168}$$

where a_1 is the lift curve slope of the tailplane and a_2 is the lift curve slope with respect to elevator angle η. The corresponding drag coefficient may be expressed

$$C_{D_T} = C_{D_{0_T}} + k_T C_{L_T}^2 \tag{13.169}$$

where all of the parameters in equation (13.169) are tailplane dependent.

$\mathring{X}_\eta = \dfrac{\partial X}{\partial \eta}$ *Axial force due to elevator*

It is assumed that for a small elevator deflection, consistent with a small perturbation, the resulting axial force perturbation arises from the drag change associated with the tailplane only. Whence

$$X \equiv X_T = -D_T = -\frac{1}{2}\rho V^2 S_T C_{D_T} \tag{13.170}$$

Thus

$$\mathring{X}_\eta = \frac{\partial X_T}{\partial \eta} = -\frac{1}{2}\rho V^2 S_T \frac{\partial C_{D_T}}{\partial \eta} \tag{13.171}$$

Substitute for C_{D_T}, from equation (13.169), into equation (13.171) to obtain

$$\mathring{X}_\eta = \frac{\partial X_T}{\partial \eta} = -\rho V^2 S_T k_T C_{L_T} \frac{\partial C_{L_T}}{\partial \eta} \tag{13.172}$$

For a small perturbation, in the limit $V \cong V_0$, from equation (13.168) $\partial C_{L_T}/\partial \eta \cong a_2$ and equation (13.172) may be written

$$\mathring{X}_\eta = -\rho V_0^2 S_T k_T C_{L_T} a_2 \tag{13.173}$$

With reference to Appendix 1, the dimensionless form of the derivative is given by

$$X_\eta = \frac{\mathring{X}_\eta}{\frac{1}{2}\rho V_0^2 S} = -2\frac{S_T}{S} k_T C_{L_T} a_2 \tag{13.174}$$

$\mathring{Z}_\eta = \dfrac{\partial Z}{\partial \eta}$ *Normal force due to elevator*

As before, it is assumed that for a small elevator deflection the resulting normal force perturbation arises from the lift change associated with the tailplane only. Whence

$$Z \equiv Z_T = -L_T = -\frac{1}{2}\rho V^2 S_T C_{L_T} \tag{13.175}$$

Thus

$$\mathring{Z}_\eta = \frac{\partial Z_T}{\partial \eta} = -\frac{1}{2}\rho V^2 S_T \frac{\partial C_{L_T}}{\partial \eta} \tag{13.176}$$

Substitute for C_{L_T}, from equation (13.168), to obtain

$$\mathring{Z}_\eta = \frac{\partial Z_T}{\partial \eta} = -\frac{1}{2}\rho V^2 S_T a_2 \tag{13.177}$$

For a small perturbation, in the limit $V \cong V_0$ and with reference to Appendix 1, the dimensionless form of the derivative is given by

$$Z_\eta = \frac{\mathring{Z}_\eta}{\frac{1}{2}\rho V_0^2 S} = -\frac{S_T}{S} a_2 \tag{13.178}$$

$\mathring{M}_\eta = \dfrac{\partial M}{\partial \eta}$ *Pitching moment due to elevator*

It is assumed that the pitching moment resulting from elevator deflection is due entirely to the moment of the tailplane lift about the *cg*. Hence

$$M \equiv M_T = -L_T l_T = -\frac{1}{2}\rho V^2 S_T l_T C_{L_T} \tag{13.179}$$

Thus, it follows that

$$\mathring{M}_\eta = \frac{\partial M_T}{\partial \eta} = -\frac{1}{2}\rho V^2 S_T l_T \frac{\partial C_{L_T}}{\partial \eta} = \mathring{Z}_\eta l_T \tag{13.180}$$

With reference to Appendix 1 the dimensionless form of the derivative is given by

$$M_\eta = \frac{\mathring{M}_\eta}{\frac{1}{2}\rho V_0^2 S\bar{c}} = -\frac{S_T l_T}{S\bar{c}} a_2 = -\bar{V}_T a_2 \tag{13.181}$$

where $\bar{V}_T$ is the tail volume ratio.

References

Babister, A. W. 1961: *Aircraft Stability and Control.* Pergamon Press, Oxford.

Babister, A. W. 1980: *Aircraft Dynamic Stability and Response.* Pergamon Press, Oxford.

ESDU: *Aerodynamics.* (Especially, *Volume 9—Stability of Aircraft.*) Engineering Sciences Data, ESDU International Ltd, London.

Hancock, G. J. 1995: *An Introduction to the Flight Dynamics of Rigid Aeroplanes.* Ellis Horwood Ltd, Hemel Hempstead.

Appendix 1

Definitions of Aerodynamic Stability and Control Derivatives

Notes

(i) The derivatives given in Tables A1.5 to A1.8 are all referred to *generalized body axes*, and $U_e = V_0 \cos\theta_e$ and $W_e = V_0 \sin\theta_e$. In the particular case when the derivatives are referred to wind axes, $\theta_e = 0$ and the following simplifications can be made: $U_e = V_0$, $W_e = 0$, $\sin\theta_e = 0$ and $\cos\theta_e = 1$.

(ii) The equivalent algebraic expressions in Tables A1.5 to A1.8 were derived with the aid of the computer program *Mathcad 4.0* which includes a facility for symbolic calculation.

(iii) In Tables A1.5, A1.6, A1.7 and A1.8 normalized mass and inertias are used which are defined as follows

$$m' = \frac{m}{\frac{1}{2}\rho V_0 S}$$

$$I'_x = \frac{I_x}{\frac{1}{2}\rho V_0 S b}$$

$$I'_y = \frac{I_y}{\frac{1}{2}\rho V_0 S \bar{\bar{c}}}$$

$$I'_z = \frac{I_z}{\frac{1}{2}\rho V_0 S b}$$

$$I'_{xz} = \frac{I_{xz}}{\frac{1}{2}\rho V_0 S b}$$

Table A1.1 Longitudinal aerodynamic stability derivatives

Dimensionless	Multiplier	Dimensional
X_u	$\frac{1}{2}\rho V_0 S$	$\overset{\circ}{X}_u$
X_w	$\frac{1}{2}\rho V_0 S$	$\overset{\circ}{X}_w$
$X_{\dot{w}}$	$\frac{1}{2}\rho S\bar{\bar{c}}$	$\overset{\circ}{X}_{\dot{w}}$
X_q	$\frac{1}{2}\rho V_0 S\bar{\bar{c}}$	$\overset{\circ}{X}_q$
Z_u	$\frac{1}{2}\rho V_0 S$	$\overset{\circ}{Z}_u$
Z_w	$\frac{1}{2}\rho V_0 S$	$\overset{\circ}{Z}_w$
$Z_{\dot{w}}$	$\frac{1}{2}\rho S\bar{\bar{c}}$	$\overset{\circ}{Z}_{\dot{w}}$
Z_q	$\frac{1}{2}\rho V_0 S\bar{\bar{c}}$	$\overset{\circ}{Z}_q$
M_u	$\frac{1}{2}\rho V_0 S\bar{\bar{c}}$	$\overset{\circ}{M}_u$
M_w	$\frac{1}{2}\rho V_0 S\bar{\bar{c}}$	$\overset{\circ}{M}_w$
$M_{\dot{w}}$	$\frac{1}{2}\rho S\bar{\bar{c}}^2$	$\overset{\circ}{M}_{\dot{w}}$
M_q	$\frac{1}{2}\rho V_0 S\bar{\bar{c}}^2$	$\overset{\circ}{M}_q$

Table A1.2 Longitudinal control derivatives

Dimensionless	Multiplier	Dimensional
X_η	$\frac{1}{2}\rho V_0^2 S$	$\overset{\circ}{X}_\eta$
Z_η	$\frac{1}{2}\rho V_0^2 S$	$\overset{\circ}{Z}_\eta$
M_η	$\frac{1}{2}\rho V_0^2 S\bar{\bar{c}}$	$\overset{\circ}{M}_\eta$
X_τ	1	$\overset{\circ}{X}_\tau$
Z_τ	1	$\overset{\circ}{Z}_\tau$
M_τ	$\bar{\bar{c}}$	$\overset{\circ}{M}_\tau$

Table A1.3 Lateral aerodynamic stability derivatives

Dimensionless	Multiplier	Dimensional
Y_v	$\frac{1}{2}\rho V_0 S$	$\overset{\circ}{Y}_v$
Y_p	$\frac{1}{2}\rho V_0 Sb$	$\overset{\circ}{Y}_p$
Y_r	$\frac{1}{2}\rho V_0 Sb$	$\overset{\circ}{Y}_r$
L_v	$\frac{1}{2}\rho V_0 Sb$	$\overset{\circ}{L}_v$
L_p	$\frac{1}{2}\rho V_0 Sb^2$	$\overset{\circ}{L}_p$
L_r	$\frac{1}{2}\rho V_0 Sb^2$	$\overset{\circ}{L}_r$
N_v	$\frac{1}{2}\rho V_0 Sb$	$\overset{\circ}{N}_v$
N_p	$\frac{1}{2}\rho V_0 Sb^2$	$\overset{\circ}{N}_p$
N_r	$\frac{1}{2}\rho V_0 Sb^2$	$\overset{\circ}{N}_r$

Table A1.4 Lateral aerodynamic control derivatives

Dimensionless	Multiplier	Dimensional
Y_ξ	$\frac{1}{2}\rho V_0^2 S$	$\overset{\circ}{Y}_\xi$
L_ξ	$\frac{1}{2}\rho V_0^2 Sb$	$\overset{\circ}{L}_\xi$
N_ξ	$\frac{1}{2}\rho V_0^2 Sb$	$\overset{\circ}{N}_\xi$
Y_ζ	$\frac{1}{2}\rho V_0^2 S$	$\overset{\circ}{Y}_\zeta$
L_ζ	$\frac{1}{2}\rho V_0^2 Sb$	$\overset{\circ}{L}_\zeta$
N_ζ	$\frac{1}{2}\rho V_0^2 Sb$	$\overset{\circ}{N}_\zeta$

Table A1.5 Concise longitudinal aerodynamic stability derivatives

Concise derivative	Equivalent expressions: in terms of dimensional derivatives	Equivalent expressions: in terms of dimensionless derivatives
x_u	$\frac{\mathring{X}_u}{m} + \frac{\mathring{X}_{\dot{w}}\mathring{Z}_u}{m(m-\mathring{Z}_{\dot{w}})}$	$\frac{X_u}{m'} + \frac{\frac{\bar{c}}{V_0}X_{\dot{w}}Z_u}{m'\left(m' - \frac{\bar{c}}{V_0}Z_{\dot{w}}\right)}$
z_u	$\frac{\mathring{Z}_u}{m-\mathring{Z}_{\dot{w}}}$	$\frac{Z_u}{m' - \frac{\bar{c}}{V_0}Z_{\dot{w}}}$
m_u	$\frac{\mathring{M}_u}{I_y} + \frac{\mathring{Z}_u\mathring{M}_{\dot{w}}}{I_y(m-\mathring{Z}_{\dot{w}})}$	$\frac{M_u}{I'_y} + \frac{\frac{\bar{c}}{V_0}M_{\dot{w}}Z_u}{I'_y(m' - \frac{\bar{c}}{V_0}Z_{\dot{w}})}$
x_w	$\frac{\mathring{X}_w}{m} + \frac{\mathring{X}_{\dot{w}}\mathring{Z}_w}{m(m-\mathring{Z}_{\dot{w}})}$	$\frac{X_w}{m'} + \frac{\frac{\bar{c}}{V_0}X_{\dot{w}}Z_w}{m'\left(m' - \frac{\bar{c}}{V_0}Z_{\dot{w}}\right)}$
z_w	$\frac{\mathring{Z}_w}{m-\mathring{Z}_{\dot{w}}}$	$\frac{Z_w}{m' - \frac{\bar{c}}{V_0}Z_{\dot{w}}}$
m_w	$\frac{\mathring{M}_w}{I_y} + \frac{\mathring{Z}_w\mathring{M}_{\dot{w}}}{I_y(m-\mathring{Z}_{\dot{w}})}$	$\frac{M_w}{I'_y} + \frac{\frac{\bar{c}}{V_0}M_{\dot{w}}Z_w}{I'_y(m' - \frac{\bar{c}}{V_0}Z_{\dot{w}})}$
x_q	$\frac{\mathring{X}_q - mW_e}{m} + \frac{(\mathring{Z}_q + mU_e)\mathring{X}_{\dot{w}}}{m(m-\mathring{Z}_{\dot{w}})}$	$\frac{\bar{\bar{c}}X_q - m'W_e}{m'} + \frac{(\bar{\bar{c}}Z_q + m'U_e)\frac{\bar{c}}{V_0}X_{\dot{w}}}{m'\left(m' - \frac{\bar{c}}{V_0}Z_{\dot{w}}\right)}$
z_q	$\frac{\mathring{Z}_q + mU_e}{m-\mathring{Z}_{\dot{w}}}$	$\frac{\bar{\bar{c}}Z_q + m'U_e}{m' - \frac{\bar{c}}{V_0}Z_{\dot{w}}}$
m_q	$\frac{\mathring{M}_q}{I_y} + \frac{(\mathring{Z}_q + mU_e)\mathring{M}_{\dot{w}}}{I_y(m-\mathring{Z}_{\dot{w}})}$	$\frac{\bar{\bar{c}}M_q}{I'_y} + \frac{(\bar{\bar{c}}Z_q + m'U_e)\frac{\bar{c}}{V_0}M_{\dot{w}}}{I'_y\left(m' - \frac{\bar{c}}{V_0}Z_{\dot{w}}\right)}$
x_θ	$-g\cos\theta_e - \frac{\mathring{X}_{\dot{w}}g\sin\theta_e}{m-\mathring{Z}_{\dot{w}}}$	$-g\cos\theta_e - \frac{\frac{\bar{c}}{V_0}X_{\dot{w}}g\sin\theta_e}{m' - \frac{\bar{c}}{V_0}Z_{\dot{w}}}$
z_θ	$-\frac{mg\sin\theta_e}{m-\mathring{Z}_{\dot{w}}}$	$-\frac{m'g\sin\theta_e}{m' - \frac{\bar{c}}{V_0}Z_{\dot{w}}}$
m_θ	$-\frac{\mathring{M}_{\dot{w}}mg\sin\theta_e}{I_y(m-\mathring{Z}_{\dot{w}})}$	$-\frac{\frac{\bar{c}}{V_0}M_{\dot{w}}m'g\sin\theta_e}{I'_y\left(m' - \frac{\bar{c}}{V_0}Z_{\dot{w}}\right)}$

Table A1.6 Concise longitudinal control derivatives

Concise derivative	Equivalent expressions	
	in terms of dimensional derivatives	in terms of dimensionless derivatives
x_η	$\frac{\mathring{X}_\eta}{m} + \frac{\mathring{X}_{\dot{w}}\mathring{Z}_\eta}{m(m-\mathring{Z}_{\dot{w}})}$	$\frac{V_0 X_\eta}{m'} + \frac{\frac{\bar{c}}{V_0}X_{\dot{w}}Z_\eta}{m'\left(m' - \frac{\bar{c}}{V_0}Z_{\dot{w}}\right)}$
z_η	$\frac{\mathring{Z}_\eta}{m-\mathring{Z}_{\dot{w}}}$	$\frac{V_0 Z_\eta}{m' - \frac{\bar{c}}{V_0}Z_{\dot{w}}}$
m_η	$\frac{\mathring{M}_\eta}{I_y} + \frac{\mathring{M}_{\dot{w}}\mathring{Z}_\eta}{I_y(m-\mathring{Z}_{\dot{w}})}$	$\frac{V_0 M_\eta}{I'_y} + \frac{\bar{c}M_{\dot{w}}Z_\eta}{I'_y\left(m' - \frac{\bar{c}}{V_0}Z_{\dot{w}}\right)}$
x_τ	$\frac{\mathring{X}_\tau}{m} + \frac{\mathring{X}_{\dot{w}}\mathring{Z}_\tau}{m(m-\mathring{Z}_{\dot{w}})}$	$\frac{V_0 X_\tau}{m'} + \frac{\frac{\bar{c}}{V_0}X_{\dot{w}}Z_\tau}{m'\left(m' - \frac{\bar{c}}{V_0}Z_{\dot{w}}\right)}$
z_τ	$\frac{\mathring{Z}_\tau}{m-\mathring{Z}_{\dot{w}}}$	$\frac{V_0 Z_\tau}{m' - \frac{\bar{c}}{V_0}Z_{\dot{w}}}$
m_τ	$\frac{\mathring{M}_\tau}{I_y} + \frac{\mathring{M}_{\dot{w}}\mathring{Z}_\tau}{I_y(m-\mathring{Z}_{\dot{w}})}$	$\frac{V_0 M_\tau}{I'_y} + \frac{\bar{c}M_{\dot{w}}Z_\tau}{I'_y\left(m' - \frac{\bar{c}}{V_0}Z_{\dot{w}}\right)}$

Table A1.7 Concise lateral aerodynamic stability derivatives

Concise derivative	Equivalent expressions	
	in terms of dimensional derivatives	in terms of dimensionless derivatives
y_v	$\frac{\mathring{Y}_v}{m}$	$\frac{Y_v}{m'}$
y_p	$\frac{(\mathring{Y}_p + mW_e)}{m}$	$\frac{(bY_p + m'W_e)}{m'}$
y_r	$\frac{(\mathring{Y}_r - mU_e)}{m}$	$\frac{(bY_r - m'U_e)}{m'}$
y_ϕ	$g\cos\theta_e$	$g\cos\theta_e$
y_ψ	$g\sin\theta_e$	$g\sin\theta_e$
l_v	$\frac{(I_z\mathring{L}_v + I_{xz}\mathring{N}_v)}{(I_xI_z - I_{xz}^2)}$	$\frac{(I'_zL_v + I'_{xz}N_v)}{(I'_xI'_z - I'^2_{xz})}$
l_p	$\frac{(I_z\mathring{L}_p + I_{xz}\mathring{N}_p)}{(I_xI_z - I_{xz}^2)}$	$\frac{(I'_zL_p + I'_{xz}N_p)}{(I'_xI'_z - I'^2_{xz})}$
l_r	$\frac{(I_z\mathring{L}_r + I_{xz}\mathring{N}_r)}{(I_xI_z - I_{xz}^2)}$	$\frac{(I'_zL_r + I'_{xz}N_r)}{(I'_xI'_z - I'^2_{xz})}$
l_ϕ	0	0
l_ψ	0	0
n_v	$\frac{(I_x\mathring{N}_v + I_{xz}\mathring{L}_v)}{(I_xI_z - I_{xz}^2)}$	$\frac{(I'_xN_v + I'_{xz}L_v)}{(I'_xI'_z - I'^2_{xz})}$
n_p	$\frac{(I_x\mathring{N}_p + I_{xz}\mathring{L}_p)}{(I_xI_z - I_{xz}^2)}$	$\frac{(I'_xN_p + I'_{xz}L_p)}{(I'_xI'_z - I'^2_{xz})}$
n_r	$\frac{(I_x\mathring{N}_r + I_{xz}\mathring{L}_r)}{(I_xI_z - I_{xz}^2)}$	$\frac{(I'_xN_r + I'_{xz}L_r)}{(I'_xI'_z - I'^2_{xz})}$
n_ϕ	0	0
n_ψ	0	0

Table A1.8 Concise lateral control derivatives

Concise derivative	Equivalent expressions	
	in terms of dimensional derivatives	in terms of dimensionless derivatives
y_ξ	$\frac{\mathring{Y}_\xi}{m}$	$\frac{V_0 Y_\xi}{m'}$
l_ξ	$\frac{(I_z \mathring{L}_\xi + I_{xz} \mathring{N}_\xi)}{(I_x I_z - I_{xz}^2)}$	$\frac{V_0(I'_z L_\xi + I'_{xz} N_\xi)}{(I'_x I'_z - I'^2_{xz})}$
n_ξ	$\frac{(I_x \mathring{N}_\xi + I_{xz} \mathring{L}_\xi)}{(I_x I_z - I_{xz}^2)}$	$\frac{V_0(I'_x N_\xi + I'_{xz} L_\xi)}{(I'_x I'_z - I'^2_{xz})}$
y_ζ	$\frac{\mathring{Y}_\zeta}{m}$	$\frac{V_0 Y_\zeta}{m'}$
l_ζ	$\frac{(I_z \mathring{L}_\xi + I_{xz} \mathring{N}_\zeta)}{(I_x I_z - I_{xz}^2)}$	$\frac{V_0(I'_z L_\zeta + I'_{xz} N_\zeta)}{(I'_x I'_z - I'^2_{xz})}$
n_ζ	$\frac{(I_x \mathring{N}_\zeta + I_{xz} \mathring{L}_\zeta)}{(I_x I_z - I_{xz}^2)}$	$\frac{V_0(I'_x N_\zeta + I'_{xz} L_\zeta)}{(I'_x I'_z - I'^2_{xz})}$

Appendix 2

Aircraft Response Transfer Functions Referred to Aircraft Body Axes

1. Longitudinal response transfer functions in terms of dimensional derivatives

The following longitudinal numerator polynomials describe the motion of the aircraft in response to elevator η input. To obtain the numerators describing the response to engine thrust input it is simply necessary to replace the subscript η with τ.

	Common denominator polynomial $\Delta(s) = as^4 + bs^3 + cs^2 + ds + e$
a	$mI_y(m - \mathring{Z}_{\dot{w}})$
b	$I_y(\mathring{X}_u\mathring{Z}_{\dot{w}} - \mathring{X}_{\dot{w}}\mathring{Z}_u) - mI_y(\mathring{X}_u + \mathring{Z}_w) - mM_{\dot{w}}(\mathring{Z}_q + mU_e)$ $- m\mathring{M}_q(m - \mathring{Z}_{\dot{w}})$
c	$I_y(\mathring{X}_u\mathring{Z}_w - \mathring{X}_w\mathring{Z}_u) + (\mathring{X}_u\mathring{M}_{\dot{w}} - \mathring{X}_{\dot{w}}\mathring{M}_u)(\mathring{Z}_q + mU_e)$ $+ \mathring{Z}_u(\mathring{X}_{\dot{w}}\mathring{M}_q - \mathring{X}_q\mathring{M}_{\dot{w}}) + (\mathring{X}_u\mathring{M}_q - \mathring{X}_q\mathring{M}_u)(m - \mathring{Z}_{\dot{w}})$ $+ m(\mathring{M}_q\mathring{Z}_w - \mathring{M}_w\mathring{Z}_q) + mW_e(\mathring{M}_{\dot{w}}\mathring{Z}_u - \mathring{M}_u\mathring{Z}_{\dot{w}})$ $+ m^2(\mathring{M}_{\dot{w}}g\sin\theta_e + W_e\mathring{M}_u - U_e\mathring{M}_w)$
d	$(\mathring{X}_u\mathring{M}_w - \mathring{X}_w\mathring{M}_u)(\mathring{Z}_q + mU_e)$ $+ (\mathring{M}_u\mathring{Z}_w - \mathring{M}_w\mathring{Z}_u)(\mathring{X}_q - mW_e) + \mathring{M}_q(\mathring{X}_w\mathring{Z}_u - \mathring{X}_u\mathring{Z}_w)$ $+ mg\cos\theta_e(\mathring{M}_{\dot{w}}\mathring{Z}_u + \mathring{M}_u(m - \mathring{Z}_{\dot{w}})) + mg\sin\theta_e(\mathring{X}_{\dot{w}}\mathring{M}_u - \mathring{X}_u\mathring{M}_{\dot{w}} + m\mathring{M}_w)$
e	$mg\sin\theta_e(\mathring{X}_w\mathring{M}_u - \mathring{X}_u\mathring{M}_w) + mg\cos\theta_e(\mathring{M}_w\mathring{Z}_u - \mathring{M}_u\mathring{Z}_w)$

Numerator polynomial $N_\eta^u(s) = as^3 + bs^2 + cs + d$	
a	$I_y(\mathring{X}_{\dot{w}}\mathring{Z}_\eta + \mathring{X}_\eta(m - \mathring{Z}_{\dot{w}}))$
b	$\mathring{X}_\eta(-I_y\mathring{Z}_w - \mathring{M}_{\dot{w}}(\mathring{Z}_q + mU_e) - \mathring{M}_q(m - \mathring{Z}_{\dot{w}}))$ $+ \mathring{Z}_\eta(I_y\mathring{X}_w - \mathring{X}_{\dot{w}}\mathring{M}_q + \mathring{M}_{\dot{w}}(\mathring{X}_q - mW_e))$ $+ \mathring{M}_\eta((\mathring{X}_q - mW_e)(m - \mathring{Z}_{\dot{w}}) + \mathring{X}_{\dot{w}}(\mathring{Z}_q + mU_e))$
c	$\mathring{X}_\eta(\mathring{Z}_w\mathring{M}_q - \mathring{M}_w(\mathring{Z}_q + mU_e) + mg\sin\theta_e\mathring{M}_{\dot{w}})$ $+ \mathring{Z}_\eta(\mathring{M}_w(\mathring{X}_q - mW_e) - \mathring{X}_w\mathring{M}_q - mg\cos\theta_e\mathring{M}_{\dot{w}})$ $+ \mathring{M}_\eta(\mathring{X}_w(\mathring{Z}_q + mU_e) - \mathring{Z}_w(\mathring{X}_q - mW_e) - mg\cos\theta_e(m - \mathring{Z}_{\dot{w}}) - mg\sin\theta_e\mathring{X}_{\dot{w}})$
d	$\mathring{X}_\eta\mathring{M}_w mg\sin\theta_e - \mathring{Z}_\eta\mathring{M}_w mg\cos\theta_e + \mathring{M}_\eta(\mathring{Z}_w mg\cos\theta_e - \mathring{X}_w mg\sin\theta_e)$

Numerator polynomial $N_\eta^w(s) = as^3 + bs^2 + cs + d$	
a	$mI_y\mathring{Z}_\eta$
b	$I_y\mathring{X}_\eta\mathring{Z}_u - \mathring{Z}_\eta(I_y\mathring{X}_u + m\mathring{M}_q) + m\mathring{M}_\eta(\mathring{Z}_q + mU_e)$
c	$\mathring{X}_\eta(\mathring{M}_u(\mathring{Z}_q + mU_e) - \mathring{Z}_u\mathring{M}_q) + \mathring{Z}_\eta(\mathring{X}_u\mathring{M}_q - \mathring{M}_u(\mathring{X}_q - mW_e))$ $+ \mathring{M}_\eta(\mathring{Z}_u(\mathring{X}_q - mW_e) - \mathring{X}_u(\mathring{Z}_q + mU_e) - m^2g\sin\theta_e)$
d	$-\mathring{X}_\eta\mathring{M}_u mg\sin\theta_e + \mathring{Z}_\eta\mathring{M}_u mg\cos\theta_e + \mathring{M}_\eta(\mathring{X}_u mg\sin\theta_e - \mathring{Z}_u mg\cos\theta_e)$

Numerator polynomials $N_\eta^q(s) = s(as^2 + bs + c)$ and $N_\eta^\theta(s) = as^2 + bs + c$	
a	$m\mathring{Z}_\eta\mathring{M}_{\dot{w}} + m\mathring{M}_\eta(m - \mathring{Z}_{\dot{w}})$
b	$\mathring{X}_\eta(\mathring{Z}_u\mathring{M}_{\dot{w}} + \mathring{M}_u(m - \mathring{Z}_{\dot{w}})) + \mathring{Z}_\eta(m\mathring{M}_w - \mathring{X}_u\mathring{M}_{\dot{w}} + \mathring{M}_u\mathring{X}_{\dot{w}})$ $+ \mathring{M}_\eta(-\mathring{X}_u(m - \mathring{Z}_{\dot{w}}) - \mathring{Z}_u\mathring{X}_{\dot{w}} - m\mathring{Z}_w)$
c	$\mathring{X}_\eta(\mathring{Z}_u\mathring{M}_w - \mathring{M}_u\mathring{Z}_w) + \mathring{Z}_\eta(\mathring{X}_w\mathring{M}_u - \mathring{M}_w\mathring{X}_u) + \mathring{M}_\eta(\mathring{X}_u\mathring{Z}_w - \mathring{Z}_u\mathring{X}_w)$

2. Lateral-directional response transfer functions in terms of dimensional derivatives

The following lateral-directional numerator polynomials describe the motion of the aircraft in response to aileron ξ input. To obtain the numerators describing the response to rudder input it is simply necessary to replace the subscript ξ with ζ.

	Denominator polynomial $\Delta(s) = s(as^4 + bs^3 + cs^2 + ds + e)$
a	$m(I_x I_z - I_{xz}^2)$
b	$-\mathring{Y}_v(I_x I_z - I_{xz}^2) - m(I_x \mathring{N}_r + I_{xz}\mathring{L}_r) - m(I_z \mathring{L}_p + I_{xz}\mathring{N}_p)$
c	$\mathring{Y}_v(I_x \mathring{N}_r + I_{xz}\mathring{L}_r) + \mathring{Y}_v(I_z \mathring{L}_p + I_{xz}\mathring{N}_p) - (\mathring{Y}_p + mW_e)(I_z \mathring{L}_v + I_{xz}\mathring{N}_v)$ $-(\mathring{Y}_r - mU_e)(I_x \mathring{N}_v + I_{xz}\mathring{L}_v) + m(\mathring{L}_p \mathring{N}_r - \mathring{L}_r \mathring{N}_p)$
d	$\mathring{Y}_v(\mathring{L}_r \mathring{N}_p - \mathring{L}_p \mathring{N}_r) + (\mathring{Y}_p + mW_e)(\mathring{L}_v \mathring{N}_r - \mathring{L}_r \mathring{N}_v)$ $+(\mathring{Y}_r - mU_e)(\mathring{L}_p \mathring{N}_v - \mathring{L}_v \mathring{N}_p)$ $-mg\cos\theta_e(I_z \mathring{L}_v + I_{xz}\mathring{N}_v) - mg\sin\theta_e(I_x \mathring{N}_v + I_{xz}\mathring{L}_v)$
e	$mg\cos\theta_e(\mathring{L}_v \mathring{N}_r - \mathring{L}_r \mathring{N}_v) + mg\sin\theta_e(\mathring{L}_p \mathring{N}_v - \mathring{L}_v \mathring{N}_p)$

	Numerator polynomial $N_\xi^v(s) = s(as^3 + bs^2 + cs + d)$
a	$\mathring{Y}_\xi(I_x I_z - I_{xz}^2)$
b	$\mathring{Y}_\xi(-I_x \mathring{N}_r - I_z \mathring{L}_p - I_{xz}(\mathring{L}_r + \mathring{N}_p)) + \mathring{L}_\xi(I_z(\mathring{Y}_p + mW_e) + I_{xz}(\mathring{Y}_r - mU_e))$ $+\mathring{N}_\xi(I_x(\mathring{Y}_r - mU_e) + I_{xz}(\mathring{Y}_p + mW_e))$
c	$\mathring{Y}_\xi(\mathring{L}_p \mathring{N}_r - \mathring{L}_r \mathring{N}_p)$ $+\mathring{L}_\xi(\mathring{N}_p(\mathring{Y}_r - mU_e) - \mathring{N}_r(\mathring{Y}_p + mW_e) + mg(I_z\cos\theta_e + I_{xz}\sin\theta_e))$ $+\mathring{N}_\xi(\mathring{L}_r(\mathring{Y}_p + mW_e) - \mathring{L}_p(\mathring{Y}_r - mU_e) + mg(I_x\sin\theta_e + I_{xz}\cos\theta_e))$
d	$\mathring{L}_\xi(\mathring{N}_p mg\sin\theta_e - \mathring{N}_r mg\cos\theta_e) + \mathring{N}_\xi(\mathring{L}_r mg\cos\theta_e - \mathring{L}_p mg\sin\theta_e)$

Numerator polynomials $N_\xi^p(s) = s(as^3 + bs^2 + cs + d)$ and $N_\xi^\phi(s) = as^3 + bs^2 + cs + d$	
a	$m(I_z\mathring{L}_\xi + I_{xz}\mathring{N}_\xi)$
b	$\mathring{Y}_\xi(I_z\mathring{L}_v + I_{xz}\mathring{N}_v) + \mathring{L}_\xi(-I_z\mathring{Y}_v - m\mathring{N}_r) + \mathring{N}_\xi(m\mathring{L}_r - I_{xz}\mathring{Y}_v)$
c	$\mathring{Y}_\xi(\mathring{L}_r\mathring{N}_v - \mathring{L}_v\mathring{N}_r) + \mathring{L}_\xi(\mathring{N}_r\mathring{Y}_v - \mathring{N}_v\mathring{Y}_r + mU_e\mathring{N}_v)$ $+ \mathring{N}_\xi(\mathring{L}_v\mathring{Y}_r - \mathring{L}_r\mathring{Y}_v - mU_e\mathring{L}_v)$
d	$mg\sin\theta_e(\mathring{L}_v\mathring{N}_\xi - \mathring{L}_\xi\mathring{N}_v)$

Numerator polynomials $N_\xi^r(s) = s(as^3 + bs^2 + cs + d)$ and $N_\xi^\psi(s) = as^3 + bs^2 + cs + d$	
a	$m(I_x\mathring{N}_\xi + I_{xz}\mathring{L}_\xi)$
b	$\mathring{Y}_\xi(I_x\mathring{N}_v + I_{xz}\mathring{L}_v) + \mathring{L}_\xi(m\mathring{N}_p - I_{xz}\mathring{Y}_v) - \mathring{N}_\xi(I_x\mathring{Y}_v + m\mathring{L}_p)$
c	$\mathring{Y}_\xi(\mathring{L}_v\mathring{N}_p - \mathring{L}_p\mathring{N}_v) + \mathring{L}_\xi(\mathring{N}_v\mathring{Y}_p - \mathring{N}_p\mathring{Y}_v + mW_e\mathring{N}_v)$ $+ \mathring{N}_\xi(\mathring{L}_p\mathring{Y}_v - \mathring{L}_v\mathring{Y}_p - mW_e\mathring{L}_v)$
d	$mg\cos\theta_e(\mathring{L}_\xi\mathring{N}_v - \mathring{L}_v\mathring{N}_\xi)$

3. Longitudinal response transfer functions in terms of concise derivatives

Again the longitudinal numerator polynomials describe the motion of the aircraft in response to elevator η input. To obtain the numerators describing the response to engine thrust input it is simply necessary to replace the subscript η with τ.

Common denominator polynomial $\Delta(s) = as^4 + bs^3 + cs^2 + ds + e$	
a	1
b	$-(m_q + x_u + z_w)$
c	$(m_q z_w - m_w z_q) + (m_q x_u - m_u x_q) + (x_u z_w - x_w z_u) - m_\theta$
d	$(m_\theta x_u - m_u x_\theta) + (m_\theta z_w - m_w z_\theta) + m_q(x_w z_u - x_u z_w) + x_q(m_u z_w - m_w z_u) + z_q(m_w x_u - m_u x_w)$
e	$m_\theta(x_w z_u - x_u z_w) + x_\theta(m_u z_w - m_w z_u) + z_\theta(m_w x_u - m_u x_w)$

Numerator polynomial $N_\eta^u(s) = as^3 + bs^2 + cs + d$	
a	x_η
b	$m_\eta x_q - x_\eta(m_q + z_w) + z_\eta x_w$
c	$m_\eta(x_w z_q - x_q z_w + x_\theta) + x_\eta(m_q z_w - m_w z_q - m_\theta) + z_\eta(m_w x_q - m_q x_w)$
d	$m_\eta(x_w z_\theta - x_\theta z_w) + x_\eta(m_\theta z_w - m_w z_\theta) + z_\eta(m_w x_\theta - m_\theta x_w)$

Numerator polynomial $N_\eta^w(s) = as^3 + bs^2 + cs + d$	
a	z_η
b	$m_\eta z_q + x_\eta z_u - z_\eta(m_q + x_u)$
c	$m_\eta(x_q z_u - x_u z_q + z_\theta) + x_\eta(m_u z_q - m_q z_u) + z_\eta(m_q x_u - m_u x_q - m_\theta)$
d	$m_\eta(x_\theta z_u - x_u z_\theta) + x_\eta(m_u z_\theta - m_\theta z_u) + z_\eta(m_\theta x_u - m_u x_\theta)$

Numerator polynomials $N_\eta^q(s) = s(as^2 + bs + c)$ and $N_\eta^\theta(s) = as^2 + bs + c$	
a	m_η
b	$-m_\eta(x_u + z_w) + x_\eta m_u + z_\eta m_w$
c	$m_\eta(x_u z_w - x_w z_u) + x_\eta(m_w z_u - m_u z_w) + z_\eta(m_u x_w - m_w x_u)$

4. Lateral-directional response transfer functions in terms of concise derivatives

As before, the lateral-directional numerator polynomials describe the motion of the aircraft in response to aileron ξ input. To obtain the numerators describing the response to rudder input it is simply necessary to replace the subscript ξ with ζ.

Denominator polynomial $\Delta(s) = as^5 + bs^4 + cs^3 + ds^2 + es + f$	
a	1
b	$-(l_p + n_r + y_v)$
c	$(l_p n_r - l_r n_p) + (n_r y_v - n_v y_r) + (l_p y_v - l_v y_p) - (l_\phi + n_\psi)$
d	$(l_p n_\psi - l_\psi n_p) + (l_\phi n_r - l_r n_\phi) + l_v(n_r y_p - n_p y_r - y_\phi)$ $+ n_v(l_p y_r - l_r y_p - y_\psi) + y_v(l_r n_p - l_p n_r + l_\phi + n_\psi)$
e	$(l_\phi n_\psi - l_\psi n_\phi) + l_v((n_r y_\phi - n_\phi y_r) + (n_\psi y_p - n_p y_\psi))$ $+ n_v((l_\phi y_r - l_r y_\phi) + (l_p y_\psi - l_\psi y_p)) + y_v((l_r n_\phi - l_\phi n_r) + (l_\psi n_p - l_p n_\psi))$
f	$l_v(n_\psi y_\phi - n_\phi y_\psi) + n_v(l_\phi y_\psi - l_\psi y_\phi) + y_v(l_\psi n_\phi - l_\phi n_\psi)$

Numerator polynomial $N^v_\xi(s) = as^4 + bs^3 + cs^2 + ds + e$	
a	y_ξ
b	$l_\xi y_p + n_\xi y_r - y_\xi(l_p + n_r)$
c	$l_\xi(n_p y_r - n_r y_p + y_\phi) + n_\xi(l_r y_p - l_p y_r + y_\psi) + y_\xi(l_p n_r - l_r n_p - l_\phi - n\psi)$
d	$l_\xi(n_\phi y_r - n_r y_\phi + n_p y_\psi - n_\psi y_p) + n_\xi(l_r y_\phi - l_\phi y_r + l_\psi y_p - l_p y_\psi) + y_\xi(l_\phi n_r - l_r n_\phi + l_p n_\psi - l_\psi n_p)$
e	$l_\xi(n_\phi y_\psi - n_\psi y_\phi) + n_\xi(l_\psi y_\phi - l_\phi y_\psi) + y_\xi(l_\phi n_\psi - l_\psi n_\phi)$

Numerator polynomials $N^p_\xi(s) = s(as^3 + bs^2 + cs + d)$ and $N^\phi_\xi(s) = as^3 + bs^2 + cs + d$	
a	l_ξ
b	$-l_\xi(n_r + y_v) + n_\xi l_r + y_\xi l_v$
c	$l_\xi(n_r y_v - n_v y_r - n_\psi) + n_\xi(l_v y_r - l_r y_v + l_\psi) + y_\xi(l_r n_v - l_v n_r)$
d	$l_\xi(n_\psi y_v - n_v y_\psi) + n_\xi(l_v y_\psi - l_\psi y_v) + y_\xi(l_\psi n_v - l_v n_\psi)$

Numerator polynomials $N^r_\xi(s) = s(as^3 + bs^2 + cs + d)$ and $N^\psi_\xi(s) = as^3 + bs^2 + cs + d$	
a	n_ξ
b	$l_\xi n_p - n_\xi(l_p + y_v) + y_\xi n_v$
c	$l_\xi(n_v y_p - n_p y_v + n_\phi) + n_\xi(l_p y_v - l_v y_p - l_\phi) + y_\xi(l_v n_p - l_p n_v)$
d	$l_\xi(n_v y_\phi - n_\phi y_v) + n_\xi(l_\phi y_v - l_v y_\phi) + y_\xi(l_v n_\phi - l_\phi n_v)$

Appendix 3

Units, Conversions and Constants

Table A3.1 Factors for conversion from Imperial to SI units

Parameter	Symbol	Imperial unit	Equivalent SI unit
mass	m	1 slug	14.594 kg
length	l	1 ft	0.3048 m
velocity	V	1 ft/s	0.3048 m/s
acceleration	a	1 ft/s^2	0.3048 m/s^2
force	F	1 lb	4.448 N
moment	M	1 lb ft	1.356 N m
density	ρ	1 slug/ft^3	515.383 kg/m^3
inertia	I	1 slug ft^2	1.3558 kg m^2

Table A3.2 Useful constants

Constant	Symbol	Imperial units	SI units
1 knot	kt	1.689 ft/s	0.515 m/s
Sea level air density	ρ_0	0.00238 slug/ft^3	1.225 kg/m^3
Speed of sound at sea level	a_0	1116.44 ft/s	340.29 m/s
Radian	rad	57.3°	57.3°
Gravitational acceleration	g	32.17 ft/s^2	9.81 m/s^2

Appendix 4

A Very Short Table of Laplace Transforms

	$F(t)$	$f(s)$
1	1	$\frac{1}{s}$
2	e^{at}	$\frac{1}{s-a}$
3	$\sin kt$	$\frac{k}{s^2+k^2}$
4	$\cos kt$	$\frac{s}{s^2+k^2}$
5	$e^{-at}\sin kt$	$\frac{k}{(s+a)^2+k^2}$
6	$e^{-at}\cos kt$	$\frac{(s+a)}{(s+a)^2+k^2}$

Appendix 5

The Dynamics of a Linear Second Order System

The solution of the linearized small perturbation equations of motion of an aircraft contains recognizable classical second order system terms. A review of the dynamics of a second order system is therefore useful as an aid to the correct interpretation of the solution of the aircraft equations of motion.

Consider the classical mass–spring–damper system whose motion is described by the equation of motion

$$m\ddot{x}(t) + c\dot{x}(t) + kx(t) = f(t) \tag{A5.1}$$

where $x(t)$ is the displacement of the mass and $f(t)$ is the forcing function. The constants of the system comprise the mass m, the viscous damping c and the spring stiffness k.

Classical unforced motion results when the forcing $f(t)$ is made zero, the mass is displaced by A, say, and then released. Equation (A5.1) may then be written

$$m\ddot{x}(t) + c\dot{x}(t) + kx(t) = 0 \tag{A5.2}$$

and the initial conditions are defined, $\dot{x}(0) = 0$ and $x(0) = A$. The time response of the motion of the mass may be found by solving equation (A5.2) subject to the constraints imposed by the initial conditions. This is readily achieved with the aid of the Laplace transform.

Thus

$$\begin{aligned} \mathrm{L}\{m\ddot{x}(t) + c\dot{x}(t) + kx(t)\} &= m(s^2x(s) - sx(0) - \dot{x}(0)) + c(sx(s) - x(0)) + kx(s) \\ &= m(s^2x(s) - sA) + c(sx(s) - A) + kx(s) = 0 \end{aligned}$$

which, after some rearrangement, may be written

$$x(s) = \frac{A(ms + c)}{(ms^2 + cs + k)} \tag{A5.3}$$

Or, alternatively

$$x(s) = \frac{A(s + 2\zeta\omega)}{(s^2 + 2\zeta\omega s + \omega)} \tag{A5.4}$$

where

$$\left.\begin{aligned} 2\zeta\omega &= \frac{c}{m} \\ \omega^2 &= \frac{k}{m} \\ \zeta &= \text{system damping ratio} \\ \omega &= \text{system undamped natural frequency} \end{aligned}\right\} \tag{A5.5}$$

The time response $x(t)$ may be obtained by determining the inverse Laplace transform of equation (A5.4) and the form of the solution obviously depends on the magnitudes of the physical constants of the system m, c and k. The characteristic equation of the system is given by equating the denominator of equation (A5.3) or (A5.4) to zero

$$ms^2 + cs + k = 0 \tag{A5.6}$$

or, equivalently

$$s^2 + 2\zeta\omega s + \omega^2 = 0 \tag{A5.7}$$

To facilitate the determination of the inverse Laplace transform of equation (A5.4), the denominator is first factorized and the expression on the right-hand side is split into partial fractions. Whence

$$\begin{aligned} x(s) &= \frac{A(s+2\zeta\omega)}{(s+\omega(\zeta+\sqrt{\zeta^2-1}))(s+\omega(\zeta-\sqrt{\zeta^2-1}))} \\ &= \frac{A}{2}\left(\frac{\left(1+\frac{\zeta}{\sqrt{\zeta^2-1}}\right)}{(s+\omega(\zeta+\sqrt{\zeta^2-1}))} + \frac{\left(1-\frac{\zeta}{\sqrt{\zeta^2-1}}\right)}{(s+\omega(\zeta-\sqrt{\zeta^2-1}))}\right) \end{aligned} \tag{A5.8}$$

With reference to the table of transform pairs, Appendix 4, transform pair 2, the inverse Laplace transform of equation (A5.8) is readily obtained

$$x(t) = \frac{Ae^{-\omega\zeta t}}{2}\left(\left(1+\frac{\zeta}{\sqrt{\zeta^2-1}}\right)e^{-\omega t\sqrt{\zeta^2-1}} + \left(1-\frac{\zeta}{\sqrt{\zeta^2-1}}\right)e^{\omega t\sqrt{\zeta^2-1}}\right) \tag{A5.9}$$

Equation (A5.9) is the general solution describing the unforced motion of the mass and the type of response depends on the value of the damping ratio.

(i) When $\zeta = 0$ equation (A5.9) reduces to

$$x(t) = \frac{A}{2}(e^{-j\omega t} + e^{j\omega t}) = A\cos\omega t \tag{A5.10}$$

which describes *undamped harmonic motion* or, alternatively, a *neutrally stable system.*

(ii) When $0 < \zeta < 1$ equation (A5.9) may be modified by writing

$$\omega_n = \omega\sqrt{1-\zeta^2}$$

where ω_n is the damped natural frequency. Thus the solution is given by

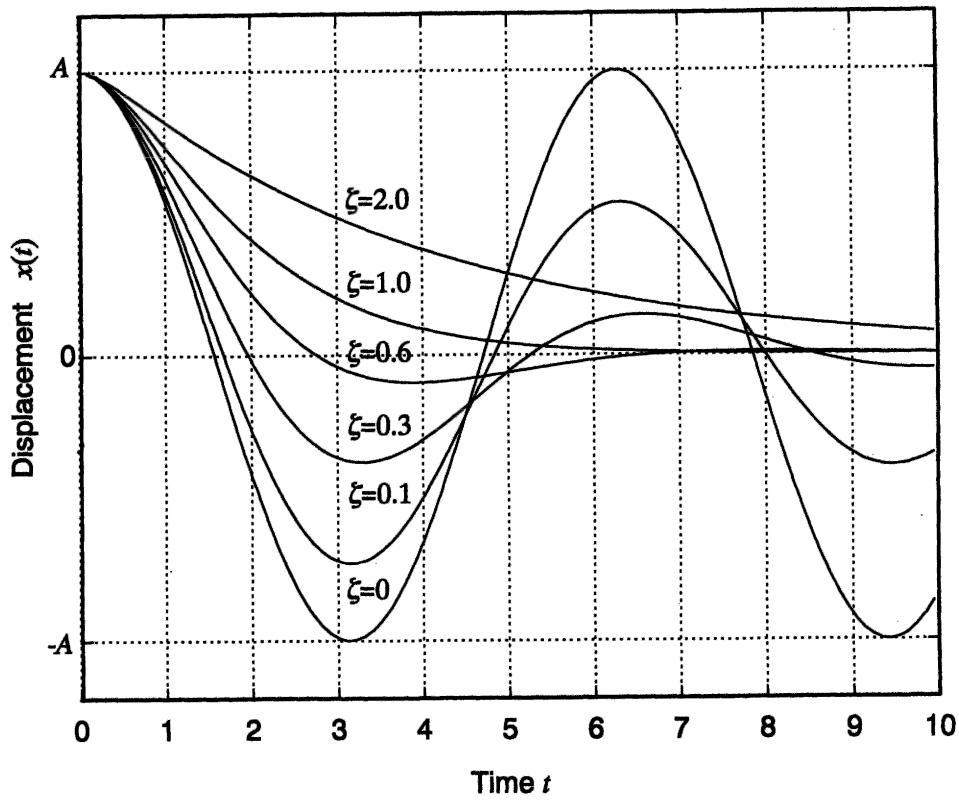

Fig. A5.1 Typical second order system responses

$$x(t) = \frac{Ae^{-\omega\zeta t}}{2}\left(\left(1+\frac{j\zeta}{\sqrt{1-\zeta^2}}\right)e^{-j\omega_n t}+\left(1-\frac{j\zeta}{\sqrt{1-\zeta^2}}\right)e^{-j\omega_n t}\right)$$

$$= Ae^{-\omega\zeta t}\left(\cos\omega_n t - \frac{\omega\zeta}{\omega_n}\sin\omega_n t\right) \qquad \text{(A5.11)}$$

which describes *damped harmonic motion.*

(iii) When $\zeta = 1$ the coefficients of the exponential terms in equation (A5.9) become infinite. However, by expressing the exponentials as series and by letting $\zeta \to 1$, it may be shown that the damped natural frequency ω_n tends to zero and the solution is given by

$$x(t) = Ae^{-\omega t}(1 - \omega t) \qquad \text{(A5.12)}$$

(iv) When $\zeta > 1$ the solution is given by equation (A5.9) directly and is thus a function of a number of exponential terms. The motion thus described is non-oscillatory and is exponentially convergent.

Typical response time histories for a range of values of damping ratio are shown in Fig. A5.1.

It is important to note that the type of response is governed entirely by the damping ratio and undamped natural frequency which, in turn, determine the roots of the

Table A5.1 Summary of a stable system

Damping ratio	Roots of characteristic equation	Type of response
$\zeta = 0$	$(s+j\omega)(s-j\omega) = 0$ Complex with zero real part	Undamped sinusoidal oscillation with frequency ω
$0 < \zeta < 1$	$(s+\omega\zeta+j\omega_n)(s+\omega\zeta-j\omega_n) = 0$ Complex with non-zero real part	Damped sinusoidal oscillation with frequency $\omega_n = \omega\sqrt{1-\zeta^2}$
$\zeta = 1$	$(s+\omega)^2 = 0$ Repeated real roots	Exponential convergence of form $e^{-\omega t}(1-\omega t)$.
$\zeta > 1$	$(s+r_1)(s+r_2) = 0$ Real roots where $r_1 = \omega(\zeta+\sqrt{\zeta^2-1})$ $r_2 = \omega(\zeta-\sqrt{\zeta^2-1})$	Exponential convergence of general form, $k_1e^{-r_1t} + k_2e^{-r_2t}$

characteristic equation, (A5.6) or (A5.7). Thus, dynamic properties of the system may be directly attributed to the physical properties of the system. Consequently, the type of unforced response may be ascertained simply by inspection of the characteristic equation. A summary of these observations for a stable system is given in Table A5.1.

The classical mass–spring–damper system is always stable, but rather more general systems which demonstrate similar properties may not necessarily be stable. For a more general interpretation including unstable systems in which $\zeta < 0$, it is sufficient only to note that the types of solution are similar except that the motion they describe is divergent rather than convergent. Aeroplanes typically demonstrate both stable and unstable characteristics which are conveniently described by this simple linear second order model.

Appendix 6

Approximate Expressions for the Dimensionless Aerodynamic Stability and Control Derivatives

Table A6.1 Longitudinal aerodynamic stability derivatives

Small perturbation derivatives referred to aircraft wind axes			
Derivative	Description	Expression	Comments
X_u eq (13.16)	Axial force due to velocity	$-2C_D - V_0\frac{\partial C_D}{\partial V} + \frac{1}{\frac{1}{2}\rho V_0 S}\frac{\partial \tau}{\partial V}$	Drag and thrust effects due to velocity perturbation
X_w eq (13.27)	Axial force due to 'incidence'	$C_L - \frac{\partial C_D}{\partial \alpha}$	Lift and drag effects due to incidence perturbation
X_q eq (13.46)	Axial force due to pitch rate	$-\bar{V}_T\frac{\partial C_{D_T}}{\partial \alpha_T}$	Tailplane drag effect, usually negligible
$X_{\dot{w}}$ eq (13.68)	Axial force due to downwash lag	$-\bar{V}_T\frac{\partial C_{D_T}}{\partial \alpha_T}\frac{d\varepsilon}{d\alpha} \equiv X_q\frac{d\varepsilon}{d\alpha}$	Tailplane drag due to downwash lag effect (added mass effect)
Z_u eq (13.21)	Normal force due to velocity	$-2C_L - V_0\frac{\partial C_L}{\partial V}$	Lift effects due to velocity perturbation
Z_w eq (13.30)	Normal force due to 'incidence'	$-C_D - \frac{\partial C_L}{\partial \alpha}$	Lift and drag effects due to incidence perturbation
Z_q eq (13.51)	Normal force due to pitch rate	$-\bar{V}_T a_1$	Tailplane lift effect
$Z_{\dot{w}}$ eq (13.72)	Normal force due to downwash lag	$-\bar{V}_T a_1\frac{d\varepsilon}{d\alpha} = Z_q\frac{d\varepsilon}{d\alpha}$	Tailplane lift due to downwash lag effect (added mass effect)
M_u eq (13.34)	Pitching moment due to velocity	$V_0\frac{\partial C_m}{\partial V}$	Mach dependent, small at low speed
M_w eq (13.39)	Pitching moment due to 'incidence'	$\frac{dC_m}{d\alpha} = -aK_n$	Pitch stiffness, dependent on static margin
M_q eq (13.55)	Pitching moment due to pitch rate	$-\bar{V}_T a_1\frac{l_T}{\bar{c}} \equiv Z_q\frac{l_T}{\bar{c}}$	Pitch damping, due mainly to tailplane
$M_{\dot{w}}$ eq (13.76)	Pitching moment due to downwash lag	$-\bar{V}_T a_1\frac{l_T}{\bar{c}}\frac{d\varepsilon}{d\alpha} \equiv M_q\frac{d\varepsilon}{d\alpha}$	Pitch damping due to downwash lag effect at tailplane

Table A6.2 Lateral aerodynamic stability derivatives

Small perturbation derivatives referred to aircraft wind axes			
Derivative	Description	Expression	Comments
Y_v eq (13.82)	Sideforce due to sideslip	$\left(\frac{S_B}{S}y_B - \frac{S_F}{S}a_{1_F}\right)$	Always negative and hence stabilizing
L_v eq (13.92) eq (13.105) eq (13.108)	Rolling moment due to sideslip	(i) wing with dihedral $-\frac{1}{Ss}\int_0^s c_y a_y \Gamma y \mathrm{d}y$ (ii) wing with aft sweep $-\frac{2C_L \tan \Lambda_{1/4}}{Ss}\int_0^s c_y y \mathrm{d}y$ (iii) fin contribution $-a_{1_F}\bar{V}_F\frac{h_F}{l_F}$	Lateral static stability, determined by total dihedral effect. Many contributions most of which are difficult to estimate reliably. Most accessible approximate contributions given.
N_v eq (13.112)	Yawing moment due to sideslip	(i) fin contribution $a_{1_F}\bar{V}_F$	Natural weathercock stability, dominated by fin effect
Y_p eq (13.117)	Sideforce due to roll rate	(i) fin contribution $-\frac{1}{Sb}\int_0^{H_F} a_h c_h h \mathrm{d}h$	Fin effect dominates, often negligible
L_p eq (13.128)	Rolling moment due to roll rate	(i) wing contribution $-\frac{1}{2Ss^2}\int_0^s (a_y + C_{D_y}) c_y y^2 \mathrm{d}y$	Roll damping wing effects dominate but fin and tailplane contribute
N_p eq (13.137)	Yawing moment due to roll rate	(i) wing contribution $-\frac{1}{2Ss^2}\int_0^s \left(C_{L_y} - \frac{\mathrm{d}C_D}{\mathrm{d}\alpha_y}\right) c_y y^2 \mathrm{d}y$	
Y_r eq (13.142)	Sideforce due to yaw rate	(i) fin contribution $\bar{V}_F a_{1_F}$	Many contributions, but often negligible
L_r eq (13.150) eq (13.155)	Rolling moment due to yaw rate	(i) wing contribution $\frac{1}{Ss^2}\int_0^s C_{L_y} c_y y^2 \mathrm{d}y$ (ii) fin contribution $a_{1_F}\bar{V}_F\frac{h_F}{b} \equiv -L_{v(\mathrm{fin})}\frac{l_F}{b}$	
N_r eq (13.162) eq (13.167)	Yawing moment due to yaw rate	(i) wing contribution $-\frac{1}{Ss^2}\int_0^s C_{D_y} c_y y^2 \mathrm{d}y$ (ii) fin contribution $-a_{1_F}\bar{V}_F\frac{l_F}{b} = -\frac{l_F}{b}N_{v(\mathrm{fin})}$	Yaw damping, for large aspect ratio rectangular wing, wing contribution is approximately $C_D/6$

Table A6.3 Longitudinal aerodynamic control derivatives

Small perturbation derivatives referred to aircraft wind axes			
Derivative	Description	Expression	Comments
X_η eq (13.174)	Axial force due to elevator	$-2\frac{S_T}{S}k_T C_{L_T} a_2$	Usually insignificantly small
Z_η eq (13.178)	Normal force due to elevator	$-\frac{S_T}{S}a_2$	
M_η eq (13.181)	Pitching moment due to elevator	$-\bar{V}_T a_2$	Principal measure of pitch control power

Appendix 7

The Transformation of Aerodynamic Stability Derivatives from a Body Axes Reference to a Wind Axes Reference

1. Introduction

Aerodynamic stability derivatives are usually quoted with respect to a system of body axes or with respect to a system of wind axes. When the derivatives are quoted with respect to one system of axes and it is desired to work with the equations of motion referred to a different system of axes, then the derivatives must be transformed to the system of axes of interest. Fortunately, the transformation of aerodynamic derivatives from one axis system to another is a relatively straightforward procedure using the transformation relationships discussed in Chapter 2. The procedure for transforming derivatives from a body axes reference to a wind axes reference is illustrated below. However, the procedure can be applied for transforming derivatives between any two systems of reference axes provided their angular relationship is known.

In steady level symmetric flight a system of body axes differs from a system of wind axes by the body incidence α_e only as shown in Fig. 2.2. In the following sections small perturbation force and velocity components, X, Y, Z and u, v, w respectively, are indicated in the usual way where, here, the subscript denotes the reference axes. Small perturbation moment and angular velocity components, L, M, N and p, q, r, respectively, are also most conveniently represented by vectors as described in Chapter 2. Again the subscript denotes the reference axes system.

2. Force and moment transformation

The transformation of the aerodynamic force components from a *body to wind axes* reference may be obtained directly by the application of the inverse direction cosine matrix, as given by equation (2.13). Writing $\theta = \alpha_e$ and $\phi = \psi = 0$ since level symmetric flight is assumed then

$$\begin{bmatrix} X_w \\ Y_w \\ Z_w \end{bmatrix} = \begin{bmatrix} \cos\alpha_e & 0 & \sin\alpha_e \\ 0 & 1 & 0 \\ -\sin\alpha_e & 0 & \cos\alpha_e \end{bmatrix} \begin{bmatrix} X_b \\ Y_b \\ Z_b \end{bmatrix} \tag{A7.1}$$

Similarly, the aerodynamic moments transformation may be written

$$\begin{bmatrix} L_w \\ M_w \\ N_w \end{bmatrix} = \begin{bmatrix} \cos\alpha_e & 0 & \sin\alpha_e \\ 0 & 1 & 0 \\ -\sin\alpha_e & 0 & \cos\alpha_e \end{bmatrix} \begin{bmatrix} L_b \\ M_b \\ N_b \end{bmatrix} \tag{A7.2}$$

3. Aerodynamic stability derivative transformations

3.1 FORCE–VELOCITY DERIVATIVES

Consider the situation when the aerodynamic force components comprise only those terms involving the force–velocity derivatives. Then, referred to wind axes

$$\begin{bmatrix} X_w \\ Y_w \\ Z_w \end{bmatrix} = \begin{bmatrix} \mathring{X}_{u_w} & 0 & \mathring{X}_{w_w} \\ 0 & \mathring{Y}_{v_w} & 0 \\ \mathring{Z}_{u_w} & 0 & \mathring{X}_{w_w} \end{bmatrix} \begin{bmatrix} u_w \\ v_w \\ w_w \end{bmatrix} \tag{A7.3}$$

and referred to body axes

$$\begin{bmatrix} X_b \\ Y_b \\ Z_b \end{bmatrix} = \begin{bmatrix} \mathring{X}_{u_b} & 0 & \mathring{X}_{w_b} \\ 0 & \mathring{Y}_{v_b} & 0 \\ \mathring{Z}_{u_b} & 0 & \mathring{X}_{w_b} \end{bmatrix} \begin{bmatrix} u_b \\ v_b \\ w_b \end{bmatrix} \tag{A7.4}$$

Substitute equations (A7.3) and (A7.4) into equation (A7.1)

$$\begin{bmatrix} \mathring{X}_{u_w} & 0 & \mathring{X}_{w_w} \\ 0 & \mathring{Y}_{v_w} & 0 \\ \mathring{Z}_{u_w} & 0 & \mathring{X}_{w_w} \end{bmatrix} \begin{bmatrix} u_w \\ v_w \\ w_w \end{bmatrix} = \begin{bmatrix} \cos\alpha_e & 0 & \sin\alpha_e \\ 0 & 1 & 0 \\ -\sin\alpha_e & 0 & \cos\alpha_e \end{bmatrix} \begin{bmatrix} \mathring{X}_{u_b} & 0 & \mathring{X}_{w_b} \\ 0 & \mathring{Y}_{v_b} & 0 \\ \mathring{Z}_{u_b} & 0 & \mathring{X}_{w_b} \end{bmatrix} \begin{bmatrix} u_b \\ v_b \\ w_b \end{bmatrix} \tag{A7.5}$$

Now the transformation of linear velocity components from a *wind to body axes* reference may be obtained directly from the application of the direction cosine matrix, equation (2.12), with the same constraints as above

$$\begin{bmatrix} u_b \\ v_b \\ w_b \end{bmatrix} = \begin{bmatrix} \cos\alpha_e & 0 & -\sin\alpha_e \\ 0 & 1 & 0 \\ \sin\alpha_e & 0 & \cos\alpha_e \end{bmatrix} \begin{bmatrix} u_w \\ v_w \\ w_w \end{bmatrix} \tag{A7.6}$$

Substitute the velocity vector referred to body axes, given by equation (A7.6), into equation (A7.5) and cancel the velocity vectors referred to wind axes to obtain

$$\begin{bmatrix} \mathring{X}_{u_w} & 0 & \mathring{X}_{w_w} \\ 0 & \mathring{Y}_{v_w} & 0 \\ \mathring{Z}_{u_w} & 0 & \mathring{X}_{w_w} \end{bmatrix} = \begin{bmatrix} \cos\alpha_e & 0 & \sin\alpha_e \\ 0 & 1 & 0 \\ -\sin\alpha_e & 0 & \cos\alpha_e \end{bmatrix} \begin{bmatrix} \mathring{X}_{u_b} & 0 & \mathring{X}_{w_b} \\ 0 & \mathring{Y}_{v_b} & 0 \\ \mathring{Z}_{u_b} & 0 & \mathring{X}_{w_b} \end{bmatrix} \begin{bmatrix} \cos\alpha_e & 0 & -\sin\alpha_e \\ 0 & 1 & 0 \\ \sin\alpha_e & 0 & \cos\alpha_e \end{bmatrix}$$

or, after multiplying the matrices on the right-hand side, the following transformations are obtained

$$\left.\begin{aligned}
\mathring{X}_{u_w} &= \mathring{X}_{u_b}\cos^2\alpha_e + \mathring{Z}_{w_b}\sin^2\alpha_e + (\mathring{X}_{w_b} + \mathring{Z}_{u_b})\sin\alpha_e\cos\alpha_e \\
\mathring{X}_{w_w} &= \mathring{X}_{w_b}\cos^2\alpha_e - \mathring{Z}_{u_b}\sin^2\alpha_e - (\mathring{X}_{u_b} - \mathring{Z}_{w_b})\sin\alpha_e\cos\alpha_e \\
\mathring{Y}_{v_w} &= \mathring{Y}_{v_b} \\
\mathring{Z}_{u_w} &= \mathring{Z}_{u_b}\cos^2\alpha_e - \mathring{X}_{w_b}\sin^2\alpha_e - (\mathring{X}_{u_b} - \mathring{Z}_{w_b})\sin\alpha_e\cos\alpha_e \\
\mathring{Z}_{w_w} &= \mathring{Z}_{w_b}\cos^2\alpha_e + \mathring{X}_{u_b}\sin^2\alpha_e - (\mathring{X}_{w_b} + \mathring{Z}_{u_b})\sin\alpha_e\cos\alpha_e
\end{aligned}\right\} \quad \text{(A7.7)}$$

3.2 *MOMENT–VELOCITY DERIVATIVES*

Consider now the situation when the aerodynamic moment components comprise only those terms involving the moment–velocity derivatives. Then, referred to wind axes

$$\begin{bmatrix} L_w \\ M_w \\ N_w \end{bmatrix} = \begin{bmatrix} 0 & \mathring{L}_{v_w} & 0 \\ \mathring{M}_{u_w} & & \mathring{M}_{w_w} \\ 0 & \mathring{N}_{v_w} & 0 \end{bmatrix} \begin{bmatrix} u_w \\ v_w \\ w_w \end{bmatrix} \quad \text{(A7.8)}$$

and referred to body axes

$$\begin{bmatrix} L_b \\ M_b \\ N_b \end{bmatrix} = \begin{bmatrix} 0 & \mathring{L}_{v_b} & 0 \\ \mathring{M}_{u_b} & & \mathring{M}_{w_b} \\ 0 & \mathring{N}_{v_b} & 0 \end{bmatrix} \begin{bmatrix} u_b \\ v_b \\ w_b \end{bmatrix} \quad \text{(A7.9)}$$

Substitute equations (A7.8) and (A7.9) into equation (A7.2)

$$\begin{bmatrix} 0 & \mathring{L}_{v_w} & 0 \\ \mathring{M}_{u_w} & & \mathring{M}_{w_w} \\ 0 & \mathring{N}_{v_w} & 0 \end{bmatrix} \begin{bmatrix} u_w \\ v_w \\ w_w \end{bmatrix} = \begin{bmatrix} \cos\alpha_e & 0 & \sin\alpha_e \\ 0 & 1 & 0 \\ -\sin\alpha_e & 0 & \cos\alpha_e \end{bmatrix} \begin{bmatrix} 0 & \mathring{L}_{v_b} & 0 \\ \mathring{M}_{u_b} & & \mathring{M}_{w_b} \\ 0 & \mathring{N}_{v_b} & 0 \end{bmatrix} \begin{bmatrix} u_b \\ v_b \\ w_b \end{bmatrix} \quad \text{(A7.10)}$$

As before, the transformation of linear velocity components from a *wind to body axes* reference is given by equation (A7.6). Substitute the velocity vector referred to body axes, given by equation (A7.6), into equation (A7.10). Again, the velocity vectors referred to wind axes cancel and after multiplying the matrices on the right-hand side the following transformations are obtained

$$\left.\begin{aligned}
\mathring{L}_{v_w} &= \mathring{L}_{v_b}\cos\alpha_e + \mathring{N}_{v_b}\sin\alpha_e \\
\mathring{M}_{u_w} &= \mathring{M}_{u_b}\cos\alpha_e + \mathring{M}_{w_b}\sin\alpha_e \\
\mathring{M}_{w_w} &= \mathring{M}_{w_b}\cos\alpha_e - \mathring{M}_{u_b}\sin\alpha_e \\
\mathring{N}_{v_w} &= \mathring{N}_{v_b}\cos\alpha_e - \mathring{L}_{v_b}\sin\alpha_e
\end{aligned}\right\} \quad \text{(A7.11)}$$

3.3 *FORCE–ROTARY DERIVATIVES*

Consider now the situation when the aerodynamic force components comprise only those terms involving the force–angular velocity derivatives, more commonly referred to as the force–rotary derivatives. Then, referred to wind axes

$$\begin{bmatrix} X_w \\ Y_w \\ Z_w \end{bmatrix} = \begin{bmatrix} 0 & \mathring{X}_{q_w} & 0 \\ \mathring{Y}_{p_w} & 0 & \mathring{Y}_{r_w} \\ 0 & \mathring{Z}_{q_w} & 0 \end{bmatrix} \begin{bmatrix} p_w \\ q_w \\ r_w \end{bmatrix} \tag{A7.12}$$

and referred to body axes

$$\begin{bmatrix} X_b \\ Y_b \\ Z_b \end{bmatrix} = \begin{bmatrix} 0 & \mathring{X}_{q_b} & 0 \\ \mathring{Y}_{p_b} & 0 & \mathring{Y}_{r_b} \\ 0 & \mathring{Z}_{q_b} & 0 \end{bmatrix} \begin{bmatrix} p_b \\ q_b \\ r_b \end{bmatrix} \tag{A7.13}$$

Substitute equations (A7.12) and (A7.13) into equation (A7.1)

$$\begin{bmatrix} 0 & \mathring{X}_{q_w} & 0 \\ \mathring{Y}_{p_w} & 0 & \mathring{Y}_{r_w} \\ 0 & \mathring{Z}_{q_w} & 0 \end{bmatrix} \begin{bmatrix} p_w \\ q_w \\ r_w \end{bmatrix} = \begin{bmatrix} \cos\alpha_e & 0 & \sin\alpha_e \\ 0 & 1 & 0 \\ -\sin\alpha_e & 0 & \cos\alpha_e \end{bmatrix} \begin{bmatrix} 0 & \mathring{X}_{q_b} & 0 \\ \mathring{Y}_{p_b} & 0 & \mathring{Y}_{r_b} \\ 0 & \mathring{Z}_{q_b} & 0 \end{bmatrix} \begin{bmatrix} p_b \\ q_b \\ r_b \end{bmatrix} \tag{A7.14}$$

Now, with reference to Chapter 2, the treatment of angular velocity components as vectors enables their transformation from a *wind to body axes* reference to be obtained as before by the direct application of the direction cosine matrix, equation (2.12). Thus, with the same constraints as above

$$\begin{bmatrix} p_b \\ q_b \\ r_b \end{bmatrix} = \begin{bmatrix} \cos\alpha_e & 0 & -\sin\alpha_e \\ 0 & 1 & 0 \\ \sin\alpha_e & 0 & \cos\alpha_e \end{bmatrix} \begin{bmatrix} p_w \\ q_w \\ r_w \end{bmatrix} \tag{A7.15}$$

Substitute the angular velocity vector referred to body axes, given by equation (A7.15), into equation (A7.14) and cancel the velocity vectors referred to wind axes to obtain

$$\begin{bmatrix} 0 & \mathring{X}_{q_w} & 0 \\ \mathring{Y}_{p_w} & 0 & \mathring{Y}_{r_w} \\ 0 & \mathring{Z}_{q_w} & 0 \end{bmatrix} = \begin{bmatrix} \cos\alpha_e & 0 & \sin\alpha_e \\ 0 & 1 & 0 \\ -\sin\alpha_e & 0 & \cos\alpha_e \end{bmatrix} \begin{bmatrix} 0 & \mathring{X}_{q_b} & 0 \\ \mathring{Y}_{p_b} & 0 & \mathring{Y}_{r_b} \\ 0 & \mathring{Z}_{q_b} & 0 \end{bmatrix} \begin{bmatrix} \cos\alpha_e & 0 & -\sin\alpha_e \\ 0 & 1 & 0 \\ \sin\alpha_e & 0 & \cos\alpha_e \end{bmatrix}$$

or, after multiplying the matrices on the right-hand side, the following transformations are obtained

$$\left.\begin{aligned} \mathring{X}_{q_w} &= \mathring{X}_{q_b}\cos\alpha_e + \mathring{Z}_{q_b}\sin\alpha_e \\ \mathring{Y}_{p_w} &= \mathring{Y}_{p_b}\cos\alpha_e + \mathring{Y}_{r_b}\sin\alpha_e \\ \mathring{Y}_{r_w} &= \mathring{Y}_{r_b}\cos\alpha_e - \mathring{Y}_{p_b}\sin\alpha_e \\ \mathring{Z}_{q_w} &= \mathring{Z}_{q_b}\cos\alpha_e - \mathring{X}_{q_b}\sin\alpha_e \end{aligned}\right\} \tag{A7.16}$$

3.4 MOMENT–ROTARY DERIVATIVES

Consider now the situation when the aerodynamic moment components comprise only those terms involving the moment–angular velocity derivatives, or moment–rotary derivatives. Then, referred to wind axes

$$\begin{bmatrix} L_w \\ M_w \\ N_w \end{bmatrix} = \begin{bmatrix} \mathring{L}_{p_w} & 0 & \mathring{L}_{r_w} \\ 0 & \mathring{M}_{q_w} & 0 \\ \mathring{N}_{p_w} & 0 & \mathring{N}_{r_w} \end{bmatrix} \begin{bmatrix} p_w \\ q_w \\ r_w \end{bmatrix} \tag{A7.17}$$

and referred to body axes

$$\begin{bmatrix} L_b \\ M_b \\ N_b \end{bmatrix} = \begin{bmatrix} \mathring{L}_{p_b} & 0 & \mathring{L}_{r_b} \\ 0 & \mathring{M}_{q_b} & 0 \\ \mathring{N}_{p_b} & 0 & \mathring{N}_{r_b} \end{bmatrix} \begin{bmatrix} p_b \\ q_b \\ r_b \end{bmatrix} \tag{A7.18}$$

Substitute equations (A7.17) and (A7.18) into equation (A7.2)

$$\begin{bmatrix} \mathring{L}_{p_w} & 0 & \mathring{L}_{r_w} \\ 0 & \mathring{M}_{q_w} & 0 \\ \mathring{N}_{p_w} & 0 & \mathring{N}_{r_w} \end{bmatrix} \begin{bmatrix} p_w \\ q_w \\ r_w \end{bmatrix} = \begin{bmatrix} \cos\alpha_e & 0 & \sin\alpha_e \\ 0 & 1 & 0 \\ -\sin\alpha_e & 0 & \cos\alpha_e \end{bmatrix} \begin{bmatrix} \mathring{L}_{p_b} & 0 & \mathring{L}_{r_b} \\ 0 & \mathring{M}_{q_b} & 0 \\ \mathring{N}_{p_b} & 0 & \mathring{N}_{r_b} \end{bmatrix} \begin{bmatrix} p_b \\ q_b \\ r_b \end{bmatrix} \tag{A7.19}$$

As before, the transformation of angular velocity components from a *wind to body axes* reference is given by equation (A7.15). Substitute the angular velocity vector referred to body axes, given by equation (A7.15), into equation (A7.19). Again, the angular velocity vectors referred to wind axes cancel and after multiplying the matrices on the right-hand side the following transformations are obtained

$$\left.\begin{aligned} \mathring{L}_{p_w} &= \mathring{L}_{p_b}\cos^2\alpha_e + \mathring{N}_{r_b}\sin^2\alpha_e + (\mathring{L}_{r_b} + \mathring{N}_{p_b})\sin\alpha_e\cos\alpha_e \\ \mathring{L}_{r_w} &= \mathring{L}_{r_b}\cos^2\alpha_e - \mathring{N}_{p_b}\sin^2\alpha_e - (\mathring{L}_{p_b} - \mathring{N}_{r_b})\sin\alpha_e\cos\alpha_e \\ \mathring{M}_{q_w} &= \mathring{M}_{q_b} \\ \mathring{N}_{p_w} &= \mathring{N}_{p_b}\cos^2\alpha_e - \mathring{L}_{r_b}\sin^2\alpha_e - (\mathring{L}_{p_b} - \mathring{N}_{r_b})\sin\alpha_e\cos\alpha_e \\ \mathring{N}_{r_w} &= \mathring{N}_{r_b}\cos^2\alpha_e + \mathring{L}_{p_b}\sin^2\alpha_e - (\mathring{L}_{r_b} + \mathring{N}_{p_b})\sin\alpha_e\cos\alpha_e \end{aligned}\right\} \tag{A7.20}$$

3.5 FORCE–ACCELERATION DERIVATIVES

The force–acceleration derivatives are calculated in exactly the same way as the force–velocity derivatives. However, in this case, the aerodynamic force components referred to wind axes are given by

$$\begin{bmatrix} X_w \\ Y_w \\ Z_w \end{bmatrix} = \begin{bmatrix} 0 & 0 & \mathring{X}_{\dot{w}_w} \\ 0 & 0 & 0 \\ 0 & 0 & \mathring{Z}_{\dot{w}_w} \end{bmatrix} \begin{bmatrix} \dot{u}_w \\ \dot{v}_w \\ \dot{w}_w \end{bmatrix} \tag{A7.21}$$

and referred to body axes

$$\begin{bmatrix} X_b \\ Y_b \\ Z_b \end{bmatrix} = \begin{bmatrix} 0 & 0 & \mathring{X}_{\dot{w}_b} \\ 0 & 0 & 0 \\ 0 & 0 & \mathring{Z}_{\dot{w}_b} \end{bmatrix} \begin{bmatrix} \dot{u}_b \\ \dot{v}_b \\ \dot{w}_b \end{bmatrix} \tag{A7.22}$$

Equations (A7.21) and (A7.22) are substituted into equation (A7.1), the velocity vectors become acceleration vectors and, after some algebraic manipulation, the following transformations are obtained

$$\left.\begin{aligned} \mathring{X}_{\dot{w}_w} &= \mathring{X}_{\dot{w}_b}\cos^2\alpha_e + \mathring{Z}_{\dot{w}_b}\sin\alpha_e\cos\alpha_e \\ \mathring{Z}_{\dot{w}_w} &= \mathring{Z}_{\dot{w}_b}\cos^2\alpha_e - \mathring{X}_{\dot{w}_b}\sin\alpha_e\cos\alpha_e \end{aligned}\right\} \tag{A7.23}$$

3.6 MOMENT–ACCELERATION DERIVATIVES

The moment–acceleration derivatives are calculated in exactly the same way as the moment–velocity derivatives. However, in this case, the aerodynamic moment components referred to wind axes are given by

$$\begin{bmatrix} L_w \\ M_w \\ N_w \end{bmatrix} = \begin{bmatrix} 0 & 0 & 0 \\ 0 & 0 & \mathring{M}_{\dot{w}_w} \\ 0 & 0 & 0 \end{bmatrix} \begin{bmatrix} \dot{u}_w \\ \dot{v}_w \\ \dot{w}_w \end{bmatrix} \tag{A7.24}$$

and referred to body axes

$$\begin{bmatrix} L_b \\ M_b \\ N_b \end{bmatrix} = \begin{bmatrix} 0 & 0 & 0 \\ 0 & 0 & \mathring{M}_{\dot{w}_b} \\ 0 & 0 & 0 \end{bmatrix} \begin{bmatrix} \dot{u}_b \\ \dot{v}_b \\ \dot{w}_b \end{bmatrix} \tag{A7.25}$$

Equations (A7.24) and (A7.25) are substituted into equation (A7.2), the velocity vectors become acceleration vectors and, after some algebraic manipulation, the following transformation is obtained

$$\mathring{M}_{\dot{w}_w} = \mathring{M}_{\dot{w}_b}\cos\alpha_e \tag{A7.26}$$

3.7 AERODYNAMIC CONTROL DERIVATIVES

The aerodynamic control derivatives are most easily dealt with by denoting a general control input δ. The transformation of the control force derivatives from a *body to wind axes* reference then follows directly from equation (A7.1) by writing

$$\begin{bmatrix} \mathring{X}_{\delta_w} \\ \mathring{Y}_{\delta_w} \\ \mathring{Z}_{\delta_w} \end{bmatrix}\delta = \begin{bmatrix} \cos\alpha_e & 0 & \sin\alpha_e \\ 0 & 1 & 0 \\ -\sin\alpha_e & 0 & \cos\alpha_e \end{bmatrix} \begin{bmatrix} \mathring{X}_{\delta_b} \\ \mathring{Y}_{\delta_b} \\ \mathring{Z}_{\delta_b} \end{bmatrix}\delta \tag{A7.27}$$

The corresponding transformation of the control moment derivatives follows directly from equation (A7.2) by writing

$$\begin{bmatrix} \mathring{L}_{\delta_w} \\ \mathring{M}_{\delta_w} \\ \mathring{N}_{\delta_w} \end{bmatrix}\delta = \begin{bmatrix} \cos\alpha_e & 0 & \sin\alpha_e \\ 0 & 1 & 0 \\ -\sin\alpha_e & 0 & \cos\alpha_e \end{bmatrix} \begin{bmatrix} \mathring{L}_{\delta_b} \\ \mathring{M}_{\delta_b} \\ \mathring{N}_{\delta_b} \end{bmatrix}\delta \tag{A7.28}$$

The specific control derivative transformations are then obtained by substituting elevator angle η, aileron angle ξ, rudder angle ζ, thrust τ and so on, in place of δ in

equations (A7.27) and (A7.28). Bearing in mind that the longitudinal and lateral equations of motion are decoupled then it follows that

$$\left.\begin{aligned} \mathring{X}_{\eta_w} &= \mathring{X}_{\eta_b}\cos\alpha_e + \mathring{Z}_{\eta_b}\sin\alpha_e \\ \mathring{Z}_{\eta_w} &= \mathring{Z}_{\eta_b}\cos\alpha_e - \mathring{X}_{\eta_b}\sin\alpha_e \\ \mathring{M}_{\eta_w} &= \mathring{M}_{\eta_b} \end{aligned}\right\} \tag{A7.29}$$

and

$$\left.\begin{aligned} \mathring{Y}_{\xi_w} &= \mathring{Y}_{\xi_b} \\ \mathring{L}_{\xi_w} &= \mathring{L}_{\xi_b}\cos\alpha_e + \mathring{N}_{\xi_b}\sin\alpha_e \\ \mathring{N}_{\xi_w} &= \mathring{N}_{\xi_b}\cos\alpha_e - \mathring{L}_{\xi_b}\sin\alpha_e \end{aligned}\right\} \tag{A7.30}$$

By writing τ in place of η in equation (A7.29) the thrust control derivative transformations are obtained. Similarly, by writing ζ in place of ξ in equation (A7.30) the rudder control derivative transformations are obtained.

4. Summary

The *body to wind axes* derivative transformations described above are summarized in Table A7.1. The transformations from *wind to body axes* are easily obtained by the inverse procedure and these are summarized in Table A7.2 for convenience. The corresponding control derivative transformations are summarized in Tables A7.3 and A7.4.

Table A7.1 Body axes to wind axes derivative transformations

Wind axes	Body axes
$\mathring{X}_{u_w}$	$\mathring{X}_{u_b}\cos^2\alpha_e + \mathring{Z}_{w_b}\sin^2\alpha_e + (\mathring{X}_{w_b} + \mathring{Z}_{u_b})\sin\alpha_e\cos\alpha_e$
$\mathring{X}_{w_w}$	$\mathring{X}_{w_b}\cos^2\alpha_e - \mathring{Z}_{u_b}\sin^2\alpha_e - (\mathring{X}_{u_b} - \mathring{Z}_{w_b})\sin\alpha_e\cos\alpha_e$
$\mathring{Y}_{v_w}$	$\mathring{Y}_{v_b}$
$\mathring{Z}_{u_w}$	$\mathring{Z}_{u_b}\cos^2\alpha_e - \mathring{X}_{w_b}\sin^2\alpha_e - (\mathring{X}_{u_b} - \mathring{Z}_{w_b})\sin\alpha_e\cos\alpha_e$
$\mathring{Z}_{w_w}$	$\mathring{Z}_{w_b}\cos^2\alpha_e + \mathring{X}_{u_b}\sin^2\alpha_e - (\mathring{X}_{w_b} + \mathring{Z}_{u_b})\sin\alpha_e\cos\alpha_e$
$\mathring{L}_{v_w}$	$\mathring{L}_{v_b}\cos\alpha_e + \mathring{N}_{v_b}\sin\alpha_e$
$\mathring{M}_{u_w}$	$\mathring{M}_{u_b}\cos\alpha_e + \mathring{M}_{w_b}\sin\alpha_e$
$\mathring{M}_{w_w}$	$\mathring{M}_{w_b}\cos\alpha_e - \mathring{M}_{u_b}\sin\alpha_e$
$\mathring{N}_{v_w}$	$\mathring{N}_{v_b}\cos\alpha_e - \mathring{L}_{v_b}\sin\alpha_e$
$\mathring{X}_{q_w}$	$\mathring{X}_{q_b}\cos\alpha_e + \mathring{Z}_{q_b}\sin\alpha_e$
$\mathring{Y}_{p_w}$	$\mathring{Y}_{p_b}\cos\alpha_e + \mathring{Y}_{r_b}\sin\alpha_e$
$\mathring{Y}_{r_w}$	$\mathring{Y}_{r_b}\cos\alpha_e - \mathring{Y}_{p_b}\sin\alpha_e$
$\mathring{Z}_{q_w}$	$\mathring{Z}_{q_b}\cos\alpha_e - \mathring{X}_{q_b}\sin\alpha_e$
$\mathring{L}_{p_w}$	$\mathring{L}_{p_b}\cos^2\alpha_e + \mathring{N}_{r_b}\sin^2\alpha_e + (\mathring{L}_{r_b} + \mathring{N}_{p_b})\sin\alpha_e\cos\alpha_e$
$\mathring{L}_{r_w}$	$\mathring{L}_{r_b}\cos^2\alpha_e - \mathring{N}_{p_b}\sin^2\alpha_e - (\mathring{L}_{p_b} - \mathring{N}_{r_b})\sin\alpha_e\cos\alpha_e$
$\mathring{M}_{q_w}$	$\mathring{M}_{q_b}$
$\mathring{N}_{p_w}$	$\mathring{N}_{p_b}\cos^2\alpha_e - \mathring{L}_{r_b}\sin^2\alpha_e - (\mathring{L}_{p_b} - \mathring{N}_{r_b})\sin\alpha_e\cos\alpha_e$
$\mathring{N}_{r_w}$	$\mathring{N}_{r_b}\cos^2\alpha_e + \mathring{L}_{p_b}\sin^2\alpha_e - (\mathring{L}_{r_b} + \mathring{N}_{p_b})\sin\alpha_e\cos\alpha_e$
$\mathring{X}_{\dot{w}_w}$	$\mathring{X}_{\dot{w}_b}\cos^2\alpha_e + \mathring{Z}_{\dot{w}_b}\sin\alpha_e\cos\alpha_e$
$\mathring{Z}_{\dot{w}_w}$	$\mathring{Z}_{\dot{w}_b}\cos^2\alpha_e - \mathring{X}_{\dot{w}_b}\sin\alpha_e\cos\alpha_e$
$\mathring{M}_{\dot{w}_w}$	$\mathring{M}_{\dot{w}_b}\cos\alpha_e$
$\mathring{X}_{\eta_w}$	$\mathring{X}_{\eta_b}\cos\alpha_e + \mathring{Z}_{\eta_b}\sin\alpha_e$
$\mathring{Z}_{\eta_w}$	$\mathring{Z}_{\eta_b}\cos\alpha_e - \mathring{X}_{\eta_b}\sin\alpha_e$

Table A7.2 Wind axes to body axes derivative transformations

Body axes	Wind axes
$\mathring{X}_{u_b}$	$\mathring{X}_{u_w}\cos^2\alpha_e + \mathring{Z}_{w_w}\sin^2\alpha_e - (\mathring{X}_{w_w} + \mathring{Z}_{u_w})\sin\alpha_e\cos\alpha_e$
$\mathring{X}_{w_b}$	$\mathring{X}_{w_w}\cos^2\alpha_e - \mathring{Z}_{u_w}\sin^2\alpha_e + (\mathring{X}_{u_w} - \mathring{Z}_{w_w})\sin\alpha_e\cos\alpha_e$
$\mathring{Y}_{v_b}$	$\mathring{Y}_{v_w}$
$\mathring{Z}_{u_b}$	$\mathring{Z}_{u_w}\cos^2\alpha_e - \mathring{X}_{w_w}\sin^2\alpha_e + (\mathring{X}_{u_w} - \mathring{Z}_{w_w})\sin\alpha_e\cos\alpha_e$
$\mathring{Z}_{w_b}$	$\mathring{Z}_{w_w}\cos^2\alpha_e + \mathring{X}_{u_w}\sin^2\alpha_e + (\mathring{X}_{w_w} + \mathring{Z}_{u_w})\sin\alpha_e\cos\alpha_e$
$\mathring{L}_{v_b}$	$\mathring{L}_{v_w}\cos\alpha_e - \mathring{N}_{v_w}\sin\alpha_e$
$\mathring{M}_{u_b}$	$\mathring{M}_{u_w}\cos\alpha_e - \mathring{M}_{w_w}\sin\alpha_e$
$\mathring{M}_{w_b}$	$\mathring{M}_{w_w}\cos\alpha_e + \mathring{M}_{u_w}\sin\alpha_e$
$\mathring{N}_{v_b}$	$\mathring{N}_{v_w}\cos\alpha_e + \mathring{L}_{v_w}\sin\alpha_e$
$\mathring{X}_{q_b}$	$\mathring{X}_{q_w}\cos\alpha_e - \mathring{Z}_{q_w}\sin\alpha_e$
$\mathring{Y}_{p_b}$	$\mathring{Y}_{p_w}\cos\alpha_e - \mathring{Y}_{r_w}\sin\alpha_e$
$\mathring{Y}_{r_b}$	$\mathring{Y}_{r_w}\cos\alpha_e + \mathring{Y}_{p_w}\sin\alpha_e$
$\mathring{Z}_{q_b}$	$\mathring{Z}_{q_w}\cos\alpha_e + \mathring{X}_{q_w}\sin\alpha_e$
$\mathring{L}_{p_b}$	$\mathring{L}_{p_w}\cos^2\alpha_e + \mathring{N}_{r_w}\sin^2\alpha_e - (\mathring{L}_{r_w} + \mathring{N}_{p_w})\sin\alpha_e\cos\alpha_e$
$\mathring{L}_{r_b}$	$\mathring{L}_{r_w}\cos^2\alpha_e - \mathring{N}_{p_w}\sin^2\alpha_e + (\mathring{L}_{p_w} - \mathring{N}_{r_w})\sin\alpha_e\cos\alpha_e$
$\mathring{M}_{q_b}$	$\mathring{M}_{q_w}$
$\mathring{N}_{p_b}$	$\mathring{N}_{p_w}\cos^2\alpha_e - \mathring{L}_{r_w}\sin^2\alpha_e + (\mathring{L}_{p_w} - \mathring{N}_{r_w})\sin\alpha_e\cos\alpha_e$
$\mathring{N}_{r_b}$	$\mathring{N}_{r_w}\cos^2\alpha_e + \mathring{L}_{p_w}\sin^2\alpha_e + (\mathring{L}_{r_w} + \mathring{N}_{p_w})\sin\alpha_e\cos\alpha_e$
$\mathring{X}_{\dot{w}_b}$	$\mathring{X}_{\dot{w}_w}\cos^2\alpha_e - \mathring{Z}_{\dot{w}_w}\sin\alpha_e\cos\alpha_e$
$\mathring{Z}_{\dot{w}_b}$	$\mathring{Z}_{\dot{w}_w}\cos^2\alpha_e + \mathring{X}_{\dot{w}_w}\sin\alpha_e\cos\alpha_e$
$\mathring{M}_{\dot{w}_b}$	$\mathring{M}_{\dot{w}_w}\cos\alpha_e$

In the two following tables it is simply necessary to write η, τ, ξ or ζ in place of δ as appropriate.

Table A7.3 Body axes to wind axes control derivative transformations

Wind axes	Body axes
$\mathring{X}_{\delta_w}$	$\mathring{X}_{\delta_b} \cos\alpha_e + \mathring{Z}_{\delta_b} \sin\alpha_e$
$\mathring{Y}_{\delta_w}$	$\mathring{Y}_{\delta_b}$
$\mathring{Z}_{\delta_w}$	$\mathring{Z}_{\delta_b} \cos\alpha_e - \mathring{X}_{\delta_b} \sin\alpha_e$
$\mathring{L}_{\delta_w}$	$\mathring{L}_{\delta_b} \cos\alpha_e + \mathring{N}_{\delta_b} \sin\alpha_e$
$\mathring{M}_{\delta_w}$	$\mathring{M}_{\delta_b}$
$\mathring{N}_{\delta_w}$	$\mathring{N}_{\delta_b} \cos\alpha_e - \mathring{L}_{\delta_b} \sin\alpha_e$

Table A7.4 Wind axes to body axes control derivative transformations

Body axes	Wind axes
$\mathring{X}_{\delta_b}$	$\mathring{X}_{\delta_w} \cos\alpha_e - \mathring{Z}_{\delta_w} \sin\alpha_e$
$\mathring{Y}_{\delta_b}$	$\mathring{Y}_{\delta_w}$
$\mathring{Z}_{\delta_b}$	$\mathring{Z}_{\delta_w} \cos\alpha_e + \mathring{X}_{\delta_w} \sin\alpha_e$
$\mathring{L}_{\delta_b}$	$\mathring{L}_{\delta_w} \cos\alpha_e - \mathring{N}_{\delta_w} \sin\alpha_e$
$\mathring{M}_{\delta_b}$	$\mathring{M}_{\delta_w}$
$\mathring{N}_{\delta_b}$	$\mathring{N}_{\delta_w} \cos\alpha_e + \mathring{L}_{\delta_w} \sin\alpha_e$

Appendix 8

The Transformation of the Moments and Products of Inertia from a Body Axes Reference to a Wind Axes Reference

1. Introduction

In the same way that it is sometimes necessary to transform the aerodynamic stability and control derivatives from a body axes reference to a wind axes reference, and vice versa, it is also necessary to transform the corresponding moments and products of inertia. Again, the procedure is very straightforward and makes use of the transformation relationships discussed in Chapter 2. It is assumed that the body axes and wind axes in question have a common origin at the *cg* of the aeroplane and that it is in steady level symmetric flight. Thus, the axes differ by the steady body incidence α_e only as shown in Fig. 2.2.

2. Coordinate transformation

2.1 BODY TO WIND AXES

A set of coordinates in a body axes system (x_b, y_b, z_b) may be transformed into the equivalent set in a wind axes system (x_w, y_w, z_w) by application of the inverse direction cosine matrix given by equation (2.13). Writing $\theta = \alpha_e$ and $\phi = \psi = 0$, since level symmetric flight is assumed, then

$$\begin{bmatrix} x_w \\ y_w \\ z_w \end{bmatrix} = \begin{bmatrix} \cos\alpha_e & 0 & \sin\alpha_e \\ 0 & 1 & 0 \\ -\sin\alpha_e & 0 & \cos\alpha_e \end{bmatrix} \begin{bmatrix} x_b \\ y_b \\ z_b \end{bmatrix} \tag{A8.1}$$

or

$$\left.\begin{aligned} x_w &= x_b \cos\alpha_e + z_b \sin\alpha_e \\ y_w &= y_b \\ z_w &= z_b \cos\alpha_e - x_b \sin\alpha_e \end{aligned}\right\} \tag{A8.2}$$

2.2 WIND TO BODY AXES

A set of coordinates in a wind axes system (x_w, y_w, z_w) may be transformed into the equivalent set in a body axes system (x_b, y_b, z_b) by application of the direction cosine

Appendix 8

The Transformation of the Moments and Products of Inertia from a Body Axes Reference to a Wind Axes Reference

1. Introduction

In the same way that it is sometimes necessary to transform the aerodynamic stability and control derivatives from a body axes reference to a wind axes reference, and vice versa, it is also necessary to transform the corresponding moments and products of inertia. Again, the procedure is very straightforward and makes use of the transformation relationships discussed in Chapter 2. It is assumed that the body axes and wind axes in question have a common origin at the *cg* of the aeroplane and that it is in steady level symmetric flight. Thus, the axes differ by the steady body incidence α_e only as shown in Fig. 2.2.

2. Coordinate transformation

2.1 BODY TO WIND AXES

A set of coordinates in a body axes system (x_b, y_b, z_b) may be transformed into the equivalent set in a wind axes system (x_w, y_w, z_w) by application of the inverse direction cosine matrix given by equation (2.13). Writing $\theta = \alpha_e$ and $\phi = \psi = 0$, since level symmetric flight is assumed, then

$$\begin{bmatrix} x_w \\ y_w \\ z_w \end{bmatrix} = \begin{bmatrix} \cos\alpha_e & 0 & \sin\alpha_e \\ 0 & 1 & 0 \\ -\sin\alpha_e & 0 & \cos\alpha_e \end{bmatrix} \begin{bmatrix} x_b \\ y_b \\ z_b \end{bmatrix} \tag{A8.1}$$

or

$$\left.\begin{aligned} x_w &= x_b \cos\alpha_e + z_b \sin\alpha_e \\ y_w &= y_b \\ z_w &= z_b \cos\alpha_e - x_b \sin\alpha_e \end{aligned}\right\} \tag{A8.2}$$

2.2 WIND TO BODY AXES

A set of coordinates in a wind axes system (x_w, y_w, z_w) may be transformed into the equivalent set in a body axes system (x_b, y_b, z_b) by application of the direction cosine

matrix given by equation (2.12). Again, writing $\theta = \alpha_e$ and $\phi = \psi = 0$ since level symmetric flight is assumed, then

$$\begin{bmatrix} x_b \\ y_b \\ z_b \end{bmatrix} = \begin{bmatrix} \cos\alpha_e & 0 & -\sin\alpha_e \\ 0 & 1 & 0 \\ \sin\alpha_e & 0 & \cos\alpha_e \end{bmatrix} \begin{bmatrix} x_w \\ y_w \\ z_w \end{bmatrix} \tag{A8.3}$$

which is simply the inverse of equation (A8.1). Alternatively

$$\left.\begin{aligned} x_b &= x_w \cos\alpha_e - z_w \sin\alpha_e \\ y_b &= y_w \\ z_b &= z_w \cos\alpha_e + x_w \sin\alpha_e \end{aligned}\right\} \tag{A8.4}$$

3. The transformation of the moment of inertia in roll from a body axes reference to a wind axes reference

The moment of inertia in roll is defined in Chapter 4, Table 4.1, and may be written when referenced to a system of wind axes

$$I_{x_w} = \sum \delta m(y_w^2 + z_w^2) \tag{A8.5}$$

Substitute for y_w and z_w from equations (A8.2) to obtain

$$I_{x_w} = \sum \delta m(y_b^2 + z_b^2) + \sum \delta m(x_b^2 - z_b^2)\sin^2\alpha_e - 2\sum \delta m x_b z_b \sin\alpha_e \cos\alpha_e \tag{A8.6}$$

Add the following null expression to the right-hand side of equation (A8.6)

$$\sum \delta m(y_b^2 + z_b^2)\sin^2\alpha_e - \sum \delta m(y_b^2 + z_b^2)\sin^2\alpha_e$$

and rearrange to obtain

$$I_{x_w} = \sum \delta m(y_b^2 + z_b^2)\cos^2\alpha_e + \sum \delta m(x_b^2 + y_b^2)\sin^2\alpha_e - 2\sum \delta m x_b z_b \sin\alpha_e \cos\alpha_e \tag{A8.7}$$

Referring to the definitions of moments and products of inertia in Chapter 4, Table 4.1, equation (A8.7) may be rewritten

$$I_{x_w} = I_{x_b}\cos^2\alpha_e + I_{z_b}\sin^2\alpha_e - 2I_{xz_b}\sin\alpha_e \cos\alpha_e \tag{A8.8}$$

Equation (A8.8) therefore describes the inertia transformation from a body axes reference to a wind axes reference.

This simple procedure may be repeated to obtain all of the moment and product of inertia transformations from a body axes reference to a wind axes reference. The inverse procedure, using the coordinate transformations given by equations (A8.4), is equally straightforward to apply to obtain the corresponding transformations from a wind axes reference to a body axes reference.

4. Summary

The *body to wind axes* moments and products of inertia transformations are summarized in Table A8.1. The corresponding transformations from *wind to body axes* obtained by the inverse procedure are summarized in Table A8.2.

Table A8.1 Moment and product of inertia transformations from a body to wind axes reference

Wind axes	Body axes
I_{x_w}	$I_{x_b}\cos^2\alpha_e + I_{z_b}\sin^2\alpha_e - 2I_{xz_b}\sin\alpha_e\cos\alpha_e$
I_{y_w}	I_{y_b}
I_{z_w}	$I_{z_b}\cos^2\alpha_e + I_{x_b}\sin^2\alpha_e + 2I_{xz_b}\sin\alpha_e\cos\alpha_e$
I_{xy_w}	$I_{xy_b}\cos\alpha_e + I_{yz_b}\sin\alpha_e$
I_{xz_w}	$I_{xz_b}(\cos^2\alpha_e - \sin^2\alpha_e) + (I_{x_b} - I_{z_b})\sin\alpha_e\cos\alpha_e$
I_{yz_w}	$I_{yz_b}\cos\alpha_e - I_{xy_b}\sin\alpha_e$

Table A8.2 Moment and product of inertia transformations from a wind to body axes reference

Body axes	Wind axes
I_{x_b}	$I_{x_w}\cos^2\alpha_e + I_{z_w}\sin^2\alpha_e + 2I_{xz_w}\sin\alpha_e\cos\alpha_e$
I_{y_b}	I_{y_w}
I_{z_b}	$I_{z_w}\cos^2\alpha_e + I_{x_w}\sin^2\alpha_e - 2I_{xz_w}\sin\alpha_e\cos\alpha_e$
I_{xy_b}	$I_{xy_w}\cos\alpha_e - I_{yz_w}\sin\alpha_e$
I_{xz_b}	$I_{xz_w}(\cos^2\alpha_e - \sin^2\alpha_e) + (I_{z_w} - I_{x_w})\sin\alpha_e\cos\alpha_e$
I_{yz_b}	$I_{yz_w}\cos\alpha_e + I_{xy_w}\sin\alpha_e$

Appendix 9
The Root Locus Plot

1. Mathematical background

Given the general closed loop system transfer function

$$\frac{r(s)}{c(s)} = \frac{G(s)}{1 + G(s)H(s)} \tag{A9.1}$$

where r is the response to a command input c, $G(s)$ is the transfer function of the open loop system and $H(s)$ is the transfer function of the feedback controller located in the feedback path. The closed loop characteristic equation is given by the denominator of equation (A9.1)

$$1 + G(s)H(s) = 0 \tag{A9.2}$$

Now, in general, the transfer function product $G(s)H(s)$ will itself be a transfer function and may be expressed as the ratio of two polynomials

$$G(s)H(s) = \frac{K_1(1 + sT_1)(1 + sT_3)\dots}{s^n(1 + sT_2)(1 + sT_4)\dots} \tag{A9.3}$$

or, alternatively,

$$G(s)H(s) = \frac{K(s + 1/T_1)(s + 1/T_3)\dots}{s^n(s + 1/T_2)(s + 1/T_4)\dots} \tag{A9.4}$$

where the gain constant is given by

$$K = \frac{K_1 T_1 T_3 \dots}{T_2 T_4 \dots} \tag{A9.5}$$

Each factor in equation (A9.4) may be expressed alternatively in terms of magnitude and phase, assuming sinusoidal command and response such that $s = j\omega$, for example

$$(s + 1/T_1) = A_1 e^{j\phi_1} \tag{A9.6}$$

whence, equation (A9.4) may be written

$$G(s)H(s) = \frac{KA_1A_3\dots e^{j[(\phi_1+\phi_3+\dots)-(n\phi_0+\phi_2+\phi_4+\dots)]}}{A_0^n A_2 A_4 \dots} \equiv Ae^{j\phi} \tag{A9.7}$$

where the total magnitude A is given by

$$A = \frac{KA_1A_3\ldots}{A_0^nA_2A_4\ldots} \tag{A9.8}$$

and the total phase is given by

$$\phi = (\phi_1 + \phi_3 + \ldots) - (n\phi_0 + \phi_2 + \phi_4 + \ldots) \tag{A9.9}$$

Thus, the characteristic equation (A9.2) may be written

$$1 + G(s)H(s) \equiv 1 + Ae^{j\phi} = 0 \tag{A9.10}$$

which has the solution

$$Ae^{j\phi} = -1 \tag{A9.11}$$

For the solution of equation (A9.11) to exist two conditions must be satisfied.

(i) The *angle condition*

$$\phi = (\phi_1 + \phi_3 + \ldots) - (n\phi_0 + \phi_2 + \phi_4 + \ldots) = (2k+1)180° \tag{A9.12}$$

where $k = 0, \pm1, \pm2, \pm3, \ldots$.

(ii) The *magnitude condition*

$$|G(s)H(s)| = A = \frac{KA_1A_3\ldots}{A_0^nA_2A_4\ldots} = 1 \tag{A9.13}$$

Thus, any point in the s-plane where the conditions defined by both equations (A9.12) and (A9.13) are satisfied defines a root of the characteristic equation. By finding all such points in the s-plane a locus of the roots of the characteristic equation may be constructed. In fact, the root loci may be identified merely by satisfying the angle condition only; the loci may then be *calibrated* by applying the magnitude condition to selected points of interest on the loci.

2. The rules for constructing a root locus plot

The simple closed loop system of interest is defined by the structure shown in Fig. A9.1. The object is to establish how the roots of the closed loop transfer function are governed by the choice of feedback gain K_r. The *open loop* transfer function of the system is known at the outset and comprises the product of the transfer functions of all the system components in the loop

$$K_rG(s)H(s) \tag{A9.14}$$

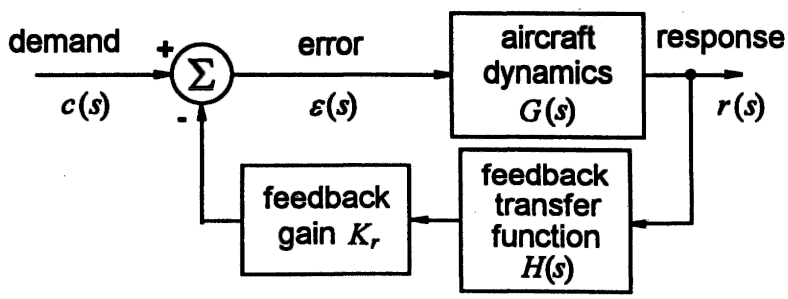

Fig. A9.1 A simple closed loop system

The corresponding *closed loop* transfer function is

$$\frac{r(s)}{c(s)} = \frac{G(s)}{1 + K_r G(s)H(s)} \tag{A9.15}$$

The root locus plot is constructed from the open loop transfer function (A9.14) which should be in factorized form for convenience. The *zeros* are the numerator roots and the *poles* are the denominator roots of (A9.14). When plotting the root loci on the *s*-plane it is often convenient to choose the same numerical scales for both the real and imaginary axes.

RULE 1

Continuous curves which comprise the branches of the locus start at the poles of $G(s)H(s)$ where the gain $K_r = 0$. The branches of the locus terminate at the zeros of $G(s)H(s)$, or at infinity, where the gain $K_r = \infty$.

RULE 2

The locus includes all points on the real axis to the left of an odd number of poles plus zeros.

RULE 3

As $K_r \to \infty$, the branches of the locus become asymptotic to straight lines with angles

$$\frac{(2k+1)180^\circ}{n_p - n_z} \qquad k = 0, \pm 1, \pm 2, \pm 3, \ldots$$

where

n_p = number of poles

n_z = number of zeros

RULE 4

The asymptotes radiate from a point on the real axis called the *centre of gravity* (*cg*) of the plot, which is determined by

$$cg = \frac{\sum \text{poles} - \sum \text{zeros}}{n_p - n_z}$$

RULE 5

The loci *break in* to, or *break away* from, points on the real axis located between pairs of zeros or pairs of poles respectively. Two methods may be used to estimate the locations of the break-in or break-away points on the real axis. The first method is approximate and gives results of acceptable accuracy for the majority of cases. The second method is exact and may be used when the first method gives unsatisfactory results.

(i) Method 1

Step 1. Select a test point on the real axis in the vicinity of a known break-in or break-away point.

Step 2. Measure the distances from the test point to each real axis pole and zero. Assign a negative sign to the pole distances, a positive sign to the zero distances and calculate the reciprocals of the distances.

Step 3. Calculate the sum of the reciprocals for all poles and zeros to the left of the test point and calculate the sum of the reciprocals for all poles and zeros to the right of the test point.

Step 4 The test point is a break-in or break-away point when the left and right reciprocal sums are equal.

Step 5. Choose a new test point and iterate until the break-in or break-away point is obtained with acceptable accuracy.

Step 6. Note that this method may give inaccurate results when complex poles and zeros lie close to the real axis.

(ii) Method 2

Step 1. Denote the open loop transfer function

$$G(s)H(s) = \frac{A(s)}{B(s)} \tag{A9.16}$$

Step 2. Define a function $F(s)$

$$F(s) = B(s)\frac{dA(s)}{ds} - A(s)\frac{dB(s)}{ds} \tag{A9.17}$$

Step 3. The roots of $F(s)$ include all the break-in or break-away points.

RULE 6

Loci branching in to, or away from, the real axis do so at $\pm 90°$ to the real axis.

RULE 7

The angle of departure of a locus from a complex pole, or the angle of arrival at a complex zero, is given by

$$\phi = \sum(\text{angles to all other zeros}) - \sum(\text{angles to all other poles}) - 180° \tag{A9.18}$$

An example is illustrated in Fig. A9.2.

Thus, with reference to Fig. A9.2, the angle of departure of the locus from complex pole p_1 is given by

$$\phi = (\theta_1 + \theta_3 + \theta_5) - (\theta_2 + \theta_4) - 180° \tag{A9.19}$$

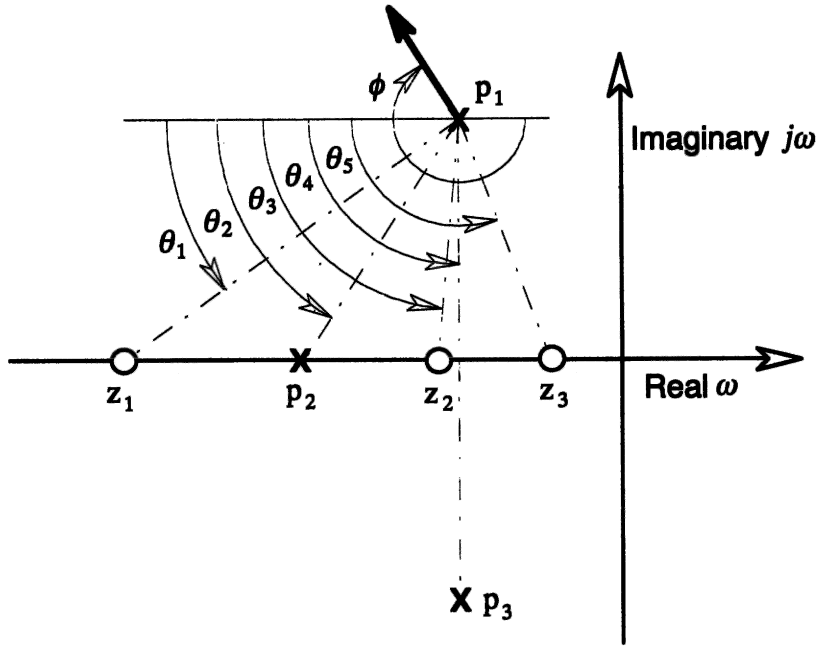

Fig. A9.2 Example of the locus departure angle from a complex pole

RULE 8

The total loop gain at any point on a locus is given by

$$\text{gain} = \frac{\prod(\text{distances from test point to poles})}{\prod(\text{distances from test point to zeros})} \tag{A9.20}$$

Note that if the system under investigation has no zeros then the denominator of expression (A9.20) is taken to be unity.

Index

Page numbers representing figures are in **bold**; tables are in *italics*